UNIVERSITAT POLITÈCNICA DE CATALUNYA
BARCELONATECH
Escola Tècnica Superior d'Enginyeria
Industrial de Barcelona

IONIC COMPLEXES OF NATURALLY-OCCURRING BIOPOLYMERS AND CATIONIC SURFACTANTS: A PLATFORM FOR INDUSTRIAL AND BIOMEDICAL APPLICATIONS

Ph.D. Thesis presented by Ana Gamarra Montes
Directed by Prof. Dr. Sebastián Muñoz-Guerra
Barcelona, Julio 2018

ABSTRACT

In recent years, the increasing public concern about the environmental pollution caused by persistent plastic wastes has stimulated the interest in replacing synthetic polymers by biopolymers. The term biopolymer refers to polymers that are either renewable or biodegradable or both. Biopolymers are capable of bio-assimilation at accelerated rates so they are biocompatible with the environment. Furthermore, it is of exceptional interest their sustainability; the renewable origin of biopolymers makes them inexhaustible in contrast with the uncertain accessibility at medium-term of synthetic polymers produced from fossil sources. Nevertheless, biopolymers often have inferior properties compared to commodity polymers. Modification is a way to improve properties and achieve property combinations required for specific applications. Therefore the synthesis, characterization and property evaluation of new biopolymers derivatives are essential tasks that have to be done for the development of new materials able to replace the traditional plastics in areas such as industrial, medical, food, consumer products, and pharmaceutical applications.

In the present Thesis, the chemical modification of two kinds of carboxylic biopolymers has been studied to respond to the necessity of creating new biopolymer derivatives with advanced properties at reasonable cost. Poly (γ-glutamic acid) (**PGGA**) and hyaluronic acid (**HyA**) were the biopolymers selected for their capacity to form stable ionic complexes with cationic surfactants to generate stable materials with new properties. These complexes are currently object of intensive research in our group due to their outstanding features. They are easily prepared and they tend to be self-assembled in well-ordered amphiphilic structures able to respond reversibly to thermal effects. This behaviour is of high scientific interest and of practical relevance in the design of medical devices for thermally and chemically controlled store and delivery of drugs.

The main goal of this Thesis is the preparation of ionic complexes of the two mentioned polyacids using different cationic surfactants depending on the desired final properties. The first part of the work is devoted to provide physicochemical knowledge of the structure and properties of alkyltrimethylphosphonium surfactants which have potential interest for novel applications. Then these surfactants were coupled to both PGGA and HyA to obtain the respective ionic complexes with biocide activity and higher thermal stability than those made of their ammonium analogs. PGGA complexes, abbreviated as ***n*ATMP·PGGA**, have high interest as food preserving and packaging applications having as main advantage the edibility of this polymer and the possibility of improving their basic properties through blending with nanoclays. On the

other hand, HyA complexes, ***n*ATMP·HyA**, are useful to obtain HyA derivatives with antimicrobial activity. In addition, the preparation of nanoparticles of *n*ATMP·HyA with antimicrobial properties was carried out using the ionotropic gelation method.

The second part of the Thesis was devoted to the preparation of "greener" complexes of hyaluronic acid. For this regard, alkanoylcholine surfactants were used to prepare the ionic complexes ***n*ACh·HyA**. These complexes constitute a highly promising biocompatible/biodegradable platform for the design of systems suitable for drug transport and targeting delivery in anticancer chemotherapy because it was demonstrated that non-cytotoxic nanoparticles can be prepared with these systems.

The third part of the Thesis is dedicated to explore the preparation of biocompatible antimicrobial complexes using as cationic surfactant one of the most potent food preservative agents that is well-known today, that is the ethyl $^{\alpha}$*N*-lauroyl *L*-arginate chloride surfactant (also known as LAE). These complexes (**LAE·PGGA** and **LAE·HyA**) are shown to be potential candidates to develop antimicrobial edible films and hyaluronic-based antimicrobial materials, respectively.

Key words: Poly(γ-glutamic acid) (PGGA), hyaluronic acid (HyA), biotechnological polymer, ionic polymer complex, tetraalkylphosphonium surfactant, ethyl $^{\alpha}$N-lauroyl L-arginate chloride, antimicrobial biopolymers, alkanoylcholines.

RESUMEN

En los últimos años se ha producido un aumento de la preocupación sobre la contaminación producida por plásticos persistentes que ha estimulado el interés de remplazar los polímeros sintéticos por biopolímeros. El término biopolímero se refiere a polímeros que son o bien renovables o biodegradables o ambos. Los biopolímeros son capaces de ser bioasimilados a velocidades aceleradas, por tanto, son biocompatibles con el medio ambiente. Además, es de excepcional interés su sustentabilidad; el origen renovable de los biopolímeros les hace inagotables al contrario que los polímeros sintéticos que al ser producidos a partir de fuentes fósiles tienen una incierta accesibilidad a medio plazo. Sin embargo, los biopolímeros a menudo tienen propiedades inferiores si les comparamos con los polímeros habituales. La modificación es una vía para mejorar las propiedades y alcanzar las combinaciones de propiedades requeridas para aplicaciones específicas. Por tanto, la síntesis, caracterización y evaluación de propiedades de nuevos derivados de biopolímeros son tareas esenciales que se tienen que realizar para el desarrollo de nuevos materiales capaces de remplazar los plásticos tradicionales en sectores tales como la industria química, la automoción, medicina, alimentación, productos de consumo y aplicaciones farmacéuticas.

En la presente Tesis, se ha estudiado la modificación química de dos tipos de biopolímeros carboxílicos para responder a la necesidad de crear nuevos derivados de biopolímeros con propiedades avanzadas y un precio razonable. El ácido poly (γ-glutámico) (**PGGA**) y el ácido hialurónico (**HyA**) fueron seleccionados por su capacidad para formar complejos iónicos estables con surfactantes catiónicos para generar materiales estables con nuevas propiedades. Estos complejos son actualmente objeto de intensa investigación en nuestro grupo debido a sus propiedades destacadas. Estos complejos son fácilmente preparados y tienden a autoensamblarse en estructuras anfifílicas ordenadas capaces de responder reversiblemente a efectos térmicos. Este comportamiento es de elevado interés científico y de relevancia práctica en el diseño de dispositivos médicos para el almacenamiento y liberación de fármacos de manera térmica y químicamente controlada.

El principal objetivo de esta Tesis es la preparación de complejos iónicos de los dos poliácidos mencionados usando diferentes surfactantes catiónicos dependiendo de las propiedades finales deseadas. La primera parte del trabajo está dedicada a proporcionar el conocimiento fisico-químico de la estructura y propiedades de los surfactantes de alquiltrimetilfosfonio, los cuales tienen un interés potencial para nuevas

aplicaciones. Después estos surfactantes fueron acoplados a ambos, el PGGA y el HyA para obtener los respectivos complejos iónicos con propiedades biocidas y mayor estabilidad térmica que aquellos complejos preparados a partir de sus análogos de amonio. Los complejos de PGGA, abreviados como ***n*ATMP·PGGA**, tienen un alto interés como preservadores de alimentos y aplicaciones de envasado teniendo como principal ventaja la comestibilidad de este polímero y la posibilidad de mejorar sus propiedades básicas mezclándoles con nanoarcillas. Por otro lado, los complejos de HyA, ***n*ATMP·HyA**, son útiles para obtener derivados del ácido hialurónico con actividad antimicrobiana. Además, se ha llevado a cabo la preparación de nanopartículas de *n*ATMP·HyA con propiedades antimicrobianas utilizando el método "ionotropic gelation".

La segunda parte de la Tesis se dedicó a la preparación de complejos sostenibles de ácido hialurónico. Para ello se utilizaron surfactantes de alcanoilcolinas para preparar los complejos iónicos ***n*ACh·HyA**. Estos complejos constituyen una prometedora plataforma biocompatible/biodegradable para el diseño de sistemas capaces del transporte y liberación específica de fármacos anticancerígenos en quimioterapias porque se ha demostrado que se pueden preparar nanopartículas no-toxicas con estos sistemas.

La tercera parte de la Tesis está dedicada a explorar la preparación de complejos biocompatibles con propiedades antimicrobianas utilizando como surfactante catiónico uno de los preservantes alimenticios más potentes de los que se conoce actualmente, el cloruro de etil $^{\alpha}$*N*-lauroil *L*-arginato (también conocido como LAE). Estos complejos (**LAE·PGGA** y **LAE·HyA**) son candidatos potenciales para desarrollar films comestibles con propiedades antimicrobianas y materiales de ácido hialurónico con propiedades antimicrobianas, respectivamente.

Palabras clave: ácido poli(γ-glutámico) (PGGA), ácido hialurónico (HyA), polímeros biotecnológicos, complejos poliméricos iónicos, surfactante de tetraalquilfosfonio, cloruro de $^{\alpha}$N-lauroil L-arginato, biopolímeros con propiedades antimicrobianas, alcanoilcolinas.

RESUM

En els últims anys s'ha produït un augment de la preocupació sobre la contaminació produïda pels plàstics persistents que ha estimulat l'interès per reemplaçar els polímers sintètics pels biopolímers. El terme biopolímer es refereix als polímers que són o bé renovables o biodegradables, o ambdós. A més, és de excepcional interès la seva sostenibilitat; l'origen renovable dels biopolímers els fa inesgotables al contrari dels polímers sintètics, que al ser produïts a partir de fonts fòssils presenten una accessibilitat incerta a mig termini. No obstant, els biopolímers presenten de vegades unes propietats inferiors si se'ls comparem amb els polímers tradicionals. La modificació és una vía per millorer les propietats i arribar a les combinacions de propietats requerides per a aplicacions específiques. Per tant, la síntesi, caracterització i avaluació de propietats de nous derivats de biopolímers són tasques essencials que s'han de realitzar pel desenvolupament de nous materials capaços de reemplaçar els plàstics tradicionals en sectors com ara la indústria química, medicina, alimentació, productes de consum i farmàcia.

En la present Tesi, s'ha estudiat la modificació química de dos tipus de biopolímers carboxílics per respondre a la necessitat de crear derivats de biopolímers amb propietats avançades i a un preu raonable. L'àcid poli(glutamic) (**PGGA**) i l'àcid hialurònic (**HyA**) van ser seleccionats per la seva capacitat per formar complexes iònics estables amb surfactants catiònics per generar materials estables amb noves propietats. Aquests complexes es preparen fàcilment i tendeixen a autoassemblar-se en estructures amfifíliques ordenades, capaços de respondre reversiblement a efectes tèrmics. Aquest comportament és d'elevat interès científic i de rellevància pràctica en el disseny de dispositius mèdics per l'emmagatzematge i alliberament de fàrmacs de manera tèrmica i químicament controlada.

El principal objectiu d'aquesta Tesi es la preparació de complexes iònics dels dos poliàcids mencionats utilitzant diferents surfactants catiònics depenent de les propietats finals desitjades. La primera part del treball està dedicada a proporcionar el coneixement físic-químic de l'estructura i propietats dels surfactants d'alquiltrimetilfosfoni, els quals tenen un interès potencial per a noves aplicacions. Posteriorment, aquests surfactants foren acoblats als dos biopolímers, PGGA i HyA, per obtenir els respectius complexes iònics amb propietats biocides i de major estabilitat tèrmica que aquells complexes preparats a partir dels seus anàlegs d'amoni. Els complexes de PGGA, abreviats com ***n*ATMP·PGGA**, tenen un alt interès com a preservadors d'aliments i aplicacions de envasat tenint com a principal avantatge la

comestibilitat d'aquest polímer i la possibilitat de millorar les seves propietats bàsiques mesclant aquests compostos amb nanoargiles. Per altra banda, els complexes de HyA, ***n*ATMP·HyA**, són útils per obtenir derivats de l'àcid hialurònic amb activitat antimicrobiana. A més, s'ha dut a terme la preparació de nanopartícules de nATMP·HyA amb propietats antimicrobianes utilitzant el mètode "ionotropic gelation".

La segona part de la Tesi es va focalitzar en la preparació de complexes sostenibles d'àcid hialurònic. Per a realitzar-ho es van utilitzar surfactants d'alcanoilcolines per preparar els complexes iònics ***n*ACh·HyA.** Aquests complexes constitueixen una prometedora plataforma biocompatible/biodegradable pel disseny de sistemes capaços de transportar i alliberar de forma específica els fàrmacs anticancerígens de quimioteràpia.

La tercera part de la Tesi està dedicada a explorar la preparació de complexes biocompatibles amb propietats antimicrobianes utilitzant com a surfactant catiònic un dels preservants alimentaris més potents que es coneixen actualment, el **LAE**. Aquests complexes (**LAE·PGGA** i **LAE·HyA**) són candidats potencials per desenvolupar films comestibles amb propietats microbianes i materials d'àcid hialurònic amb propietats antimicrobianes, respectivament.

Paraules clau: àcid poli(γ-glutàmic (PGGA), àcid hialurònic (HyA), polímers biotecnològics, complexes polimèrics iònics, surfactant de tetraalquilfosfoni, clorur de αN-lauroil L-arginat, biopolímers amb propietats antimicrobianes, alcanoilcolines.

GLOSSARY

ACh Alkanoylcholine
ATMA Alkyltrimethlyammonium
ATMP Alkyltrimethlyphosphonium
CEC Cation exchange capacity
CFU Colony forming units
cmc Critical micelle concentration
$\mathbf{d_{001}}$ Interplanar Bragg spacing
DDS Drug delivery system
DLS Dynamic light scattering
DMSO Dimethyl sulfoxide
DOX Doxorubicin
DSC Differential scanning calorimetry
ε Elongation at break
E Elastic modulus
FBS Fetal bovine serum
FTIR Fourier transform infrared spectroscopy
$\Delta\mathbf{H}$ Enthalpy
$\Delta\mathbf{H_c}$ Crystallization enthalpy
$\Delta\mathbf{H_m}$ Melting enthalpy
HLB Hydrophily lipophile balance
HyA Hyaluronic acid
L or L_0 Lamellar spacing
LAE Ethyl $^{\alpha}$N-lauroyl L-arginate chloride
LAE·HyA Complexes of LAE and hyaluronic acid
LAE·PGGA Complexes of LAE and glutamic acid
Na·MMT Montmorillonite of sodium
$\mathbf{M_n}$ Number-average molecular weight
$\mathbf{M_w}$ Weight-average molecular weight
n Number of carbons in hydrocarbon chain
***n*ACh·HyA** Complexes of choline salts and hyaluronic acid
***n*ACh·HyA·NPs** Nanoparticles of *n*ACh·HyA complexes
***n*ATMP·HyA** Complexes of alkyltrimethylphosphonium salts and hyaluronic acid
***n*ATMP·HyA·NPs** Nanoparticles of *n*ATMP·HyA complexes
***n*ATMP·PGGA** Complexes of alkyltrimethylphosphonium salts and PGGA
***n*ATMP·PGGA·*X*%MMT** Nanocomposites of complexes *n*ATMP·PGGA and modified Na·MMT
NCD Non-crystalline diffraction
n.d. Not determined
$\mathbf{n_c}$ Number of crystallized methylenes
NPs Nanoparticles
NMR Nuclear magnetic resonance
OD Optical density
OMLS Organically modified layered silicate
P(D)GGA Poly(γ,D-glutamic acid)
P(L)GGA Poly(γ,L-glutamic acid)
PBS Phosphate buffered saline
PDA Potato dextrose agar
PDB Potato dextrose broth
PenStrep Penicillin streptomycin
PGGA Poly(γ-glutamic acid)
Ph-I Structural phase at room temperature
Ph-II Structural phase at medium temperature
Ph-III Structural phase at high temperature
Ph-Is Structural phase of isotropic phase at the highest temperature
POM Polarizing optical microscopy
σ Tensile strength
SAXS Small angle X-ray scattering

SI Supporting information
T_c Crystallization temperature
T^o In TGA, onset temperature
T_{max} In TGA, temperature for maximum decomposition rate
TEM Transmission electron microscopy
T_g Glass transition temperature
TGA Termogravimetric analysis
T_{Krafft} Krafft temperature
T_m Melting temperature
TSA Triptic soy agar
TSB Triptic soy broth
υ Wavenumber
W In TGA, remaining final weight
WAXS Wide angle X-ray scattering
XRD X-ray diffraction

INDEX

Chapter I. Objectives and outline of the Thesis

Biopolymers are organic polymers synthesized by living organisms. Most abundant biopolymers are polysaccharides, proteins, and polynucleotides (such as the nucleic acids DNA and RNA). Other biopolymers exist in nature in very specific organisms or/and in very limited amounts, as it is the case of polyterpenes and polyesters. However the term biopolymer has been recently widened to include those polymers that are produced by classical chemical synthesis but starting from renewable bio-based monomers such as polylactic acid, or those that are produced by cultured microorganisms or genetically modified bacteria, such as poly(γ-glutamic acid) and polyalkanoates.

Biopolymers are potential candidates for replacing fossil-derived polymers mainly due to their sustainability, biodegradability and biocompatibility. Despite the advantages that biopolymers offer, they often have inferior general properties compared to traditional polymers. Modification is a way to improve their behaviour and achieve property combinations suitable for satisfying new specific applications. Therefore the preparation, characterization and property evaluation of new biopolymers derivatives is essential for the development of sustainable materials able to replace the petrochemical polymers in areas such as agriculture, food, biomedicine, pharmacy and even as commodity plastics. Between the techniques used for modifying biopolymers (incorporation of fillers, blending…), chemical modification embrace a number of possibilities including side-group reaction, copolymerization, grafting, complexation and reactive blending.

The approach used in this Thesis is coupling of anionic biopolymers with organocationic compounds, which has recently been revealed as an efficient and simple way to produce stable biopolymer derivatives. The modified biopolymers are ionic complexes that not only display self-assembling properties, but they are also able to be processed by both wet and dry methods. Depending on the cationic compound used for coupling, different properties will be achieved.

Two biopolymers have been chosen for this study, namely poly (γ-glutamic acid) (PGGA) and hyaluronic acid (HyA). PGGA has been the focus of plenty researches due to its outstanding properties such as water affinity, biodegradability and biocompatibility. However, the production and spreading of this polypeptide is severely limited mainly due to its poor stability in humid environments and its incapacity for being processed. For this reason, diverse chemical modifications of PGGA have been

explored with the purpose of increasing the potential industrial applications of its derivatives.

HyA is a naturally occurring polysaccharide which is ubiquitous in the human body. It has demonstrated to have relevant properties including biodegradability, biocompatibility, high water sorption and retention, and ability to interact specifically with cells and other living tissues. Consequently, it has recently attracted a high attention, especially in the biomedical field. Nevertheless, hyaluronic acid is highly soluble at room temperature and has a high rate of elimination and recovery turnover. Therefore, the chemical modification of HyA is necessary to fulfill the requirements for each application. A number of strategies for the chemical modification of HyA for improving its physicochemical properties through carboxyl and hydroxyl groups have been developed. Similarly to PGGA, the strategy used in this Thesis for obtaining HyA derivatives has been ionic coupling with cationic surfactants. Three kinds of cationic compounds have been used, namely trialkylphosphonium (*n*ATMP), arginine (LAE) and choline (*n*ACh) derived surfactants. The two first families are interesting to obtain HyA derivatives with antimicrobial activity to ensure that HyA displays antimicrobial and antiviral properties which is a property that is not clear. The *n*ACh·HyA complexes are potential candidates in the design of medical devices for thermally controlled store and delivery of drugs because their biocompatibility and the possibility of preparing NPs through nanoprecipitation.

1. General objective

The general objective of the Thesis is carrying out the modification of two kinds of biopolymers, namely poly(γ-glutamic acid) (PGGA) and hyaluronic acid (HyA), by ionic coupling with organocationic compounds with the aim at improving the properties of these biopolymers and so increasing their number of applications.

2. Specific objectives

The specific objectives of this Thesis are enumerated as follows:

1. Synthesis and fully characterization including thermal properties of alkyltrimethylphosphonium surfactants (*n*ATMP with *n* being the number of carbon atoms contained in the alkyl chain and taking even values from 12 to 22) to be used for coupling with the biopolymers of choice.

2. Synthesis and chemical characterization of ionic complexes of PGGA and *n*ATMP surfactants with *n* ranging from 12 to 22, abbreviated as *n*ATMP·PGGA. Structural and thermal analysis of these complexes and critical comparison of results with those available for complexes made of their analogues

alkyltrimethylammonium surfactants (*n*ATMA·PGGA) previously studied in our group. Evaluation of their antimicrobial activity and improvement of their properties *via* nanocomposite preparation for the potential development of these films for active packaging applications.

3. Synthesis, chemical characterization and thermal behavior of complexes of hyaluronic acid and *n*ATMP surfactants (abbreviated as *n*ATMP·HyA with *n* = 12-22). Structural analysis of these complexes, as both films and nanoparticles Evaluation of the antimicrobial properties of *n*ATMP·HyA complexes as films or as NPs for the development of hyaluronic-based antimicrobial materials.

4. Synthesis, chemical characterization and thermal behavior of fully bio-based ionic complexes made of hyaluronic acid and alkanoylcholines as cationic surfactants (*n*ACh·HyA with *n*=12-18). Structural analysis of these complexes, as both films and nanoparticles. Evaluation of these complexes embracing both cytotoxicity and drug encapsulation and release assays, with the aim at providing a biocompatible/biodegradable platforms for drug transport and targeting delivery in anticancer chemotherapy.

5. Synthesis and chemical characterization of antimicrobial ionic complexes made of PGGA or HyA and the commercial biocide agent LAE. Evaluation of the bactericide activity of these complexes as a function of both biopolymer used and content in the active agent.

3. Outline

The present work is structured in seven chapters as follows:

Chapter 1. This chapter informs on the objectives and the outline of the Thesis

Chapter 2. This chapter contains a general introduction to the polymeric ionic complexes and their state of art.

Chapter 3. In this chapter, the collection of synthesis methodologies and techniques used for the characterization of the complexes are described.

Chapter 4. This chapter reports on the synthesis and physicochemical study of alkyltrimethylphosphonium surfactants used for coupling in this work.

Chapter 5. This chapter deals with the preparation and characterization of ionic complexes of poly(γ-glutamic acid) and alkyltrimethylphosphonium as well as their nanocomposites made with modified layered nanoclays.

Chapter 6. This chapter of the Thesis is also concerned with the preparation and study of complexes made of *n*ATMP surfactants but this time using hyaluronic acid as biopolymer and including the preparation and characterization of nanoparticles.

Chapter 7. This chapter is devoted to the preparation and characterization of fully-biobased complexes made of hyaluronic acid and alkanoylcholine surfactants, and the preparation of their nanoparticles and their preliminary evaluation as drug delivery systems.

Chapter 8. The last chapter describes the preparation of antimicrobial complexes of both PGGA and HyA with the antimicrobial agent LAE to develop antimicrobial-edible films.

In the annex part, the supplementary information of Chapters IV, V, VI, VII and VIII is collected (Annexes: A, B, C, D and E).

Chapter II. Introduction

1. Biotechnological biopolymers

1.1. Poly (γ-glutamic acid)

Poly (γ-glutamic acid) (PGGA or γ-PGA)) is a naturally occurring polypeptide that is commercially produced by microbial methods. It is actually an homopolyamide that has the backbone structure of nylon 4 with a carboxylic group substituted at C4 (Scheme 1.1). PGGA was first discovered in 1935 by Ivánovics and Bruckner (Bruckner et al., 1937) in the capsule of *B. anthracis* which was released into the medium on autoclaving, or on aging and autolysis of the cells. It was considered as a toxic polymer until it was discovered by Fuiji (Fuiji, 1963) in a Japanese traditional food called ‘‘natto’’ (Figure 1.1) as a very beneficial food because it increases the uptake in the small intestine of some active substances (Kashima et al., 2006).

Figure 1.1. Soybean fermented with *Bacillus natto*.

The well-known biodegradability and non-toxicity displayed by this biopolymer are the main factors promoting its study as biomaterial. It is also a water-soluble and edible polyelectrolyte.

1.1.1. Chemical structure and physicochemical properties

γ-PGGA is a polypeptide made of D- and L-glutamic units. The enantiomeric composition (the D/L monomer ratio) depends on the organism and the conditions employed in the process but it normally oscillates between 1/1 and 2/1. Enantiomerically pure D and L homopolymers are obtained from *B. anthracis* and *Natrialbaa egyptiaca*, respectively (Pérez-Camero et al., 1999; Martínez de Ilarduya et al., 2002). Manipulating the enantiomeric composition of PGGA allows altering its

properties (Shih et al., 2003). For example, enantiomerically pure PGGA is soluble in EtOH, whereas PGGA containing equimolar amounts of L and D enantiomers is not soluble in this solvent (Candela, 2006).

PGGA is isomer of α-PGGA (α-PGA, poly(α-glutamic acid), which is one of the most interesting poly(α-aminoacid)s due to its structure and biochemistry incidence. In α-PGA the attachment of the carboxylic group is in position α, whereas in γ-PGA it is in position γ.

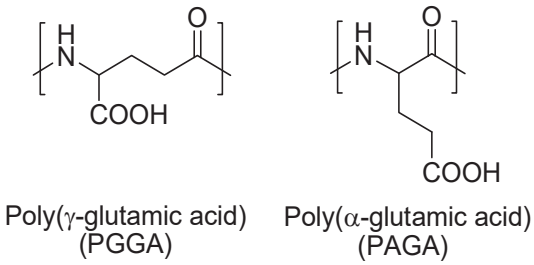

Scheme 1.1. Chemical structure of poly(γ-glutamic acid) and its isomer poly(α-glutamic acid).

PGGA is an optically active polyelectrolyte and its specific rotation depends on the D/L ratio and has a T_g around 50 ºC. PGGA has a pK_a= 2.27 so it will be ionized or not depending on the pH. As a result, pH is a critical factor for the solubility and structure of PGGA (Figure 1.2). At low pH values, PGGA is protonated and the polymer adopts a structure of α-helix. The protonated form is soluble in organic solvents such as dimethylsulfoxide (DMSO) (Kubota et al., 1992), hexamethylphosphoramide (HMPA) (Shah et al., 1995) or warm dimethylformamide (DMF) and *N*-methylpyrrolidone (NMP) (Kubota et al., 1993). When the pH is higher, around 5.1, the PGGA is in ionized form. At this pH PGGA adopts the random coil arrangement. This PGGA is soluble in water but non-soluble in MeOH, EtOH or DMSO.

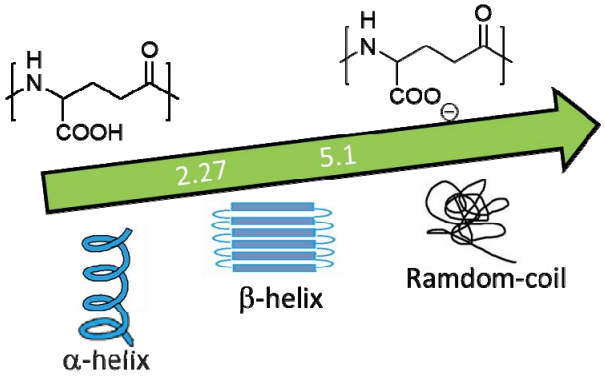

Figure 1.2. PGGA arrangement adopted depending on pH.

1.1.2. Degradability of PGGA

The degradability is a critical parameter that has to be studied before using a biopolymer because its properties will depend on its molecular mass. For instance PGGA generally has a relatively high molecular weight (M_w ~10^5–8×10^6 Da), which can limit its industrial applications due to its high viscosity, unmanageable rheology, and difficult chemical modification (Shih et al., 2001). To overcome this drawback its necessary to diminish its M_w. Recently, acid or alkaline hydrolysis, ultrasonic degradation and microbial or enzymatic degradation have been used to alter the molecular weight of PGGA (Shih et al., 2001). Hydrolysis of PGGA can be carried out in either basic (Kubota et al., 1996) or acidic (Shah et al.,1992) media through a random chain scission mechanism. Controlled hydrolysis of PGGA in which samples with M_w below 500,000 were obtained was patented (Hiruta et al., 1994). The hydrolytic degradation rate can be raised by increasing the temperature or using ultrasonic irradiation. The latter provides an interesting alternative because it allows reducing both the molecular weight and polydispersity of PGGA without disturbing the chemical composition of the polymer (Pérez-Camero et al., 1999). In principle polyglutamic acids should be expected to be readily degraded by enzymatic hydrolysis. However PGGA which is only susceptible to be degraded by γ-glutamyldepolymerases (Troy, 1973). On the contrary, α-PGA is insensitive to these enzymes but sensitive to proteases, such as pepsine, tripsine or quimiotripsine, which are the responsible of its digestion in humans.

Regarding the thermal stability of PGGA, Kubota *et al.* (Kubota et al., 1995) reported that PGGA is stable to heating up to 210 ºC, where melting and decomposition happen at the same time. The mechanism of the thermal degradation of PGGA was proposed by Portilla-Arias *et al.* (Portilla-Arias et al., 2007). It consists of an unzipping mechanism with generation of pyroglutamic acid (Scheme 1.2).

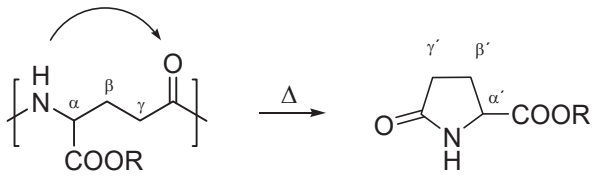

Scheme 1.2. Thermal degradation mechanism of PGGA with generation of pyroglutamic acid.

1.1.3. Synthesis of PGGA

The production of PGGA has been undertaken by several researchers. PGGA may be produced by both biosynthetic and chemical processes. Microbial biosynthesis of PGGA can be carried out by different kinds of bacteria. Depending on the used bacteria different stereochemical polymers are obtained. The first studies were carried

out by Thorne *et al.* (Thorne et al., 1954). They used *B. anthracis* species and obtained an enantiomerically pure poly(D,γ–glutamic acid). Nevertheless this bacteria has a pathogenic nature so *Bacillus subtilis* (Ho et al., 2006) and *Bacillus licheniformis (*Yoon et al., 2000) are the species mostly used for production of PGGA. Mixtures of the two enantiomeric forms with a more or less racemic composition are obtained when these bacteria were used (Buescher et al., 2007). According to the biosynthetic mechanism, the most consistent one is that proposed by Kunioka (Kunioka et al., 1997) (Scheme 1.3). This mechanism is based on the L-glutamic acid that is generated in the tricarboxylic acid cycle (TCA cycle) with α-ketoglutaric as a direct precursor (Ko et al., 1998). This mechanism incorporates the pyruvic cycle proposed by Thorne *et al.* (Thorne et al., 1954) in 1954. In brief, a partial stereochemical inversion leading to D-glutamic acid takes place by the action of pyruvic/ketoglucaric acid with the interactive concourse of the pair D/L-alanine. The polymerization of D/L-enantiomeric mixtures of glutamic acid finally occurs by the action of PGGA polymerase.

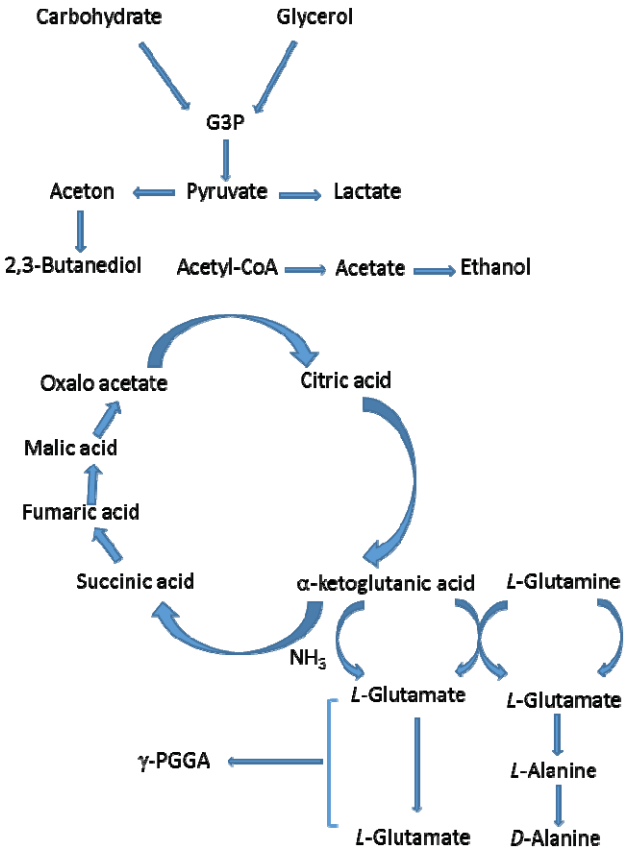

Scheme 1.3. Microbial biosynthesis of PGGA.

The chemical synthesis of PGGA is also feasible. Different methods have been reported but all of them are so complex that cannot be used at industrial scale. Waley and Bruckner synthesis (Ivánovics et al., 1937) was based on the polycondensation of glutamic acid with protected α-carboxyl groups and activated γ-carboxyl groups. Nevertheless, PGGA derivatives predominantly cyclized into pyroglutamate by intramolecular condensation (Katjar et al., 1969). Afterwards they obtained PGGA through polycondensation of the PGGA ester derivative without cyclization because the α-carboxyl group was protected with alkyl esters (Hollosi et al., 1969). Sanda et al. (Sanda et al., 2001) obtained the polymer through a new route that includes a previous transesterification followed by hydrogenation (Scheme 1.4).

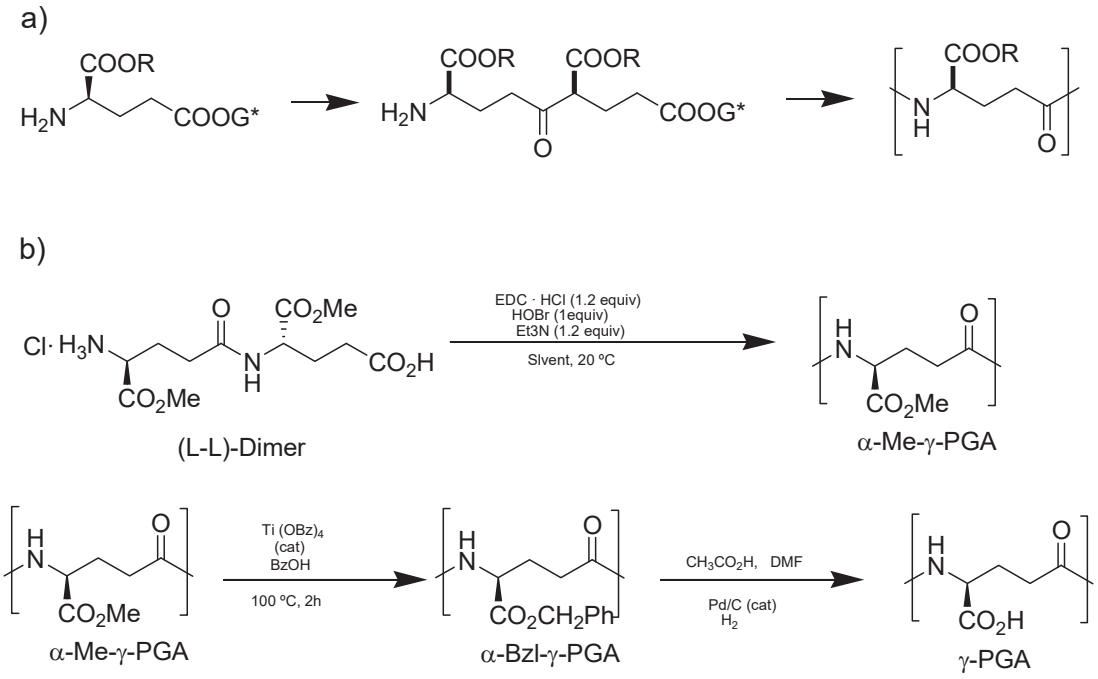

Scheme 1.4. Chemical synthesis of PGGA through polycondensation of the PGGA ester (a) and through transesterification and hydrogenation (b).

1.1.4. PGGA derivatives

The high solubility of PGGA in water is a severe limitation for many applications that can be overcome by chemical modification. The different approaches applied to date for the modification of PGGA regarding its use for the development of bioplastics suitable for active packaging and biomaterials have been recently reviewed by Muñoz-Guerra *et al. (*Muñoz-Guerra et al., 2013). Both, esterification (Kubota et al., 1992; Shah et al., 1995; Morillo et al., 2001; Morillo et al., 2003) and amidation (Kunioka et al., 1997; Akagi et al., 2006) of the carboxyl side group of PGGA are known to lead to water non-soluble derivatives suitable for being processed by applying either humid or

dry methods. Nevertheless, the covalent modification of PGGA is a tricky procedure that usually implies long reaction times as well as the use of large amounts of solvents and reagents that in most of cases are of unsatisfactory sustainability. Ionic coupling of PGGA with cationic surfactants affords a third option to prepare non-soluble water PGGA (Antonietti et al., 1994a). These complexes are resistant to water and well stable to heating and tend to self-assemble in supramolecular structures of both academic and practical interest. Such complexes are readily prepared by just mixing aqueous solutions of the polyacid and the surfactant, and they are usually made of stoichiometric or nearly stoichiometric ratios of the two components. Among them, interestingly ionic coupling of PGGA with cationic alkyltrimethylammonium surfactants bearing long alkyl chains (*n*ATMA·PGGA) has been recently revealed to be an efficient approach to produce PGGA derivatives with attractive properties (Pérez-Camero et al., 2004; García-Álvarez et al., 2005).

1.1.5. Applications of PGGA

PGGA is a potential candidate for replacing the flocculants currently used in the market such as polyacrilic acids, which degrade slowly in water releasing toxic substances. This application is possible due to the solubility of PGGA in water and its capacity for interacting with cations. This property makes PGGA a suitable polymer for waste-water treatment since both, inorganic and organic suspended materials can be removed by flocculation and coagulation (Shih et al., 2001). PGGA can also be utilized to reduce the environmental risks related to the presence of heavy metals. It has been demonstrated the metal-binding affinity of the PGGA to a variety of metals including Ni^{+2}, Cu^{+2}, Mn^{+2}, Al^{+3}, $Cr^{+3}$and U^{+4} (McLean et al., 1990). Recently Bhattacharyyal *et al.*(Bhattacharyya et al., 1998) discovered that membranes containing attached PGGA have extremely high retention capacity for heavy metals.

In medicine, PGGA is highly promising because it is biodegradable, edible, and non-toxic towards human and environment. Hence it has been suggested to be a good candidate for curable biological adhesive (Buescher et al., 2007) and as drug, vaccine or gene carriers (Dekie et al., 2000; Markland et al., 1999; Richard et al., 2001). For instance, PGGA could replace the fibrin-biological adhesives which are currently widely used for wound closure in surgery, tissue adhesion and control of massive bleeding (Otani et al., 1996). As carrier for different active molecules, PGGA has been proposed to be used to transport prostaglandin (PGE). This compound is clinically used for peripherial vascular disturbance treatment and hepatitis therapy but it cannot be administrated alone due to its undesired side effects, low solubility and stability. Hashida developed in 1999 a galactosylated-PGGA carrier which keeps the PGE

activity avoiding its drawbacks (Hashida et al., 1999). PGGA can also be used to deliver chemotherapeutic agents such as Paclitaxel. Paclitaxel is a natural antimicrotubule agent which has a potent antitumor activity but it is insoluble in water. Thanks to PGGA a Paclitaxel derivative which is water-soluble and retains its high antitumor activity could be formulated (Li et al., 1998).

Furthermore, PGGA is interesting for applications in agriculture and, taking into account its biocompatibility, in cosmetics and dermatology (Lee et al., 2014). These applications require hydrogels which can be prepared with PGGA due to the high density of hydrogen bonds in its structure (Kunioka, 1993; Kunioka et al., 1995).

Another interesting outcome of this polymer is in the food field. PGGA not only is an effective cryoprotectant for frozen food, but also it has a taste weaker than the commonly used cryoprotectants such as saccharides, inorganic salts and aminoacids. PGGA is usually used as a bitterness-relieving agent to mask the bitter or weird taste of some food. Other applications of PGGA in food are the following: i) PGGA accelerates the absorption of minerals (Tanimoto et al., 1996); ii) PGGA prevents of aging and improve the texture of bakery products (Konno et al., 1988) and iii) PGGA can be used as ice-cream stabilizer (Daninippon Pharmaceutica Co, 1972). As animal food additive, PGGA promotes absorption of minerals, increases the strength of egg shells, and improve the phosphorous assimilation (Ajinomoto. Co. Inc, 1997).

1.2. Hyaluronic acid

Hyaluronic acid (HyA) is a naturally occurring unbranched polysaccharide. It can be designed as glycoaminoglycan because its structure is composed by D-glucuronic acid and D-*N*-acetylglucosamine (Scheme 1.5.) It is one of the main constituents of the extracellular matrix and it is found throughout connective, epithelial and neural tissues. Significant amounts of HyA are also found in lung, kidney and muscle tissues.

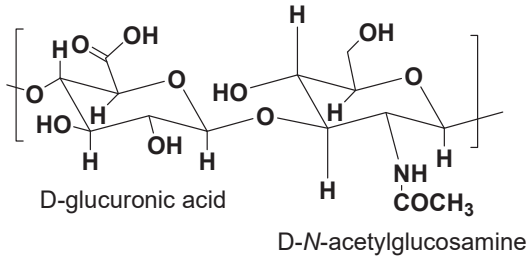

Scheme 1.5. Chemical structure of hyaluronic acid (HyA).

It was isolated in 1934 by Meyer and Palmer (Meyer et al., 1934) from bovine vitreous humour and since then it has attracted a high attention because its properties including biodegradability, biocompatibility, solubility in water, high water sorption and

retention, and its ability to interact with cells and other living tissue. Consequently, hyaluronic acid is very useful for the development of biomedical applications. Nevertheless, hyaluronic acid is highly soluble at room temperature and has a high rate of elimination and recovering turnover. Therefore, chemical modification and crosslinking of HyA are necessary for fitting the properties to each desired application.

1.2.1. Chemical structure and physicochemical properties of hyaluronic acid

The structure of hyaluronic acid, as previously mentioned, consists of an alternating disaccharide repeat of D-glucuronic acid and *N*-acetyl-D-glucosamine, where the pyranose rings are connected by β-1,3 bonds. The repeating units are bonded with a β-1,4 glycosidic bond (see Scheme 1.6a). The HyA arrangement and its ability to form supramolecular structures are important features for explaining some of its physico-chemical properties and understanding its biological functions. Since sugar rings of hyaluronic acid bear bulky groups (OH, COOH, $NHCOCH_3$), the free rotation around glycosidic bonds is restricted making that the whole chain is rigid. Axial positions are occupied by hydrogen atoms making this region hydrophobic (Scheme 1.6a). Secondary and tertiary structures can be adopted when hydrogen bonds are formed between atoms of functional groups contained in a single molecule or in different molecules (Heatley et al., 1988). Secondary structure is described as a single stand left-handed helix with two disaccharide residues per turn (2-fold-helix) (Scheme 1.6b). These 2-fold single helices are capable of forming a tertiary structure through the interaction between hydrophobic areas of HyA chain. This structure is described as a β-sheet based in 2-fold helices (Scheme 1.6c).

In water solutions of HyA, molecules of water are involved in the formation of the H-bonds. Therefore, water acts as a stabilizer of the secondary structure making that solutions of HyA display very unusual rheological properties and are exceedingly lubricious and very hydrophilic. These properties depend on the concentration and the molecular weight of HyA. At low concentrations, these chains entangle with each other contributing to the unusual rheological properties displayed by this biopolymer due to its high and shear-dependent viscosity (Laurent et al., 1996). When concentration increases, an enhancement of the viscoelasticity and elasticity is observed for hyaluronan solutions and for high molecular weight (>1 MDa) (Hargittai et al.,2008), an infinite network is form so HyA appearance is like a gel. This doesn't occur under physiological conditions because gelification is avoided whatever the concentration of HyA is (Garg et al., 2004). Other consequences of these interactions are the non-newtonian viscoelasticity properties of HyA solution (Kobayashi et al., 1994). Because of these interactions, molecules of HyA occupy large hydrodynamic volume making

that HyA self-associate by forming anti parallel double helices, bundles and ropes. As a result, a coil structure is formed that traps approximately one thousand times its weight in water (Cowman et al., 2005).

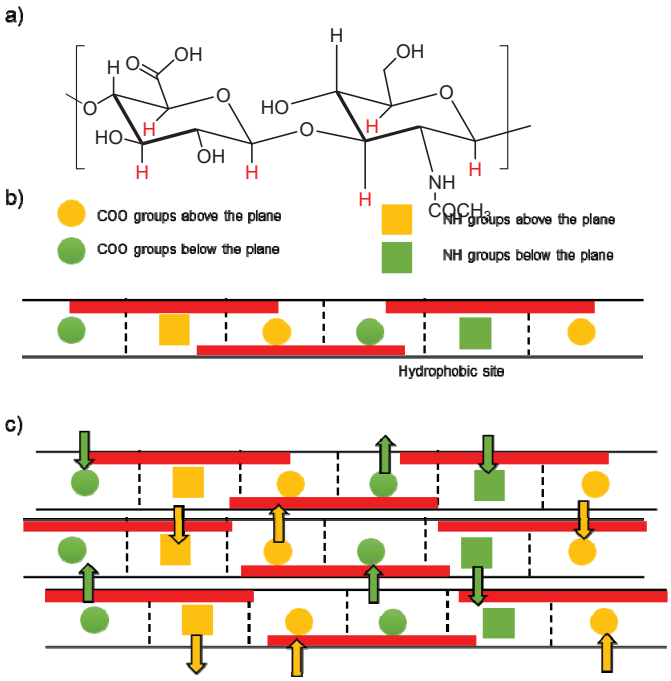

Scheme 1.6. Molecular formula of hyaluronic acid disaccharide unit (a), Secondary (b) and tertiary (c) structure of hyaluronan.

The pK_a of this polysaccharide is around 3.0. Thus, changes in the pH will provide different ionization grades. For instance, at physiological pH the carboxylate groups are deprotonated so hundreds of negative charges will be fixed to each chain, which will be balanced with different cations. The pH changes will influence the number of charges and finally the organization of the chains, and their interactions with the surroundings. Therefore some HyA properties including rheological properties and the solubility in water will be affected by pH. As a result, HyA is water non-soluble when converted into an uncharged polymer (Toole, 2004).

HyA is involved in several biological functions such as supporting the viscoelasticity of liquid connective tissues in the joint synovial and eye vitreous fluids and controlling biomechanical properties of tissues and water transport (Necas et al., 2008). It also performs several structural tasks in the extracellular matrix (ECM) as it binds to cell proteins and other component through specific and non-specific interactions. Several cell receptors (such as CD44, RHAMM, TSG6, GHAP, ICAM-1 and LYVE-1) interact with HyA influencing cellular processes like cell detachment, mitosis, migration, tumor development and metastasis, and inflammation (Toole et al., 2002; Hascall et al., 2004; Necas et al., 2008).

Molecular weight of HyA is known to play an important role in some HyA functions. For instance, HyA can stimulate gene expression in macrophages, endothelial cells and certain epithelial cells (Necas et al., 2008). This properties only are possible when HyA has only low/intermediate molecular weight ($2 \cdot 10^4$-$4.5 \cdot 10^5$ Da). Wound-healing process also depends on the molecular weight of HyA. Low molecular weight HyA (products of HyA degradation) was identified to contribute in the scar formation process whereas scar formation was diminished if high molecular weight HyA was found during fetal wound healing. The findings also suggested that high molecular weight HyA favored cell quiescence and supported tissue integrity, whereas production of HyA fragments signaled injury and initiated the inflammatory response (Chen et al., 1999; Garg et al., 2004; Necas et al., 2008).

1.2.2. Degradation of hyaluronic acid

Degradation of HyA can occur via enzymatic or non-enzymatic reaction. Enzymatic degradation is produced by three types of enzymes: hyaluronidase, β-D-glucuronidase and β-*N*-acetylhexosaminidase. Hyaluronidase cleaves high molecular weight HyA into smaller fragments while the other two enzymes degrade the fragments by removing the non-reducing terminal sugars (Stern et al., 2007; Necas et al., 2008; Volpi et al., 2009). Non-enzymatic degradation can be carried out through different mechanisms including shear or thermal stress, acidic/alkaline hydrolysis and oxidation. Ultrasonication degrades HyA in a non-random way. It was reported that high molecular weight HyA is degraded slower than low molecular weight when HyA is subjected to ultrasonication (Garg et al., 2004; Stern et al., 2007). Heating is another way to degrade HyA. Rheological studies on HyA solutions showed that the degradation and viscosity of HyA increase exponentially as a function of temperature. Acidic/alkaline hydrolysis degrades HyA in a random way (Scheme 1.7). Acidic hydrolysis degrades the glucuronic acid moiety whereas alkaline hydrolysis occurs on *N*-acetylglucosamine units (Tokita et al., 1995). HyA can also been degraded via oxidation in a random way by the presence of reactive oxygen species as superoxide anions, hydroxyl radicals and hydrochlorides. This kind of degradation can arise in several inflammatory and degenerative processes such as arthritis in which these reactive oxygen species are produced, but the mechanisms of action are still largely undefined (Garg et al., 2004; Stern et al., 2007).

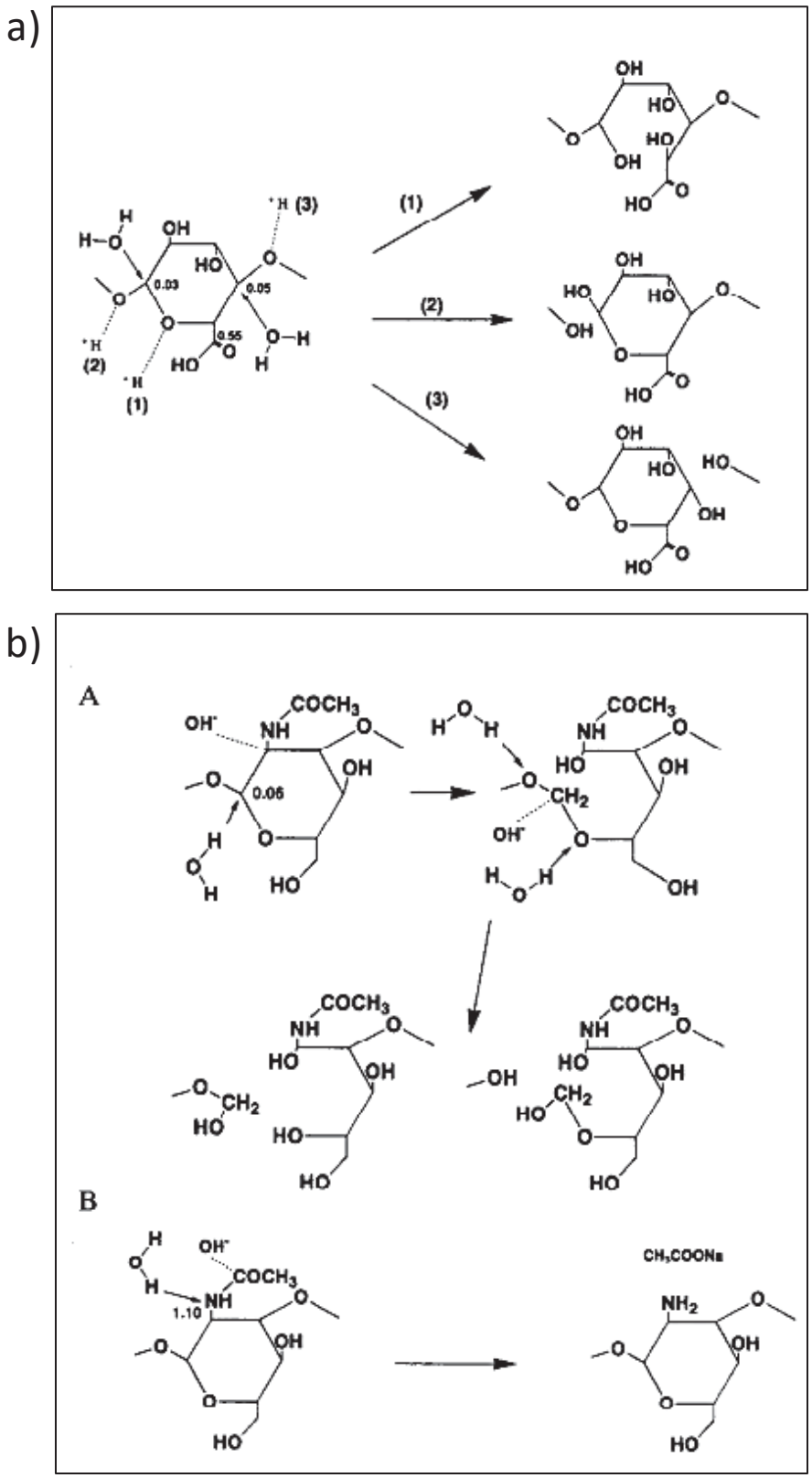

Scheme 1.7. Hydrolysis reaction mechanism of HyA in acidic conditions (a) and basic conditions (b): Figures are electron densities of LUMO taking from (Tokita et al., 1995).

1.2.3. HyA derivatives

A number of strategies for the chemical modification and crosslinking of HyA for improving its physicochemical properties, have been developed (Balazs et al., 1987; Kuo et al., 1991; Luo et al., 2000).

Chemical modifications are classified depending on which functional group (the carboxylic acid of glucuronic acid, the primary or secondary hydroxyl groups, and the *N*-acetyl group) is modified (Scheme 1.8). Carboxylic groups have been modified by carbodiimide-mediated reactions, esterification, and amidation. Hydroxyl groups have been modified by etherification, divinylsulfone crosslinking, esterification, and bis-epoxide crosslinking. These HyA derivatives can be categorized as *monolithic* and *living* HyA. Monolithic HyA derivatives cannot form new chemical bonds in the presence of cells or tissues, and must be processed and fabricated into different forms. In contrast, living derivatives of HyA can form new covalent bonds in the presence of cells and tissues allowing HyA the possibility of being further crosslinked which is essential for multiple medical applications.

Another way of modification is coupling of HyA with cationic surfactants (Scheme 1.8b). It has been reported out that this modification give rise to stable comb-like polymers able to self-assemble in amphiphilic layered structures and respond reversibly to thermal effects (Macknight et al., 1998). In these sense, our group has recently undertaken the research of HyA complexes made of HyA and tetraalkylammonium surfactants, and shown that these complexes have a layered biphasic structure with the hydrophilic main chain and the hydrophobic side chain clearly separated in organized nano-domains (Tolentino et al., 2013; Battistini et al., 2013, 2014, 2017).

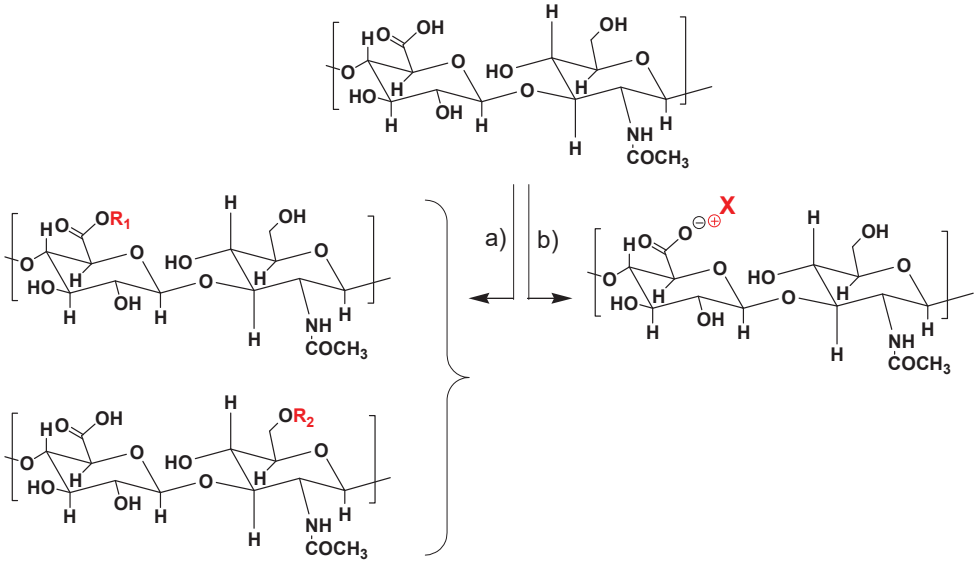

Scheme 1.8. Chemical modification of hyaluronic acid by means of bonding covalent bonds (a) or by coupling with cationic surfactants (b).

1.2.4. Applications of hyaluronic acid

The unique viscoelastic nature of HyA along with its biocompatibility and non-immunogenicity has led to its use in a number of clinical applications: *a) HyA as tissue engineering.* Since hyaluronic acid is one of the main components of body tissues, its potential for tissue engineering applications has been highly touted. Chemical crosslinking of HyA allows HyA displaying desirable mechanical properties, extending the HyA degradation process *in vivo,* and providing long term stability. Thus chemical crosslinking HyA has been used for multiple applications including orthopedics, cardiovascular medicine and dermatology (Allison et al., 2006). The introduction of functional groups used for radical polymerization such as acrylates and methacrylates give rise a HyA susceptible to photopolymerization. This photocrosslinked HyA forms hydrogels with a range of degradation and material properties which can be used in different application such as cartilage tissue engineering, cardiac repair, molecule delivery, valvular enginery, control of stem cell behavior and microdevices (Baier et al., 2011). Benzyl derivatives of HyA can be used for the development of scaffolds based on HyA. These scaffolds are hydrophobic, degrade at predictable rates and can be used for chondrocytes in cartilage engineering. HyA crosslinked with divinyl sulfones (DVS) in the presence of ultraviolet light allows obtaining scaffolds for surfaces contacting blood (Ibrahim et al., 2010). Thiol modification of HyA carboxylate groups has been reported to give rise HyA hydrogels that are useful for regenerative applications. These hydrogels are biocompatible and are formed spontaneously when exposure to air (Shu et al., 2002; Shu et al., 2003; Burdick et al., 2011). *b) HyA as dermal filler*. HyA has been approved by Food and Drug Administration (FDA) as a dermal filler. Since its launch in Europe in 1996, HyA has become the gold standard as filler for treating wrinkles, hydrating skin and increasing volume (Andre, 2008). In 2006, cosmetic injections of HyA were known to be the second most popular non-surgical procedure for women and the third for men (Monheit et al., 2007; Brandt et al., 2008; Buck et al., 2009). As HyA has a short half-life is necessary its crosslinking to extend duration as a dermal filler (Kablick et al., 2009). The two crosslinkers employed are 1,4-butanediol diglycidil ether and divinyl sulfone. Despite improving resistance to degradation and increase the duration of the treatment, current HyA-based dermal fillers have a maximum treatment duration up to 12 months. To extent the treatment duration, HyA with higher molecular weight or more crosslinking is necessary. Nevertheless, the injectability of these HyA fillers would be more difficult which would be an important drawback (Andre, 2008). *c) HyA in osteoarthritis (OA) treatment.* Osteoarthritis is the most common disease associated with aging affecting about 70 % of people with 65 years old or over. HyA has been proposed as a potential candidate

because it is the main component of synovial fluid. In 1970s the first study on the application of HyA for human knee were performed by Rydell and Balazs. In 1974 Peyron and Balazs (Balazs, 1993) injected different volumes of HyA into 23 knees and observed a reduction of pain and increase of patient function. In 1997, HyA was approved by FDA as viscosupplementation for OA treatment. Since then, HyA has been accepted as a common therapy for reducing pain associated with OA (Moreland, 2003) and several HyA supplements are available in the market. Nevertheless it is still necessary the development of products with enhance injectability and yet reasonable viscoelastic behavior. d*) HyA as a drug delivery system.* Nowadays HyA has received much attention as a tool for drug delivery system development because of its potential properties including its mucoadhesive property and safety. HyA has been used as a drug delivery carrier in both non-parenteral and parenteral routes. The non-parenteral application includes the ocular and nasal delivery systems. On the other hand, its use in parenteral systems has been considered important as in the case of sustained release formulation of protein drugs through subcutaneous injection (Jin et al., 2010). HyA is one of the major components of the extracellular matrix and is the main ligand for CD44 and RHAMM, which are over-expressed in a variety of tumor cell surfaces including human breast epithelial cells, colon cancer, lung cancer and acute leukemia cells (Culty et al., 1994). Therefore, anticancer drug targeting to tumor cells and tumor metastases can be accomplished by HyA derivatives via the HyA receptor-mediated uptake of these drugs. Furthermore, the solubilization, stabilization and release of anticancer drug can be improved due to their coupling to HyA (Luo et al., 2002; Auzenne et al., 2007; Choi et al., 2010; Battistini et al., 2014).

2. Surfactants

The word surfactant is a contraction of the term surface-active agent (SAA). That is surfactants are amphiphilic molecules with two mutually insoluble portions. This means that they are made of two counterparts differing in polarity and with opposite affinity for water which are called hydrophilic and hydrophobic counterparts, respectively. The hydrophilic part is often called the head-group and the hydrophobic part is called the tail group (Figure 2.1). Surfactants are also known as tensioactive agents because they tend to adsorb at surfaces and interfaces of immiscible phases.

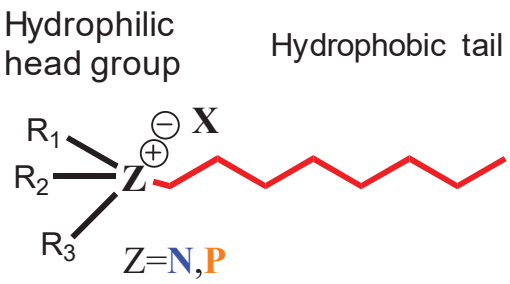

Figure 2.1. Schematic illustration of the surfactant structure.

2.1. Classification and properties of surfactants

Surfactants are broadly classified according to their polar head group nature: anionic (negatively charged; *e.g.* salts of fatty acids), cationic (positively charged; *e.g.* alkylamines or quaternary ammonium salts), nonionic (neutral; *e.g.* polyethylene oxide based surfactants) or amphoteric (its charge changes as a function of pH; *e.g.* amino acids, betaines and phospholipid derived surfactants).

Surfactant structure endows them with unusual physicochemical properties. The hydrophilic and hydrophobic parts make the surfactant surface active in the sense that it tends to be located at interfaces between polar and non-polar media, so that the hydrophilic part is solvated in the polar medium and the hydrophobic part in the non-polar medium. The first important distinguishing property is its ability to lower the free energy at a liquid/air interface or two immiscible liquids. The latter property is the one that allows a surfactant to be used as an emulsifier.

The degree of surfactant concentration at an interface depends on the surfactant structure and also on the chemical nature of the two phases that meet at the interface. Therefore, there is not a universally good surfactant, suitable for all uses (Holmberg et al., 2003). However with the empirical scale of HLB (HydrophileLipophile Balance) the applications of some surfactants can be predicted (Table 2.1) (Becher, 1985).

Table 2.1. Application of surfactants depending on their HLB values.

HLB number	Application
3-6	W/O emulsions
7-9	Wetting agents
8-15	O/W emulsions
13-15	Detergent
15-18	Solubilizer

A fundamental property of surfactants is their ability to self-associate through an aggregation process known as micellization above some specific narrow concentration range (depending on M_w and shape of the hydrophobic counterpart). The concentration

at which these micelles start to be formed is called the critical micelle concentration (*cmc*). Below their *cmc* surfactants are dissolved in water as monomers. Above their *cmc* micelles are formed. Micelles consist of ordered aggregates made of *c.a.* 50-150 surfactant molecules. In water, the hydrophobic chains are oriented inward away from the aqueous phase. This is relevant for solubilize poorly water-soluble molecules. Inverse micelles with an opposite orientation of the molecules are formed when the liquid is non-polar liquids; in this case, water soluble molecules can be solubilize in oils.

At higher concentrations, surfactants may also associate to form mesomorphic phases, a state intermediate between the liquid and the crystalline state, termed lyotropic liquid crystal. Lyotropic structures include cubic, hexagonal cylindrical and lamellar arrays (Figure 2.2). The rheological (viscoelastic) properties of surfactants vary considerably from shear thinning to thixotropic and this is why they have been extensively used in food emulsions. Another notable feature is their ability to form particles with very different sizes, which have been profited for oral administration of drugs.

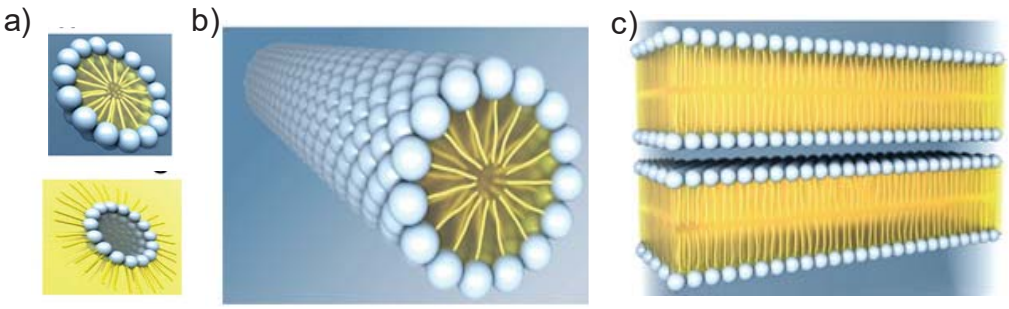

Figure 2.2. Surfactant aggregation as micelle (a), cylindrical array (b) and lamellar arrangement (c).

2.2. Ammonium surfactants

Tetraalkylammonium salts are well-known cationic surfactants. These amphiphilic molecules aggregate in aqueous solution to micelles and at higher concentrations to lyotropic mesophases (Demus 1998). Furthermore, they exhibit high surface activity and excellent adsorptive and bacterial properties. Therefore, tetraalkylammonium surfactants have been widely applied in detergent (Asadov et al., 2012), emulsification (Naves et al., 2013), phase transfer catalysis (Wang et al., 2013), materials synthesis.

Scheme 2.1. Chemical structure of cetyltrimethylammonium bromide.

(Salaikov et al., 2012; Ye et al., 2012), separation (Guo et al., 2012), corrosion inhibitors for metal (Hegazy et al., 2014), sterilization (Mowery et al., 2009) and so on .

Long-chain quaternary ammonium salts, such as the typical cetyltrimethylammonium bromide (Scheme 2.1), form layered crystalline structures (Iwamoto et al., 1981). This structure is formed through the electrostatic interaction of quaternary centers with halide anions. As a result, bidimensional polar layers sandwiched between the long alkyl chain layers are obtained. Upon heating these quaternaries are transformed, through a solid-solid phase transition, to another layered structure, viewed as a mesophase (Iwamoto et al., 1981) in which although the hydrocarbon chains are "melted" the ionic bonding inside the polar layers remains practically intact. Thus free molecular motion of the amphiphiles is prevented by the rigidity of the ionic layers. It has also been found that *n*-alkyltrimethylammonium halides decompose after the clearing point in the presence of nitrogen (Iwamoto et al., 1981) or even before the clearing point in atmospheric oxygen.

2.3. Phosphonium surfactants

Tetraalkylphosphonium salts (Scheme 2.2) bearing long alkyl chains constitute a family of cationic amphiphiles comparable to the widely known tetraalkylammonium family but much less studied because their synthesis is more difficult. As tetraalkylammonium salts, tetraalkylphosphonium salts are able to form thermotropic mesophases and are able to take up similar arrangements than ammonium surfactants but covering broader domains of temperatures and displaying higher clearing points (Kanazawa et al., 1997). Fortunately, the characterization of the high-temperature phases found in phosphonium surfactants is feasible thanks to the good thermal stability displayed by these systems. The arrangement consists of an amphiphilic array of the phosphonium or ammonium-halide ionic pairs aligned in layers and the hydrophobic alkyl chains in a more or less extended conformation filling the interlayer spacing (Kamitori et al., 1997). Nevertheless, the literature dealing with the structure and thermal behaviour of phosphonium-based surfactants is scarce (Axenov et al., 2011).

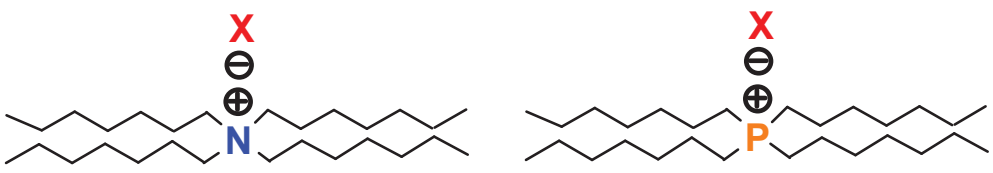

Scheme 2.2. Chemical formula of tetraalkylammonium and tetraalkylphosphonium salts.

Reports of alkyltributylphosphonium halides date back the 1980s, when Knifton published the use of some molten tetrabutylphosphonium bromide salts (Knifton, 1988) which granted him several patents (Knifton, 1981, 1982a, 1982b). Then, alkyltributylphosphonium halides were applied in the late 80s as biocides or as compounds with microbiological activity (Donofrir et al., 1989). Despite the impact of Knifton's studies, it was not until 1990 when tributylphosphine was started to be produced at large scale. Since then, most attention in the literature has been given to the trihexyltetradecylphosphonium halide surfactants as they are commercially available within a range of different anions, and also relatively cheap (Bradaric et al., 2003).

Nowadays, tetraalkylphosphonium surfactants have recently become the focus of a good number of investigations because they offer superior properties in some aspects when they are compared with tetraalkylammonium surfactants. Tetraalkylphosphonium salts have phase transfer capability, electrostatic properties and are generally less dense than water, which can be beneficial in processes that involve decanting steps.

In addition, quaternary organophosphonium compounds are particularly attractive as ionic liquids because they display high thermal stability (Xie et al., 2002) and may be designed with a wide diversity of structures, some of them being able to melt at sub-ambient temperatures (Fraser et al., 2009). Their applications as solvents (McNulty et al., 2002; Gerritsma et al., 2004; Ito et al., 2004), phase transfer catalysts (Ramnial et al., 2005) or exfoliation agents for nanoclays (Panek et al., 2006; Byrne et al., 2007; Hedley et al., 2007) among others, have been recently explored for some of these compounds. They are also interesting as building blocks in the design of antimicrobial materials since it has been proved that they are less cytotoxic than organoammonium compounds (Cieniecka-Rosłonkiewicz et al., 2005; Kumar et al., 2009).

Scheme 2.3. Chemical formula of tetraalkylphosphonium salts containing one long alkyl chain.

Nevertheless, the literature dealing with the structure and thermal behaviour of phosphonium-based surfactants is still scarce, a meagre situation that is evidenced when compared with the vast amount of information that has been amassed on commercialized surfactants based on tetraalkylammonium salts (Binnemans, 2005). Such comparative backwardness is mainly due to the synthesis difficulties associated to phosphorous chemistry, as well as to the restricted availability of the

trialkylphosphines that are commonly used as starting materials. The few studies carried out to date on phosphonium-based surfactants concern salts bearing two, three or four long alkyl chains (Kanazawa et al., 1997; Abdallah et al., 1999, 2000; Adamová et al., 2011), whereas only there is one study about phosphonium salts containing only one long alkyl chain (Scheme 2.3) which was devoted to evaluate the antimicrobial properties of such compounds (Kanazawa et al., 1994).

2.4. Choline surfactants

Choline, 2-hydroxyethyl)trimethyl ammonium salt, is a naturally occurring compound of extreme biological relevance as a precursor of neurotransmitters and membrane constituents (Blusztajn et al., 1883). What is more, it has been classified as essential nutrient by the Food and Nutrition Board of the Institute of Medicine, National Academy of Sciences for optimal brain development (Blusztajn et al., 1998). In addition, choline is biocompatible and able to biodegrade both in living organisms (Kortstee, 1970) and in the environment (Gorke et al., 2008). Consequently, choline derivatives are extensively investigated specifically in field of green, sustainable chemistry. Choline based ionic liquids are extensively applied in many chemical processes (Plechkova et al., 2008; Liu et al., 2015).

Choline based ionic surfactants are nowadays of more interest for their potential as suitable components for develop green materials. In addition they are distinguished for displaying low Krafft temperatures (Klein et al., 2008; Klein et al., 2009). Among them choline-based surfactants derived of fatty acid esters *i.e* alkanoylcholines (Scheme 2.4) are of high interest. Alkanoylcholines compounds are derivatives from naturally occurring phospholipids like lecithin that is produced by living organisms. That is alkanoylcholines belongs to one of the bio-surfactants groups. Alkanoylcholines are known to display certain biological activity (Ahlstrom et al., 1995), as well as highly appreciated medical properties properties (Schneider et al., 1957; Alexander et al., 1989; Carelli et al., 2001; Patel, 2003;). For instance, alcanoylcholines have proven to display therapeutic effect in brain and cognitive related illnesses such as Alzheimer disease (Carelli, et al., 2001; Patel, 2003) showing also a better penetration through the Blood Brain Barrier (BBB). In addition, an enhancement in drug absorption by different human tissues is achieve due to the ester group of alkanoylcholines (Alexander et al., 1990). Consequently, alkanoylcholines are promising compounds for development of biomaterials.

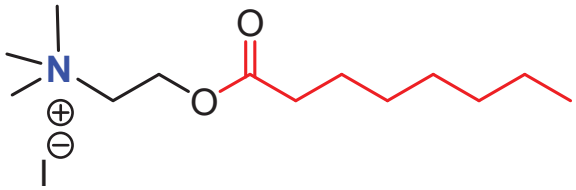

Scheme 2.4. Chemical structure of *n*-alkanoylcholine.

Long-chain alkanoylcholines have demonstrated having a microbiocidal activity similar to that observed in quaternary ammonium salts (Ahlstrom et al., 1995). This behaviour is due to the quaternary ammonium functionality in the head group of alkanoylcholines. However alkanoylcholines have the advantage of being non-toxic, which is one of the main problems found when quaternary ammonium salts are used. This is possible because the alkanoylcholines compounds have an ester bond between the ammonium and the long alkyl chain making the molecule sensible to certain hydrolytic enzymes such as butyrylcholine estearase (BchE) (Scheme 2.5) (Chelminska-Bertilsson et al., 1993). Thus alkanoylcholines are hydrolysed into biocompatible products once that the antimicrobial effect has been exerted (Mansbach et al., 1992; Saitoh et al., 1992). This property makes them potentially valuable to replace traditional tetraalkylammonium compounds in personal care products (Watson et al., 2012).

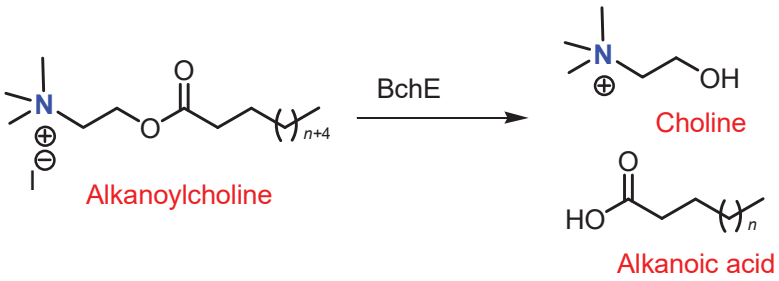

Scheme 2.5. Enzymatic hydrolysis of long-chain alkanoylcholines catalyzed by BChE.

2.5. LAE surfactant

LAE (ethyl $^{\alpha}$*N*-lauroyl L-arginate chloride), which is one of the most potent food preservative agents today known, have a wide antimicrobial activity against multiple microorganism. This antimicrobial effectiveness results from its structure and surfactant properties (Rodriguez et al., 2004). LAE is a guanidinium-based compound derived from lauric acid, *L*-arginine and ethanol (Scheme 2.6). Its molecular weight is 421.03 Da and its molecular formula $C_{20}H_{41}N_4O_3Cl$, as monohydrochloride salt. As surfactant, it is a cationic surfactant, has a Krafft temperature of > 5 ºC, surface tension of 30.1 $mN \cdot m^{-1}$ and *cmc* of $6.0 \cdot 10^{-3}$ M.

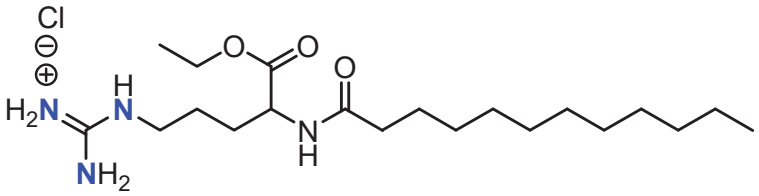

Scheme 2.6. Chemical formula of ethyl $^{\alpha}$*N*-lauroyl L-arginate chloride (LAE).

LAE was first synthesized from lauric acid, L-arginine and ethanol in Barcelona in 1984 by the Higher Council of Scientific Research (Infante, 1984) and was then patented and commercialized by the Vedeqsa Lamirsa Group in Spain. In 2005, LAE was classified by the Food and Drug Administration (FDA) as GRAS (Generally Recognized as Safe) as food preservative at concentrations up to 200 ppm. In 2007, LAE was evaluated as antimicrobial in meat and poultry products by the US Department of Agriculture (USDA).

The high antimicrobial activity of LAE has been attributed to the cationic charge of this surfactant which interacts with cell membranes of microorganisms causing disturbances in membrane potential modifying the metabolic processes of microorganisms but without causing cellular lysis (Rodriguez et al., 2004). In addition, it has been shown that LAE shows antimicrobial activity in a range of pH 3–7 (Asker et al., 2011). Its durability and solubility also depend on the pH. At pH= 4 the half-life of LAE was longer than one year at 25 ºC, but it decreases to 57 days at pH= 7 and 34 h at pH= 9 (European Food Safety, 2007).

LAE is only soluble at pH<4.5 because at higher pH it has a high ionic strength that makes it to precipitate. Furthermore, LAE has a low oil-water equilibrium partition coefficient (K_{OW} < 0.1), which means it tends to concentrate in the aqueous phase of products, where most bacterial action occurs (Ruckman et al., 2004). LAE has been verified to be nontoxic and is rapidly metabolized to amino acid arginine by hydrolysis of the ethyl ester and lauroyl amide functions. The arginine subsequently is further metabolized to ornithine and urea and eventually to CO_2 through normal mammalian biochemical pathways (Scheme 2.7) (Ruckman et al., 2004; Hawkins et al., 2009). According to these outstanding features, LAE is becoming a product widely used for pharmaceuticals, cosmetics and food conservation (Luchansky et al., 2005; Asker et al., 2011). As antimicrobial agent, LAE can't be used in all food matrices, that is, LAE is an active cationic surfactant and therefore can interact with many anionic food compounds (Bonnaud et al., 2010). In addition it has a bitter taste at high concentration, which may affect the organoleptic properties of some food products. However, the use of LAE as food packaging is still limited. Several studies have been

done in this regard to prepare antimicrobial coatings or films that incorporate LAE (Muriel-Galet et al., 2012; Higuera et al., 2013).

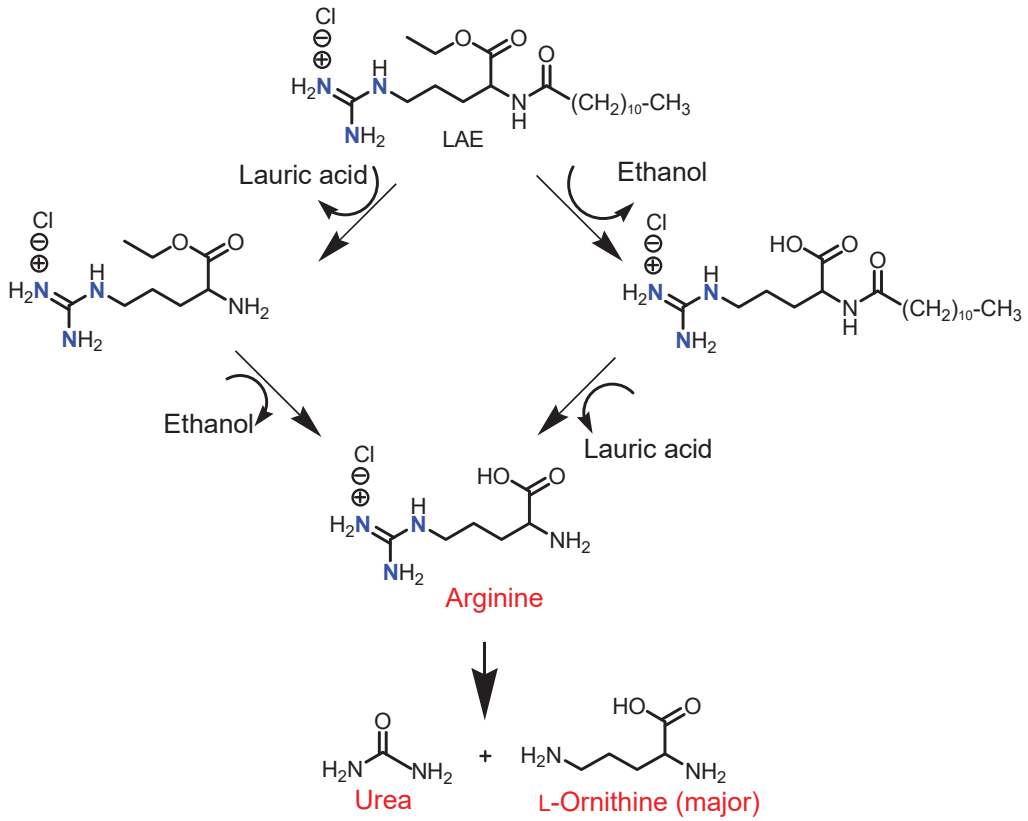

Scheme 2.7. Postulated pathway for the *in vivo* mammalian metabolism of LAE (Hawkins et al. , 2009).

The aim of these studies is prolonging the microbial shelf-life of food products without modifying their organoleptic properties through improving traditional packaging by the use of the newly developed films as an inner coating of the package wall (Appendini et al., 2002). Specifically they want to improve the durability of refrigerated products because the stipulated time given by manufacturer after the package is opened and stored under refrigerated conditions is only 2 days.

3. Polyelectrolyte-surfactant complexes

Polyelectrolyte-surfactant complexes are the best known self-assembling synthetic materials. They consist of charged polymer chains (polyelectrolytes) and oppositely charged small amphiphilic molecules (surfactants).

Self-assembly is defined as spontaneous intermolecular association via non-covalent bonds (*e.g.,* electrostatic interactions, hydrogen bonds, or hydrophobic interactions), resulting in thermodynamically stable, well-defined supramolecular structures with dimensions ranging from 10 nm to 10 μm (Lehn, 1990). Self-assembly

offers a number of advantages over chemical synthesis involving formation of covalent bonds: i) it does not require complicated preparative procedures, ii) the reactions are typically fast, iii) the resulting structures may be capable of reversible adaptive rearrangement in response to changes in environment (*e.g.*, solvent or temperature) and iv) control of assembly processes opens fascinating possibilities in the manipulation of materials properties on the molecular scale, which may be particularly important for fabrication of multifunctional materials for technological applications. Self-organizing systems are widely represented in nature, *e.g.*, double-helical structures of nucleic acids and bilayers of lipids within cell membranes, with organization and intimately linked function (Ringsdorf et al., 1991).

Polyelectrolyte-surfactant complexes formed by binding surfactants to polyelectrolytes of opposite charges has been reported to be a highly cooperative process in which the cooperative binding range is restricted to the early stage of binding. It is known that the presence of polyelectrolytes induces aggregation of the opposite charged surfactant (Abuin et al., 1984). As in the case of self-assembly, the aggregation starts in a narrow concentration range (critical aggregation concentration), which is usually a few orders of magnitude below the *cmc* of the surfactant (Read, 1972). Above *cmc*, polyelectrolytes most often interact with oppositely charged surfactants so strongly that irreversible macroscopic phase separation occurs. Dubin *et al.* (Dubin et al., 1983) showed that such strong electrostatic interactions could be attenuated by diluting the surface charge of ionic surfactant micelles with non-ionic surfactant. This results in the formation of soluble polyelectrolyte-surfactant complexes. Consequently, it become possible to identify a critical micellar surface charge necessary for complex formation and its square-route dependence on ionic strength (Li et al., 1994). In the solid state, stoichiometric polyelectrolyte-surfactant complexes lead to the spontaneous formation of highly organized assemblies with lamellar structures (Antonietti et al., 1994a).

3.1. Structure and properties of polyelectrolyte-surfactant complexes

Polyelectrolyte-surfactant complexes are prepared through an ion-exchange reaction driven by electrostatic attraction between the polymer chain units and the surfactant ions. If dilute aqueous solutions of the two components are mixed, complexes are formed spontaneously (Ibragimova et al., 1986; Goddard et al., 1993). The complexation reaction occurs at concentration considerably lower than the critical micelle concentration (*cmc*) of the surfactant and is highly cooperative.

Several structures of complexes has been described in the literature (Higashi et al., 1986; Decher et al., 1991; Mao et al., 1993) depending on the preparation procedure: i)

monolayer films are formed when an amphiphile is spread on an aqueous solution of an oppositely charged polyelectrolyte; ii) multilayer films are prepared by successive adsorption of a surfactant and a polyelectrolyte on a solid substrate and iii) complexes with liquid crystalline mesophases are obtained when solutions of polyelectrolytes with flexible chains and oppositely charged small amphiphiles with mesogenic groups are mixed in polar organic solvents. Such complexes exhibit liquid crystalline mesophases characteristic of the bound amphiphile, while the polymer chains enhance the thermal stability and mechanical properties of the ordered structures (Ujiie et al., 1990; Bazuin et al., 1994).

Depending on the polymer to surfactant ratio, the complexes formed are either stoichiometric or non-stoichiometric (Ibragimova et al., 1986; Goddard et al., 1993) Non-stoichiometric complexes containing an excess of either charged polymer chain units or surfactant molecules are generally soluble in water (Figure 3.1a). The formation and structure of those containing an excess of polyelectrolyte chain units have been studied in detail (Ibragimova et al., 1986; Goddard et al., 1993). Such complexes form “mixed micelles” consisting of clusters of hydrophobic surfactant chains surrounded by the polar polyelectrolyte backbone. In addition, they are able to solubilize nonpolar organic molecules in water solutions, which have a number of technological applications (Goddard et al., 1993).

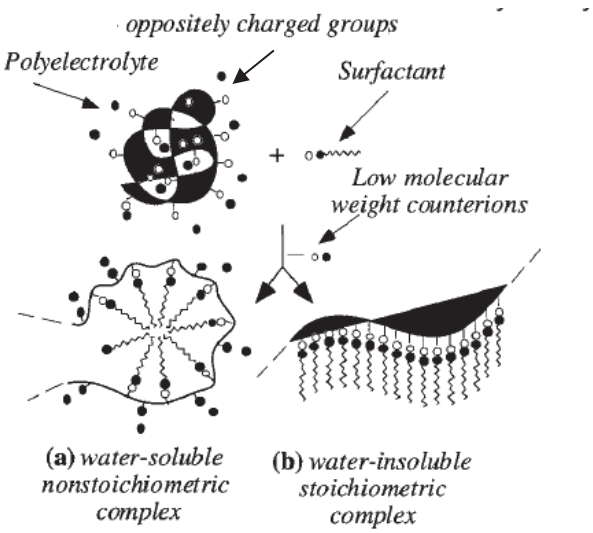

Figure 3.1. Scheme of formation of polyelectrolyte-surfactant complexes in aqueous solutions (Macknight et al.,1998).

On the other hand, stoichiometric complexes are insoluble in water (Figure 3.1b) because the ionic groups of polyelectrolyte and surfactant are shielded from solvent by nonpolar parts of the complex. Such complexes are obtained when equimolar amounts of charged polymer chain units and surfactant molecules are mixed in water. Until recently, the interest in these complexes has been limited; however, the discovery of

such complexes with outstanding properties has dramatically increased the interest for this area. Among their properties, it is the simplicity of their synthesis and their solubility in organic solvents. Furthermore, the ability of such complexes to combine the properties of polymers with those of amphiphilies together with the wide variety of available polyelectrolytes and surfactants, provide attractive opportunities for preparation of materials with adjustable macroscopic properties. For instance, polymer components can provide mechanical strength and thermal stability, while the surfactants retain their tendency to assemble in layered structures and their ability to crystallize.

3.2. Applications of polyelectrolyte-surfactant complexes

These systems are particularly promising as materials for molecular composites, separation membranes, solubilization, and compatibilization. For instance, fluoropolymers, like poly(tetrafluoroethylene) (PTFE, Teflon ®), are distinguished due to their low surface tension that is, their capacity of generating non-sticky surfaces that are repellent to both water and oily liquid phases. However, they are insoluble and have high flowing temperatures that avoid their processability. Complexes of polyelectrolytes with fluorinated surfactants offer a solution to processing problems because thanks to the polar moieties they are soluble and the arrangement of fluorocarbon tails in layers results in even lower surface tension than PTFE (Antonietti et al., 1996; Zhou et al., 1998). Certain polyelectrolytes are able to form highly organized structures with DNA (Rädler et al., 1997) and so they have been object of attention in several studies related to gene therapy (Zhu et al., 2010). Nevertheless, the most promising application is probably as carriers to protect active molecules and transport by body fluids. The self-assembly and amphiphilicity make polyelectrolyte-surfactant suitable biomaterials for either as simple drug carriers or even as targeting systems with an active role. One interesting example are NPs made of cationic polyelectrolytes and retinoic acid. Retinoic acid is a metabolite of Vitamin A so it is involved in the proliferation and differentiation of epithelial tissues, and can be used in the treatment of dermatological disorders such as acne, psoriasis and hyperkeratosis. (Packer et al., 1994). Furthermore, its role in the treatment of malignant-tumours or brain function is being widely investigated. In order to preserve its genuine properties, non-damaging immobilization of retinoic acid is necessary during administration. One way of overcoming this limitation is by binding to positive polyelectrolytes (instead of proteins as occurs in nature). Thünemann *et al.* reported complexes of retinoic acid with PEI (Polyethylenimine) (Thünemann, 2000) and polyamino acids (Thünemann et al., 2000). In both cases, they prepared NPs containing retinoic acid to transport it

safely. Other kinds of NPs useful as potential drug delivery systems have been prepared using different techniques (Thünemann et al., 2001).

3.3. State of art

The study of stoichiometric polyelectrolyte-surfactant complexes has been mainly focused on two polymer families: conventional synthetic charged polymers, such as modified polystyrene (Ruokolainen et al, 1999) or poly(acrylic acid) (Antonietti et al. 1994b) and bio-polyelectrolytes, such as polypeptides.

Ponomarenko *et al.* (Ponomarenko et al., 1996) reported the solid state properties of stoichiometric complexes formed by synthetic polypeptide sodium poly(α,L-glutamate) and the oppositely charged surfactant dodecyl- and cetyl-trimethylammonium bromides. They showed that the polypeptide in these complexes adopts the α-helical conformation, and that the alkyl chains were organized in two different ways: long alkyl chains of the surfactant are able to crystallize separately in a hexagonal lattice, whereas the shorter ones (below 16 carbon atoms) remain in a disordered state. A similar behaviour is displayed by the long alkyl esters of poly(α,L-glutamic acid) (Akagi et al., 2010), although in this case the minimum number of alkyl carbons required to crystallize is lower.

Ionic comb-like complexes started to be investigated two decades ago by our group. Pérez-Camero *et al.* (Pérez-Camero et al., 2004) and García-Álvarez *et al.* (García-Álvarez et al., 2005) prepared stoichiometric or quasi-stoichiometric complexes made from poly(γ,D-glutamic acid) or poly(γ,DL-glutamic acid) and alkyltrimethylammonium bromides, *n*ATMA·Br. Such complexes were prepared by precipitation when aqueous solutions of Na·PGGA and *n*ATMA·Br were mixed (Scheme 3.1).

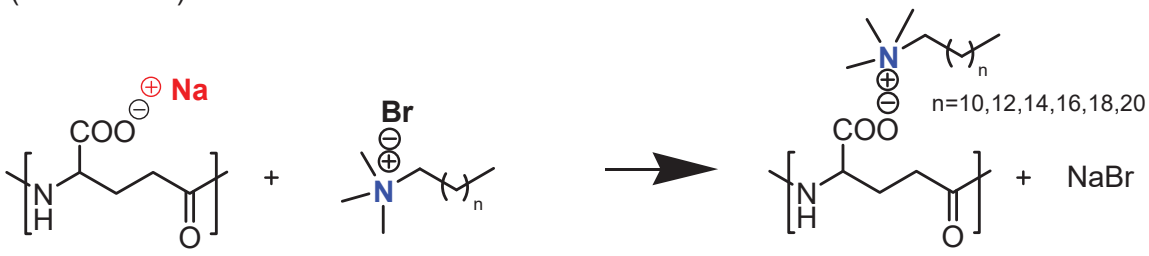

Scheme 3.1. Coupling reaction of *n*ATMA·Br with Na·PGGA leading to *n*ATMA·PGGA ionic complexes.

The thermal behavior and structural properties of these complexes was extensively studied , and results can be summarized as: i) all complexes are thermal stable up to 200 ºC; ii) DSC analysis showed that the shortest alkyl chains did not show any thermal transition from 0 ºC to degradation temperature. Conversely, a well-defined peak between 50 and 80 ºC, depending on the alkyl chain length, appeared in the

thermograms of the *n*ATMA·PGGA complexes with *n*=18, 20 and 22. This is the peak corresponding to the melting of the crystallized paraffin phase; iii) it was ascertained by X-ray diffraction that these complexes adopt the layered biphasic structure typical of comb-like polymers, which is schematically depicted in Figure 3.2. The window spacing of the layered structure ranged between 3.0 and 4.5 nm depending on the length of the alkyl chain. The chains of *n*ATMA·PGGA complexes with *n*= 18, 20 and 22 are partially crystallized in a pseudo-hexagonal lattice. Whereas those of complexes with $n \leq 16$ are uncrystallized; iv) The melting-crystallization transition involving the paraffinic phase can be closely followed by SAXS/WAXS and is also detected by ^{13}C-NMR spectroscopy (Yamanobe et al., 1988) as an anti-to-gauche interconversion of methylenes. The interlamellar spacing is expanded after heating in the case of D-PGGA complexes, whereas a shrinkage has been observed for those made of D,L-PGGA (Pérez-Camero et al., 2004; García-Álvarez et al., 2005).

Figure 3.2. Lamellar biphasic structure characteristic of comb-like ionic complexes of PGGA (García-Álvarez et al., 2005).

More recently, Portilla-Arias *et al.* (Portilla-Arias et al., 2007b) have described *n*ATMA·PMLA complexes made of poly (L-malic acid) and *n*ATMA surfactants; these complexes display almost exactly the same structure and properties than those made of PGGA.

Nevertheless, in spite of the potential applications of these ionic complexes as biomaterials, the lack of biocompatibility of the surfactants could be a drawback for their use in biomedical applications. For this reason, Tolentino *et al.* (Tolentino et al., 2013) have recently described ionic complexes of PGGA with bio-surfactants derived from choline, which resulted to be the first comb-like ionic system entirely made of bio-based components. These complexes, *n*ACh·PGGA (Scheme 3.2), were made from PGGA and alkanoylcholines (*n*ACh) derived from fatty acids. Alkanoylcholines have been proved to be less toxic than alkyltrimethylammonium compounds (Klein et al., 2008; Tischer et al., 2012) and able to display therapeutic activity in the treatment of the Alzheimer disease (Carelli et al., 2001) and certain gastro-intestinal disorders (Alexander et al., 1989). *n*ACh·PGGA complexes were also self-assembled in layered

amphiphilic structures able to respond reversibly to thermal effects. In addition, nACh·PGGA complexes formed nanoparticles of 50-100 nm which were able to encapsulate different drugs including both neutral (theophiline and carbamazepine) and ionic (doxorubicine) drugs. The entrappingf and releasing of these drugs was low and fast for the former and high and slow for the latter (Tolentino et al., 2014). Therefore *n*ACh·PGGA complexes are candidates of exceptional interest in the design of medical devices for thermally controlled store and delivery of drugs.

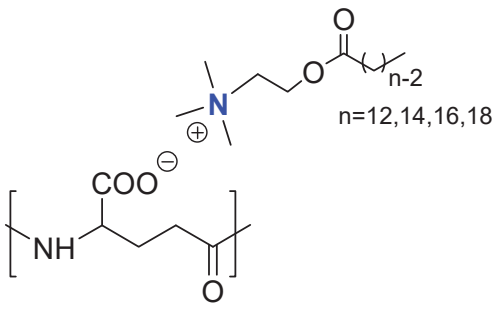

Scheme 3.2. Chemical structure of nACh·PGGA complexes.

4. Polymer nanocomposites

Composite materials are solid multiphase materials in which one phase is continues and is called matrix, while the other is filler material, which make the dispread phase. Composites offer unusual combinations of component materials properties such as weight, strength, stiffness, permeability, electrical, biodegradability and optical properties that is difficult to attain separately by individual components (Giannelis, 1996).

Composites that are gaining importance are nanocomposites in which the combination of a filler with nanoscale dimension and high aspect ratio with its nanoscale dispersion within polymer matrix leads to significant improvements in the polymer properties at very low filler volume fractions. As a result of lower filler using, the macroscopic homogeneity and low density of primary polymer are retained, as well as it's opacity in the final nanocomposite system (Mittal, 2009). Although the term nanocomposite represents a new field in material science and technology, the nanocomposites have actually been used for centuries by the nature. Bones, shells and wood are some examples of strong nanocomposites made by nature (Hussain et al., 2006). The "new nanocomposite science" was started by the Toyota report (Usuki et al., 1993) on the superior improvement in the properties of nylon-6 by the preparation of exfoliated nylon-6/clay nanocomposites and has been continued by more recent studies with carbon nanotubes, carbon nanofillers, exfoliated graphite,

nanocrystaline metals and fibers modified with inorganic fillers used in polymeric composites (Pau et al., 2008). Nevertheless the filler materials mostly employed in nanocomposites are layered silicates due to their excellent availability and high aspect ratio and surface area (Nguyen et al., 2006; Pavlidou et al., 2008).

4.1. Layered silicates

Layered silicates are natural or synthetic minerals consisted of the regular stacks of aluminosilicate layers with a high aspect ratio and high surface area. The layers in clays are built when tetrahedral (T) and octahedral (O) sheets are fused together. The crystal lattice represented in Figure 4.1 is well known as 2:1 phyllosilicates which are the most common clays used for the preparation of polymer-layered silicate nanocomposites. When the aluminum cations in the octahedral layers are partially substituted by divalent magnesium, an overall negative charge is created that is counter-balanced in the interlayer by counter sodium or calcium ions. This kind of phyllosilicate is called montmorillonite (MMT) and it is featured by its capacity for exchanging (CEC) of the interlayer ions (measured as mequiv/100 mg) due to the charge created on the layers is not locally constant and varies from layer to layer (Kim et al., 2005; Tjong et al., 2006).

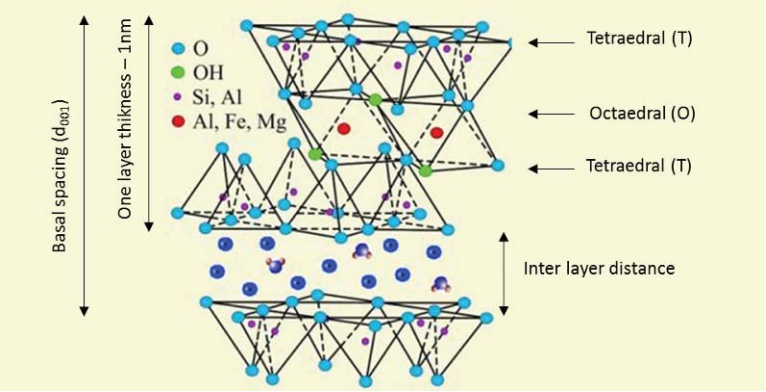

Figure 4.1. Layered structure of montmorillonite.

4.2. Modification of clays

Pristine layered silicates are hydrophilic, and therefore incompatible with hydrophobic polymers, which are the most common engineering polymers. The incompatibility is because hydrophilic clays cannot disperse within the polymer matrices and weak interactions are caused. Therefore exfoliation and preparation of dispersed stable nanocomposites with improved properties are not possible to obtain. Consequently, it is necessary to modify the clay layers with hydrophilic agents to render the clay layer more compatible with polymer chains. This can be performed

through a cation exchange process by the replacement of sodium and calcium cations present in the interlayer space or clay galleries by onium cations such as alkylammonium or alkylphosphonium cations (Figure 4.2) (Ahmad et al., 2009). The long organic chains of these surfactants not only provide hydrophobicity, but also give rise to an increase of the interlayer distance, which promotes the following intercalation of polymer chains into the galleries during nanocomposites preparation (Kim et al., 2005).

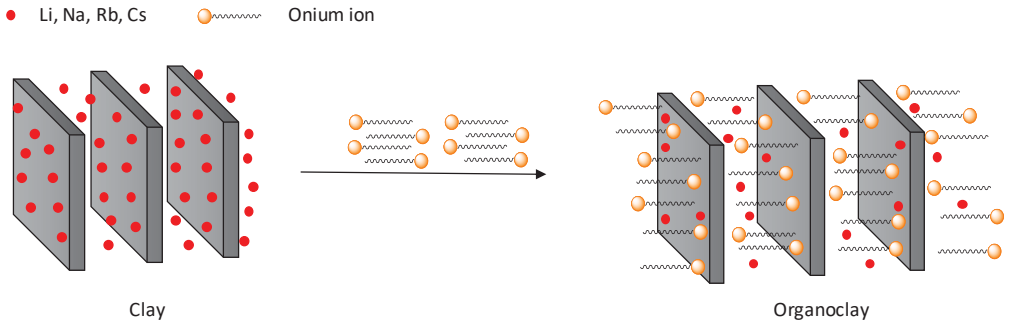

Figure 4.2. Scheme of modification of clay layers by organic-onium cations.

Onium cations can adopt monolayer, bilayer or paraffin-type aggregations in layered silicates depending on the charge density of clay layers (Figure 4.3) (Lagaly, 1986). Also increasing the temperature can lead to structures with more basal spacing due to the increasing mobility of onium molecules into the galleries. However, in a given temperature two parameters determine the equilibrium layer spacing, the charge density of layers (driving the packing) and number and size of onium chains into the interlayer space.

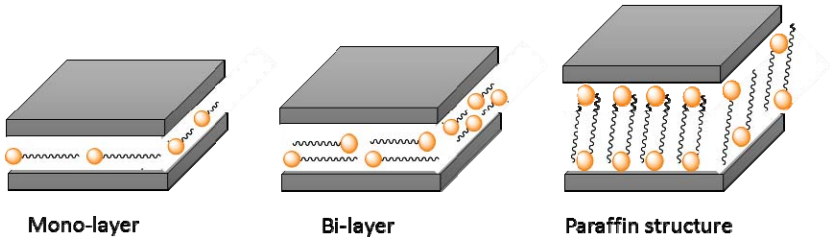

Figure 4.3. Arrangements of organic-oniums compounds into the clay galleries.

4.3. Polymer layered silicates nanocomposites

The research on this kind of nanocomposites was encouraged since Vaia *et al.* (Vaia et al., 1993) reported a simple preparation method for enhancing polymer properties by adding a few percents of filler. The procedure consisted of heating a mixture of polymer and silicate powder above T_g or T_m of the polymer. Consequently, the polymer chains were able to diffuse into the clay galleries leading to an intercalated structure of polymer and silicate.

4.3.1. Nanocomposite structure

In general, the structures of polymer/clay nanocomposites are classified according to the level of intercalation of polymer chains into the clay galleries (Figure 4.4). When affinity between polymers and clays is scarce, the polymer is unable to intercalate within the clay layers and the clay is dispersed as aggregates or particles with silicate layers stacked together. Consequently, a phase separation is obtained that makes that the properties of these composites are similar to traditional microcomposites (Okada et al., 1987; Alexandre et al., 2000).

If the affinity between the filler and the matrix is good enough, polymers chains are inserted into the inter layer space and cause an increasing of the inter-layer spacing. If the periodic array of the clay layer still exists, an intercalated nanocomposite is formed which consist of a well-ordered multi-layer hybrid morphology. If clay layers are separated one another (with interlayer distances between clay platelets around 10 nm or more) and individual layers are dispersed within the polymer matrix, an exfoliated structure is obtained. Due to the well dispersion of individual clay layers, large surface interactions between polymer and clay are produced. Consequently, an improvement in polymer properties is obtained but using clay contents lower than needed by the intercalated one (Kim et al., 2005).

The mechanical improvement observed in nanocomposites is due to the effective stress transfer from the polymer matrix to the filler through the interphase area. As exfoliated nanocomposites have larger interphase area than intercalated ones, it is well accepted that exfoliated nanocomposites show the best physical properties. Nevertheless, the most of reported polymer nanocomposites present an intercalated structure or a mixture of intercalated and exfoliated ones because the achievement of totally exfoliated clay into a polymer matrix is highly difficult (Vaia et al., 1994).

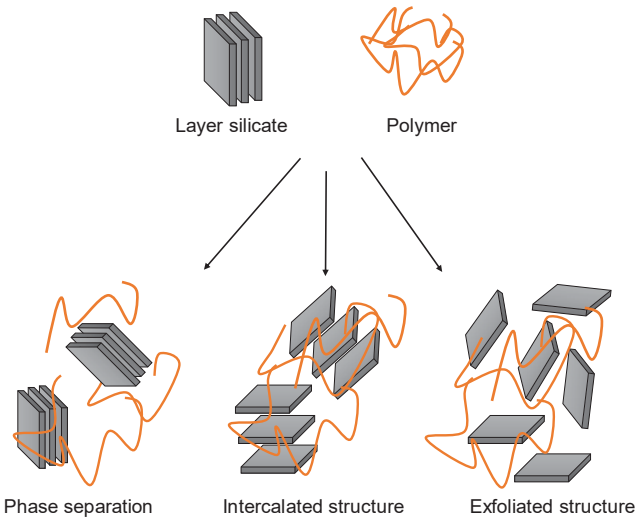

Figure 4.4. Scheme of the different structures polymer/clay nanocomposites.

4.3.2. Nanocomposite preparation methodologies

In addition to polymer characteristics such as polarity, molecular weight, hydrophobicity, reactive groups as well as clay characteristics including charge density and its modified structure and polarity, the preparation method also plays an important role in succeeding to obtain an efficient nanocomposite. Currently, there are three main procedures to produce polymer-clay nanocomposites: *in situ* intercalative polymerization, melt intercalation and solution intercalation.

In situ intercalative polymerization is a method in which the organoclay is swollen in monomer solution. Therefore, the polymerization is carried out within the clay galleries, as well as extra galleries resulting in a disordered and exfoliated structure. This method is suitable for the preparation of thermoset/clay nanocomposites and has been widely used for the epoxies and styrene polymer nanocomposites (Lan et al., 1995). The polarity of monomer and clay layers determines the diffusion rate and equilibrium concentration of monomer within the clay galleries. Consequently, the exfoliation and dispersion of clay layers can be tailored by the clay and monomer chemistry (Pavlidou et al., 2008).

Melt intercalation is a method in which clay is mixed within the polymer matrix in molten temperature. Consequently, polymer chains are intercalated or exfoliated into the galleries. In order to enhance their compatibility and therefore promote the exfoliation, clays are organically modified and polymer chains are surface modified with more polar functional groups. This methodology have many advantages, no solvent is required and is a popular method for industry (Sinha et al., 2003). The conventional methods such as extrusion and injection molding are used for dispersion of clay layers within the polymer matrix. For instance, this method is effective for the preparation of thermoplastic nanocomposites (Kornmann et al., 2001).

Solution intercalation consists of dissolving the polymer in a solvent and dispersing the clay in the same solution. The nanocomposite is obtained by solvent removal. During the solvent evaporation the entropy gained by the exit of solvent molecules from the interlayers spacing, allows the polymer chains to diffuse the layers and sandwiching. Intercalated or exfoliated structures are obtained by this method depending on the interactions between polymer and clay sheets. This technique was first used for water-soluble polymers such as polyethylene oxide (PEO), polyvinyl alcohol (PVA) or polyvinylpyrrolidone (PVP) (Aranda et al., 1992; Kim et al., 2005; Vaia et al., 1993). With regard to non-polar polymers, organic solvents are used to swell organically modified silicates and to dissolve the polymeric matrices. Intercalated nanocomposites of polyethylene (PE), polystyrene (PS), polycaprolactone (PCL) or

polylactic acid (PLA) have been obtained using this method (Aranda et al., 1992; Vaia et al., 1993; Kim et al., 2005). The environmental problems associated to the use of large amounts of non-aqueous solvents make this method inadequate for industrial preparation of non-polar polymer nanocomposites. However this method can be interesting for the preparation of bio-nanocomposites made of biopolymers produced by living organisms such as polysaccharides, polypeptides, gelatin and poly(3-hydroxybutyrate) (PHB). The formation of biopolymer nanocomposites (bio-nanocomposites) are the way to overcome the limitations that present some biopolymers such as brittleness, high gas permeability, low heat distortion temperature or low melt viscosity. This technology affords a potential for new applications of biopolymers in which an enhancement of properties is required (Kim et al., 2005; Sinha et al., 2005).

4.3.3 Properties and applications

Layered silicate nanocomposites have proven to improve many properties of neat polymers. Improvements can include a high storage modulus both in solid and molten states, increased tensile and flexural properties, increased heat distortion temperature and thermal stability, a decrease in gas permeability and flammability, increase in the biodegradation rate, and so forth (Kim et al., 2005). Nanocomposites display other specific characteristics when compared to conventional composites. One outstanding feature of nanocomposites is their transparency due to the lack of scattering by the nanometric clay particles. Resistance to scratch and ablation are also properties that have been reported to be improved by nanocomposite formation (Okada et al., 1987; Vaia et al., 1994). Property improvement is attained even at low concentrations of clay and so they are much lighter than traditional composites (Okada et al., 1987). Nowadays the potential applications for nanocomposites involve a number of technology fields including automotive sector, construction, aerospace, food packaging, electronics, biomedicine or textile (Okada et al., 1987). The first commercial polymer nanocomposite was developed for the automotive industry (Zanetti et al., 2000). It was patented by Toyota and Ube in the 90s and consisted of a Nylon 6 nanocomposite which was applied for timing belt cover because its good thermal resistance, rigidity and lightness (Usuki et al., 1993). Later these nanocomposites were used in the building of engine covers, but their expensive prices limited their expansion so that their applications were focused on high barrier materials (Walls et al., 2003). Other nanocomposites used in the automotive industry are nanocomposites based on polyolefins. They are used like materials for step assistant or structural seat backs (Zanetti et al., 2000).

Nanocomposites have become the favorite materials for beverage and food packing applications due to the improvement on the barrier properties and optical transparency exhibited by nanocomposites. Bayer, Mitsubishi and Nanocor companies have developed materials with high barrier properties suitable for packaging films and bottles using clay nanocomposites (Okada et al., 1987; Sinha et al., 2005). Nanocomposites for electrochemical or electroanalytical devices, membranes and corrosion protection are also used (Aranda et al., 2006) due to their fire retardant behavior and tailoring conductivity.

Despite their outstanding properties, production of nanocomposites is still expensive and their market expansion is slow. As a result, several big automotive companies such as Ford and Volvo, as well as chemical companies such as Honeywell and Clariant maintain great efforts in the research and development of nanocomposites with the aim of overcoming economical drawbacks (Okada et al., 1987; Sinha et al., 2005).

5. Polymeric materials with antimicrobial activity

Infections by pathogenic microorganisms including bacteria, viruses, fungi and protozoa are still a major cause of morbidity and mortality (Hall-Stoodley et al., 2004). What is more, infections kill worldwide more people than any other single cause because microorganisms are found everywhere, in air, soil and water. For instance, it has been estimated that as much as 30% of people in industrialized countries suffers yearly from a food borne disease, and that in 2000 at least two millions of people died from diarrheal diseases worldwide, the major proportion being attributable to microbial contamination of food and water (Mead et al., 1999). Because of them, there is a growing concern in many fields including medical devices, drugs, surgery equipment, health care products, water purification systems, textiles, food packagings etc (Davey et al., 2000).

There are more than 200 of active agents causing gastrointestinal illnesses, about 60% of which being due to infection by food borne bacterial pathogens. Eventually it is known that wounds always have a high risk of bacterial infection due to the invasion and proliferation of pathogenic bacteria such as *Straphylococcus aureus* (Hynes et al., 2000), which are able to produce the enzyme hyaluronidase that degrade hyaluronic acid (Stern et al., 2007) penetrating and spreading the infection to other issues (Hynes, 2004). *Salmonella spp., Campylobacter spp. and Escherichia coli* are the pathogens traditionally attracting major attention (Newell et al., 2010) but in the last two decades concerns have included not only an increasing number of additional pathogens as *L. monocytogenes*, but also the development of modified traditional strains displaying

antibiotic resistance (Lai et al., 2016). Antibiotic resistance is related to the overuse of antibiotics and the capacity of genetic adaptation of some microorganisms (Abebe et al., 2016). In fact microorganisms acquire-resistance involves numerous mechanisms (Jayaraman, 2009). As a result, effective antibiotics may not be available to treat specific infections because of multiple resistance. Consequently, attention has been especially devoted to new and emerging systems in the field of antimicrobial materials that are not easily susceptible to resistance (Engler et al., 2012).

In this sense, antimicrobial polymers are being overlooked in these days of antibiotic resistance as alternatives to antibiotics (Muñoz-Bonilla et al., 2012). These systems offer some advantages: i) polymers act as a matrix for holding the antimicrobial agents, having a great influence on the final antimicrobial activity due to the rate of biocide release which depends straightly on the hydrophilicity and molecular weight of the polymer, ii) the toxicity related to some biocides is decreased because the polymer matrix avoid the diffusion of the low molecular weight biocide into the human body, and iii) the antimicrobial activity of antimicrobial polymers is longer compared to the activity of free biocides.

During the last decade there has been a notable development in the field of polymeric materials with antimicrobial activity (Hetrick et al., 2006; Santos et al., 2016). Specifically polymers containing antimicrobial agents such as metals, cationic salts or halogen atoms in their structure have been extensively explored to produce antimicrobial materials. It is the easiest way to ensure the antimicrobial activity of the polymer without the necessity of carrying out a chemical modification (Muñoz-Bonilla et al., 2012). Strain dependence of antibacterial activity is known to be originated from differences in cell wall structures of bacteria (Costerton et al., 1975; Kanazawa et al., 1993). Gram-positive bacteria possess a relatively simple cell wall structure which is composed mainly of peptidoglycan and teichoic acid (Figure 5.1). On the other hand, the structure of the cell wall of Gram-negative bacteria is much more complicated than that of Gram-positive species. The peptidoglycan layer is rather thin, but there is an outer membrane outside the peptidoglycan layer that is composed mainly of lipopolysaccharides and phospholipids. The role of this outer membrane is to protect the bacterial cell from attack by foreign compounds, such as disinfectants (Costerton et al., 1975). Hydrophobicity has been confirmed to be critical for the antibacterial activity of cationic disinfectants (Kanazawa et al., 1993). By increasing the hydrophobicity of the cationic biocides, their interaction with the cytoplasmic membrane is largely enhanced. Accordingly, it is expected that surfactants having the longest alkyl chains would display the highest antibacterial activity (Kanazawa et al., 1994).

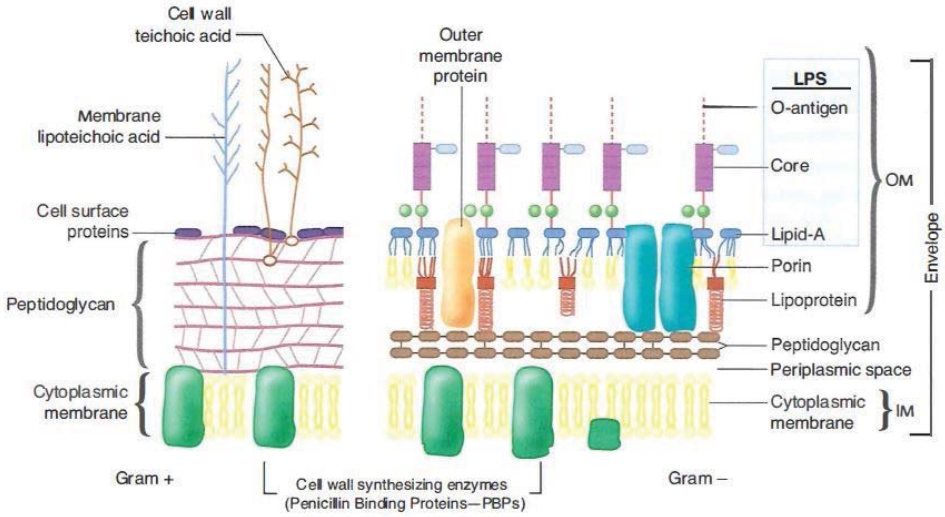

Figure 5.1. Cross-sectional diagram showing major differences between cell envelope of mammalian cell and various microbial families (Engler et al., 2012).

PGGA is an excellent candidate for designing antimicrobial polymeric materials for food packaging due to its edibility and innocuity. As mentioned before, this biopolymer is edible and its polyanionic nature makes it very suitable for the efficient loading of organocationic compounds *via* ionic coupling (Pérez-Camero et al., 2004; García-Álvarez et al., 2005; Portilla-Arias et al., 2007b). Furthermore, the capacity of PGGA to inhibit by itself the growth of some pathogenic bacteria has been also announced (Lee et al., 2014). Nevertheless, the references on the application of PGGA in food packaging are very scarce in the accessible literature (Siracusa et al., 2008).

HyA has attached quite attention as antimicrobial polymer because its capacity to cleavage some bacteria that produce hyaluronidases *e.g. S. aureus* (Baier et al., 2013). Despite the bacteriostatic activity found in HyA (Pirnazar et al., 1999; Ardizzoni et al., 2011), infections are not still completely avoided in some medical applications such as contact lenses (Rah, 2011) and wound dressings (Teh et al.,2012). The antimicrobial activity of the polysaccharide is not clear and seems to depend on the concentration and molecular weight of HyA and on bacterial species (Ardizzoni et al., 2011). Therefore, HyA must be used in combination with antimicrobial agents to ensure its antimicrobial effect. HyA-silver nanoparticles and HyA coupled with polyhexanide (Kemp et al., 2009; Baier et al., 2013) and nisin polypeptide (Lequeux et al., 2014) are representative examples of such materials.

5.1. Polysaccharide-based nanoparticles for biocides and drug release applications

To date, a significant number of reports on the activity of antibiotic-conjugated polymeric NPs against various infections, including those caused by drug-resistant pathogens, have been published (Engler et al., 2012). The antimicrobial mechanism of

action of NPs is generally described as adhering to one of three models: oxidative stress induction (Gurunathan et al., 2012), metal ion release (Nagy et al., 2011), or non-oxidative mechanisms (Leung et al., 2014). These three types of mechanisms can occur simultaneously. Due to the size of NPs which is in the nanometer scale range, their use shows the following advantages: i) NPs have demonstrated a broad-spectrum of antibacterial properties against both Gram-positive and Gram-negative bacteria, ii) the antibiotic resistance mechanisms are irrelevant for NPs because the mode of action of NPs is the direct contact with the bacterial cell wall, without needing to penetrate the cell, which makes that NPs are less prone to promoting resistance in bacteria than antibiotics, and iii) biofilms (that is matrices consisting of extracellular polymeric substance that accumulates and surrounds bacterial cells (Mah et al., 2001), acting as a barrier to diffusion by trapping and degrading antibiotic molecules) may be destroyed by increasing the local NPs concentration.

NPs have also attained a significant impact on clinical chemotherapy in the last two decades (Allen et al., 2004; Wagner et al., 2006). Advantages in nanoparticle drug delivery, particularly at the systemic level, include longer circulation half-lives, improved pharmacokinetics and reduced side effects (Davis et al., 2008). In cancer treatments, nanoparticles can rely on the enhanced permeability and retention effect caused by leaky tumor vasculatures for better drug accumulation at the tumor sites. At biocompatible nanoscale drug carriers have enabled more efficient and safer delivery of a myriad of drugs in specific site drug delivery. A wide variety of nanocarriers (bearing dissolved, encapsulated and linked drugs) have been developed for drug delivery purposes (Figure 5.2): for example, self-assembled carriers with vesicular (liposomes, niosomes or polymeric vesicles) or micellar morphology (polymeric micelles), nanoparticular aggregates (made of lipids, hydrophobic polymers, hydrogels), single molecules (dendrimers, carbon nanotubes, linear polymers), viruses and inorganic core-shell nanoparticles (Conniot et al., 2014).

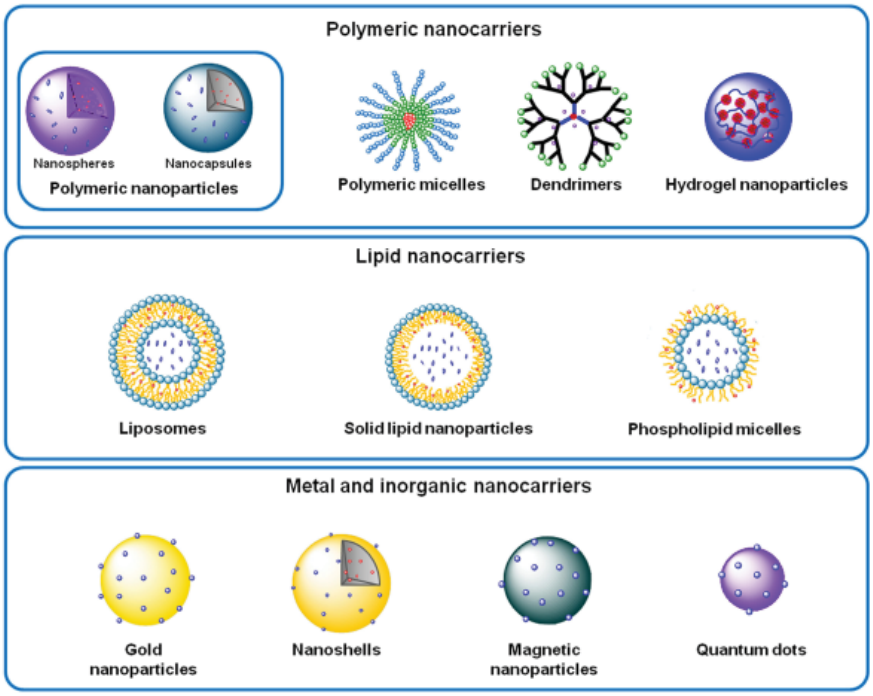

Figure 5.2. Representative types of nanocarriers for drug delivery.

Polymers are particularly favoured as nanocarriers and among them, polysaccharides are the compounds of choice for the preparation of nanoparticles for drug delivery that must meet very specific requirements such as a) biocompatibility, b) appropriate mechanical strength c) degradation kinetics matching the biological process, d) chemical, structural and application versatility, e) capacity of loading a variety of drugs, contrast agents, and nucleic acids, both non-covalently and covalently. f) improving targetability by surface modification with ligands and antibodies (Peer et al., 2007).

Polysaccharides are found in abundance in a diverse range of natural sources and therefore they have the advantage of being relatively inexpensive. For instance, alginate and carraggenan have algal origins; cellulose, pectine and guar gum have plant origins; dextran and xanthan gum have microbial origins; and hyaluronan, chondroitin and heparin have animal origins (Mizrahy et al., 2012).

Nanoparticles made of hyaluronic acid (HyA) are of particular relevance to this Thesis. HyA is a naturally-occurring glycosaminoglycan that is concentrated in regions of high cell division (*e.g.* cancer). In addition, HyA plays an instructive role via HyA receptors on the cell surface (mainly CD44 and RHAMM) (Ouasti et al., 2012). Taking into account these features together with the fact that HyA is biocompatible, biodegradable, non-toxic and non-inflammatory, there is a widespread interest in HyA nanoparticles as drug carrier (Knudson et al., 1993; Brown et al., 2005; Choi et al.,

2010). In general, three main methodologies have been exploited so far for the design of HyA-based nanoparticles (Figure 5.3) (Knudson et al., 1993): i) Conjugates of low weight HyA with drugs, ii) nanoparticle carriers where HyA is placed on the surface and drugs are physically incorporated in the bulk, and iii) HyA nanogels, which are an intermediate system between the two formers.

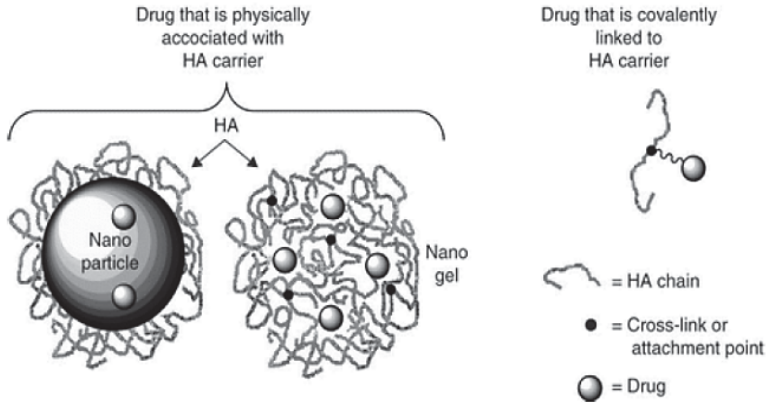

Figure 5.3. Main types of HyA-based nanocarriersl. Taken from (Knudson et al., 1993).

6. References

Abdallah, D. J., Bachman, R. E., Perlstein, J., Weiss, R. G. (1999). Crystal structures of symmetrical tetra n-alkyl ammonium and phosphonium halides. Dissection of competing interactions leading to “biradial” and “tetraradial” shapes. J. Phys. Chem. B, 103(43), 9269–9278.

Abdallah, D. J., Robertson, A., Hsu, H., Weiss, R. G. (2000). Smectic liquid-crystalline phases of quaternary group (especially phosphonium) salts with three equivalent long n -alkyl chains. How do layered assemblies form in liquid-crystalline and crystalline phases? J. Am. Chem. Soc. 122(8), 3053–3062.

Abebe, E., Tegegne, B., Tibebu, S. (2016). A review on molecular mechanisms of bacterial resistance to antibiotics. European J. Appl. Sci. 8(5), 301–310.

Abuin, E. B., Scaiano, J. C. (1984). Exploratory study of the effect of polyelectrolyte surfactant aggregates on photochemical behavior. J. Am. Chem. Soc. 106(21), 6274–6283.

Adamová, G., Gardas, R. L., Rebelo, L. P. N., Robertson, A. J., Seddon, K. R. (2011). Alkyltrioctylphosphonium chloride ionic liquids: synthesis and physicochemical properties. Dalt. Trans. 40(47), 12750–12764.

Ahlstrom, B., Chelminska-Bertilsson, M., Thompson, R. A., Edebo, L. (1995). Long-chain alkanoylcholines, a new category of soft antimicrobial agents that are enzymatically degradable. Antimicrob. Agents Chemother. 39(1), 50–55.

Ahmad, M. B., Hoidy, W. H., Nor Azowa, B. I., Al-Mulla, E. A. J. (2009). Modification of montmorillonite by new surfactants J. Eng. amp; Appl. Sci. 4(3), 184–188.

Ajinomoto Co. Inc (1997). The use of poly-gamma-glutamic acid for preparing an agent for increasing the phosphorus assimilation. Patent EP0838160A1.

Akagi, T., Higashi, M., Kaneko, T., Kida, T., Akashi, M. (2006). Hydrolytic and enzymatic degradation of nanoparticles based on amphiphilic poly(γ-glutamic acid)-graft -L-phenylalanine copolymers. Biomacromolecules, 7(1), 297–303.

Akagi, T., Watanabe, K., Kim, H., Akashi, M. (2010). Stabilization of polyion complex nanoparticles composed of poly(amino acid) using hydrophobic interactions. Langmuir, 26(4), 2406–2413.

Al-Saleh, M. H., Sundararaj, U. (2010). Processing-microstructure-property relationship in conductive polymer nanocomposites. Polymer, 51(12), 2740–2747.

Alexander, J., Fix, J. A (1989). Enhancement of absorption of drugs from gastrointestinal tract using choline ester salts - US Pat. 4,822,773.

Alexander, J., Fix, J. A., Repta, A. J. (1990). Choline esters as absorption-enhancing agents for drug delivery through mucous membranes of the nasal, buccal, sublingual and vaginal cavities. Patent, US4963556.

Alexandre, M., Dubois, P. (2000). Polymer-layered silicate nanocomposites: preparation, properties and uses of a new class of materials. Mater. Sci. Eng. 28(1–2), 1–63.

Allen, T. M., Cullis, P. R. (2004). Drug delivery systems: entering the mainstream. Science, 303(5665), 1818–1822.

Allison, D. D., Grande-Allen, K. J. (2006). Review. Hyaluronan: a powerful tissue engineering tool. Tissue Eng. 12, 2131–2140.

Andre, P. (2008). New trends in face rejuvenation by hyaluronic acid injections. J. Cosmet. Dermatol. 7(4), 251–258.

Antonietti, M., Conrad, J., Thünemann, A. (1994a). Polyelectrolyte-surfactant complexes: a new type of solid, mesomorphous materials. Macromolecules, 27(21), 6007–6011.

Antonietti, M., Conrad, J. (1994b). Synthesis of very highly ordered liquid crystalline phases by complex formation of polyacrylic acid with cationic surfactants. Angew. Chemie Int. Edit. 33(18), 1869–1870.

Antonietti, M., Henke, S., Thünemann, A. (1996). Highly ordered materials with ultra-low surface energies: polyelectrolyte-surfactant, complexes with fluorinated surfactants. Adv. Mater. 8(1), 41–45.

Appendini, P., Hotchkiss, J. H. (2002). Review of antimicrobial food packaging. Innov. Food Sci. Emerg. Technol. 3(2), 113–126.

Aranda, P., Ruiz-Hitzky, E. (1992). Poly(ethylene oxide)-silicate intercalation materials. Chem. Mater. 4(6), 1395–1403.

Aranda, P., Darder, M., Fernández-Saavedra, R., López-Blanco, M. (2006). Relevance of polymer– and biopolymer–clay nanocomposites in electrochemical and electroanalytical applications. Thin Solid Film, 495(1–2), 104–112.

Ardizzoni, A., Neglia, R. G., Baschieri, M. C., Cermelli, C., Caratozzolo, M., Righi, E., Blasi, E. (2011). Influence of hyaluronic acid on bacterial and fungal species, including clinically relevant opportunistic pathogens. J. Mater. Sci. Mater. Med. 22(10), 2329–2338.

Asadov, Z. H., Rahimov, R. A., Ahmadova G. A., Mammadova, K. A. (2012). Synthesis, surface active and thermodynamic parameters of novel quaternary ammonium salts. J. Surfactants Deterg. 15, 721-727.

Asker, D., Weiss, J., McClements, D. J. (2011). Formation and stabilization of antimicrobial delivery systems based on electrostatic complexes of cationic−non-ionic mixed micelles and anionic polysaccharides. J. Agric. Food Chem. 59(3), 1041–1049.

Auzenne, E., Ghosh, S. C., Khodadadian, M., Rivera, B., Farquhar, D., Price, R. E., Klostergaard, J. (2007). Hyaluronic acid- paclitaxel: antitumor efficacy against CD44(+) human ovarian carcinoma xenografts. Neoplasia, 9(6), 479–486.

Axenov, K. V., Laschat, S. (2011). Thermotropic ionic liquid crystals. Materials, 4(12), 206–259.

Baier Leach, J., Bivens, K. A., Patrick, C. W., Schmidt, C. E. (2003). Photocrosslinked hyaluronic acid hydrogels: Natural, biodegradable tissue engineering scaffolds. Biotechnol. Bioeng. 82(5), 578–589.

Baier, G., Cavallaro, A., Vasilev, K., Mailänder, V., Musyanovych, A., Landfester, K. (2013). Enzyme responsive hyaluronic acid nanocapsules containing polyhexanide and their exposure to bacteria to prevent infection. Biomacromolecules, 14(4), 1103–1112.

Balazs, E., Leshchiner, A. (1987). Cross-linked gels of hyaluronic acid and products containing such gels. US4582865A US Grant.

Balazs E.A., Denlinger J.L. (1993) Viscosupplementation: a new concept in the treatment of osteoarthritis. J. Rheumatol. 39, 3–9.

Bazuin, C. G.; Brandys, F. A.; Eve, T. M.; Plante, M. (1994). Use of noncovalent interactions to form novel liquid crystalline polymeric materials. Macromol. Symp. 84(1), 183-196.

Becher, P. (1985). Encyclopedia of emulsion technology, volume 2: applications. Wiley Subscription Services, Inc., A Wiley Company.

Bhattacharyya, D., Hestekin, J., Brushaber, P., Cullen, L., Bachas, L., Sikdar, S. (1998). Novel poly-glutamic acid functionalized microfiltration membranes for sorption of heavy metals at high capacity. J. Memb. Sci. 141(1), 121–135.

Binnemans, K. (2005). Ionic liquid crystals. Chem. Rev. 105(11), 4148–4204.

Blusztajn, Jan K.; Wurtman, R. J. (1883). Choline and cholinergic neurons. Science, 221(4611), 614–20.

Blusztajn, J. K., Wurtman, R. J. (1998). Choline, a vital amine. Science, 281, 794–795.

Bonnaud, M., Weiss, J., McClements, D. J. (2010). Interaction of a food-grade cationic surfactant (Lauric Arginate) with food-grade biopolymers (pectin, carrageenan, xanthan, alginate, dextran, and chitosan). J. Agric. Food Chem. 58(17), 9770–9777.

Bradaric, C. J., Downard, A., Kennedy, C., Robertson, A. J., Zhou, Y. (2003). Industrial preparation of phosphonium ionic liquids. Green Chem. 5(2), 143-152.

Brandt, F. S., Cazzaniga, A. (2008). Hyaluronic acid gel fillers in the management of facial aging. Clin. Interv. Aging. (1), 153–159.

Brown, M. B., Jones, S. A. (2005). Hyaluronic acid: a unique topical vehicle for the localized delivery of drugs to the skin. J. Eur. Acad. Dermatology Venereol. 19(3), 308–318.

Bruckner, V., Ivanovics, G. (1937). Chemische und immunologische Studien uber den Mechanismus der milzbrandinfektin und Immunitat; die chemische Struktur der Kapselsubstanz des Milzbrandbazillus und der serologisch identischen spezifischen Subtanz des Bazillus mesentericus. Z. Immunitatsforsch, 304-318.

Buck, D. W., Alam, M., Kim, J. Y. S. (2009). Injectable fillers for facial rejuvenation: a review. J. Plast. Reconstr. Aesthetic Surg. 62(1), 11–18.

Buescher, J. M., Margaritis, A. (2007). Microbial biosynthesis of polyglutamic acid biopolymer and applications in the biopharmaceutical, biomedical and food industries. Crit. Rev. Biotechnol. 27(1), 1–19.

Burdick, J. A., Prestwich, G. D. (2011). Hyaluronic acid hydrogels for biomedical applications. Adv. Mater. 23, H41–H56.

Byrne, C., McNally, T. (2007). Ionic liquid modification of layered silicates for enhanced thermal stability. Macromol. Rapid Commun. 28, 780–784.

Candela T. F. A. (2006). Poly-gamma-glutamate in bacteria. Mol. Microbiol. 60(5), 1091–1098.

Carelli, V., Liberatore, F., Scipione, L., Cardellini, M., Rotiroti, Domenicantonio Rispoli, V. (2001). Choline derivatives for the treatment of Alzheimer's disease. Patent-WO0181296.

Chelminska-Bertilsson, M., Allenmark, S., Edebo, L. (1993). Butyrylcholinesterase activity towards long-chain alkanoylcholines: kinetics and mechanism. Biochim. Biophys. Acta - Protein Struct. Mol. Enzymol. 1202(1), 56–60.

Chen, W. Y. J., Abatangelo, G. (1999). Functions of hyaluronan in wound repair. Wound Repair Regen. 7(2), 79–89.

Choi, K. Y., Chung, H., Min, K. H., Yoon, H. Y., Kim, K., Park, J. H., Jeong, S. Y. (2010). Self-assembled hyaluronic acid nanoparticles for active tumor targeting. Biomaterials, 31(1), 106–114.

Cieniecka-Rosłonkiewicz, A., Pernak, J., Kubis-Feder, J., Ramani, A., Robertson, A. J., Seddon, K. R. (2005). Synthesis, anti-microbial activities and anti-electrostatic properties of phosphonium-based ionic liquids. Green Chem. 7(12), 855–862.

Conniot, J., Silva, J. M., Fernandes, J. G., Silva, L. C., Gaspar, R., Brocchini, S., Barata, T. S. (2014). Cancer immunotherapy: nanodelivery approaches for immune cell targeting and tracking. Front. Chem. 2(105), 1-27.

Costerton, J. W., Cheng, K. J. (1975). The role of the bacterial cell envelope in antibiotic resistance. J. Antimicrob. Chemother. 1(4), 363–77.

Cowman, M. K., Matsuoka, S. (2005). Experimental approaches to hyaluronan structure. Carbohydr. Res. 340(5), 791–809.

Culty, M., Shizari, M., Thompson, E. W., Underhill, C. B. (1994). Binding and degradation of hyaluronan by human breast cancer cell lines expressing different forms of CD44: Correlation with invasive potential. J. Cell. Physiol. 160(2), 275–286.

Daninippon Pharmaceutica Co, L. (1972). Ice-cream stabilizer. Patent EP0090356A1.

Davey, M. E., O'toole, G. A. (2000). Microbial biofilms: from ecology to molecular genetics. Microbiol. Mol. Biol. Rev. 64(4), 847–67.

Davis, M. E., Chen, Z., Shin, D. M. (2008). Nanoparticle therapeutics: an emerging treatment modality for cancer. Nat. Rev. Drug Discov. 7(9), 771–782.

Decher, G.; Hong, J. Makromol. Chem., (1991). Buildup of ultrathin multilayer films by a self-assembly process: consecutive adsorption of anionic and cationic bipolar amphiphiles on charged surfaces, Makromol. Symp.46, 321-327.

Dekie, L., Toncheva, V., Dubruel, P., Schacht, E. H., Barrett, L., Seymour, L. W. (2000). Poly-L-glutamic acid derivatives as vectors for gene therapy. J. Control. Release, 65(1–2), 187–202.

Demus, D., Goodby, J., Gray, G. W., Spies, H.-W., Vill, V. (1998) Eds.; Wiley-VCH: Weinheim, 3, Chapter VII, p 341.

Donofrir, D. K., Whitekettle, W. K. (1989). Biocidal compositions and use thereof containing a synergistic mixture of n-tributyl tetradecyl phosphonium chloride and bis(tributyl) tin oxide. US Patent 4835143.

Dubin, P. L., Oteri, R. (1983). Association of polyelectrolytes with oppositely charged mixed micelles. J. Colloid Interface Sci. 95(2), 453–461.

Engler, A. C., Wiradharma, N., Ong, Z. Y., Coady, D. J., Hedrick, J. L., Yang, Y. Y. (2012). Emerging trends in macromolecular antimicrobials to fight multi-drug-resistant infections. Nano Today, 7(3), 201–222.

European Food Safety Authority. (2007). Call for expressions of interest for a position within the (parma).

Fraser, K. J., MacFarlane, D. R. (2009). Phosphonium-based ionic liquids : an overview. Aust. J. Chem., 62, 309–321.

Fuiji, H. (1963). Formation of mucilage by Bacillus natto. Nippon Nogei Kagaku. Kaishi. 37, 615-618.

García-Álvarez, M., Álvarez, J., Alla, A., Martínez de Ilarduya, A., Herranz, C., Muñoz-Guerra, S. (2005). Comb-like ionic complexes of cationic surfactants with bacterial poly(γ-glutamic acid) of racemic composition. Macromol. Biosci. 5(1), 30–38.

Garg, H. G., Hales, C. A. (2004). Chemistry and biology of hyaluronan. El sevier.

Gerritsma, D. A., Robertson, A., McNulty, J., Capretta, A. (2004). Heck reactions of aryl halides in phosphonium salt ionic liquids: Library screening and applications. Tetrahedron Lett. 45(41), 7629–7631.

Giannelis, E. P. (1996). Polymer layered silicate nanocomposites. Adv. Mater. 8(1), 29–35.

Goddard, E. D., Ananthapadmanabhan, K. P. (1993). Interactions of surfactants with polymers and proteins. CRC Press, Boca Raton, FL, 1-427.

Gorke, J. T., Srienc, F., Kazlauskas, R. J. (2008). Hydrolase-catalyzed biotransformations in deep eutectic solvents. Chem. Comm. (10), 1235–1237.

Guo, W., Hou, Y., Wu, W., Ren, S., Tian, S., Marsh, K. N. (2013). Separation of phenol from model oils with quaternary ammonium salts via forming deep eutectic solvents. Green Chem. 15, 226-229.

Gurunathan, S., Woong Han, J., Abdal Daye, A., Eppakayala, V., Kim, J. (2012). Oxidative stress-mediated antibacterial activity of graphene oxide and reduced graphene oxide in pseudomonas aeruginosa. Int. J. Nanomed. 7, 5901–5914.

Hall-Stoodley, L., Costerton, J. W., Stoodley, P. (2004). Bacterial biofilms: from the natural environment to infectious diseases. Nat. Rev. Microbiol. 2, 95–108.

Hargittai, I., Hargittai, M. (2008). Molecular structure of hyaluronan: an introduction. Struct Chem, 19, 697–717.

Hascall, V. C., Majors, A. K., De La Motte, C. A., Evanko, S. P., Wang, A., Drazba, J. A., Wight, T. N. (2004). Intracellular hyaluronan: a new frontier for inflammation? Biochim. Biophys. Acta. 1673(1–2), 3–12.

Hashida, M., Akamatsu, K., Nishikawa, M., Yamashita, F., Takakura, Y. (1999). Design of polymeric prodrugs of prostaglandin E1 having galactose residue for hepatocyte targeting. J. Control. Release, 62(1–2), 253–262.

Hawkins, D. R., Rocabayera, X., Ruckman, S., Segret, R., Shaw, D. (2009). Metabolism and pharmacokinetics of ethyl $^{\alpha}$N-lauroyl-L-arginate hydrochloride in human volunteers. Food Chem. Toxicol. 47(11), 2711–2715.

Heatley, F., Scott, J. E. (1988). A water molecule participates in the secondary structure of hyaluronan. Biochem. J., 254(2), 489–493.

Hedley, C. B., Yuan, G., Theng, B. K. G. (2007). Thermal analysis of montmorillonites modified with quaternary phosphonium and ammonium surfactants Appl. Clay Sci. 35(3–4), 180–188.

Hegazy, M. A., Abdallah, M., Awad, M. K. (2014). Three novel di-quaternary ammonium salts as corrosion inhibitors for API X65 steel pipeline in acidic solution. Part I: Experimental results. Rezk, Corros Sci. 81, 54-64.

Hetrick, E. M., Schoenfisch, M. H. (2006). Reducing implant-related infections: active release strategies. Chem. Soc. Rev. 35(9), 780-789.

Higashi, N.; Kunitake, T. (1986). Stabilization and facilitated deposition of surface monolayersof fluorocarvon amphiphiles through polyion complex formation. Chem. Lett., 15 (1),105-108.

Higueras, L., López-Carballo, G., Hernández-Muñoz, P., Gavara, R., Rollini, M. (2013). Development of a novel antimicrobial film based on chitosan with LAE (ethyl-N-dodecanoyl-L-arginate) and its application to fresh chicken. nt. J. Food Microbiol. 165(3), 339–345.

Hiruta, O., Hasegawa, N., Oonishi, Y. (1994). Low-molecule weight γ-polyglutamic acid manufacture with acid or alkali. JP Patent 94/112332.

Ho, G.H., Ho, T.I., Hsieh, K.H., Su, Y.C., Lin, P.Y., Yang, J., Yang, S.C. (2006). γ-polyglutamic acid produced by bacillus subtilis (natto): structural characteristics, chemical properties and biological functionalities. J. Chin. Chem. Soc., 53, 1363–1384.

Hoel M, K. S. (1996). Depletion of fossil fuels and the impacts of global warming. Resour. Energy Econ. 18(2), 115–136.

Hollosi, M., Kajtar, M., Bruckner, V. (1969). Improved syntheses of stereoisomeric poly-gamma-glutamic acids .2. Syntheses via polybenzyl and poly-t-butyl esters. Acta Chim. Acad. Sci.Hungaricae, 62(3), 305.

Holmberg, K., Jönsson, B., Kronberg, B., Lindman, B. (2003). Surfactants and polymers in aqueous solution. J. W. A, LTD: Chichester, England 157-174.

Hussain, F., Hojjati, M., Okamoto, M., Gorga, R. E. (2006). Review article: polymer-matrix nanocomposites, processing, manufacturing, and application: an overview. J. Compos. Mater. 40(17), 1511–1575.

Hynes, W. L., Walton, S. L. (2000). Hyaluronidases of Gram-positive bacteria. FEMS Microbio. Lett. 183(2), 201–207.

Hynes, W. (2004). Virulence factors of the group A streptococci and genes that regulate their expression. Front. Biosci. 9, 3399–3433.

Ibragimova, Z. K., Kasaikin, V., Zezin, A., Kabanov, V. (1986). Non-stoichiometric polyelectrolyte complexes of polyacrylic acid and cationic surfactants. Polym. Sci. U.S.S.R., 28(8), 1826–1833.

Ibrahim, S., Kang, Q. K., Ramamurthi, A. (2010). The impact of hyaluronic acid oligomer content on physical, mechanical, and biologic properties of divinyl sulfone-crosslinked hyaluronic acid hydrogels. J. Biomed. Mater. Res. Part A, 94(2), 355-370.

Infante, R., Garcia Dominguez, J., Erra, P., Julia, R., Prats, M. (1984). Surface active molecules: preparation and properties of long chain n-acyl-l-alpha-amino-omega-guanidine alkyl acid derivatives. Int. J. Cosmet. Sci. 6(6), 275–282.

Ito, N., Arzhantsev, S., Heitz, M., Maroncelli, M. (2004). Solvation dynamics and rotation of coumarin in alkylphosphonium ionic liquids. J. Phys. Chem. B, 108, 5771–5777.

Ivánovics, G., Brucknerm, V. (1937). Chemische und immunologische Studien über den Mechanimus der Milzbrandinfektion und Immunitat; die chemische Struktur der Kapdelsubstanz des Milzbrandbasillus und der serologisch identischen spezifischen Substanz des Bacillus mesentericus. Z. Immunitatsforsch, 90, 304–318.

Iwamoto, K., Ohnuki, Y., Sawada, K., Seno, M. (1981). Solid-solid phase transitions of long-chain n-alkyltrimethylammonium halides. Mol. Cryst. Liq. Cryst. 73, 95-103.

Jayaraman, R. (2009). Antibiotic resistance: an overview of mechanisms and a paradigm shift. Curr. Sci. 96(11), 1475–1484.

Jin, Y. J., Ubonvan, T., Kim, D.D. (2010). Hyaluronic acid in drug delivery systems. . Pharm. Investig. 40, 33–43.

Kablik, J., Monheit, G. D., Yu, L., Chang, G., Gershkovich, J. (2009). Comparative physical properties of hyaluronic acid dermal fillers. Dermatologic Surg. 35(1), 302–312.

Kamitori, S., Sumimoto, Y., Vongbupnimit, K., Noguchi, K. Okuyama, K. (1997). Molecular and crystal structures of dodecyltrimethylammonium bromide and its complex with p-phenylphenol. Mol. Cryst. Liq. Cryst., 300, 31–43.

Kanazawa, A., Ikeda, T., Endo, T. (1993). Novel polycationic biocides. Synthesis and antibacterial activity of polymeric phosphonium salts. Journal of Polymer Science, Part A: Polym. Chem. 31(2), 335–343.

Kanazawa, A., Ikeda, T., Endo, T. (1994). Synthesis and antimicrobial activity of dimethyl- and trimethyl-substituted phosphonium salts with alkyl chains of various lengths. Antimicrob. Agents Chemother. 38(5), 945–952.

Kanazawa, A., Tsutsumi, O., Ikeda, T., Nagase, Y. (1997). Novel thermotropic liquid crystals without a rigid core formed by amphiphiles having phosphonium ions. J. Am. Chem. Soc. 119(33), 7670–7675.

Kashima, N., Furuta, L., Tanabe, I. (2006). Permeability enhancer. Patent US20060025346.

Katjar, M., Bruckner, V. (1969). Improved syntheses of stereoiomeric polygamma-glutamic acids. I. Syntheses via polymethylesters. Acta Chim. Acad. Sci. Hung., 62, 191–212.

Kemp, M. M., Kumar, A., Clement, D., Ajayan, P., Mousa, S., Linhardt, R. J. (2009). Hyaluronan- and heparin-reduced silver nanoparticles with antimicrobial properties. Nanomed. 4(4), 421–429.

Kim, Y., White, J. L. (2005). Formation of polymer nanocomposites with various organoclays. J. Appl. Polym. Sci. 96(5), 1888–1896.

Klein, R., Touraud, D., Kunz, W. (2008). Choline carboxylate surfactants: biocompatible and highly soluble in water. Green Chem. 10(4), 433–435.

Klein, R., Kellermeier, M., Drechsler, M., Touraud, D., Kunz, W. (2009). Solubilisation of stearic acid by the organic base choline hydroxide. Colloids Surfaces A Physicochem. Eng. Asp. 338 (1–3), 129–134.

Knifton, J. F. (1981). Manufacture of ethylene glycol from synthesis gas. United States Patent 4265828.

Knifton, J. F. (1982a). Manufacture of alkanols from synthesis gas. United States Patent 4332914.

Knifton, J. F. (1982b). Process for preparing acetic and propionic acids and their esters. United States Patent 4362822.

Knifton, J. F. (1988). Homogeneous Transition-Metal Catalysis in Molten Salts. Asp. Homog. Catal. 1–58.

Knudson, C. B., Knudson, W. (1993). Hyaluronan-binding proteins in development, tissue homeostasis, and disease. FASEB J. 7(13), 1233–1241.

Ko, Y. H., Gross, R. A. (1998). Effects of glucose and glycerol on γ-poly(glutamic acid) formation by Bacillus licheniformis ATCC 9945a. Biotechnol. Bioeng. 57(4), 430–437

Kobayashi, Y., Okamoto, A., Nishinari, K. (1994). Viscoelasticity of hyaluronic acid with different molecular weights. Biorheology, 31(3), 235–244.

Konno, A., Taguchi, T., Yamaguchi, T. (1988). New use of polyglutamic acid for foods. Patent EP0284386B.

Kornmann, X., Lindberg, H., Berglund, L. A. (2001). Synthesis of epoxy–clay nanocomposites. Influence of the nature of the curing agent on structure. Polymer, 42(10), 4493–4499.

Kortstee, G. J. J. (1970). Arch. Microbiol. 71(3), 235–244.

Kubota H., Fukuda H., Takebe H. E. T. (1992). Poly-gamma-glutamic acid ester and shaped body thereof. Patent Number(s) US5118784.

Kubota, H., Nambu, Y. Endo, T. (1993). Some properties of poly(gamma-glutamic acid) produced by microorganism. Nippon Kagaku Kaishi, 8, 973–977.

Kubota, H., Nambu, Y., Endo, T. (1995). Convenient esterification of poly(γ-glutamic acid) produced by microorganism with alkyl halides and their thermal properties. Journal of Polym. Sci. Part A: Polym. Chem. 33(1), 85–88.

Kubota, H., Nambu, Y., Endo, T. (1996). Alkaline hydrolysis of poly(γ-glutamic acid) produced by microorganism. J. Polym. Sci. Part A: Polym. Chem. 34(7), 1347–1351.

Kumar, V., Malhotra, S. V. (2009). Study on the potential anti-cancer activity of phosphonium and ammonium-based ionic liquids. Bioorg. Med. Chem. Lett. 19(16), 4643–4646.

Kunioka, M. (1993). Properties of hydrogels prepared by gamma-irradiation in microbial poly(gamma-glutamic acid) aqueous-solutions. Kobunshi Ronbunshu, 50(10), 755–760.

Kunioka, M., Choi, H. J. (1995). Properties of biodegradable hydrogels prepared by γ–irradiation of microbial poly(ε-lysine) aqueous solutions. J. Appl. Polym. Sci. 58(4), 801–806.

Kunioka, M., Furusawa, K. (1997). Poly(γ-glutamic acid) hydrogel prepared from microbial poly(γ-glutamic acid) and alkanediamine with water-soluble carbodiimide. J. Appl. Polym. Sci. 65(10), 1889–1896.

Kuo, J. W., Swann, D. A., Prestwich, G. D. (1991). Chemical modification of hyaluronic acid by carbodiimides. Bioconj. Chem. 2(4), 232–241.

Lagaly, G. (1986). Interaction of alkylamines with different types of layered compounds. Solid State Ionics, 22(1), 43–51.

Lai, E. P. C., Iqbal, Z., Avis, T. J. (2016). Combating Antimicrobial Resistance in Foodborne Microorganisms. J. Food Prot. 79(2), 321–336.

Lan, T., Kaviratna, P. D., Pinnavaia, T. J. (1995). Mechanism of clay tactoid exfoliation in epoxy-clay nanocomposites. Chem. Mater. 7 (11), 2144–2150.

Laurent, T. C., Laurent, U. B. G., Fraser, J. R. E. (1996). The structure and function of hyaluronan: An overview, Immunol. Cell Biol. 74(2), A1–A7.

Lee, N., Go, T., Lee, S., Jeong, S., Park, G., Hong, C., Son, H. (2014). In vitro evaluation of new functional properties of poly-γ-glutamic acid produced by Bacillus subtilis D7. J. Biol. Sci. 21(2), 153–158.

Lehn, J. M. (1990). Perspectives in supramolecular chemistry—from molecular recognition towards molecular information processing and self-organization. Angew. Chemie Int. Ed. English. 29 (11), 1304–1319.

Lequeux, I., Ducasse, E., Jouenne, T., Thebault, P. (2014). Addition of antimicrobial properties to hyaluronic acid by grafting of antimicrobial peptide. Eur. Polym. J. 51(1), 182–190.

Leung, Y. H., Ng, A. M. C., Xu, X., Shen, Z., Gethings, I. A., Wong, M. T., Leung, F. C. C. (2014). Mechanisms of antibacterial activity of mgo: non-ros mediated toxicity of mgo nanoparticles towards Escherichia coli. Small, 10(6), 1171–1183.

Li, Y., Xia, J., Dubin, P. L. (1994). Complex formation between polyelectrolyte and oppositely charged mixed micelles: static and dynamic light scattering study of the effect of polyelectrolyte molecular weight and concentration. Macromolecules, 27(24), 7049–7055.

Li, C., Yu, D. F., Newman, R. A., Cabral, F., Stephens, L. C., Hunter, N., Wallace, S. (1998). Complete regression of well-established tumors using a novel water-soluble poly(L-glutamic acid)-paclitaxel conjugate. Cancer Res. 58(11), 2404–2409.

Liu, P., Hao, J. W., Mo, L.P., Zhang, Z.H. (2015). Recent advances in the application of deep eutectic solvents as sustainable media as well as catalysts in organic reactions. RSC Adv. 5(60), 48675–48704.

Luchansky, J. B., Call, J. E., Hristova, B., Rumery, L., Yoder, L., Oser, A. (2005). Viability of Listeria monocytogenes on commercially-prepared hams surface treated with acidic calcium sulfate and lauric arginate and stored at 4 °C. Meat Sci. 71, 92–99.

Luo, Y., Kirker, K. R., Prestwich, G. D. (2000). Cross-linked hyaluronic acid hydrogel films: new biomaterials for drug delivery. J. Control. Release, 69(1), 169–184.

Luo, Y., Bernshaw, N. J., Lu, Z.-R., Kopecek, J., Prestwich, G. D. (2002). Targeted delivery of doxorubicin by HPMA copolymer-hyaluronan bioconjugates. Pharm. Res. 19(4), 396–402.

Macknight, W. J., Ponomarenko, E. A., Tirrel, D. A. (1998). Self-assembled polyelectrolyte-surfactant complexes in nonaqueous solvents and in the solid state. Accounts Chem. 31(12), 781–788.

Mah, T. F. C., O'Toole, G. A. (2001). Mechanisms of biofilm resistance to antimicrobial agents. Trends Microbiol. 9(1), 34–39.

Mansbach, C., Dowell, R. (1992). Uptake and metabolism of circulating fatty-acids by rat intestine. Am. J. Physiol. 263(6), G927–G933.

Mao, G.; Tsao, Y.; Tirrell, M.; Davis, T. H.; Hessel, V.; Ringsdorf, H. (1993). Self-assembly of photopolymerizable bolaform amphiphile mono- and multilayers. Langmuir, 9 (12), 3461-3470.

Markland, P., Amidon, G. L., Yang, V. C. (1999). Modified polypeptides containing Î3-benzyl glutamic acid as drug delivery platforms. Int. J. Pharm. 178(2), 183–192.

Martínez de Ilarduya, A., Ittobane I., Bermúdez, M., Alla, A., El Idrissi, M., Muñoz-Guerra, S. (2002). Poly(α-alkyl γ-glutamate)s of microbial origin. 2. on the microstructure and crystal structure of poly(α-ethyl γ-glutamate)s. Biomac. 3, 1078-1086

McLean, R. J., Beauchemin, D., Clapham, L., Beveridge, T. J. (1990). Metal-binding characteristics of the gamma-glutamyl capsular polymer of bacillus licheniformis ATCC 9945. Appl. Environ. Microbiol. 56(12), 3671–3677.

McNulty, J., Capretta, A., Wilson, J., Dyck, J., Adjabeng, G., Robertson, A. (2002). Suzuki cross-coupling reactions of aryl halides in phosphonium salt ionic liquid under mild conditions. Chem. Comm. 17, 1986–1987.

Mead, P. S., Slutsker, L., Dietz, V., McCaig, L. F., Bresee, J. S., Shapiro, C., Tauxe, R. V. (1999). Food-related illness and death in the United States. Emerg. Infect. Dis. 5(5), 607–625.

Meneghetti, P., Qutubuddin, S. (2006). Synthesis, thermal properties and applications of polymer-clay nanocomposites. Thermochim. Acta. 442(1–2), 74–77.

Meyer, K., Palmer, J. W. (1934). The polysaccharide of the vitreous humor. J. Biol. Chem., 107, 629–634.

Mittal, V. (2009). Polymer layered silicate nanocomposites: A Review. Materials, 2(3), 992–1057.

Mizrahy, S., Peer, D. (2012). Polysaccharides as building blocks for nanotherapeutics. Chem. Soc. Rev., 41(7), 2623–2640.

Monheit, G. D., Prather, C. L. (2007). Hyaluronic acid fillers for the male patient. Dermatol. Ther. 20(6), 394–406.

Moreland, L. W. (2003). Intra-articular hyaluronan (hyaluronic acid) and hylans for the treatment of osteoarthritis: mechanisms of action. Arthritis Res. Ther. 5(2), 54–67.

Morillo, M., Martínez de Ilarduya, A., Alla, A. (2003). Comblike alkyl esters of biosynthetic poly (γ-glutamic acid). 2. Supramolecular structure and thermal transitions. Macromolecules, 36(20), 7567–7576.

Morillo, M., Martínez de Ilarduya, A., Muñoz-Guerra, S. (2001). Comblike alkyl esters of biosynthetic poly (γ-glutamic acid). 1. Synthesis and characterization. Macromolecules, 34(22), 7868–7875.

Mowery, B. P., Lindner, A. H., Weisblum, B., Stahl S. S., Gellman, S. H. (2009). Structure−activity relationships among random nylon-3 copolymers that mimic antibacterial host-defense peptides J. Am. Chem. Soc. 131, 9735-9745.

Muñoz-Bonilla, A., Fernández-García, M. (2012). Polymeric materials with antimicrobial activity. Prog. Polym. Sci. 37(2), 281–339.

Muñoz-Guerra, S., García-Álvarez, M., Portilla-Arias, J. A. (2013). Chemical modification of microbial poly(γ-glutamic acid): progress and perspectives. J. Renew. Mater. 1(1), 42–60.

Muriel-Galet, V., López-Carballo, G., Gavara, R., Hernández-Muñoz, P. (2012). Antimicrobial food packaging film based on the release of LAE from EVOH. Int. J. Food Microbiol. 157(2), 239–244.

Necas, J., Bartosikova, L., Brauner, P., Kolar, J. (2008). Hyaluronic acid (hyaluronan): a review. Vet. Med. 53(8), 397–411.

Naves, A. F., Palombo, R. R., Carrasco L. D. M., Carmona-Ribeiro, A. M. (2013). Antimicrobial particles from emulsion polymerization of methyl methacrylate in the presence of quaternary ammonium surfactants. Langmuir, 29, 9677-9684.

Newell, D. G., Koopmans, M., Verhoef, L., Duizer, E., Aidara-Kane, A., Sprong, H., Kruse, H. (2010). Food-borne diseases - The challenges of 20 years ago still persist while new ones continue to emerge. nt. J. Food Microbiol. 139, S3–S15.

Nguyen, Q. T., Baird, D. G. (2006). Preparation of polymer–clay nanocomposites and their properties. Adv. Polym. Technol. 25(4), 270–285.

Okada, A., Fukushima, Y., Kawasumi, M., Inagaki, S., Usuki, A., Sugiyama, S. Kurauchi, T., Kamigatio, O. (1987). Composite material and its preparation. US Patent 4739007.

Otani Y., Tabata Y. I. Y. (1996). Rapidly curable biological glue composed of gelatin and poly(L-glutamic acid). Biomaterials, 17(14), 1387–1391.

Ouasti, S., Kingham, P. J., Terenghi, G., Tirelli, N. (2012). The CD44/integrins interplay and the significance of receptor binding and representation in the uptake of RGD-functionalized hyaluronic acid. Biomaterials, 33(4), 1120–1134.

Packer, L., Ed. (1990).Antioxidant activity of retionoids.Academic Press: San Diego, CA, Vol 190.

Panek, G., Schleidt, S., Mao, Q., Wolkenhauer, M., Spiess, H. W., Jeschke, G. (2006). Heterogeneity of the surfactant layer in organically modified silicates and polymer/layered silicate composites. Macromolecules, 39, 2191–2200.

Patel, H. (2003). Use of choline derivatives for memory, learning and cognition-WO Pat. 2005018631 A1.

Paul, D. R., Robeson, L. M. (2008). Polymer nanotechnology: Nanocomposites. Polymer, 49(15), 3187–3204.

Pavlidou, S., Papaspyrides, C. D. (2008). A review on polymer–layered silicate nanocomposites. Prog. Polym. Sci. 33(12), 1119–1198.

Peer, D., Karp, J. M., Hong, S., Farokhzad, O. C., Margalit, R. Langer, R. (2007). Nanocarriers as an emerging platform for cancer therapy. Nat. Nanotechnol. 2(12), 751–760.

Pérez-Camero, G., Congregado, F., Bou, J. J., Muñoz-Guerra, S. (1999). Biosynthesis and ultrasonic degradation of bacterial poly(γ-glutamic acid). Biotechnol. Bioeng. 63(1), 110–115.

Pérez-Camero, G., García-Álvarez, M., Martínez de Ilarduya, A., Fernández, C., Campos, L., Muñoz-Guerra, S. (2004). Comblike complexes of bacterial poly(γ,D-glutamic acid) and cationic surfactants. Biomacromolecules, 5(1), 144–152.

Plechkova, N. V., Seddon, K. R. (2008). Applications of ionic liquids in the chemical industry. Chem. Soc. Rev., 37(1), 123–150.

Ponomarenko, E. A., Waddon, A. J., Tirrell, D. A., Macknight, W. J. (1996). Structure and properties of stoichiometric complexes formed by sodium poly (α,l -glutamate) and oppositely charged surfactants. Langmuir, 12(9), 2169–2172.

Portilla-Arias, J. A., García-Álvarez, M., Martínez de Ilarduya, A., Muñoz-Guerra, S. (2007a). Thermal decomposition of microbial poly(γ-glutamic acid) and poly(γ-glutamate)s. Polym. Degrad. Stab. 92(10), 1916–1924.

Portilla-Arias, J. A., García-Álvarez, M., Martínez de Ilarduya, A., Muñoz-Guerra, S. (2007b). Ionic complexes of biosynthetic poly(malic acid) and poly(glutamic acid) as prospective drug-delivery systems. Macromol. Biosci., 7(7), 897–906.

Racoviţă, Ş., Vasiliu, S., Popa, M., Luca, C. (2009). Polysaccharides based on micro- and nanoparticles obtained by ionic gelation and their applications as drug delivery systems. Rev. Roum. Chim. 54(9), 709–718.

Rädler, J. O., Koltover, I., Salditt, T., Safinya, C. R. (1997). Structure of DNA-cationic liposome complexes: DNA intercalation in multilamellar membranes in distinct interhelical packing regimes. Science, 275(5301), 810–814.

Rah, M. J. (2011). A review of hyaluronan and its ophthalmic applications. Optometry - J. Am. Optom. Assoc. 82(1), 38–43.

Ramnial, T., Ino, D. D., Clyburne, J. A. C. (2005). Phosphonium ionic liquids as reaction media for strong bases. Chem. Comm. (3), 325–327.

Read, A. D. (1972). The use of high molecular weight polyacrylamides in the selective flocculation separation of a mineral mixture. Br. Polym. J. 4(3), 253–264.

Richard, A., Margaritis, A. (2001). Poly(glutamic Acid) for biomedical applications. Crit. Rev. Biotechnol. 21(4), 219–232.

Ringsdorf, H., Schlarb, B., Venzmer, J. (1988). Molecular architecture and function of polymeric oriented systems: models for the study of organization, surface recognition, and dynamics of biomembranes. Angew. Chemie Int. Ed. English. 27(1), 113–158.

Rodriguez, E., Seguer, J., Rocabayera, X., Manresa, A. (2004). Cellular effects of monohydrochloride of L-arginine, N-alpha-lauroyl ethylester (LAE) on exposure to *Salmonella typhimurium* and *S. aureus*. J. Appl. Microbiol. 96(5), 903–912.

Ruckman, S. A., Rocabayera, X., Borzelleca, J. F., Sandusky, C. B. (2004). Toxicological and metabolic investigations of the safety of N-alpha-lauroyl-L-arginine ethyl ester monohydrochloride (LAE). Food Chem. Toxicol. 42(2), 245–59.

Ruokolainen, J., Brinke, G. Ten, Ikkala, O. (1999). Supramolecular Polymeric Materials with Hierarchical Structure-Within-Structure Morphologies. Adv. Mater. 11(9), 777–780.

Saitoh, H., Kobayashi, M., Sugawara, M., Iseki, K., Miyazaki, K. (1992). Carrier-mediated transport system for choline and its related quaternary ammonium compounds on rat intestinal brush-border membrane. Biochim. Biophys. Acta Biomembr. 1112(1), 153–160.

Salajkov´a, M., Berglund, L. A., Zhou, Q. (2012). Hydrophobic cellulose nanocrystals modified with quaternary ammonium salts. J. Mater. Chem., 22, 19798-19805.

Sanda, F., Fujiyama, T., Endo, T. (2001). Chemical synthesis of poly-γ-glutamic acid by polycondensation of γ-glutamic acid dimer: Synthesis and reaction of poly- γ-glutamic acid methyl ester. J. Polym. Sci. Part A: Polym. Chem. 39(5), 732–741.

Santos, M. R. E., Fonseca, A. C., Mendonça, P. V., Branco, R., Serra, A. C., Morais, P. V., Coelho, J. F. J. (2016). Recent developments in antimicrobial polymers: a review. Materials, 9(7), 599–632.

Schiller, J.; Fuchs, B.; Arnhold, J.; Arnold, K. (2003) Contribution of reactive oxygen species to cartilage degradation in rheumatic dis- eases: molecular pathways, diagnosis and potential therapeutic strategies. Curr. Med. Chem.10, 2123-45.

Schneider, R., Timms, A. R. (1957). Some aspects of the pharmacology of an homologous series of choline esters of fatty acids J. Pharmacol. Chemother. 12(1), 30–8.

Shafiee S, T. E. (2009). When will fossil fuel reserves be diminished? Energy Policy, 37(1), 181–189.

Shah, D., Mccarthy, S., Gross, R. (1992). New polymers derived from gamma-poly(glutamic acid). Am. Chem. Soc. 204, 249-255.

Shah, D. T., McCarthy, S. P., Gross, R. A. (1995). γ-poly(glutamic acid) esters. Pat. Number US5378807-A.

Shih, I. L., Van, Y.T. (2001). The production of poly-(gamma-glutamic acid) from microorganisms and its various applications. Bioresour Technol., 79, 207–225.

Shih, I. L., Van, Y. T., Yeh, L. C., Lin, H. G., Chang, Y. N. (2001). Production of a biopolymer flocculant from *Bacillus licheniformis* and its flocculation properties. Bioresour. Technol. 78(3), 267–272.

Shih, I. L., Van, Y.T., Sau, Y.Y. (2003). Antifreeze activities of poly(γ-glutamic acid) produced by *Bacillus licheniformis*. Biotechnol. Biofuels. 25(20), 1709–1712.

Shu, X. Z., Liu, Y., Luo, Y., Roberts, M. C., Prestwich, G. D. (2002). Disulfide cross-linked hyaluronan hydrogels. Biomacromolecules, 3(6), 1304–1311.

Shu, X. Z., Liu, Y., Palumbo, F., Prestwich, G. D. (2003). Disulfide-crosslinked hyaluronan-gelatin hydrogel films: a covalent mimic of the extracellular matrix for in vitro cell growth. Biomaterials, 24(21), 3825–3834.

Sinha Ray, S., Okamoto, M. (2003). Polymer/layered silicate nanocomposites: a review from preparation to processing. Prog. Polym. Sci. 28(11), 1539–1641.

Sinha Ray, S., Bousmina, M. (2005). Biodegradable polymers and their layered silicate nanocomposites: In greening the 21st century materials world. Prog. Polym. Sci. Prog. Mater. Sci. 50(8), 962–1079.

Siracusa, V., Rocculi, P., Romani, S., Marco, D. (2008). Biodegradable polymers for food packaging: a review. Trends Food Sci. Technol. 19(12), 634–643.

Stern, R., Kogan, G., Jedrzejas, M. J., Šoltés, L. (2007). The many ways to cleave hyaluronan. Biotechnol. Adv. 25(6), 537–557.

Tanimoto, H., Sato, H., Karasawa, M., Iwasaki, K., Oshima, A. (1996). Feed composition containing poly-glutamic acid. Patent WO1996035339A1.

Teh, B. M., Shen, Y., Friedland, P. L., Atlas, M. D., Marano, R. J. (2012). A review on the use of hyaluronic acid in tympanic membrane wound healing. Expert Opin. Biol. Ther. 12(1), 23–36.

Thorne, C. B., Gómez, C. G., Noyes, H. E., Housewright, R. D. (1954). Production of glutamyl polypeptide by *Bacillus subtilis*. J. Bacteroil., 68(3), 307–315.

Thünemann, A. (2000). Polyethylenimine complexes with retinoic acid: structure, release profiles and nanoparticles. Am. Chem. Soc. 6878–6885.

Thünemann, A., Beyermann, J. (2000). Immobilization of retinoic acid by polyamino acids: lamellar-structured nanoparticles. Am. Chem. Soc. 850–857.

Thünemann, A., General, S. (2001). Nanoparticles of polyelectrolyte-fatty acid complex: carriers for Q10 and triiodothyronine. J. Control. Release, 75, 237–247.

Tischer, M., Pradel, G., Ohlsen, K., Holzgrabe, U. (2012). Quaternary ammonium salts and their antimicrobial potential: Targets or nonspecific interactions? Chem. Med. Chem. 7, 22-31.

Tjong, S. C. (2006). Structural and mechanical properties of polymer nanocomposites. Mater. Sci. Eng. R Reports. 53(3–4), 73–197.

Tokita, Y., Okamoto, A. (1995). Hydrolytic degradation of hyaluronic acid. Polym. Degrad. Stab. 48(2), 269–273.

Tolentino, A., Alla, A., Martínez de Ilarduya, A., Muñoz-Guerra, S. (2013). Comb-like ionic complexes of hyaluronic acid with alkyltrimethylammonium surfactants. Carbohydr. Polym. 92(1), 691–696.

Tolentino, A., León, S., Alla, A., Martínez de Ilarduya, A., Muñoz-Guerra, S. (2013). Comblike ionic complexes of poly(γ-glutamic acid) and alkanoylcholines derived from fatty acids. Macromolecules, 46(4), 1607–1617.

Tolentino, A., Alla, A., Martínez de Ilarduya, A., Muñoz-Guerra, S. (2014). Complexes of poly(glutamic acid) and long-chain alkanoylcholines: nanoparticle formation and drug release. Int. J. Biol. Macromol. 66, 346–353.

Toole, B. P., Wight, T. N., Tammi, M. I. (2002). Hyaluronan-cell interactions in cancer and vascular disease. J. Biol. Chem. 277(7), 4593–4596.

Toole, B. P. (2004). Hyaluronan: from extracellular glue to pericellular cue. Nat. Rev. Cancer. 4(7), 528–539.

Troy, F. A. (1973). Chemistry and biosynthesis of the poly(glutamyl) capsule in bacillus licheniformis I. Properties of the membrane-mediated biosynthetic reactionquot; J. Biol. Chem. 248(1), 305–316.

Ujiie, S.; IImura, K. (1990). Ammonium halide type thermotropic liquid-crystallines polyethylenimines and those low-mass model compounds. Chem. Lett., 19(6), 995-998.

Usuki, A., Kawasumi, M., Kojima, Y., Okada, A., Kurauchi, T., Kamigaito, O. (1993). Swelling behavior of montmorillonite cation exchanged for ω-amino acids by caprolactam. J. Mater. Res. 8(5), 1174–1178.

Vaia, R. A., Ishii, H., Giannelis, E. P. (1993). Synthesis and properties of two-dimensional nanostructures by direct intercalation of polymer melts in layered silicates. Chem. Mater. 5(12), 1694–1696.

Vaia, R. A., Teukolsky, R. K., Giannelis, E. P. (1994). Interlayer structure and molecular environment of alkylammonium layered silicates. Chem. Mater. 6(7), 1017–1022.

Volpi, N., Schiller, J., Stern, R., Soltés, L. (2009). Role, metabolism, chemical modifications and applications of hyaluronan. Curr. Med. Chem. 16(0), 1718–1745.

Wagner, V., Dullaart, A., Bock, A. K., Zweck, A. (2006). The emerging nanomedicine landscape. Nat. Biotechnol. 24(10), 1211–1217.

Walls, H. J., Riley, M. W., Singhal, R. R., Spontak, R. J., Fedkiw, P. S., Khan, S. A. (2003). Nanocomposite electrolytes with fumed silica and hectorite clay networks: passive versus active Fillers. Adv. Funct. Mater. 13(9), 710–717.

Wang, H.Y., Zhang, J.X., Cao, D.D., Zhao, G. (2013). Enantioselective addition of thiols to imines catalyzed by thiourea–quaternary ammonium salts. ACS Catal. 3, 2218-2221.

Watson, M. K., Tezel, U., Pavlostathis, S. G. (2012). Biotransformation of alkanoylcholines under methanogenic conditions. Water Res. 46(9), 2947–2956.

Whitesides, G. M., Mathias, J. P., Seto, C. T. (1991). Molecular self-assembly and nanochemistry: a chemical strategy for the synthesis of nanostructures. Science, 254(5036), 1312–1319.

Xie, W., Xie, R., Pan, W. P., Hunter, D., Koene, B., Tan, L. S., Vaia, R. (2002). Thermal stability of quaternary phosphonium modified montmorillonites. Chem. Mater. (11), 4837–4845.

Yamanobe, T., Tsukahara, M., Komoto, T., Watanabe, J., Ando, I., Uematsu, I. Imanari, M. (1988). Conformation and dynamic aspects of poly(gamma.-n-octadecyl L-glutamate) in the solid state and liquid-crystalline state as studied by variable-temperature carbon-^{13} CP/MAS NMR spectroscopy. Macromolecules, 21(1), 48–50.

Ye, X., Jin, L., Caglayan, H., Chen, J., Xing, G., Zheng, C., Doan-Nguyen, V., Kang, Y., Engheta, N., Kagan, C. R. (2012). Improved size-tunable synthesis of monodisperse gold nanorods through the use of aromatic additives. ACS Nano, 6, 2804-2817.

Yoon, S. H., Hwan Do, J., Yup Lee, S., Nam Chang, H. (2000). Production of poly-γ-glutamic acid by fed-batch culture of Bacillus licheniformis. Biotechnol. Lett. 22(7), 585–588.

Zanetti, M., Lomakin, S., Camino, G. (2000). Polymer layered silicate nanocomposites. Macromol. Mater. Eng. 279(1), 1–9.

Zhang, R., Ni, Q. Q., Natsuki, T., Iwamoto, M. (2007). Mechanical properties of composites filled with SMA particles and short fibers. Compos. Struct. 79(1), 90–96.

Zhou, S., Burger, C., Yeh, F., Chu, B. (1998). Charge density effect of polyelectrolyte chains on the nanostructures of polyelectrolyte−surfactant complexes. Macromolecules, 31(23), 8157-8163.

Zhu, L., Mahato, R. I. (2010). Lipid and polymeric carrier-mediated nucleic acid delivery. Expert Opin. Drug Deliv. 7(10), 1209–1226.

Chapter III. Methodology

1. Synthesis of surfactants

1.1. Phosphonium surfactants

The synthesis of the alkyltrimethylphosphonium surfactants (*n*ATMP·Br) was carried out as follows. 5 mL of a 1.0 M solution of trimethylphosphine (TMP) in toluene (5 mmol) was slowly added to 1-bromoalkane (5.5 mmol) preheated at 80 ºC and under a nitrogen atmosphere. The mixture was then heated in a silicone oil bath up to 116 ºC and maintained at that temperature under stirring for a period of 18 to 24 h depending on the value of *n*. The precipitate formed at the end of the reaction period was collected by filtration. In order to remove the excess of the bromoalkane, the precipitate was repeatedly washed with toluene and then dried under vacuum for 48 h. The *n*ATMP·Br salts were recovered as white powders in yields ranging between 70 and 90%. They all were soluble in a variety of organic solvents such as chloroform and methanol, and also in water at temperatures between 20 ºC and 60 ºC depending on the length of the alkyl chain. Synthesis data for these compounds are given in full detail in the supplementary information of chapter 4.

1.2. Choline surfactants

Choline iodide esters were synthetized by adding the *N,N*-dimethylamino-2-ethanol (DMAE) to a solution of the corresponding fatty acid chloride in chloroform (100 $g \cdot L^{-1}$) and placed in an ice-bath. After 2 h of stirring, the product was neutralized with aqueous $NaHCO_3$ and separated as oil through liquid-liquid extraction. Finally, the extracted product was quaternized with an excess of methyl iodide at room temperature. Upon standing overnight the resulting alkanoylcholine iodide (*n*ACh·I) was obtained as a white precipitate that could be easily separated by filtration and washed with acetone.

2. Preparation of polyelectrolyte-surfactant complexes

The complexes made from PGGA or HyA and different kind of cationic surfactants were prepared following the methodology initially reported by Ponomarenko *et al.* (Ponomarenko et al., 1996) for the synthesis of complexes made from charged poly(α-aminoacids) and ionic surfactants, and that was later applied by us for coupling either PGGA (Pérez-Camero et al., 2004; García-Álvarez et al., 2005) or polyuronic acids (Tolentino et al., 2011, 2013) with quaternary ammonium salts bearing long alkyl chains. In brief, an aqueous solution of the cationic salt was added dropwise to a

solution of Na·PGGA or Na·HyA in water under stirring at a temperature between 25 and 70 ºC depending on the surfactant water solubility. After several hours of standing a white precipitate appeared which was isolated by centrifugation, repeatedly washed with water, and finally dried under vacuum for at least 48 h. All complexes were collected as white to pale non-hygroscopic powders.

3. Design and characterization of nanocomposites

3.1. Polymer nanocomposites

Polymer complexes were prepared for two different lengths of the alkyl chain (*n* = 12 and 20). The nanoclay used was a sodium montmorillonite clay (Na·MMT) with a Cation Exchange Capacity (CEC) of 1.35% (meq·g^{-1}).

a) Modification of montmorillonite

300 mg of dried montmorillonite (Na·MMT) were placed into 30 mL of a water-ethanol mixture (4:1 v/v) and stirred overnight at room temperature to attain a fine dispersion. Then a 0.04 M solution of the *n*ATMP·Br in water-ethanol (4:1, v/v) was added to the dispersion to have a CEC:surfactant ratio of 1:1. After stirring for 24 h at 70 ºC, the mixture was filtered and the solid repeatedly washed with a hot solution of water-ethanol (1:1, v/v) until no bromide ion traces were detected in the filtrate upon addition of 0.1 M silver nitrate solution. The collected modified organoclay (^{P}MMT) was dried overnight at room temperature and then at 120 ºC for 24 h, and finally finely grounded in a mortar and stored in a desiccator.

b) Preparation of nanocomposites

The preparation of nanocomposites was carried out in two steps. Firstly, the *n*ATMP·PGGA complexes with *n* = 12 and 20, were synthetized by adding dropwise an aqueous solution of the corresponding *n*ATMP·Br salt to an aqueous solution of Na·PGGA Secondly, the nanocomposites were prepared by mixing a 5 g·L^{-1} dispersion of ^{P}MMT in chloroform with a 0.05 M solution of the complex in the same solvent. The mixture was stirred at room temperature until no sedimentation was detected upon standing. The suspension was then concentrated by partial evaporation of the solvent and casted to render consistent films of 12ATMP·PGGA·*X*%^{P}MMT and 20ATMP·PGGA·*X*%^{P}MMT composites with ^{P}MMT contents of 3, 10, 20, 30, 50, 70 and 90%.

4. Design and characterization of nanoparticles

*n*ATMP·HyA NPs and *n*ACh·HyA NPs were generated in aqueous media by ionotropic gelation avoiding the use of organic solvents (Figure 1). The procedure is essentially the same that is applied for the preparation of the complexes but in this case surfactant to HyA ratios of 1:4 and 1:2 were used. NPs were formed by nanoprecipitation upon addition dropwise of the *n*ATMP or *n*ACh solution to the HyA solution under stirring at a temperature between 25 and 70 ºC depending on the surfactant. After further stirring for 4 h, the mixture was dialyzed against water during 24 h and the clean NPs suspension was duly characterized.

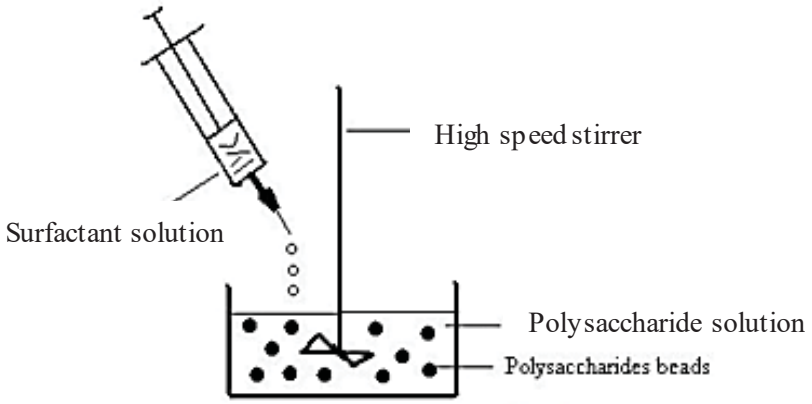

Figure 1. Schematic representation of preparation of complexes particles by applying the ionic gelation technique.

5. Measurements

5.1. Elemental analysis and spectroscopy

Elemental analyses were carried out at the Servei de Microanàlisi at IQAC (Barcelona). Tests were made in a Flash 1112 elemental microanalyser (A5) which was calibrated with appropriate standards of known composition. C, N and H contents were determined by the dynamic flash combustion method using He as carrier gas. Results were given in (w/w) percentages and in duplicates.

FTIR spectra were recorded within the 4000-600 cm^{-1} interval from powder samples on a FTIR Perkin Elmer Frontier spectrophotometer provided with a universal ATR sampling accessory for solid samples. ^{1}H and ^{13}C NMR spectra were recorded on a Bruker AMX-300 NMR instrument and using TMS as internal reference. The spectra were registered at 300.1 MHz for ^{1}H NMR and at 75.5 MHz for ^{13}C NMR MHz from samples dissolved in deuterated chloroform or deuterated methanol depending on their solubility.

5.2. Krafft temperature and critical micelle concentration (cmc)

Krafft temperatures (T_{Krafft}) were estimated visually. Samples were prepared as follows: 1% (w/w) mixtures of *n*ATMP·Br in water were heated until dissolution and then cooled down to room temperature and kept in a refrigerator at 5 ºC for 24 hours. The cooled samples were then introduced in a water bath provided with a magnetic stirring and heated up in steps of 1 ºC every 15 min. The temperature at which turbidity disappeared was taken as the approximate Krafft temperature. The *cmc* for *n* = 12, 14 and 16 were determined by ^{1}H NMR by following the evolution of the chemical shifts of specific signals of the surfactant with increasing concentration according to the procedure described in the literature (Lee 2014). Samples were dissolved in D_2O, and ^{1}H NMR spectra were recorded at the selected temperature using the sodium salt of the 3-(trimethylsilyl)-propanesulfonic acid as internal reference.

5.3. Thermal measurements

Thermogravimetric analyses were performed on a Mettler-Toledo TGA/DSC 1 Star System under a nitrogen flow of 20 mL·min^{-1} over the 30 to 600 ºC interval at a heating rate of 10 ºC·min^{-1} and using sample weights of 10-15 mg. Calorimetric measurements were performed with a Perkin-Elmer DSC 8000 instrument calibrated with indium and zinc. Sample weights of about 2-5 mg were subjected to heating-cooling cycles at a rate of 10 ºC·min^{-1} within the temperature range of 30 to 280 ºC for surfactants and -30 to 120 ºC for complexes under a nitrogen atmosphere.

5.4. Optical microscopy

Optical microscopy was carried out on an Olympus BX51 polarizing optical microscope equipped with a digital camera and a Linkam THMS-600 hot stage provided with a nitrogen gas circulating system to avoid contact with air and humidity. Samples for observation were prepared by casting 1-5% (w/v) chloroform or methanol solutions of the surfactants or complexes on a microscope square glass coverslip and the dried film covered with another slide.

5.5. X-ray diffraction

X-ray diffraction (XRD) using conventional light was performed in the “Centres Científics i Tecnològics de la Universitat de Barcelona” (CCiT). XRD patterns were registered at room temperature from powder samples, either coming directly from synthesis or previously heated at selected temperatures. The diffractometer used was a PANalytical X’Pert PRO MPD theta/theta with Cu(K_α) radiation (λ = 0.15418 nm). The reflections collected were those appearing in the 1º ≤ θ ≤ 15º range.

Real time X-ray diffraction studies were carried out using X-ray synchrotron radiation at the BL11 beamline (Non-Crystalline Diffraction (NCD), at ALBA (Cerdanyola del Vallès, Barcelona, Spain). Both SAXS and WAXS were taken simultaneously from powder samples subjected to heating-cooling cycles at rates of 10 or 0.5 ºC·min^{-1}. The energy employed corresponded to a 0.10 nm wavelength, and spectra were calibrated with silver behenate (AgBh) and Cr_2O_3 for SAXS and WAXS, respectively.

5.6. Single-crystal analysis

The 12ATMP·Br surfactant was subjected to structural analysis using a monocrystal that was grown by the vapor-diffusion technique at 20 ºC. The applied procedure was as follows: A solution of the surfactant (0.5 mg·mL^{-1}) in $CHCl_3$:EtOAc (90:10) was prepared and distributed in a multi-well plate, which was then placed in a closed chamber and left to evaporate under a EtOAc saturated atmosphere. After several days a unique large monocrystal of 0.45 x 0.14 x 0.10 mm dimensions suitable for XRD analysis was formed. The selected crystal was mounted on a D8 Venture diffractometer provided with a multilayer monochromator Mo-K_α radiation (λ = 0.071073 nm), and the generated scattering was collected with an area detector Photon 100 CMOS. Unit cell parameters were determined from 7111 reflections within the θ range of 2.23° to 25.14°. Intensities of 25,175 reflections collected within the 2.23°-25.39° angular range were measured. The structure was solved by direct methods and refined by least-squared method (SHELXL-97 program) (Sheldrick, 2008). A detailed description of the methodology used for the structure analysis is given in the ESI file attached to this paper.

5.7. Mechanical properties

Mechanical properties were measured at 25 ºC and at a stretching rate of 10 m·min^{-1} on a Zwick 2.5/TN1S testing machine. The young modulus (E), maximum tensile stress (σ_{max}), and the strain at break were determined for each sample in triplicate.

5.8. Films preparation

Films preparation was carried out by casting a solution of the desired complex in chloroform or methanol on 3x3 cm^2 Petri plates. After drying at room temperature, films were cut as either 1x1 cm^2 squares or discs with 5 mm diameter and further dried under vacuum for 24 h. Film thickness were estimated to be 115 ± 10 µm as measured by a Mitutoyo micrometer (Osaka, Japan).

5.9. Hydrolytic degradation and release of surfactant from complexes

For degradation studies of *n*ATMP·HyA and *n*ACh·HyA complexes, discs of selected complexes were placed in vials to which 5 mL of the corresponding buffer solution were added. In the case *n*ATMP·HyA complexes the used buffers were of Phosphate buffer pH= 7.4 either with or without enzymes added and acid phosphate buffer at pH= 5.5. Whereas for *n*ACh·HyA complexes only physiological conditions (pH=7.4, 37 ºC) with or without enzymes were selected as incubation mediums. Sealed vials were stored at 37 ºC in a heat chamber and discs were taken out at scheduled times, washed with distilled water, dried under vacuum at room temperature, and finally weighted. Chemical modifications involved in degradation were followed by NMR (for *n*ATMP·HyA complexes) or FTIR (*n*ACh·HyA complexes) analysis.

For specific measuring of the release of cationic surfactants from complexes, complexes were incubated in aqueous medium. Discs were placed into cellulose membrane tubes (2000 Da cut-off) and introduced in a vial containing 10 mL of buffer solution for a determine amount of time under gentle stirring. Assays were carried out at pH= 7.4 and 5.5 at 25 ºC, and in some cases also at pH= 7.4 at 4 ºC and 37 ºC. The amount of released surfactant was determined by measuring the absorbance of the dialysate at 208 nm (for *n*ATMP complexes) or 220 nm (for LAE complexes) at scheduled times.

5.10. Antimicrobial activity

Antimicrobial activity of complexes made of *n*ATMP·Br surfactants (*n*ATMP·PGGA and *n*ATMP·HyA films) and LAE surfactant (LAE·PGGA and LAE·HyA) was tested in vivo using different microorganisms. Bacteria for this study were selected for their widespread occurrence and well-known ability to cause food-borne diseases by uncontrolled ingestion (Newell et al., 2010). Cultures of *E. coli* NCTC 9001 isolated from human urine cystitis, *S. enterica* CECT 4594 from septicemic liver from bovine*, L. monocytogenes* ATCC 19115 from human, and *S. aureus* ATCC 6538 isolated from human lesion were obtained from the National Collection of Type Cultures (NCTC, Public Health England, UK), the Spanish Type Culture Collection (CECT, Valencia, Spain), and the American Type Culture Collection (ATCC, USA), respectively. In addition the common yeast *Candida albicans* CECT 1392 have been used in some studies.

The organisms were stored at -20 ºC in tryptic soy broth (TSB; Merck, Darmstadt, Germany) containing 50 % (v/v) glycerol until needed. To activate them a *loopful* of each bacterium was streaked on tryptic soy agar (TSA) petri dishes and incubated for 24 h at 37 ºC and then transferred to a TSB (Triptic Soy Broth) medium where they

were left to grow for 18 h at 37 ºC to assess their exponential growth. Cultures were then diluted to obtain the desired concentration. *C albicans* cells were left to grow for 18 h at 30 ºC in Potato Dextrose Broth (PDB) medium. Cultures were then diluted to obtain the desired concentration.

The antimicrobial activity of all complexes was determined in liquid culture media. Polymer specimens (1x1 cm^2 squares films) were immersed in 10 mL of TSB (PDB for *C. albicans*) containing 100 μL of each microorganism for incubation at selected temperature (37 or 22 ºC) during 24 h – 7 days depending on the complex of study. For quantification, 100 μL aliquots were removed from the suspension at scheduled times, diluted with peptone buffer solution and plated in triplicate in Petri dishes in a TSA (or PDA for *C. albicans*) culture medium. Colonies were counted after incubation at 37 °C for 24 h in triplicate. Controls without films (blank) and with unmodified PGGA or HyA films (negative controls, NC) were also tested and experiments were performed in triplicates. All the films were sterilized before using by UV light for 15 minutes. Data are represented as colony forming units per mL (CFU/mL) or logarithm of colony forming units (LogCFU). Formula for logarithm reduction value (LRV) and percentage reduction calculations are shown below (Durán et al., 2007),

$$\text{Log reduction value} = \log_{10}(A/B) \qquad \text{Percentage reduction} = [(A-B)/A]\cdot 100$$

where *A* is the number of viable bacteria in the negative control and *B* is the number of viable bacteria after treatment with the selected ionic complexes.

The antimicrobial activity on solid media of *n*ATMP·HyA films was also tested using the agar diffusion method which consists of spreading 100 μL of microorganism solution over a prepared TSA or TSB (for *C. albicans*) surface and placing the 5 mm-diameter film disk at the center of a petri dish. Plates were incubated at 37 ºC for 24 h and the diameter of the resulting inhibition zone was measured directly after the incubation period. HyA was used as negative control and all measurements were made in triplicate.

To study the effect of pH and or temperature in the antimicrobial activity of *n*ATMP·PGGA and *n*ATMP·HyA films, the growth curve of each microorganism was studied alone and in the presence of compounds released from the complexes upon incubation. Colony counting was made by photometric measurement using a Tecan's Magellan™ instrument. Firstly, each film was immersed in tubes containing 10 mL of TSB (or PDB for *C. albicans*) at pH 7.4 at 22 ºC (also 4 and 37 ºC for *n*ATMP·HyA films) or pH 5.5 at 22 ºC for 24 h. Then 200 and 100 μL (for *n*ATMP·PGGA and *n*ATMP·HyA films, respectively) of the supernatant liquid was transferred to ELISA

plates containing 2 and 100 µL (for *n*ATMP·PGGA and *n*ATMP·HyA films) of *S. aureus or E. coli* and incubated at 37 °C for 24 h under agitation. Measurements were made in triplicate at λ = 490 nm at regular periods over the whole incubation period.

For quantification the antimicrobial activity of *n*ATMP·HyA NPs, 40 µL of NPs were added to a well containing 160 µL of each microorganism and incubated for 24 h at 37 ºC. After that time, the optical density was measured at 450 nm and serial dilutions were realized to quantify by spreading on TSA or PDB petri dishes. The antimicrobial activity of *n*ATMP·HyA NPs was calculated using the following equation:

$$\text{Antimicrobial activity} = \frac{CFU\,(HyA) - CFU\,(NPs)}{CFU\,(HyA)} \cdot 100$$

where *CFU* is the Colony Forming Units counted for the three assayed microorganisms in the presence of pristine HyA (CFU (HyA), negative control) and in the presence of nATMP·HyA NPs (CFU (NPs)).

5.11. Dynamic light scattering and ζ-potential

Dynamic light scattering (DLS) for particle hydrodynamic size was performed with PSS NICOMP™ (particle sizing system, Inc. Santa Barbara, Calif., USA) and displayed values were the average of three readings. ζ-potential measurements were performed with a ZetaSizer NS (Malvern Instruments, UK) with particles suspended in deionized water and displayed values were the average of twelve readings.

5.12. Transmission electron microscopy

For TEM observation nanocomposite samples in form of films were sectioned either at room temperature (utramicrotom LEICA EM FDC7) or at -80 ºC). Ultrathin sections either unstained or stained with uranyl acetate were examined with a Tecnai F20 (200 kV) or Zeiss Libra 120 electron microscope instruments.

The nanostructure morphology of *n*ATMP·HyA and *n*ACh·HyA complexes was visualized using a Philips TECNAI 10 and Tecnai F20 transmission electron microscopes operating at 100 kV and 200 kV, respectively. Specimens were prepared by casting a solution of *n*ATMP·HyA or *n*ACh·HyA complexes in MeOH:BuOH (4:1) over a water surface. Pieces of the floating film were picked up with carbon coated grids and stained with phosphotungstic acid (PTA) previous to observation.

The structure of nanoparticle samples of both *n*ATMP·HyA and *n*ACh·HyA complexes was study using a Tecnai F20 electron microscope operating at 200 kV. For NPs visualization, drops of the suspensions were placed onto carbon coated grids and the adhered material washed with water and stained as before.

5.13. Cell viability

The cytotoxicity of *n*ACh·HyA NPs was studied *in vitro* on raw 264.7 cell line, which is one of the best-characterized mouse monocyte macrophages, using a nanoparticle concentration of 75 $\mu g \cdot mL^{-1}$ with 100.000 cells per well. Cells were incubated for 4 h and 24 h periods at 37 ºC, 5% CO_2 in cell culture medium (RPMI as cell culture media, 10% Fetal Bovine Serum (FBS), 1% of Penicillin Streptomycin (Pen Strep)) after which the number of cells alive was counted.

6. References

Durán, N., Marcato, P. D., De Souza, G. I. H., Alves, O. L., Esposito, E. (2007). Antibacterial effect of silver nanoparticles produced by fungal process on textile fabrics and their effluent treatment. J. Biomed. Nanotechnol. 3(2), 203–208.

Gamarra, A., Martínez de Ilarduya, A., Vives, M., Morató, J., Muñoz-Guerra, S. (2017). Ionic complexes of poly(γ-glutamic acid) with alkyltrimethylphosphonium surfactants. Polymer, 116, 43–54.

García-Álvarez, M., Álvarez, J., Alla, A., Martínez de Ilarduya, A., Herranz, C., Muñoz-Guerra, S. (2005). Comb-like ionic complexes of cationic surfactants with bacterial poly(γ-glutamic acid) of racemic composition. Macromol. Biosci. 5(1), 30–38.

Lee, Y. S., Woo, K. W. (1995). Micellization of aqueous cationic surfactant solutions at the micellar structure transition concentration-based upon the concept of the pseudophase separation. J. Colloid Interface Sci. 169 (1), 34–38.

Newell, D. G., Koopmans, M., Verhoef, L., Duizer, E., Aidara-Kane, A., Sprong, H., Kruse, H. (2010). Food-borne diseases-The challenges of 20 years ago still persist while new ones continue to emerge. Int. J. Food Microbiol. 139, S3–S15.

Pérez-Camero, G., García-Álvarez, M., Martínez de Ilarduya, A., Fernández, C., Campos, L., Muñoz-Guerra, S. (2004). Comblike complexes of bacterial poly(γ,D-glutamic acid) and cationic surfactants. Biomacromolecules, 5(1), 144–152.

Ponomarenko, E. A., Waddon, A. J., Tirrell, D. A., Macknight, W. J. (1996). Structure and properties of stoichiometric complexes formed by sodium poly (α,l-glutamate) and oppositely charged surfactants. Langmuir, 12(9), 2169–2172.

Sheldrick, G. M. (2008). A short history of SHELX. Acta Crystallogr. Sect. A, A64(Pt 1), 112–122.

Tolentino, A., Alla, A., Martinez de Ilarduya, A., Font-Bardia, M., Leon, S., Munoz-Guerra, S. (2014). Thermal behavior of long-chain alkanoylcholine soaps. Rsc Adv. 4, 10738–10750.

Chapter IV. Alkyltrimethylphosphonium surfactants

Abstract

Quaternary organophosphonium salts bearing long alkyl chains are cationic surfactants of interest for their physical and biological properties. In the present work, the crystal structure and thermotropic behavior of the homologous series of alkyltrimethylphosphonium bromides (*n*ATMP·Br), with the alkyl chain containing *n* even numbers of carbon atoms from 12 to 22, has been examined within the 0-300 ºC range of temperatures. These compounds showed to be resistant to heat up to above ~390 ºC. The phases adopted at different temperatures were detected by DSC, and the structural changes involved in the phase transitions have been characterized by simultaneous WAXS and SAXS carried out in real-time and by polarizing optical microscopy as well. Three or four phases were identified for *n* =12 and 14 or *n*≥ 16 respectively, in agreement with the heat exchange peaks observed by DSC. The phase existing at room temperature (Ph-I) was found to be fully crystalline and its crystal lattice was determined by single-crystal X-ray diffraction methods. Ph-II consisted of a semicrystalline structure that can be categorized as a Smectic-B phase with the crystallized ionic pairs hexagonally arranged in layers and the molten alkyl confined in the interlayer space. Ph-II of 12ATMAP·Br and 14ATMP·Br directly isotropicized upon heating at ~220 ºC whereas for *n* ≥ 16 it converted into a Smectic-A phase (Ph-III) that needed to be heated above 240 ºC to become isotropic (Ph-Is). The correlation existing between thermal behavior, phase structure and length of the alkyl side chain has been demonstrated.

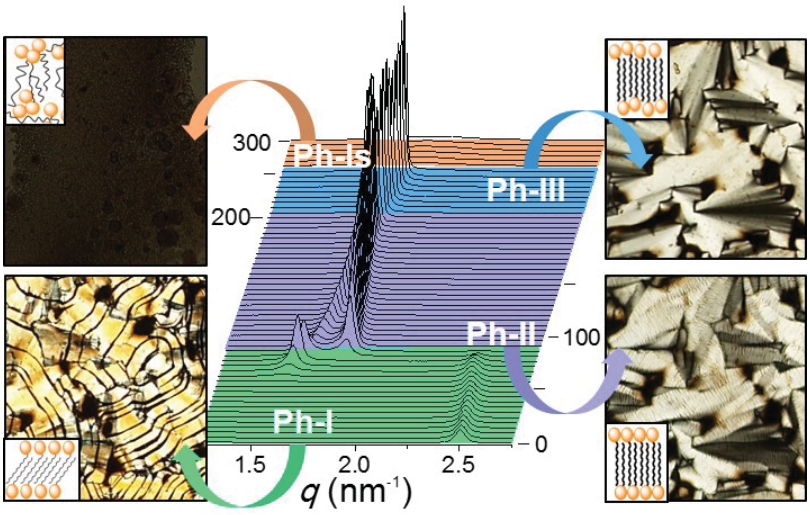

Publication derived from this work:

Gamarra, A., Urpí, L., Martínez de Ilarduya, A., Muñoz-Guerra, S. (2017). Crystalline structure and thermotropic behavior of alkyltrimethylphosphonium amphiphiles. Phys. Chem. Chem. Phys., 19, 4370–4382.

Supporting Information (SI) to this chapter in Annex A

1.1. Introduction

Tetraalkylphosphonium salts bearing long alkyl chains constitute a family of cationic amphiphiles comparable to the widely known tetraalkylammonium family but that offers superior properties in some aspects. Quaternary organophosphonium compounds are particularly attractive as ionic liquids because they display high thermal stability (Xie et al., 2002) and may be designed with a wide diversity of structures, some of them being able to melt at sub-ambient temperatures (Fraser et al., 2009). Their applications as solvents (McNulty et al., 2002; Gerritsma et al., 2004; Ito et al., 2004), phase transfer catalysts (Ramnial et al., 2005), or exfoliation agents for nanoclays (Panek et al., 2006; Byrne et al., 2007; Hedley et al., 2007), among others have been recently explored for some of these compounds. They are also interesting as building blocks in the design of antimicrobial materials since it has been proved that they are less cytotoxic than organoammonium compounds (Cieniecka-Rosłonkiewicz et al., 2005; Kumar et al., 2009). Nevertheless the research carried out to date on organophosphonium salts, an in particular on tetraalkylphosphonium ones, is much less extensive than on their ammonium analogues so that the knowledge currently available on their structure and properties is relatively limited (Binnemans, 2005). Such comparative backwardness is mainly due to the synthesis difficulties associated to phosphorous chemistry as well as to the restricted availability of the trialkylphosphines that are commonly used as starting materials.

The ability of tetraalkylammonium surfactants to form thermotropic mesophases is a well-known fact that has been investigated for a good number of systems (Axenov et al., 2011). These compounds usually adopt an amphiphilic arrangement with the ammonium-halide ionic pairs aligned in layers and the hydrophobic alkyl chains in a more or less extended conformation filling the interlayer spacing (Kamitori et al., 1997). Tetraalkylphosphonium surfactants are able to take up similar arrangements but covering broader domains of temperatures and displaying higher clearing points (Kanazawa et al., 1997). Fortunately, the characterization of the high-temperature phases found in phosphonium surfactants is feasible thanks to the good thermal stability displayed by these systems. Nevertheless, the literature dealing with the structure and thermal behavior of phosphonium-based surfactants is scarce, a meager situation that is evidenced when compared with the vast amount of information that has been amassed on commercialized surfactants based on tetraalkylammonium salts. To the best of our knowledge, the few studies carried out to date on phosphonium-based surfactants only concern salts bearing three long alkyl chains (Abdallah et al., 2000; Adamová et al., 2011) whereas no study has been addressed to examine the basic

properties of those containing only one long alkyl chain except that of Kanazawa et al. which was devoted to evaluate the antimicrobial properties of the chloride salts of some of these compounds (Kanazawa et al., 1994).

In this paper we wish to report on a series of alkyltrimethylphosphonium surfactants, abbreviated as *n*ATMP·Br (Scheme 1) with the alkyl chain being linear and containing an even number of carbon atoms (*n*) ranging from 12 to 22. The primary purpose of the work is to provide physicochemical knowledge on the structure and properties of this family of surfactants of potential interest for novel applications, in particular for the synthesis of surfactant-polymer complexes. Recently, comb-like complexes generated by ionic coupling of naturally-occurring polyelectrolytes with ionic surfactants are receiving exceptional attention (Antonietti et al., 1994). Thus complexes made of bacterially produced poly(γ-glutamic) acid or certain polyuronic acids and alkyltrimethylammonium soaps have been prepared and demonstrated to be useful for drug encapsulation and also as compatibilizers for bionanocomposites (Pérez-Camero et al., 2004; Tolentino et al., 2011, 2012, 2013, 2014). For the development of new complexes based on alkytrimethylphosphonium surfactants, the structure of these compounds should be determined and their basic properties properly evaluated. This paper includes the synthesis of the *n*ATMP·Br series, the characterization of their thermal transitions, and the structural analysis of the thermotropic phases that they are able to adopt as a function of temperature.

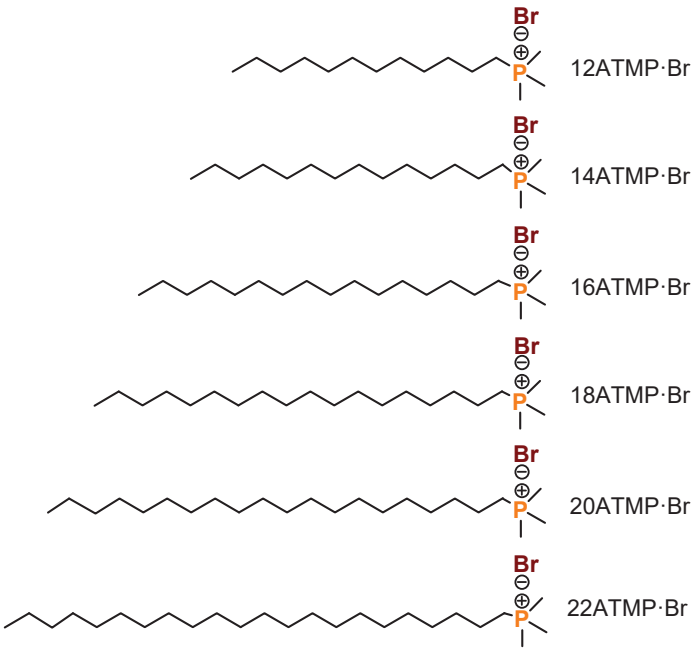

Scheme 1. Chemical formulae of *n*ATMP·Br surfactants.

1.2. Results and discussion

1.2.1. Synthesis and characterization of *n*ATMP·Br

The alkyltrimethylphosphonium bromides (*n*ATMP·Br) studied in this work were synthesized by nucleophilic reaction of trimethylphosphine onto the corresponding alkyl bromide at properly adjusted times and temperatures. Specific conditions used for reaction and yields obtained thence for every *n*ATMP·Br are detailed in Table 1. The elemental composition in carbon and hydrogen of *n*ATMP·Br was checked by combustion analysis and their chemical constitution was ascertained by both FT-IR and NMR spectroscopy. Infrared spectra showed bands at ~990 and ~715 cm^{-1} indicative of the presence of the trimethylphosphonium group (Beg et al., 1968; Witschard et al., 1963), as well as others at ~2900-2850 and ~1470 cm^{-1} arising from the C-H and C-C stretching vibrations whose absorbance decreased as the length of the long alkyl chain increased. ^{1}H and ^{13}C NMR spectra were in full agreement with the structure expected for the *n*ATMP·Br with all the observed signals being properly assigned regarding both chemical shifts and intensities. The whole collection of spectra registered from the *n*ATMP·Br series are reproduced in the SI file.

Table 1. Synthesis data of *n*ATMP·Br surfactants.

n	*t* (h)	*T* (ºC)	Yield (%)	Elemental analysis[a]		T_{Krafft}[b] (ºC)	*cmc*[c] ($mM \cdot L^{-1}$)
				C (%)	H (%)		
12	16	116	70	55.53 (55.53)	10.50 (10.59)	<0	9.9
14	17	116	80	58.03 (57.92)	10.79 (10.90)	<0	2.7
16	18	116	85	60.06 (59.96)	11.00 (11.16)	15	0.65
18	20	116	70	61.56 (61.73)	11.22 (11.38)	30	n.d
20	22	116	80	63.12 (63.26)	11.37 (11.58)	45	n.d
22	24	116	70	64.70 (64.61)	11.65 (11.75)	55	n.d

[a]In parenthesis, calculated values for the expected compositions. [b]Visually estimated for a 1% (w/w) concentration. [c]Measured by ^{1}H NMR at 25 ºC.

As expected, the solubility and aggregation properties of the *n*ATMP·Br series are depending on *n*. The Krafft temperatures (T_{Krafft}) and the critical micellar concentrations (*cmc*) of the surfactants are listed in Table 1. The T_{Krafft} of the phosphonium surfactants are lower than those displayed by their ammonium analogs (Davey et al., 1998) with values falling below zero for *n* = 12 and 14. The *cmc* were measured by NMR for those members displaying T_{Krafft} below room temperature, *i.e.* for *n* = 12, 14 and 16. As expected and according to what is observed in other ionic surfactant series, the *cmc*

decreased exponentially as the length of the alkyl chain increased. It is remarkable that the values observed for this series are noticeably lower than those reported for the alkyltrimethylammonium series (Lee et al., 1995). A detailed account of *cmc* determination carried out by the NMR method is given in the SI file.

1.2.2. Thermal stability

The TGA traces recorded from *n*ATMP·Br surfactants under an inert atmosphere are depicted in Figure 1, and the most relevant thermal decomposition parameters measured either directly on these traces or from their derivative curves (SI file) are listed in Table 2.

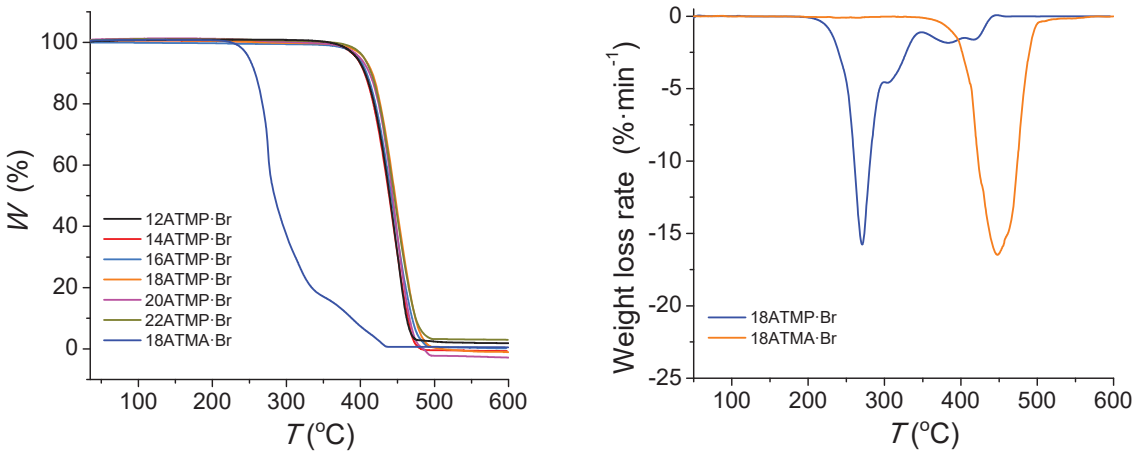

Figure 1. Left: TGA traces of the *n*ATMP·Br series recorded under a nitrogen atmosphere.The trace produced by octadecyltrimethylammonium bromide (18ATMA·Br) is included for comparison. Right: Compared derivative traces of 18ATMP·Br and 18ATMA·Br.

Decomposition temperatures corresponding to a 5% loss of the initial weight ($^{\circ}T_d$) were above 390 ºC, and maximum decomposition rate temperatures were observed in the 440-445 ºC range with a slight trend towards higher values as the length of the alkyl chain increased. Only one peak is displayed in the derivative plots indicating that decomposition takes place cleanly in one single step with almost negligible residual weight. This behavior contrasts with the thermal decomposition reported for octadecyltrimethylammonium bromide (18ATMA·Br), which displays a $^{\circ}T_d$ below 200 ºC and decomposes through a complex mechanism whose main step takes place at temperatures below 300 ºC (Sheldrick, 2007). The trace of this compound has been included in Figure 1 for comparison and the complete collection of traces of the nATMA·Br series is included in the SI file. It is precisely the great thermal stability displayed by the *n*ATMP·Br surfactants that makes them particularly appealing for their use as clay modifiers in the design of nanocomposites with high resistance to heat (Patel et al., 2007). An isothermal assay carried out with 18ATMP·Br revealed that this

compound lost less than 2% of its original weight after heating at 280 ºC for three days under an inert atmosphere (SI).

1.2.3. Thermal transitions

The DSC analysis on *n*ATMP·Br was aimed at bringing out the occurrence of thermal transitions, and it consisted of recording three heating-cooling cycles over the -30 to 300 ºC range for each surfactant. The recorded DSC traces are depicted in Figure 2, and temperatures and enthalpies associated to the heat exchanges observed on the traces are listed in Table 2.

Table 2. Thermal properties of *n*ATMP·Br surfactants.

	TGA[a]			DSC[b]								
				1st Heating			Cooling			2nd Heating		
n	$^{o}T_d$ (ºC)	$^{max}T_d$ (ºC)	*W* (%)	I/II	II/III	III/Is	II/I	III/II	Is/III	I/II	II/III	III/Is
12	395	443	~1	66 (39.0)	← 215 → (12.1)		40 (-14.0)	← 212 → (-11.5)		59 (20.6)	← 214 → (11.5)	
14	395	443	~0	75 (44.7)	← 225 → (11.3)		59 (-13.2)	← 218 → (-11.4)		73 (21.2)	← 225 → (10.9)	
16	398	443	~0	84 (49.5)	228 (10.4)	241 (1.5)	68 (-18.4)	224 (-10.9)	240 (-1.6)	75 (21.2)	228 (10.7)	242 (1.6)
18	399	444	~1	89 (60.6)	227 (10.1)	260 (1.6)	76 (-23.1)	220 (-11.3)	258 (-1.6)	84 (24.3)	227 (10.1)	260 (1.5)
20	400	445	~0	91 (69.2)	223 (10.0)	263 (1.3)	80 (-27.6)	217 (-11.3)	264 (-1.1)	87 (28.9)	224 (10.3)	268 (1.2)
22	405	445	~3	99 (76.0)	225 (10.8)	271 (1.5)	90 (-31.7)	218 (-10.4)	271 (-1.2)	96 (33.5)	225 (10.1)	271 (1.2)

[a] $^{o}T_d$ = onset decomposition temperature for 5% of weight loss; $^{max}T_d$ = maximum rate decomposition temperature; *W* = remaining weight after heating at 600 ºC. [b] Temperatures (ºC) and enthalpies (kJ·mol^{-1}, in parenthesis) observed at heating and cooling for the indicated phase transitions.

.

Two main endothermal peaks were observed on the first heating traces within the 60-100 ºC and 210-225 ºC ranges, respectively, both of them reappearing after cooling and reheating, and two exothermal peaks were also observed on their respective cooling traces at somewhat lower temperatures. It is noticed that the transition occurring in the low temperature region (below 100 ºC) required a significant supercooling (~10-25 ºC) that steadily enlarged as the length of the alkyl chain diminished, and produced a material showing at the second heating an endothermic peak with the enthalpy reduced in about 30-40% of its initial value. These features strongly suggest that this transition must involve the interconversion between a crystal phase (Ph-I) and a molten phase (Ph-II) through a melting-crystallization process that is homogenously nucleated.

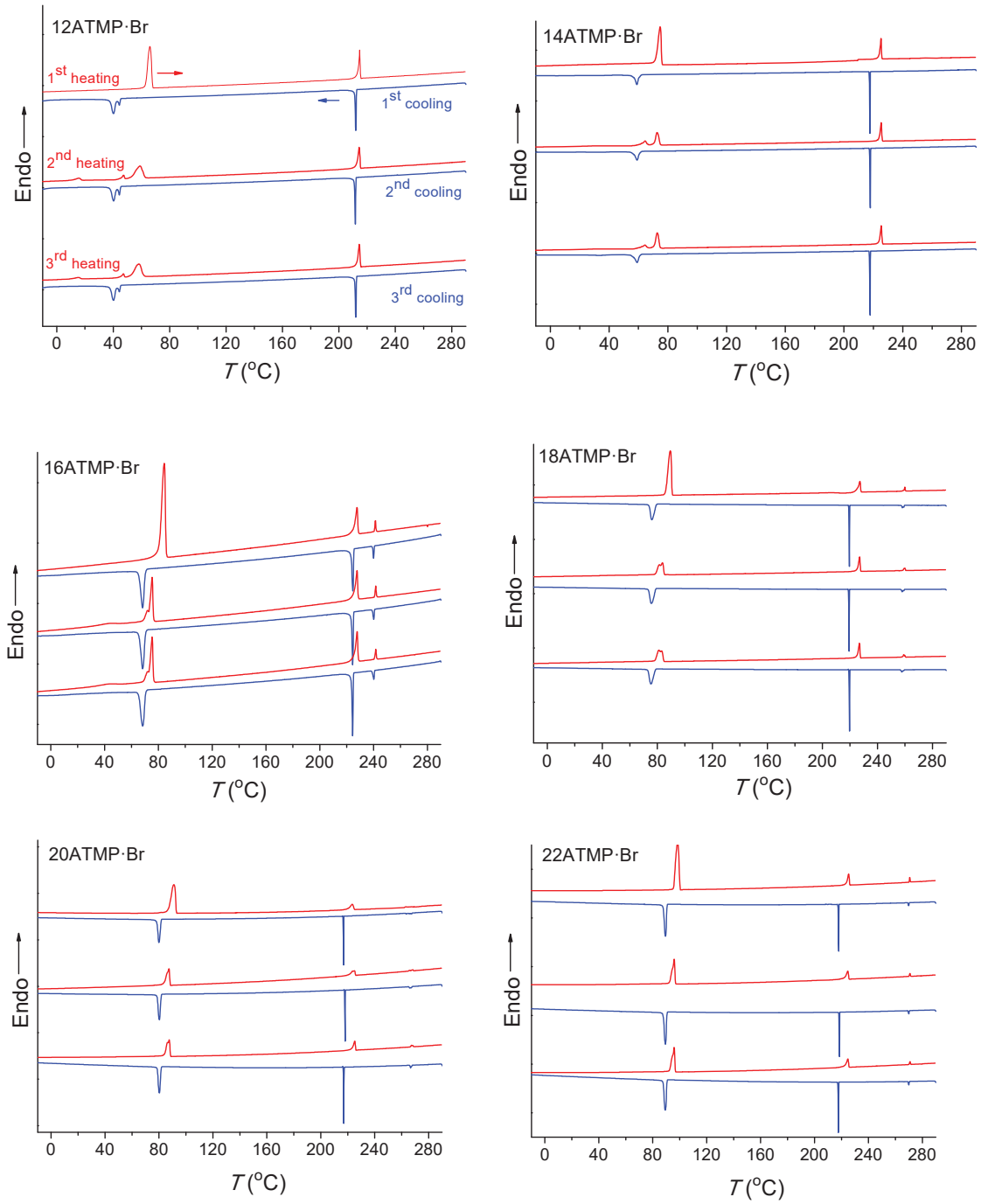

Figure. 2. DSC traces of *n*ATMP·Br at successive heating-cooling cycles over the -30 ºC to 280 ºC interval.

Peak doubling occasionally observed for the Ph-I/Ph-II transition deserves additional comments. The main endothermal peak arising from this transition at the second and third heating traces of both 12ATMP·Br and 14ATMP·Br is accompanied by a second minor peak appearing at lower temperatures. The two peaks seem to move closer to each other as n increases so that a single sharp peak is only present for

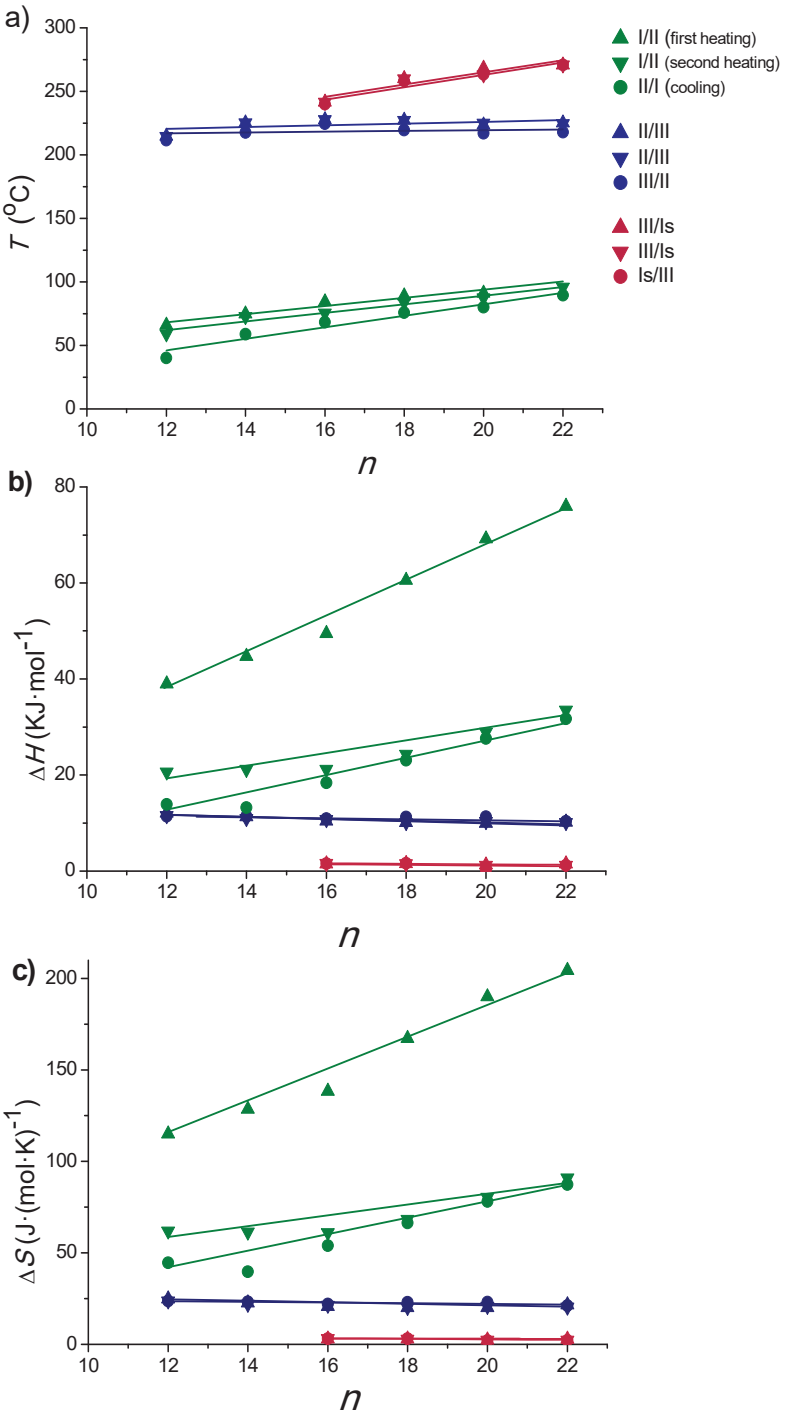

Figure 3. Phase transition temperatures (a), enthalpies (b) and entropies (c) of *n*ATMP·Br surfactants as a function of *n*. In (b) the Δ*H* negative values registered at cooling are represented in positive for a closer comparison with the Δ*H* values registered at heating.

highest values of n. On the other hand, 12ATMP·Br is the only surfactant showing a double peak for the exotherm appearing for this transition at the cooling traces. The presence of double melting should be associated with the existence of two crystallite populations differing in size or/and crystal structure and that could crystallize in one or two stages depending on the mechanismimplied in their nucleation. As it will be demonstrated below by polarizing optical microscopy, phase II generated upon cooling is not structurally homogeneous due to the slow conversion rate of phase III. Such heterogeneity may be the reason for the complexity observed for the heat exchange involved in the Ph-I/Ph-II transition. This point will be further discussed in the section dealing with the thermotropic behavior of the high temperature phases.

At difference with that observed at lower temperatures, the second heat exchange taking place above 200 ºC showed almost negligible supercooling, and the initial endothermal peak was almost exactly reproduced in the second heating trace with both position and intensity essentially preserved at the original values. The transition associated to this peaks-pair should imply therefore an interconversion between two liquid-crystal phases (Ph-II and Ph-III) that must be very closely interrelated. In addition to these two transitions, a third endo/exo heat exchange was detectable for *n*ATMP·Br with $n \geq 16$ when heated above 240 ºC. This third transition takes place at temperatures steadily increasing with *n* and involves a very small heat exchange (~1-1.5 $kJ \cdot mol^{-1}$) that is not appreciably depending on *n*, and that reverses without perceivable supercooling. As it will be seen below, this peak is associated to the isotropization of Ph-III taking place in *n*ATMP·Br with $n \geq 16$.

Temperatures, enthalpies and entropies involved in the thermal transitions observed for *n*ATMP·Br are plotted against *n* in Figure 3. The almost linear trend followed by the three parameters as a function of *n* becomes clearly apparent in these plots and the comparative analysis of the plotted data provides insight into the nature of the transitions: a) the sloping linear dependence of the Ph-I/Ph-II transition parameters, both T and ΔH, on *n* is consistent with the occurrence of a process entailing the melting/crystallization of the polymethylene chain. b) In contrast, the invariance observed for these parameters in the Ph-II/Ph-III interconversion indicates that the trimethylphosphonium group must be the counterpart of the surfactant mainly implied in the rearrangement taking place in this transition with the alkyl chain playing an irrelevant role. On the other hand, the linear dependence on *n* of the Ph-III/Ph-Is transition temperature and the very small enthalpy therein involved suggest the occurrence of an entropically driven process leading to the complete disordering of the system. It is interesting to note that extrapolation of the *T*-*n* straight line of Ph-III/Ph-Is to *n* values of 14 and 12 includes the corresponding points of the Ph-II/Ph-III line. It

could be therefore interpreted that for these two surfactants, Ph-II is directly converted into Ph-Is without going through Ph-III; Ph-III is envisaged then as an intermediate phase that has only existence when the alkyl chains are sufficiently long. A scheme of the existence domains of the different phases is depicted in Figure 4.

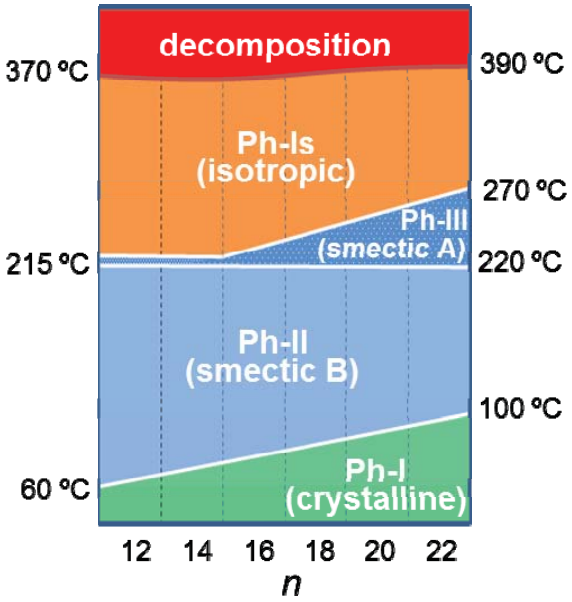

Figure 4. Domains of existence of *n*ATMP·Br phases. Temperatures are approximately indicated.

1.2.4. Crystal structure of *n*ATMP·Br at room temperature (phase I)

Phase I (Ph-I) is the phase adopted by *n*ATMP·Br surfactants at room temperature over a domain of existence that extends up to 60-100 ºC depending on *n*. The scattering produced by this phase when subjected to X-ray diffraction (XRD) consists of a profile made of multiple discrete peaks characteristic of a crystalline state. In the SAXS region (≥1.5 nm), a very sharp strong peak corresponding to a repeat ranging from 1.8 up to 2.8 nm is conspicuously observed as *n* increases from 12 to 22 (Figure 5a). According to what is known for other related surfactants as those made of a trimethylammonium group bearing a long polymethylene chain (Iwamoto et al., 1981), such spacing is interpreted as arising from the periodical distance (*L*) characteristic of the layered biphasic structure usually adopted by these compounds. On the other hand, the diffraction observed for *n*ATMP·Br in the WAXS region (~0.7-0.3 nm) consists of a good number of peaks of varying intensity with most of them being shared by the whole series (Figure 5b), which strongly suggests that the same crystal structure is very probably adopted in all cases. It should be noted that some slight mismatching is more than reasonable to occur since minor deviations in the crystal lattice dimensions of *n*ATMP·Br must be expected due to differences in alkyl chain length.

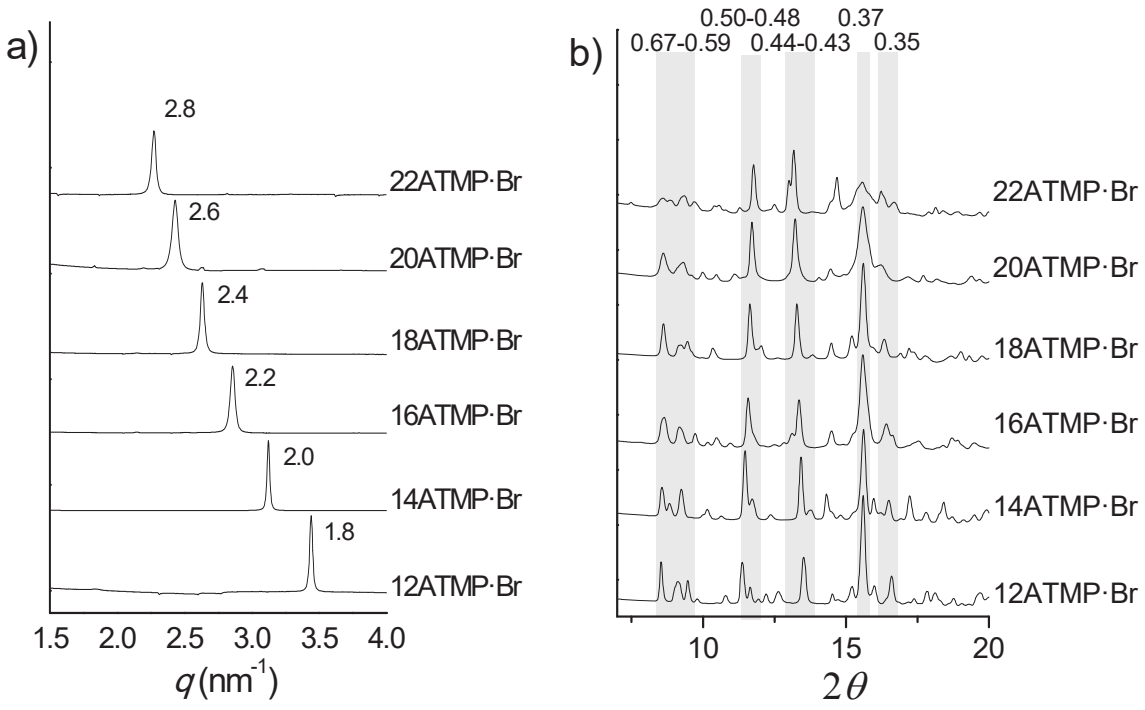

Figure 5. Compared powder X-ray diffraction profiles of *n*ATMP·Br recorded at 25 ºC. a) SAXS region showing the sharp reflections that arise from the periodical spacing characteristic of the layered structure. b) WAXS region with shaded stripes embracing the 2θ intervals that show similar scattering. In both plots, spacings are indicated in nm.

Upon precipitation from organic solution *n*ATMP·Br rendered a microcrystalline powder with diffracting properties characteristic of Ph-I. In order to resolve the structure of this phase, a monocrystal suitable for single-crystal XRD analysis was grown from 12ATMP·Br using the vapor-diffusion method in complete absence of humidity. A picture of the analyzed crystal together with a full account of the crystallographic data collected and handled in this study is given in the SI file. 12ATMP·Br crystallized in a monoclinic lattice belonging to $P2_1/c$ space group, with cell parameters: a = 1.829 nm, b = 0.797 nm, c = 1.267 nm, β = 93.113º, and with a single molecule in the asymmetric unit. The compound crystallized without any solvent molecule included. An ORTEP representation of the 12ATMP·Br molecule in the conformation adopted in the crystal together as well as list of atomic coordinates and torsion angles are given in the SI file. The alkyl chain is in a fully extended conformation and the phosphonium group deviates slightly from the average atomic plane defined for the chain. The same molecular arrangement has been found for the crystal structure of dodecylammonium bromide (Lundén, 1974).

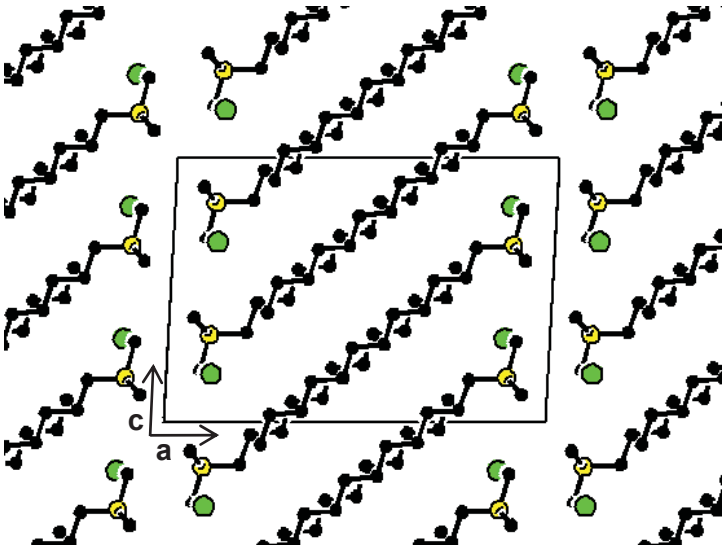

Figure 6. View of the 12ATMP·Br crystal (Ph-I) projected along the *b*-axis with the unit cell outlined. Code colors: bromide in green, phosphorous in yellow, carbon in black; hydrogens have been omitted for clarity.

A representation of the crystal structure of 12ATMP·Br as viewed along the *b*-axis is depicted in Figure 6. The alkyl chain is oriented approximately parallel to the *ac* diagonal and molecules are packed in a biphasic array of alternating hydrophilic and hydrophobic layers. The hydrophilic layer is constituted by the trimethylphosphonium bromide groups and is approximately parallel to the *bc* plane of the crystal. Conversely, the hydrophobic domain contains the dodecyl chains, which are tilted about 30º to the plane defined by the phosphonium bromide ionic pairs. A similar conformation and packing were found for hexadecyltrimethylammonium bromide (Campanelli et al., 1986) although it should be mentioned that there are other reported cases in which the long alkyl chain was not fully extended (Ermolaev et al., 2010; Wang et al., 2014). In this structure, the bromide ion is surrounded by five surfactant molecules but interacts with only one phosphonium atom which is separated by a distance of ~0.413 nm. Such a distance is in agreement with that found in the trimethyl-2-phenylethylphosphonium bromide crystal (0.415 nm) (Riddell et al., 1997) but significant shorter than that reported for tetra-decylphosphonium bromide (0.486 nm) (Abdallah et al., 1999).

In Figure 7 the powder XRD pattern simulated for a crystal lattice of 12ATMP·Br by means of the CERIUS^2 4.9 program (Accelrys Inc) (Accelrys CERIUS^2 Manual, 2003) is compared to the pattern experimentally recorded from a powder sample of this surfactant obtained by precipitation from toluene. The crystal lattice used for simulation was modelled on the basis of the crystal unit cell determined by single crystal analysis. The extremely high coincidence attained between simulated and experimental profiles, including both SAXS and WAXS regions, leads to ascertain without ambiguity that the

crystal structure adopted by 12ATMP·Br at room temperature (Ph-I) must be the same as that found in the monocrystal prepared by diffusion-evaporation.

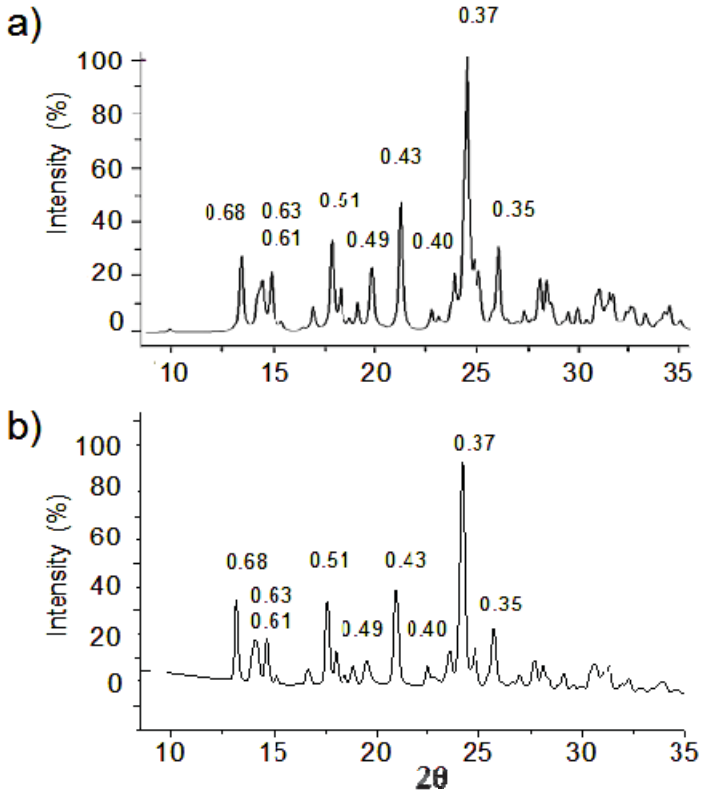

Figure 7. Compared powder X-ray diffraction profiles of 12ATMP·Br in Ph-I. a) Profile simulated for the monoclinic crystal lattice found in the monocrystal. b) Profile experimentally obtained from the powder sample.

The respective crystal lattices were then modelled for all the other members of the *n*ATMP·Br series by taking the 12ATMP·Br monoclinic crystal structure as starting point. The methylene units necessary to appropriately enlarge the alkyl chain were added and the unit cell size was accordingly readjusted by changing both *a* and β parameters, while keeping *b* and *c* at the same value that they have in 12ATMP·Br. The XRD powder profiles obtained by simulation of the crystal lattices built for *n*ATMP·Br for *n* = 14 to 22 showed again an extreme similarity with those experimentally recorded from their respective powder samples, which allowed us to conclude that the monoclinic crystal structure determined for 12ATMP·Br can be successfully extrapolated to the whole series. The unit cell parameters resulting for each *n*ATMP·Br surfactant are provided in the SI file, and a comparison of the XRD spacings calculated for such unit cells with those experimentally observed is provided in Table 3.

1.2.5. Thermotropic behaviour of *n*ATMP·Br (phases II, III and Is)

The thermal transitions between the *n*ATMP·Br phases that were identified by DSC were then examined by XRD with synchrotron radiation. For this purpose, simultaneous SAXS and WAXS spectra were recorded at real time from each surfactant subjected to heating/cooling at a rate of 10 ºC·min^{-1} within the 10-300 ºC range. The heating traces registered every 5 ºC increasing interval are shown in Figure 8 for 14ATMP·Br and 20ATMP·Br surfactants. In both cases clear changes were observed at the two scattering regions in agreement with the heat exchange peaks present in their respective DSC traces. In the SAXS region of 14ATMP·Br, the initial peak initially appearing at 2.0 nm jumped to 2.7 nm and it increased in intensity when the temperature reached ~75 ºC. Simultaneously, the multiple-peak scattering observed at room temperature at the WAXS region was reduced to three small groups of peaks centered at around 0.62, 0.36 and 0.31 nm. This patterns can be made to correspond to a two-dimensional pseudo-hexagonal array of *a* = 0.72 nm that characterizes Ph-II. A similar behavior was observed for 20ATMP·Br with the transition temperature being ~90 ºC in agreement with DSC results, and the long spacing peak jumping in this case from 2.6 nm to 3.5 nm. Nevertheless the SAXS response given by 14ATMP·Br and

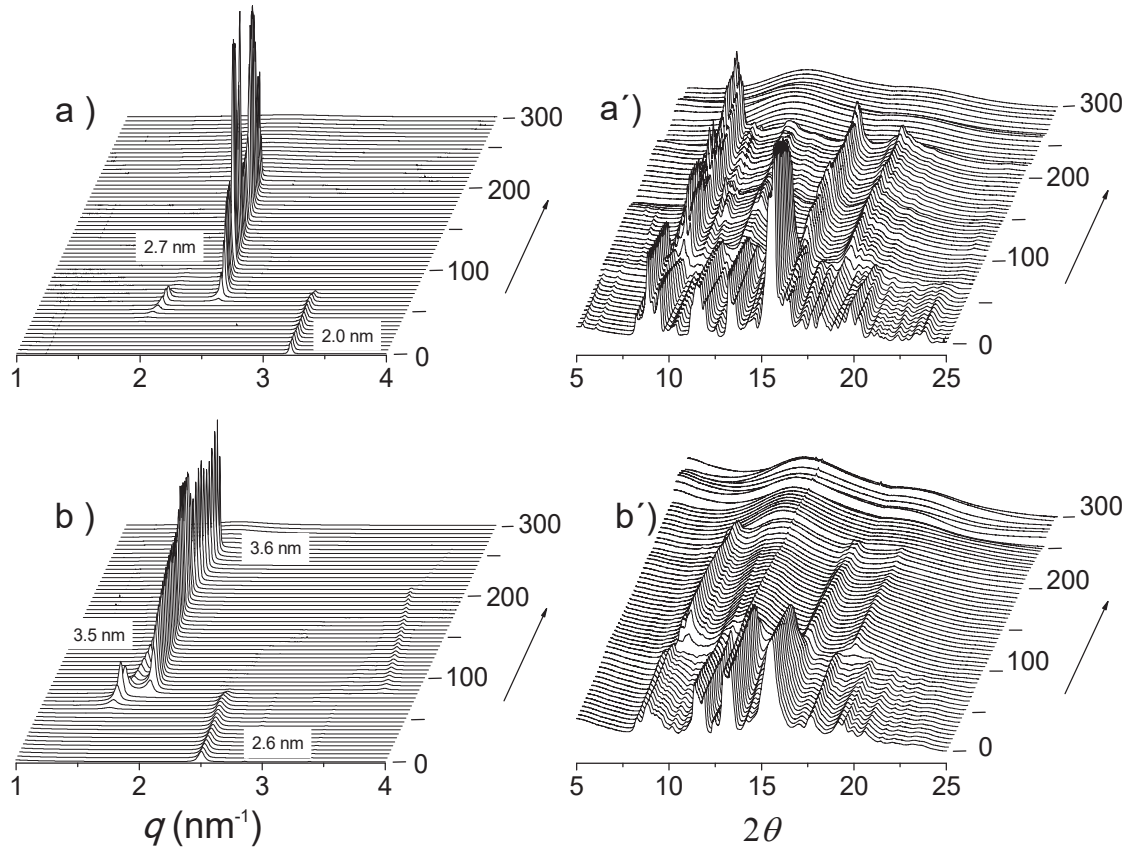

Figure 8. SAXS (left) and WAXS (right) plots from 14ATMP·Br (a) and 20ATMP·Br (b) registered during heating over the 0-300 ºC interval.

20ATMP·Br to heating in the high temperature region, *i.e.* above 200 ºC, was different. In the former case, the 2.7 nm peak disappeared at ~220 ºC, whereas in the latter, the 3.5 nm peak remained practically unchanged in intensity and slightly shifted to a spacing of 3.6 nm to eventually disappears when temperature was around to 265 ºC. Such differences provide evidence the occurrence of an additional thermotropic phase (Ph-III) previous to isotropization (Ph-Is) in 20ATMP·Br, and are consistent with the small endothermal peak that is detected in the examined by thermal XRD at real time by applying heating/cooling cycles at rates between 5 and 0.5 ºC min^{-1}. DSC trace of this compound but that is absent in the case of 14ATMP·Br. Comparable results were attained in the thermal XRD analysis of the others *n*ATMP·Br with 12ATMP·Br following the diffraction pattern observed for 14ATMP·Br and the remaining ones displaying a behavior similar to 20ATMP·Br (available in the SI file). It was observed that Ph-III and Ph-II were atmolt instantaneously recovered upon cooling from Ph-Is and Ph-III (or Ph-Is for *n* = 12 and 14) respectively, but the conversion of Ph-II into Ph-I was found to be incomplete within the applied time scale. However Ph-I could be fully recovered from Ph-II after several hours of standing at room temperature. The complete collection of XRD plots including both SAXS and WAXS profiles registered during heating/cooling cycles for the whole series is available in the SI file.

Table 3. Observed and calculated *d*-spacings for the three phases of *n*ATMP·Br.[a]

n	**12**		**14**		**16**		**18**		**20**		**22**	
					Phase I							
	Obs.	Calc.	Obs.	Calc.	Obs.	Calc.	Obs.	Calc.	Obs.	Calc.	Obs.	Calc.
[b] *L*	1.8	1.8	2.0	2.0	2.2	2.2	2.4	2.4	2.6	2.6	2.8	2.8
hkl												
002	0.63m	0.63 (9)	0.63w	0.63 (5)	n.o	0.62 (3)	0.62m	0.62 (3)	n.o	-	n.o	-
011	0.67m	0.67 (32)	0.67m	0.67 (22)	0.67m	0.67 (21)	0.67m	0.67 (29)	0.67m	0.67 (13)	0.67m	0.66 (11)
012	0.50m	0.50 (15)	0.50m	0.49 (14)	0.50m	0.49 (12)	0.49m	0.49 (8)	0.49s	0.48 (7)	0.49s	0.48 (5)
013	0.37s	0.37 (22)	0.37s	0.37 (18)	0.37s	0.37 (17)	0.37s	0.37 (12)	0.37s	0.37 (9)	0.37s	0.37 (7)
121		0.37 (100)		0.37 (100)		0.37 (100)		0.37 (100)		0.37 (100)		0.37 (100)
020	0.40w	0.40 (9)	0.40m	0.40 (4)	0.40m	0.40 (15)	0.40m	-	0.40m	0.40 (10)	0.40m	0.40 (11)
$10\bar{2}$	0.61m	0.61 (10)	0.62m	0.62 (12)	0.63m	0.63 (10)	0.63m	0.64 (7)	0.63m	0.63 (4)	0.62m	0.63 (3)
221	0.35m	0.35 (34)	0.35m	0.35 (29)	0.35m	0.35 (23)	0.35m	0.35 (22)	0.35m	0.36 (18)	0.35m	0.36 (17)
302	0.43m	0.43 (53)	0.43m	0.44 (55)	0.43m	0.44 (51)	0.43m	0.44 (52)	0.44s	0.44 (44)	0.44s	0.45 (45)
					Phase II							
L	2.4		2.7		2.9		3.2		3.5		3.7	
hkl												
010	0.63-0.62		0.64-0.60		0.62-0.60		0.65-0.62		0.64-0.62		0.64-0.62	
011	0.36		0.36		0.36		0.36		0.36		0.36	
020	0.31		0.31		0.31		0.31		0.31		0.31	
					Phase III							
L	-		-		3.0		3.3		3.6		3.8	

[a] The intensity of peaks (in parenthesis) are visually estimated for observed reflexions and given in normalized % for calculated reflexions.

[b] *L* is referred to the spacing of the *hkl* = 100.

The textures of the phases characterized for *n*ATMP·Br were evidenced by polarizing optical microscopy observation carried out on heated/cooled samples along the same temperature ranges than used for DSC and XRD analysis. Representative optical micrographs of the three phases adopted by 14ATMP·Br are shown in Figure 9. Pictures were taken from the same area of the surfactant film (initially Ph-I), which was first heated to 250 ºC for isotropization (Ph-Is) and then slowly cooled down to room temperature to recover Ph-I by passing through Ph-II. The observed differences in texture for Ph-I before and after treatment are reasonable due to differences in thermal history and also to a probably incomplete conversion of Ph-II. The texture displayed by Ph-II at 150 ºC is indicative of a smectic arrangement although no so clearly as to be able to identify the smectic phase that is dealing with.

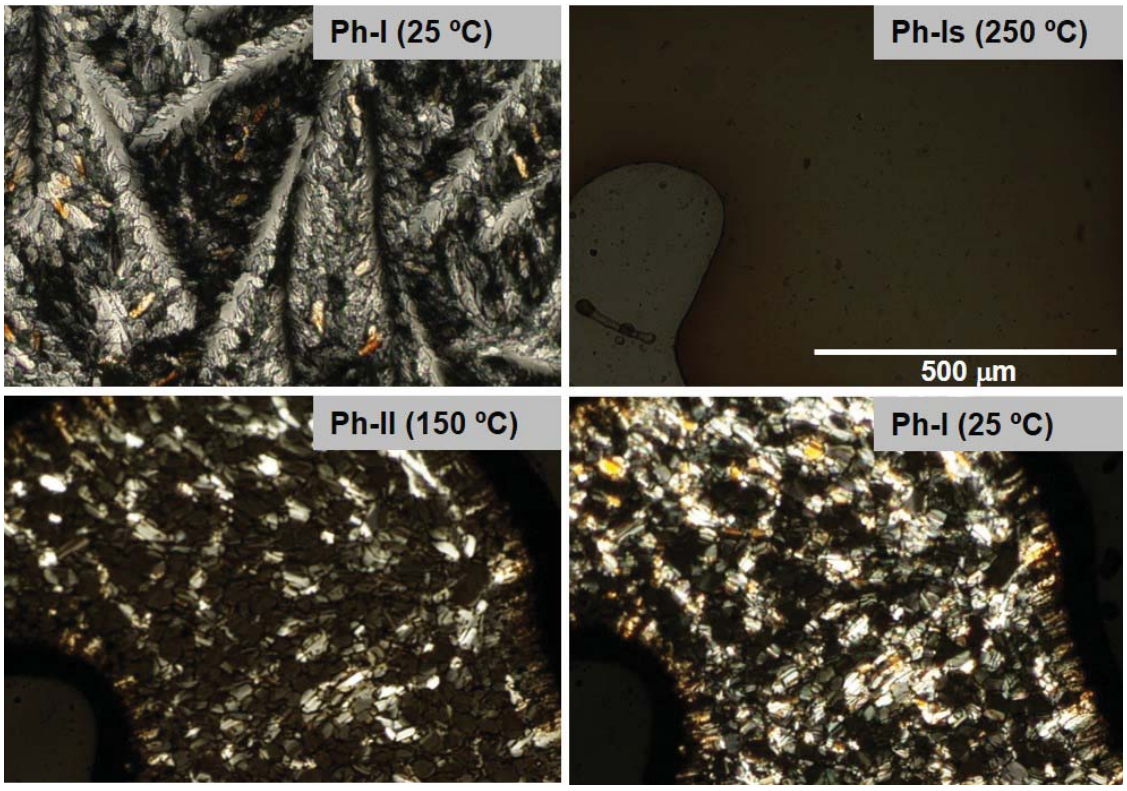

Figure 9. POM micrographs of the three phases of 14ATMP·Br recorded at the indicated temperatures.

The POM pictures recorded from 20ATMP·Br following a similar protocol are depicted in Figure 10. In this case the four phases previously identified for this compound by DSC and XRD were clearly brought into evidence. The initial microcrystalline powder of Ph-I that is observed at room temperature was first isotropicized at 300 ºC (Ph-Is). Upon cooling at 230 ºC the isotropic phase converted into Ph-III displaying a focal-conical fan-like texture characteristic of a Smectic-A structure. Upon further cooling to 190 ºC, the morphology slightly changed to show a more polygonal texture lacking fan shapes but consistent with the occurrence of a

Smectic-B phase (Ph-II). A careful inspection of the pictures recorded along the whole Ph-II domain of temperatures, reveals for this phase the presence of frequent non-regular striations that intensify as temperature decreases. The Ph-I recovered by cooling at 30 ºC displays conspicuous black stripes reminiscent of the striations present in Ph-II. This is a very interesting observation that brings out the close structural interrelation between the semicrystalline Ph-II and the full crystalline Ph-I and that could account for the complexity observed for the heat exchange observed for the Ph-I/Ph-II transition by DSC (Figure 2). A complete assortment of POM pictures illustrating the phase textures for the whole series of *n*ATMP·Br is included in the SI.

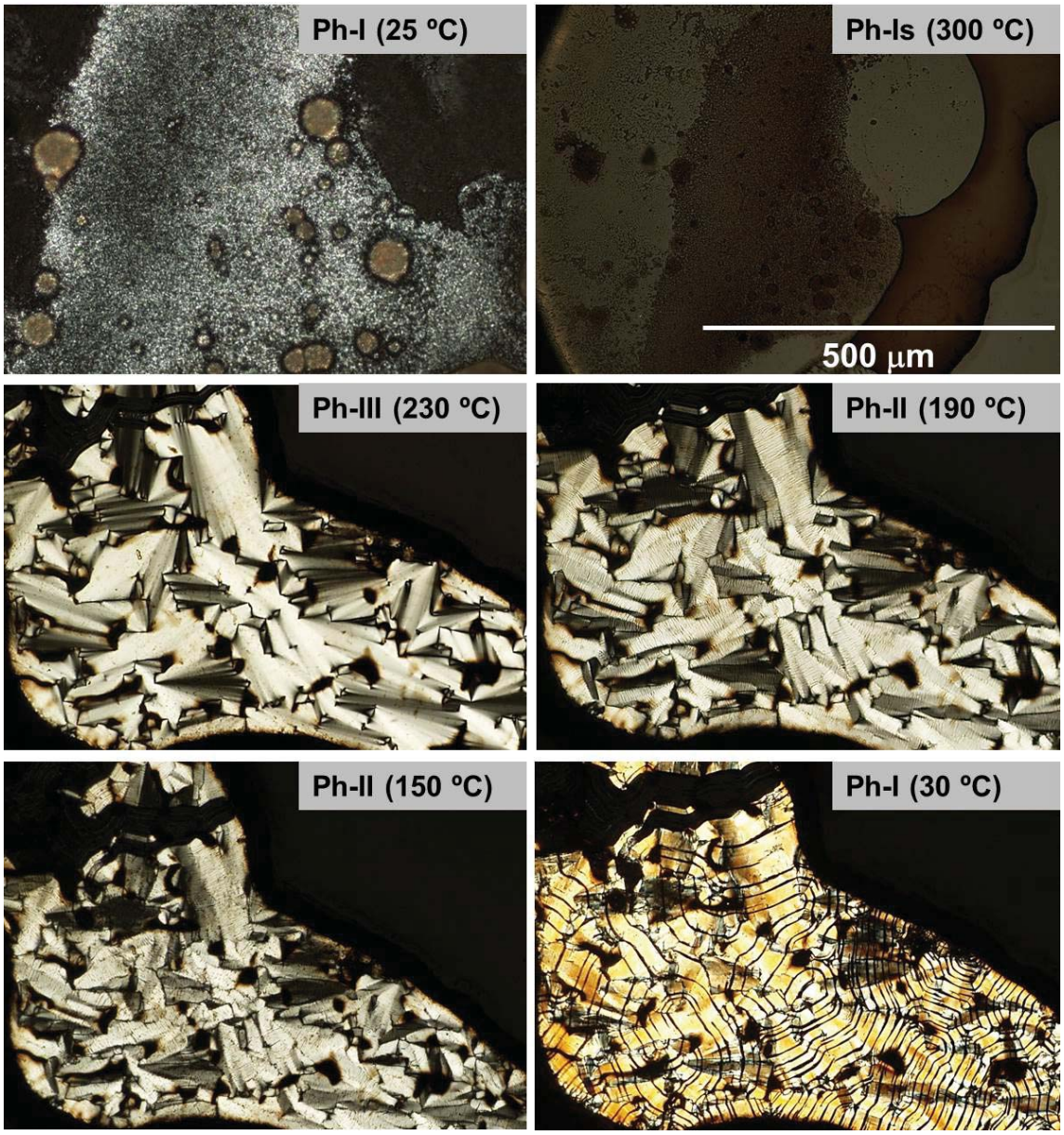

Figure 10. POM micrographs of the four phases of 20ATMP·Br recorded at the indicated temperatures.

1.2.6. Molecular arrangements in the *n*ATMP·Br phases

The *L* values for the *n*ATMP·Br phases displaying long-range order are plotted against *n* in Figure 11. A remarkable feature of this plot is that an almost straight linear fitting is observed for every phase and that lines with very similar equations in both the gradient and the *L*-intercept are displayed for the phases formed upon heating (Ph-II and Ph-III). On the other hand, the *L*-*n* points for Ph-I become almost perfectly aligned along a straight line that is significantly displaced downwards and has a slightly smaller slope. The graphical analysis of the *L*-*n* plots reveals relevant details of the phases geometry as they are the thickness of both the polar layer containing the trimethylphosphonium pairs (L_0) and the paraffinic layer containing the long alkyl chains (L-L_0). The ratio of L-L_0 to the length of the alkyl chain in *all-trans* conformation (l) gives indication of the shortening undergone by the structure due to chain tilting, degree of interpenetration or occurrence of *gauche* conformation effects. The results of these calculations are compared in Table 4.

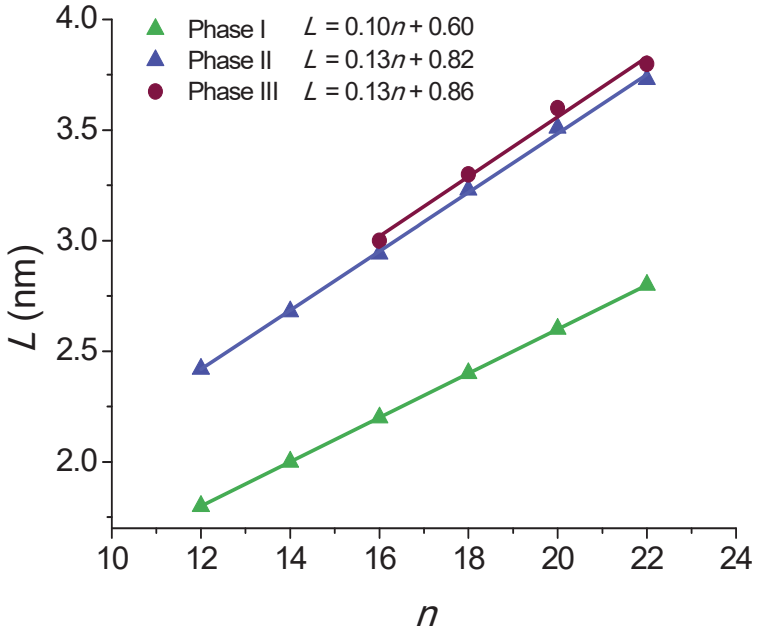

Figure 11. Plot of the long spacing *L* measured by SAXS against *n* for the crystalline and liquid-crystal phases found in *n*ATMP·Br.

The *L*-*n* straight line for Ph-I has a slope of 0.1 nm/CH_2 and an *L*-intercept of 0.6 nm. The shrinkage ratio of the paraffinic layer is pretty constant along the series with a value of 0.80. These data are in full agreement with the molecular arrangement put forward for the crystal structure of these compounds on the basis of the monocrystal XRD analysis of 12ATMP·Br, i.e. the alkyl chains are crystallized in an almost fully interdigitated arrangement and are tilted about 37º with respect to the basal plane of the structure. Furthermore the ionic layer thickness of 0.6 nm defined by the *L*-intercept

is also consistent with the molecular volume calculated for the trimethylphosphonium-bromide pair as it is arranged in the crystal.

The geometric parameters resulting from the analysis of the Ph-II plot are clearly different from those calculated for Ph-I. The large expansion in *L* taking place when Ph-I converts into Ph-II entails a considerable enlargement of L_0 in spite that line slope becomes now about 0.13 nm per CH_2. Also the $(L\text{-}L_0)/l$ ratio is larger for Ph-II than for Ph-I attaining now a value close to unity. These values are in agreement with a layered structure in which the alkyl chains are still fully or almost fully interdigitated and standing approximately normal to the basal plane of the structure. The larger thickness displayed by the polar layer can be explained by assuming that a rearrangement has occurred in the packing of the ion pairs within this layer. According to data provided by XRD it is reasonable to interpret therefore that Ph-II consists of a "semicrystalline" phase (Smectic-B) in which the polar heads of the surfactant remain crystallized in a pseudo-hexagonal array whereas the alkyl tails with a quasi-extended conformation are side-by-side packed without crystalline order.

Table 4. Geometrical parameters for the *n*ATMP·Br phases.

		Phase I			Phase II			Phase III		
n	*l*[a]	*L*[b]	L_o[c]	$(L\text{-}L_0)/l$	*L*	L_o	$(L\text{-}L_0)/l$	*L*	L_o	$(L\text{-}L_0)/l$
12	1.5	1.8	0.6	0.80	2.4	0.82	1.06		-	-
14	1.75	2.0	0.6	0.80	2.7	0.82	1.06	-	-	-
16	2.0	2.2	0.6	0.80	2.9	0.82	1.06	3.0	0.86	1.06
18	2.25	2.4	0.6	0.80	3.2	0.82	1.06	3.3	0.86	1.06
20	2.5	2.6	0.6	0.80	3.5	0.82	1.06	3.6	0.86	1.06
22	2.75	2.8	0.6	0.80	3.7	0.82	1.06	3.8	0.86	1.06

[a]Length of the alkyl chain in fully extended conformation. [b]Interplanar scacing experimentally observed by SAXS. [c]Thickness of the Me_3P^+ Br^- ionic-pair layer.

Ph-III is only observed for *n*ATMP·Br with $n \geq 16$. The graphical differences found between *L*-*n* plots of Ph-II and Ph-III are non-relevant and only entail a small expansion (less than ~5%) in both *L* and L_0. However, the scattering produced by Ph-III in the WAXS region merely consists of a broad plateau centered on ~0.5 nm without showing any vestige of discrete scattering characteristic of crystalline material. The structure of this phase is therefore envisaged as a smetic-A phase in which the trimethylphosphonium bromides continue to be confined in layers but without crystalline order and the alkyl chains are filling the interlayer paraffinic space in an arrangement close to that adopted in Ph-II.

A simple scheme sketching approximately the molecular arrangements adopted in Ph-I, Ph-II and Ph-III of *n*ATMP·Br is depicted in Figure12. Accordingly the description of the thermal phase conversion process can be envisaged as follows: The I/II transition involves melting/crystallization of the paraffinic layer together with a slight rearrangement of the phosphonium-bromide pairs, which converts the monoclinic lattice present in Ph-I into the two-dimensional pseudo-hexagonal array present in Ph-II and *vice versa*. The transition from Ph-II to Ph-III implies the complete melting of the ionic layer and probably an increased disordering of the paraffinic core although the polymethylene chains must remain essentially extended to maintain the long periodicity revealed by SAXS. Finally, a complete disordering takes places when Ph-III is converted in the isotropic phase Ph-Is. The direct conversion of Ph-II into Ph-Is that is observed for 12ATMP·Br and 14ATMP·Br is thought to be due to the incapacity of these compounds to generate a stable Ph-III because the insufficient length that the polymethylene chain has in these cases. No evidence indirectly suggesting the presence of disordered mesoscopic structures in the Ph-Is of *n*ATMP·Br has been met along this work. Further specific studies supported by microcalorimetry and spectroscopy should be made in order to discard definitively the occurrence of such structures in these surfactants.

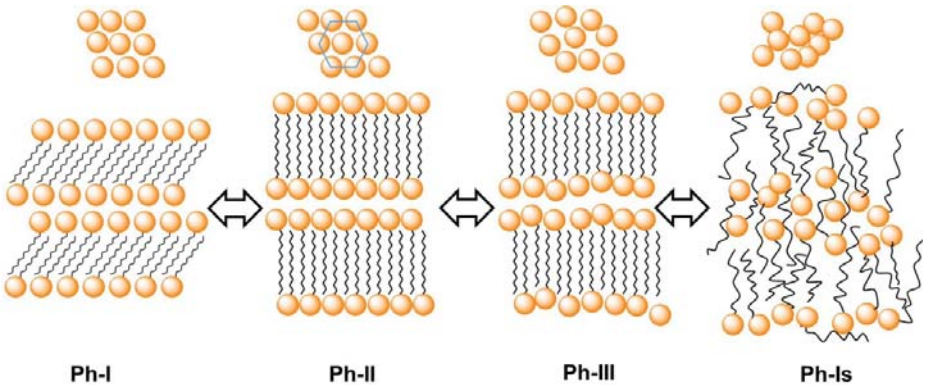

Figure 12. Scheme of the molecular arrangements adopted in in the *n*ATMP·Br phases. On the top the array adopted by the polar heads in the 001 planes are depicted. Note that it pass from oblique in Ph-I to pesudo-hexagonal in Ph-II to become disordered in Phase-III.

1.3. Conclusions

A series of alkyltrimethylphosphonium bromides (*n*ATMP·Br) bearing linear alkyl chains with an even number (*n*) of carbon atoms from 12 to 22 have been synthesized and chemically characterized. These amphiphilic compounds have Krafft temperatures steadily going up from below 0 up to 55 ºC for increasing values of *n*, and they show cmc lower than those reported for their alkyltrimethylammonium bromide analogs. *n*ATMP·Br appear to be highly thermally stable compounds with onset decomposition temperatures close to 400 ºC. Their response to heating within the 0–300 ºC range of temperatures involves two or three thermotropic transitions depending on *n*. At room temperature, all nATMP·Br crystallize in a monoclinic lattice with the Me_3P·Br ionic heads arranged in layers and the long alkyl chains in a fully extended conformation, filling the interlayer spacing with a tilted orientation. This crystalline phase is converted upon heating into a Smectic-B phase that maintains a similar stratified arrangement but with the alkyl chains in the molten state. For $n \geq 16$, the Smectic-B phase changes to Smectic-A when heated around 225 ºC to become finally isotropic when temperatures increase above 240 ºC. For $n = 12$ and 14, isotropization occurs at 215–220 ºC without formation of the Smectic-A phase. All the thermal transitions observed for nATMP·Br are reversible but proceed at moderate rates in particular when they take place at low temperatures.

1.4. References

Abdallah, D. J., Bachman, R. E., Perlstein, J., Weiss, R. G. (1999). Crystal structures of symmetrical t etra *n*-alkyl ammonium and phosphonium halides. Dissection of competing interactions leading to “biradial” and “tetraradial” shapes. J. Phys. Chem. B, 103(43), 9269–9278.

Abdallah, D. J., Robertson, A., Hsu, H., Weiss, R. G. (2000). Smectic liquid-crystalline phases of quaternary group (especially phosphonium) salts with three equivalent long *n*-alkyl chains. How do layered assemblies form in liquid-crystalline and crystalline phases? J. Am. Chem. Soc. 122(8), 3053–3062.

Accelrys Cerius2 Manual, 4.9 ed., Accelrys Inc., 2003.

Adamová, G., Gardas, R. L., Rebelo, L. P. N., Robertson, A. J., Seddon, K. R. (2011). Alkyltrioctylphosphonium chloride ionic liquids: synthesis and physicochemical properties. Dalton Trans. 40(47), 12750–12764.

Antonietti, M., Conrad, J., Thünemann, A. (1994). Polyelectrolyte-surfactant complexes: a new type of solid, mesomorphous materials. Macromolecules, 27(21), 6007–6011.

Axenov, K. V., Laschat, S. (2011). Thermotropic ionic liquid crystals. Materials, 4(12), 206–259.

Beg, M. A. A., Samiuzzaman. (1968). Spectroscopic studies of organophosphorus compounds-II : infrared and ultraviolet spectra of phosphonium compounds and their structures. Tetrahedron, 24, 191–198.

Binnemans, K. (2005). Ionic liquid crystals. Chem. Rev., 105(11), 4148–4204.

Byrne, C., McNally, T. (2007). Ionic liquid modification of layered silicates for enhanced thermal stability. Macromol. Rapid Commun. 28, 780–784.

Campanelli, A. R., Scaramuzza, L. (1986). Hexadecyltrimethylammonium bromide. Sect. C: Cryst. Struct. Commun. C42(10), 1380–1383.

Cieniecka-Rosłonkiewicz, A., Pernak, J., Kubis-Feder, J., Ramani, A., Robertson, A. J., Seddon, K. R. (2005). Synthesis, anti-microbial activities and anti-electrostatic properties of phosphonium-based ionic liquids. Green Chem. 7(12), 855–862.

Davey, T. W., Ducker, W. A, Hayman, A. R., Simpson, J. (1998). Krafft temperature depression in quaternary ammonium bromide surfactants. Langmuir, 14(6), 3210–3213.

Ermolaev, V., Miluykov, V., Rizvanov, I., Krivolapov, D., Zvereva, E., Katsyuba, S., Schmutzler, R. (2010). Phosphonium ionic liquids based on bulky phosphines: synthesis, structure and properties. Dalton Trans. 39(23), 5564–5571.

Fraser, K. J., MacFarlane, D. R. (2009). Phosphonium-based ionic liquids : an overview. Aust. J. Chem., 62, 309–321.

Gerritsma, D. A., Robertson, A., McNulty, J., Capretta, A. (2004). Heck reactions of aryl halides in phosphonium salt ionic liquids: Library screening and applications. Tetrahedron Lett. 45(41), 7629–7631.

Hedley, C. B., Yuan, G., Theng, B. K. G. (2007). Thermal analysis of montmorillonites modified with quaternary phosphonium and ammonium surfactants. Appl. Clay Sci. 35(3–4), 180–188.

Ito, N., Arzhantsev, S., Heitz, M., Maroncelli, M. (2004). Solvation dynamics and rotation of coumarin 153 in alkylphosphonium ionic liquids. J. Phys. Chem. B, 108, 5771–5777.

Iwamoto, K., Ohnuki, Y., Sawada, K., Seno, M. (1981). Solid-solid phase transitions of long-chain *n*-alkyltrimethylammonium halides. Mol. Cryst. Liq. Cryst. 73(1–2), 95–103.

Kamitori, S., Sumimoto, Y., Vongbupnimit, K., Noguchi, K., Okuyama, K. (1997). Molecular and crystal structures of dodecyltrimethylammonium bromide and its complex with p-phenylphenol. Mol. Cryst. Liq. Cryst., 300, 31–43.

Kanazawa, A., Tsutsumi, O., Ikeda, T., Nagase, Y. (1997). Novel thermotropic liquid crystals without a rigid core formed by amphiphiles having phosphonium ions. J. Am. Chem. Soc. 119(33), 7670–7675.

Kumar, V., Malhotra, S. V. (2009). Study on the potential anti-cancer activity of phosphonium and ammonium-based ionic liquids. Bioorg. Med. Chem. Lett. 9(16), 4643–4646.

Lee, y.s, Woo, K. W. (1995). Micellization of aqueous cationic surfactantsolutions at the micellar structure transition concentration–Based upon the concept of the pseudophase separation. J. Colloid Interface Sci. 169(1), 34–38.

Lundén, B. M. (1974). The crystal structure of *n*-dodecylamrnonium bromide. Acta Crystallogr. B30, 1756–1760.

McNulty, J., Capretta, A., Wilson, J., Dyck, J., Adjabeng, G., Robertson, A. (2002). Suzuki cross-coupling reactions of aryl halides in phosphonium salt ionic liquid under mild conditions. Chem. Comm. 17, 1986–1987.

Panek, G., Schleidt, S., Mao, Q., Wolkenhauer, M., Spiess, H. W., Jeschke, G. (2006). Heterogeneity of the surfactant layer in organically modified silicates and polymer/layered silicate composites. Macromolecules, 39, 2191–2200.

Patel, H. a., Somani, R. S., Bajaj, H. C., Jasra, R. V. (2007). Preparation and characterization of phosphonium montmorillonite with enhanced thermal stability. Appl. Clay Sci. 35, 194–200.

Pérez-Camero, G., García-Álvarez, M., Martínez de Ilarduya, A., Fernández, C., Campos, L., Muñoz-Guerra, S. (2004). Comblike complexes of bacterial poly(γ,D-glutamic acid) and cationic surfactants. Biomacromolecules, 5(1), 144–152.

Ramnial, T., Ino, D. D., Clyburne, J. A. C. (2005). Phosphonium ionic liquids as reaction media for strong bases. Chem. Comm. 3, 325–327.

Riddell, F. G., Rogerson, M., Turnbull, W. B., Fülöp, F. (1997). Intramolecular motions in crystalline phosphonium salts studied by 31P and 13C CP–MAS NMR spectroscopy. J. Chem. Soc., Perkin Trans. 2, (1), 95–100.

Sheldrick, G. M. (2007, January). A short history of SHELX. Acta Crystallogr. Sect. A, 64, 112–122.

Tolentino, A., Alla, A., Martínez de Ilarduya, A., Muñoz-Guerra, S. (2011). Comb-like ionic complexes of pectinic and alginic acids with alkyltrimethylammonium surfactants. Carbohydr. Polym. 86(2), 484–490.

Tolentino, A., Alla, A., Muñoz-Guerra, S. (2012). Nanocomposites of comb-like ionic complexes of bacterial poly(glutamic acid) with nanoclays. Eur. Polym. J. 48(11), 1838–1845.

Tolentino, A., Alla, A., Martínez de Ilarduya, A., Muñoz-Guerra, S. (2013). Comb-like ionic complexes of hyaluronic acid with alkyltrimethylammonium surfactants. Carbohydr. Polym. 92(1), 691–696.

Tolentino, A., Alla, A., Martínez de Ilarduya, A., Muñoz-Guerra, S. (2014). Complexes of poly(glutamic acid) and long-chain alkanoylcholines: Nanoparticle formation and drug release. Int. J. Biol. Macromol. 66, 346–353.

Wang, C. M., Chang, T. Y., Chiu, C. W., Lin, H. M., Lii, K. H. (2014). New nanostructured zinc phosphite templated by cetyltrimethylammonium cations: synthesis, crystal structure, adsorption, and photoluminescence properties. Inorg. Chem. 53(7), 3266–3268.

Witschard, G., Griffin, C. E. (1963). Infrared absorption characteristics of alkyl and aryl substituted phosphonium salts. Spectrochim. Acta, 19(1958), 1905–1910.

Xie, W., Xie, R., Pan, W. P., Hunter, D., Koene, B., Tan, L. S., Vaia, R. (2002). Thermal stability of quaternary phosphonium modified montmorillonites. Chem. Mater. 14(11), 4837–4845.

Chapter V. Ionic complexes of poly(γ-glutamic acid) and their nanocomposites

Poly(γ-glutamic acid) (PGGA) is a naturally-occurring polyelectrolyte which is biodegradable, biocompatible and even edible, and in addition, easily accessible by microbial biosynthesis. The chemical modification of PGGA towards compounds suitable for biomaterial applications is currently an issue of primary interest.

Stoichiometric ionic complexes of PGGA with cationic surfactants are compounds with a comb-like architecture that are able to self-assemble in layered amphiphilic nanostructures able to display thermo-responsive properties. These compounds have a remarkable interest for novel technological applications.

We have shown some years ago that stoichiometric or quasi-stoichiometric complexes made from poly(γ,D-glutamic acid) or poly(γ,DL-glutamic acid) and alkyltrimethylammonium bromides, *n*ATMA·Br, have a biphasic stable arrangement with the hydrophilic main chain and the hydrophobic side chain clearly separated in organized nano-domains. Such structures are layered structures with a window spacing between 3.0 and 4.5 nm depending on the length of the alkyl chain. The chains of *n*ATMA·PGGA complexes with *n*=18, 20 and 22 are partially crystallized in a pseudo-hexagonal lattice. Whereas those of complexes with $n \leq 16$ are uncrystallized.

In this chapter we wish to report on comb-like ionic complexes made of PGGA and alkyltrimethylphosphonium soaps, abbreviated as *n*ATMP·PGGA with two main objectives. Firstly it is of fundamental interest to know if the replacement of nitrogen by phosphorous may have significant influence on the ionic PGGA-surfactant complexes regarding essential aspects as crystallizability, formation of the layered structure and response to heating effects. Secondly, phosphonium surfactants are known to be much more resistant to temperature than their ammonium analogs and also to exert a more strong biocide activity. These properties will be relevant for the potential utilization of *n*ATMP·PGGA as extruded films in active coating and packaging applications.

In the second part of the chapter, the topic of interest is the study of nanocomposites of PGGA with montmorillonite clays (MMT) using alkyltrimethylphosphonium surfactants as compatibilizers. Recently, our group have reported on nanocomposites made from *n*ATMA·PGGA complexes and a tetraalkylammonium modified montmorillonite (*n*ATMA·PGGA·MMT), and shown that these nanocomposites may occur along a full range of compositions and display largely improved thermal and mechanical properties. Our efforts are now addressed to extend the study to similar (*n*ATMP·PGGA·MMT) hybrids made from alkylphosphonium

compounds because the replacement of nitrogen by phosphorous will render much more thermally stable nanocomposites.

V.1. Ionic complexes of poly(γ-glutamic acid) with alkyltrimethylphosphonium surfactants

Abstract: A series of ionic complexes with a comb-like architecture and a nearly stoichiometric composition were prepared from bacterial poly(γ,DL-glutamic acid) (PGGA) and alkyltrimethyl phosphonium bromides (*n*ATMP·Br) bearing long linear alkyl chains with even numbers of carbon atoms (*n*) ranging from 12 to 22. The *n*ATMP·PGGA complexes were non-water soluble but readily soluble in organic solvents, and they displayed a high thermal stability. Combined DSC and XRD studies revealed that these complexes adopted an amphiphilic layered structure with the polypeptide chain and the alkyl chain separated in two differentiated phases with a nanoperiodicity that increased steadily with the length of the alkyl chain. The paraffinic phase was found to be partially crystallized in an extent that decreased with *n*, so that complexes with *n* = 12 and 14 did not show any sign of crystallinity whereas those with *n* from 16 to 22 showed crystalline melting in the ~30-70 ºC range. The structural transitions taking place by temperature effects were characterized by simultaneous SAXS/WAXS using synchrotron radiation at real time. In all cases, a shortening of the layer periodicity occurred upon heating with recovering of the initial structure after cooling. *n*ATMP·PGGA with *n* ≤ 16 showed strong antimicrobial activity against both *E. coli* and *S. aureus,* a property that could be related to the weak dissociation of the complexes happening upon incubation in water. The structure and properties of these complexes where comparatively discussed taking as reference their analog complexes made from PGGA and alkyltrimethylammonium bromides already studied by us.

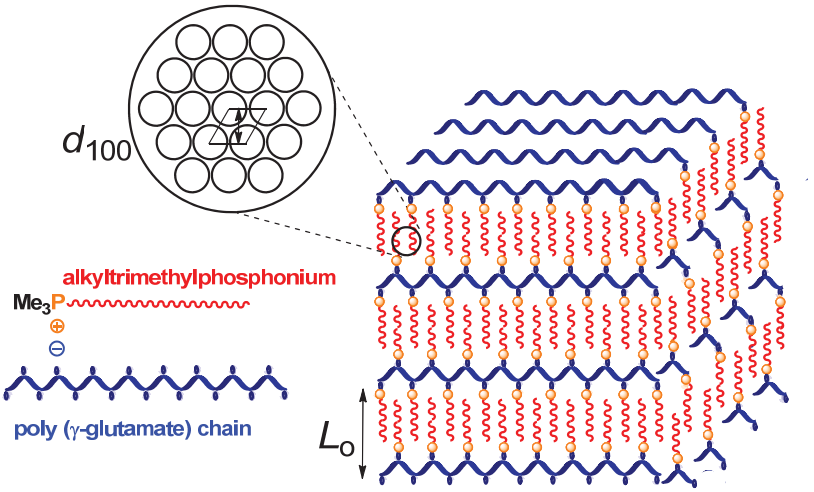

Publication derived from this work:

Gamarra, A., Martínez de Ilarduya, A., Vives, M., Morató, J., Muñoz-Guerra, S. (2017). Ionic complexes of poly(γ-glutamic acid) with alkyltrimethylphosphonium surfactants. Polymer, 116, 43-54.

Supporting Information (SI) to this chapter in Annex B.1

1.1. Introduction

Poly(γ-glutamic acid) (PGGA) is an emerging biopolymer that attracts plenty of research due to its outstanding properties such as water affinity, biodegradability and biocompatibility, in addition to be functionalized (Muñoz-Guerra et al., 2013). Nevertheless, the industrial production and commercial spreading of this poly(γ-peptide) becomes seriously limited by its poor stability in humid environments and its incapacity for being processed. A diversity of modifications of PGGA consisting mainly on esterification (Kubota et al., 1992; Shah et al., 1995; Muñoz-Guerra et al., 2013) or amidation (Kunioka et al., 1997; Akagi et al., 2006; Muñoz-Guerra et al., 2013) of the carboxylic side groups have been reported as convenient approaches to render non-water soluble polymers able to be processed by applying either humid or dried methods. Nevertheless, the covalent modification of PGGA is a tricky procedure that usually implies long reaction times as well as the use of large amounts of solvents and reagents that in most of cases are of unsatisfactory sustainability.

Coupling of carboxylic polypeptides with cationic surfactants has proven to be a very convenient route to produce comb-like ionic complexes that are resistant to water and well stable to heating, and that tend to be self-assembled in supramolecular structures of both academic and practical interest (Antonietti et al., 1994). Such complexes are readily prepared by just mixing aqueous solutions of the polyacid and the surfactant, and they are usually made of stoichiometric or nearly stoichiometric ratios of the two components. Around ten years ago we described for the first time the ionic complexes made of PGGA, either nearly racemic (García-Álvarez et al., 2005) or largely enriched in the D-enantiomer (Pérez-Camero et al., 2004), and alkyltrimethylammonium surfactants (*n*ATMA) bearing linear alkyl chains with numbers of carbons (*n*) from 12 to 22. It was then ascertained by different methods that these complexes (*n*ATMA·PGGA) adopted an amphiphilic layered structure consisting of two separated phases, a hydrophilic one lodging the polypeptide chains and a hydrophobic other integrated by the alkyl side chains. This structure was found to be highly sensitive to temperature showing reversible dimensional changes upon heating or cooling within the 20-70 ºC range. The potential of these complexes as thermoresponsive carriers for hydrophobic active compound has been repeatedly claimed (Pérez-Camero et al., 2004), and their capacity for improving the compatibility of PGGA and nanoclays in layered nanocomposites has been clearly demonstrated (Tolentino et al., 2012). More recently ionic complexes of PGGA of varying stoichiometry have been made using alkanoylcholines derived from fatty acids as counterions (Tolentino et al., 2013). These entirely bio-based complexes are also arranged in a layered structure with features

similar to those found for *n*ATMA·PGGA complexes. Furthermore non-stoichiometric choline derived complexes were used for building biodegradable nanoparticles of 50–100 nm which were able to charge efficiently and deliver under control different kind of drugs of therapeutic interest (Tolentino et al., 2014).

In this study we wish to report on comb-like ionic complexes made by coupling racemic PGGA with alkyltrimethylphosphonium soaps, abbreviated *n*ATMP·PGGA where *n* stands for the number of carbon atoms contained in the linear alkyl chain taking even values from 12 up to 22. The structure and thermotropic behavior of the organophosphonium salts (*n*ATMP·Br) used in this work have been examined in detail in a recently published paper (Gamarra et al., 2017). Two main reasons among others have encouraged us to undertake the present study. Firstly it is of fundamental interest to know if the replacement of nitrogen by phosphorous, which is a much more bulky atom, may have significant influence on the ionic PGGA-surfactant complexes regarding essential aspects as crystallizability, formation of the layered structure and response to heating effects. Secondly alkyltrimethylphosphonium compounds are known to be much more resistant to temperature than their ammonium analogs (Xie et al., 2002) and also to exert a more strong biocide activity (Kanazawa et al., 1994). These properties will be relevant for the behavior of their complexes with PGGA which should be expected therefore to show high thermal stability and intense antimicrobial activity, both properties being of interest for the potential utilization of *n*ATMP·PGGA as extruded films in active coating and packaging applications.

1.2. Results and discussion

1.2.1. Synthesis and chemical characterization of *n*ATMP·PGGA complexes

The coupling reaction between Na·PGGA and *n*ATMP·Br leading to *n*ATMP·PGGA ionic complexes with *n* even values from 12 to 22 is depicted in Scheme 1. The reaction conditions used and the results obtained for the six complexes prepared in this work are compared in Table 1. The temperature used for mixing was the minimum required to have the alkyltrimethylphosphonium salt well dissolved in water. *cmc* values for *n*ATMP·Br surfactants with *n* = 12, 14 and 16 at 25 ºC have been reported to go down from ~10 to ~0.6 mM for increasing values of *n* (Gamarra et al., 2017). At the concentrations used for the preparation of their corresponding *n*ATMP·PGGA complexes (75, 50 and 10 mM, respectively), the surfactant must be in the form of micelles when it is made to contact with the polyelectrolyte. Unfortunately, no data are available for $n \geq 18$ but lower *cmc* values should be expected for longer alkyl chains. Although the higher temperatures used in the preparation of complexes

for *n* = 18, 20 and 22 prevent from attaining a definite conclusion, it can be assumed that the surfactant is in the micellar state in these cases too.

Equimolecular amounts of polyacid and surfactant were mixed in all cases with higher concentration solutions used for lower values of *n* in order to optimize complex precipitation. In spite of that, yields were found to oscillate between 70 and 90% with the lower values corresponding to surfactants bearing shorter alkyl chains. The solubility behavior displayed by *n*ATMP·PGGA was found to be similar to that observed for the ionic complexes made of PGGA and alkyltrimethylammonium surfactants, *i.e.* they are soluble in organic solvents such as, chloroform, methanol, ethanol, TFE or DMSO but non-water soluble.

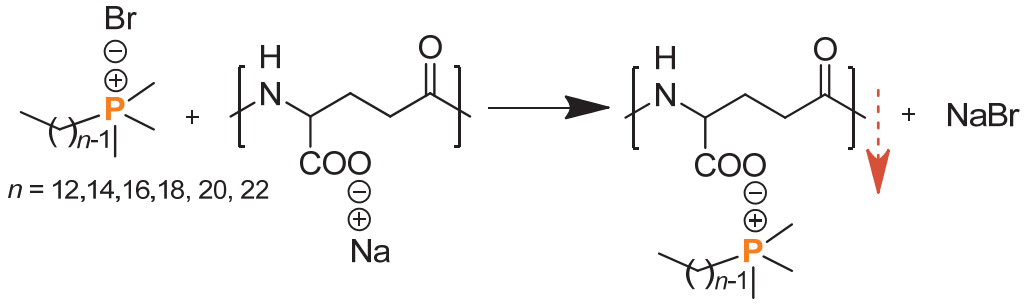

Scheme 1. Coupling reaction of alkyltrimethylphosphonium bromides with Na·PGGA leading to *n*ATMP·PGGA ionic complexes.

The chemical constitution of the *n*ATMP·PGGA complexes was assessed by both FTIR and NMR spectroscopies. Infrared spectra showed characteristic bands at 3280 cm^{-1} (N-H stretching),1635 and 1540 cm^{-1} (Amide I and Amide II), the all three arising from the amide groups of PGGA, in addition to strong bands at 1590 and 1400 cm^{-1} attributed to the asymmetric and symmetric stretching modes of the carboxylate group. As expected bands at 2900, 2850 and 1470 cm^{-1} characteristic of alkyl groups were observed with their intensity steadily increasing with the length of the alkyl chain. On the other hand, conspicuous sharp bands appearing at 990 and 715 cm^{-1} were attributable to the P-C stretching vibrations occurring in the alkylphosphonium groups. The FTIR spectra of Na·PGGA, 18ATMP·Br and 18ATMP·PGGA complex as well as those registered from the whole *n*ATMP·PGGA series are comparatively reproduced in the SI file.

Table 1. Results for the preparation of *n*ATMP·PGGA complexes.

R$Me_3P·Br$	Complex	Mixing conditions[a]		Yield (%)	Composition[b]
		c (M)	*T* (ºC)		
-$C_{12}H_{25}$	12ATMP·PGGA	0.075	25	70	1.0:1.0
-$C_{14}H_{29}$	14ATMP·PGGA	0.05	25	80	1.1:1.0
-$C_{16}H_{33}$	16ATMP·PGGA	0.01	30	80	1.2:1.0
-$C_{18}H_{37}$	18ATMP·PGGA	0.01	45	85	1.2:1.0
-$C_{20}H_{41}$	20ATMP·PGGA	0.01	55	90	1.3:1.0
-$C_{22}H_{45}$	22ATMP·PGGA	0.01	65	90	1.3:1.0

[a]Molar concentration and temperature used for mixing.
[b]Molar ratio of *n*ATMP to PGGA in the complex as determined by NMR.

The ^{1}H NMR spectra of the *n*ATMP·PGGA complexes are compared in Figure 1 with indication of peak assignments. Non assignable signals present in these spectra are negligible both in number and intensity, indicating therefore that complexes have been prepared with high purity. The ^{13}C NMR spectra, which are accessible in the SI file, corroborated the chemical constitution of these complexes.

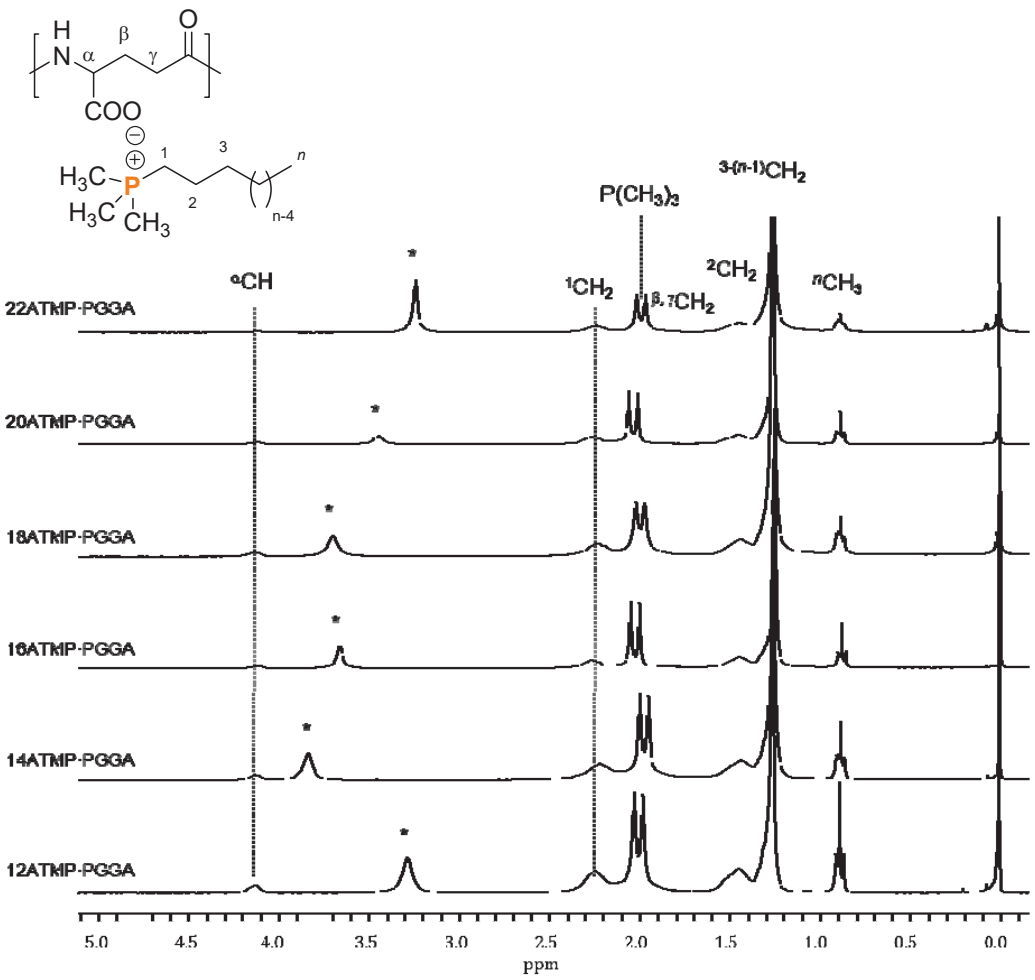

Figure 1. Compared ^{1}H NMR spectra of *n*ATMP·PGGA in $CDCl_3$. (*) Peak arising from residual water.

The composition of the complexes was estimated by comparing the area of the PGGA α-CH signal appearing at 4.1 ppm with that of the signals located in the 1.2-1.5 ppm range which arise from the 2 to *n*-1 methylene protons contained in the phosphonium alkyl chain. The results afforded by this quantitative analysis revealed that the ratio of surfactant to polyacid in the complexes oscillated between 1.0 and 1.3 with values increasing with the length of the alkyl side chain (Table 1). Deviations from stoichiometry are very likely due to the coprecipitation of certain amounts of uncoupled surfactant, a process that should become more significant as the solubility of the ATMP·Br salt in water decreases.

1.2.2. Thermal properties of *n*ATMP·PGGA complexes

The resistance to heat of *n*ATMP·PGGA complexes under an inert atmosphere was systematically examined by TGA. The recorded traces for the whole series together with their corresponding derivative curves are shown in Figure 2, and the most significant thermal parameters are collected in Table 2. *n*ATMP·Br compounds are distinguished by displaying a high thermal stability with onset degradation temperatures (°T_d) around 400 ºC, a behavior that strongly contrasts with that shown by their *n*ATMA·Br analogs that start to decompose at temperatures between 200 ºC and 250 ºC (Kanazawa et al., 1997). On the other hand, PGGA is a relatively thermosensitive polymer that shows appreciable decomposition when heated above 200 ºC (Kubota, et al., 1995). The TGA analysis of *n*ATMP·PGGA complexes revealed that these compounds follow a thermal decomposition pattern which is the result of the reciprocal influence of their two components. In fact, upon gradual heating of the complexes, weight loss initiated at temperatures slightly below 300 ºC, which are values intermediate between those observed for PGGA and *n*ATMP·Br.

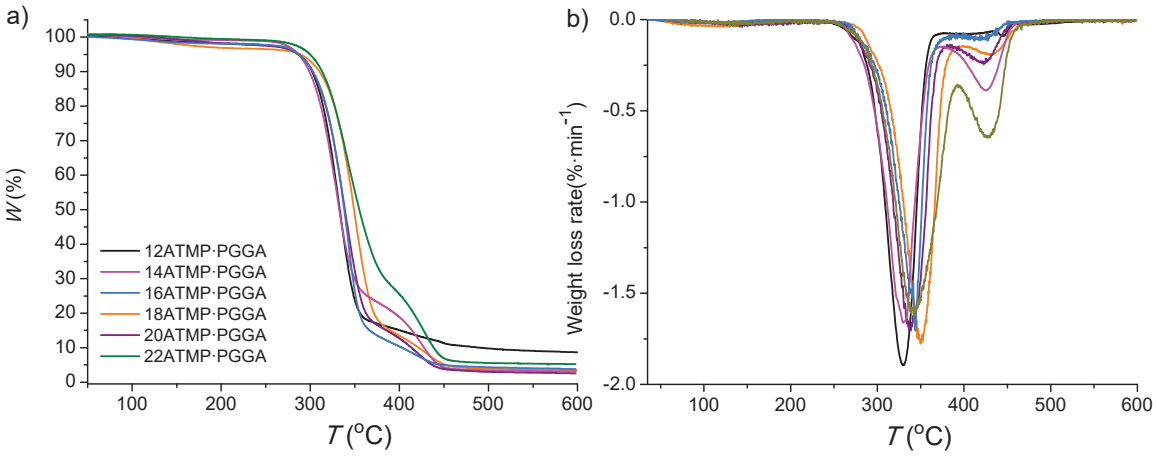

Figure 2. Comparison of the TGA traces for the whole series of *n*ATMP·PGGA complexes (a) and their derivatives curves (b).

Table 2. Thermal parameters of *n*ATMP·PGGA complexes.

n	TGA[a]			DSC[b]								
				1st Heating			Cooling		2nd Heating			
	$^{o}T_d$ (ºC)	$^{max}T_d$ (ºC)	*W* (%)	T_m (ºC)	ΔH_m (kcal·mol^{-1})	n_c	T_c (ºC)	ΔH_c (kcal·mol^{-1})	T_m (ºC)	ΔH_m (kcal·mol^{-1})	n_c	
12	284	331/423	18/9	-	-	-	-	-	-	-	-	
14	285	335/424	18/3	-	-	-	-	-	-	-	-	
16	285	343/424	15/4	38	0.38	-	-	-	-	-	-	
18	285	345/427	17/4	51	4.0	4.9	28	-2.5	35	2.3	2.9	
20	286	345/427	19/5	63	5.8	6.9	47	-4.2	62	4.1	4.9	
22	301	347/431	29/5	72	7.3	8.9	58	-6.0	72	5.6	6.9	

[a] $^{o}T_d$ and $^{max}T_d$: onset and maximum rate decomposition temperatures; *W*: remaining weight at the end of each step.
[b] T_m and T_c: Melting and crystallization temperatures; ΔH_m and ΔH_c: melting and crystallization enthalpies; n_c: calculated number of crystallized methylene units.

Decomposition proceeded through two stages with maximum loss weight rates at the temperature ranges of 330-350 ºC and 420-430 ºC respectively, to leave less than 10% of residual weight and the end of the assay. It is noteworthy to recall that the *n*ATMA·PGGA complexes made from alkyltrimethylammonium surfactants display a similar thermal degradation pattern but with all decomposition temperatures displaced nearly 100 ºC lower (Pérez-Camero et al., 2004; García-Álvarez et al., 2005). The mechanism proposed for the pyrolysis of these complexes entailed the splitting of the complex ionic pair with concomitant generation of pyroglutamic acid at the first step followed by the decomposition of the surfactant counterpart at the second step (Portilla-Arias et al., 2007). Although no similar study has been undertaken in the present work for *n*ATMP·PGGA complexes, it does make sense to assume that both types of complexes should decompose through a similar mechanism. What is clearly evidenced anyway is the higher effect on PGGA thermal stability exerted by the alkylphosphonium surfactants when compared to their alkylammonium analogs.

The DSC study carried out on the *n*ATMP·PGGA complexes in this work has been addressed to identify the occurrence of reversible thermal transitions implying either melting or crystallization. It must be noticed that glass transition has never been observed for this kind of complexes previously reported either by us (Pérez-Camero et al., 2004; García-Álvarez et al., 2005; Tolentino et al., 2011, 2012, 2013a, 2013b) or by others (Ponomarenko et al., 1996). In fact, no sign of slope change characteristic of T_g was detected in the DSC traces of *n*ATMP·PGGA complexes registered over the -100 to 200 ºC range using different heating/cooling rates. For such purpose, samples were subjected to heating-cooling-heating cycles along the 25-120 ºC range since preliminary assays had revealed that all the observed heat exchange peaks were located between 30 ºC and 80 ºC. As it is shown in Figure 3a, only complexes with $n \geq$

16 showed melting peaks, which appear at temperatures steadily increasing from 38 ºC (n =16) up to 72 ºC (n = 22). Upon cooling from 120 ºC, exothermal peaks characteristic of crystallization were observed only for $n \geq 18$ with a supercooling of around 20 ºC. Their corresponding melting peaks were reproduced on the second heating traces at temperatures not far from those observed at first heating (Table 2). For illustrating graphically this transition the traces recorded for 22ATMP·PGGA are depicted in Figure 3b and those recorded for n = 18 and 20 have been included in the SI file.

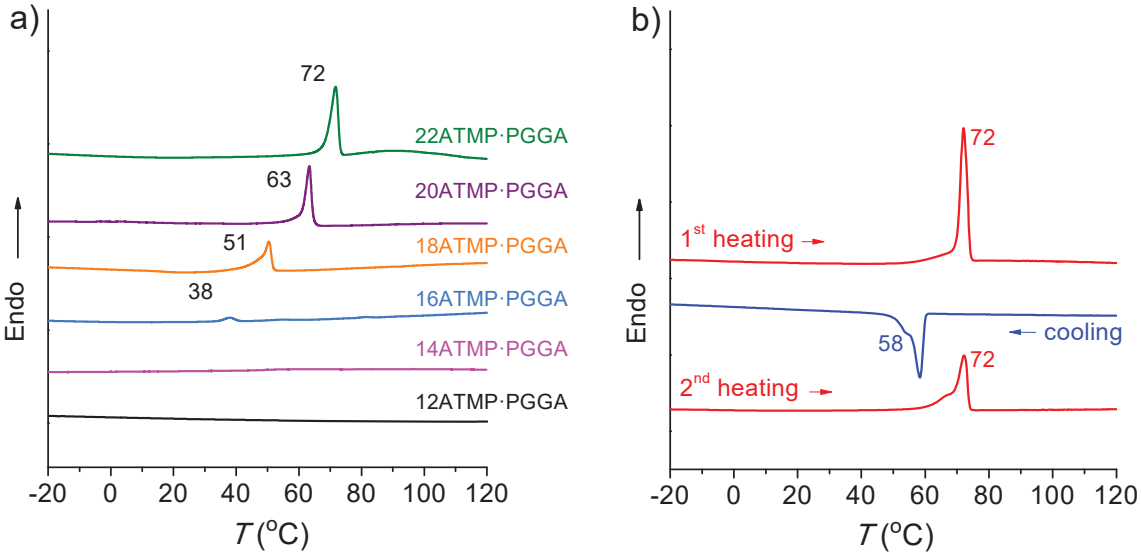

Figure 3. First heating DSC traces of the whole set of *n*ATMP·PGGA complexes (a) and DSC traces of the 22ATMP·PGGA along the heating-cooling-heating cycle (b).

According to data previously reported for other PGGA ionic complexes bearing long alkyl side chains (Pérez-Camero et al., 2004; García-Álvarez et al., 2005), the heat exchanges observed by DSC for *n*ATMP·PGGA must be related to the occurrence of a melting-crystallization process involving exclusively the paraffinic phase. The graphical representation of T_m against n reveals an almost linear dependence between these two variables with an increment of around 5 ºC for every carbon atom that is added to the alkyl chain (Figure 4a). Also the variation of ΔH_m with n follows a similar dependence for the complexes showing crystallization except for n =16, which deviates down from linearity. The same trend was found for the melting of the complexes crystallized by cooling the heated samples although the enthalpy was in these cases about two kcal·mol^{-1} smaller (Figure 4b). The individual methylene (ΔH_m^{CH2}) and non-methylene (ΔH_m^0) contributions to the experimentally observed melting enthalpy are respectively given by the slope and the y-axis intercept at n = 0 of the linear ΔH_m-n plots (Jordan et al., 1971). The resulting values are around 0.8 kcal·mol^{-1}·CH_2^{-1} for

ΔH_m^{CH2} and 10-12 kcal·mol^{-1} for ΔH_m^0 pointing that the crystallized alkyl chains must be packed in a pseudo-hexagonal array (Broadhurst, 1962) and that only a fraction of the chain is included in the crystal phase. As it is seen in Table 2 and plotted in Figure 4b, the amount of crystallized methylene units in crystallized *n*ATMP·PGGA samples oscillates between 3 and 9 (corresponding to chain fractions between 17% and 42%) depending on chain length and crystallization conditions.

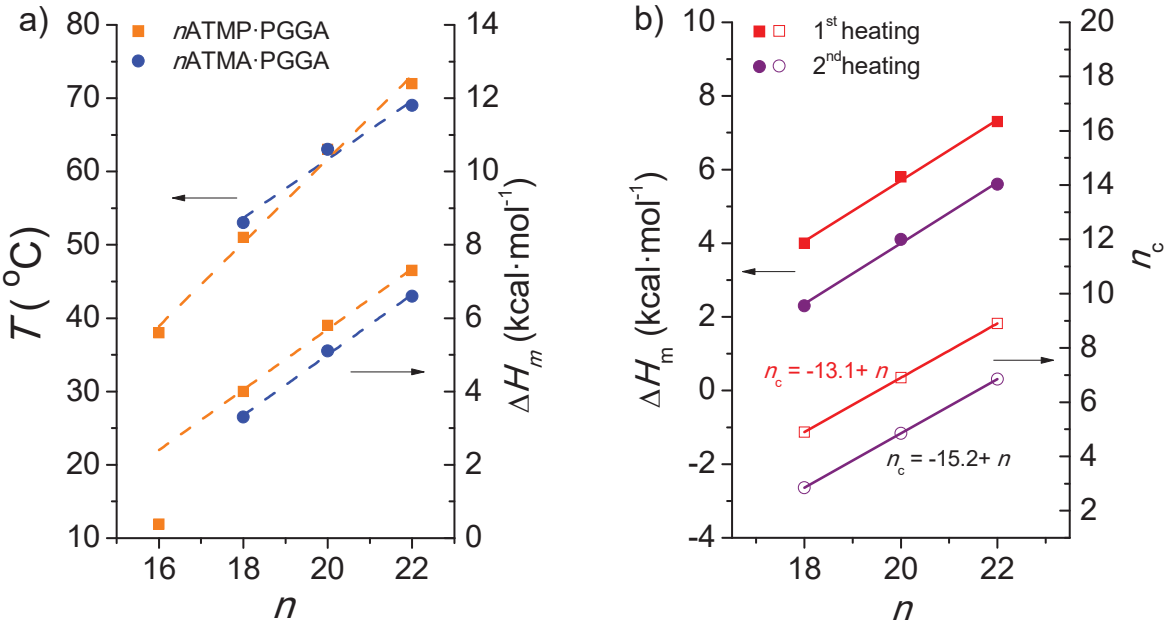

Figure 4. a) Melting temperatures and enthalpies experimentally observed on the heating DSC traces recorded from pristine samples of *n*ATMP·PGGA and *n*ATMA·PGGA for *n*= 16, 18, 20 and 22. b) ΔH_m and number of crystallized methylenes (n_c) of 18, 20 and 22ATMP·PGGA complexes against the number of carbons contained in the alkyl chain for both pristine samples and samples crystallized from the melt.

The trend observed for crystallinity and crystallizability in *n*ATMP·PGGA as the length of the alkyl chain changes is a feature of general application to all the comb-like PGGA derivatives studied to date including ionic-complexes (Pérez-Camero et al., 2004; García-Álvarez et al., 2005; Tolentino et al., 2013b) and poly(α-alkyl γ-glutamate)s as well (Morillo et al., 2001). For comparison, the DSC data reported for the *n*ATMA·PGGA series have been also plotted in Figure 4a. As it can be seen the behavior of the two series regarding both melting temperatures and enthalpies are very similar although slightly higher values are invariable found for the *n*ATMP·PGGA complexes.

1.2.3. Supramolecular structure of *n*ATMP·PGGA complexes

The *n*ATMP·PGGA complexes have a comb-like architecture with a strongly marked amphiphilic constitution. The PGGA polypeptide chain including the attached carboxylate-phosphonium ionic pairs composes the hydrophilic part whereas the

hydrophobic part is made of the pending long linear alky side chains. According to what has been repeatedly reported for other similar systems (Pérez-Camero et al., 2004; García-Álvarez et al., 2005; Tolentino et al., 2013b), the precipitation of these complexes from water taking place in situ as they are formed upon mixing their components is expected to happen through a self-assembling process. In fact, X-ray diffraction of the *n*ATMP·PGGA precipitates produced discrete light scattering characteristic of a well-organized material. The SAXS and WAXS profiles recorded from the complexes are compared in Figure 5 for the whole series. In the small-angle region (Figure 5a), a strong peak corresponding to a spacing ranging between 3 and 5 nm is conspicuously observed for all the complexes, which is accompanied by a second minor one for the exceptional case of 18ATMP·PGGA. In line with the study carried out earlier on other ionic complexes of PGGA, these peaks

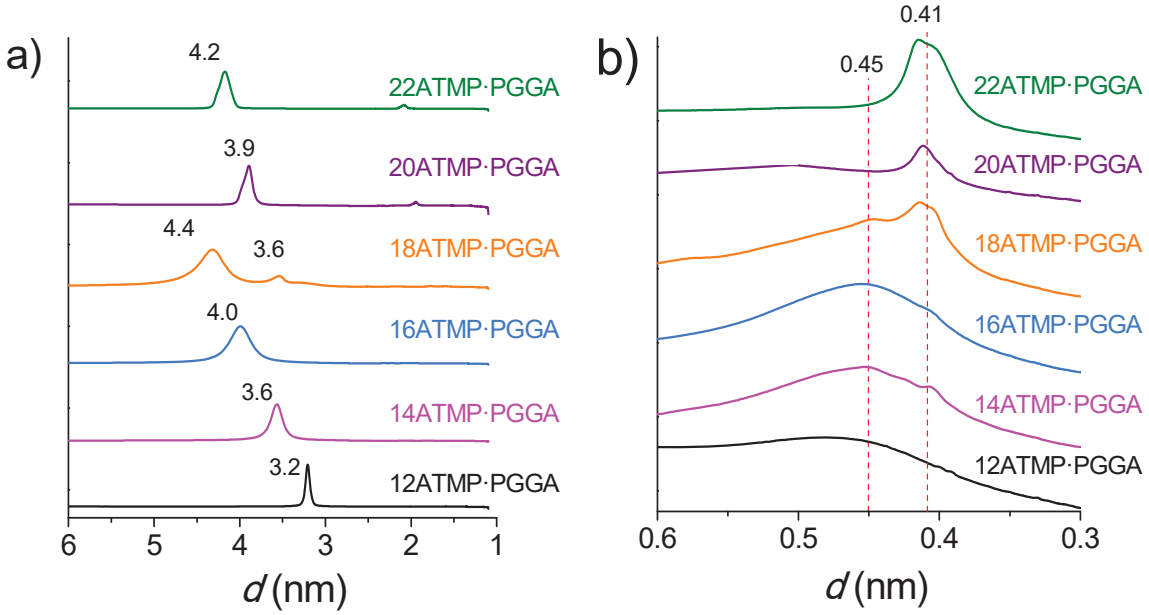

Figure 5. XRD profiles recorded at room temperature from *n*ATMP·PGGA in the SAXS (a) and WAXS regions (b).

appearing at low angles are interpreted as arising from the periodical spacing of a structure made of alternating polypeptidic and paraffinic layers with a window that steadily increases with the length of the alkyl side chain. In fact, the plot of the long spacing (*L*) values measured by SAXS against *n* (Figure 6) reveals that the periodicity of the layered structure varies almost linearly with *n* along the whole *n*ATMP·PGGA series but showing an abrupt discontinuity at *n* = 18. The *L*-*n* straight line fitting the complexes with *n* = 22, 20 and 18 (lower *L* value) displays a positive slope of ~0.15 nm·CH_2^{-1} whereas complexes with *n* =12, 14, 16 and 18 (higher *L* value) fit in a straight line that is displaced to higher *L* values and is inclined ~0.2 nm·CH_2^{-1}. Approximately

the same *L*-intercept at *n* = 0 results for the two lines with a value of 0.8-0.9 nm which is interpreted as the thickness of the polypeptidic layer with the trimethylphosphonium groups therein included. No experimental data supporting a plausible explanation for the function discontinuity observed in this plot have been attained. A modification in the supramolecular arrangement of the complexes entailing a change in tilting or/and interdigitation of the alkyl side chains could be the reason for the observed jump. Also the presence of crystallinity detected for $n \geq 18$ could be invoked to explain the *L* contraction undergone by these complexes. The dual *L* value displayed exclusively by *n* = 18 would indicate the occurrence of more than one structure or phase for the specific case of the 18ATMP·PGGA complex. It should be noticed that this behavior is also displayed by complexes made of hyaluronic acid and alkyltrimethylphosphonium surfactants (unpublished results) whereas a single straight line is found when complexes are made of alkyltrimethylammonium surfactants for both PGGA and hyaluronic acid. It seems therefore that it is the replacement of nitrogen by phosphorus that is behind the observed difference.

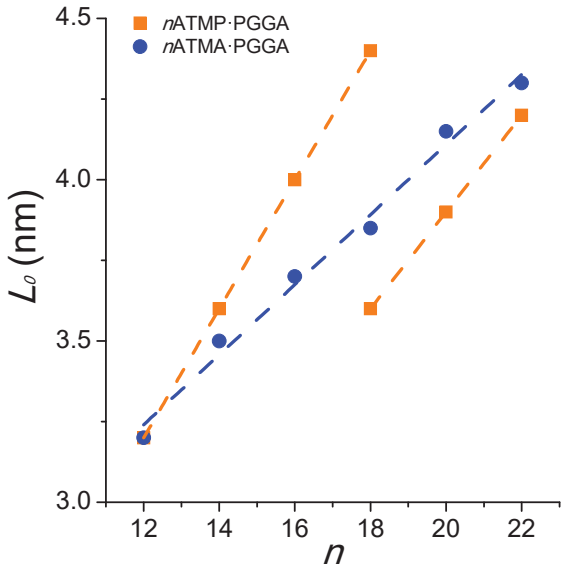

Figure 6. Interlayer spacings observed at room temperature for *n*ATMP·PGGA as a function of *n*. Data reported for the *n*ATMA·PGGA [8] have been included for comparison.

The XRD data collected in the WAXS region afforded additional distinguishing structural information between the two groups of complexes (Figure 5b). The profiles recorded for 20ATMP·PGGA and 22ATMP·PGGA show a discrete peak at ~0.41 nm (d_{100}) characteristic of a paraffinic phase crystallized in a pseudo-hexagonal array of chains separated to one another by an average distance of about 0.47 nm (a_0). On the contrary, a broad signal characteristic of amorphous scattering and centered around 0.45 nm is the most prominent feature observed on the profiles produced by complexes with *n* = 12, 14 and 16. The WAXS profile of 18ATMP·PGGA show both discrete and

diffuse scattering with comparable intensities revealing that crystallized as well as non-crystallized paraffinic material must be present in this complex in similar amounts.

No evidence on the conformation adopted by the polypeptide chain in the *n*ATMP·PGGA complexes is provided in this paper. Unfortunately, the information that could be provided by X-ray diffraction is probably masked by the strong scattering arising from the layered structure. The tendency of optically pure PGGA to be arranged in a helix is known for long. It was Rydon (Rydon, 1964) who first put forward a helical conformation of α-helix type for PGGA in the un-ionized state, a proposal that has been recently confirmed by molecular dynamics studies (Zanuy et al., 1998). Nevertheless, on the basis of dichroic infrared analysis carried out on 18ATMA·PGGA (Pérez-Camero et al., 2004), it was found that the conformation most probably adopted by PGGA in this kind of ionic complexes is a slightly folded conformation not far from the β-form of polypeptides, in which the carboxylate side groups become conveniently distributed in the space to allow an efficient packing of the alkyl side chains (Pérez-Camero et al., 2004). In the absence of any opposing evidence, there are reasons to assume that this conformation must be present in the *n*ATMP·PGGA too. The thickness that is estimated for the polypeptidic layer would be rather small to accommodate an α-helix, and the racemic composition of the PGGA used for building these complexes is in principle incompatible with any regular helical arrangement.

On the basis of the structure previously reported for other comb-like ionic complexes of PGGA (Pérez-Camero et al., 2004; García-Álvarez et al., 2005;) and with the support of the XRD results described above, a model may be proposed for the layered structure of *n*ATMP·PGGA which is drawn in Figure 7. This model is essentially identical to that proposed for *n*ATMA·PGGA with the difference that the trimethylammonium group is here replaced by the bulkier trimethylphosphonium one. It should be noted that although the alkyl chains are aligned with an orientation normal to the basal plane of the structure, they may be crystallized (*n* = 22 to 18) or not (*n* =18 to 12) and that in the former case, only a fraction of the chain will be in the crystalline state. Note also that the distance between carboxylate groups in one fully extended PGGA chain is ~0.6 nm whereas the longitudinally aligned alkyl chains are averagely separated by 0.47 nm or 0.45 nm depending whether they are crystallized or not. Fitting the paraffin phase to the polypeptidic layer will imply therefore a slight shrinkage of the PGGA chain in about 20% as well as deep interdigitation of the alkyl chains stemming from neighboring layers. The PGGA chains within the same layer would be connected to one another by hydrogen bonding the neighboring amide groups.

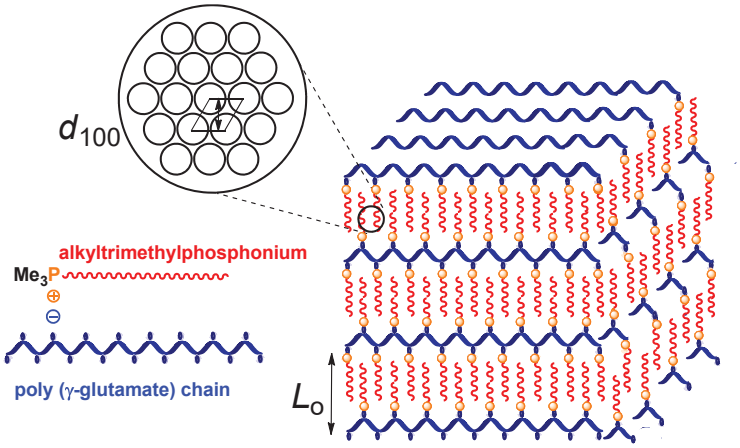

Figure 7. Model for the layered structure adopted by *n*ATMP·PGGA complexes.

The occurrence of liquid-crystal or semicrystalline phases for *n*ATMP·PGGA complexes at room temperature corresponding to compositions for which the parafiinic phase was crystallized or not was supported by POM. Mosaic texture characteristic of a smectic structure was clearly identified for 12ATMP·PGGA whereas well-developed spherulitic morphologies indicative of semicrystalline material were observed for 20ATMP·PGGA and 22ATMP·PGGA. The textures exhibited by the complexes with *n* = 14, 16 and 18 were more difficult to interpret probably because they reflect the occurrence of more than one phase coexisting in the material at the temperature at which images were taken. A complete collection of POM pictures including the whole series of complexes is given in the SI file.

1.2.4. Temperature effects on the structure of *n*ATMP·PGGA complexes

The effect of temperature on the layered structure adopted by the *n*ATMP·PGGA complexes was examined by XRD at real time using synchrotron radiation. Samples were subjected to heating-cooling-heating cycles covering the 10 ºC to 120 ºC range at a heating/cooling rate of 10 ºC·min^{-1}. The spacings observed at the beginning and the end of each run for every complex are compared in Table 3, and the charts showing the evolution of the scattering profile in both SAXS and WAXS regions for every 3 ºC of temperature change are included in the SI file. General features observed in these X-ray thermodiffractograms are a decreasing trend of the periodical long spacing of the structure as temperature raised and an almost complete reversibility of the occurring changes after cooling. However, more or less significant differences were observed among the members of the series, which are consistent with the results obtained by DSC. It should be noticed that almost identical results were obtained for the two components of the extreme pairs, *i.e* 12ATMP·PGGA/14ATMP·PGGA and

Table 3. X-ray diffraction data (in nm) of *n*ATMP·PGGA complexes recorded at different temperatures.

n	SAXS			WAXS		
	$L^{10ºC}$	$L^{120ºC}$	$L^{10ºC}$	$d_{100}{}^{10ºC}$	$d_{100}{}^{120ºC}$	$d_{100}{}^{10ºC}$
12	3.2	3.0	3.3	0.45	0.45	0.45
14	3.6	3.4	3.7	0.45 (0.41)	0.45	0.45
16	4.0	(3.7), 3.6	(3.9), 3.6	0.45, (0.41)	0.45	0.45
18	4.4 (3.6)	3.9, (3.3)	3.9, (3.4)	0.45, 0.41	0.45	0.45
20	3.9	3.8	3.9	0.41	0.45	0.41
22	4.2	4.0	4.1	0.41	0.45	0.41

L: interlamellar distance; d_{100}: interplanar spacing of the crystallized paraffinic phase; in parenthesis, values for very weak peaks.

22ATMP·PGGA/20ATMP·PGGA, whereas clear differences were evidenced between the two pairs.The charts for *n*= 12 and *n* = 22, which are taken as representatives of each pair, are shown in Figure 9 and 10, respectively. The SAXS profiles recorded for 12ATMP·PGGA at 10 ºC show a sharp peak corresponding to a spacing of 3.2 nm that moves evenly down until 3.0 nm at 120 ºC and that reverses to near the initial value upon cooling (Figure 8a). The WAXS scattering produced by this complex is completely insensitive to temperature effects so that the flat profile initially recorded is maintained invariable along the whole heating-cooling-reheating cycle (Figure 8b). Exactly the same pattern of behavior was found for 14ATMP·PGGA with the initial SAXS peak appearing in this case at 3.6 nm and going down to 3.4 nm at 120 ºC. Conversely the response to temperature of 22ATMP·PGGA was significantly different both in SAXS and WAXS (Figure 9). The SAXS peak at 4.2 nm present at 10 ºC also moved slightly to down values but in this case with a jump taking place at the surrounding of 70 ºC (Figure 9a), which is the melting temperature detected by DSC for this complex. The WAXS chart (Figure 9b) shows how the 0.41 nm peak characteristic of the crystallized paraffinic phase disappears at the melting temperature and is then recovered after cooling down to the initial temperature. Exactly the same pattern of behavior was found for 20ATMP·PGGA with the initial SAXS peak appearing in this case at 3.9 nm and going down to 3.8 nm at 120 ºC.

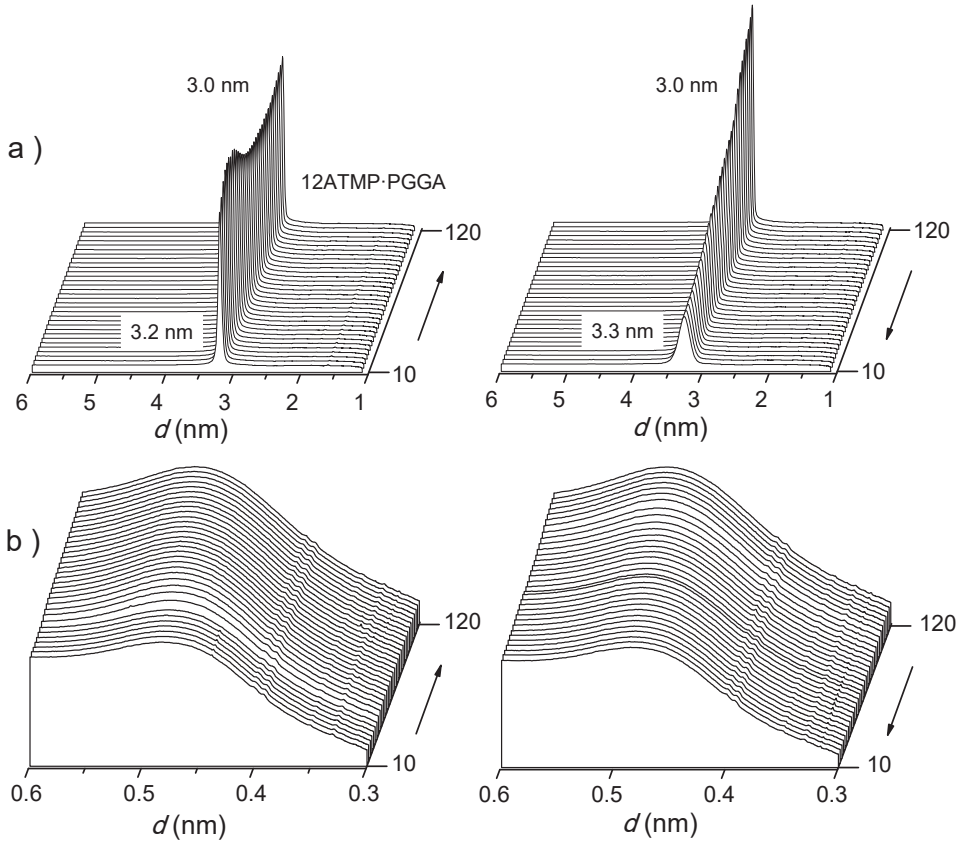

Figure 8. SAXS (a) and WAXS (b) profiles of 12ATMP·PGGA at heating (left) and cooling (right).

The behavior observed for both 16ATMP·PGGA and 18ATMP·PGGA is more intricate not only due to the presence of significant amounts of both crystallized and non-crystallized material. Furthermore the implication of more than two supramolecular arrangements in the heating-cooling process cannot be discarded. In these cases two peaks are observed in the SAXS profiles either from the beginning or after heating, and the discrete peak initially present in WAXS was not recovered after cooling the heated sample (see SI file). Although reversible dimensional changes also happen for these intermediate complexes when they are subjected to heating and cooling, and a melting-crystallization process is in some extent also involved, the interpretation of such changes is not easy. A more detailed analysis by XRD in combination with calorimetric and polarizing optical microscopy should be made in order to achieve a sounded explanation for the structural transformations detected for these two complexes.

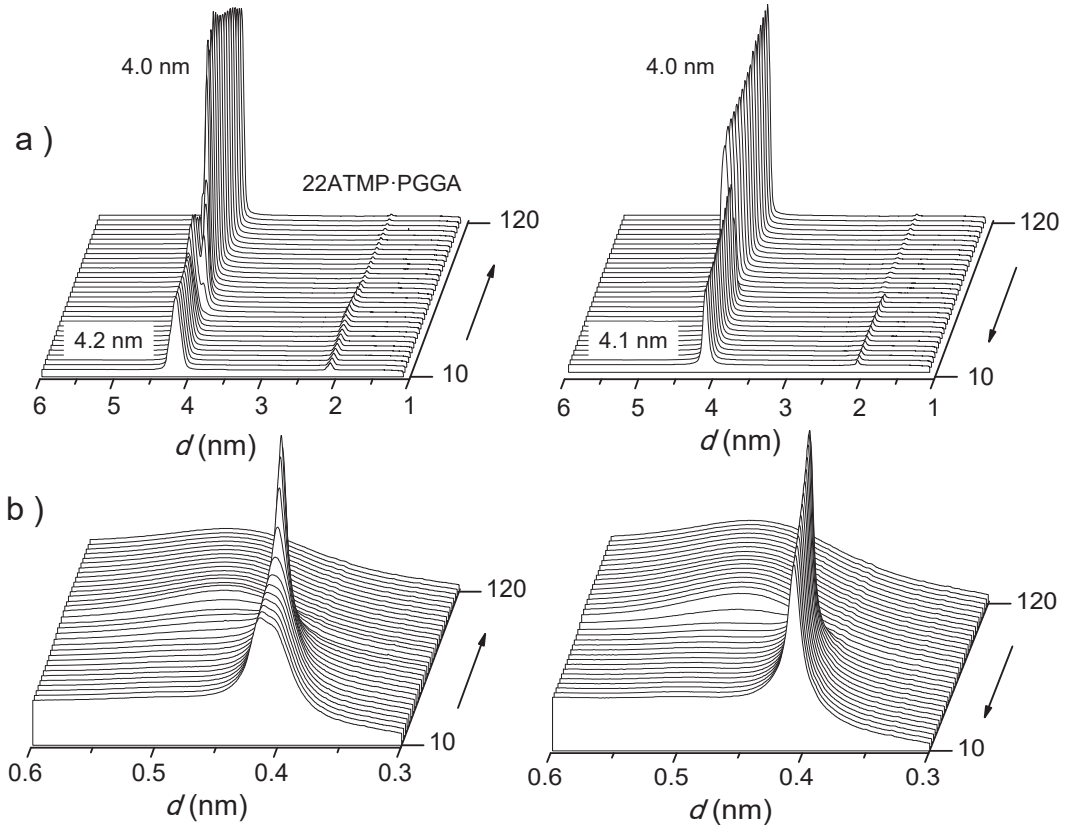

Figure 9. SAXS (a) and WAXS (b) profiles of 22ATMP·PGGA at heating (left) and cooling (right).

1.2.5. Dissociation of *n*ATMP·PGGA complexes in aqueous environment and antimicrobial activity

The ionic nature of the *n*ATMP·PGGA complexes make them to be in thermodynamic equilibrium with their ionic components when they are in an aqueous environment. The intrinsic extent of the equilibrium for the different members of the series will be mainly determined by both the water solubility of the trimethylalkylphosphonium cation and the ability of PGGA to be homogeneously mixed with water either by partial swelling of sequentially charged segments or even by solubilization of the whole chain after sufficient ionization. The dissociation of the complexes upon incubation in water was estimated by measuring the absorbance at 208 nm as a function of time and the profiles obtained for the whole series along a period of seven days at pH 7.0 and 5.0 are represented in Figure 10. It should be minded that both PGGA and the trimethylphosphonium cation are able to absorb at the applied wavelength so that the observed absorbance is due to the presence of the two ionic species. However, absorptivity has essentially the same value for the two species which prevents to determine by this method the ratio at which they are present in the solution. Nevertheless, a comparative inspection of the results allows to state that a)

Complex dissociation decreases with the length of the alkyl chain so that it becomes only significant for *n* values lower than 18. This is a much expected result given the strong dependence of surfactant solubility on *n*. b) For all complexes the amount of released ions is higher at pH 7.0 than at pH 5.0. This is a rather striking result since one could expect that a more protonated polyacid occurring at lower pH would facilitate the release of the organocation. However the ionization degrees at pH 5 and 7 of PGGA (pKa 2.27) are >99.9% and 99.9999% respectively so that the influence of ionization on the release of the surfactant at any of these two pH's may be considered negligible. Furthermore the visual inspection of the complex film after incubation revealed more apparent changes at pH 7 than at pH 5 (an illustrative picture has been included in the SI associated to this chaper). c) The maximum dissociation extent happens for 12ATMP·PGGA at pH 7.0 but the ionic concentration in water is smaller than 10% of the initial complex concentration.

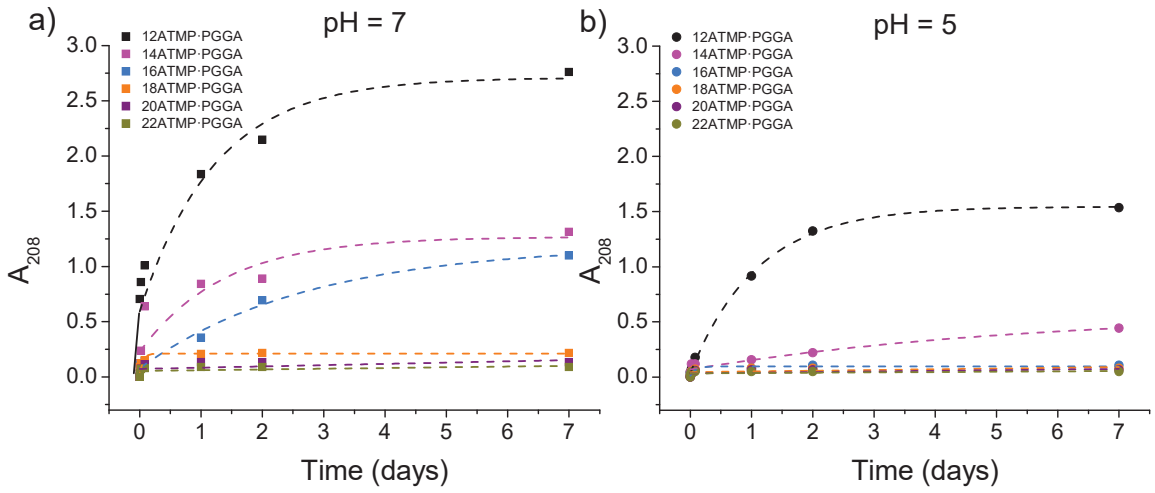

Figure 10. Dissociation of *n*ATMP·PGGA complexes in water at pH 7 (a) and 5 (b).

The biocide activity of organic quaternary salts is a well-known fact that has been widely reported and that is currently exploited for building a diversity of materials and formulations with bactericide or/and fungicide properties (Muñoz-Bonilla et al., 2012). Organophosphonium salts are particularly efficient in this regard and their use in the preparation of polymeric materials with biocide activity has been accomplished by different approaches that include blending, surface attachment or covalent incorporation into the polymer chain either in the backbone or as pending side groups (Kanazawa et al., Endo, 1993; Popa et al., 2011; Qiu et al., 2014; Xue et al., 2015). Given the capacity of the *n*ATMP·PGGA complexes to render consistent films suitable for coating or packaging, it was interesting to explore the antimicrobial activity of such films. For this preliminary study, two common bacteria, Gram-negative *E. coli* and

Gram-positive *S. aureus* at pH 5 and pH 7 were selected for the assays, and two methods differing in the way that the active agent contacts the bacteria were applied. The bacterial growth inhibition estimated by counting of the colonies along time either visually or by turbidimetry was taken as a measure of the biocide activity.

In the first method, the microorganism growth evolution with time was followed while the complex film was immersed in the bacteria suspension. Results obtained for the whole series and for neat PGGA are compared in Figure 11. Taken the control (assay carried out in absence of polymer) as reference it becomes evident that at the scale of time used, complexes for $n \geq 20$ and also PGGA are fully inactive under the two assayed pHs, and that 18ATMP·PGGA shows only weak activity against *E. coli* at pH 5. On the contrary, complexes for n = 12, 14 and 16 display a general strong antibacterial activity at pH 7 with almost total growth inhibition after 24 h of incubation except for the case of 16ATMP·PGGA that needed several days for a complete disappearance of the colonies. The activity of these complexes at pH 5.0 was in general lower than a pH 7.0 and much higher against *S. aureus*.

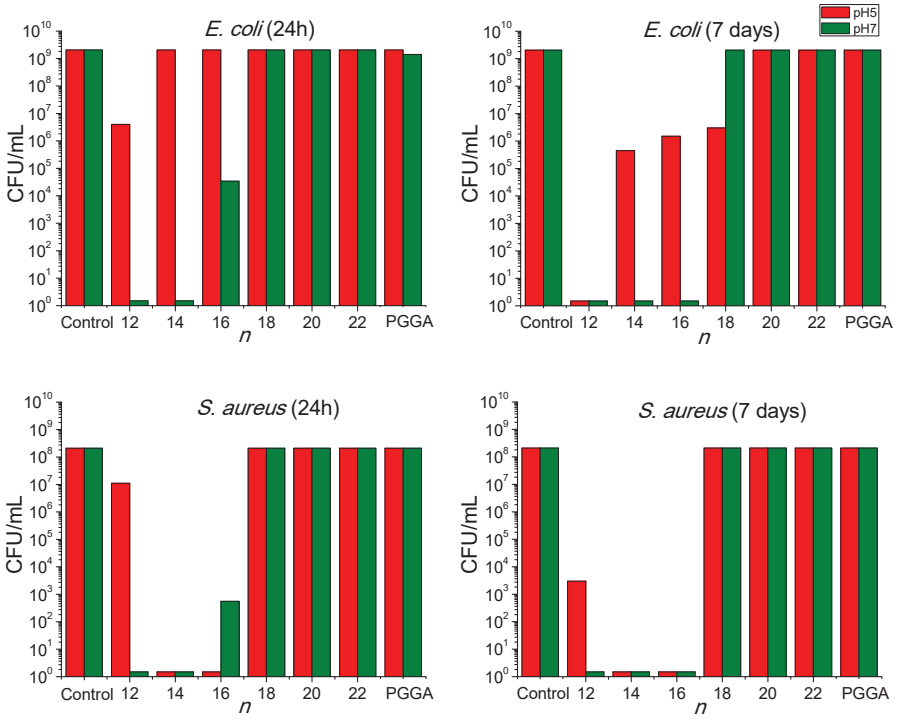

Figure 11. Bactericide activity against *E. coli* and *S. aureus* of *n*ATMP·PGGA films after incubation for 24 h and 7 days at the two indicated pHs. The antimicrobial effectiveness is expressed as the visually estimated concentration of colonies forming units.

The results obtained after application of the second method are shown in Figure 12. In this case, the direct contact of films with bacteria was avoided and the biocide activity was measured for the species leached from *n*ATMP·PGGA films to the

supernatant after incubation for five days. The resulting microbial activity was very similar to that obtained by the first method but the general behavior was even more systematic. The supernatants recovered from *n*ATMP·PGGA complexes with $n \leq 16$ were fully efficient in killing the bacteria so total inhibition was effective since the beginning. For $n = 20$ and 22, the curves were similar to those obtained for the control displaying the typical growth evolution in three or four phases, (lag, exponential, stationary and death), which indicates the total inactivity of these complexes against the two assayed bacterial species. The behavior displayed by 18ATMP·PGGA was somewhat erratic; in this case a strong antimicrobial activity was shown except when tested against *E. coli* at pH 5 which is in disagreement with results obtained in the former assay.

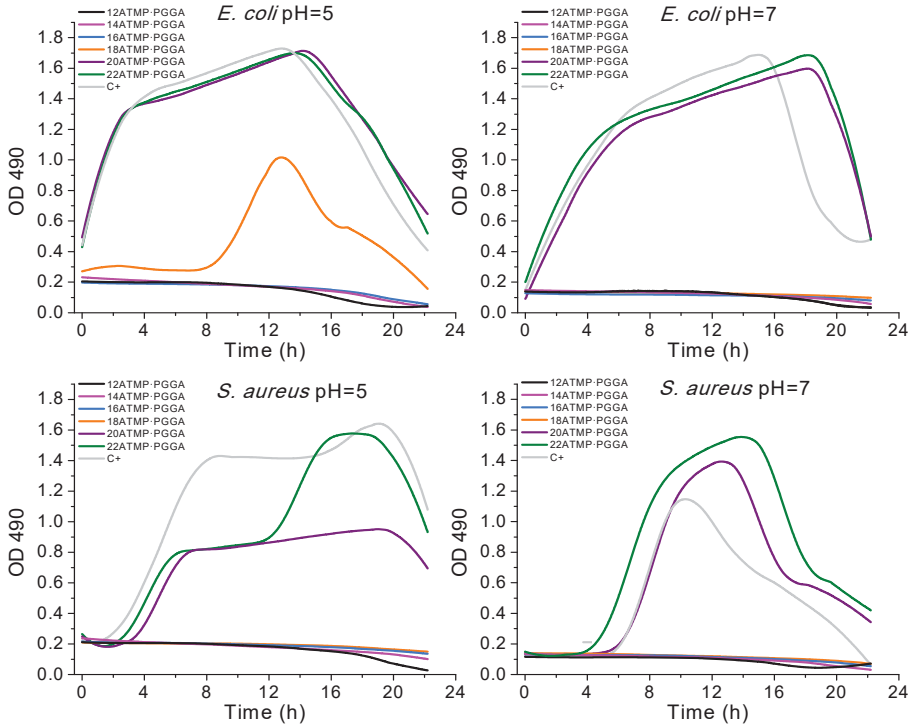

Figure 12. Bactericide activity of the supernatant recovered from *n*ATMP·PGGA films incubated for 5 days at the two indicated pHs. The antimicrobial activity was measured along 24 h and is expressed as the reduction in optical absorption at 490 nm.

The unquestionable conclusion that can be drawn from the results obtained from the biocide assays is that *n*ATMP·PGGA complexes with short alkyl side chains (n = 12, 14 and 16) display strong antimicrobial activity against both Gram-positive and Gram-negative bacteria. Such activity must be associated to the organophosphonium counterpart which is partially delivered to the aqueous environment upon incubation. It can be inferred therefore that the bactericide activity of *n*ATMP·PGGA complexes is

eventually determined by the water solubility of the surfactant implied in each case, and in less extent by the influence of incubation conditions on the stability of the complex.

1.3. Conclusions

Comb-like ionic complexes (*n*ATMP·PGGA) could be successfully prepared by mixing aqueous solutions of PGGA and alkyltrimethylphosphonium bromides with linear alkyl chains containing even numbers of carbon atoms ranging from 12 to 22. The ionic composition of the complexes was nearly stoichiometric with deviations being larger for longer alkyl chains. The complexes were non-soluble in water but readily soluble in organic solvents. These complexes based on organophosphonium cations displayed excellent thermal stability with onset decomposition temperatures near to 300 ºC, which are about 100 ºC higher than those reported for similar complexes made from alkyltrimethylammonium surfactants. *n*ATMP·PGGA complexes are arranged in a amphiphilic structure that follows the same biphasic layer pattern described for their ammonium analogs and displays a similar trend for the crystallization of the paraffinic phase. However, higher melting enthalpies were observed for these complexes indicating that a larger fraction of the polymethylene segment is able to crystallize when the alkyl chain is attached to the phosphorous atom. The response of the *n*ATMP·PGGA complexes to temperature changes consists of a reversible shortening of the layer periodicity in about 5% of the original value upon heating from the 10 to 120 ºC, which is exactly opposite to what happens in the ammonium complexes. Finally it has been evidenced that the *n*ATMP·PGGA with *n* = 12, 14 and 16 display strong bactericide activity as a consequence of the weak release of the alkyltrimethylphosphonium species that take place in such complexes when incubated in an aqueous environment. The combination of this property with the ability to form films by either hot-pressing or casting confers on these complexes potential for being used in active coating or packaging applications.

1.4. References

Akagi, T., Higashi, M., Kaneko, T., Kida, T., Akashi, M. (2006). Hydrolytic and enzymatic degradation of nanoparticles based on amphiphilic poly(γ-glutamic acid)-graft -*L*-phenylalanine copolymers. Biomacromolecules, 7(1), 297–303.

Antonietti, M., Conrad, J., Thünemann, A. (1994a). Polyelectrolyte-surfactant complexes: a new type of solid, mesomorphous materials. Macromolecules, 27(21), 6007–6011.

Broadhurst, M. G. (1962). An analysis of the solid phase behavior of the normal paraffins. Phys. Chem. 66A, No.3 (3), 241–249.

Gamarra, A., Urpí, L., Martínez de Ilarduya, A., Muñoz-Guerra, S. (2017). Crystalline structure and thermotropic behavior of alkyltrimethylphosphonium amphiphiles. Phys. Chem. Chem. Phys., 19, 4370-4382.

García-Álvarez, M., Álvarez, J., Alla, A., Martínez de Ilarduya, A., Herranz, C., Muñoz-Guerra, S. (2005). Comb-like ionic complexes of cationic surfactants with bacterial poly(γ-glutamic acid) of racemic composition. Macromol. Biosci. 5(1), 30–38.

Jordan, E. F., Feldeisen, D. W., Wrigley, A. N. (1971). Side-chain crystallinity. I. Heats of fusion and melting transitions on selected homopolymers having long side chains. J. Polym. Sci. Part A-1 Polym. Chem. 9(7), 1835–1851.

Kanazawa, A., Ikeda, T., Endo, T. (1993). Novel polycationic biocides. Synthesis and antibacterial activity of polymeric phosphonium salts. J. Polym. Sci. Part A Polym. Chem. 31(2), 335–343.

Kanazawa, A., Ikeda, T., Endo, T. (1994). Synthesis and antimicrobial activity of dimethyl- and trimethyl-substituted phosphonium salts with alkyl chains of various lengths. Antimicrob. Agents Chemother. 38(5), 945–952.

Kanazawa, A., Tsutsumi, O., Ikeda, T., Nagase, Y. (1997). Novel thermotropic liquid crystals without a rigid core formed by amphiphiles having phosphonium ions. J. Am. Chem. Soc. 119(33), 7670–7675.

Kubota, H., Nambu, Y., Endo, T. (1995). Convenient esterification of poly(γ-glutamic acid) produced by microorganism with alkyl halides and their thermal properties. J. Polym. Sci. Part A Polym. Chem. 33(1), 85–88.

Kubota, H., Fukuda, H., Takebe, H. (1992).Pat. Number US5118784. Meiji Seika Kabushiki Kaisha.

Kunioka, M., Furusawa, K. (1997). Poly(γ-glutamic acid) hydrogel prepared from microbial poly(γ-glutamic acid) and alkanediamine with water-soluble carbodiimide. J. Appl. Polym. Chem., 65(10), 1889–1896.

Morillo, M., Martínez de Ilarduya, A., Muñoz-Guerra, S. (2001). Comblike alkyl esters of biosynthetic poly (γ-glutamic acid). Synthesis and characterization. Macromolecules, 34(22), 7868–7875.

Muñoz-Bonilla, A., Fernández-García, M. (2012). Progress in polymer science polymeric materials with antimicrobial activity. Prog. Polym. Sci., 37, 281–339.

Muñoz-Guerra, S., García-Alvarez, M., Portilla-Arias, J. A. (2013). Chemical modification of microbial poly(γ-glutamic acid). J. Renew. Mater. 1(1), 42–60.

Pérez-Camero, G., García-Álvarez, M., Martínez de Ilarduya, A., Fernández, C., Campos, L., Muñoz-Guerra, S. (2004). Comblike complexes of bacterial poly(γ,D-glutamic acid) and cationic surfactants. Biomacromolecules, 5(1), 144–152.

Ponomarenko, E. A., Waddon, A. J., Tirrell, D. A., Macknight, W. J. (1996). Structure and properties of stoichiometric complexes formed by sodium poly (α,l -glutamate) and oppositely charged surfactants. Langmuir, 12(9), 2169–2172.

Popa, A., Crisan, M., Visa, A., Ilia, G. (2011). Effect of a phosphonium salt grafted on polymers on cucumber germination and initial growth. Braz. Arch. Biol. Technol. 54(1), 107–112.

Portilla-Arias, J. A., García-Alvarez, M., Martínez de Ilarduya, A., Muñoz-Guerra, S. (2007). Thermal decomposition of microbial poly(γ-glutamic acid) and poly(γ-glutamate)s. Polym. Degrad. Stab. 92(10), 1916–1924.

Qiu, T., Zeng, Q., Ao, N. (2014). Preparation and characterization of chlorinated nature rubber (CNR) based polymeric quaternary phosphonium salt bactericide. Mater. Lett. 122, 13-16.

Rydon, H. N. (1964). 260. Polypeptides. Part X. The optical rotatory dispersion of poly-γ-D-glutamic acid. J. Chem. Soc., 1328–1333.

Shah, D. T., McCarthy, S. P., Gross, R. A. (1995). γ-poly(glutamic acid) esters. Pat. Number US5378807-A. Univ Massachusetts Lowell (UMAC-C).

Tolentino, A., Alla, A., Martínez de Ilarduya, A., Muñoz-Guerra, S. (2011). Comb-like ionic complexes of pectinic and alginic acids with alkyltrimethylammonium surfactants. Carbohydr. Polym. 86(2), 484–490.

Tolentino, A., Alla, A., Muñoz-Guerra, S. (2012). Nanocomposites of comb-like ionic complexes of bacterial poly(glutamic acid) with nanoclays. Eur. Polym. J. 48(11), 1838–1845.

Tolentino, A., Alla, A., Martínez de Ilarduya, A., Muñoz-Guerra, S. (2013a). Comb-like ionic complexes of hyaluronic acid with alkyltrimethylammonium surfactants. Carbohydr. Polym. 92(1), 691–696.

Tolentino, A., León, S., Alla, A., Martínez de Ilarduya, A., Muñoz-Guerra, S. (2013b). Comblike ionic complexes of poly(γ-glutamic acid) and alkanoylcholines derived from fatty acids. Macromolecules, 46(4), 1607–1617.

Tolentino, A., Alla, A., Martínez de Ilarduya, A., Muñoz-Guerra, S. (2014). Complexes of polyglutamic acid and long-chain alkanoylcholines: nanoparticle formation and drug release. J. Biol. Macromol. 66, 346–353.

Xie, W., Xie, R., Pan, W. P., Hunter, D., Koene, B., Tan, L. S., Vaia, R. (2002). Thermal stability of quaternary phosphonium modified montmorillonites. Chem. Mater. 14(11), 4837–4845.

Xue, Y., Xiao, H., Zhang, Y. (2015). Antimicrobial polymeric materials with quaternary ammonium and phosphonium salts. Int. J. Mol. Sci. 16(2), 3626–3655.

Zanuy, D., Alemán, C., Muñoz-Guerra, S. (1998). On the helical conformation of un-ionized poly(γ-*D*-glutamic acid). Int. J. Biol. Macromol. 23(3), 175–184.

V.2. Nanocomposites of microbial polyglutamic acid and nanoclays compatibilized by organophosphonium surfactants

Abstract:

Ionic coupling of bacterial poly(γ-glutamic acid) (PGGA) with alkyltrimethylphosphonium surfactants has been reported to render comb-like PGGA complexes with a biphasic layered structure displaying periodicity at nanoscopic scale. In this work, nanocomposites made of PGGA and montmorillonite, and covering a wide variety of compositions, were prepared by using either dodecyl- or eicosyl-trimethylphosphonium surfactant as a third component with a double purpose, *i.e.* ionic complexation of PGGA and organo-modification of the nanoclay. TGA analysis ascertained the compositions of these three-component nanocomposites and evidenced their excellent thermal stability. The nanocomposite structure with PGGA and clay more or less intercalated according to composition and thermal history was evidenced by both XRD and TEM. Simultaneous thermal SAXS/WAXS analysis at real time revealed extensive intermixing of the two phases that became notably enhanced by heating treatment. Thermal transitions characteristic of the surfactant-PGGA complex were not significantly altered in the nanocomposites, but elastic moduli and strength to yield were found to increase proportionally to the content of clay.

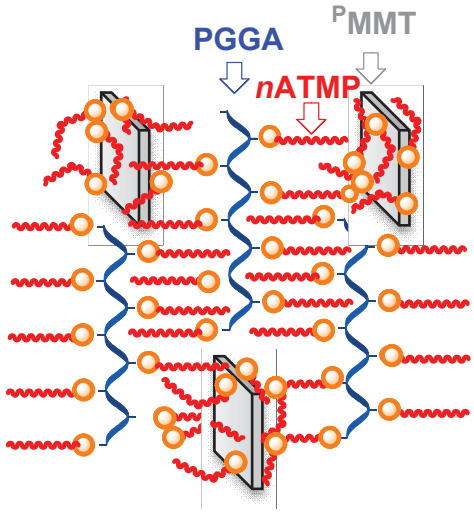

Publication derived from this work:

Gamarra, A., Muñoz-Guerra S., Urpí, L.; Galbis, E., Galbis, J.A. (2018). *Nanocomposites of microbial polyglutamic acid and nanoclays compatibilized by organophosphonium surfactants*. Macromol. Chem. Phys. doi.or/10.1002/mac0.201800083.

Supporting Information (SI) to this chapter in Annex B.2

2.1. Introduction

Poly(γ-glutamic acid) (PGGA or -PGA) is an emerging biopolymer of great interest because its multiple potential applications in the food, biomedical, healthcare and water-treatment fields (Bajaj et al., 2011; Gross, 1998). PGGA has been subjected to diverse chemical modifications with the main purpose of obtaining materials with better processing properties (Pérez-Camero et al., 2004). Coupling of PGGA with quaternary alkylammonium or alkylphosphonium surfactants leading to stoichiometric or nearly stoichiometric ionic complexes with a comb-like molecular architecture has been the approach chosen reiteratively by us for such purpose (Pérez-Camero et al., 2004; García-Álvarez et al., 2005; Gamarra et al., 2017). These complexes are well stable to heat, water-resistant, and soluble in organic compounds, but their mechanical properties need to be improved if they are intended to be used in active packaging or coating applications (Peelman et al., 2013). Addition of small amounts of nanoclays to a polymer is an attractive way of doing to improve its physical properties (Tjong, 2006; Mittal, 2009;). The efficacy of this technique is critically determined by the compatibility of the two components (Kim et al., 2005; Ahmad et al., 2009). Modification of either the polymer or the clay is the strategy commonly applied to improve compatibility and attaining therefore successful results (Panek et al., 2006; Ahmad et al., 2009). Ion-exchange of pristine clays with quaternary tetraalkylammonium salts is the method commonly preferred to render organoclays suitable for extensive intercalation with relatively hydrophobic polymers (Wu et al., 2008; Singla et al., 2012).

Several polyglutamic-based nanocomposites of different nature and prepared by different techniques have been reported in the recent literature. PGGA/silica nanocomposite with interest for bone regeneration (Poologasundarampillai et al., 2014) as well as POSS/gelatin-PGGA hydrogel with mechanical properties suitable for soft tissue engineering (Renò et al., 2013) are examples of hybrid materials made of PGGA that have been examined for their potential as biomaterials. Layered double hydroxides based nanocomposites of PGGA (Chiang et al., 2011) were successfully prepared by the anion exchange method. It has been demonstrated that the layered structure was preserved in these nanocomposites with barely changes concerning dehydration and contraction of the interlayer distances (Chiang et al., 2012). However, nanocomposites made of polyglutamic acid and laminar nanoclays are scarce. To our knowledge, nanocomposites made of PGGA and Cloisite 30B is the only case of nanocomposites based on laminar silicates that is found in the accessible literature (Tolentino et al., 2012, 2013). These nanocomposites were made of PGGA and Cloisite 30B with the polyacid previously coupled with alkyltrimethylammonium

surfactants (*n*ATMA) (Tolentino et al., 2012, 2013). *n*ATMA·PGGA·CL30B nanocomposites displayed improved mechanical properties, in particular for certain specific compositions at which an exfoliated structure seemed to be formed. The detailed structural study of these compounds carried out by combining XRD and TEM revealed that the polymer and the clay were homogeneously mixed for a wide range of compositions, and brought into evidence the successful role played by the *n*ATMA surfactant as compatibilizing agent.

In the present work we wish to report a study similar to that made of *n*ATMA·PGGA·CL30B but using montmorillonite instead of cloisite and alkyltrimethylphosphonium surfactants (*n*ATMP) for modification of both the polyacid and the nanoclay. The strategy followed for the preparation of these nanocomposites (*n*ATMP·PGGA·*X*(%)^{P}MMT is schemed in Figure 1. By applying this strategy, two series of nanocomposites differing in the length of the long alkyl group of ATMP, namely dodecyl and eicosyl, have been prepared for the full range of compositions and systematically examined with regard to their structure, thermal properties and mechanical behavior. Organophosphonium compounds are particularly convenient for building nanocomposites because, in addition to show noticeable biocide activity (Cieniecka-Rosłonkiewicz et al., 2005), their thermal stability is significantly higher than that of their ammonium analogues (Xie et al., 2002). To our knowledge, no study entailing the modification of the two components of the nanocomposite, the polymer and the clay, with a common agent has been reported so far.

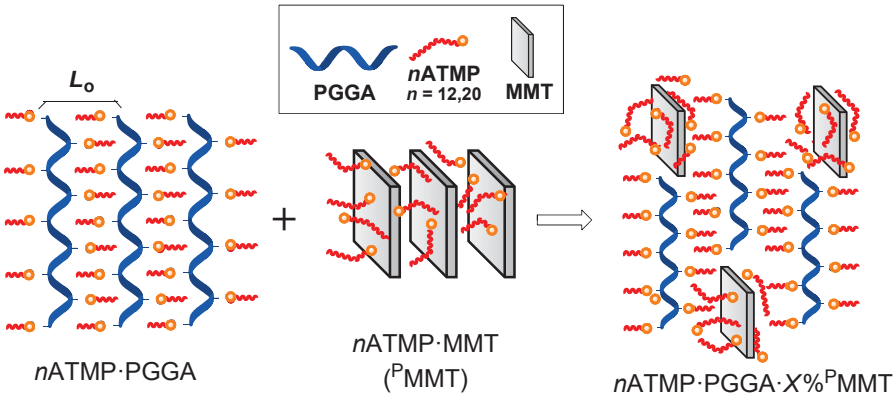

Figure 1. Strategy applied for the preparation of PGGA/MMT nanocomposites compatibilized by alkyltrimethylphosphonium surfactants. *n*ATMP: alkyltrimethyl phosphonium with number of carbon atoms *n* in the long alkyl chain being 12 or 20; PGGA: poly(γ-glutamic acid); MMT: pristine montmorillonite; ^{P}MMT: organophosphonium modified montmorillonite; *X*%: weight percent of ^{P}MMT in the nanocomposite.

2.2. Results and discussion

2.2.1. Alkyltrimethylphosphonium modified montmorillonites (^{P}MMT)

The replacement of sodium ions present in Na·MMT clay by alkyltrimethylphosphonium ions was successfully attained for the two surfactants used, *i.e.* 12ATMP and 20ATMP. The replacement was clearly evidenced by well perceivable changes taking place in the FTIR spectra, in particular those implying intensity variations of the characteristic C-H and C-P stretching bands at 2850-2950 cm^{-1} and 715 cm^{-1}, respectively. These spectra are provided in Figure SI-1 (in the supplementary information file linked to this chapter).

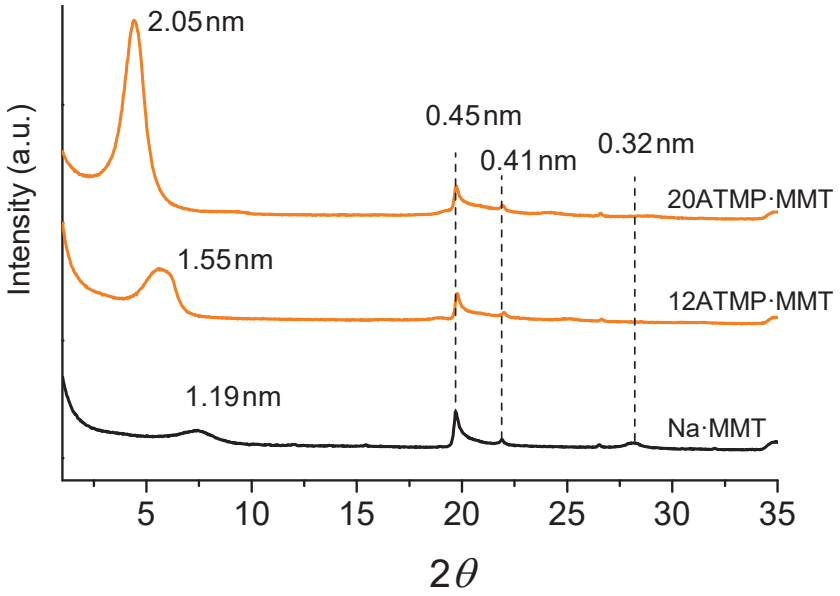

Figure 2. Powder XRD profiles of ^{P}MMT modified with 12ATMP and 20ATMP surfactants compared to that arising from the unmodified clay (Na·MMT).

The insertion of the organophosphonium ions in the clay galleries is expected to produce an enlargement of the interlayer spacing of the clay more or less proportional to the length of the alkyl group of the surfactant (Seyidoglu et al., 2015). The effect of such modification is clearly reflected in the X-ray diffraction profiles depicted in Figure 2. In fact the peak originally seen at 1.19 nm attributed to the layer periodicity of the clay moved up to 1.55 nm and 2.05 nm upon modification with 12ATMP and 20ATMP, respectively. It is worth noting that this peak not only increased in spacing but also in intensity and sharpness indicating that a greater electronic density fluctuation and interlayer spacing uniformity were attained in the nanoclay upon modification. On the other hand, the sharp 0.45 and 0.41 nm peaks arising from the clay crystal lattice remained unchanged in the modified montmorillonite indicating that the crystal structure of the aluminosilicate layer has been fully preserved.

The thermogravimetry analysis (TGA) of the ^{P}MMT not only provided information about the effect of modification on thermal stability but also allowed making an approximate estimation of the amount of surfactant incorporated in the clay. The TGA traces recorded under inert atmosphere from the montmorillonites before and after modification are depicted in Figure 3a where the traces for the 12ATMP·Br and 20ATMP·Br have been also included for comparison. The weight remaining after heating 12ATMP·MMT and 20ATMP·MMT at 800 ºC was 77% and 72% of the initial sample weight, respectively, whereas the weight lost by Na·MMT was only about 5%. The weight left by the surfactants subjected to the same treatment was almost negligible (about 1-2%). It can be inferred from these data that the loss of organic material in the pyrolysis of 12ATMP·MMT and 20ATMP·MMT was around 30% and 25%, respectively, in acceptable correspondence with which could be expected taking into account the difference in molecular weight of the two surfactants. According to these values, the molar contents of surfactant incorporated in the ^{P}MMT were calculated to be about $0.85 \cdot 10^{-3}$ and $0.77 \cdot 10^{-3}$ mol·g^{-1} for 12ATMP and 20ATMP respectively, which correspond to a replacement of sodium ions of about 60-70%.

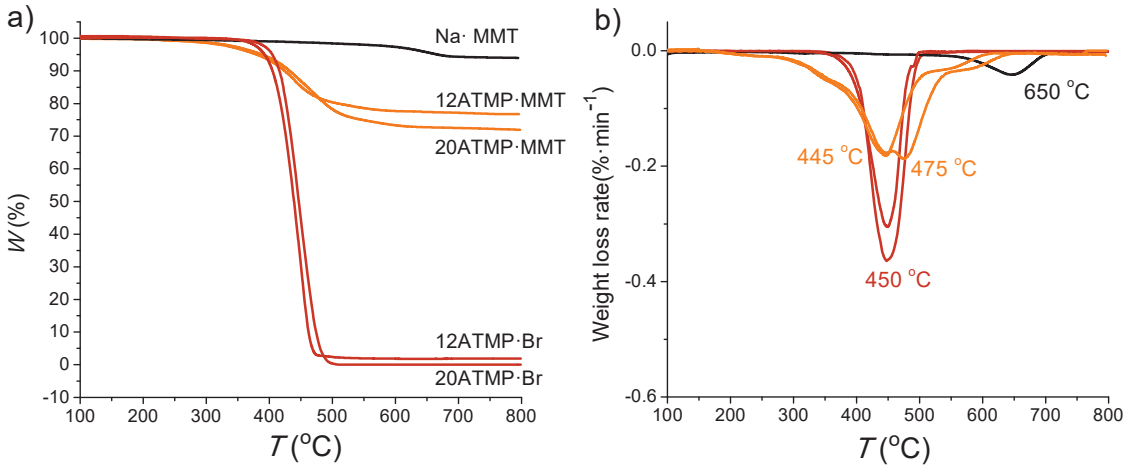

Figure 3. a) TGA traces of ^{P}MMT modified with 12ATMP·Br and 20ATMP·Br surfactants recorded under inert atmosphere. b) Derivative curves indicating temperatures at which decomposition takes place at maximum rate. Data for the *n*ATMP·Br surfactants with *n* = 12 and 20, and unmodified Na·MMT have been included for comparison.

The traces shown in Figure 3a also reveal that modification with alkyltrimethylphosphonium causes a decreasing of the resistance to heat of the montmorillonite with the onset decomposition temperature falling from above 600 ºC for Na·MMT to below 400 ºC for the ^{P}MMT. Such decay in thermal stability is obviously due to the sensitivity to heating of the organic counterpart which usually is unable to bear temperatures above 350 ºC. On the other hand, derivative TGA curves (Figure 3b) show that, at difference with Na·MMT, the mechanism operating in the decomposition of the modified montmorillonites consists of several steps with the

lowest temperature one taking place at 450 ºC, which is coincident with the temperature recorded for maximum rate decomposition of the surfactants. It should be remarked however that the depressing effect on the thermal resistance of the montmorillonite observed here is much less pronounced than in the case of modification made with analogue alkyltrimethylammonium compounds (Xie et al., 2001). The higher thermal resistance displayed by organophosphonium modified montmorillonites is a well-recognized merit of these systems that has been mentioned in several occasions (Patel et al., 2007).

2.2.2. Nanocomposites of PGGA and MMT compatibilized by *n*ATMP

According to the scheme depicted in Figure 1, firstly *n*ATMP·PGGA complexes were prepared by coupling of Na·PGGA with the corresponding *n*ATMP·Br. These complexes have been previously studied by us and characterized in great detail (Gamarra et al., 2017). The nanocomposites were prepared by mixing the chloroform solution of the complex with the corresponding ^{P}MMT suspended in the same solvent. Intercalation of PGGA and MMT is thus favored because the alkyltrimethylphosphonium cations not only neutralize the negative charges of both the polypeptide and the silicate, but also create hydrophobic interactions between the two phases. By this way, two series of nanocomposites, abbreviated *n*ATMP·PGGA·*X*%^{P}MMT, with *n* = 12 and 20, and covering a full range of PGGA/MMT compositions, were successfully prepared.

2.2.3. Thermal analysis of *n*ATMP·PGGA·X%PMMT nanocomposites

The TGA traces recorded for the two nanocomposite series (*n* = 12 and 20), including the two ^{P}MMT modified clays (*X*= 100%) as well as the two *n*ATMP·PGGA complexes (*X* = 0%), are compared in Figure 4, and the more relevant thermal decomposition parameters afforded by this analysis are listed in Table 1. TGA results indicated that decomposition of these nanocomposites induced by heating was found to proceed along two steps following a pattern similar to that displayed by the *n*ATMP·PGGA complexes (Gamarra et al., 2017).

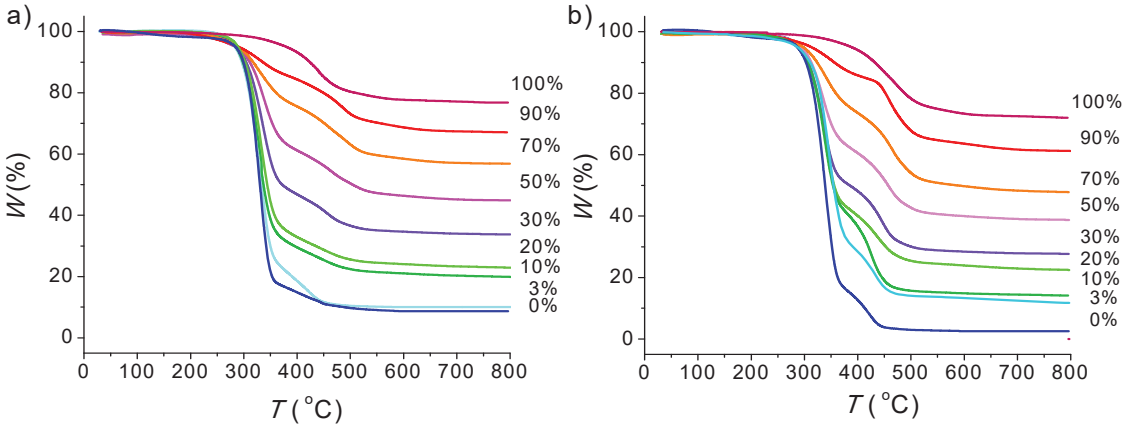

Figure 4. Compared TGA traces of the 12ATMP·PGGA·*X*%^{P}MMT series (a) and 20ATMP·PGGA·*X*%^{P}MMT series (b) recorded under inert atmosphere.

Table 1. Compositions and thermal parameters of *n*ATMP·PGGA·*X*%^{P}MMT composites.

*n*ATMP·PGGA·*X*%^{P}MMT			TGA[c]			DSC[d]		
X% [a]	*n*	*MMT*% [b]	$^{o}T_d$	$^{max}T_d$	W_{exp} (W_{calc})	$^{1}T_m$ (ΔH_m)	T_c (ΔH_c)	$^{2}T_m$ (ΔH_m)
0	12	0	284	331/423	9 (9)	-	-	-
	20	0	286	345/427	5 (5)	63 (5.8)	47 (-4.2)	62 (4.1)
3	12	2.3	286	330/422	12 (11.0)	-	-	-
	20	2.2	285	333/425	11 (7.1)	62 (5.7)	56 (-4.2)	60 (5.4)
10	12	7.7	286	330/424	17 (15.8)	-	-	-
	20	7.2	286	333/426	14 (11.7)	62 (5.5)	55 (-4.6)	59 (5.3)
20	12	15.4	286	330/435	23 (22.6)	-	-	-
	20	14.4	288	333/436	23 (18.4)	62 (5.7)	50 (-5.0)	60 (5.3)
30	12	23.1	286	329/442	34 (29.4)	-	-	-
	20	21.6	290	333/443	28 (25.1)	62 (5.9)	50 (-5.2)	60 (5.0)
50	12	38.5	287	329/450	44 (43.0)	-	-	-
	20	36.0	295	333/454	39 (38.5)	59 (5.9)	50 (-4.1)	60 (5.0)
70	12	53.9	290	332/460	57 (56.6)	-	-	-
	20	50.4	298	334/461	48 (51.9)	59 (6.0)	43 (-3.7)	57 (5.0)
90	12	69.3	295	347/490	67 (70.2)	-	-	-
	20	64.8	307	357/490	61 (65.3)	58 (6.1)	28 (-2.8)	52 (6.8)
100	12	77	380	445/560	77 (77.0)	-	-	-
	20	72	387	475/590	72 (72.0)	-	-	-

[a] Nominal content (%) in ^{P}MMT according to the used formulation.
[b] Content in MMT (%) in the nanocomposite calculated on the basis of its content in 12ATMP·MMT and 20ATMP·MMT as determined by TGA.
[c] $^{o}T_{d,5\%}$ and $^{max}T_d$: onset for 5% of weight loss and maximum rate decomposition temperatures in ºC. 1 and 2 refer to first and second decomposition step, respectively; *W*: remaining weight (%) at the end of the decomposition process. In parenthesis, the remaining weight calculated according to the nominal composition.
[d] T_m and T_c: Melting and crystallization temperatures in ºC; ΔH_m and ΔH_c: melting and crystallization enthalpies in kcal·mol^{-1}. 1 and 2 refer to first and second heating, respectively.

The onset temperature $^{o}T_d$ (5% of weight loss) and the two maximum rate decomposition temperatures $^{max}T_{d1}$ and $^{max}T_{d2}$ recorded for 12ATMP·PGGA·*X*%^{P}MMT and 20ATMP·PGGA·*X*%^{P}MMT are plotted against the content in ^{P}MMT in Figure 5a over the whole range of compositions. The three temperatures were observed to increase with the content in ^{P}MMT, very slightly for $^{o}T_d$ and $^{max}T_{d1}$ but much more noticeable for $^{max}T_{d2}$. It is worthy to compare these results with those found in the TGA analysis of the nanocomposites made of PGGA and Cloisite 30B with added alkyltrimethylammonium surfactants (Tolentino, Alla, Muñoz-Guerra, 2012). Both $^{o}T_d$ and $^{max}T_{d1}$ follow a similar trend in the two systems although values for the organophosphonium-based ones are about 100 ºC higher. Conversely, the evolution observed for $^{max}T_{d2}$ is opposite since it decreased with the increase of clay content in the organoammonium-based PGGA nanocomposites.

The mechanism of the thermal decomposition of *n*ATMA·PGGA complexes happening in the two first steps was studied in some detail and reported to consist of splitting of the ionic complex followed by cyclodepolymerization of PGGA (Portilla-Arias et al., 2007). Given the close similarities of the TGA results obtained for the two systems, a similar mechanism could be reasonably assumed to operate not only in *n*ATMP·PGGA complexes but also in nanocomposites in the earlier degradation stages. On the contrary, the notable divergence found for $^{max}T_{d2}$ is not easily explainable since the large number of reactions happening at high temperature makes difficult to rationalize the information collected for this step. On the other hand, the weight lost by nanocomposites after being heated at 800 ºC is plotted in Figure 5b against their ^{P}MMT content, and compared to the content of organics calculated for each composition. An excellent correlation between experimental and calculated values was found for the two series.

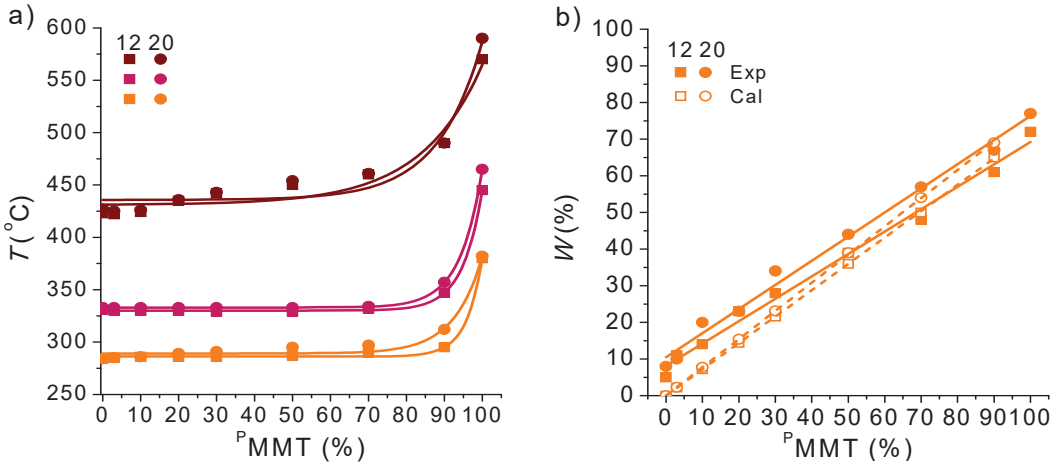

Figure 5. Plots of TGA data recorded for 12ATMP·PGGA·*X*%^{P}MMT and 20ATMP·PGGA·*X*%^{P}MMT series. Evolution of onset and maximum rate decomposition temperatures (a), and remaining weights (b) with nanocomposite composition.

The thermal behavior of nanocomposites regarding melting-crystallization was examined by DSC. It is known that *n*ATMP·PGGA complexes display crystallinity only for *n* = 16, 18, 20 and 22, which is associated to the ordered close packing adopted by the polymethylene chains (Gamarra et al., 2017). Accordingly, the DSC analysis of 12ATMP·PGGA·*X*%^{P}MMT nanocomposites did not show melting for whichever composition due to the unability of dodecyl chains to crystallize. On the contrary, the DSC analysis of the 20ATMP·PGGA·*X*%^{P}MMT series showed melting peaks indicative of the presence of crystallinity for all compositions. The DSC traces recorded at heating from previously melted samples are depicted in Figure 6a. A well-defined endotherm, which is interpreted to arise from melting of the crystal phase made of eicosyl chains, was observed at temperatures close to ~60 ºC with the peak area steadily decreasing with the content in ^{P}MMT. Melting temperatures and enthalpies measured for the whole series are listed in Table 1 and in Figure 6b, the peak enthalpy expressed as both J·g^{-1} and kcal·mol^{-1}, is plotted against the nominal content in ^{P}MMT.

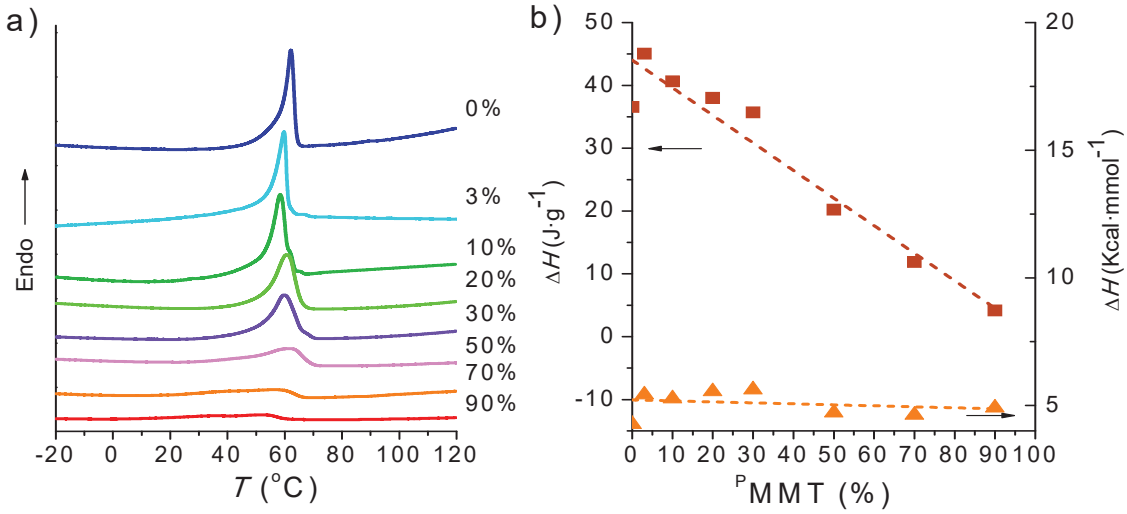

Figure 6. a) Second heating traces of 20ATMP·PGGA·*X*%^{P}MMT composites for the indicated compositions in ^{P}MMT. b) Melting enthalpy measured for the whole series and expressed on both weight-basis and mole-basis.

ΔH decreased almost linearly with composition when referred to sample weight but it stayed almost constant when it was expressed on the molar basis. It can be concluded therefore that the effect of the clay on the genuine crystallinity of the complex was practically negligible, and that the eicosyl chains belonging to the *n*ATMP used for clay modification are non-crystallized in the nanocomposite, *i.e*. the crystallinity observed in the nanocomposite is exclusively associated to the alkyl chains of the *n*ATMP coupled with PGGA.

2.2.4. Stress-strain behavior

The effect of composition on the stress-strain behavior of the *n*ATMP·PGGA·*X*%^{P}MMT nanocomposites is shown in Figure 7, and values measured for the characteristic mechanical parameters are accessible in Table SI-1 of the SI file. As it should be expected from the non-crystallized state of the dodecyl chains, the tensile behavior displayed by 12ATMP·PGGA complex is typical of a rubber with elastic modulus (E) and stress to yield (σ) showing values about 2 MPa and 0.2 MPa, respectively. These parameters are significantly higher (about 16 MPa and 0.8 MPa) for the 20ATMP·PGGA due to the crystallinity present in this complex provided by the crystallization of the paraffinic phase. In both cases, the material is susceptible to be stretched in a large extension without requiring much additional stress. The effect of the presence of ^{P}MMT was found to be essentially the same in the two nanocomposite series. Both E and σ increased almost steadily with the content in ^{P}MMT to reach finally one or two orders higher when X exceeded 50%. Such changes evidenced the strong positive influence of the clay on the stiffness and strength of the material. On the contrary, the effect on elongation was in overall to diminish the ductility of the original complex as it is known to usually happen in nanoclay-based polymer nanocomposites (Tjong, 2006). This effect was found to be much more apparent in the case of the 20ATMP·PGGA *X*%^{P}MMT where the elongation to break fell down from about 1500% in the complex to about 2% in the composite containing 70% of ^{P}MMT. As a result of such embrittling effect, nanocomposites with contents in ^{P}MMT higher than 50% were found to be unsuitable for stress-strain testing.

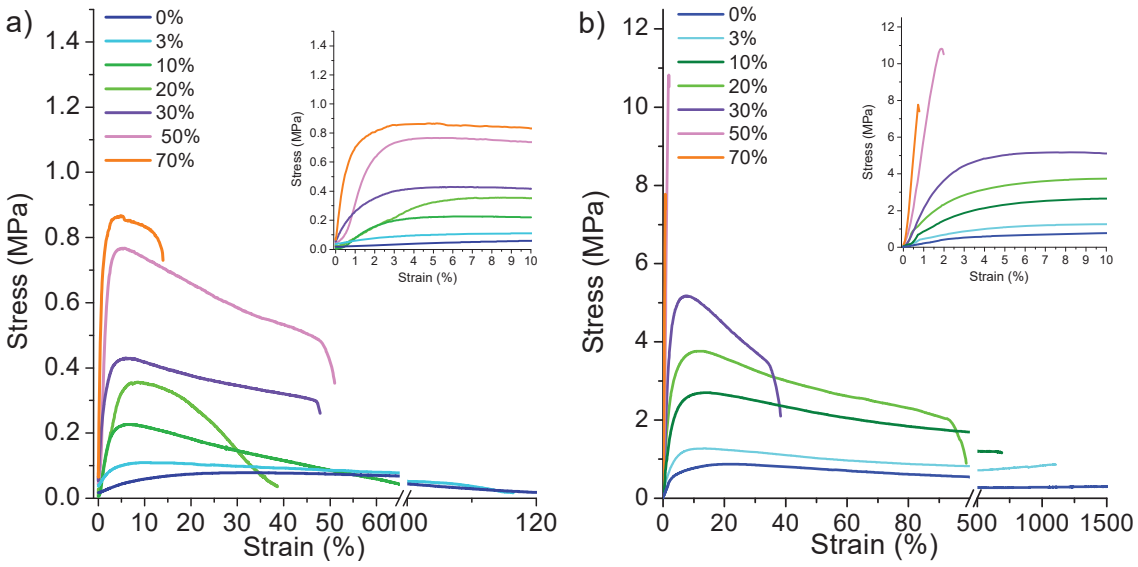

Figure 7. Stress–strain plots of 12ATMP·PGGA·*X*%^{P}MMT (a) and 20ATMP·PGGA·*X*%^{P}MMT (b) nanocomposite series. Insets: region of low deformation (up to 10%) showing clearly the steady increasing of the elastic modulus with the content in ^{P}MMT.

2.2.5. Structural analysis by XRD and TEM

The XRD profiles registered for the whole series of *n*ATMP·PGGA·*X*%^{P}MMT, including both the pristine complexes and the modified montmorillonites ^{P}MMT, for *n* = 12 and 20, are compared in Figures 8. SAXS providing information on the interlayer distance of the nanocomposites for different compositions are presented in Figure 8a and 8b. The sharp peak observed at 3.2 nm (*n* = 12) or 3.9 nm (*n* = 20) is known to arise from the long spacing characteristic of the complex (Gamarra et al., 2017). The evolution of this peak with the content in ^{P}MMT follows a similar pattern in the two series, *i.e*. it broadens and moves upwards to finally disappears. These changes are consistent with the occurrence of intercalated hybrid structures in which the interlayer distance increases in fluctuation and spacing with increasing content of clay.

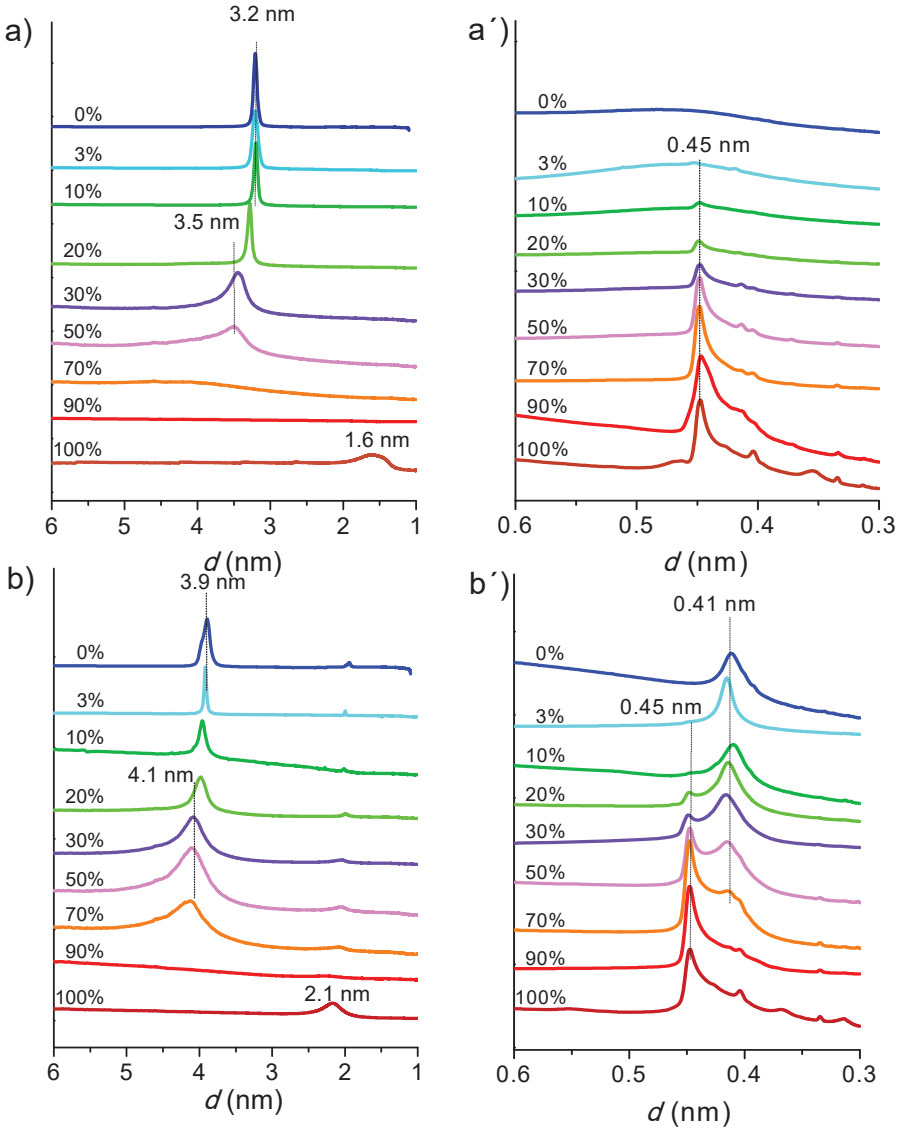

Figure 8. Compared XRD profiles recorded at 25 ºC for 12ATMP·PGGA·*X*%^{P}MMT series (a, a‘) and 20ATMP·PGGA·*X*%^{P}MMT series (b,b‘). SAXS (a,b) and WAXS (a‘,b‘).

On the other hand, the peak characteristic of ^{P}MMT observed at 1.6 nm (*n* = 12) or 2.1 nm (*n* = 20) became undetectable as soon as the presence of the complex reached 10-20%. The fact that the characteristic peaks of the complex and ^{P}MMT were not simultaneously observed in any profile is taken as indicative of the compatibility of the two components over the whole range of compositions.

The WAXS profiles shown in Figure 8a‘ and 8b‘ are clearly different for the two composite series as it should be expected from the different alkyl length present in each case. No discrete scattering was observed for the 12ATMP·PGGA complex whereas a rather sharp peak at 0.41 nm caracteristic of the crystallized paraffinic phase is conspicuous in the profile of 20ATMP·PGGA. This peak is arising from the crystallized paraffinic phase made of eicosyl chains and is clearly detectable in nanocomposites with contents in ^{P}MMT up to around 50%. On the other hand, the 0.45 nm peak arising from the aluminosilicate crystal structure was observed for the two series up to contents in ^{P}MMT so low as 10%. These observations are in full agreement with the results obtained by DSC and support the above conclusion stating that the crystallinity of the paraffinic phase initially present in the complex becomes preserved in the nanocomposites.

Samples of 20ATMP·PGGA·*X*%^{P}MMT were examined by TEM in order to have a direct view of the nanomorphology of these nanocomposites. Ultrathin sections were cut from thin films at either room temperature or at -80 ºC and observed either unstained or stained with uranyl acetate. Low magnification images showed a good dispersion of the clay in the nanocomposite whereas high magnification images revealed the presence of the layered structure characteristic of these compounds (Figures SI-2 and SI-3 in the SI file).

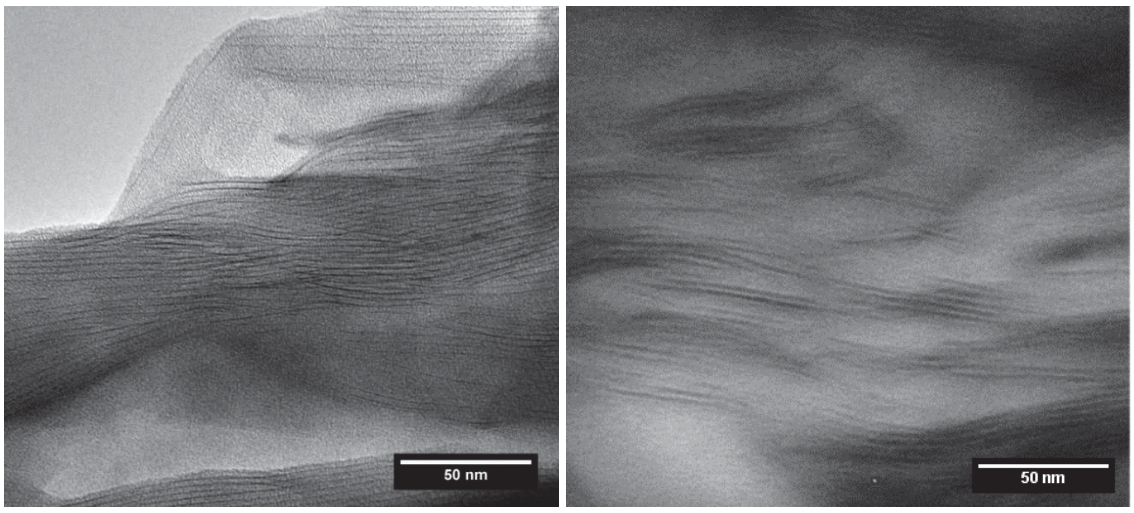

Figure 9. TEM images of 20ATMP·PGGA·50%^{P}MMT (a) and 20ATMP·PGGA ·30%^{P}MMT.

However the simultaneous observation of the complex and the clay with good definition is not feasible due to contrast effects and only faint images clearly displaying the presence of the two phases became available after staining with uranyl acetate (Figure SI-4 in the SI file). The observation of the stratified structure showing the clay layers separated by distances fluctuating between 3 and 5 nm, which is consistent with data collected by XRD are clearly visible in images taken from unstained sections at high magnification (Figure 9).

2.2.6. Thermal effects on the nanocomposite structure

*n*ATMP·PGGA complexes are known to display well defined phase transitions that take place reversibly when they are heated at rather low temperatures, *i.e*. between 30 and 80 ºC depending on *n*. To see if this behavior is retained in the *n*ATMP·PGGA·*X*%^{P}MMT nanocomposites, a variable temperature XRD analysis of a selection of these compounds was performed at real time using synchrotron radiation. Both SAXS and WAXS profiles were registered in parallel from samples subjected to heating and cooling over the 10-120 ºC range at a rate of 10 ºC·min^{-1}. The results obtained from 20ATMP·PGGA·50%^{P}MMT, which can be taken as representative of the whole family, are shown in Figure 10.

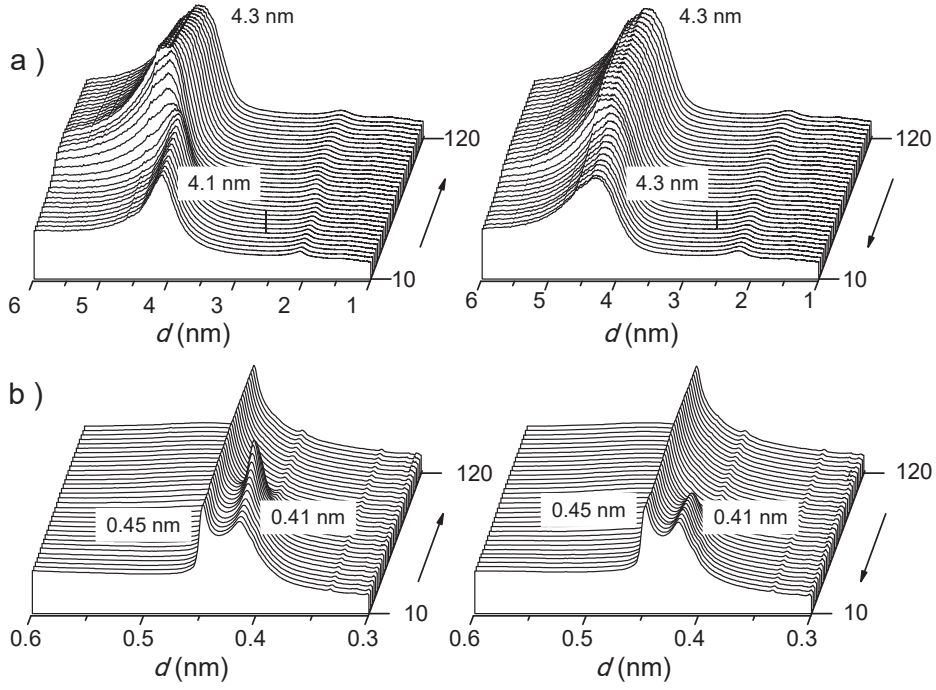

Figure 10. Evolution of SAXS (a) and WAXS (b) profiles of 20ATMP·PGGA·50%^{P}MMT at heating (left) and cooling (right) within the indicated range of temperatures.

As it is seen in the SAXS plot of Figure 10a, the characteristic long spacing peak of 20ATMP·PGGA·50%^{P}MMT appearing at 4.1 nm remained unaltered upon heating until temperature reached 50-60 ºC where it broadened and moved up to 4.3 nm. This

pattern remained unchanged on further heating up to 120 ºC and after cooling to room temperature. The evolution of the scattering produced by 20ATMP·PGGA·50%^{P}MMT within the wide angle region as a function of temperature is shown in Figure 10b. The 0.41 nm and 0.45 nm peaks present on the initial profile, which arise from the crystalline subphases of the complex and the clay respectively, were fully recovered at the end of the applied heating/cooling cycle.

Note that the 0.45 nm peak remained unchanged throughout the whole treatment as it is expected from the integrity of the aluminosilicate crystal over the applied temperature range.On the contrary the 0.41 nm peak arising from the paraphinic phase of the complex vanished upon heating at 50-60 ºC to reappear after cooling with the same initial features. It is well known that this peak corresponds to the basic interplanarspacing of the crystal lattice (monoclinic or hexagonal)(Broadhurst, 1962) adopted by the eicosyl chains. The behavior pattern displayed by this peak is in agreement with the occurrence of a melting-crystallization process taking place in the nanocomposite with similar characteristics as that known to occur in the neat complex. Similar analyses of 20ATMP·PGGA·*X*%^{P}MMT and 12ATMP·PGGA·*X*%PMMT were carried out for all the other compositions. The behavior observed was in all cases consistent with that described above and in agreement with what could be expected from the values of *n* and *X* of each nanocomposite (see Figures SI-5 to S-I-10 in the SI file).

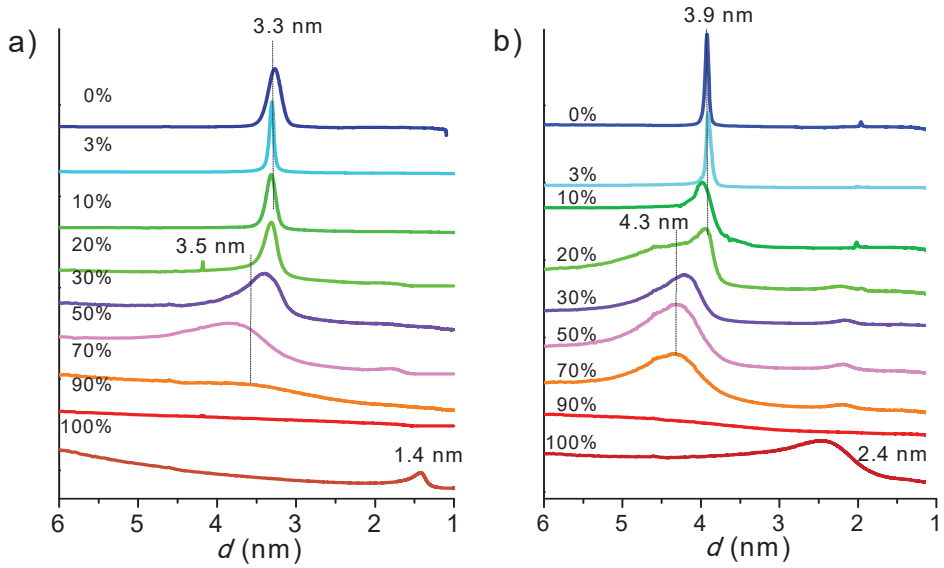

Figure 11. Compared SAXS profiles of the 12ATMP·PGGA·*X*%^{P}MMT (a) and 20ATMP·PGGA·*X*%^{P}MMT (b) series recorded at 25 ºC after being subjected to the heating/cooling cycle.

The effect of heating on the structure of nanocomposites can be readily appraised by the changes produced in the SAXS profiles recorded after the heating treatment, which can be readily made by comparing Figure 11 with Figure 8. Noticeable

differences concerning both position and width of the peaks located in the ~3-4 nm region are apparent between the plots contained in the two figures for each pair of *n* and *X* values. After the heating treatment, peaks moved to lower Bragg angles and spread over a much wider interval to the point that it disappeared completely for contents in ^{P}MMT above 70%. The increasing and broadening of the interlayer spacings taking place irreversibly by heating is interpreted to be a consequence of the improved mixing of the polypeptidic and clay phases. The thickening of the layered structure by heating effect could be ascertained by TEM (Figure SI-11 in the SI file) as an increasing of the interlayer spacing taking place in sections that were heated at 100 ºC during 2 hours previous to observation. Apparently, the main entropically-driven mixing process is kinetically activated at high temperatures because the alkyl chains surfactant attached to both PGGA and MMT attain greater mobility and are able to improve the compatibility of the two phases with greater efficiency.

2.3. Conclusions

Montmorillonite clay has been successfully modified using alkyltrimethylphosphonium surfactants bearing alkyl chains with *n* = 12 and 20 carbon atoms. Organoclays with notably widened galleries and stable up to temperatures near to 300 ºC were prepared. Mixing of the modified montmorillonites with PGGA previously ionically coupled with the same surfactants allowed the preparation of homogeneous nanocomposites over the whole range of compositions. XRD and TEM evidenced the occurrence of extensive intercalation of the two components. The thermal behavior characteristic of the surfactant-PGGA complexes was retained in the nanocomposites which showed increasing of the long interlayer spacing in all cases and only reversible melting-crystallization for *n* = 20. Furthermore the degree of intercalation could be further increased by heating treatment. Elastic modulus and strength of the PGGA complex were notably enhanced by the presence of the organoclay although their ductility was drastically reduced. It is finally concluded that the efficient mixing of the clay with the polypeptide was feasible due to the compatibilizing effect of the alkyltrimethylphosphonium surfactants used for both complexation of PGGA and modification of the nanoclay.

2.4. References

Ahmad, M. B., Hoidy, W. H., Nor Azowa, B. I., Al-Mulla, E. A. J. (2009). Modification of montmorillonite by new surfactants. J. Eng. Appl. Sci. 4(3), 184–188.

Bajaj, I., Singhal, R. (2011). Poly (glutamic acid) – An emerging biopolymer of commercial interest. Bioresour. Technol. 102(10), 5551–5561.

Broadhurst, M. G. (1962). An analysis of the solid phase behavior of the normal paraffins. Phys. Chem. 66A, No.3(3), 241–249.

Chiang, M.F., Chen, E. C., Wu, T.M. (2012). Preparation, mechanical properties and thermal stability of poly(l-lactide)/γ-polyglutamate-modified layered double hydroxide nanocomposites. Polym. Degrad. Stab. 97(6), 995–1001.

Chiang, M.F., Wu, T. M. (2011). Intercalation of γ-PGA in Mg/Al layered double hydroxides: An in situ WAXD and FTIR investigation. Appl. Clay Sci. 51(3), 330–334.

Cieniecka-Rosłonkiewicz, A., Pernak, J., Kubis-Feder, J., Ramani, A., Robertson, A. J., Seddon, K. R. (2005). Synthesis, anti-microbial activities and anti-electrostatic properties of phosphonium-based ionic liquids. Green Chem. 7(12), 855–862.

Gamarra, A., Martínez de Ilarduya, A., Vives, M., Morató, J., Muñoz-Guerra, S. (2017). Ionic complexes of poly(γ-glutamic acid) with alkyltrimethylphosphonium surfactants. Polymer, 116, 43–54.

García-Álvarez, M., Álvarez, J., Alla, A., Martínez de Ilarduya, A., Herranz, C., Muñoz-Guerra, S. (2005). Comb-like ionic complexes of cationic surfactants with bacterial poly(γ-glutamic acid) of racemic composition. Macromol. Biosci. 5(1), 30–38.

Gross, R. A. (1998). Biopolymers from renewable resources. Springer.

Kim, Y., White, J. L. (2005). Formation of polymer nanocomposites with various organoclays. J. Appl. Polym. Sci. 96(5), 1888–1896.

Mittal, V. (2009). Polymer Layered Silicate Nanocomposites: A Review. Materials, 2(3), 992–1057.

Panek, G., Schleidt, S., Mao, Q., Wolkenhauer, M., Spiess, H. W., Jeschke, G. (2006). Heterogeneity of the surfactant layer in organically modified silicates and polymer/layered silicate composites. Macromolecules, 39, 2191–2200.

Patel, H. A., Somani, R. S., Bajaj, H. C., Jasra, R. V. (2007). Preparation and characterization of phosphonium montmorillonite with enhanced thermal stability. Applied Clay Science, 35, 194–200.

Peelman, N., Ragaert, P., De Meulenaer, B., Adons, D., Peeters, R., Cardon, L., Van Impe, F, D. F. (2013). Application of bioplastics for food packaging. Trends Food Sci. Technol. 32(2), 128–141.

Pérez-Camero, G., García-Álvarez, M., Martínez de Ilarduya, A., Fernández, C., Campos, L., Muñoz-Guerra, S. (2004). Comblike complexes of bacterial poly(γ,D-glutamic acid) and cationic surfactants. Biomacromolecules, 5(1), 144–152.

Poologasundarampillai, G., Yu, B., Tsigkou, O., Wang, D., Romer, F., Bhakhri, V., Jones, J. R. (2014). Poly(γ-glutamic acid)/silica hybrids with calcium incorporated in the silica network by use of a calcium alkoxide precursor. Chem. - Eur. J. 20(26), 8149–8160.

Portilla-Arias, J. A., García-Alvarez, M., Martínez de Ilarduya, A., Muñoz-Guerra, S. (2007). Thermal decomposition of microbial poly(γ-glutamic acid) and poly(γ-glutamate)s. Polym. Degrad. Stab. 92(10), 1916–1924.

Renò, F., Carniato, F., Rizzi, M., Marchese, L., Laus, M., Antonioli, D. (2013). POSS/gelatin-polyglutamic acid hydrogel composites: Preparation, biological and mechanical characterization. J. Appl. Polym. Sci. 129(2), 699–706.

Seyidoglu, T., Yilmazer, U. (2015). Modification and characterization of bentonite with quaternary ammonium and phosphonium salts and its use in polypropylene nanocomposites. J. Thermoplast. Compos. Mater. 28(1), 86–110.

Singla, P., Mehta, R., Upadhyay, S. N. (2012). Clay Modification by the Use of Organic Cations. Green Sustainable Chem. 2, 21–25.

Tjong, S. C. (2006). Structural and mechanical properties of polymer nanocomposites. Mater. Sci. Eng., R. 53(3), 73–197.

Tolentino, A., Alla, A., Muñoz-Guerra, S. (2012). Nanocomposites of comb-like ionic complexes of bacterial poly(glutamic acid) with nanoclays. Eur. Polym. J. 48(11), 1838–1845.

Tolentino, A., León, S., Alla, A., Martínez De Ilarduya, A., Muñoz-Guerra, S. (2013). The structure of poly(γ-glutamic acid)/nanoclay hybrids compatibilized by alkylammonium surfactants. Eur. Polym. J., 49(9), 2596–2609.

Wu, T., Xie, T., Yang, G. (2008). Preparation of exfoliated polyacrylic clay nanocomposites with high loading : an investigation into the intercalation of ammonium-terminated polyacrylic acid and polyacrylates. J. Polym. Sci. Part B Polym. Phys. 46(21) 2335–2340.

Xie, W., Gao, Z., Pan, W. P., Hunter, D., Singh, a., Vaia, R. (2001). Thermal degradation chemistry of alkyl quaternary ammonium Montmorillonite. Chem. Mater. 13(9), 2979–2990.

Xie, W., Xie, R., Pan, W. P., Hunter, D., Koene, B., Tan, L. S., Vaia, R. (2002). Thermal stability of quaternary phosphonium modified montmorillonites. Chem. Mater. 14(11), 4837–4845.

Chapter VI. Ionic complexes of hyaluronic acid and phosphonium surfactants

Hyaluronic acid (HyA) is a linear polysaccharide ubiquitous in the human body. Its potential properties including high capacity for holding water, high viscoelasticity, its inherent biocompatibility and biodegradability, make HyA a suitable biomaterial for medical and pharmaceutical applications. Nevertheless, hyaluronic acid is highly soluble at room temperature and has a high rate of elimination and turnover. Therefore, the chemical modification and crosslinking of HyA is necessary for fitting the properties of each application. In this sense, coupling of HyA with cationic surfactants has been widely reported to give rise stable comb-like systems able to self-assemble in amphiphilic structures. These structures are made of two phases, one paraffinic and the other that alternate in layers with a periodicity of several nanometers. The nanoscopic dimensions of such structures are able to respond reversibly to thermal effects. Consequently, this new HyA derivatives are potentially useful to design medical devices with transport activity.

In this chapter tetraalkylphosphonium salts (*n*ATMP, *n*= 12,14,16,18,20,22) have been coupled to HyA to generate stable ionic complexes (*n*ATMP·HyA NPs) with a comb-like architecture and characterize them. The study is parallel to that recently published by us on the ionic complexes of HyA with alkyltrimethylammonium bromide salts (*n*ATMA) with the purpose of evaluating the advantages and disadvantages that derive from the replacement of organoammonium by organophosphonium counter ion in the building of the complexes. As mention before, tetraalkylphosphonium compounds are known to be much more resistant to temperature than their ammonium analogs and to display stronger biocide activity. Therefore, these ionic complexes are expected to have higher thermal stability and antimicrobial properties compared to those made by *n*ATMA salts. Accordingly coupling salts to HyA is a good way to ensure that HyA have antimicrobial properties because despite knowing that HyA is able to exert bacteriostatic, the biocide effect of this polysaccharide is not clear and seems to depend on the molecular weight and concentration.

In the second part of the chapter, the nanoparticle preparation of *n*ATMP·HyA NPs, was carried out. It is known that ionic complexes are able to form nanoparticles of adequate flowing stability in aqueous environments and controlled degradability due to their amphiphillicity. Ionotropic gelation technique was used to prepare *n*ATMP·HyA NPs with different sizes (n=16, 18 and 22) and morphologies. This methodology is a simple procedure in which NPs are obtained without adding additives. These NPs are

also expected to have antimicrobial properties and so the advantages of these materials to target bacteria as an alternative to antibiotics. Between the main advantages of antimicrobial NPs are i) their broad-spectrum antibacterial properties against both Gram-positive and Gram-negative bacteria; ii) their direct contact with bacterial cell wall without the need to penetrate it to kill the micrroorganims; iii) their high effectively because,,as their size is in the nanometer scale, they offer the possibility of increasing the local NPs concentration.

VI.1. Amphiphilic ionic complexes of hyaluronic acid with organophosphonium compounds and their antimicrobial activity

Abstract:

Amphiphilic ionic complexes of hyaluronic acid and alkyltrimethylphosphonium soaps with alkyl chains containing even numbers of carbons from 12 to 22 have been produced. The complexes have a nearly stoichiometric composition, are non-water soluble, and are stable to heat up to temperatures of above 200 ºC. They adopt amphiphilic structures with the paraffinic and the polysaccharide phases separated in ordered nanometric arrangements with periodicities ranging between 3 and 5 nm depending on *n.* The paraffinic phase in complexes with $n \geq 18$ was crystallized and showed melting at temperatures between 58 and 70 ºC. The complexes decomposed upon incubation in water under physiological conditions, and undergone extensive biodegradation by the action of hyaluronases. Biocide assays carried out in both solid and liquid media demonstrated a high antimicrobial activity of the complexes against Gram-positive *S. aureus* but only moderate against Gram-negative *E. coli* and *C. albicans* fungi.

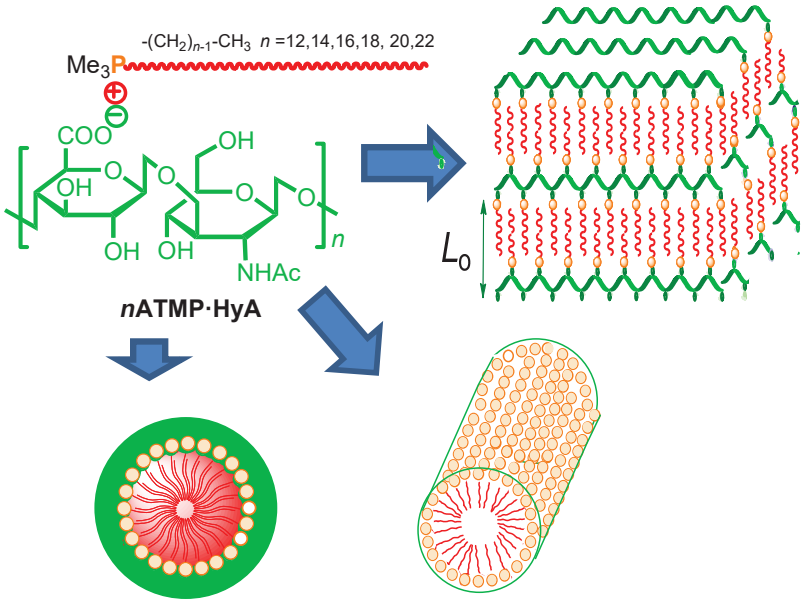

Publication derived from this work:

Gamarra, A., Forés, E., Morató, J., Muñoz-Guerra, S. Amphiphilic ionic complexes of hyaluronic acid with organophosphonium compounds and their antimicrobial activity (To be submitted to Int. J. Biolog. Macromol. (Elsevier).

Supporting Information (SI) to this chapter in Annex C.1

1.1. Introduction

Hyaluronic acid (HyA) is a linear polysaccharide, which is ubiquitous in the human body. Its high viscoelasticity and great capacity for holding water, as well as its inherent biocompatibility and biodegradability, are properties that make HyA an outstanding biomaterial for medical and pharmaceutical applications (Baier et al., 2003; Luo et al., 2000). Furthermore, hyaluronic acid is also important in the regulation of injury associated reactions because it promotes early inflammation, which is a critical step for starting wound healing (Vazquez et al., 2003; Gao et al., 2008). A number of strategies for the chemical modification of HyA addressed to improving its physicochemical properties, most of them based on the reaction of carboxyl or hydroxyl groups have been developed (Balazs et al., 1987; Kuo et al., 1991; Luo et al., 2000). A valid alternative approach for the modification of HyA is its coupling with cationic surfactants. It has been widely reported that this type of modification carried out on polyelectrolytes (either polypeptides or polyuronic acids) gives rise to stable comb-like ionically-linked systems able to self-assemble in amphiphilic structures (Antonietti et al., 1994; Tolentino et al., 2013). These structures consist of two phases, one paraffinic and the other made of the biopolymer, that alternate in layers with a periodicity of several nanometers. Interestingly, the nanometric dimensions of such structures are reversibly responsive to thermal effects. Consequently, these derivatives are potentially useful to design medical devices with temperature-depending transport activity (Macknight et al., 1998).

According to what has been noticed in a recent investigation, HyA is able to exert bacteriostatic effects and also to display antimicrobial and antiviral properties (Pirnazar et al., 1999; Ardizzoni et al., 2011). However, as it has been reported by a number of authors, the biocide effect of this polysaccharide is not clear and it seems to critically depend on molecular weight and concentration in solution. It is therefore advisable that HyA is used in combination with well recognized antimicrobial agents in order to avoid such dependences and ensure its bacteriostatic effect. Nisin, silver and polyhexanide are among others, active compounds that have been added to HyA to make it an efficient antimicrobial system (Kemp et al., 2009; Baier et al., 2013; Lequeux et al., 2014).

In this study tetraalkylphosphonium surfactants have been coupled to HyA to generate stable ionic complexes with comb-like architecture and antimicrobial properties. The biocide activity of quaternary salts has been widely demonstrated (Muñoz-Bonilla et al., 2012), and organophosphonium salts are particularly efficient in this regard (Kanazawa et al., 1994). In fact, these compounds have been extensively

used in the preparation of polymeric materials displaying remarkable antimicrobial activity (Kanazawa et al., 1993; Popa et al., 2011; Qiu et al., 2014; Xue et al., 2015). Furthermore organophosphonium compounds are known to be much more resistant to temperature than their organoammonium analogs (Xie et al., 2002). In this work, alkyltrimethylphosphonium bromide soaps, abbreviated as *n*ATMP·Br, with *n* standing for the number of carbon atoms contained in the linear alkyl chain and taking even values from 12 to 22, have been coupled with HyA to give the *n*ATMP·HyA complexes. The study is parallel to that recently published by us on the ionic complexes of HyA with alkyltrimethylammonium bromide salts (*n*ATMA·Br), and it has been conceived with the purpose of evaluating the advantages and disadvantages that derive from the replacement of organoammonium by organophosphonium surfactant concerning the structure and properties of the complexes. Firstly a detailed chemical characterization of *n*ATMP·HyA including their thermal stability was performed. Then the nanostructure adopted by the complexes and their thermal behavior were examined in detail since significant differences between the two complexes series in these regards should be expected from the much bigger size of the phosphorous atom respect to the nitrogen one. Finally the antimicrobial activity against bacteria, including Gram-negative and Gram-positive bacteria, as well as against a fungus, was evaluate to ascertain to what extent the biocide activity of *n*ATMP surfactants is retained once that ionic complexes are formed.

1.2. Results and discussion

1.2.1. Synthesis and chemical characterization of *n*ATMP·HyA complexes

The coupling reaction of *n*ATMP·Br and Na·HyA (Scheme 1) provided the ionic *n*ATMP·HyA complexes with *n* even values from 12 to 22. The solubility displayed by the *n*ATMP·HyA complexes was in agreement with what should be expected for polymers with a strong amphiphilic character, *i.e.* they were soluble in methanol but non-soluble in either water or chloroform. The reaction conditions used for this synthesis and the results therein obtained are presented in Table 1.

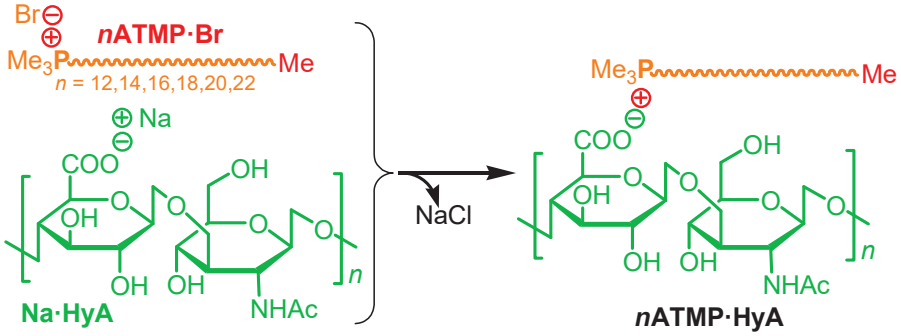

Scheme 1. Coupling of *n*ATMP·Br surfactants with HyA leading to *n*ATMP·HyA complexes.

Table 1. Results for the preparation of *n*ATMP·HyA complexes.

*n*ATMP·HyA	Mixing conditions		Yield	Elemental analysis[c]			Composition[d]
	c (M)[a]	*T* (ºC)[b]	(%)	C (%)	H (%)	N (%)	ATMP:HyA:H_2O
12ATMP·HyA	0.075	25	55	53.3 (52.8)	8.5 (8.9)	2.0 (2.1)	1.0:1.0:2.0
14ATMP·HyA	0.05	25	65	56.5 (55.6)	9.4 (9.0)	1.9 (2.1)	1.0:1.0:1.0
16ATMP·HyA	0.01	25	70	57.0 (57.3)	9.6 (9.3)	1.8 (1.9)	1.0:1.0:0.75
18ATMP·HyA	0.01	45	75	58.6 (58.6)	10.1 (9.4)	1.7 (1.9)	1.0:1.0:0.5
20ATMP·HyA	0.01	55	85	59.6 (59.7)	10.2 (9.7)	1.6 (1.8)	1.05:1.0:0.5
22ATMP·HyA	0.01	65	90	60.7 (60.8)	10.5 (9.9)	1.5 (1.7)	1.1:1.0:0.5

[a] Molar concentration of the two solutions mixed to form the complex.
[b] Mixing temperature selected according to the surfactant solubility in water.
[c] Experimental percentages of C, H and N. The calculated values are indicated in parenthesis.
[d] Ratio of *n*ATMP to HyA in the complex consistent with elemental analysis after including 0.5-2 molecules of H_2O.

In all cases, equimolar amounts of polyacid and surfactant were mixed at the minimum temperature required to have the alkyltrimethylphosphonium salt fully dissolved in water. Yields ranged between 55 and 90% with values increasing steadily with the length of the surfactant alkyl tail. Yields of complexes with lower values of *n* could not be enhanced despite using higher concentration solutions.

The chemical constitution of the *n*ATMP·HyA complexes was ascertained by both FTIR and NMR spectroscopies. As an example of the information provided by FTIR, the spectrum of 18ATMP·HyA together with those of the sodium salt of hyaluronic acid (Na·HyA) and octadecyltrimethylphosphonium bromide (18ATMP·Br) are represented in Figure 1a. The spectrum recorded from the complex showed the characteristic bands of hyaluronic acid at 3340 cm^{-1} (O-H and N-H stretching), 1616 and 1410 cm^{-1} (asymmetric and symmetric C-O stretching modes of the planar carboxyl groups), 1653, 1563 and 1320 cm^{-1} (amide I, II, and III bands, respectively) and 1040 cm^{-1} (C-O-C stretching) (Gilli et al.,1994; Alkrad et al., 2003; Wu, 2012). Additionally the two bands at 990 and 715 cm^{-1} which are attributable to the P-C stretching vibrations in the alkylphosphonium groups (Witschard et al., 1963; Beg et al., 1968), were present with strong intensity. On the contrary, and as it should be much expected, the band appearing at 1745 cm^{-1} in the spectrum of Na·HyA which is associated to the C=O stretching mode of the sodium carboxylate group (Haxaire et al., 2003), was absent in the spectrum of the complex. The spectra recorded for the whole series of complexes are comparatively represented in Figure 1b where the close similitude existing among them can be appreciated. The only difference clearly noticed was that concerning the

intensity of the C-H stretching bands appearing at ~2900 and ~2850 cm^{-1}, which as expected, increased steadily with the value of *n*. The ^{1}H NMR spectrum recorded from the 18ATMP·HyA complex is reproduced in Figure 2 and the collection recorded from the whole series may be inspected in Figure SI-1. In these spectra, all the signals arising from both the polyacid and surfactant counterparts could be properly assigned according to the chemical structure expected for the complexes. However, signal overlapping and too much broadening, the latter probably due to the restricted mobility of the HyA chain, prevented determining with reliability the complex composition by signal area quantification.

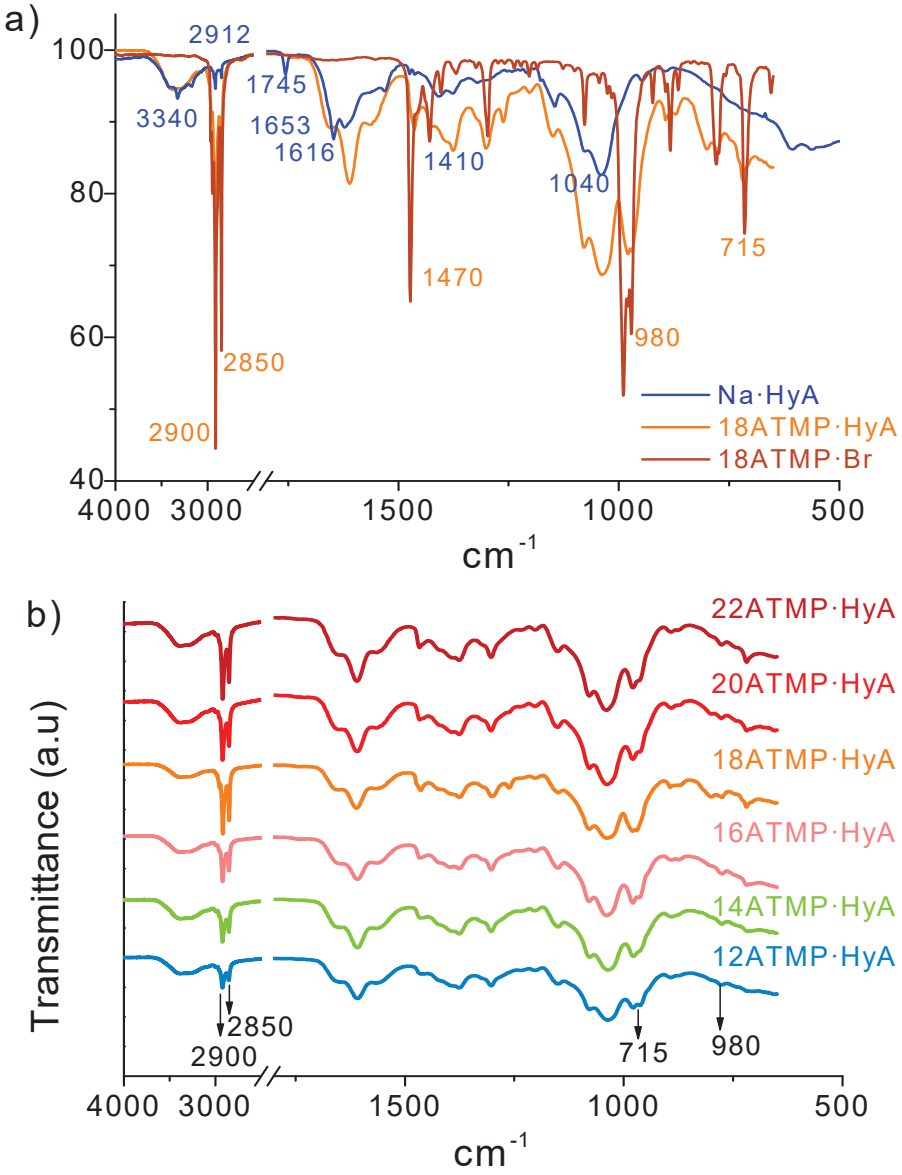

Figure 1. FTIR recorded at 25 ºC from a) 18ATMP·Br, Na·HyA and 18ATMP·HyA complex, and b) the whole series of *n*ATMP·HyA complexes.

Nevertheless, an approximate evaluation of the composition of the complexes could be made on the basis of the atomic composition provided by the combustion analysis data by assuming that a certain amount of water is adsorbed in the complex. The resulting values are given in Table 1 and a graphical representation of the reasonably acceptable compositional domain in terms of surfactant/hyaluronic acid ratio and adsorbed water is depicted in Figure SI-2. The *n*ATMP:HyA ratio in *n*ATMP·HyA complexes oscillated between 1.0 and 1.1 with values slightly increasing with the length of the alkyl side chain. The amount of water present in these complexes ranged between 0.5 to 2 moles per mole of HyA, as it was inferred by fitting experimental and calculated atom percentages in the elemental analysis. As expected, the longer is the alkyl chain, the lower is the amount of water that is adsorbed in the complex.

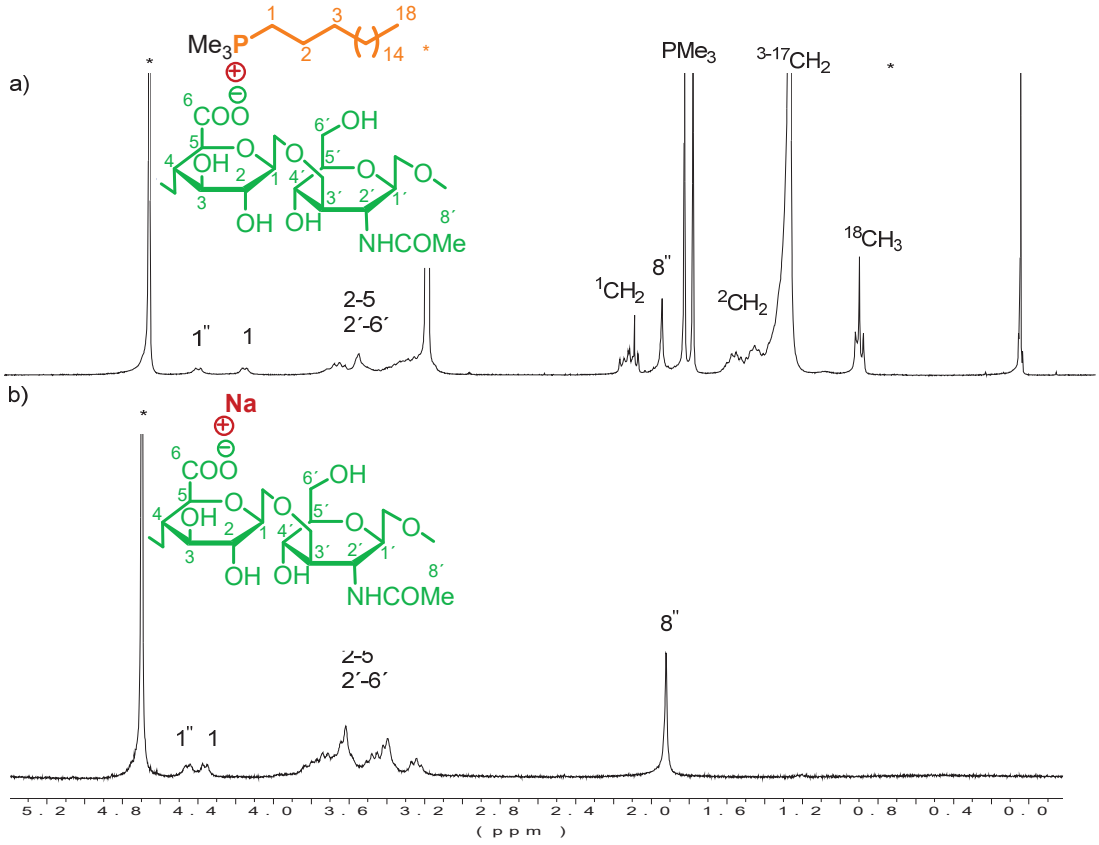

Figure 2. ^{1}H NMR spectra of 18ATMP·HyA complex in MeOD (a) and hyaluronic acid in D_2O (b) recorded at 25 ºC. *Residual protons of deuterated solvents.

1.2.2. Thermal properties of *n*ATMP·HyA complexes

The thermal stability of *n*ATMP·HyA complexes under an inert atmosphere was examined by TGA. The most significant thermogravimetric parameters are collected in Table 2 and the recorded traces for the whole series together with their corresponding derivative curves are shown in Figure 3. All traces presented in Figure 3a show a slight weight loss at temperatures around 100 ºC which is interpreted as due to the release of adsorbed water. Onset thermal decomposition temperatures are between 200 and 210 ºC which is the range in which HyA starts to decompose (Figure SI-3) but they are much lower than the $^{o}T_d$ reported for *n*ATMP·Br surfactants (Kanazawa et al., 1997; Gamarra et al., 2017a). Apparently the thermal stability of HyA is not improved by the presence of the organophosphonium counterpart, which is a result contrary to that reported for poly(γ-glutamic acid) coupled with the same surfactants (Gamarra et al., 2017b).

Table 2. Thermal parameters of *n*ATMP·HyA complexes.

Complex	**TGA**[a]			**DSC**[b]								
				1st Heating			Cooling		2nd Heating			
	$^{o}T_d$ (ºC)	$^{max}T_d$ (ºC)	*W* (%)	T_m (ºC)	ΔH_m (Kcal·mol^{-1})	n_c	T_m (ºC)	ΔH_m (Kcal·mol^{-1})	T_m (ºC)	ΔH_m (Kcal·mol^{-1})	n_c
12ATMP·HyA	207	219/306/430	12	-	-	-			-	-	-
14ATMP·HyA	205	219/312/432	11	-	-	-			-	-	-
16ATMP·HyA	200	219/330/437	9	-	-	-			-	-	-
18ATMP·HyA	209	219/340/437	10	58	1.9	2	43	1.2	48	1.1	1
20ATMP·HyA	203	216/350/437	11	67	3.1	4	62	1.4	64	2.1	3
22ATMP·HyA	205	216/350/437	7	70	5.2	6	65	3.7	69	4.5	5

[a] $^{o}T_d$ and $^{max}T_d$: onset and maximum rate decomposition temperatures; *W*: remaining weight at 600 ºC.
[b] DSC traces recorded in the -20-80 ºC interval; T_m: melting temperature; ΔH_m: melting enthalpy; n_c: calculated number of crystallized methylenes in the alkyl chain.

The derivative curves shown in Figure 3b clearly revealed that thermal decomposition proceeded in all cases trough a multi-stage process involving at least three stages with maximum loss weight rates at temperatures in the 215-220 ºC, 300-350 ºC and 430-440 ºC ranges, respectively, to leave less than 10 % of the initial mass at the end of the whole process. The $^{max}T_d$ for the first stage appeared fairly constant along the whole series of complexes indicating that decomposition of the hyaluronic acid must be the main process taking place at this stage. Conversely, the second and third maximum decomposition temperatures increased steadily with *n,* suggesting that decomposition of the surfactant should be involved in the two last stages. The molecular mechanism of the thermal degradation of the *n*ATMA·PGGA complexes has been studied in detail and reported to proceed through two stages, the former taking

place at temperatures increasing with *n* and involving the simultaneous decomposition of the complex and the polyacid (Portilla-Arias et al., 2007). On the other hand, *n*ATMA·HyA complexes have been reported to decompose through a multi-stage process with the $^{max}T_d$ for the first stage being almost constant at a value within the 215-225 ºC range (Tolentino et al., 2013). Unfortunately, the thermal decomposition of neither HyA nor their derivatives has been studied in detail and the information accessible on this topic is scarce (Lowry et al., 1994; Caspersen et al., 2014). At this moment, little more can be said about the mechanism operating in the thermal decomposition of *n*ATMP·HyA complexes.

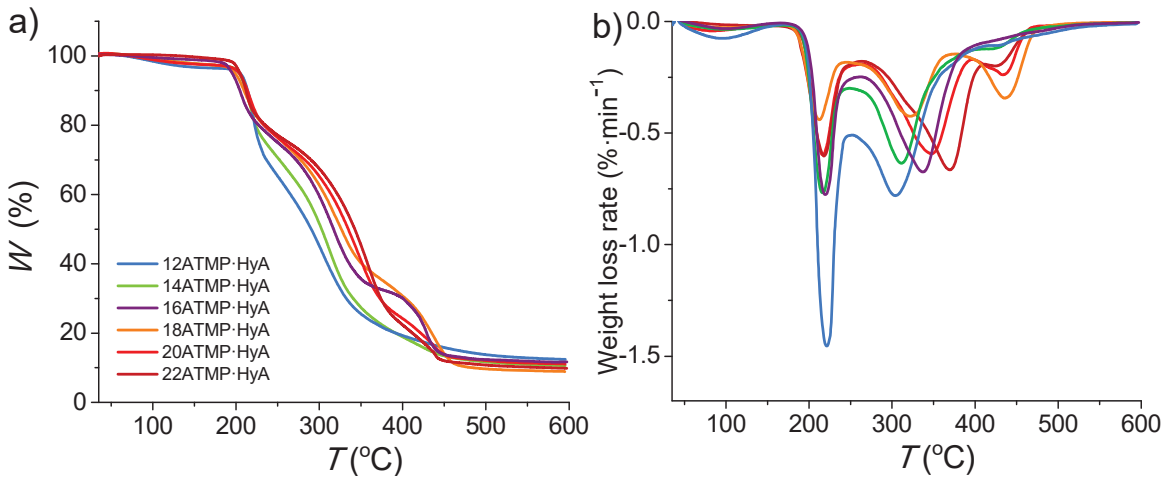

Figure 3. TGA traces of *n*ATMP·HyA complexes (a) and their derivative curves (b).

The DSC study was performed by subjecting the *n*ATMP·HyA samples to heating-cooling cycles over the -30-120 ºC range. As it is shown in Figure 4a, only heating traces of complexes with $n \geq 18$ showed endothermic peaks, which appear at temperatures steadily increasing from 55 ºC up to 70 ºC. According to what is well known for other related ionic complexes (Pérez-Camero et al., 2004; García-Álvarez et al., 2005), such endothermic peaks must be associated to the melting of the paraffinic phase made of crystallized alkyl chains. Comparison of these results with those reported for *n*ATMP·PGGA complexes, in which crystallinity could be observed for $n \geq 16$ (Gamarra et al., 2017b), led to infer that, compared to PGGA, HyA is more effective in disturbing the lateral arrangement required by the alkyl chains to crystallize.

Recrystallization of *n*ATMP·HyA from the melt was highly depending on the temperature at which the sample was previously heated. Figure 4b shows that no crystallization occurred in 18ATMP·HyA upon cooling from 120 ºC whereas melting peaks could be partially recovered when the first heating was limited to 80 ºC. Similar results were obtained for 20ATMP·HyA and 22ATMP·HyA complexes (Figure SI-4). Such a different behavior is doubtlessly a consequence of the nucleating effect that is

able to operate in samples subjected to moderate overheating. Melting temperatures and enthalpies measured for the recrystallized samples are given in Table 2.

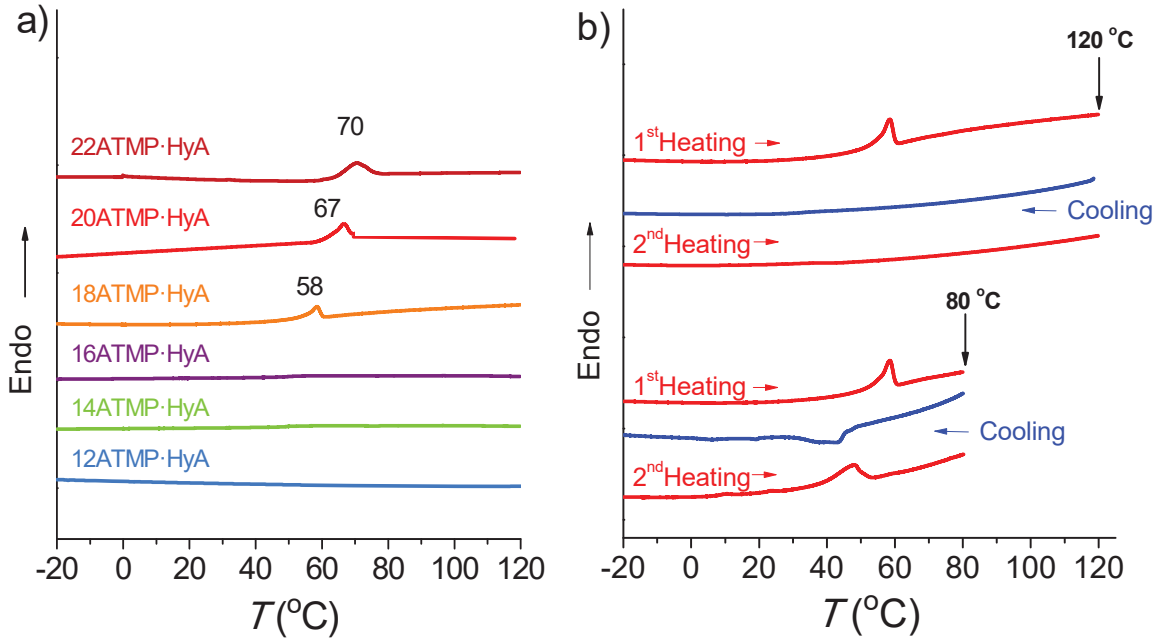

Figure 4. a) First heating DSC traces of *n*ATMP·HyA complexes. b) DSC traces of 18ATMP·HyA complex recording at heating and cooling within the -20-120 ºC and -20-80 ºC intervals.

The graphical representation of ΔH_m against n (Figure 5) revealed an almost linear dependence between these two variables. The equation resulting from these data provides the individual methylene (ΔH_m^{CH2}) and non-methylene (ΔH_m^0) contributions to the experimentally observed melting enthalpy as the slope and the *y*-axis intercept at n = 0, respectively (Broadhurst, 1962; Jordan et al., 1971). The average amount of crystallized methylene units per alkyl chain is given by $n_c = K+n$, where–n_c is the minimum number needed for crystallization. As it is represented in Figure 5 and given in Table 2, n_c oscillates between 1 and 6 depending on chain length and thermal history. These values are much lower than those reported for *n*ATMP·PGGA complexes (Gamarra et al., 2017b) but comparable to those reported for *n*ATMA·HyA (Tolentino et al., 2013), which confirm the different influence of the polymer chain on the crystallizability of the attached surfactant.

.

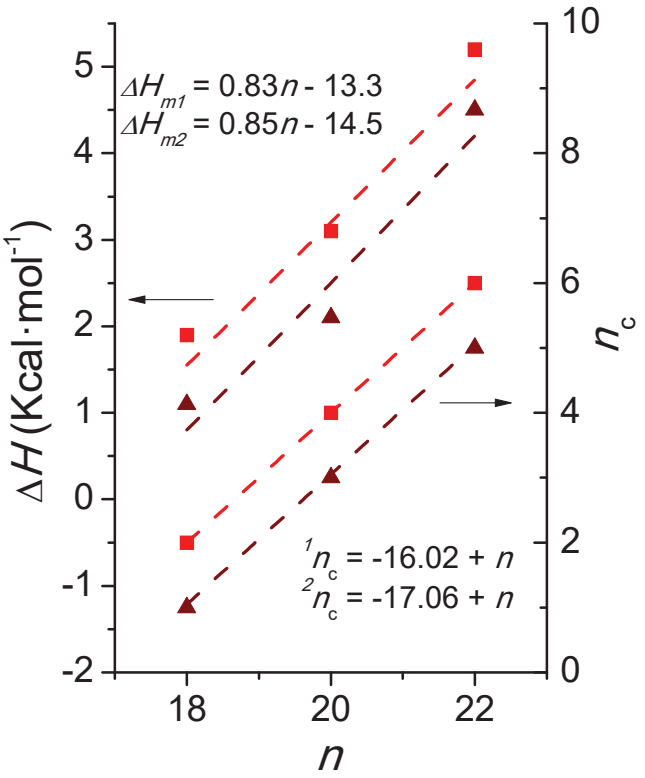

Figure 5. Plots of melting enthalpy (ΔH_m) and number of crystallized methylenes (n_c) for 18, 20 and 22ATMP·HyA complexes against the number of carbons contained in the alkyl side chain. Squares and triangles refer to values obtained in the first heating and the second heating of samples crystallized from samples previously heated at 80 ºC.

1.2.3. Structural of *n*ATMP·HyA complexes. Temperature effects

To gather information on both the supramolecular structure and the packing of the alkyl side chains in *n*ATMP·HyA, as well as to evaluate the effect of heating on the structure, these complexes were examined at real time by X-ray diffraction at variable temperature. Wide and small angle scattering (WAXS and SAXS, respectively) were simultaneously recorded from samples subjected to heating or cooling over the 10-120 ºC interval.

1.2.3.1 XRD and TEM analysis at room temperature.

The SAXS and WAXS profiles recorded at 25 ºC from the whole series are compared in Figure 6, and the spacings measured at different temperatures are collected in Table 3. The scattering produced in the SAXS region by all the complexes (Figure 6a) consisted of three main peaks with spacings between 3 and 5 nm and variable intensity. According to a number of studies carried out on similar comb-like amphiphilic systems (Pérez-Camero et al., 2004; Tolentino et al., 2013), this scattering is interpreted to arise from the periodicity of the biphasic nanostructure in which the complexes become self-assembled. In previously examined cases, a stratified structure

with the polyelectrolyte and the paraffinic moiety of the surfactant separated in two phases that alternate regularly with an interlayer spacing that increases monotonically with the length of the alkyl chain, was commonly described.

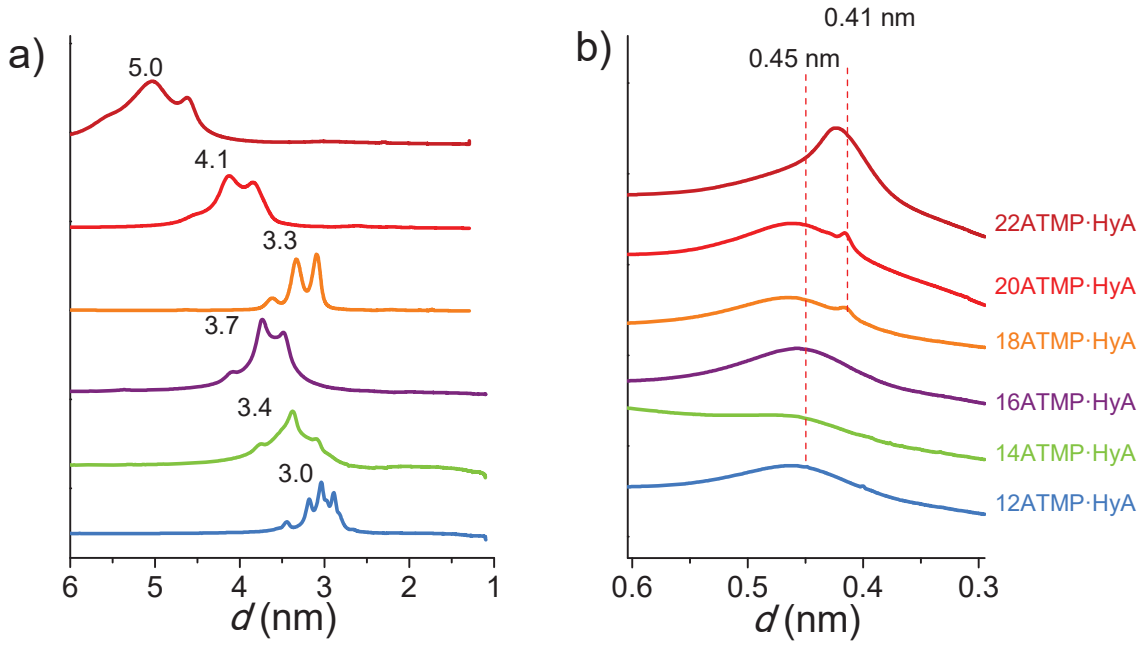

Figure 6. XRD profiles recorded at room temperature from *n*ATMP·HyA in the SAXS (a) and WAXS regions (b).

Table 3. X-ray diffraction data of *n*ATMP·HyA complexes.

Complex	SAXS[a]			WAXS		
	$L_0^{10ºC}$	$L_0^{120ºC}$	$L_0^{10ºC}$	$d_{100}^{10ºC}$	$d_{100}^{120ºC}$	$d_{100}^{10ºC}$
12ATMP·HyA	3.45, **3.15**, 2.90	3.44, 3.18, 2.88	3.39, 3.12, 2.84	0.45	0.45	0.45
14ATMP·HyA	3.75, **3.40**, 3.10	3.79, 3.39, 3.12	3.68, 3.35, 3.08	0.45	0.45	0.45
16ATMP·HyA	4.06, **3.71**, 3.38	4.35, 3.91, 3.44	4.37, 3.89, 3.42	0.45	0.45	0.45
18ATMP·HyA	3.66, **3.36**, 3.05	3.76, 3.44, 3.76	3.78, 3.43, 3.77	0.41	0.45	0.45
20ATMP·HyA	4.57, **4.14**, 3.82	4.55, 4.18, 3.96	4.45, 4.13, 3.86	0.41	0.45	0.45
22ATMP·HyA	5.52, **5.06**, 4.60	5.61, 5.07, 4.67	5.48, 4.98, 4.49	0.41	0.45	0.45

[a]Main peaks in bold

In the present case however the occurrence of multiple scattering is indicative of a more complex structure. Interestingly, an approximate ratio of 1:1.1:1.2 is assessed for the spacings associated to the three peaks seen in SAXS indicating that a close structural interrelation must exists among them. Furthermore, linear correlations are detected for the spacings of complexes with $n \leq 16$ and for the complexes with $n \geq 18$. A mixture of different arrangements all them fitting in a common structural pattern may be in principle consistent with SAXS results. On the other hand, the scattering exhibited in the WAXS region (Figure 6b) for all the complexes consisted of a broad scattering centered on ~0.45 nm, which is known to be characteristic of a disordered packing of

the polymethylene chains. In addition 18ATMP·HyA, 20ATMP·HyA and 22ATMP·HyA showed a shoulder at ~0.41 nm that is associated to the pseudo hexagonal lattice commonly adopted by the paraffinic phase in this type of complexes (Pérez-Camero et al., 2004).

The TEM examination of films of these complexes prepared by casting on a water surface provided useful information that greatly helped the interpretation of X-rays diffraction results. Representative micrographs recorded from films of 16ATMP·HyA and 22ATMP·HyA are shown in Figure 7. In both cases, a banded texture with an average periodicity oscillating between 3 and 6 nm was clearly observed in good agreement with the spacings observed by SAXS. It is worthy noticing the waving appearance observed in the case of 16ATMP·HyA, which is reminiscent of the typical finger-print texture displayed by soft phospholipid membranes. On the contrary, the essentially straight traces observed for 22ATMP·HyA indicate the presence of a much stiffer structure in this complex.

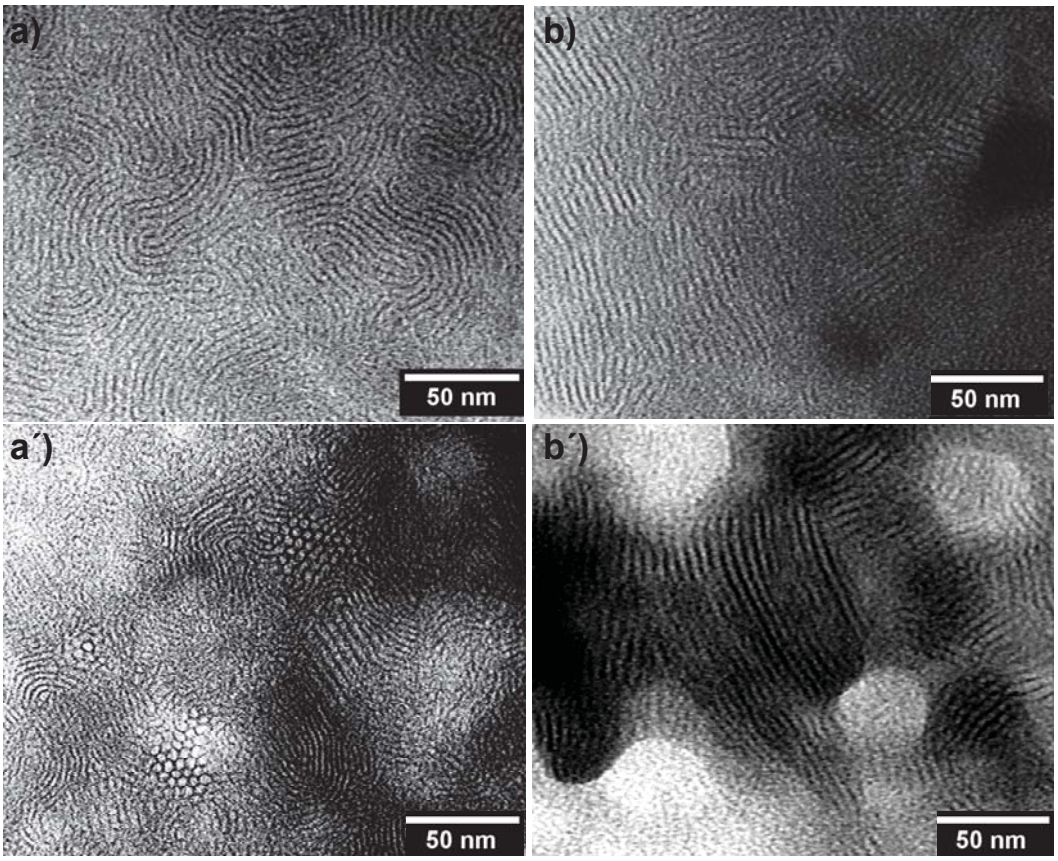

Figure 7. TEM micrographs of 16ATMP·HyA (a and a´) and 22ATMP·HyA (b and b´) films obtained by casting.

1.2.3.2 Temperature effects on the structure of *n*ATMP·HyA complexes

The effect of temperature on the structure of *n*ATMP·HyA complexes was examined by XRD at real time using synchrotron radiation. Samples were subjected to heating-cooling cycles from 10 ºC to 120 ºC at a heating/cooling rate of 10 ºC·min^{-1}. Spacings observed at the beginning and the end of each run for the whole series of complexes is compared in Table 3. The detailed changes taking place on the X-ray diffraction profiles of 16ATMP·HyA and 22ATMP·HyA, with temperature in both SAXS and WAXS regions, are shown in Figures 8 y 9, respectively. Similar graphical representations for all the other complexes are included in Figures SI-7-SI-10 of the SM file.

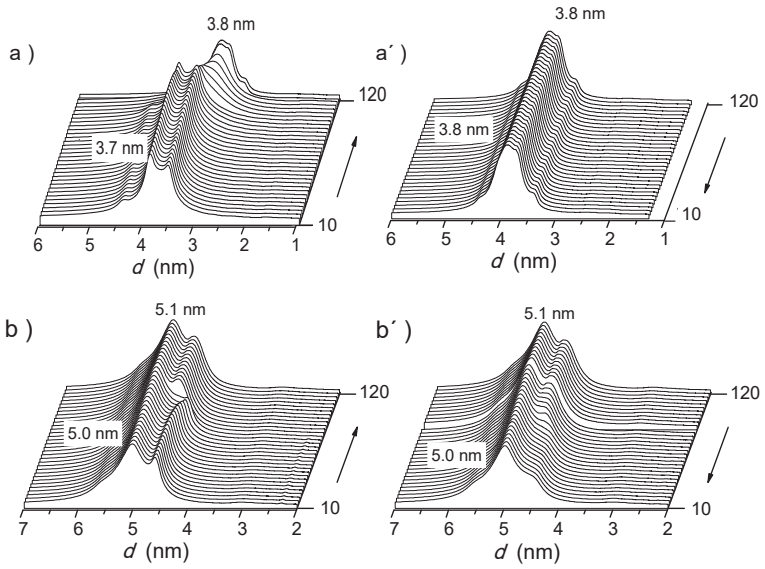

Figure 8. SAXS and WAXS profiles of 16ATMP·HyA and 22ATMP·HyA at heating (a and b) and cooling (a´and b´) along 10-120 ºC range.

The general behavior observed in the SAXS profiles is a slight change in the L_0 spacings with temperature that does not follows any recognizable trend along the series for none of the observed peaks. This result strongly contrasts with those observed for analog complexes made from PGGA where a clear L_0 change effect is shared by the whole series upon heating or cooling. On the contrary, significant differences were observed in WAXS profiles among the members of the series. WAXS profiles of complexes with $n \leq 16$ hardly changed with temperature so that the initial profile observed at 10 ºC was maintained invariable along the whole heating-cooling cycle (Figure 9a and 9a´). Conversely, WAXS profiles of complexes with $n \geq 18$ were sensitive to heating with the 0.41 nm peak characteristic of the crystallized paraffinic phase disappearing at the melting temperature. At 120 ºC the broad peak at 0.45 nm characteristic of a disordered phase was the only one observed for all complexes. After

cooling, the peak at 0.41 nm was barely recovered (Figure 9b´) revealing the poor crystallinity of these complexes.

To appraise more accurately the reversibility of the melting-cooling process of *n*ATMP·HyA complexes with $n \geq 18$, XRD of 22ATMP·HyA was registered from samples subjected to a heating-cooling cycle over the 10-80 ºC range. The changes seen in SAXS were similar to that observed when samples were initially heated at 120 ºC but WAXS profiles revealed that the complex was able to crystallize under these conditions (Figure SI-11). These results give support to those obtained by DSC previously described, and confirm the critical importance of the self-nucleating process on the ability of the surfactant alkyl chain to crystallize in these complexes.

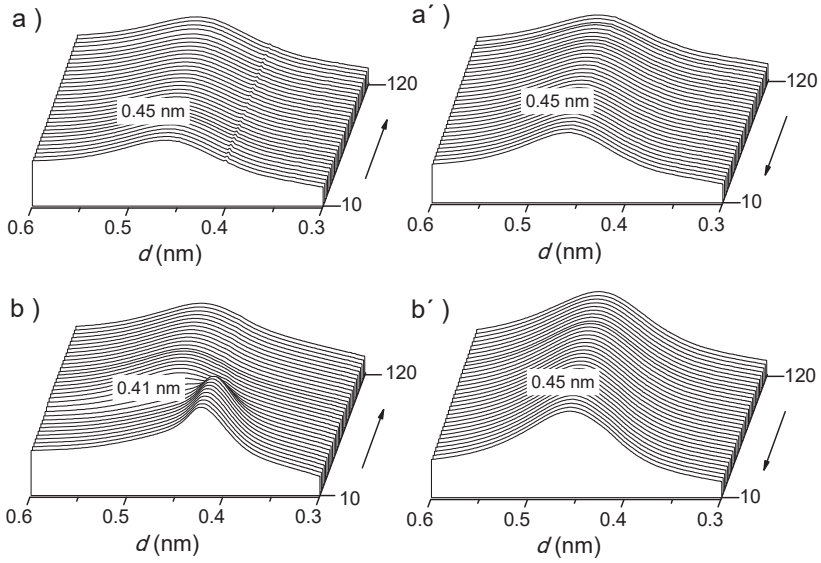

Figure 9. SAXS and WAXS profiles of 16ATMP·HyA and 22ATMP·HyA at heating (a and b) and cooling (a´and b´) along 10-120 ºC range.

1.2.4. Decomposition of *n*ATMP·HyA complexes in aqueous environment

The changes in sample weight of two *n*ATMP·HyA complexes differing in *n*, *i.e.* 16ATMP·HyA and 22ATMP·HyA, upon incubation in an aqueous environment were comparatively examined under different conditions in order to evaluate the effect of the length of the alkyl chain, pH and enzymes on their susceptibility to water attack. Both dissociation of the ionic pair and hydrolysis of the polysaccharide chain are expected to occur in more or less extent by the action of water. The weight losses taking place at pH 5.5 and 7.4, in the latter case with or without enzymes added, are plotted in Figure 10a. The results clearly revealed that the complexes with *n*= 16 decomposed faster than those with *n*= 22 at both pH. This is more than reasonable since the paraffinic moiety of the surfactant is expected to hinder the access of water to the polymer main

chain. It was also shown that decomposition proceeded at much higher rates at physiological pH than at acidic pH for the two complexes. In fact, both complexes lost only 10% of their initial weight at pH=5.5 along the whole incubation period whereas at pH=7.4 the lost weight was near 40 % and 20 % for 16ATMP·HyA and 22ATMP·HyA, respectively. The action of enzymes was really noticeable since weight losses arrived to be more than 50% when the complexes were incubated in the presence of hyaluronidases. This result is remarkable since it demonstrated that HyA continues being sensitive to enzymes after being ionically coupled with organophosphonium compounds (West et al., 1985).

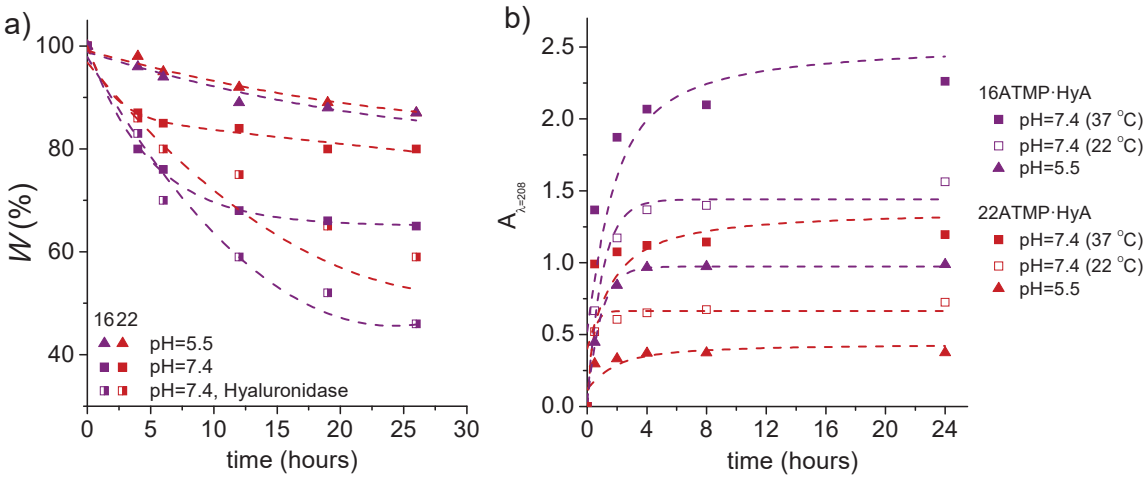

Figurre 10. a) Weight loss undergone by *n*ATMP·HyA complexes with *n* =16 and 22 upon incubation at 37 ºC at different pH and either with or without enzymes added. b) Release of the *n*ATMP for *n* = 16 and 22 from their respective *n*ATMP·HyA complexes under the indicated conditions.

The release of ATMP from *n*ATMP·HyA complexes was studied as a prediction of their biocide activity. Although the capability of HyA to repress the growth of certain microorganisms has been claimed by different authors, the biocide activity of the complexes is expected to be essentially determined by the organophosphonium counterpart. The more surfactant is released to the aqueous environment, the higher will be the antimicrobial activity displayed by the *n*ATMP·HyA complexes. ATMP is released as a consequence of the dissociation undergone by the ionic pair and the releasing rate will depend on the water solubility of both trimethylalkylphosphonium cation and HyA as well as on incubation conditions. The dissociation of complexes in water with concomitant release of the surfactant was estimated by measuring the increase of absorbance at 208 nm of the incubation medium as a function of time for a total period of 24 h at either 22 ºC (pH 5.5 and 7.4) or 37 ºC (pH 7.4). The results are plotted in Figure 10b where it is clearly seen how the dissociation equilibrium was reached after 4-6 hours of incubation. A simple comparison of the resulting curves brings into evidence also that 16ATMP was released faster than 22ATMP whichever

were the conditions used. This is quite reasonable given the relative solubility in water of the two surfactants. Regarding pH and temperature, maximum dissociation was found to happen at pH 7.4 at 37 ºC. Whereas the favourable effect of temperature on release rate does not need supporting explanation, the greater dissociation observed at neutral conditions for the two complexes should be related to the effect that pH has on the solubility of the surfactant.

NMR analysis provided valuable information in support of the results obtained from weight loss and absorbance measurements (Figure SI-12). The ^{1}H NMR spectra of discs residues remaining after incubation showed scarce differences with those recorded from the initial ones. It does mean that no chemical changes other than hydrolysis of HyA took place upon incubation. The observed weight loss must correspond therefore to the release of *n*ATMP·HyA short fragments generated by hydrolysis of the polysaccharide chain with enough low molecular weight as to be water-soluble. This is in agreement with what was seen on the spectra recorded from the releasing medium which showed surfactant signals only when enzymes were used for degradation.

1.2.5. Antimicrobial activity of *n*ATMP·HyA complexes

The antimicrobial activity of films of *n*ATMP·HyA complexes was evaluated against bacteria *S. aureus* (Gram-positive) and *E. coli* (Gram-negative) and against the common yeast *C. albicans* by using both solid and liquid media methodologies. 16ATMP·HyA and 22ATMP·HyA complexes were selected for this study.

Results obtained with the solid-medium method using agar as substrate are gathered in Table 4 where the diameter of the inhibition area observed for every microorganism is compared for the two complexes and uncoupled HyA. No inhibition area was observed at any case when culture was performed on HyA which is taken as indicative of the inactivity of this compound against the tested microorganisms. On the contrary, a considerable growth inhibiting capacity against bacteria was displayed by both 16ATMP·HyA and 22ATMP·HyA, which was found stronger for the former when *S. aureus* was the microorganism assayed. This result is very according to expectations since the high biocide effectivity of cationic surfactants against Gram-positive bacteria is a well-known fact (Vaara, 1992). The results obtained for *C. albicans* revealed a poor activity of 16ATMP·HyA against this fungi, which arrived to be inappreciable for 22ATMP·HyA.

Table 4. Antimicrobial activity of *n*ATMP·HyA films against bacteria and fungi.[a]

Microorganism	HyA	16ATMP·HyA	22ATMP·HyA
S. aureus	0 ± 0.0	29.5 ± 0.9	11.9 ± 0.5
E. coli	0 ± 0.0	15.1 ± 0.3	11.0 ± 0.9
C. albicans	0 ± 0.0	8.3 ± 0.2	0 ± 0.0

[a] Evaluated on a solid medium at 37 °C for 24 h. Zones of growth inhibition (mm) showing antimicrobial activity; film size 5 mm, plate diameter 90 mm. Values for zone of growth inhibition are presented as mean ± SD for triplicates.

Results obtained from biocide assays using liquid media are compared in Figure 11, and pictures showing the appearance displayed by the incubation medium along the different assays are provided in Figure SI-13. The representation of Log(CFU) (Colonia Forming Units) at scheduled incubation times for 16ATMP·HyA and 22ATMP·HyA and their respective surfactants as well as for HyA depicted in Figure 11 provides a clear assessment of the biocide capacity of the complexes. Values of Log(CFU) measured at different times for the different assayed systems are collected in Table SI-1 together with the Log(RV) (Reduction Value) and PR (Percentage of Reduction) values calculated therefrom. In agreement with results afforded by solid media assays, the highest antibacterial activity was displayed by 16ATMP·HyA against *S. aureus* with a total growth inhibition after only 2 h. An even faster activity was shown by this complex against *E. coli* reaching an almost total inhibition after 30 min. The behaviour displayed by 22ATMP·HyA was significantly different. The inhibition capacity of this complex against *S. aureus* was also very strong showing a PR of 99.998% after 24 h but its efficiency against *E.coli* was poor with a PR of only 11% after 24 h. Regarding the antifungal activity, results obtained against *C. albicans* revealed a remarkable inhibitory capacity for 16ATMP·HyA that dramatically decreased for 22ATMP·HyA.

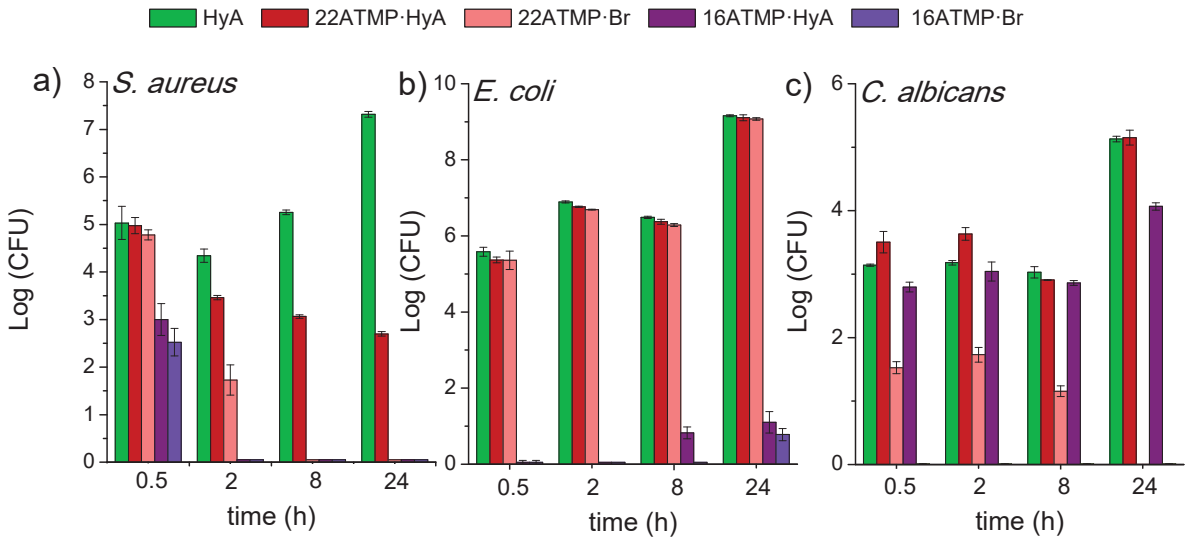

Figure 11. Antimicrobial activity of 16ATMP·Br, 22ATMP·Br and their complexes with HyA in liquid media against *S. aureus* (a) and *E. coli* (b).

In order to ascertain that the activity displayed by the complexes mainly arose from the compounds that were released to the incubation medium, the growth of microorganisms in the supernatants used for incubating the complexes films was examined. Results obtained in this study are depicted in Figure 12 where the growth rate measured as OD at 490 nm, is plotted against time for the two bacteria. The curves obtained in the absence of biocide activity (blank and HyA supernatants) clearly displayed the typical growth evolution profile consisting of lag, exponential and stationary phases. Curves obtained for the supernatants of 16ATMP·HyA and 22ATMP·HyA films were much flatter, in particular for the former complex, revealing the biocide effect of the dissolved species.

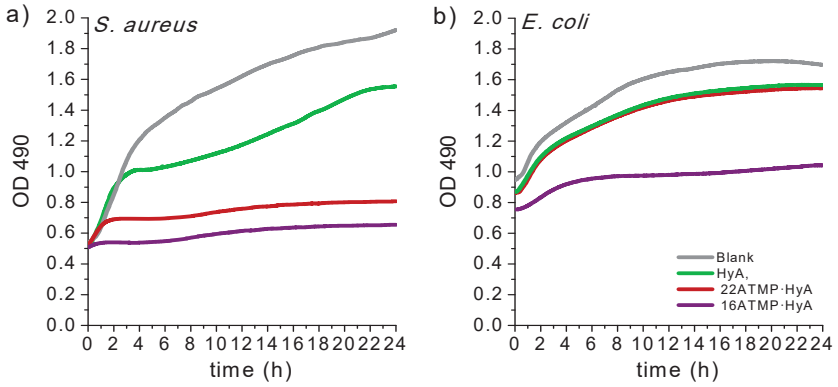

Fig.12. Bactericide activity along 24 h of the supernatant of *n*ATMP·HyA films for *n* = 16 and 22. The antimicrobial activity is expressed by the optical density measured at 490 nm.

1.3. Conclusions

Almost stoichiometric *n*ATMP·HyA complexes have been successfully produced by ionic coupling of hyaluronic acid (HyA) with alkyltrimethylphosphonium bromide soaps (*n*ATMP·Br, *n* =12-22). The structure and thermal properties of these complexes have been examined as a function of *n* and compared with data reported for their analogous complexes made from poly(γ-glutamic acid) (*n*ATMP·PGGA). As their analogues, *n*ATMP·HyA complexes are non-water soluble and also adopt a nanoscopic biphasic arrangement in the solid state. However, noticeable differences have been found between the two series as a consequence of the replacement of the polypeptide by the polysaccharide as the polyanionic counterpart of the complex. The thermal stability of *n*ATMP·HyA, although high, is about 100 ºC lower than that of *n*ATMP·PGGA, most probably due to the intrinsic low resistance to heat of HyA. Also the crystallizability of the HyA derived complexes is poorer than that of the PGGA derived ones as it is reflected in the lower fraction of methylene units that are able to crystallize and in the higher difficulty found to crystallize from the melt. The greater

disturbing effect of HyA on crystallization is readily understandable taking into account its bulkiness and high interactive capacity by hydrogen bonding. Contrary to what happens in *n*ATMP·PGGA, self-assembling of *n*ATMP·HyA takes place in a much more complex way with generation of more than one biphasic nanostructure that differ among them in the reciprocal arrangement adopted by the surfactant and the biopolymer phases. The response of the *n*ATMP·HyA structure to heating effect is insignificant at the nanoscale level whereas a slight contraction was invariably observed for *n*ATMP·PGGA. Both series of complexes decomposed by the action of water with a similar response to pH changes but the complexes made of HyA showed an extensive degradation in the presence of enzymes. The bactericide activity shown by the two series is similar with a higher intensity when Gram-positive bacteria are concerned. *n*ATMP·HyA complexes display also fungicide activity, a property that was not evaluated for the complexes made of PGGA. In both cases, the biocide activity was found to arise from the organophosphonium compounds that are released to water upon incubation. The summarized conclusion that may be drawn from these parallel studies is that *n*ATMP·HyA and *n*ATMP·PGGA complexes are not significantly different in either structure or properties including the biocide activity. Both of them are therefore acceptable options for the design of biocompatible/biodegradable films, the preference for one or another being dictated by other complementary properties, such as mechanical or barrier properties and stability in humid environments that should be evaluated in future studies.

1.4. References

Alkrad, J.A., Mrestani, Y., Stroehl, D., Wartewig, S., Neubert, R. (2003). Characterization of enzymatically digested hyaluronic acid using NMR, raman, IR, and UV-Vis spectroscopies. J. Pharm. Biomed. Anal. 31 (3), 545–550.

Antonietti, M., Conrad, J., Thünemann, A. (1994). Polyelectrolyte-surfactant complexes: a new type of solid, mesomorphous material. Macromolecules, 27(21), 6007–6011.

Ardizzoni, A., Neglia, R. G., Baschieri, M. C., Cermelli, C., Caratozzolo, M., Righi, E., Blasi, E. (2011). Influence of hyaluronic acid on bacterial and fungal species, including clinically relevant opportunistic pathogens. J. Mater. Sci. Mater. Med. 22(10), 2329–2338.

Baier Leach, J., Bivens, K. A., Patrick, C. W., Schmidt, C. E. (2003). Photocrosslinked hyaluronic acid hydrogels: Natural, biodegradable tissue engineering scaffolds. Biotech. Bioeng. 82(5), 578–589.

Baier, G., Cavallo, A., Vasilev, K., Mailänder, V., Musyanovych, A., Landfester, K. (2013). Enzyme responsive hyaluronic acid nanocapsules containing polyhexanide and

their exposure to bacteria to prevent Infection" Biomacromolecules, 14, 1103-1112.

Balazs, E., Leshchiner. (1987). A. Cross-linked gels of hyaluronic acid and products containing such gels. US4582865A US Grant.

Beg, M. A. A., Samiuzzaman. (1968). Spectroscopic studies of organophosphorus compounds--II : Infrared and ultraviolet spectra of phosphonium compounds and their structures. Tetrahedron, 24, 191–198.

Broadhurst, M. G. (1962). An analysis of the solid phase behavior of the normal paraffins. Phys. Chem. 66A, No.3(3), 241–249.

Caspersen, M. B., Roubroeks, J. P., Liu, Q., Huang, S., Fogh, J., Zhao, R., Tømmeraas, K. (2014). Thermal degradation and stability of sodium hyaluronate in solid state. Carbohydr. Polym. 107 (1), 25–30.

Gamarra, A., Urpí, L., Martínez de Ilarduya, A., Muñoz-Guerra, S. (2017a). Crystalline structure and thermotropic behavior of alkyltrimethylphosphonium amphiphiles. Phys. Chem. Chem. Phys. 19, 4370–4382.

Gamarra, A., Martínez de Ilarduya, A., Vives, M., Morató, J., Muñoz-Guerra, S. (2017b). Ionic complexes of poly(γ-glutamic acid) with alkyltrimethylphosphonium surfactants. Polymer, 116, 43–54.

Gao, F., Yang, C.X., Mo, W., Liu, Y.W., He, Y.Q. (2008). Hyaluronan oligosaccharides are potential stimulators to angiogenesis via RHAMM mediated signal pathway in wound healing. Clin. Investig. Med. 31 (3), 106–116.

García-Álvarez, M., Álvarez, J., Alla, A., Martínez de Ilarduya, A., Herranz, C., Muñoz-Guerra, S. (2005). Comb-like ionic complexes of cationic surfactants with bacterial poly(γ-glutamic acid) of racemic composition. Macromol. Biosci. 5(1), 30–38.

Gilli, R., Kacuráková, M., Mathlouthi, M., Navarini, L., Paoletti, S. (1994). FTIR studies of sodium hyaluronate and its oligomers in the amorphous solid phase and in aqueous solution. Carbohydr. Res. 263 (2), 315–326.

Haxaire, K., Maréchal, Y., Milas, M., Rinaudo, M. (2003). Hydration of polysaccharide hyaluronan observed by IR spectrometry. I. Preliminary experiments and band assignments. Biopolymers, 72(1), 10–20.

Jordan, E.F., Feldeisen, D. W., Wrigley, A. N.(1971). Side-chain crystallinity. I. Heats of fusion and melting transitions on selected homopolymers having long side chains. J. Polym. Sci. Part A-1 Polym. Chem. 9 (7), 1835–1851.

Kanazawa, A., Ikeda, T., Endo, T. (1993). Novel polycationic biocides. Synthesis and antibacterial activity of polymeric phosphonium salts. J. Polym. Sci. Part A Polym. Chem. 31(2), 335–343.

Kanazawa, A., Ikeda, T., Endo, T. (1994). Synthesis and antimicrobial activity of dimethyl- and trimethyl-substituted phosphonium salts with alkyl chains of various lengths. Antimicrob. Agents Chemother. 38(5), 945–952.

Kanazawa, A., Tsutsumi, O., Ikeda, T., Nagase, Y. (1997). Novel thermotropic liquid crystals without a rigid core formed by amphiphiles having phosphonium ions. J. Am. Chem. Soc. 119(33), 7670–7675.

Kemp, M. M., Kumar, A., Clement, D., Ajayan, P., Mousa, S., Linhardt, R. J. (2009).

Hyaluronan- and heparin-reduced silver nanoparticles with antimicrobial properties. Nanomedicine, 4(4), 421–429.

Kuo, J. W., Swann, D.A., Prestwich, G.D. (1991). Chemical modification of hyaluronic acid by carbodiimides. Bioconjug. Chem. 2 (4), 232–241.

Lequeux, I., Ducasse, E., Jouenne, T., Thebault, P. (2014). Addition of antimicrobial properties to hyaluronic acid by grafting of antimicrobial peptide. Eur. Polym. J. 51(1), 182–190.

Lowry, K.M., Beavers, E.M. (1994). Thermal stability of sodium hyaluronate in aqueous solution. J. Biomed. Mater. Res. 28 (10), 1239–1244.

Luo, Y., Kirker, K. R., Prestwich, G.D. (2000). Cross-linked hyaluronic acid hydrogel films: new biomaterials for drug delivery. J. Control. Release, 69 (1), 169–184.

Macknight, W. J., Ponomarenko, E. A., Tirrel, D. A. (1998). Self-assembled polyelectrolyte-surfactant complexes in nonaqueous solvents and in the solid state. Accounts Chem. 31(12), 781–788.

Muñoz-Bonilla, A., Fernández-García, M. (2012). Polymeric materials with antimicrobial activity. Prog. Polym. Sci 37(2), 281–339.

Pérez-Camero, G., García-Álvarez, M., Martínez de Ilarduya, A., Fernández, C., Campos, L., Muñoz-Guerra, S. (2004). Comblike complexes of bacterial poly(γ,D-glutamic acid) and cationic surfactants. Biomacromolecules, 5(1), 144–152.

Pirnazar, P., Wolinsky, L., Nachnani, S., Haake, S., Pilloni, A., Bernard, G. W. (1999). Bacteriostatic effects of hyaluronic acid. J. Periodontol. 70(4), 370–374.

Ponomarenko, E. A., Waddon, A. J., Tirrell, D. A., Macknight, W. J. (1996). Structure and properties of stoichiometric complexes formed by sodium poly (α,l -glutamate) and oppositely charged surfactants. Langmuir, 12(9), 2169–2172.

Popa, A., Crisan, M., Visa, A., Ilia, G. (2011). Effect of a phosphonium salt grafted on polymers on cucumber germination and initial growth. Braz. Arch. Biol. Technol. 54(1), 107–112.

Portilla-Arias, J. A., García-Alvarez, M., Martínez de Ilarduya, A., Muñoz-Guerra, S. (2007). Thermal decomposition of microbial poly(γ-glutamic acid) and poly(γ-glutamate)s. Polym. Degrad. Stab. 92(10), 1916–1924.

Qiu, T., Zeng, Q., Ao, N. (2014). Preparation and characterization of chlorinated nature rubber (CNR) based polymeric quaternary phosphonium salt bactericide. Materials Letters, 122, 13–16.

Tolentino, A., Alla, A., Martínez de Ilarduya, A., Muñoz-Guerra, S. (2011). Comb-like ionic complexes of pectinic and alginic acids with alkyltrimethylammonium surfactants. Carbohydr. Polym. 86(2), 484–490.

Tolentino, A., Alla, A., Martínez de Ilarduya, A., Muñoz-Guerra, S. (2013). Comb-like ionic complexes of hyaluronic acid with alkyltrimethylammonium surfactants. Carbohydr. Polym. 92(1), 691–696.

Vaara, M. (1992). Agents that increase the permeability of the outer membrane. Microbiol. Rev. 56(3), 395–411.

Vazquez, J.R., Short, B., Findlow, A.H., Nixon, B.P., Boulton, A.J.M., Armstrong, D.G. (2003). Outcomes of hyaluronan therapy in diabetic foot wounds. Diabetes Res. Clin. Pract. 59 (2), 123–127.

West, D. C., Hampson, I. N., Arnold, F., Kumar, S. (1985). Angiogenesis induced by degradation products of hyaluronic acid. Science, 228(4705), 1324–1326. 0

Witschard, G., Griffin, C. E. (1963). Infrared absorption characteristics of alkyl and aryl substituted phosphonium salts. Spectrochim. Acta, 19(1958), 1905–1910.

Wu, Y. (2012). Preparation of low-molecular-weight hyaluronic acid by ozone treatment. Carbohydr. Polym. 89 (2), 709–712.

Xie, W., Xie, R., Pan, W. P., Hunter, D., Koene, B., Tan, L. S., Vaia, R. (2002). Thermal stability of quaternary phosphonium modified montmorillonites. Chem. Mater. 14(11), 4837–4845.

Xue, Y., Xiao, H., Zhang, Y. (2015). Antimicrobial polymeric materials with quaternary ammonium and phosphonium salts. Int. J. Mol. Sci. 16(2), 3626–3655.

VI.2. Antimicrobial nanoparticles made of alkyltrimethyl-phosphonium hyaluronic acid complexes

Abstract:

Three alkyltrimethylphosphonium surfactants (*n*ATMP·Br, *n* = 16, 18 and 22 carbon atoms) were coupled with hyaluronic acid (HyA) to obtain non-stoichiometric ionic complexes (*n*ATMP·HyA) in the form of nanoparticles (NPs) by applying the ionotropic gelation technique. NPs had a size around 100 nm and displayed high negative ζ-potential. The complex in these NPs was organized in nano-arrangements reminiscent of the amphiphilic biphasic structure described for films made of nearly stoichiometric *n*ATMP·HyA complexes. Both a lamellar structure and a quasi-hexagonal packing of either cylinders or spheres are adopted in these NPs. The antimicrobial activity of *n*ATMP·HyA NPs was evaluated against Gram-positive and Gram-negative bacteria (*S. aureus* and *E. coli*) and a common yeast (*C. albicans*). It was found that all *n*ATMP·HyA NPs were effective against *S. aureus* whereas only those made of 16ATMP·HyA showed antimicrobial activity against *E. coli* and *C. albicans*.

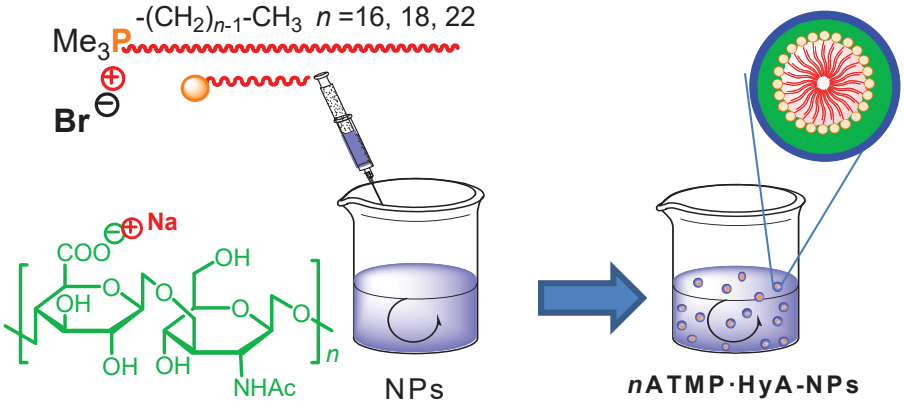

Publication derived from this work:

Gamarra, A., Forés,. E., Morató, J., Muñoz-Guerra, S. Antimicrobial nanoparticles made of alkyltrimethylphosphonium-hyaluronic acid complexes (To be submitted to Eur. Polym. J.). (Elsevier).

Supporting Information (SI) to this chapter in Annex C.2

2.1. Introduction

Infections by pathogenic microorganisms including bacteria, viruses, fungi and protozoa are still a major cause of morbidity and mortality (Hall-Stoodley et al., 2004). Because of that, there is a growing concern about the development of infection-resistant products as medical devices, drugs, surgery equipment, health care products, water purification systems, textiles, food packaging films etc. (Davey et al., 2000). Wounds suffer from the particularly high risk of bacterial infection due to the invasion and proliferation of certain pathogenic bacteria such as *Staphylococcus aureus* (Hynes et al., 2000), that are able to produce the enzyme hyaluronidase which degrades hyaluronic acid (Stern et al., 2007) penetrating and spreading the infection to other issues (Hynes, 2004). Antibiotics have been the preferred treatment method to fight bacterial infections due to their cost-effectiveness. However, super-bacteria have emerged in the last decades (Abebe et al., 2016), which are resistant to nearly all antibiotics because abusing of these drugs (Jayaraman, 2009). Another challenge is the tendency of bacteria to form biofilms which act as a barrier of diffusion by trapping and degrading antibiotic molecules (Mah e al., 2001). These problems have generated the necessity of developing new systems in the field of antimicrobial materials that are able to reach the target efficiently and creating resistance as less as possible (Engler et al., 2012).

Antibacterial active nanoparticles (NPs) are increasingly used to target bacteria as an alternative to antibiotics. To date, a significant number of reports on the activity of antibiotic-conjugated polymeric NPs against various infections, including those caused by drug-resistant pathogens, have been published (Engler et al., 2012).Due to the nanometric size of NPs their use offers valuable advantages as: i) a broad-spectrum of antibacterial properties against both Gram-positive and Gram-negative species is displayed, ii) the antibiotic resistance mechanisms become irrelevant because they interact with bacteria cell wall without needing to penetrate the cell, and iii) effectivity against bacteria may be enhanced by increasing their local concentration (Nagy et al., 2011; Gurunathan, et al., 2012; Leung et al., 2014).

Hyaluronic acid (HyA) is a naturally occurring mucopolysaccharide consisting of alternating units of β-1,4-D-glucuronic acid and β-1,3-*N*-acetyl-D-glucosamine. It is found in the extracellular matrix of connective tissues in the human body where it is the major component of the synovial fluid (Schanté et al., 2011). Due to its high capacity for holding water and inherent biocompatibility and biodegradability, HyA is used in a wide range of medical and pharmaceutical applications (Balazs, 2008; Yeom et al., 2010; Burdick et al., 2011). Interestingly, hyaluronic acid promotes early inflammation,

which is critical for starting wound healing (Vazquez et al., 2003; Gao et al., 2008; Campo et al., 2010;) and shows bacteriostatic effects (Pirnazar et al., 1999). Because of the latter, HyA has attracted much attention because its capacity to cleavage bacteria that produce hyaluronidases (Baier et al., 2013) *e.g. S. aureus.* Despite the bacteriostatic effect found in HyA (Pirnazar et al., 1999; Ardizzoni et al., 2011), the antimicrobial activity of this polysaccharide is not clear and seems to depend on its molecular weight and its concentration in the bacterial species (Ardizzoni et al., 2011). Therefore, HyA must be used in combination with antimicrobial agents to ensure its antimicrobial effect. HyA-silver nanoparticles and HyA coupled with polyhexanide (Kemp et al., 2009; Baier et al., 2013) and nisin polypeptide (Lequeux et al., 2014) are representative examples of such materials.

In this study alkyltrimethylphosphonium soaps have been coupled to HyA to obtain HyA-based NPs (*n*ATMP·HyA NPs). Organophosphonium compounds are particularly convenient for building antibacterial NPs because they show noticeable biocide activity (Cieniecka-Rosłonkiewicz et al., 2005), specifically against Gram-positive bacteria (Costerton et al., 1975). Consequently these NPs are expected to have antimicrobial properties which would made them particularly striking for developing antimicrobial devices to treat microorganisms infections (Jayaraman, 2009; WHO, 2012). It is known that ionic complexes are able to form nanoparticles with satisfactory flowing stability in aqueous environments and also to display water degradability adjustable by their amphiphillicity (Tolentino et al., 2014). In this work the ionotropic gelation technique was used to prepare *n*ATMP·HyA NPs (with *n*= 16, 18 and 22) with different sizes and morphologies. This methodology is a simple procedure in which NPs are obtained in a water environment without adding additives (Patil et al., 2010). The prepared NPs were characterized by FTIR and DLS and their structure examined by combination of XRD and TEM. Finally, their antimicrobial activity against bacteria and fungi was evaluated.

2.2. Results and discussion

2.2.1. *n*ATMP·HyA NPs

As it is schematically depicted in Figure 1, the ionotropic gelation technique *was* used for the preparation of *n*ATMP·HyA NPs with *n* = 16, 18 and 22 and covering a full range of ATMP:HyA molar ratios. Furthermore three sets of concentrations of the mixing solutions were tested. The results obtained from these exploratory experiments regarding the formation of stable emulsion are summarized in Table SI-1 of the Supplementary Material (SM) file. It can be concluded that the more diluted solutions were used, the higher was the amount of *n*ATMP that could be added without evolving precipitation and also that higher amounts were in general needed for surfactants bearing shorter alkyl chains. The NPs selected for further study were obtained using the highest concentration and *n*ATMP:HyA ratio allowable for each selected *n* value, *i.e.* 0.6:1.0 for 16ATMP·HyA and 0.5:10 or 0.2:1.0 for *n*ATMP·HyA with *n*=18 and 22.

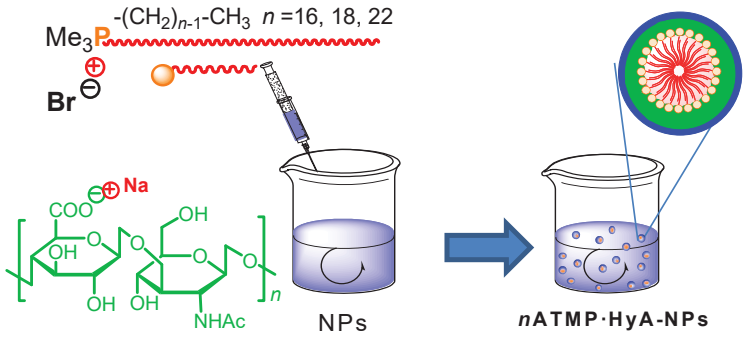

Figure 1. Scheme of the preparation procedure used for obtaining the *n*ATMP·HyA NPs.

The chemical structure of *n*ATMP·HyA NPs was ascertained by FTIR. As it can be seen in Figure 2, the FTIR spectra of *n*ATMP·HyA NPs showed the characteristic absorptions of both, hyaluronate (Alkrad et al., 2003) and surfactant counterparts (Witschard et al., 1963; Beg et al., 1968). Most conspicuous bands due to HyA include those at 3340 cm^{-1} (O-H and N-H stretching), 2912 cm^{-1} (C-H stretching) and 1620, 1410 and 1045 cm^{-1} (asymmetric C-O and symmetric C-O stretching modes of the carboxyl and C-O-C groups) (Gilli et al., 1994). The presence of organophosphonium moieties in the complexes is supported by the presence of strong to medium intensity bands at 980 and 715 cm^{-1} which are attributable to the P-C stretching vibrations. The C-H stretching vibration bands appearing at 2900–2850 cm^{-1} with intensity steadily increasing with *n*, are fully consistent with the presences of ATMP in the complex.

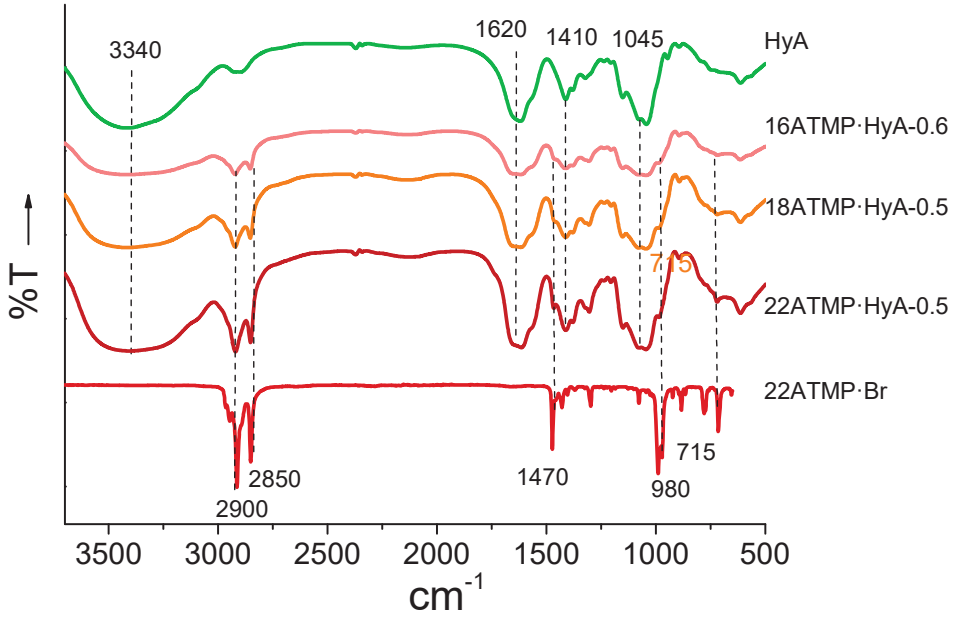

Figure 2. FTIR spectra of HyA, 22ATMP surfactant and *n*ATMP·HyA NPs.

2.2.2. *n*ATMP·HyA NPs characterization

*n*ATMP·HyA NPs were analysed by DLS and ζ potential measurements to determine their size and ζ potential, respectively. As it can be seen in Table 1, all the prepared NPs displayed a negative ζ potential with sizes in the 100-150 nm range showing a slight increasing with concentration (Figure 3a). The changes in size taking place along time when the NPs were suspended in water at different pH's were also measured in order to determine their stability. Only small changes in size were observed after 30 days of incubation at pH ranging between 4 and 9 (Figures 3b and 3c).

Table 1. NPs prepared with varying compositions under different experimental conditions.

	*n*ATMP·HyA NPs					
	n= 16	*n*= 18		*n*= 22		
*n*ATMP: HyA ratio	0.6	0.2	0.5	0.2	0.5	0.2
*n*ATMP/Na·HyA[a]	0.8/2	1/1(H)	1/1(H)	1/1(H)	1/1(H)	0.2/0.2 (L)
T (ºC)	40	50	50	65-70	65-70	65-70
Size (nm)	298	114	124	250	134	126
STD[b] (%)	41	37	30	30	30	20
ζ potential (mV)	-30.6	-21.2	-26.2	-24.7	-24.7	-18.8

[a]Concentration (mg·mL^{-1}) of the *n*ATMP and HyA aqueous solutions mixed for coupling. In parenthesis: H: high concentration; L: low concentration.
[b]Standard deviation of DLS experiment after three measurements per sample.

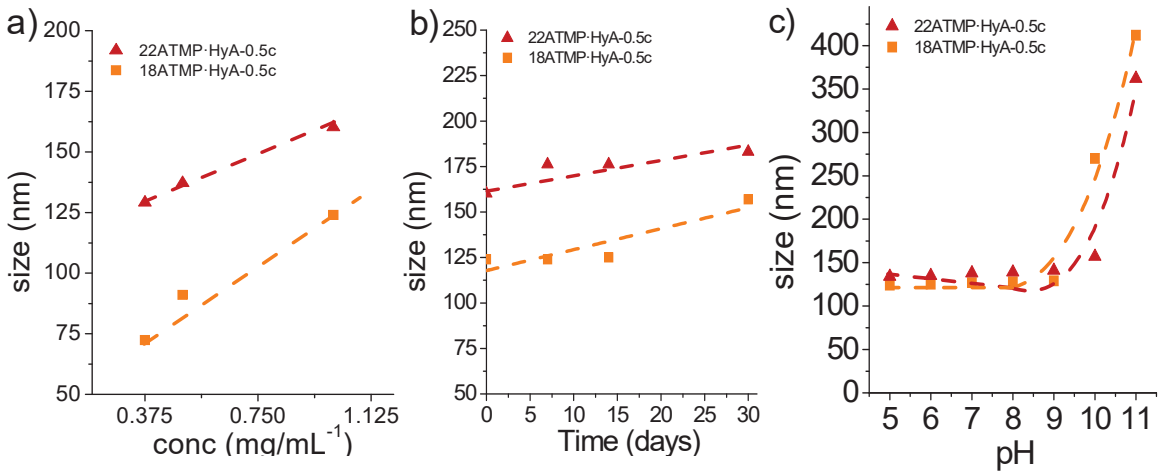

Figure 3. Changes in size displayed by *n*ATMP·HyA NPs with *n*=18 and 22 (prepared with a ATMP:HyA ratio of 0.5:1.0) as a function of the indicated variables: a) concentration of the mixing solutions used for coupling, b) storing time, and c) pH.

2.2.3. Structure of *n*ATMP·HyA NPs

The structure of *n*ATMP·HyA NPs was examined by XRD and TEM. XRD was carried out with simultaneous recording of the scattering produced in the wide and small angle regions (WAXS and SAXS, respectively). In the SAXS region a strong scattering could be observed for all *n*ATMP·HyA NPs revealing the presence of a well-organized nanostructure with a periodicity ranging between 4.4 and 5.5 nm range depending on *n* (Figure 4a). The SAXS spacings values plotted as a function of n showed an almost linear trend very similar to that previously observed for the films of these complexes. In the WAXS region, the profiles displayed a broad peak at 0.45 nm for the whole series of nATMP·HyA NPs (Figure 4b) that led to conclude that that the alkyl chains are not crystallized for any length.

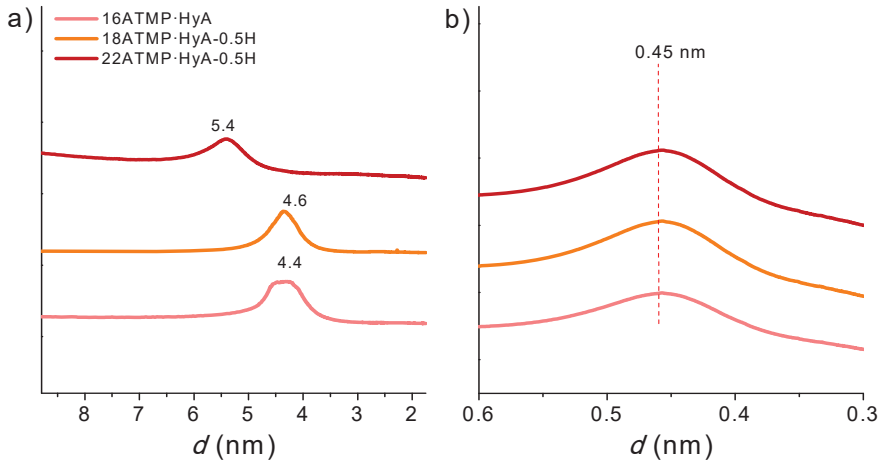

Figure 4. XRD patterns of 16, 18 and 22ATMP·HyA observed in SAXS (a) and WAXS (b) regions.

The dependence of the XRD on the conditions used for NP preparation is depicted in Figure 5. Significant variations in the long spacing observed in SAXS were appreciated among the NPs with different ATMP:HyA ratios (0.2 or 0.5) or prepared from mixing solutions with different component concentrations (1 M or 0.2 M) (Figure 5a). In WAXS, it was observed that only NPs made of ATMP:HyA 0.2L (Figure 4b) showed a sharp peak at 0.41-0.42 nm characteristic of the crystallized paraffinic phase. On the contrary, a broad signal at 0.45 nm characteristic of a disordered paraffinic phase was observed for the all other three NPs types in the WAXS region. These results are indicative of the determinant influence of the composition and preparation factors on the nanometric arrangement adopted by the complex in the nanoparticle. It is known that lamellae, cylinders or spheres are basic arrangements frequently adopted by these types of complexes, which are then packed in nanometric arrays well recognizable by TEM.

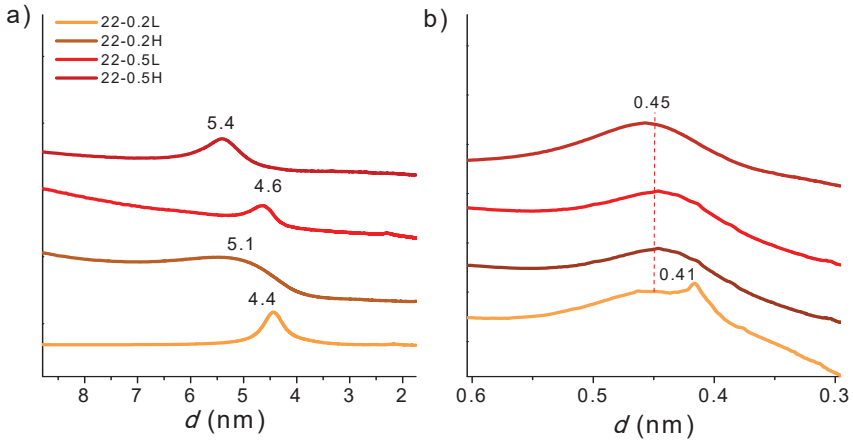

Figure 5. XRD patterns of 22ATMP·HyA in SAXS (a) and WAXS (b) regions.

For a morphological characterization of the arrangement adopted by the *n*ATMP·HyA NPs, TEM micrographs were took from a selection of them (Figure 6). As it can be seen in Figure 6a, the 22ATMP·HyA NPs with a ATMP:HyA ratio of 0.2 that were obtained from 0.2 M mixing solutions (L, low concentration) are vermicular entities ostensibly showing the layered structure typical of the complexes. In fact the average repeating distance displayed by these particles was 4.1 nm as measured by optical diffraction (Figure 7a). This value is consistent with the 4.4 nm spacing determined by SAXS provided that a slight shrinkage of the NP took place under the vacuum used for observation. On the other hand, more or less spherical particles with diameters oscillating between 50 and 150 nm were observed for NPs made of 22ATMP·HyA 0.2H complexes. These NPs display a granular texture with grains arranged in either a hexagonal or longitudinal array compatible with a packing of spheres or cylinders (Figure 6b). The periodicity values measured by OD for these NPs are around 5.0-5.5

nm which are close to those observed by SAXS (Fifure 7.b). Analogous results to the laters were obtained when a ratio of 0.2:1.0 at high concentration (0.2H) and a ratio of 0.5:1.0 and low concentration (0.5L) were used (Figure SI-1).

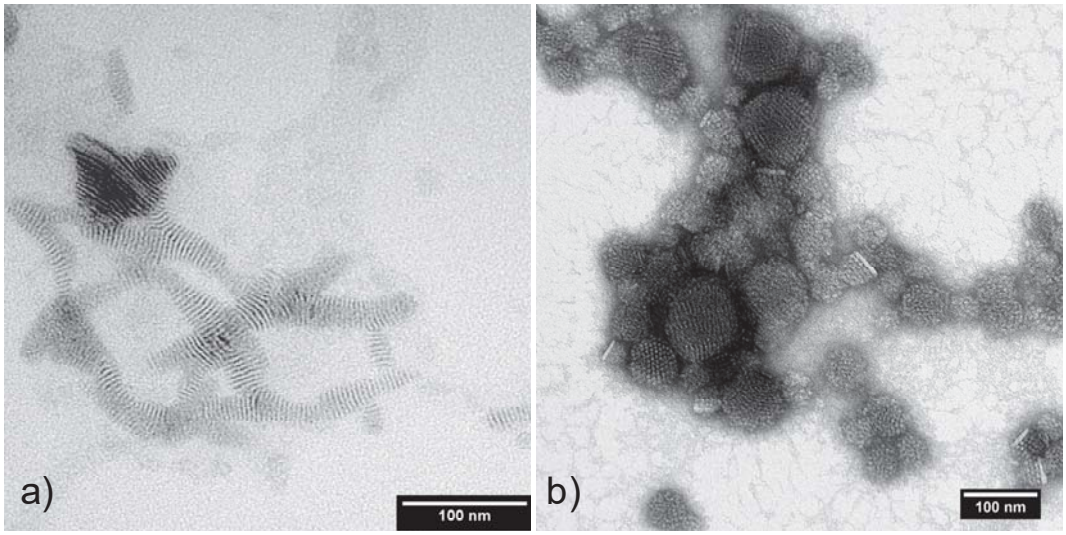

Figure 6. TEM micrographs of nanoparticles made of 22ATMP·HyA 0.2L(a) and 0.5H (b).

Similar results were obtained for *n*ATMP·HyA NPs with *n* = 16 and 18, which also showed lamellar or hexagonal arrays depending on compositional or preparative factors (Figure SI-2 and SI-3 in the SI File). Also in these cases the optical diffraction analysis of selected areas of the TEM images provided spacing values consistent with those measured by SAXS (Figures SI-2 and SI-4). The structural multiplicity observed for 22ATMP·HyA NPs is a striking behaviour that is not shared by comb-like ionic complexes (Pérez-Camero et al., 2004; Tolentino et al., 2013), but that has is shared by films of the *n*ATMP·HyA complexes previously studied by us.

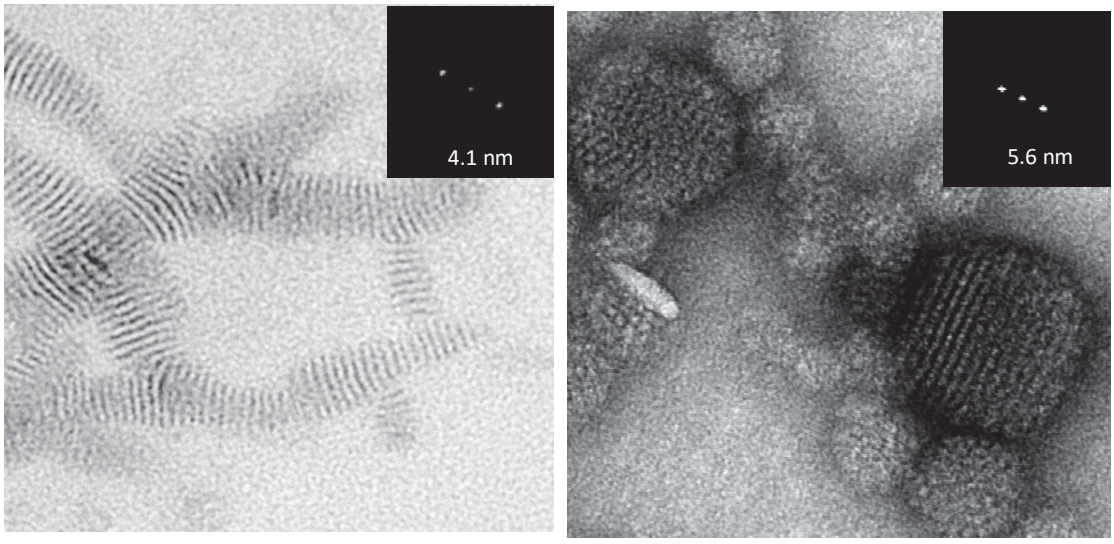

Figure 7. Optical diffraction (OD) of NPs of 22ATMP·HyA complexes differing in composition or/and preparation conditions**.** 22ATMP·HyA 0.2L (a) and 22ATMP·HyA 0.5H (b).

2.2.4. Antimicrobial activity of *n*ATMP·HyA NPs

The antimicrobial activity of *n*ATMP·HyA nanoparticles against *S. aureus* (Gram-positive) and *E. coli* (Gram-negative) bacteria and the common yeast *C. albicans* was evaluated. Quantification was carried out by measuring the optical density at 490 nm after 24 h of incubation at 37 ºC. Pristine Na·HyA was used as negative control for antimicrobial efficiency calculations.

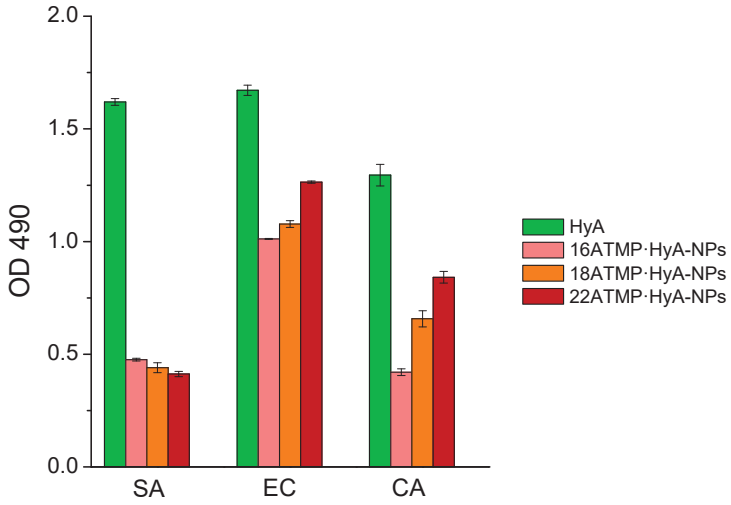

Figure 8. Bactericide activity of *n*ATMP·HyA NPs for *n*=16, 18 and 22 with a ATMP:HyA ratio of 0.5. The activity is expressed as the decrease in the optical density observed at 490 nm after incubation of the microorganism in the presence of NPs for a period of 24 h at 37 ºC.

The variations in the optical density observed for the three assayed microorganisms are depicted in Figure 8 and 9, and the calculated efficiency for every system is given in Table 3. . According to expectations, NPs prepared with a 0.5 ATMP:HyA ratio displayed much higher biocide activity than those with a ratio of 0.2. Regarding the length of the alkyl chain of the surfactant, NPs made of 22ATMP·HyA are those displaying the highest activity against *S. aureus* with a percentage of reduction (PR) of ~90% whereas values of ~88% and ~85% were attained for *n* = 18 and 16, respectively. This is a reasonable result because it has been shown that the longest the alkyl chain is, the highest is the biocide activity of the tetraalkylphosphonium salts (Kanazawa et al., 1994). The antimicrobial activity against *E. coli* and *C. albicans* was found to be not only less intense than for *S. aureus* but also to show an opposite correlation with the value of *n*. In fact, 16ATMP·HyA NPs showed the highest bioactivity in these cases with PR values of about 78% and 85% for *E. coli* and *C. albicans*, respectively, whereas values below 50% were found for 22ATMP·HyA. The particularly high efficiency shown by *n*ATMP·HyA NPs against *S. aureus* is in agreement with the well-recognized strong biocide effect that cationic surfactants have against Gram-positive bacteria (Vaara, 1992). The results obtained for 22ATMP·HyA NPs with ATMP·HyA ratio of 0.2:1.0 revealed a decrease in the

antimicrobial activity against the three microorganisms. This makes sense because the amount of *n*ATMP, which is the actual biocide agent, is lower in these NPs.

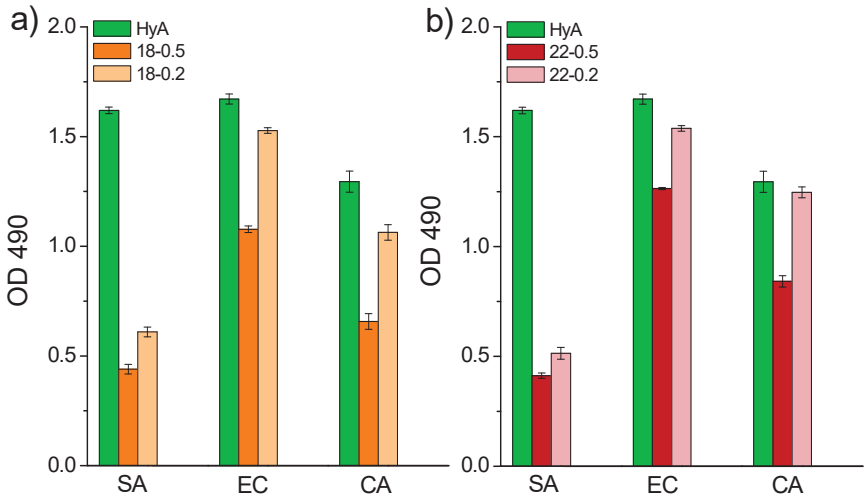

Figure 9. Compared bactericide activity of *n*ATMP·HyA NPs with *n*= 18 (a) and 22 (b) with *n*ATMP:HyA ratios of 0.5:1.0 and 0.2:1.0. Thes NP were generated at a complex concentration of 1 mg·m^{-1}. The activity is expressed as the decrease in the optical density observed at 490 nm after incubation of the microorganism in the presence of NPs for 24 h at 37 ºC.

Table 3. Antimicrobial activity of *n*ATMP·HyA NPs against different microorganisms.

Microorganism	Conc.	16ATMP·HyA (0.5)	18ATMP·HyA		22ATMP·HyA	
		16-0.5	18-0.2	18-0.5	22-0.2	22-0.5
S. aureus	1.0:1.0	85.28	75.31	87.99	55.9	90.03
E. coli	1.0:1.0	77.84	16.93	70.07	15.74	48.03
C. albicans	1.0:1.0	85.45	22.61	62.244	29.12	44.30

[a]Antibacterial activity expressed as the percentage of reduction calculated with the equation previously indicated.

2.3. Conclusions

Three different *n*ATMP·Br salts (*n* = 16, 18 and 22) were coupled to HyA to obtain *n*ATMP·HyA nanoparticles (*n*ATMP·HyA NPs) using the ionotropic gelation technique in water. The NPs have a hydrodynamic radius of around 100-200 nm and a negative *ζ*-potential. The arrangements adopted by the *n*ATMP·HyA complexes in these NPs are similar to that reported for films. Packing in layers, spheres and cylinders have been detected and their occurrence is determined by complex composition and preparation conditions. Only NPs with lamellar structure showed the crystallization of the alkyl chains which seems to be a property privative of such structure. The evaluation of the antimicrobial activity of these NPs against Gram-positive and Gram-negative bacteria (*S. aureus* and *E. coli*) and common yeast *C. albicans* revealed their

high efficiency against *S. aureus*. On the contrary, only 16ATMP·HyA NPs showed antimicrobial activity with moderate intensity against *E. coli* and *C. albicans*.

2.4. References

Abebe, E., Tegegne, B., Tibebu, S. (2016). A review on molecular mechanisms of bacterial resistance to antibiotics. Eur. J.Appl. Sci. 8(5), 301–310.

Alkrad, J.A., Mrestani, Y., Stroehl, D., Wartewig, S., Neubert, R. (2003). Characterization of enzymatically digested hyaluronic acid using NMR, raman, IR, and UV-Vis spectroscopies. J. Pharm. Biomed. Anal. 31 (3), 545–550.

Ardizzoni, A., Neglia, R. G., Baschieri, M. C., Cermelli, C., Caratozzolo, M., Righi, E., Blasi, E. (2011). Influence of hyaluronic acid on bacterial and fungal species, including clinically relevant opportunistic pathogens. J. Mater. Sci. Mater. Med. 22(10), 2329–2338.

Baier, G., Cavallo, A., Vasilev, K., Mailänder, V., Musyanovych, A., Landfester, K. (2013). Enzyme responsive hyaluronic acid nanocapsules containing polyhexanide and their exposure to bacteria to prevent Infection. Biomacromolecules, 14, 1103-1112.

Balazs, E. (2008). Hyaluronan as an ophthalmic viscoelastic device. Curr. Pharma. Biotechnol. 9(4), 236–238.

Beg, M. A. A., Samiuzzaman. (1968). Spectroscopic studies of organophosphorus compounds--II : Infrared and ultraviolet spectra of phosphonium compounds and their structures. Tetrahedron, 24, 191–198.

Burdick, J. A., Prestwich, G. D. (2011). Hyaluronic acid hydrogels for biomedical applications. Adv. Mater. 23(12), H41–H56.

Campo, G. M., Avenoso, A., Campo, S., D'Ascola, A., Nastasi, G., Calatroni, A. (2010). Small hyaluronan oligosaccharides induce inflammation by engaging both toll-like-4 and CD44 receptors in human chondrocytes. Biochemi. Pharmacol. 80(4), 480–490.

Cieniecka-Rosłonkiewicz, A., Pernak, J., Kubis-Feder, J., Ramani, A., Robertson, A. J., Seddon, K. R. (2005). Synthesis, anti-microbial activities and anti-electrostatic properties of phosphonium-based ionic liquids. Green Chem. 7(12), 855–862.

Costerton, J. W., Cheng, K. J. (1975). The role of the bacterial cell envelope in antibiotic resistance. J. Antimicrob. Chemother. 1(4), 363–77.

Davey, M. E., O'toole, G. A. (2000). Microbial biofilms: from ecology to molecular genetics. Microbiol. Mol. Biol. Rev. 64(4), 847–67.

Engler, A. C., Wiradharma, N., Ong, Z. Y., Coady, D. J., Hedrick, J. L., Yang, Y. Y. (2012). Emerging trends in macromolecular antimicrobials to fight multi-drug-resistant infections. Nano Today, 7(3), 201–222.

Gamarra, A., Urpí, L., Martínez de Ilarduya, A., Muñoz-Guerra, S. (2017a). Crystalline structure and thermotropic behavior of alkyltrimethylphosphonium amphiphiles. Phys. Chem. Chem. Phys. 19, 4370–4382.

Gao, F., Yang, C.X., Mo, W., Liu, Y.W., He, Y.Q. (2008). Hyaluronan oligosaccharides are potential stimulators to angiogenesis via RHAMM mediated signal pathway in

wound healing. Clin. Investig. Med. 31 (3), 106–116.

Gilli, R., Kacuráková, M., Mathlouthi, M., Navarini, L., Paoletti, S. (1994). FTIR studies of sodium hyaluronate and its oligomers in the amorphous solid phase and in aqueous solution. Carbohydr. Res. 263 (2), 315–326.

Gurunathan, S., Woong Han, J., Abdal Daye, A., Eppakayala, V., Kim, J. (2012). Oxidative stress-mediated antibacterial activity of graphene oxide and reduced graphene oxide in Pseudomonas aeruginosa. Int. J. Nanomedicine, 7, 5901–5914.

Hall-Stoodley, L., Costerton, J. W., Stoodley, P. (2004). Bacterial biofilms: from the natural environment to infectious diseases. Nat. Rev. Microbiol. 2, 95–108.

Hynes, W. (2004). Virulence factors of the group A streptococci and genes that regulate their expression. Front. Biosci. 9, 3399–433.

Hynes, W. L., Walton, S. L. (2000). Hyaluronidases of Gram-positive bacteria. FEMS Microbiol. Lett. 183(2), 201–7.

Jayaraman, R. (2009). Antibiotic resistance: an overview of mechanisms and a paradigm shift. Curr. Sci. 96(11), 1475–1484.

Kanazawa, A., Ikeda, T., Endo, T. (1994). Synthesis and antimicrobial activity of dimethyl- and trimethyl-substituted phosphonium salts with alkyl chains of various lengths. Antimicrob. Agents Chemother. 38(5), 945–952.

Kemp, M. M., Kumar, A., Clement, D., Ajayan, P., Mousa, S., Linhardt, R. J. (2009). Hyaluronan- and heparin-reduced silver nanoparticles with antimicrobial properties. Nanomedicine, 4(4), 421–429.

Lequeux, I., Ducasse, E., Jouenne, T., Thebault, P. (2014). Addition of antimicrobial properties to hyaluronic acid by grafting of antimicrobial peptide. Eur. Polym. J. 51(1), 182–190.

Leung, Y. H., Ng, A. M. C., Xu, X., Shen, Z., Gethings, L. A., Wong, M. T. Leung, F. C. C. (2014). Mechanisms of antibacterial activity of mgo: non-ros mediated toxicity of mgo nanoparticles towards escherichia coli. Small, 10(6), 1171–1183.

Mah, T.F. C., O'Toole, G. A. (2001). Mechanisms of biofilm resistance to antimicrobial agents. Trend Microbiol. 9(1), 34–39.

Nagy A, Harrison A, Sabbani S, Munson RS, Jr, Dutta PK, W. W. (2011). Silver nanoparticles embedded in zeolite membranes: release of silver ions and mechanism of antibacterial action. Int. J. Nanomedicine, 6, 1833–1852.

Patil, J. S., Kamalapur, M. V., Marapur, S. C., Kadam, D. V. (2010). Ionotropic gelation and polyelectrolyte complexation: The novel techniques to design hydrogel particulate sustained, modulated drug delivery system: A review. Dig. J. Nanomater. Biostructure, 5(1), 241–248.

Pérez-Camero, G., García-Álvarez, M., Martínez de Ilarduya, A., Fernández, C., Campos, L., Muñoz-Guerra, S. (2004). Comblike complexes of bacterial poly(γ,D-glutamic acid) and cationic surfactants. Biomacromolecules, 5(1), 144–152.

Pirnazar, P., Wolinsky, L., Nachnani, S., Haake, S., Pilloni, A., Bernard, G. W. (1999). Bacteriostatic effects of hyaluronic acid. J. Periodontol. 70(4), 370–374.

Schanté, C. E., Zuber, G., Herlin, C., Vandamme, T. F. (2011). Chemical modifications of hyaluronic acid for the synthesis of derivatives for a broad range of biomedical applications. Carbohydr. Polym. 85, 469–489.

Stern, R., Kogan, G., Jedrzejas, M. J., Šoltés, L. (2007). The many ways to cleave hyaluronan. Biotechnol. Adv. 25(6), 537–557.

Tolentino, A., Alla, A., Martínez de Ilarduya, A., Muñoz-Guerra, S. (2013a). Comb-like ionic complexes of hyaluronic acid with alkyltrimethylammonium surfactants. Carbohydr. Polym. 92(1), 691–696.

Tolentino, A., Alla, A., Martínez de Ilarduya, A., Muñoz-Guerra, S. (2014). Complexes of poly(glutamic acid) and long-chain alkanoylcholines: Nanoparticle formation and drug release. Int. J. Biol. Macromol. 66, 346–353.

Vaara, M. (1992). Agents that increase the permeability of the outer membrane. Microbiol. Rev. 56(3), 395–411.

Vazquez, J.R., Short, B., Findlow, A.H., Nixon, B.P., Boulton, A.J.M., Armstrong, D.G. (2003). Outcomes of hyaluronan therapy in diabetic foot wounds. Diabetes Res. Clin. Pract. 59 (2), 123–127.

WHO. (2012). The evolving threat of antimicrobial resistance: Options for action, WHO, Press,Geneva.

Witschard, G., Griffin, C. E. (1963). Infrared absorption characteristics of alkyl and aryl substituted phosphonium salts. Spectrochim. Acta, 19(1958), 1905–1910.

Yeom, J., Bhang, S. H., Kim, B.-S., Seo, M. S., Hwang, E. J., Cho, I. H., Hahn, S. K. (2010). Effect of cross-linking reagents for hyaluronic acid hydrogel dermal fillers on tissue augmentation and regeneration. Bioconjug. Chem. 21(2), 240–247.

Chapter VII. Ionic complexes of hyaluronic acid and choline surfactants

Abstract

Non-toxic alkanoylcholine soaps (*n*ACh) were synthesized from choline and fatty acids with numbers of carbons *n* equal to 12, 14, 16 and 18, the latter including both saturated and 9-*cis* unsaturated alkanoyl chains. Coupling of *n*ACh with hyaluronic acid (HyA) rendered nearly stoichiometric comb-like ionic complexes *n*ACh·HyA that were non-water soluble. The complexes were thermally stable up to temperatures above 200 ºC but readily degraded by water, in particular when hyaluronidases were present in the aqueous medium. In the solid state, these complexes were self-assembled in a biphasic layered structure in which the surfactant and the polysaccharide phases were alternating regularly with a periodicity dependent on the length of the alkanoyl chain. The paraffinic phase was found to be crystallized in saturated complexes with $n \geq 14$ but only 18ACh·HyA showed reversible melting-crystallization when subjected to cyclic heating-cooling treatment. Nanoparticles of 18ACh·HyA with diameters in the 50-150 nm range were prepared by ionotropic gelation. These nanoparticles were also structured in layers, swelled slowly in water, and were shown to be non-cytotoxic in *in vitro* assays against macrophages cells. It was also shown that the anticancer drug Doxorrubicin was efficiently encapsulated in both films and NPs of 18ACh·HyA complexes and its release shown to be almost linear and complete after one day of incubation in physiological medium. The *n*ACh·HyA complexes constitute a highly promising biocompatible/biodegradable platform for the design of systems suitable for drug transport and targeting delivery in anticancer chemotherapy.

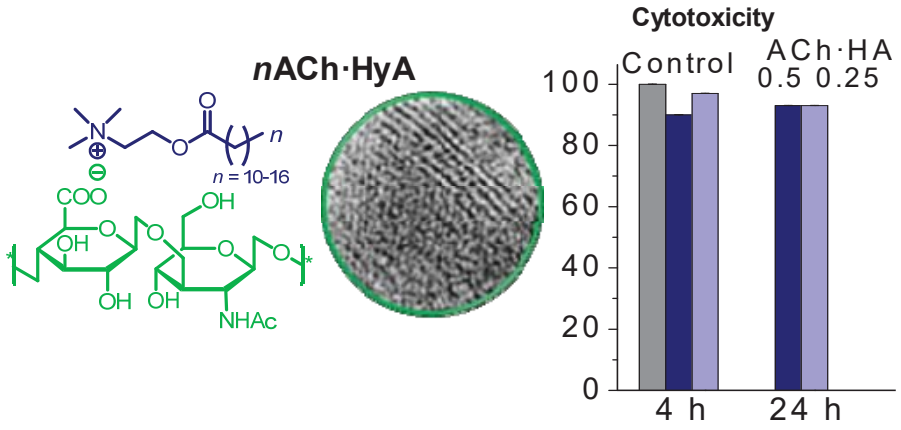

Publication derived from this work:

Gamarra, A., Muñoz-Guerra, A., Martínez de Iylladuya, A., Therein-Aubin, H., Landfester, K. (2018) Comb-like ionic complexes of hyaluronic acid and alkanoylcholine surfactants as platform for drug delivery systems. (Submitted to Biomacromolecules).

Supporting Information (SI) to this chapter in Annex D

1.1. Introduction

Ionic coupling of building blocks of different nature such as polyelectrolytes, surfactants, clusters and others, is a powerful tool to easily create self-assembled nanostructures (Faul et al., 2003). Due to the simplicity of the synthesis procedure, these hybrid compounds are receiving (Faul et al., 2003) large interest for the development of new smart applications (Kötz et al., 2001; Faul et al., 2003). Polyelectrolyte-surfactant complexes constitute an outstanding subclass of these compounds that distinguished themselves because they combine the ability of ionic surfactants to form highly ordered mesophases with the mechanical stability characteristic of polymers (Thünemann et al., 2004). Polymer ionic complexes have been extensively reviewed and their relative ease of preparation and interest as biomaterials, specifically as drug delivery systems, frequently highlighted (Kötz et al., 2001; Thünemann et al., 2001; Faul et al., 2003; Elsabee et al., 2009).

Ponomarenko et al. (Macknight et al., 1996) studied complexes made of poly(α,L-glutamate) and alkyltrimethylammonium surfactants bearing long alkyl chains (C12, C16 and C18), and reported that in the solid state, these complexes adopt a biphasic structure with the hydrophobic side chains and the hydrophilic polymer main chain clearly separated in organized nano-domains. More recently, ionic complexes of naturally occurring poly(γ-glutamic acid) (PGGA), and different kinds of cationic surfactants including alkyltrimethylammonium (ATMA), alkyltrimethylphosphonium (ATMP) and alkanoylcholine (ACh) halides, have been systematically studied (Pérez-Camero et al., 2004; García-Álvarez et al., 2005; Tolentino et al., 2013a; Gamarra et al., 2017) Also, the ionic complexes of certain polyuronic acids with organocationic compounds have been examined (Tolentino et al., 2011, 2013b). In all cases, the surfactant-biopolymer complex was found to be able to self-assemble in the characteristic layered arrangement although displaying more or less structural differences depending on the constitution of the two components.

Hyaluronic acid (HyA) is a mucopolysaccharide which is ubiquitous in the human body (Necas et al., 2008). Nowadays HyA is receiving great attention as a biomaterial for medical and pharmaceutical applications due to its distinctive properties such as good mucoadhesion, high viscoelasticity, excellent biocompatibility and biodegradability, and extraordinary capacity for holding water (Laurent et al., 1996; Jin et al., 2010). HyA is easily able to promote inflammation and consequently it plays an important role in the regulation of injury associated reactions (Vazquez et al., 2003; Gao et al., 2008). In addition, since HyA is the main ligand for CD44 and RHAMM receptors, which are over-expressed in a variety of tumor cell surfaces (Culty et al.,

1994), it is therefore well suitable for drug targeting in anticancer chemotherapy. However, HyA is highly soluble in water at room temperature, is degraded at a high rate and is also subject to a high renovation turnover. A number of strategies based on the chemical modification of HyA have been developed for overcoming such limitations and widening its potential applications (Balazs et al., 1987; Kuo et al., 1991; Luo, et al., 2000). In this sense, complexes of HyA with several organocationic compounds including drugs have been examined by Battistini et al., (Battistini et al., 2013, 2014, 2017) as a way toward the design of efficient drug delivery systems based on ionic complex dissociation. Also enzyme responsive HyA nanocapsules containing biocide agents have been described (Grützner et al., 2015).

In this paper, we wish to report on complexes made of HyA and cationic surfactants derived from choline, specifically alkanoylcholines, abbreviated as *n*ACh, derived from fatty acids with a number of carbon atoms *n* of 12, 14, 16 and 18, the later including both stearic and oleic acids (Scheme 1). Alkanoylcholines are compounds that are closely related to naturally occurring phospholipids like lecithin that belongs to one of the bio-surfactants groups. Alkanoylcholines are known to display certain biological activity (Ahlstrom et al., 1995) as well as highly appreciated medical properties (Schneider et al., 1957; Alexander et al., 1989; Carelli et al., 2001; Patel, 2003). At difference with alkyltrimethylammonium surfactants, alkanoylcholine surfactants are claimed to be harmless for living organisms since it has been proved that they are readily hydrolysed by butyrylcholine esterase generating common components of human metabolism (Chelminska-Bertilsson et al., 1993) The combination of ACh with HyA to produce *n*ACh·HyA complexes is therefore considered as an excellent approach toward the design of biocompatible systems for targeting drug delivery on tumoral cells. These complexes are expected to be structurally similar to complexes made of tetraalkylammonium surfactants and PGGA which are known to adopt the characteristic layered nanostructure with the hydrophilic and the hydrophobic counterparts separated into two well-differentiated phases (Tolentino et al., 2013a). The *n*ACh·HyA complexes are synthesized and characterized in detail with a special emphasis placed on the dependence of their structure and properties on the length of the alkanoyl group. Finally, nanoparticles of *n*ACh·HyA complexes were prepared, their cytotoxicity *in vitro* evaluated, and the loading and release of the anticancer drug Doxorubicin examined.

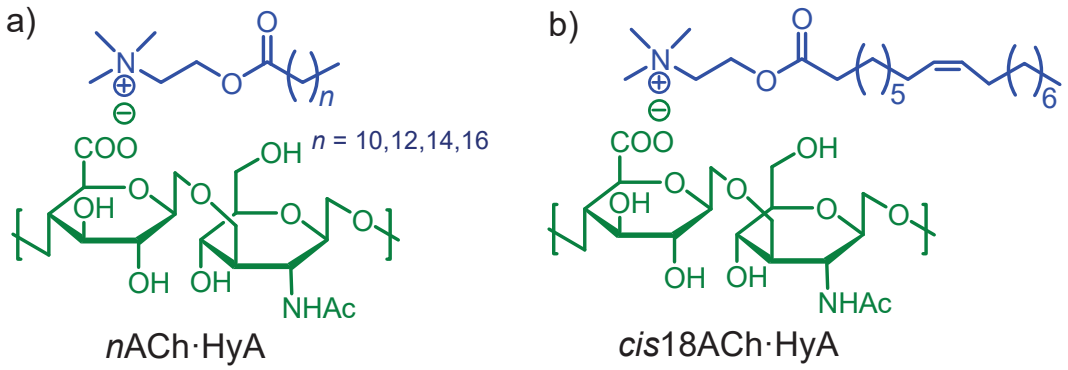

Scheme 1. Chemical structure of the ionic complexes made of HyA and choline esters of saturated (a) and unsaturated (b) fatty acids.

1.2. Results and discussion

1.2.1. Synthesis and chemical characterization of *n*ACh·HyA complexes

The synthesis of the *n*ACh·I (for *n* = 12, 14, 16, 18 and *cis*-18) surfactants was successfully carried out by following the method previously reported (Tolentino et al., 2014a). All the surfactants were obtained in good yields as white powders. The chemical constitution and purity of *n*ACh·I was assessed by ^{1}H and ^{13}C NMR spectroscopy (SI, Figures SI-1 and SI-2).

*n*ACh·HyA complexes were obtained as white precipitates by slow mixing of the aqueous solutions of HyA and surfactant at the minimum temperature required for dissolving the latter. Yields between 70 and 90% were attained by using a 0.01 M concentration for the two solutions except in the case of 12ACh·HyA, where it was raised to 0.02 M for improving the yield which increased from 45% up to 70%. The whole set of *n*ACh·HyA complexes showed the typical solubility behavior of polymers with a strong amphiphilic character, *i.e.* they were soluble in methanol but non-soluble in neither water nor chloroform.

Table 1. Results for the preparation of *n*ACh·HyA complexes.

Complex	Mixing conditions		Yield (%)	Color	Composition[c]
	c (M)[a]	*T* (ºC)[b]			
12ACh·HyA	0.02	45	70	white	1.1:1.0
14ACh·HyA	0.01	55	77	white	1.2:1.0
16ACh·HyA	0.01	65	85	white	1.3:1.0
18ACh·HyA	0.01	70	90	white	1.3:1.0
*cis*18ACh·HyA	0.01	40	84	white	1.0:1.0

[a] Concentration of the two solutions mixed to form the complex.
[b] Temperature selected according to the surfactant solubility in water.
[c] Molar ratio of *n*ACh to HyA in the complex.

The chemical characterization of *n*ACh·HyA complexes was performed by both FTIR and ^{1}H NMR spectroscopies.The FTIR spectra recorded for the whole set of *n*ACh·HyA are compared in Figure 1 together with those of Na·HyA and 18ACh·I. As expected, the spectra of all complexes contain the bands characteristic of the two components with intensities according to the composition. Thus the characteristic broad adsorption of hyaluronic acid at 3300 cm^{-1} that arises from N-H and O-H stretching vibrations appears with an intensity that decays with the increasing value of *n* and that arrives to be almost imperceptible for values of 16 and 18. A similar behavior is observed for the 1030 cm^{-1} band which is characteristic of the glycosidic C-O-C group (Gilli, et al., 1994; Alkrad et al., 2003; Wu, 2012), as well as for the ~1650 cm^{-1} group of bands attributed to the different stretching modes of the N-CO structure present in the acetamide group of HyA. On the other hand, the bands typical of *n*ACh·I surfactants at 1738 and 1165 cm^{-1} (C=O and C-O stretching), 950 cm^{-1} (C-C-stretching vibrations) and 1470, 725 cm^{-1} (CH_2 scissoring and rocking vibrations, respectively) are visible in every spectrum and their intensities increasing with the value of *n*. The spectrum of *cis*-18ACh·HyA fits well in the general trend with the remarkable specific presence of the weak band at ~3005 cm^{-1} that arises from the C-H stretching vibration associated to the double bond (Svatoš et al., 1997).

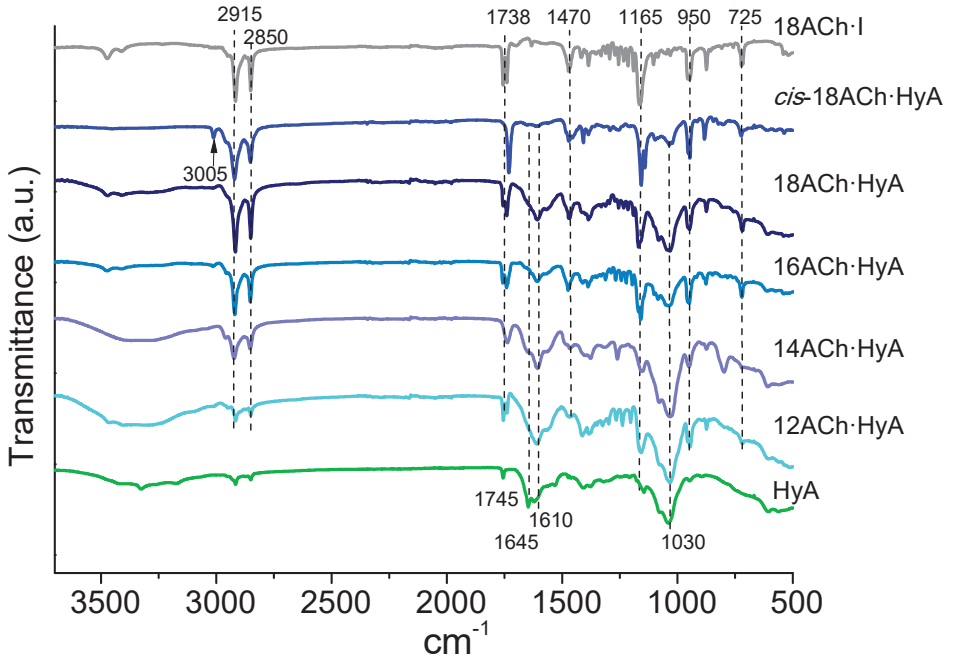

Figure 1. FTIR spectra of the whole set of *n*ACh·HyA complexes. The spectra of Na·HyA and 18ACh·I are included for reference.

The NMR spectroscopy analysis ascertained the chemical constitution of the *n*ACh·HyA complexes (SI, Figures SI-3 and SI-4). The ^{1}H NMR spectra of 18ACh·HyA and *cis*18ACh·HyA are shown in Figure 2 to illustrate the differences observed between saturated and unsaturated complexes. The later contains all the signals observed for the former in addition to two new signals characteristic of the double bond (^{9,10}CH= at 5.2-5.6 ppm and $^{8,11}CH_2$ –CH=, at 1.8-2.2 ppm). The contents of *n*ACh and HyA in the complexes were determined by ^{1}H NMR on the basis of the area ratio of the signal arising from the interior methylenes of the alkyl chain of the surfactant ($^{3\text{-}17}CH_2$, at 1.0-1.7 ppm) to the signal attributed to methyl protons of the acetamide group of HyA (CH_3, at 2.0 ppm). The results obtained by these calculations revealed that *n*ACh·HyA complexes have a nearly stoichiometric composition with *n*ACh to HyA ratios between of 1.0 and 1.3 (Table 1).

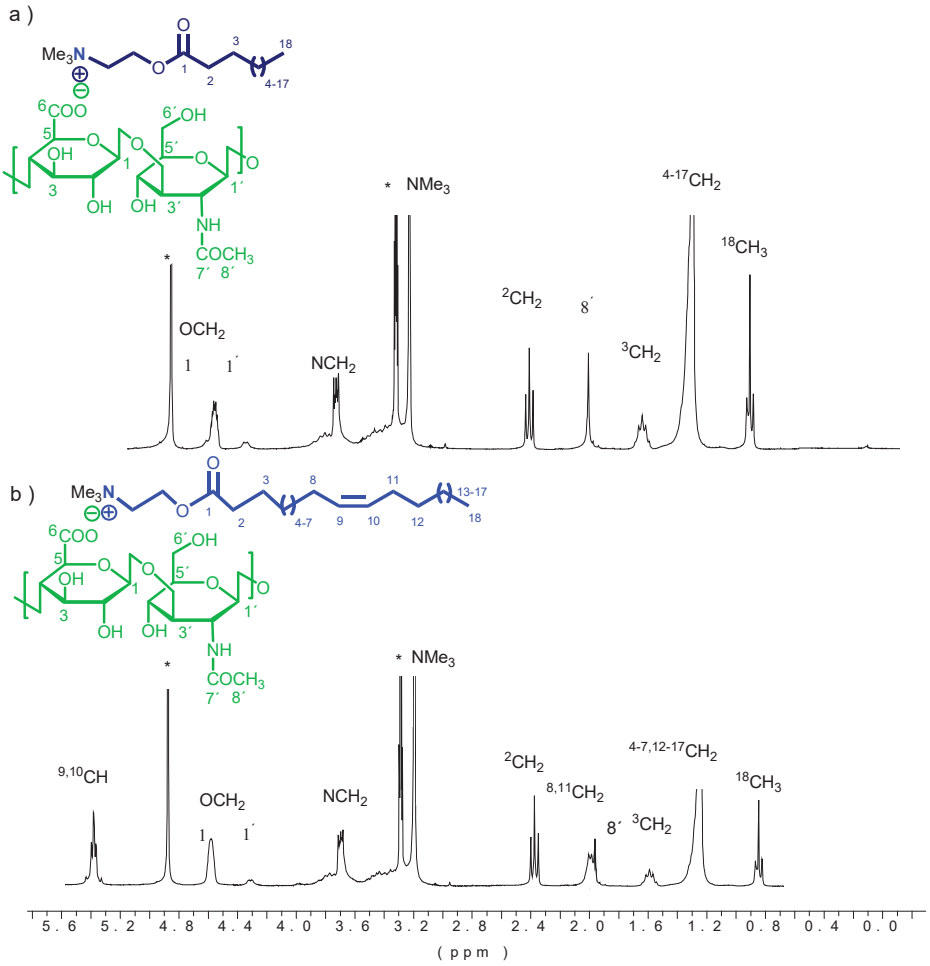

Figure 2. ^{1}H NMR spectra of 18ACh·HyA (a) and *cis*18ACh·HyA (b) complexes recorded in MeOD.

1.2.2. Thermal properties of *n*ACh·HyA complexes

The thermal behavior of *n*ACh·HyA complexes was examined by TGA and DSC, and data obtained by these analyses are summarized in Table 2. The TGA traces recorded from all the samples, as well as their derivatives curves, are shown in Figure 3. The thermal decomposition started to be detectable at 190-210 ºC revealing that both *n*ACh and HyA, which have an onset decomposition temperature at ca. 200 ºC, (Caspersen et al., 2014; Tolentino et al., 2014) retained their thermal stability after complexation. The first derivative of the TGA curves (Figure 3b) shows that saturated *n*ACh·HyA complexes decomposed through a process that involves two steps, the first one at a temperature between 220-226 ºC and the second one between 255-290 ºC. All these complexes left a residual weight of 12-14% after being heated at 600 ºC. $^{max}T_d$ for the first step were within the 220-226 ºC range, which are values close to the $^{max}T_d$ of HyA. Conversely, $^{max}T_d$ of the second step were well above 250 ºC and increased steadily with *n,* suggesting that decomposition of the alkanoyl chain of the surfactant must take place in this step.

Table 2. Thermal parameters of *n*ACh·HyA.

Complex	TGA[a]			DSC[b]						
				1st Heating			Cooling		2nd Heating	
	$^{o}T_d$ (ºC)	$^{max}T_d$ (ºC)	*W* (%)	T_m (ºC)	ΔH_m (Kcal·mol^{-1})	n_c	T_c (ºC)	ΔH_c (Kcal·mol^{-1})	T_m (ºC)	ΔH_m (Kcal·mol^{-1})
12ACh·HyA	200	220/255	14	-	-	-			-	-
14ACh·HyA	205	222/265	14	50	0.8	1	-	-	-	-
16ACh·HyA	212	226/272	14	55	1.9	3	-	-	-	-
18ACh·HyA	216	226/290	12	65	3.9	5	49	-2.2	56	2.0
*cis*18ACh·HyA	194	211/274/334	11	-	-	-	-	-	-	-
HyA	200	228	35	-	-	-	-	-	-	-

[a] $^{o}T_d$ onset for 5% of weight loss and $^{max}T_d$ maximum rate decomposition temperatures. *W*: remaining weight at 600 ºC.
[b] Data taken from DSC traces; T_m and T_c: Melting and crystallization temperatures (ºC); ΔH_m and ΔH_c: melting and crystallization enthalpies. n_c : calculated average number of crystallized methylenes.

The TGA behavior observed for the nACh·HyA series has clear concomitances with those reported for both nACh·PGGA10 and nATMA·HyA13 series suggesting that a similar thermal decomposition mechanism pattern could be shared by the three types of complexes. Unfortunately, little more can be said on mechanism details because, at difference to what happens with PGGA whose thermal decomposition has been extensively studied (David et al., 1968; Portilla-Arias et al., 2007) the knowledge available on this regards for HyA is very scarce (Lowry et al., 1994; Caspersen et al., 2014).

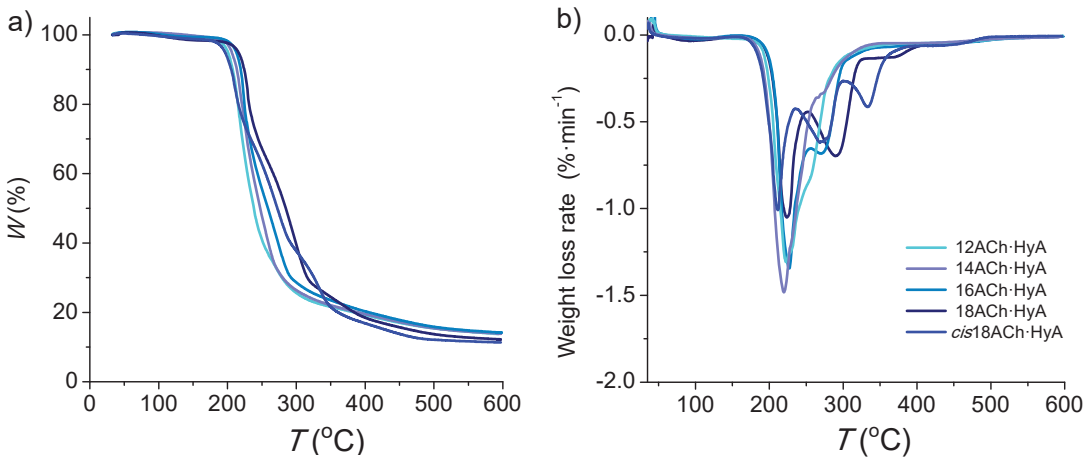

Figure 3. Comparison of the TGA traces for the whole set of *n*ACh·HyA complexes (a) and their derivatives curves (b).

Results for *cis*18ACh·HyA were found to deviate significantly from the pattern observed for the *n*ACh·HyA series, which may be attributed to the presence of the double bond in the hydrocarbon tail of the oleyl-derived surfactant. In this case, the TGA derivative curve shows an additional third decomposition step in the 330-340 ºC range which probably is the consequence of the higher heat resistance that could be expected for the double bond.

The DSC traces for the whole set of complexes are compared in Figure 4a showing that saturated complexes with $n \geq 14$ contain endothermic peaks at temperatures steadily increasing from 50 ºC up to 65 ºC with the value of *n*. According to what is generally accepted for the thermal behavior of comb-like ionic polymer complexes (Pérez-Camero et al., 2004; García-Álvarez et al., 2005; Tolentino et al., 2013a; 2013b), the observed endothermic peaks are associated to the melting of the paraffinic phase of the complex composed of the alkyl chains of the surfactant. The enthalpy of these peaks diminished with *n* indicating that, as expected, crystallinity decreased with the length of the alkyl chain length. It is noticeable that these melting enthalpy values are much lower than those reported for *n*ACh·PGGA (Tolentino et al., 2013a) revealing that HyA is more effective than PGGA in disturbing the molecular arrangement required by the alkanoyl chains to crystallize. On the other hand, the enthalpy values observed here for *n*ACh·HyA are larger than those reported for *n*ATMA·HyA (Tolentino et al., 2013b) indicating that the flexible ester bond of the alkanoylcholine acts as a flexible spacer between the polysaccharide and the polymethylene chain and favours the accommodation of the alkyl chains into the crystal lattice of the paraffinic phase.

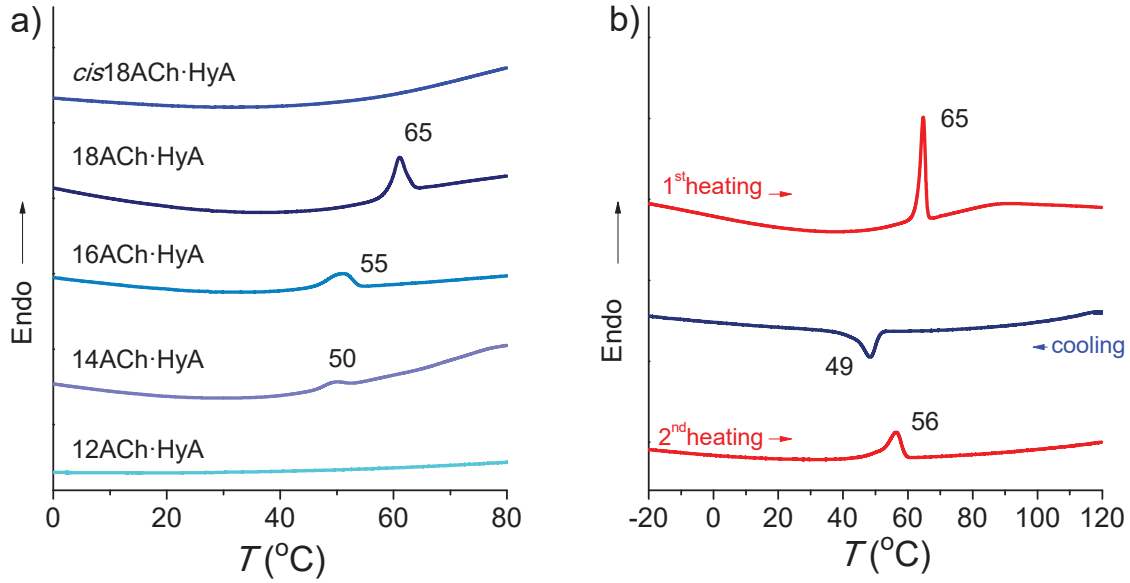

Figure 4. a) Heating DSC traces of the *n*ACh·HyA complexes and b) Heating-cooling DSC traces for 18ACh·HyA.

Upon cooling from 120 ºC, only 18ACh·HyA was able to crystallize confirming the dependence of crystallinity on *n* (Figure 4b). The *cis*18ACh·HyA complex did not show any sign of melting or crystallization according to what could be largely expected from the hindrance effect that the double bond in *cis* configuration exerts on the arrangement of the hydrocarbon tail. Melting temperatures and enthalpies measured along the heating-cooling cycles for the whole set of complexes are given in Table 2.

Melting enthalpy may be used for calculating the number of carbons that are crystallized in the alkyl chain of each complex (Jordan et al., 1971). Plotting ΔH_m against *n* (Figure 5) results in the linear equation $\Delta H_m = \Delta H_{end} + nk$, where ΔH_{end} and *k* are constants reflecting the contribution made to the heat of fusion by the methyl end group and each methylene added to the alkyl chain, respectively. A slope (*k*) of 0.78 kcal·mol^{-1}CH$_2^{-1}$ was found for the first heating, which is in good accordance with the values found for analogous complexes made of PGGA and alkanoylcholines (Tolentino et al., 2013a). In agreement with the fusion enthalpy values reported for the different lattices adopted by paraffinic crystals (Morillo et al., 2003; Pérez-Camero et al., 2004; García-Álvarez et al., 2005) the *k* value found here suggests that the polymethylene chains of *n*ACh·HyA complexes must be packed in a pseudohexagonal crystal lattice. The minimum number of methylenes (n_m) in the chain required for crystallization may be estimated by taking $\Delta H_m = 0$ in the ΔH_m *vs* *n* plot, and the average number of methylenes (n_c) that are crystallized in one chain is given by n-n_m. The resulting values for pristine complexes samples are given in Table 3 showing that the percentage of

carbons crystallized in the alkyl chain decreased with its length, to the point that no crystallization was perceived for 12ACh·HyA.

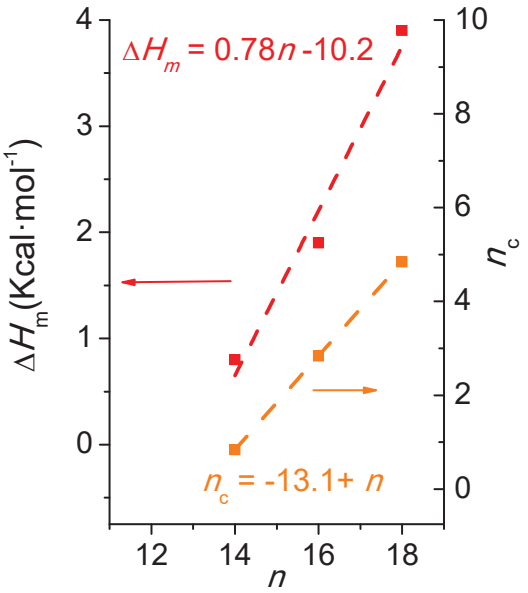

Figure 5. Melting enthalpy (left), and number of crystallized methylenes (right) against the number of carbons contained in the alkyl chain of *n*ACh·HyA complexes.

1.2.3. Structural of *n*ACh·HyA complexes

The structure of *n*ACh·HyA including both crystallinity and mesoscopic order was studied by XRD recorded simultaneously at both small and wide angles (SAXS and WAXS). The profiles recorded in the SAXS region displayed a sharp peak within the 3.9-4.7 nm range with a spacing that steadily moved upwards (higher spacing) with the increasing length of the alkanoyl chain (Figure 6a). According to other similar comb-like ionic polymer complexes made of either PGGA or HyA, this spacing is associated to the periodical distance (L_o) of a biphasic layered structure in which the polysaccharide and the surfactant phases are alternating regularly (Pérez-Camero et al., 2004; Tolentino et al., 2013b). In Figure 7 the L_o distances in *n*ACh·HyA complexes are represented as a function of *n* and are compared with those reported for *n*ACh·PGGA. In both cases an almost linear fitting was attained with a similar slope of 0.12 nm·CH_2^{-1}, but with a significant increase in the periodical distance when the polypeptide was replaced by the polysaccharide. The observed slope corresponds approximately to an increase of half of the C-C-C backbone projection height per additional methylene unit. The expansion observed in the value of L_o for n = 0 is fully related to the difference in the contour length of these two biopolymers.

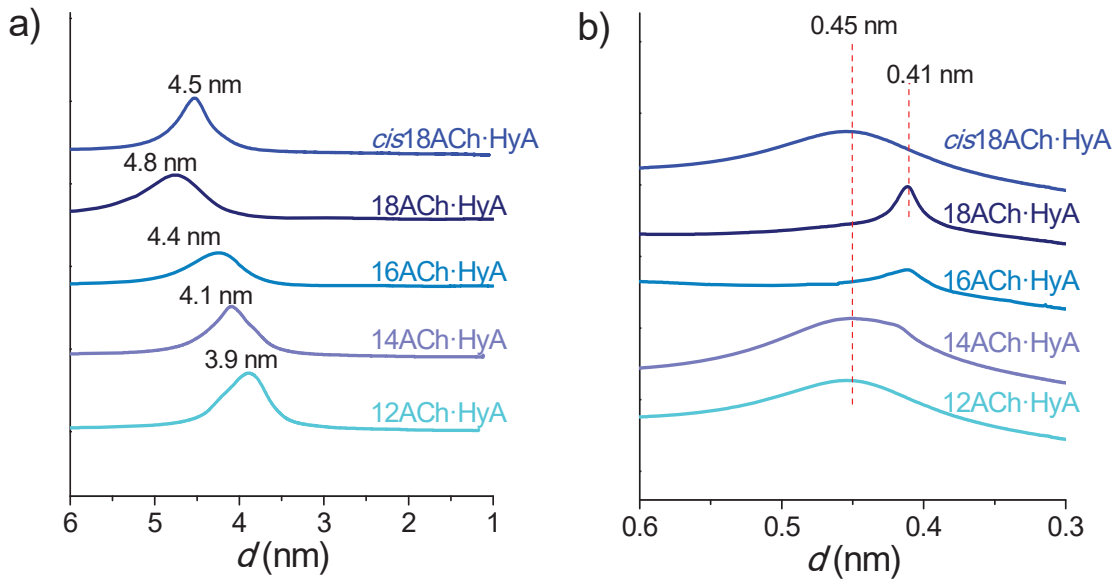

Figure 6. XRD profiles of *n*ACh·HyA recorded at room temperature in the SAXS (a) and WAXS regions (b).

The occurrence of the biphasic arrangement inferred from SAXS results was ascertained by TEM. Electron micrographs taken from films of the 18ACh·HyA prepared by casting on water showed clearly a striated structure corresponding to a layered structure with a periodicity that, as measured by optical diffraction, coincided with that defined by SAXS of this complex (Figure SI-5 in the SI file).

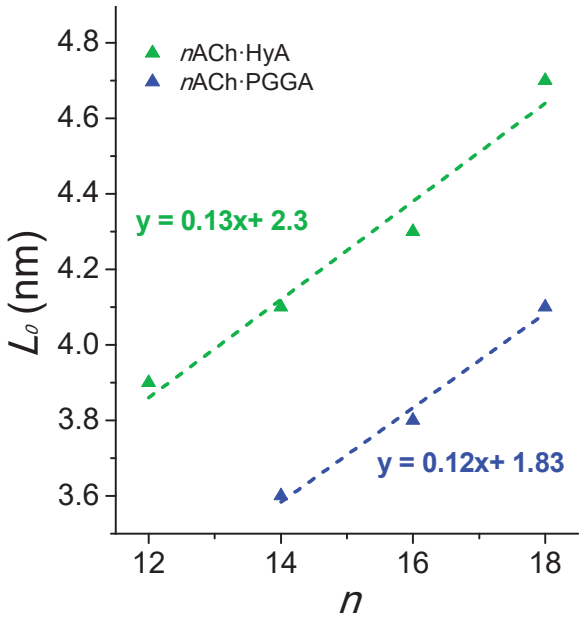

Figure 7. Plot of L_o against *n* for *n*ACh·HyA and *n*ACh·PGGA complexes. Values for the latter have been taken from reference (Tolentino et al., 2013a).

The X-ray scattering recorded in the WAXS region (Figure 6b) provided a clear indication of the order attained in the paraffinic phase in *n*ACh·HyA complexes. The results obtained are in full agreement with those obtained by DSC. Complexes with *n* = 16 and 18 displayed a well-distinct peak at 0.41-0.42 nm which is characteristic of a crystalline state. On the contrary, the WAXS profiles recorded from both 12ACh·HyA and *cis*18ACh·HyA showed a broad peak at 0.45 nm indicating that the alkanoyl chain remained uncrystallised in these complexes, in the former because the polymethylene chain is too short and in the latter because of the disturbing presence of the double bond in a *cis*-configuration. The profile recorded from 14ACh·HyA is predominantly amorphous but showed a small shoulder at 0.41 nm indicative of the presence of a minor fraction of crystallized material. According to the degree of order attained by the paraffinic phase, either a semicrystalline or a liquid-crystal state is adopted by the complex, which can be characterized by POM. Optical micrographs displaying the "batonnet" texture suggestive of the presence of a Smectic-A phase for 12ACh·HyA, and the spherulitic morphology typical of semicrystalline polymers for 18ACh·HyA are shown in Figure SI-6 in the SI file.

1.2.4. Temperature effects on the structure of *n*ACh·HyA.

To evaluate the effect of heating on the structure of the *n*ACh·HyA complexes, they were examined by real-time X-ray diffraction at variable temperatures over the 10-120 ºC interval using synchrotron radiation. Data obtained from this study are collected in Table 3. The SAXS and WAXS profiles recorded along the applied heating-cooling cycle are displayed in Figures 8 and 9 for representative examples (18ACh·HyA and *cis*18ACh·HyA), and the profiles for all the other complexes are provided in the SI file (Figures SI-7 and SI-8).

Table 3. X-ray diffraction data of *n*ATMP·PGGA complexes.

Complex	SAXS			WAXS		
	$L_0^{10ºC}$	$L_0^{120ºC}$	$L_0^{10ºC}$	$d_{100}^{10ºC}$	$d_{100}^{120ºC}$	$d_{100}^{10ºC}$
12ACh·HyA	3.9	3.7	3.8	0.45	0.45	0.45
14ACh·HyA	4.1	3.8	3.8	0.45 (0.41)	0.45	0.45
16ACh·HyA	4.3	4.4	4.2	0.41	0.45	0.45
18ACh·HyA	4.7	4.8	4.7	0.41	0.45	0.41
*cis*18ACh·HyA	4.5	4.5	4.4	0.45	0.45	0.45

L_0 (lamellar spacing) and d_{100} (interplanar spacing) of the paraffinic phase measured at 10 ºC (initial), 120 ºC, and 10 ºC (after cooling).

The changes observed in the scattering profiles of 18ACh·HyA produced in the WAXS region (Figure 8) are in full agreement with the melting-crystallization process

taking place in this complex at temperatures between 50 and 70 ºC. The sharp peak at 0.41 nm disappeared at ~60 ºC and a broad peak at 0.45 appeared instead. This change is indicative of melting of the paraffinic lattice into a disordered structure in which chains are separated by an average distance of 0.45 nm. During cooling, the 0.41 nm reappeared at around 50 ºC to melt at 56 ºC after reheating, a result that brings into evidence the reversibility of the melting-crystallization process in this complex. On the contrary, the WAXS profile of *cis*18ACh·HyA barely changed along the heating-cooling cycle as it should be expected for a disordered phase. The changes observed during heating for the other complexes fit well in one of these two patterns depending on the degree of order attained by the alkanoyl chain in each case. During cooling none of the complexes showed a recovery of the 0.41 peak so that reversibility seems to be unique of the 18ACh·HyA complex.

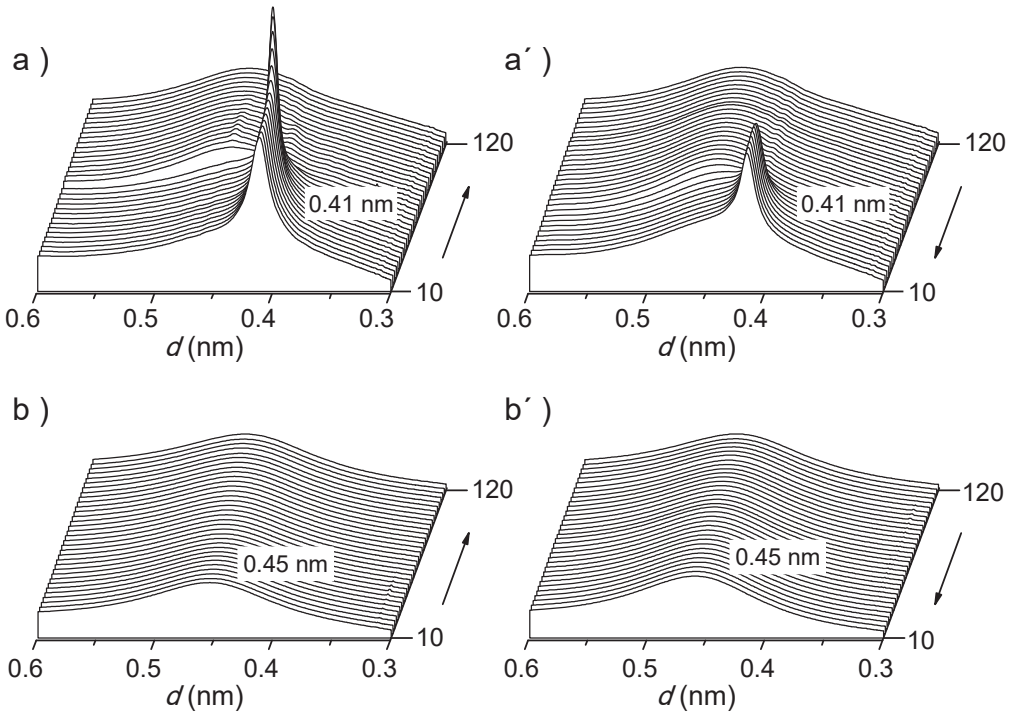

Figure 8. WAXS profiles of 18ACh·HyA (top) and *cis*18ACh·HyA (bottom) at heating (a and b) and cooling (a‘ and b´) along 10-120 ºC range.

The SAXS profiles produced by 18ACh·HyA and *cis*18ACh·HyA complexes are depicted in Figure 9. The changes taking place in the long spacing peaks after heating at 120 ºC are very slight in both cases. In fact, no shift was perceived for *cis*18ACh·HyA whereas a small increasing in the spacing of around 0.1 nm could be observed for 18ACh·HyA. It is worth to mention that the change observed for 18ACh·HyA happened abruptly at ~60 ºC revealing that the rearrangement involved in

this expansion must be associated to the melting of the paraffinic phase. After cooling the initial spacing was recovered although the peak lost some intensity and became slightly broader indicating that the original order must be reduced. As expected, the behavior observed for 16ACh·HyA is almost the same as for 18ACh·HyA whereas in the cases of both 12ACh·HyA and 14ACh·HyA, a small contraction took place upon heating and was not recovered after cooling (Figures SI-7 and SI-8 in SI). The different response given by the complexes to temperature changes can be accounted by their differences in the arrangement of the alkanoyl chain, and it is in agreement with the behavior observed for other closely related complexes previously studied (Pérez-Camero et al., 2004; Tolentino et al., 2013a, 2013b).

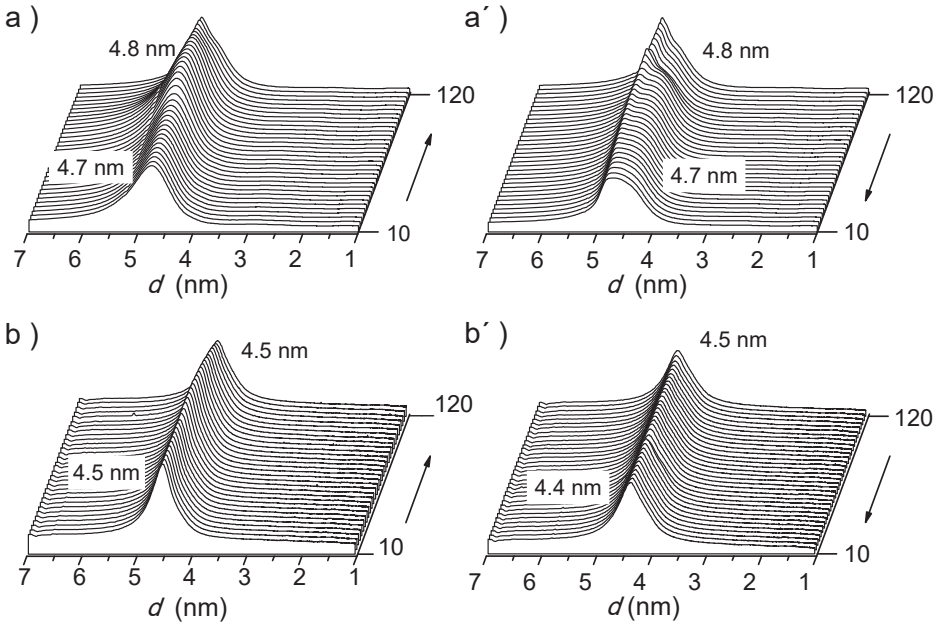

Figure 9. SAXS profiles of 18ACh·HyA (top) and *cis*18ACh·HyA (bottom) at heating (a and b) and cooling (a´and b´) along 10-120 ºC range.

1.2.5. Decomposition of *n*ACh·HyA complexes in aqueous environment

Since *n*ACh·HyA complexes are designed for building nanocarriers to be used in aqueous environments, a study addressed to investigate their response to water was performed. For that purpose, 12ACh·HyA and 18ACh·HyA complexes were incubated under physiological conditions both in the presence and in the absence of hyaluronidases, and the changes taking place with time in the weight, composition, and chemical constitution of the incubated samples were evaluated. In Figure 10, the sample weight remaining after incubation is plotted against the incubation time for the two complexes. 12ACh·HyA appeared to be highly sensitive to the presence of water so disintegration started in the first several hours of incubation and was almost

complete after three days. The weight loss was much faster in the presence of hyaluronidases with the sample fully disintegrating after 24 h. The attack of water on 18ACh·HyA was much less aggressive so that only about 30% of the original weight was lost after three weeks of incubation. As before, the presence of hyaluronidases speeded up the degradation process, so that the weight loss was ca. 60% after such period of time. The much greater stability displayed by 18ACh·HyA is undoubtedly due to the long alkanoyl surfactant chains which largely hindered the water action onto the complex. Not only the hydrophobicity is increased but when *n* = 18 the complex becomes also partially crystalline. It is worthy to notice that the water degradation observed for *n*ACh·HyA complexes is much faster than that for their analogues made of PGGA, a difference that is reasonable when taking into account the greater capacity of hyaluronic acid to swell which makes easier the uptake of water by the complex (Shu ett al., 2004; Kablik et al., 2009). The FTIR spectra recorded from the residual samples collected at increasing incubation times are compared in Figure SI-9 of the SI file. Strikingly, the chemical composition remained essentially unchanged and no band indicative of hydrolysis of the choline stearate was detected. On the contrary, bands arising from the hyaluronic acid increased in intensity, in particular, those associated to end groups generated upon hydrolysis of the polysaccharide. Therefore, it is preliminary concluded that decomposition involves mainly the breaking of the HyA chain with the subsequent release of ACh-coupled oligosaccharides to the aqueous medium. According to what has been reported to occur in similar complexes (Portilla-Arias et al., 2007; Tolentino et al., 2014) it is likely that the decoupling of the ionic pair ACh-Hyal happens to some extent, either in the original complex or in the oligomeric species generated by hydrolysis.

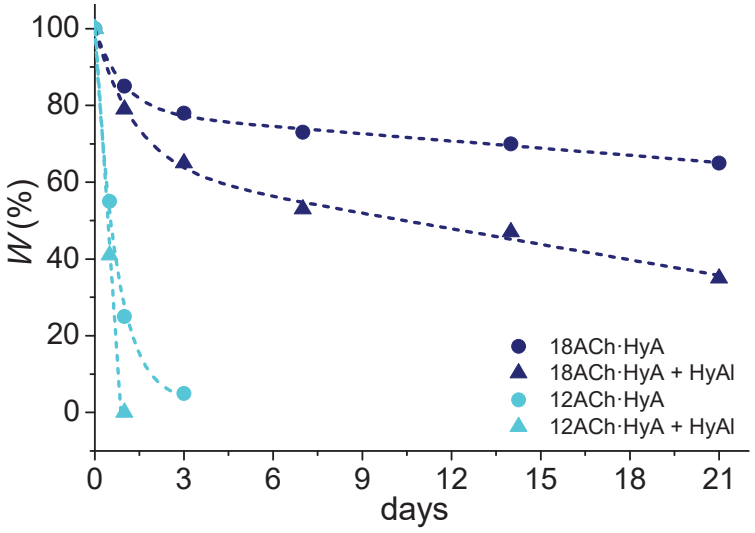

Figure 10. Weight loss undergone by *n*ACh·HyA complexes with n =12 and 18 upon incubation at pH = 7.4 at 37 ºC with and without enzymes added.

1.2.6. *n*ACh·HyA nanoparticles: Characterization, stability and cytotoxicity

We have previously showed that ionic complexes made of PGGA and alkanoylcholines are able to self-assemble in nanoparticles with acceptable stability in suspension and controlled degradability in aqueous environments (Tolentino et al., 2014). The preparation of nanoparticles of *n*ACh·HyA for 18ACh and *cis*18ACh surfactants has been realized using the ionotropic gelation technique. Different experimental conditions were explored to optimize the self-assembly of the complex in NPs whose details are given in Table SI-1 of the SI file. Nanoparticles made of 18ACh·HyA or *cis*18ACh·HyA with a surfactant-to-HyA ratios of 0.25 and 0.5, which were prepared by using a concentration of 0.1% (w/w) for the two aqueous solutions, were those displaying the best shape and size. The most relevant parameters measured for these particles are given in Table 4. No great differences were found between the two types of NPs with hydrodynamic diameters ranging between 135 and 156 nm and the larger size corresponding to those with ACh/HyA ratio of 0.25, which is according to the higher degree of swelling reasonably expected for the NPs with such composition. The ζ potential significantly increased for lower contents in surfactant as it should be expected since a higher concentration of free carboxylic groups will remain on the NP surface at lower surfactant concentration. In addition, differences in ζ potential between 18ACh·HyA and *cis*18ACh NPs were negligible indicating that the presence of the double bond affects significantly neither the size nor the charge of the NPs.

Table 4. Parameters for *n*ACh·HyA nanoparticles.

Parameters	18ACh·HyA		*cis*18ACh·HyA	
	18ACh·HyA-0.25	18ACh·HyA-0.5	18ACh·HyA-0.25	18ACh·HyA-0.5
Na·HyA (wt.%)	0.1	0.1	0.1	0.1
*n*ACh (wt.%)	0.1	0.1	0.1	0.1
ACh:HyA	0.25:1.0	0.5:1.0	0.5:1.0	0.5:1.0
T (ºC)	65	65	35	35
Size (nm)[b]	149	143	156	135
STD (%)[b]	34	35	29	34
ζ potential (mV)	-28.9	-25.7	-29.3	-25.7

[a] Concentration of the aqueous solutions used for gelation.
[b] Average hydrodynamic diameter obtained by DLS measurements in water.
[c] Standard deviation for DLS data.

The NPs made of 18ACh·HyA and *cis*18ACh·HyA NPs with a ACh:HyA ratio of 0.5:1.0 as visualized by TEM are shown in Figure 11 and similar pictures taken for NPs with the ACh:HyA ratio of 0.25:1.0 can be found in Figure SI-10 of the SI file. These micrographs show essentially spherical particles, most of them with diameters between

50 and 100 nm, which values are much smaller than those measured by DLS. Such differences in size are interpreted to be due to the drying underwent by the NPs under the vacuum applied for their observation in the microscope, and also to the fact that the hydrodynamic radio is measured by DLS. Similar sizes are observed for both 18ACh·HyA and *cis*18ACh·HyA NPs in the TEM images despite the differences observed by DLS. This is fully consistent with the results expected from the deswelling of the gel NPs. A close inspection of the TEM images showed the existence of some organization of the complex in the NPs at the nanometric scale. The 18ACh·HyA nanoparticle seen on the inset of Figure 11a displays a layered arrangement with a periodicity (measured by optical diffraction) of 4.7 nm, almost coincident with the value measured by SAXS for the film of this complex. A similar analysis of the NPs made of *cis*18ACh·HyA revealed a granular texture (inset of Figure 11b) indicative of some nanometric organization different to that observed for the 18ACh·HyA complex.

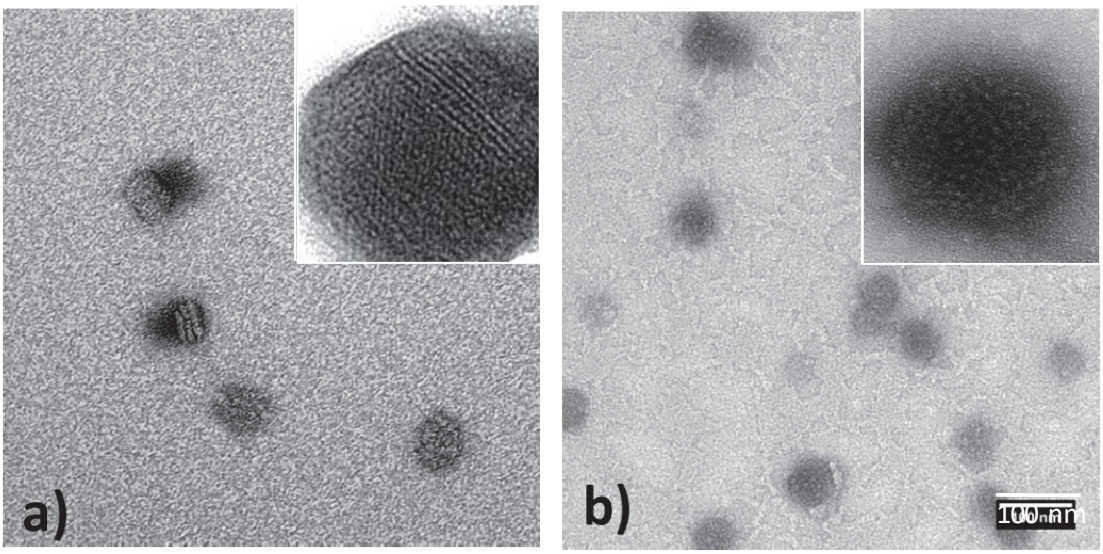

Figure 11. TEM micrographs of NPs made of 18ACh·HyA (a) and *cis*18ACh·HyA (b) with a ACh:HyA ratio of 0.5:1.0. Insets: High magnification pictures showing signs of nanometric ordering.

The stability in water of the NPs was evaluated by measuring the changes in size taking place after incubation for 15 and 30 days at 25 ºC (Figure 12). It was observed that incubation induced an increase of the NP diameter in more than twofold along with a considerable broadening in dispersity. This effect was less pronounced for *cis*18ACh·HyA NPs, which is in principle a striking result since an easier water diffusion could be expected to happen in these amorphous NPs. However it cannot be discarded that aggregation of 18ACh·HyA NPs can be favoured due to the occurrence of specific interactions between the crystalline phases of these NPs leading to further crystallization.

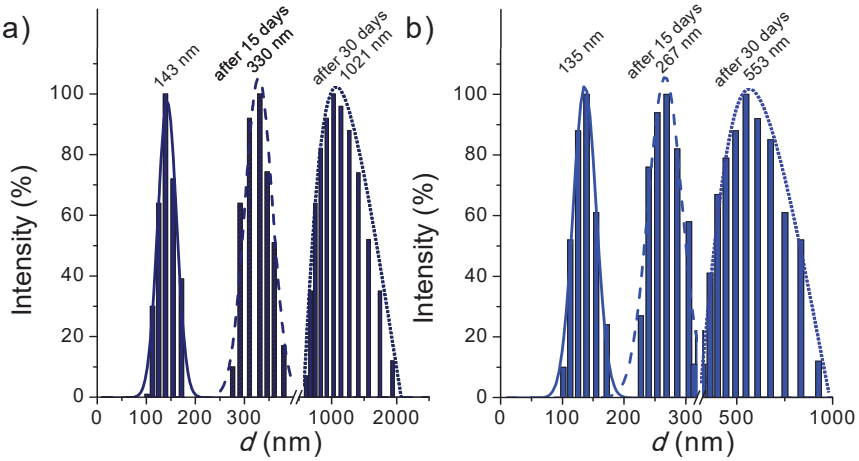

Figura 12. Size evolution of 18ACh·HyA (a) and *cis*18ACh·HyA (b) NPs along incubation time.

The cytotoxicity of 18ACh·HyA and *cis*18ACh·HyA nanoparticles with ACh:HyA ratios of 0.5:1.0 and 0.25:1.0 was evaluated in an *in vitro* study on the raw mouse macrophages 264.7 cell line using a nanoparticle concentration of 75 μg·mL^{-1} and 100,000 cells per well. Cells were incubated for 4 and 24 h at 37 ºC, in a cell culture medium (RPMI, 10% FBS, 1% PenStrep) containing 5% of CO_2. The number of cells still alive after the sheduled incubation times were counted and compared with those present in the control. As it can be seen in Figure 13, percentages of alive cells were over 80% for either 4 h or 24 h of incubation for all the types of NP assayed indicating that none of them displays significant toxicity. Nevertheless, a slight influence of the composition on toxicity may be observed at short times of incubation. The percentage of alive cells after contact for 4 h with NPs made of 0.5:1.0 complexes was 80-90% compared to the close 100% of surviving when the 0.25:1.0 ratio was used. These differences however almost vanished after 24 h of exposition with percentages of remaining alive cells being close to 100% and nearly independent of composition.

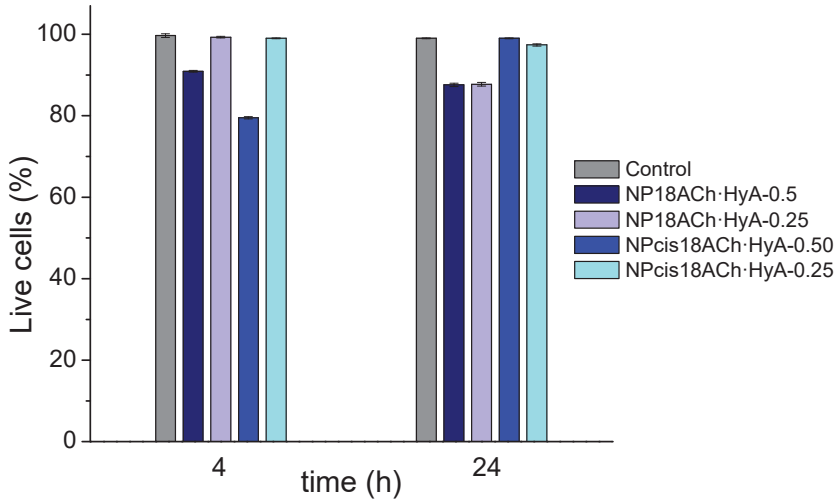

Figure 13. Cell viability of mouse macrophages cell lines 264.7 after exposure to 18ACh·HyA and *cis*18ACh·HyA NPs with different Ach·HyA ratios. Standard deviations are less than 0.3.

1.2.7. *n*ACh·HyA nanoparticles as nanocarriers: DOX loading and releasing

A preliminary study of the potential use of *n*ACh·HyA complexes as drug delivery systems was performed by the loading and releasing of DOX from both films and NPs made of 18ACh·HyA and *cis*18ACh·HyA. In all cases, the amount of DOX added for loading was around 5% of the complex. The loading efficiency was 100% and 83% for films and NPs, respectively. The delivery study was performed by incubation of the loaded films and NPs in PBS at room temperature and following the drug release along time by UV spectroscopy. The releasing profiles obtained for the two complexes are represented in Figure 14 which reveals the following: a) In all cases DOX release started at time 0 with almost no burst, b) drug delivery happened at high rate and was faster in films, c) delivery rate differences between 18ACh·HyA and *cis*18ACh·HyA complexes were not significant, and d) complete delivery of DOX was accomplished in 24 h whereas only 60% of the drug loaded in NPs was released by that time. The different kinetic behaviour displayed by the two systems, films and NPs, may be due to the degree of ionic drug-HyA interaction attained in each case. Since films were formed from complexes to which DOX was then added, the coupling of the drug with HyA is expected to occur in a lesser extent than in NPs, which were built upon simultaneous coupling of DOX and the alkanoylcholine with the polyacid. The DOX-HyA ionic interaction prevailing in this system would delay the release of the drug compared to films where DOX is only physically adsorbed.

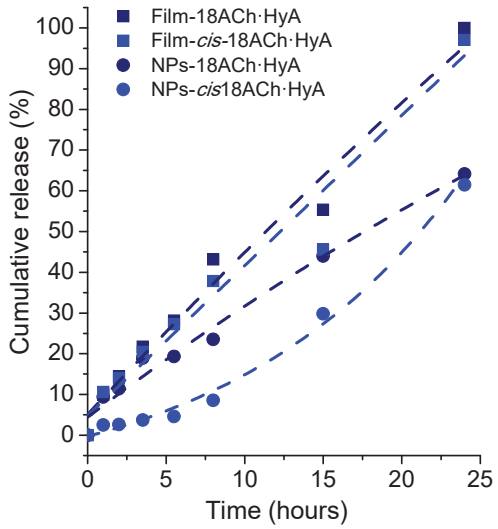

Figure 14. Drug release from 18ACh·HyA and *cis*18ACh·HyA complexes as films or NPs after being incubated at pH 7.4 and 37 ºC.

1.3. Conclusions

Ionic complexes of hyaluronic acid and alkanoylcholine surfactants (*n*ACh·HyA) with a nearly stoichiometric composition and a comb-like architecture could be successfully synthesized by applying the general coupling procedure. The *n*ACh·HyA complexes were water-insoluble and stable up to ca. 200 ºC. These complexes adopted in the solid state an amphiphilic nanometric structure with the polysaccharide and the surfactant segregated in two phases that alternate regularly with a periodicity of about 4-5 nm. Since the two components of *n*ACh·HyA are biocompatible and biodegradable, and the complexes tend to self-assemble with the paraffinic phase segregated in a separated domain, they stand out as good candidates for building nanocarriers for both hydrophobic, neutral, and ionically charged drugs. Spherical nanoparticles with diameters ca. 150 nm could be prepared by ionotropic gelation from the complexes derived from stearoyl and oleoyl choline with ACh:HyA ratios of 0.5 and 0.25. These nanoparticles were stable for a few days in aqueous emulsion to finally precipitate after one month of incubation. The cytotoxicity study carried out on these NPs has shown that they are biocompatible. Loading and releasing assays of DOX on NPs of 18ACh·HyA and *cis*18ACh·HyA demonstrated a high loading efficiency and a fast drug delivery upon incubation under physiological conditions. The final conclusion is that *n*ACh·HyA complexes may be considered a highly promising biocompatible/biodegradable platform for the design of systems suitable for drug transport and targeted delivery in anticancer chemotherapy.

1.4. References

Ahlstrom, B., Chelminska-Bertilsson, M., Thompson, R. A., Edebo, L. (1995). Long-chain alkanoylcholines, a new category of soft antimicrobial agents that are enzymatically degradable. Antimicrob. Agents Chemother. 39 (1), 50–55.

Alkrad, J.A., Mrestani, Y., Stroehl, D., Wartewig, S., Neubert, R. (2003). Characterization of enzymatically digested hyaluronic acid using NMR, raman, IR, and UV-Vis spectroscopies. J. Pharm. Biomed. Anal. 31 (3), 545–550.

Alexander, J., Fix. J.A. (1989). Enhancement of absorption of drugs from gastrointestinal tract using choline ester salts - US Pat. 4,822,773.

Baier, G., Cavallo, A., Vasilev, K., Mailänder, V., Musyanovych, A., Landfester, K. (2013) “Enzyme responsive hyaluronic acid nanocapsules containing polyhexanide and their exposure to bacteria to prevent Infection” Biomacromolecules, 14, 1103-1112.

Balazs, E., Leshchiner. (1987). A. Cross-linked gels of hyaluronic acid and products containing such gels. US4582865A US Grant, December 6

Battistini, F.D., Olivera, M.E., Manzo, R.H. (2013). Equilibrium and release properties of hyaluronic acid–drug complexes. Eur. J. Pharm. Sci. 49 (4), 588–594.

Battistini, F.D., Flores-Martín, J., Olivera, M.E., Genti-Raimondi, S., Manzo, R. H. (2014). Hyaluronan as drug carrier. the in vitro efficacy and selectivity of hyaluronan–doxorubicin complexes to affect the viability of overexpressing CD44 receptor cells. Eur. J. Pharm. Sci. 2014, 65, 122–129.

Battistini, F.D., Tártara, L.I., Boiero, C., Guzmán, M.L., Luciani-Giaccobbe, L.C., Palma, S.D., Allemandi, D. A., Manzo, R.H., Olivera, M.E. (2017) The role of hyaluronan as a drug carrier to enhance the bioavailability of extended release ophthalmic formulations. hyaluronan-timolol ionic complexes as a model case. Eur. J. Pharm. Sci. 105, 188–194.

Carelli, V., Liberatore, F., Scipione, L., Cardellini, M., Rotiroti, Domenicantonio Rispoli, V. (2001). Choline derivatives for the treatment of alzheimer's disease - Patent-WO0181296.

Caspersen, M. B., Roubroeks, J. P., Liu, Q., Huang, S., Fogh, J., Zhao, R., Tømmeraas, K. (2014). Thermal degradation and stability of sodium hyaluronate in solid state. Carbohydr. Polym. 107 (1), 25–30.

Chelminska-Bertilsson, M., Allenmark, S., Edebo, L. Butyrylcholinesterase activity towards long-chain alkanoylcholines: kinetics and mechanism. (1993). Biochim. Biophys. Acta - Protein Struct. Mol. Enzymol. 1202 (1), 56–60.

Culty, M., Shizari, M., Thompson, E.W., Underhill, C.B. (1994). Binding and degradation of hyaluronan by human breast cancer cell lines expressing different forms of CD44: correlation with invasive potential. J. Cell. Physiol. 160 (2), 275–286.

Elsabee, M.Z., Morsi, R.E., Al-Sabagh, A.M. (2009). Surface active properties of chitosan and its derivatives. Colloids Surfaces B Biointerfaces, 74 (1), 1–16.

Faul, C.F.J., Antonietti, M. (2003). Ionic Self-Assembly: Facile Synthesis of Supramolecular Materials. Adv. Mater. 15 (9), 673–683.

Gamarra, A., Martínez de Ilarduya, A., Vives, M., Morató, J., Muñoz-Guerra, S. (2017). Ionic complexes of poly(γ-glutamic acid) with alkyltrimethylphosphonium surfactants. Polymer, 116, 43–54.

Gao, F., Yang, C.X., Mo, W., Liu, Y.W., He, Y.Q. (2008). Hyaluronan oligosaccharides are potential stimulators to angiogenesis via RHAMM mediated signal pathway in wound healing. Clin. Investig. Med. 31 (3), 106–116.

García-Álvarez, M., Álvarez, J., Alla, A., Martínez de Ilarduya, A., Herranz, C., Muñoz-Guerra, S. (2005). Comb-like ionic complexes of cationic surfactants with bacterial poly(γ-glutamic acid) of racemic composition. Macromol. Biosci. 5(1), 30–38.

Gilli, R., Kacuráková, M., Mathlouthi, M., Navarini, L., Paoletti, S. (1994). FTIR studies of sodium hyaluronate and its oligomers in the amorphous solid phase and in aqueous solution. Carbohydr. Res. 263 (2), 315–326.

Jin, Y. J., Ubonvan, T., Kim, D. D. (2010). Hyaluronic acid in drug delivery systems. J. Pharm. Investig. 40, 33–43.

Jordan, E.F., Feldeisen, D. W., Wrigley, A. N.(1971). Side-chain crystallinity. I. Heats of fusion and melting transitions on selected homopolymers having long side chains. J. Polym. Sci. Part A-1 Polym. Chem. 9 (7), 1835–1851.

Kablik, J., Monheit, G.D., Yu, L., Chang, G., Gershkovich, J. (2009). Comparative physical properties of hyaluronic acid dermal fillers. Dermatologic Surg. 35 (Sup 1), 302–312.

Kuo, J. W., Swann, D.A., Prestwich, G.D. (1991). Chemical modification of hyaluronic acid by carbodiimides. Bioconjug. Chem. 2 (4), 232–241.

Laurent, T.C., Laurent, U.B.G., Fraser, J.R.E. (1996). The structure and function of hyaluronan: an overview. Immunol. Cell Biol. 74 (2), A1–A7.

Lowry, K.M., Beavers, E.M. (1994). Thermal stability of sodium hyaluronate in aqueous solution. J. Biomed. Mater. Res. 28 (10), 1239–1244.

Luo, Y., Kirker, K. R., Prestwich, G.D. (2000). Cross-linked hyaluronic acid hydrogel films: new biomaterials for drug delivery. J. Control. Release, 69 (1), 169–184.

Morillo, M., Martínez de Ilarduya, A., Alla, A. (2003). Comb-like alkyl esters of biosynthetic poly (γ-glutamic acid). 2. Supramolecular structure and thermal transitions. Macromolecules, 36 (20), 7567–7576.

Necas, J., Bartosikova, L., Brauner, P., Kolar, J. (2008). Hyaluronic acid (hyaluronan): a review. Vet. Med. 53 (8), 397–411.

Patel, H. (2003). Use of choline derivatives for memory, learning and cognition-WO Pat. 2005018631 A1.

Pérez-Camero, G., García-Álvarez, M., Martínez de Ilarduya, A., Fernández, C., Campos, L., Muñoz-Guerra, S. (2004). Comblike complexes of bacterial poly(γ,D-glutamic acid) and cationic surfactants. Biomacromolecules, 5(1), 144–152.

Portilla-Arias, J. A., García-Alvarez, M., Martínez de Ilarduya, A., Muñoz-Guerra, S. (2007). Ionic complexes of biosynthetic poly(malic acid) and poly(glutamic acid) as prospective drug-delivery systems. Macromol. Biosci. 7(7), 897–906.

Portilla-Arias, J. A., García-Alvarez, M., Martínez de Ilarduya, A., Muñoz-Guerra, S. (2007). Thermal decomposition of microbial poly(γ-glutamic acid) and poly(γ-glutamate)s. Polym. Degrad. Stab. 92(10), 1916–1924.

Schneider, R., Timms, A.R. (1957) Some aspects of the pharmacology of an homologous series of choline esters of fatty acids. Br. J. Pharmacol. Chemother. 12 (1), 30–38.

Svatoš, A., Attygalle, A. B. (1997). Characterization of vinyl-substituted, carbon−carbon double bonds by GC/FT-IR Analysis. Anal. Chem. 69 (10), 1827–1836.

Shu, X.Z., Liu, Y., Palumbo, F.S., Luo, Y., Prestwich, G.D. (2004). In situ crosslinkable hyaluronan hydrogels for tissue engineering. Biomaterials, 25, 1339–1348.

Tolentino, A., Alla, A., Martínez de Ilarduya, A., Muñoz-Guerra, S. (2011). Comb-like ionic complexes of pectinic and alginic acids with alkyltrimethylammonium surfactants. Carbohydr. Polym. 86(2), 484–490.

Tolentino, A., León, S., Alla, A., Martínez de Ilarduya, A., Muñoz-Guerra, S. (2013a). Comblike ionic complexes of poly(γ-glutamic acid) and alkanoylcholines derived from fatty acids. Macromolecules, 46(4), 1607–1617.

Tolentino, A., Alla, A., Martínez de Ilarduya, A., Muñoz-Guerra, S. (2013b). Comb-like ionic complexes of hyaluronic acid with alkyltrimethylammonium surfactants. Carbohydr. Polym. 92(1), 691–696.

Tolentino, A., Alla, A., Martinez de Ilarduya, A., Font-Bardia, M., Leon, S., Munoz-Guerra, S. (2014a). Thermal behavior of long-chain alkanoylcholine soaps. Rsc Adv. 4, 10738–10750.

Tolentino, A., Alla, A., Martínez de Ilarduya, A., Muñoz-Guerra, S. (2014b). Complexes of poly(glutamic acid) and long-chain alkanoylcholines: Nanoparticle formation and drug release. Int. J. Biol. Macromol. 66, 346–353.

Vazquez, J.R., Short, B., Findlow, A.H., Nixon, B.P., Boulton, A.J.M., Armstrong, D.G. (2003). Outcomes of hyaluronan therapy in diabetic foot wounds. Diabetes Res. Clin. Pract. 59 (2), 123–127.

Wu, Y. (2012). Preparation of low-molecular-weight hyaluronic acid by ozone treatment. Carbohydr. Polym. 89 (2), 709–712.

Chapter VIII. Ionic complexes of poly(γ-glutamic acid and hyaluronic acid with LAE surfactant

Traditional food packaging methods do not always provide the required shelf-life to allow a satisfactory commercialization of foods. Active packaging with antioxidant or antimicrobial properties can improve fresh food stability and potentially offer shelf-life extension to certain foods. In this sense, polymers that contain antimicrobial agents are very attractive in active packaging applications since their characteristic properties such as permeation, sorption and migration can constitute the mechanism of action of the active packaging system.

In this chapter we couple the antimicrobial surfactant LAE to both, poly(γ-glutamic acid) (PGGA) and hyaluronic acid (HyA), to achieve biocide-polymer systems based on ionic host-guest polymer complexes. As mentioned before, LAE is one of the most potent food antimicrobial agents, with a broad spectrum of antimicrobial activity. LAE is synthesized from lauric acid, *L*-arginine and ethanol and has been verified to be nontoxic because it is rapidly metabolized to amino acid arginine by hydrolysis of the ethyl ester and lauroyl amide functions. Furthermore, LAE has been classifiend as food preservative at concentration up to 200 ppm by the Food and Drug Administration (FDA). According to these outstanding features, LAE is becoming a product widely used for pharmaceuticals, cosmetics and food conservation.

The objective of this chapter is coupling LAE with two kind of biopolymers with two main objectives. On the one hand, obtaining antimicrobial polymeric materials for food packaging. For this regard, PGGA is an excellent candidate due to its edibility and innocuity. As mention before, the polyanionic nature of this biopolymer makes it very suitable for the efficient loading of organocationic compounds by ionic coupling. Furthermore, the capacity of PGGA to inhibit by itself the growth of some pathogenic bacteria has been also announced. On the other hand, obtaining HyA derivatives with antimicrobial properties. HyA has attached quite attention as antimicrobial polymer because its capacity to cleavage to some bacteria that produce hyalunonidases *e.g. S. aureus.* Despite the bacteriostatic effect found in HyA, infections are not still completely avoid in some medical applications. The reason is that the antimicrobial activity of the polysaccharide is not clear and seems to depend on the concentration and molecular weight of HyA. Therefore, HyA must be used in combination with antimicrobial agents to ensure its antimicrobial effect.

VIII.1. Antibacterial films made of ionic complexes of poly(γ-glutamic acid) and ethyl lauroyl arginate

Abstract: The biocide agent LAE (ethyl $^{\alpha}$*N*-lauroyl L-arginate chloride) was coupled with poly(γ-glutamic acid) (PGGA) to form stable ionic complexes with LAE:PGGA ratios of 1 and 0.5. The nanostructure adopted by these complexes and its response to thermal changes were examined in detail by DSC and XRD using synchrotron radiation in real time. A layered biphasic structure with LAE filling the space between polypeptidic sheets was adopted by the complexes. The complexes were stable up to above 250 ºC, non-water soluble, and able to form consistent transparent films. The release of LAE from the complexes upon incubation in aqueous buffer was examined and found to depend on both pH and complex composition. The antibacterial activity of films made of these complexes against Gram-positive (*L. monocytogenes* and *S. aureus*) and Gram-negative (*E. coli* and *S. enterica*) bacteria was evaluated and found to be very high against the formers and only moderate against the later. The bactericide activity displayed by the LAE·PGGA complexes was directly related with the amount of LAE that was released to the environment.

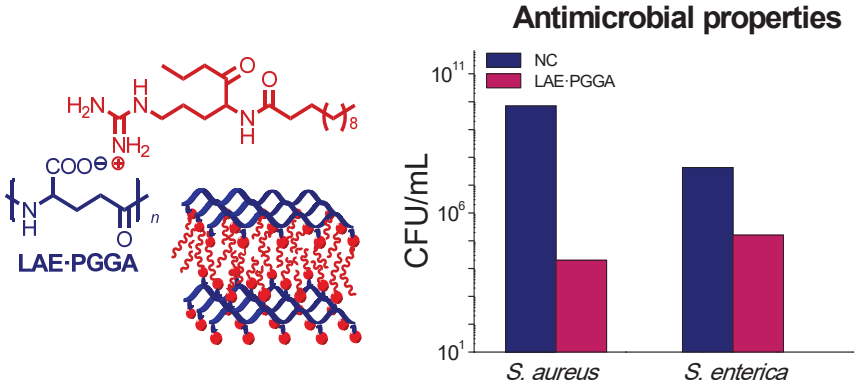

Publication derived from this work:

Gamarra, A., Missagia, B., Morató, J. Muñoz-Guerra, S. (2018). Antibacterial films made of ionic complexes of poly(γ-glutamic acid) and ethyl lauroyl arginate. Polymers, 10, 1-15.

Supporting Information (SI) to this chapter in Annex E.1

1.1. Introduction

Food safety is today an issue of major concern that is receiving great social and technological attention. It has been estimated that as much as 30% of people in industrialized countries suffer yearly from a food borne disease, and that in 2000 at least two millions of people died from diarrheal diseases worldwide, the major proportion being attributable to microbial contamination of food and water (Mead et al., 1999). There are more than 200 of active agents causing gastrointestinal illnesses, about 60% of which being due to infection by food borne bacterial pathogens. *Salmonella spp., Campylobacter spp. and Escherichia coli* are the bacteria traditionally attracting major attention (Newell et al., 2010) but in the last decades concerns have included not only an increasing number of additional pathogens as *L. monocytogenes* but also the expansion of modified traditional strains displaying antimicrobial resistance (Lai et al., 2016). The use of bactericides, both synthetic and of natural origin constitutes today the most common practice applied to prevent food spoilage so the demand for these compounds has increased considerably in these last years (Dobrucka, 2016; Fu et al., 2016). Methods followed for impregnating the targeted food with the antimicrobial agent include blending in bulk, surface treatment, and controlled delivery from active films used either for wrapping or coating the food (Appendini et al., 2002; Muñoz-Bonilla et al., 2012).

The incorporation of antimicrobials into polymeric films in contact with food to be gradually released during shelf-life has unquestionable advantages over those procedures in which the active compound is directly loaded into or onto the food. a) Deactivation of the antimicrobial by the food components is largely prevented, and b) a higher effectiveness in the inhibition of pathogens growing on the food surface, which is the most common way of food contamination, may be achieved. As a result, smaller amounts of active compounds will be required by the film activation approach to reach satisfactory outcomes. This is a very remarkable benefit since additive minimization constitutes a major challenge today for food quality and safety (Malhotra et al., 2015; Erickson et al., 2017).

In this paper we wish to report on a new antibacterial polymeric system based on an ionic polymer complex made of poly(γ-glutamic acid) (PGGA) and a guanidinium-based compound (LAE). PGGA is an emerging biopolymer that is edible and biodegradable, and that has an enormous potential as biomaterial (Patel et al., 2007). PGGA is generated by bacterial fermentation of a wide variety of substrates and it is produced at industrial scale to be used as a food complement, in healthcare and for water treatment, among others. As it is much expected for a polycarboxylic compound,

PGGA is highly hygroscopic and a number of modifications consisting mainly of esterification and amidation of the carboxylic side groups, has been reported with the purpose of making the polymer higher water-resistant (Muñoz-Guerra et al., 2013). The innocuity of PGGA makes it an excellent candidate for designing antimicrobial polymeric materials for food packaging. On the other hand, the polyanionic nature of this biopolymer makes it very suitable for the efficient loading of organocationic compounds by ionic coupling. In fact, ionic complexes of PGGA with both alkylammonium (Pérez-Camero et al., 2004; García-Álvarez et al., 2005; Portilla-Arias, et al., 2007a) and alkylphosphonium (Gamarra et al., 2017) soaps have been reported and the capacity of the later to display biocide activity has been demonstrated. Furthermore, the capacity of PGGA to inhibit by itself the growth of some pathogenic bacteria has been also announced (Lee et al., 2014). Nevertheless, the references on the application of PGGA in food packaging are very scarce in the accessible literature (Siracusa et al., 2008).

LAE (ethyl $^{\alpha}$*N*-lauroyl L-arginate) is one of the most potent food preservative agents known today that displays a broad spectrum of activity against food-borne bacteria (Becerril et al., 2013; Otero et al., 2014). The high biocide activity of LAE has been attributed to its capacity for altering the metabolic processes of microorganisms without causing cellular lysis (Rodriguez et al., 2004). LAE has been assessed to be nontoxic since after consumption it is rapidly metabolized to naturally occurring amino acids, among which arginine and ornithine appear to be majority (Ruckman et al., 2004; Hawkins et al., 2009). The Food and Drug Administration (FDA) has classified LAE as GRAS (Generally Recognized as Safe) food preservative at concentrations up to 200 ppm. Antibacterial films containing LAE were firstly prepared from synthetic polymers of common use in packaging such as PP, EVA and EVOH (Muriel-Galet et al., 2012, 2015; Otero et al., 2014). In these last years, efforts has been redirected towards the development of systems made of either bio-based polymers as PLA (Guo et al., 2014), biopolymers as chitosan (Higueras et al., 2013; Ma et al., 2016), and others (Pattanayaiying et al., 2015; Kashiri et al., 2016), which are able to be biodegraded and even fit to be eaten.

Organocationic compounds are extensively used as bactericides in a diversity of applications but their utilization in active films is severely limited by the difficulty in achieving suitable mixing with polymers commonly used for packaging. Coupling the organocation with anionic polymers is a useful approach that allows designing active films with the desired stability and releasing properties. The ionic interaction of LAE with anionic polysaccharides has been examined to evaluate the influence that these

compounds may have on its biocide activity when they are used as food ingredients (Asker et al., 2009, 2011; Loeffler et al., 2014). However, to our knowledge, no study addressed to assess the potential of ionic LAE complexes as active films has been described so far. In this work, LAE has been coupled with the polyanionic PGGA to obtain ionic stable complexes (LAE·PGGA) with antibacterial properties. Firstly the LAE·PGGA complexes are extensively characterized by physical-chemical methods (FTIR, NMR, TGA, DSC, XRD and POM) to establish their chemical and supramolecular structure. Then the dissociation of the complexes into their components upon incubation at different pH is examined. Finally the antibacterial properties of the complexes against Gram-positive bacteria (*Listeria monocytogenes and Staphylococcus aureus*) and Gram-negative bacteria (*Salmonella enterica and Escherichia coli*) are preliminary estimated in order to evaluate their potential for food preserving and packaging applications.

1.2. Results and discussion

1.2.1. Synthesis of complexes

The synthesis of the complexes of PGGA and LAE did not entail any special difficulty since they were spontaneously formed upon mixing the aqueous solutions of LAE and PGGA-Na (Scheme 1). Ionic coupling of the guanidinium cation of LAE and the carboxylate anion of PGGA resulted in non-water soluble stable complexes that precipitated from the aqueous solution upon standing. Two LAE:PGGA ratios, *i.e*. 1:1 and 1:2, were used with the purpose of evaluating the effect of composition on properties. The complexes were recovered by centrifugation in the form of white powders in 50-70% yields. Conditions used in these experiments and results attained are given in Table 1.

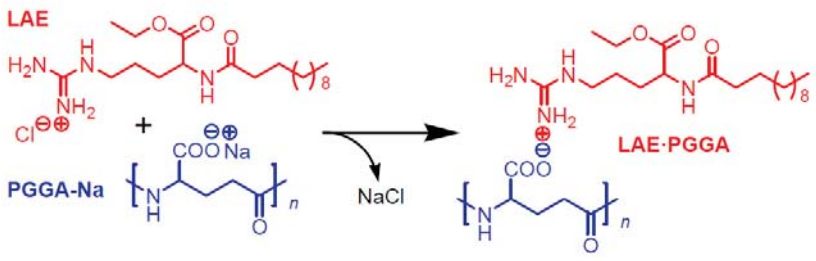

Scheme 1. Coupling reaction leading to ionic LAE·PGGA complexes.

Table 1. Results for the preparation of LAE·PGGA complexes.

Complex	LAE:PGGA[a]	Mixing conditions		Yield (%)	Color	Composition[d]
		c (M)[b]	*T* (ºC)[c]			
LAE·PGGA-1	1.0:1.0	0.01	35	70	white	0.9:1.0
LAE·PGGA-0.5	0.5:1.0	0.01	35	57	white	0.5:1.0

[a]Molar ratio of LAE to PGGA used for coupling.
[b] Concentration of the solutions mixed to form the complex.
[c] Minimum temperature at which LAE is soluble in water at the used concentration.
[d] Molar ratio of LAE to PGGA in the complex determined by ^{1}H NMR.

1.2.2. Chemical characterization

The presence of the two components in the LAE·PGGA complexes was evidenced by FTIR, as it is shown in Figure 1. The characteristic absorptions of both LAE and PGGA are present in the spectra of the complexes with the expected relative transmittance values.

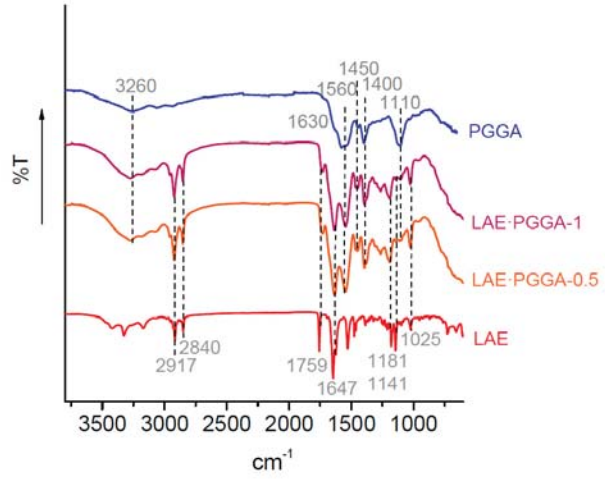

Figure 1. Compared FTIR spectra of LAE, PGGA and LAE·PGGA complexes.

The ^{1}H NMR analysis of the complexes ascertained the presence of the two components and provided an accurate quantification of their composition. The spectrum recorded from LAE·PGGA-1 is depicted in Figure 2 with indication of peak assignments. The area ratio of the signal arising from the γ-methylene of PGGA to the area of the two partially overlapped signals including the 3-11 methylenes of the lauroyl chain of LAE revealed that the actual composition of the complexes LAE·PGGA-1 and LAE·PGGA-0.5 were 0.9:1 and 0.5:1, respectively, which are values very close to those expected from the relative amounts of the two components that were used for their preparation. The ^{1}H NMR spectrum of LAE·PGGA-0.5 as well as the ^{13}C NMR of

the two complexes are shown in the Supplementary Information (SI) file associate to this chapter (Figures SI-1 and SI-2).

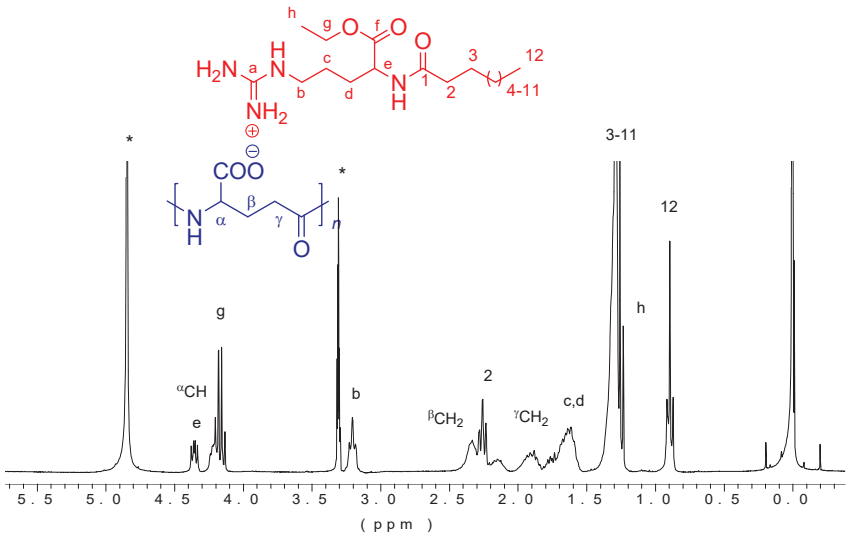

Figure 2.[1]H NMR spectra of LAE·PGGA-1 recorded at 25 °C in MeOD. *Asterisked signals are those arising from water and non-deuterated solvent.

1.2.3. Thermal properties and structure

The thermal decomposition of the LAE·PGGA complexes was examined by TGA under inert atmosphere, and possible thermal transitions were explored by DSC. The TGA traces recorded for the two complexes as well as their respective derivative curves are compared with that of LAE in Figure 3, and decomposition temperatures and remaining weights measured on these traces are given in Table 2.

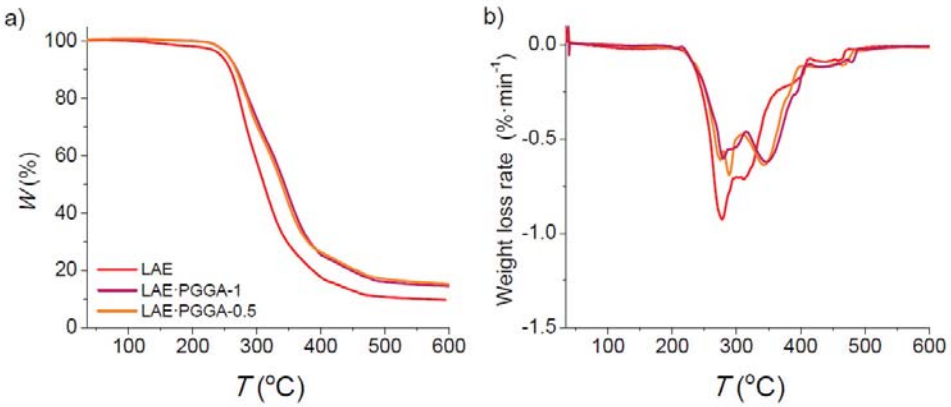

Figure 3. TGA traces (a) and derivative curves (b) of LAE and its ionic complexes with PGGA.

It was found that decomposition of the complexes started about 10 ºC above that of LAE and that the whole process happened through two stages in the three cases. Temperatures at which the first decomposition step took place at maximum rate were not very dissimilar for the three samples whereas values observed for the second step were much higher for the complexes than for LAE. The thermal decomposition of ionic

complexes of PGGA with trimethylalkylammoniun surfactants (*n*ATMA·PGGA) has been studied by us in some detail (Portilla-Arias et al., 2007b). It was then reported that *n*ATMA·PGGA started to decompose around 200 °C by decoupling of the complex, and that decomposition proceeded along two steps at rate temperatures within the 270-280 °C and 320-380 °C ranges, respectively. Given the resemblance of the overall thermal decomposition patterns of LAE·PGGA and *n*ATMA·PGGA, a similar mechanism may be assumed to occur in both types of complexes in spite that decomposition of LAE should be expected to be much more intricate than that of alkylammonium compounds.

Table 2. Thermal parameters of LAE·PGGA complexes.

	$^{o}T_d$ [a](°C)	$^{max}T_d$ [a](°C)	W [a](%)	T_m [b](°C)
LAE	245	275/311	27/10	62
LAE·PGGA-1	255	280/349	68/15	-
LAE·PGGA-0.5	253	273/342	63/16	-

[a] $^{o}T_d$ and $^{max}T_d$ are onset and maximum rate decomposition temperatures, respectively; W is the remaining weight at the end of each decomposition process.
[b] T_m is the melting temperature recorded by DSC.

1.2.4. Supramolecular structure and thermal transitions

The DSC traces recorded at heating from LAE and the complexes in the 0-200 ºC range are depicted in Figure 4. A well-defined sharp endothermal peak was observed for LAE at 62 ºC which doubtlessly arises from melting. In fact, the XRD of LAE in the wide-angle region (WAXS) produced multiple discrete scattering in the 0.3-0.5 nm range characteristic of crystalline organic material (Figure 5a). Furthermore, the examination of this sample under the polarizing optical microscope (POM), while heating revealed the presence of a typical crystalline texture that disappeared at temperatures nearly above 60 ºC (see Figure SI-3 in the SI file). On the contrary, the DSC traces of both LAE·PGGA-1 and LAE·PGGA-0.5 did not show below 100 ºC any sign indicative of crystallinity. Accordingly, no definite diffraction peak but a broad peak centered on 0.45 nm characteristic of disordered material was the only scattering detected in the WAXS of the complexes which is taken as indicative that the LAE counterpart must be in the amorphous state.

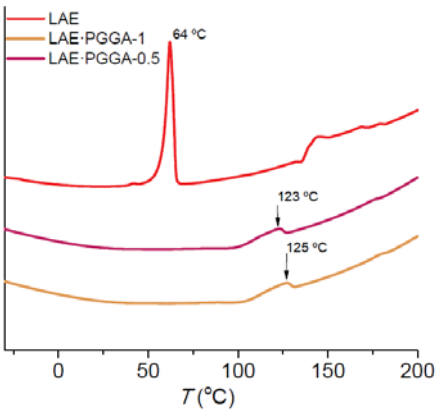

Figure 4. Differential scanning calorimety (DSC) traces of LAE and its ionic complexes with PGGA.

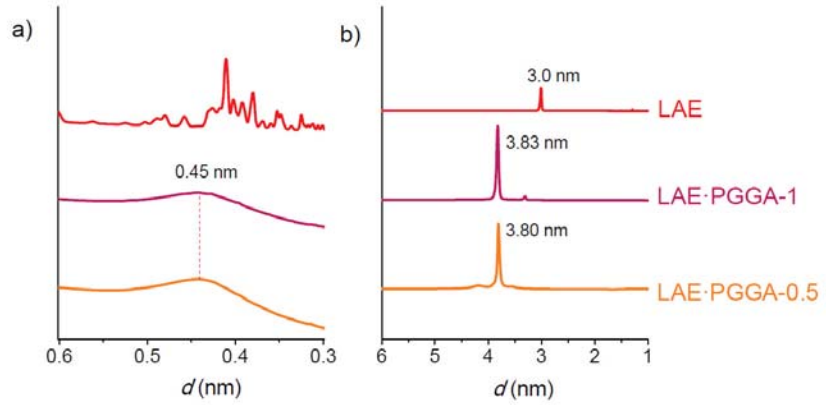

Figure 5. XRD profiles recorded from LAE and its complexes with PGGA in the wide-angle region (WAXS) (a) and small-angle region (SAXS) (b) at room temperature.

Inspection of the SAXS of the XRD patterns revealed in every case the presence of one sharp diffraction peak corresponding to a spacing of 3.0 nm for LAE and of ~3.8 nm for the complexes (Figure 5b). The presence of a peak in the ~3-4 nm range of SAXS is a distinctive characteristic of the ionic complexes made of PGGA and tetraalkylammoniun surfactants bearing long linear alkyl chains that are arranged in a biphasic structure made of alternating polypeptidic and paraffinic layers (Pérez-Camero et al., 2004; García-Álvarez et al., 2005). According to such antecedents, the ~3.8 nm spacing observed for both LAE·PGGA-1 and LAE·PGGA-0.5 can be interpreted as arising from the periodicity of the biphasic layered arrangement adopted by these complexes although the LAE moiety is in the non-crystallized state. The long spacing displayed by LAE·PGGA (~3.8 nm) is consistent with that observed for LAE (3.0 nm) since the space occupied by the PGGA layer has to be added in the complex. It is also in agreement with the long spacing reported for 12ATMA·PGGA (3.1 nm) (García-Álvarez et al., 2005) provided that the LAE non-alkyl moiety is much bulkier than the trimethylammoniun group of 12ATMA.

In order to have a deeper insight into the structure of the LAE·PGGA complexes, an XRD study at variable temperature was carried out using synchrotron radiation and spacing data measured in this study are listed in Table 3. Both WAXS and SAXS traces were simultaneously registered at real time from samples while heated or cooled over the 10-120 ºC range at a rate of 10 ºC·min^{-1}. The evolution of the SAXS and WAXS profiles recorded for LAE is shown in Figures 6a and 6a'. The scattering initially present in both regions was retained until heating up to 60 ºC to completely disappear at higher temperatures which is in full agreement with what was observed by DSC. No changes were detected after cooling (Figure SI-4, SI file) confirming the incapacity of LAE to crystallize from the melt such as was evidenced before by both DSC and POM.

The results obtained in the thermal XRD study of LAE·PGGA-1 are shown in Figures 6b and 6b'. In this case the SAXS peak at 3.83 nm was kept almost invariable over the whole temperature interval indicating that the layered arrangement present in the complex was essentially retained at the applied temperatures. In the WAXS region, the broad peak observed at 0.45 nm was unaffected by heating as it should be expected for a disordered scattering. It should be noted however that a small jump of the 3.83 peak down to 3.53 nm was observed around 60 °C. The occurrence of small jumping in the SAXS peaks in the 30-60 °C range is a frequently observed fact in the heating of comb-like ionic complexes of PGGA. Jumping may be either upwards or downwards, and it is invariably attributed to the occurrence of small rearrangements that take place in the layered structure upon melting of the alkyl chain (Tolentino et al., 2013).

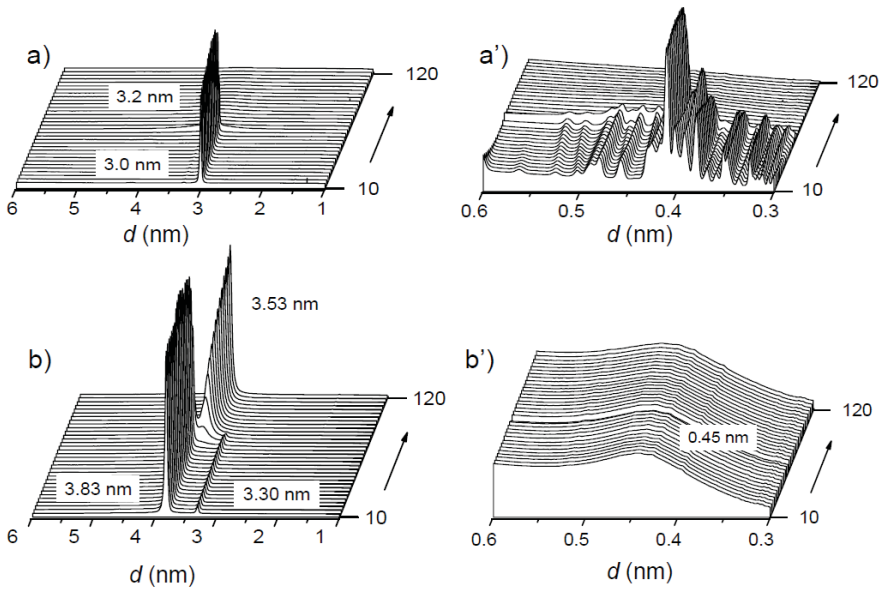

Figure 6. Evolution of the SAXS and WAXS profiles of LAE (a and a') and LAE·PGGA-1 (b and b') at heating from 10 to 120 °C.

The jump here observed for LAE·PGGA-1 cannot be explain in the same manner as for *n*ATMA·PGGA complexes since the alkyl chain of LAE is not crystallized. It may be speculated however that some spatial rearrangement could occur in the molecular assembly of the LAE nanophase involving a light shortening of the interlayer distance of the complex. In this regards, it is interesting to notice that no jump was observed for LAE·PGA-0.5 (Figure SI-5 in SI file) where the low concentration of LAE may be insufficient to adopt a close continuous packing in this phase. POM observations of LAE·PGGA-1 subjected to heating revealed an initial typical liquid-crystalline texture at room temperature that slightly changed above 60 ºC to fully disappear when temperature reached the proximities of 125-130 ºC (Figure SI-6 in SI file). This behavior is in agreement with DSC results that showed the presence of a small peak at 123 °C characteristic of a liquid crystal-isotropic phase transition.

Table 3. X-ray diffraction data of LAE·PGGA complexes.

	SAXS			WAXS		
Sample	$L_0^{10ºC}$	$L_0^{120ºC}$	$L_0^{10ºC}$	$d^{10ºC}$	$d^{120ºC}$	$d^{10ºC}$
LAE	3.0	-	-	Multiple	-	-
LAE·PGGA-1	3.8	3.5	3.5	0.45	0.45	0.45
LAE·PGGA-0.5	3.8	3.5	3.5	0.45	0.45	0.45

L_0: interlamellar distance (layered structure window).
d: interplanar distances arising from Bragg spacings.

1.2.5. LAE release and antibacterial properties

Although it has been reported that PGGA is a moderate microbiocide (Lee et al., 2014), it is the LAE counterpart of the LAE·PGGA complexes that is expected to play the main biocide activity in these systems. Accordingly, the biocide activity of the LAE·PGGA films in aqueous medium will be largely determined by the LAE concentration attained in the environment upon dissociation of the complex. To substantiate this hypothesis the accumulative amount of LAE that is released from the LAE·PGGA films to the incubation medium at 25 ºC was estimated by measuring the absorbance at 220 nm of the supernatant solution as a function of time. The results obtained from these assays for both LAE·PGGA-1 and LAE·PGGA-0.5 at different pH ranging from ~4.5 to ~9.5 are shown in Figure 7a and 7b. As it could be logically expected, the general trend is that the amount of LAE present in the buffer increased exponentially with time to finally reach a more or less constant concentration. The influence of pH on the delivery of LAE is clearly illustrated in the bar graphics shown in Figure 7c and 7d. In these plots, both the amount of LAE present in the incubation medium and the weight lost by the film is compared for the two complexes after one week of incubation at the different assayed pH. It is clearly seen that LAE is liberated

much faster at basic pH and that the minimum release rate happens at pH 5.5, a result that may be explained by taking into account the pKa of the two complex components, *i.e,* PGGA and LAE. It is also evidenced that the liberated amount of LAE is higher in LAE·PGGA-1 than in LAE·PGGA-0.5, which is much according to expectations, whereas the weight lost by the latter is significantly greater, a difference that is more ostensible at pH 9.2. This apparent conflict may be rationalized by taken into account the partial hydrolysis that it is probable undergone by PGGA upon incubation. The hydrolytic degradation of PGGA is a well-known process that is favored at higher pH (Kubota et al., 1996). This process is expected to happen more extensively in the case of LAE·PGGA-0.5 due to the higher accessibility of the PGGA backbone to water in this complex.

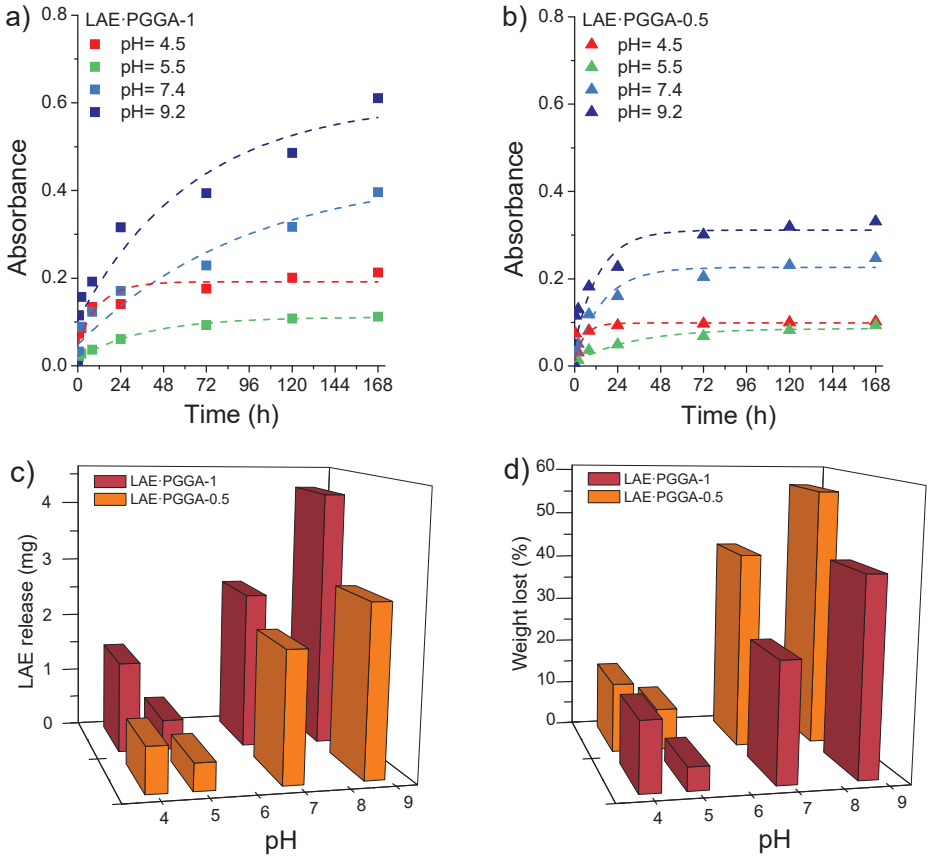

Figure 7. Dissociation of LAE·PGGA-1 (a) and LAE·PGGA-0.5 (b) complexes in aqueous buffer at the indicated pH. In c) and d) the amount of released LAE and the film weight loss are respectively compared for the two complexes after 7 days of incubation at the assayed pH.

The antibacterial activity of LAE·PGGA complexes against both Gram-negative (*S. enterica* and *E. coli*) and Gram-positive bacteria (*L. monocytogenes* and *S. aureus)* as a function of time was evaluated by the liquid medium method. Single colony of each strain was suspended into the buffer placed in essay tubes, and incubation effects were followed both visually and by measuring the optical density. The turbidity

appreciated by visual appearance of the supernatant was a preliminary indication of how the bacterial growing is affected by the presence of the complex (Figure SI-7 in the SI file). The results obtained by spectroscopic measurement are graphically depicted in Figure 8 together with those obtained for neat PGGA (negative control NC), and the blank. Average values obtained from triplicate counting and calculations are presented. Numerical data of these results expressed as Log(CFU) (logarithm of colony forming units), as well as their corresponding logarithmic reduction values (LRV) and reduction percentages (PR) calculated by means of the expressions given above are given in Table 4.

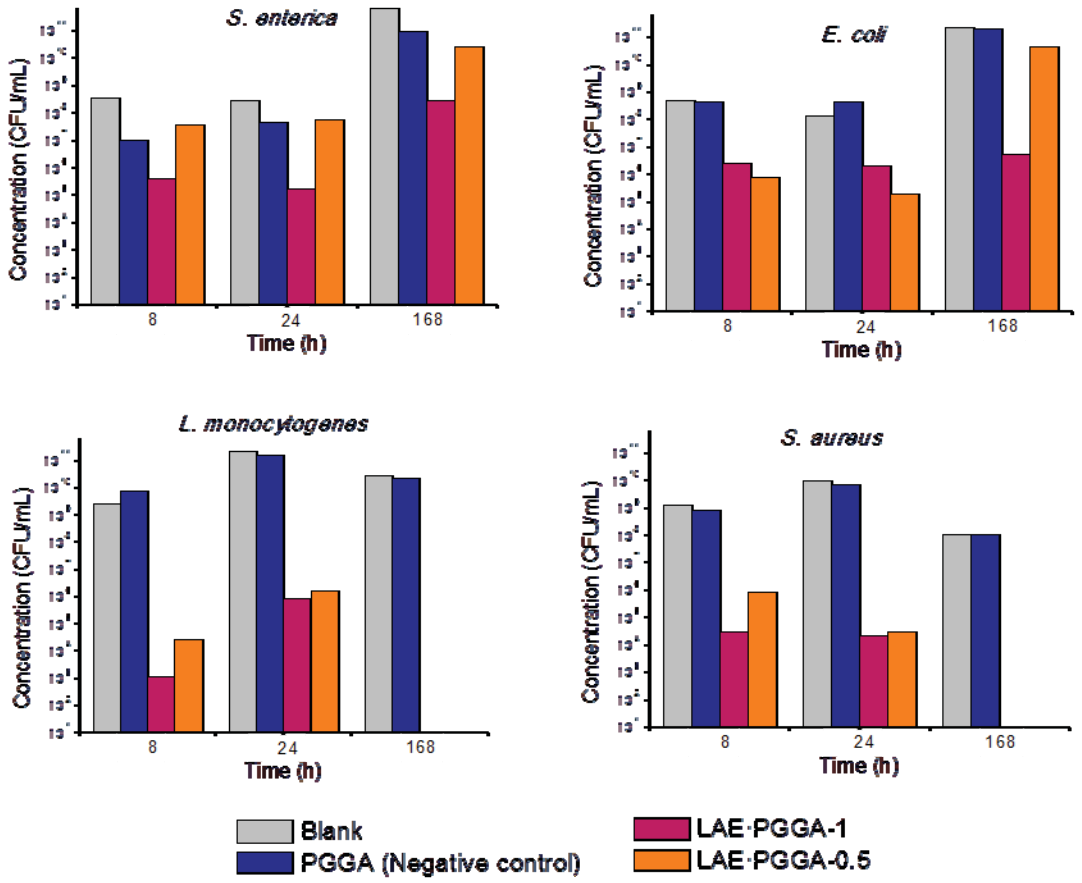

Figure 8. Antibacterial activity of LAE·PGGA-1 and LAE·PGGA-0.5 films against Gram-negative and Gram-positive bacteria expressed as concentration of colony forming units (CFU·mL^{-1}).

An overall inspection of the results obtained in the biocide activity assays leads to conclude that, in agreement with the amount of LAE that is delivered in each case, the bactericide effect is in general more pronounced for LAE·PGGA-1 than for LAE·PGGA-0.5. The higher bacterial growth reduction capacity observed for the complex containing more LAE is according to previous observations made on antimicrobial films based on LAE loaded chitosan (Higueras et al., 2013).

The two complexes displayed a similar great biocide activity against Gram-positive bacteria reaching an almost total growth inhibition for both *L. monocytogenes* and *S. aureus* after 7 days of incubation, and >99,99% of reduction after 24 hours. On the contrary both complexes were less effective against Gram-negative bacteria *(S. enterica* and *E.coli),* which is agreement with observations made by other authors on the antibacterial activity of LAE (Higueras et al., 2013; Ma et al., 2013). The LAE·PGGA-0.5 films achieved only 2.3% reduction of *S. enterica* after 24 h and 70.9% after 7 days, although the double concentrated complex reached 99.6% reduction of the same bacteria after 24 h. Since Gram-negative organisms have a greater defense system due to the outer lipopolysaccharide coat that surrounds the cell wall, the diffusion of hydrophobic compounds is expected to be much hindered than in Gram-positive species (Vaara, 1992).

Table 4. Bactericide activity of films made of LAE·PGGA complexes against Gram-negative and Gram-positive bacteria after 1 and 7 days of incubation at pH 7.4 and 37 °C.

		S. enterica		*E. coli*		*L. monocytogenes*		*S. aureus*	
		24 h	7 d	24 h	7 d	24 h	7 d	24 h	7 d
PGGA	Log (CFU)[a]	7.6	10.6	8.6	11.3	11.2	10.30	9.8	8.0
LAE·PGGA-1	Log (CFU)	5.2	8.4	6.3	6.7	3.9	total	4.3	0.3
	LRV[b]	2.4	2.5	2.3	4.6	7.3		5.5	7.7
	PR (%)[c]	99.6	99.7	99.5	>99.9	>99.9	100	>99.9	>99.9
LAE·PGGA-0.5	Log (CFU)	7.6	10.4	5.3	10.6	4.2	total	4.5	total
	LRV	0.01	0.5	3.3	0.6	7.0		5.4	
	PR (%)	2.3	70.9	99.9	76.8	>99.9	100	>99.9	100

[a] Antibacterial activity expressed as logarithm of colony forming units.
[b] Antibacterial activity expressed as log reduction value.
[c] Percentage of reduction.

Since our results were obtained from one single experiment and only one strain was used for each bacterium they should be taken as a first evaluation of the bactericide potential of these complexes. Further studies including different incubation conditions (pH, temperature, etc,), additional microorganisms, and a statistical analysis of data collected from replicated experiments will be required to attain a more definite appraisal of the biocide capacity of the LAE·PGGA system. Furthermore the possibility that a VBNC (viable but non-culturable) state is adopted by the bacteria upon the action of the bactericide cannot be completely discarded since it has been described

for some of the pathogens studied in this work (Oliver, 2005). In this case however such situation is highly improbable since LAE is a biocide in use for long time and, to our knowledge, the occurrence of dormant bacteria after the action of this agent has not been reported.

1.3. Conclusions

The widely known antimicrobial agent LAE (ethyl $^{\alpha}$*N*-lauroyl L-arginate) was ionically coupled with poly(□-glutamic acid) (PGGA) to generate host-guest ionic complexes containing either stoichiometric molar amounts of the two components or an half amount of LAE. The complexes may be used to prepare consistent films that are non-water soluble and thermally stable. Both complexes adopt a layered biphasic structure similar to that described for similar ionic complexes of PGGA made of alkyltrimethylammonium surfactants. Although LAE is a crystalline compound the LAE·PGGA complexes are essentially amorphous with the lauroyl chains staying in a disordered state. LAE is released from the complexes upon incubation in aqueous buffer at a rate that is depending on pH and in less degree on the LAE/PGGA ratio. Films of these complexes displayed antibacterial activity against both Gram positive and Gram-negative strains although the biocide effect on the former was much more ostensible. The biocide effect is motivated by both the LAE released to the aqueous environment and the fraction bounded to the complex. Since the two components that integrate the complexes are edible, these complexes offer interesting potential as antibacterial materials to be used in both food additives or packaging.

1.4. References

Appendini, P., Hotchkiss, J. H. (2002). Review of antimicrobial food packaging. Innov. Food Sci. Emerg. Technol. 3(2), 113–126.

Asker, D., Weiss, J., McClements, D. J. (2009). Analysis of the interactions of a cationic surfactant (Lauric arginate) with an anionic biopolymer (Pectin): Isothermal titration calorimetry, light scattering, and microelectrophoresis. Langmuir, 25(1), 116–122.

Asker, D., Weiss, J., McClements, D. J. (2011). Formation and stabilization of antimicrobial delivery systems based on electrostatic complexes of cationic−non-ionic mixed micelles and anionic polysaccharides. J. Agric. Food Chem. 59(3), 1041–1049.

Becerril, R., Manso, S., Nerin, C., Gómez-Lus, R. (2013). Antimicrobial activity of lauroyl arginate ethyl (LAE), against selected food-borne bacteria. Food Control, 32(2), 404–408.

Dobrucka, R. (2016). Antibacterial films made of ionic complexes of poly(γ-glutamic acid) and ethyl lauroyl arginate. Logforum, 12(4), 193–202.

Durán, N., Marcato, P. D., De Souza, G. I. H., Alves, O. L., Esposito, E. (2007). Antibacterial effect of silver nanoparticles produced by fungal process on textile fabrics and their effluent treatment. J. Biomed. Nanotechnol. 3(2), 203–208.

Erickson, M. C., Doyle, M. P. (2017). The challenges of eliminating or substituting antimicrobial preservatives in foods. Ann. Rev. Food Sci. Technol. 8(1), 371–390.

Fu, Y., Sarkar, P., Bhunia, A. K., Yao, Y. (2016). Delivery systems of antimicrobial compounds to food. Trends Food Sci. Technol. 57, 165–177.

Gamarra, A., Martínez de Ilarduya, A., Vives, M., Morató, J., Muñoz-Guerra, S. (2017b). Ionic complexes of poly(γ-glutamic acid) with alkyltrimethylphosphonium surfactants. Polymer, 116, 43–54.

García-Álvarez, M., Álvarez, J., Alla, A., Martínez de Ilarduya, A., Herranz, C., Muñoz-Guerra, S. (2005). Comb-like ionic complexes of cationic surfactants with bacterial poly(γ-glutamic acid) of racemic composition. Macromol. Biosci. 5(1), 30–38.

Guo, M., Jin, T. Z., Yang, R. (2014). Antimicrobial polylactic acid packaging films against listeria and salmonella in culture medium and on ready-to-eat Meat. Food Bioprocess Technol. 7, 3293–3307.

Hawkins, D. R., Rocabayera, X., Ruckman, S., Segret, R., Shaw, D. (2009). Metabolism and pharmacokinetics of ethyl $^{\alpha}$N-lauroyl-L-arginate hydrochloride in human volunteers. Food Chem. Toxicol. 47(11), 2711–2715.

Higueras, L., López-Carballo, G., Hernández-Muñoz, P., Gavara, R., Rollini, M. (2013). Development of a novel antimicrobial film based on chitosan with LAE (ethyl-N-dodecanoyl-L-arginate) and its application to fresh chicken. Int. J. Food Microbiol. 165(3), 339–345.

Kashiri, M., Cerisuelo, J. P., Domínguez, I., López-Carballo, G., Hernández-Muñoz, P., Gavara, R. (2016). Novel antimicrobial zein film for controlled release of lauroyl arginate (LAE). Food Hydrocoll. 61, 547–554.

Kubota, H., Fukuda, H., Takebe H, E. T. (1992). Poly-gamma-glutamic acid ester and shaped body thereof. Patent Number(s) US5118784.

Kubota, H., Nambu, Y., Endo, T. (1996). Alkaline hydrolysis of poly(γ-glutamic acid) produced by microorganism. J. Polym. Sci. Part A Polym. Chem. 34(7), 1347–1351.

Lai, E. P. C., Iqbal, Z., Avis, T. J. (2016). Combating Antimicrobial Resistance in Foodborne Microorganisms. J. Food Prot. 79(2), 321–336.

Lee, N., Go, T., Lee, S., Jeong, S., Park, G., Hong, C., Son, H. (2014). In vitro evaluation of new functional properties of poly-glutamic acid produced by Bacillus subtilis D7. Saudi J. Biol. Sci. 21(2), 153–158.

Loeffler, M., Mcclements, D. J., Mclandsborough, L., Terjung, N., Chang, Y., Weiss, J. (2014). Electrostatic interactions of cationic lauric arginate with anionic polysaccharides affect antimicrobial activity against spoilage yeasts. J. Appl. Microbiol. 117(1), 28–39.

Ma, Q., Davidson, P. M., Zhong, Q. (2013). Antimicrobial properties of lauric arginate alone or in combination with essential oils in tryptic soy broth and 2% reduced fat milk. Int. J. Food Microbiol. 166(1), 77–84.

Ma, Q., Zhang, Y., Zhong, Q. (2016). Physical and antimicrobial properties of chitosan films incorporated with lauric arginate, cinnamon oil, and ethylenediaminetetraacetate. LWT Food Sci. Technol. 65, 173–179.

Malhotra, B., Keshwani, A., Kharkwal, H. (2015). Antimicrobial food packaging: Potential and pitfalls. Front. Microbiol. 6, 1–9.

Mead, P. S., Slutsker, L., Dietz, V., McCaig, L. F., Bresee, J. S., Shapiro, C., Tauxe, R. V. (1999). Food-related illness and death in the United States. Emerg. Infect. Dis. 5(5), 607–25.

Muñoz-Bonilla, A., Fernández-García, M. (2012). Progress in polymer science polymeric materials with antimicrobial activity. Prog. Polym. Sci., 37, 281–339.

Muñoz-Guerra, S., García-Álvarez, m., portilla-arias, j. a. (2013). Chemical modification of Microbial Poly(γ-glutamic acid). J. Renew. Mater. 1(1), 42–60.

Muriel-Galet, V., López-Carballo, G., Gavara, R., Hernández-Muñoz, P. (2012). Antimicrobial food packaging film based on the release of LAE from EVOH. International Int. J. Food Microbiol. 157(2), 239–244.

Muriel-Galet, V., Cran, M. J., Bigger, S. W., Hernández-Muñoz, P., Gavara, R. (2015). Antioxidant and antimicrobial properties of ethylene vinyl alcohol copolymer films based on the release of oregano essential oil and green tea extract components. J. Food Eng. 149, 9–16.

Newell, D. G., Koopmans, M., Verhoef, L., Duizer, E., Aidara-Kane, A., Sprong, H., Kruse, H. (2010). Food-borne diseases- The challenges of 20 years ago still persist while new ones continue to emerge. Int. J. Food Microbiol. 139, S3–S15.

Oliver, J. (2005). The viable but nonculturable state in bacteria. J. Microbiol. 43, 93–100.

Otero, V., Becerril, R., Santos, J. A., Rodríguez-Calleja, J. M., Nerín, C., García-López, M. L. (2014). Evaluation of two antimicrobial packaging films against Escherichia coli O157: H7 strains invitro and during storage of a Spanish ripened sheep cheese (Zamorano). Food Control, 42, 296–302.

Pattanayaiying, R., H-Kittikun, A., Cutter, C. N. (2015). Optimization of formulations for pullulan films containing lauric arginate and nisin Z. LWT Food Sci. Technol. 63(2), 1110–1120.

Pérez-Camero, G., García-Álvarez, M., Martínez de Ilarduya, A., Fernández, C., Campos, L., Muñoz-Guerra, S. (2004). Comblike complexes of bacterial poly(γ,D-glutamic acid) and cationic surfactants. Biomacromolecules, 5(1), 144–152.

Ponomarenko, E.A., Alan J. Waddon, David A. Tirrell, MacKnight, W. J. (1996). Structure and properties of stoichiometric complexes formed by sodium poly(α,l-glutamate) and oppositely charged surfactants. Langmuir, 12(9), 2169–2172.

Portilla-Arias, J. A., García-Alvarez, M., Martínez de Ilarduya, A., Muñoz-Guerra, S. (2007a). Ionic complexes of biosynthetic poly(malic acid) and poly(glutamic acid) as prospective drug-delivery systems. Macromol. Biosci. 7(7), 897–906.

Portilla-Arias, J. A., García-Alvarez, M., Martínez de Ilarduya, A., Muñoz-Guerra, S. (2007b). Thermal decomposition of microbial poly(γ-glutamic acid) and poly(γ-glutamate)s. Polym. Degrad. Stab. 92(10), 1916–1924.

Rodriguez, E., Seguer, J., Rocabayera, X., Manresa, A. (2004). Cellular effects of monohydrochloride of L-arginine, N-alpha-lauroyl ethylester (LAE) on exposure to *Salmonella typhimurium* and *Staphylococcus aureus*. J. Appl. Microbiol. 96(5), 903–912.

Ruckman, S. A., Rocabayera, X., Borzelleca, J. F., Sandusky, C. B. (2004). Toxicological and metabolic investigations of the safety of N-alpha-lauroyl-L-arginine ethyl ester monohydrochloride (LAE). Food Chem. Toxicol. 42(2), 245–259.

Shah, D. T., McCarthy, S. P., Gross, R. A. (1995). γ-poly(glutamic acid) esters. Pat. Number US5378807-A.

Siracusa, V., Rocculi, P., Romani, S., Marco, D. (2008). Biodegradable polymers for food packaging: a review. Trends Food Sci. Technol. 19(12), 634–643.

Tolentino, A., Alla, A., Martínez de Ilarduya, A., Muñoz-Guerra, S. (2011). Comb-like ionic complexes of pectinic and alginic acids with alkyltrimethylammonium surfactants. Carbohydr. Polym. 86(2), 484–490.

Tolentino, A., León, S., Alla, A., Martínez de Ilarduya, A. Muñoz-Guerra, S. (2013). Comblike ionic complexes of poly(γ-glutamic acid) and alkanoylcholines derived from fatty acids. Macromolecules, 46(4), 1607–1617.

Vaara, M. (1992). Agents that increase the permeability of the outer membrane. Microbiol. Rev. 56(3), 395–411.

VIII.2. Ionic coupling of hyaluronic acid with ethyl *N*-lauroyl L-arginate (LAE): Structure, properties and biocide activity of complexes

Abstract:
$^{\alpha}$*N*-lauroyl L-arginate hydrochloride (LAE) was coupled with hyaluronic acid (HyA) to form ionic complexes with LAE to HyA ratios of 1:1 and 1:2. The complexes were extensively characterized by FTIR and NMR spectroscopies and their thermal properties evaluated by thermogravimetry and calorimetry. Thin films prepared from these complexes by casting displayed a smectic-like structure based on an ordered arrangement of LAE and HyA layers with a nanometric periodicity of 3.8-3.9 nm. Films immersed in water at pH 7.4 and 5.5 dissociated to deliver free LAE to the environment and reaching the equilibrium in a few hours. The biocide activity of these films against both Gram-positive and Gram-negative bacteria was preliminary assessed by the liquid medium method, and shown to be notable in both cases. The antibacterial property of the complexes was found to increase with the content of LAE and to be particularly efficient against Gram-negative *S. enterica* bacteria.

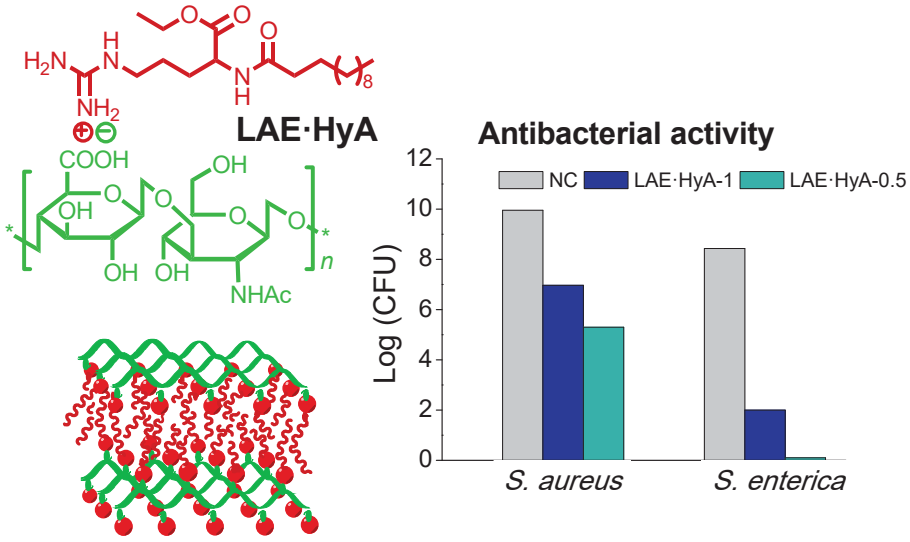

Publication derived from this work:

Gamarra, A., Missagia, B., Urpí, L., Morató, J. and Muñoz-Guerra, S. (2018). Ionic coupling of hyaluronic acid with ethyl N-lauroyl L-arginate (LAE): Structure, properties and biocide activity of complexes. Carbohydr.Polym. 197 (1), 109-116.

Supporting Information (SI) to this chapter in Annex E.2 .

2.1. Introduction

Complexation of polyelectrolytes with counter-ions of low molecular weight is a relatively simple approach recurrently used for creating materials that largely differ in properties from the parent polymer. This is so because coupling between complementary ionic building-blocks usually leads to molecular arrangements able to self-assemble in well-organized nanostructures (Macknight et al., 1998a). The complexes made of ionic polypeptides and tetraalkylsurfactants constitute a representative example of these systems (Ponomarenko et al., 1996; Macknight et al., 1998b; Pérez-Camero et al., 2004; Hanski et al., 2006). These complexes tend to adopt a layered biphasic structure with crystallinity depending on the length of the surfactant alkyl chain and a periodical spacing sensitive to temperature. Negatively charged polysaccharides, and in particular polyuronic acids, have been demonstrated to behave in a way not far from that described for anionic polypeptides. Thus coupling of alginic, pectinic and hyaluronic acids with alkyltrimethylammonium surfactants has been recently reported to render stable ionic complexes arranged in layers showing order at the nanometric scale (Tolentino et al., 2011, 2013).

In this paper we wish to report on ionic complexes made from hyaluronic acid and an arginine-based compound, namely ethyl $^{\alpha}$*N*-lauroyl L-arginate hydrochloride (LAE), which are able to display antimicrobial properties. Due to the increasing resistance of bacteria to antibiotics, bactericide polymers start to be considered today as an attractive antiseptic alternative (Engler et al., 2012). In such systems, the polymer acts as a matrix for holding and controlling the release of the antimicrobial agent so that the possible toxicity associated to the biocide is largely repressed and the period of activity increased when compared to the neat biocide. During the last decade the attention given to polymeric materials with antimicrobial activity has been very noticeable (Santos et al., 2016) and some hyaluronic acid-based materials incorporating antimicrobial agents have been found in the recent literature. HyA-silver nanoparticles and HyA coupled with polyhexanide (Kemp et al., 2009; Baier et al, 2013), and nisin polypeptide (Lequeux et al., 2014) are representative examples of such materials. To our knowledge, no study addressed to examine the ionic LAE·HyA complexes including their antimicrobial activity has been described so far.

Hyaluronic acid (HyA) is a high molecular weight mucopolysaccharide composed of repeating disaccharide units of β-1,3-*N*-acetyl D-glucosamine and β-1,4-D-glucuronic acid with a great capacity to retain moisture and to form hydrogels with excellent viscoelastic properties. Furthermore HyA is high biocompatible, non-immunogenic and susceptible to biodegradation by human hyaluronidases. HyA is always present in the

human body in small amounts, and it is widely used in medicine, cosmetic and veterinary surgery (Stern et al., 2007; Necas et al., 2008). The polysaccharide may be chemically modified to render biomaterials with properties suitable for tissue engineering (Allison et al., 2006; Burdick et al., 2011; Schanté et al., 2011). Rooster combs were the traditional source of HyA but today it is mainly produced by microbial fermentation which has boosted its applications and raised its commercial value (Liu et al., 2011). On the other hand, LAE is a synthetic surfactant consisting of an ethyl esterified arginine head with a lauroyl tail attached to the α-amino group. LAE is widely recognized as a highly powerful preservative agent for a large variety of food-borne bacteria (Becerril et al., 2013; Otero et al., 2014) a property that is due to its ability for altering the microorganisms metabolism without producing cellular disruptions (Rodriguez et al., 2004). LAE has been assessed to be nontoxic and it has been classified by FDA (Food and Drug Administration) as GRAS (Generally Recognized as Safe) at concentrations up to 200 ppm. According to their biological properties, ionic coupling of LAE with HyA is envisaged as a very convenient approach to build antimicrobial films with potential use in food preservation and design of medical antiseptic devices.

The working hypothesis for this research is that LAE·HyA complexes will be readily formed with prefixed compositions, and that they will show strong activity against pathogens because LAE will be released under control to the wet environment by water-mediated dissociation of the ionic pair. LAE and HyA are largely expected to combine ionically because both compounds have been reported to form stable ionic complexes when they enter in contact with diverse counter-ions. Thus LAE is known to interact positively with the anionic polysaccharides present in the food (Asker et al., 2009; Loeffler et al., 2014), and complexes of HyA with a diversity of organocationic compounds have been also described (Tolentino et al., 2013; Bračič et al., 2015; Chytil et al., 2016; Battistini et al., 2017). Complexes of LAE with poly(γ-glutamic acid) (LAE·PGGA) with antibacterial properties have been recently described by us (Gamarra-Montes et al., 2017).

In this paper cationic LAE is coupled with the polyanionic hyaluronic acid to obtain the ionic complexes abbreviated as LAE·HyA with LAE to HyA ratios of either 1:1 or 1:2. These complexes are extensively characterized by different techniques (FT-IR, NMR, TGA, DSC, XRD and POM) and paying detailed attention to the nanostructure. Then the release rate of LAE from complexes is estimated under different conditions and the antimicrobial properties of the films are evaluated in vitro experiments against

both Gram-positive (*L. monocytogenes* and *S. aureus)* and Gram-negative bacteria (*S. enterica* and *E.coli).*

2.2. Results and discussion

2.2.1. Synthesis of complexes

The preparation of LAE·HyA complexes was performed according to Scheme 1. Mixing at 35 ºC of the two aqueous solutions containing LAE and Na·HyA, respectively, rendered the complex as a white precipitated that could be easily recovered by centrifugation. Two LAE·HyA molar ratios, *i.e* 1:1 and 1:2, were used at mixing with the purpose of obtaining complexes with equal or half molar amount of LAE respect to HyA. The ^{1}H NMR analysis revealed that the actual compositions of the complexes were very close to those used for feeding with a slight deficiency in the cationic component. Data related with the synthesis are given in Table 1.

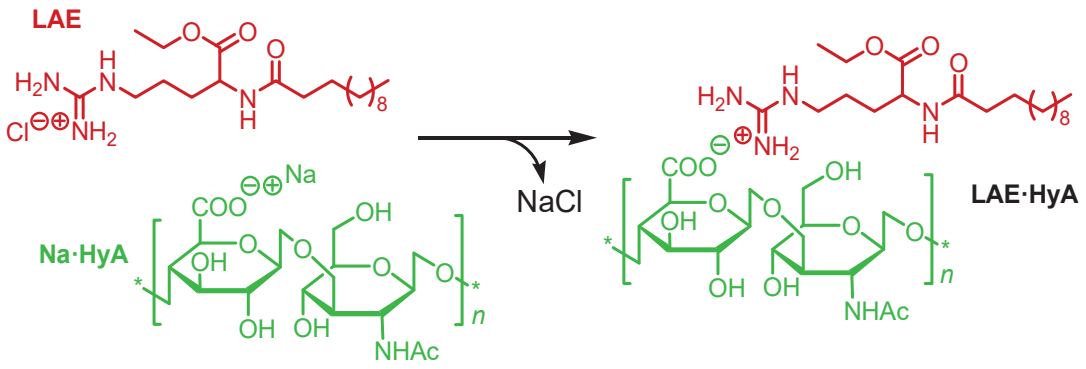

Scheme 1. Formation of LAE·HyA complexes by coupling reaction of LAE with hyaluronic acid. LAE to HyA ratios of 1:1 and 1:2 were used.

2.2.2. Chemical characterization

The FTIR spectra recorded from the LAE·HyA complexes are shown in Figure 1 together with those of Na·HyA and LAE. The spectra of the complexes include the bands characteristic of the two components with relative intensities according to composition. In fact, the digital region of these spectra over the 1800-650 cm^{-1} may be made to correspond to the overlapping of those observed for HyA and LAE with their contributions being proportional to their contents in the complexes.

Table 1. Synthesis, thermal properties and structural data.

Compound	Synthesis results				Thermal properties				X-ray diffraction data (nm)					
					TGA[d]			DSC[e]	SAXS[f]			WAXS[f]		
	c^a (M)[a]	T (ºC)[b]	Yield (%)	LAE:HyA[c]	$^{o}T_d$ (ºC)	$^{max}T_d$ (ºC)	W (%)	T_m (ºC)	$L_o^{10ºC}$	$L_o^{120ºC}$	$L_o^{10ºC}$	$d^{10ºC}$	$d^{120ºC}$	$d^{10ºC}$
HyA	-	-	-	-	200	228	35	-	n.d.	n.d.	n.d.	n.d.	n.d.	n.d.
LAE·HyA-0.5	0.02	35	70	0.4 :1.0	217	228/328	19	-	3.8	3.8	3.7	0.45	0.45	0.45
LAE·HyA-1	0.01	35	80	0.9 :1.0	228	259/328	11	-	3.9	3.9	3.8	0.45	0.45	0.45
LAE	-	-	-	-	245	275/311	10	62	3.0	-	-	m[g]	-	-

[a] Concentration of the two solutions mixed to form the complex.
[b] Mixing temperature selected according to the LAE solubility in water.
[c] Molar ratio of LAE to HyA in the complex estimated by ^{1}H NMR.
[d] $^{o}T_d$ and $^{max}T_d$: onset (5% weight loss) and maximum rate decomposition temperatures; W: remaining weight after heating at 600 ºC.
[e] T_m is the melting temperature recorded by scanning calorimetry.
[f] Small angle (SAXS) and wide angle (WAXS) X-rays scattering recorded at 10 ºC, 120 ºC and 10 ºC (after cooling) as indicated.
n.d.: not determined.
[g] Many peaks observed.

The ^{1}H NMR spectrum recorded from LAE-HyA-1 in methanol solution is reproduced in Figure 2. All signals observed in this spectrum could be consistently assigned to the chemical structure of the complex, and signals arising from the anomeric proton of the glucuronic unit of HyA and from the α-methylene protons of the lauroyl moiety of LAE (signals 1 and j) were used for determining the composition of the complex. The ^{1}H NMR spectrum of HyA and LAE-HyA-0.5 may be inspected in the SI file (Figure SI-1 and SI-2).

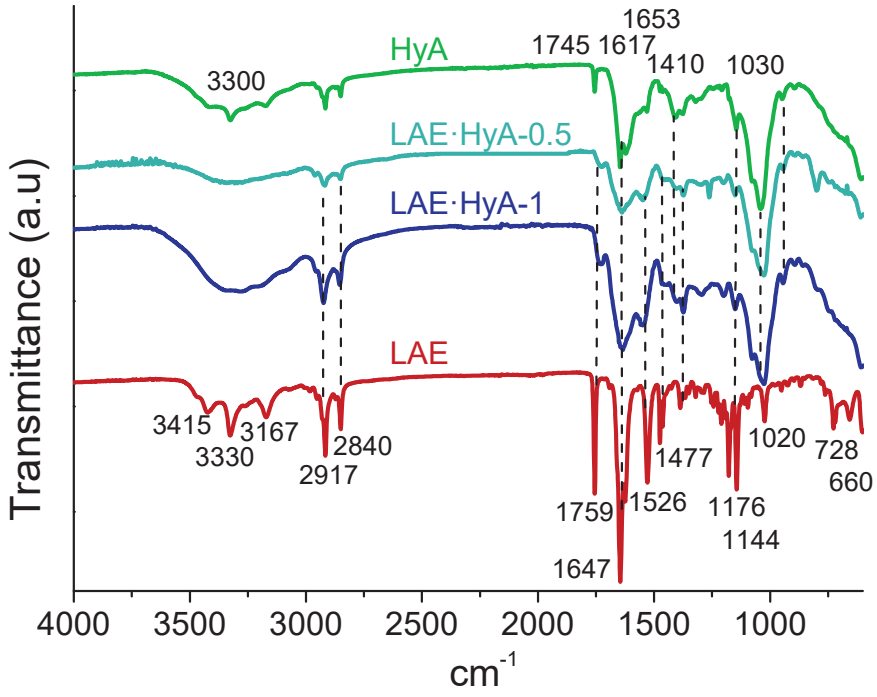

Figure 1. Comparison of FTIR spectra of LAE, HyA and their complexes with indication of most characteristic bands.

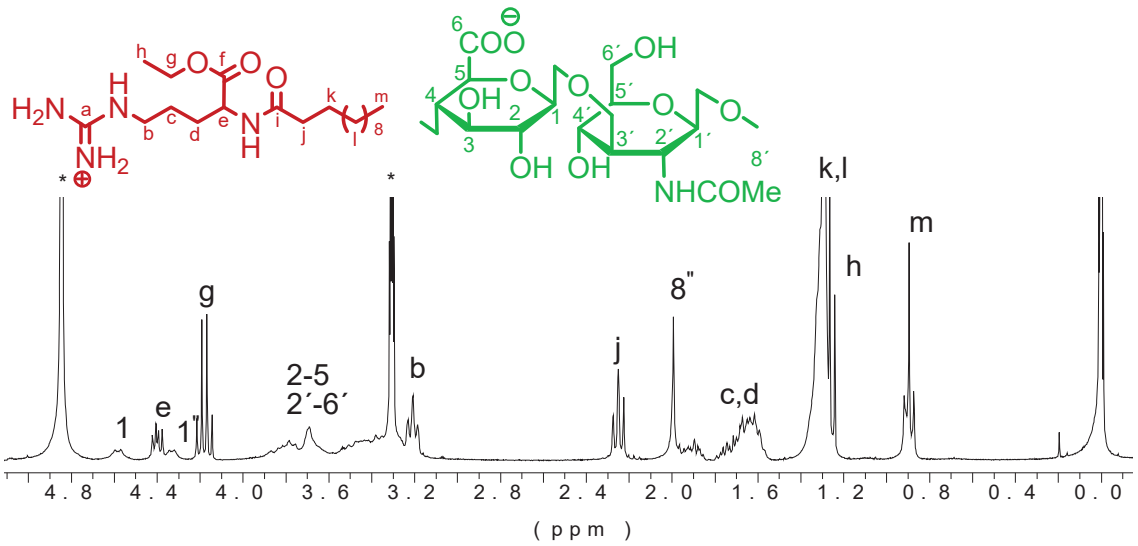

Figure 2. [1]H NMR spectrum of LAE·HyA-1 recorded in MeOD. Signals marked with asterisks are those arising from the solvent.

2.2.3. Thermal properties and structure

Firstly, the thermal stability of the complexes was evaluated by TGA. The traces registered for both LAE-HyA-1 and LAE-HyA-0.5 over the 20-600 ºC were compared with those of HyA and LAE in Figure 3a, and their respective derivative curves are represented in Figure 3b. It should be noted that the trace of HyA shows a weight loss of about 5% at temperatures around 100 ºC, which is interpreted as due to the release of the remaining adsorbed water that could not be removed by the drying treatment applied to the sample. Nevertheless, all compounds started to decompose above 200 ºC at an onset temperature that increases with the content in LAE.

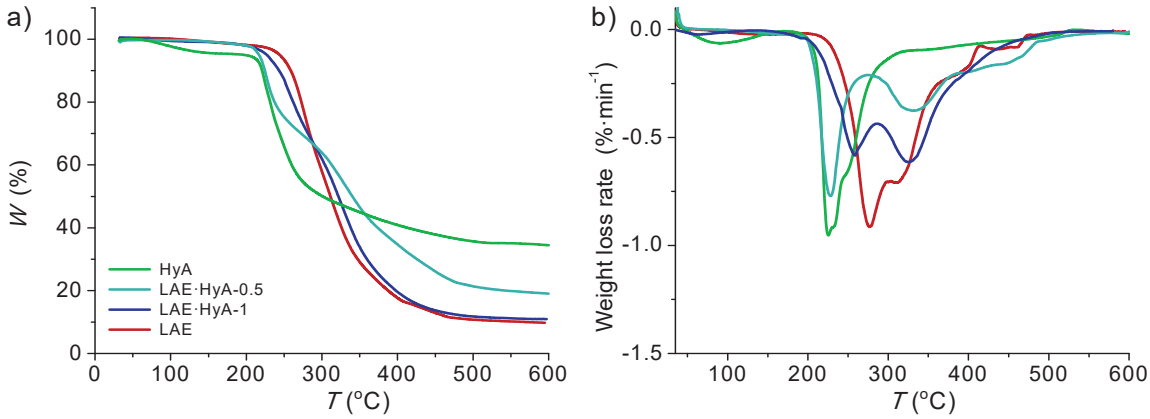

Figure 3. TGA traces of HyA, LAE and the LAE·HyA complexes recorded under an inert atmosphere (a), and their respective derivative curves (b).

Furthermore, the maximum decomposition rate in LAE took place around 50 ºC higher than for HyA. These differences are reflected in the complexes which show $^{max}T_d$ of 230 ºC and 260 ºC for LAE-HyA-0.5 and LAE-HyA-1, respectively. It can be stated on

the basis of these results that the LAE·HyA complexes could be comfortably handled in the case that usual heating processes were applied for film manufacture.

The DSC analysis (Figure 4a) revealed that only LAE shows melting transition whereas almost plain traces were registered for HyA and their complexes (the slight endotherm appreciated on the trace of HyA in the 80-120 ºC interval is very likely due to water evaporation). The crystalline nature of LAE was clearly evidenced in the spherulitic texture that is seen in films of this compound prepared by casting when they are observed by POM (Figure 4b left). Accordingly, it can be concluded that the crystallinity of LAE is lost when this compound is attached to HyA. However, POM of the LAE·HyA-1 film showed a fan-like texture typical of a smectic mesophase (Figure 4b right) indicating that complexes are ordered in a crystal liquid structure. A similar appearance was observed for the LAE·HyA-1 complex (Figure SI-3 in SI file).

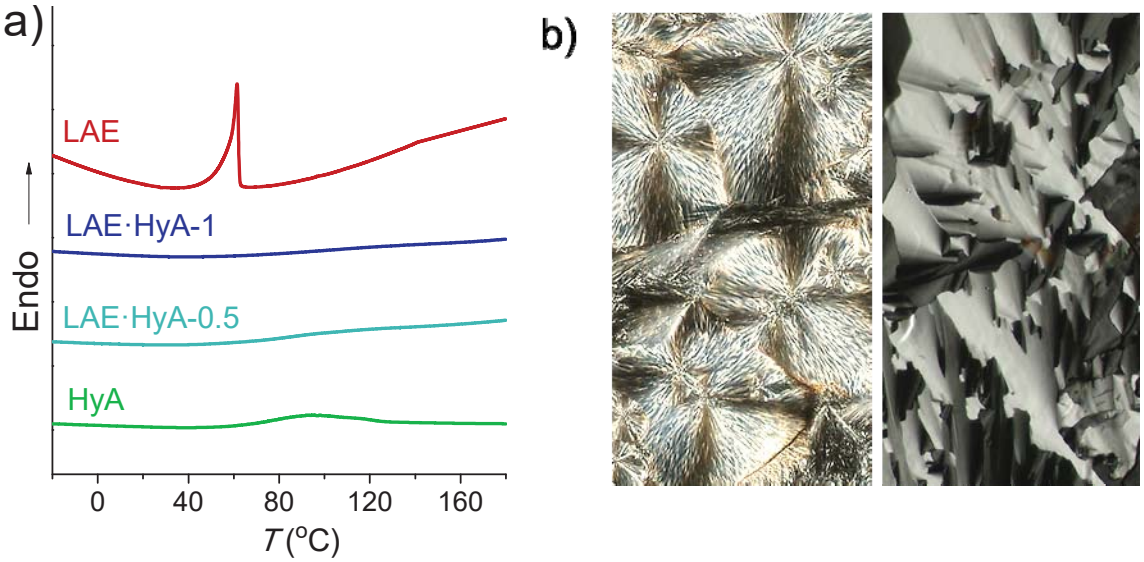

Figure 4. a) First heating DSC traces recorded from LAE and its ionic complexes. b) POM micrographs taken from LAE (left) and LAE·HyA-1 (right) thin films at 25 ºC.

The XRD scattering recorded in the WAXS region for LAE and the complexes (Figure 5a) was in full agreement with DSC results. The trace recorded for LAE contains a large number of well-defined peaks, as it should be expected for a crystalline organic compound, whereas a broad hill centered around 0.45 nm is the only alteration appearing on the traces of the complexes. In the SAXS region (Figure 5b), spectra of both LAE and complexes show an apparent sharp peak corresponding to a repeat distance of 3.0 nm for the former and around 3.9-3.8 nm for the latter. These results confirm the occurrence of an ordered arrangement at the nanometric level in the complexes in spite that they are not crystallized.

With the purpose of assessing the influence of temperature on these structures, samples of LAE and LAE·HyA-1 were subjected to a heating-cooling cycle over the 10-120 ºC range at a rate of 10 ºC·min^{-1}, and the changes taking place in the X-ray scattering were registered over the whole temperature range at real time (Figure 6). Both SAXS and WAXS signals observed for LAE fully disappeared when temperature reached 60-65 ºC, which is clear evidence that the structure melted and all the order initially present in the sample vanished. The cooling trace did not show any discrete scattering (see Figure SI-4 in the SI file) indicating that the initial structure present in LAE was not recovered. The behavior observed for LAE·HyA-1 was noticeably different. The 3.9 nm peak remained unchanged along the whole heating treatment bringing into evidence the stability of the mesophase up to temperatures close to 200 ºC. This is consistent with the observations made by POM in which the birefringence displayed by the films of LAE·HyA-1 did not vanished when subjected to heating at similar temperatures. Similar results were obtained in the XRD/POM analysis of LAE·HyA-0.5 complex (Figures SI-5 in SI). It seems reasonable to assume therefore that higher temperatures are needed to destroy the liquid crystal phase adopted by these complexes, an assumption that unfortunately cannot be tested since their thermal decomposition starts to be noticeable at 215-230 ºC. As much expected, the WAXS profiles arising from the average interatomic distances present in the disordered phase made of lauroyl chains of the LAE moiety remained unperturbed along the heating treatment.

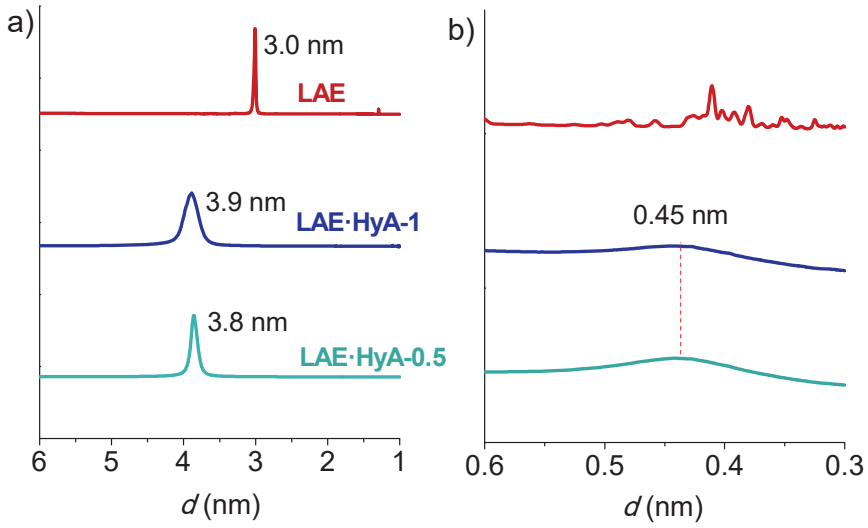

Figure 5. XRD profiles recorded at room temperature from LAE and their complexes LAE·HyA in the SAXS (a) and WAXS regions (b).

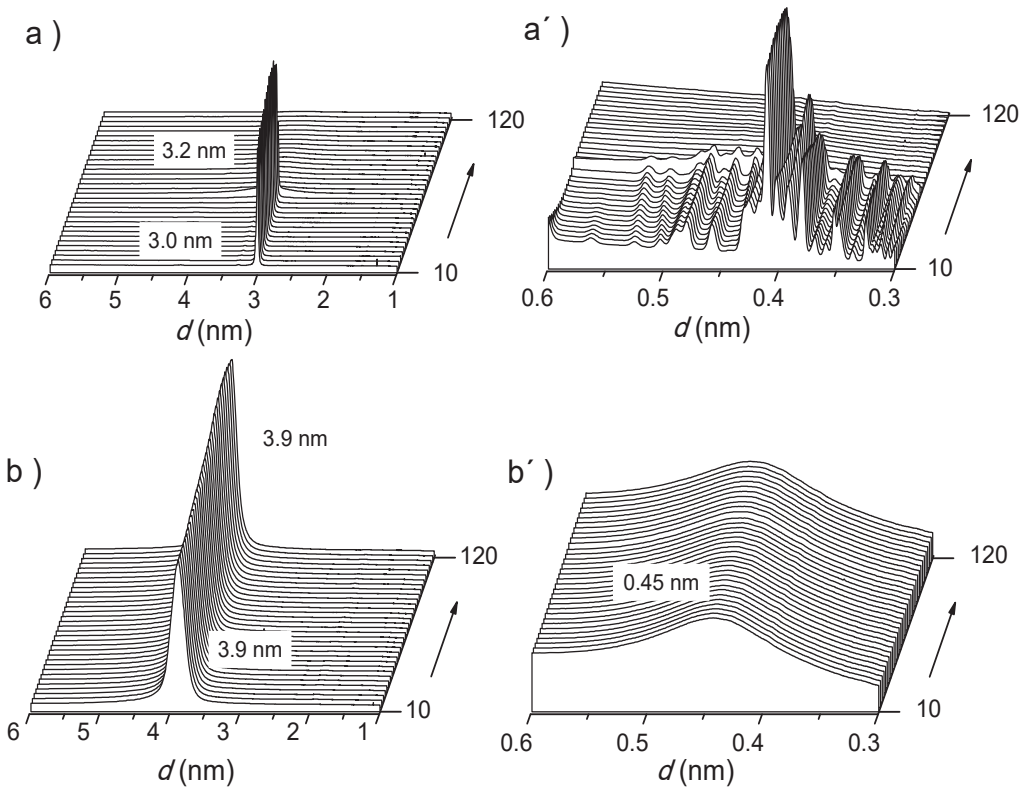

Figure 6. Evolution of the SAXS and WAXS profiles of LAE (a and a') and LAE·HyA-1 (b and b') at heating from 10 to 120 °C.

2.2.4. LAE release and antimicrobial properties

According to the hypothesis formulated for this work, the biocide activity expected for the LAE·HyA complexes should arise from the free LAE that is released to the environment as a consequence of the dissociation undergone by the ionic pair upon incubation in an aqueous medium. To evaluate the capacity of these complexes to deliver LAE under conditions commonly found in food environments, the amount of LAE that is released from both LAE·HyA-1 and LAE·HyA-0.5 and accumulated in the incubation medium at pH 7.4 and 5.5 was measured by UV absorption at 220 nm, and results are compared in Figure 7. In all cases, the dissociation equilibrium was reached within an incubation period of 4 to 8 h. The concentration of LAE attained at that time was much higher at pH 7.4 than at pH 5.5 and, as largely expected, the accumulated amount of free LAE noticeably increased with the LAE:HyA ratio in the complex. An additional experiment carried out at pH 7.4 but at a temperature of 4 ºC revealed that cooling delayed the release of LAE in an extent similar to that observed for decreasing the pH down to 5.5 (Figure SI-6 in SI).

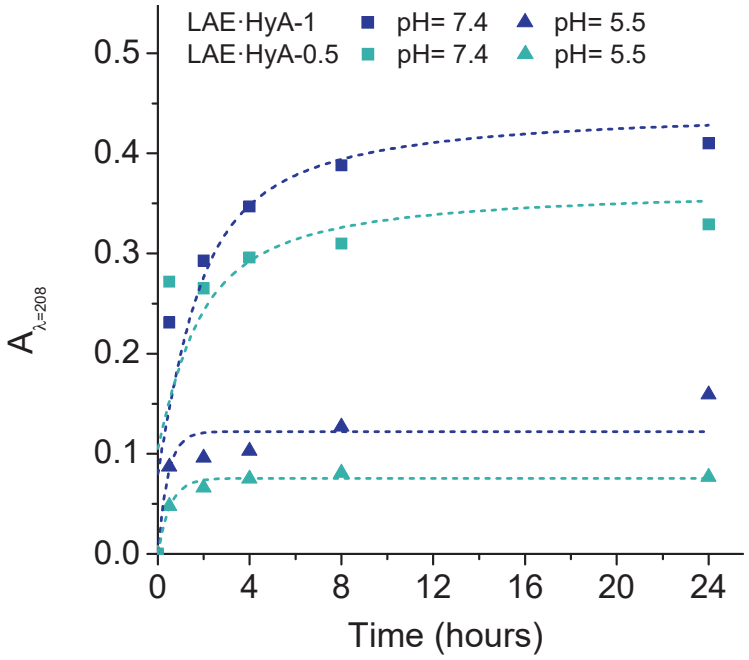

Figure 7. Dissociation of LAE·HyA complexes upon incubation in aqueous medium at pH= 7.4 and 5.5 at 25 ºC.

The bactericide activity of films made of LAE·HyA-1 and LAE·HyA-0.5 complexes at pH 7.4 and 37 ºC was evaluated by in vitro assays applying the liquid medium method and using as substrates two pairs of bacteria representatives of the Gram-positive (*L. monocytogenes* and *S. aureus*) and Gram-negative (*S. enterica* and *E. coli*) groups. A fast appraisal of the bactericidal effect could be made by visual inspection of the tubes which revealed disappearance of the initial turbidity for all the cases after 24 h of incubation (Figure SI-7, SI file). Quantitative results of these preliminary assays expressed as Log(CFU) (colony forming units), Log(RV) (reduction value) and PR (percentage of reduction) are compared in the bar graphs of Figure 8 for the four bacteria, and numerical values of these results are collected in the Table SI-1 of the SI file. As it can be inferred from the graphs, the antimicrobial activity of both, LAE·HyA-1 and LAE·HyA-0.5, is noticeable from the earlier incubation stages so they inhibited the growth of all bacteria just after 2 h of contact. This activity was found especially important against Gram-negative bacteria so that Log(RV) values of 6.6 and 4.7 for *S. enterica,* and 3.6 and 3.9 for *E. coli* was measured for LAE·HyA-1 and LAE·HyA-0.5, respectively. This result is remarkable since Gram-negative bacteria are usually less sensible to cationic surfactants than Gram-positive bacteria due to the outer lipopolysaccharide coat that surrounds the cell wall (Vaara, 1992).

The antimicrobial activity of the complexes against Gram-positive bacteria was found to be lower with Log(RV) of 0.2 and 0.4 observed for *L. monocytogenes* and 1.1 and 0.4 for *S. aureus* for LAE·HyA-1 and LAE·HyA-0.5, respectively, after 2 h of

incubation. The higher antimicrobial efficacy observed for the complex containing more LAE is quite reasonable and according to observations reported on antimicrobial films based on LAE loaded chitosan (Higueras et al., 2013). However, it was interesting to see that the antimicrobial activity of the LAE·HyA-0.5 complex against *S. aureus* became higher than that of LAE·HyA-1 when long incubation times (8 and 24 h) have elapsed. This behaviour may be convincingly explained by taking into account the observations reported by Baier et al (Baier et al., 2013) on the biocide activity of HyA-based nanocapsules containing the antimicrobial agent polyhexanide. They found that *S. aureus* was particularly sensitive to the biocide agent incorporated in such systems because its release was favored by the biodegradation of HyA, a process that happened due to the action of the hyaluronidases provided by the bacteria.

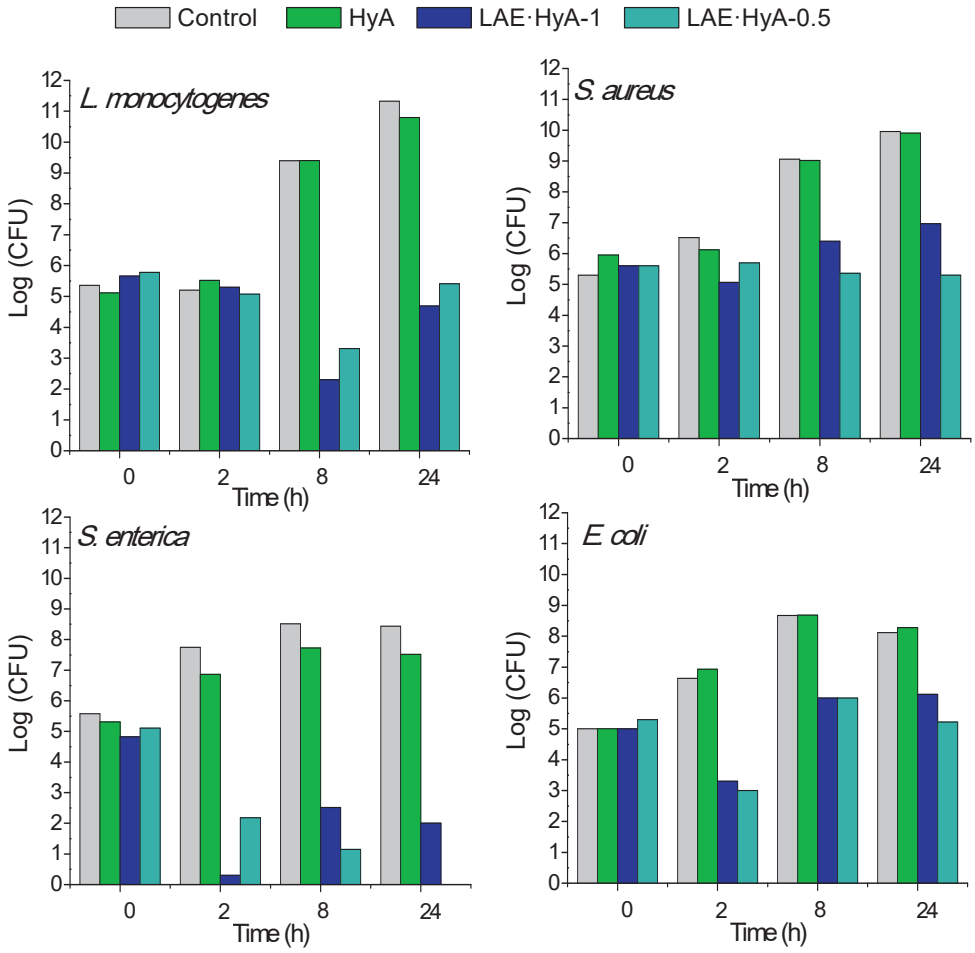

Figure 8. Antimicrobial activity of LAE·HyA-1 and LAE·HyA-0.5 films over time against Gram-positive and Gram-negative bacteria.

2.3. Conclusions

The well recognized biocide guanidinium-based compound LAE was coupled with hyaluronic acid to render ionic complexes with two compositions, *i.e* LAE:HyA = 1 and 0.5. These complexes were non-soluble in water and stable to heat up to temperatures above 200 ºC. Although the genuine crystallinity of LAE was lost when it was incorporated in the complex, a smectic liquid crystal arrangement was adopted by both LAE·HyA-1 and LAE·HyA-0.5. The nanostructure of the complexes is characterized by a periodicity of about 3.8-3.9 nm corresponding to the repeating distance of an alternating array of HyA and LAE layers in which the undecyl tail of the lauroyl group of LAE is in the disordered state. These complexes dissociated upon incubation in an aqueous medium in a range of hours providing free LAE at equilibrium concentrations depending on pH and complex composition. Films prepared from these complexes displayed significant biocide activity against both Gram-positive and Gram-negative bacteria with the highest efficiency being shown by LAE·HyA-1 against *S. enterica*.

2.4. References

Allison, D. D., Grande-Allen, K. J. (2006). Hyaluronan: a powerful tissue engineering tool. Tissue Eng. 12, 2131–2140.

Asker, D., Weiss, J., McClements, D. J. (2009). Analysis of the interactions of a cationic surfactant (lauric arginate) with an anionic biopolymer (pectin): Isothermal titration calorimetry, light scattering, and microelectrophoresis. Langmuir, 25, 116–122.

Baier, G., Cavallaro, A., Vasilev, K., Mailänder, V., Musyanovych, A., Landfester, K. (2013). Enzyme responsive hyaluronic acid nanocapsules containing polyhexanide and their exposure to bacteria to prevent infection. Biomacromolecules, 14, 1103–1112.

Battistini, F. D., Tártara, L. I., Boiero, C., Guzmán, M. L., Luciani-Giaccobbe, L. C., Palma, S. D., Allemandi D.A., Manzo, R.H., Olivera, M. E. (2017). The role of hyaluronan as a drug carrier to enhancethe bioavailability of extended release ophthalmic formulations. Hyaluronan-timolol ionic complexes as a model case. Eur. J. Pharm. Sci., 105, 188–194.

Becerril, R., Manso, S., Nerin, C., Gómez-Lus, R. (2013). Antimicrobial activity of lauroyl arginate ethyl (LAE), against selected food-borne bacteria. Food Control, 32, 404–408.

Bračič, M., Hansson, P., Pérez, L., Zemljič, L. F., Kogej, K. (2015). Interaction of sodium hyaluronate with a biocompatible cationic surfactant from lysine: a binding study. Langmuir, 3, 12043–12053.

Burdick, J. A., Prestwich, G. D. (2011). Hyaluronic acid hydrogels for biomedical applications. Adv. Mater., 23, H41–H56.

Chytil, M., Trojan, M., Kovalenko, A. (2016). Study on mutual interactions and electronic structures of hyaluronan with lysine, 6-Aminocaproic acid and arginine.

Carbohyd. Polym., 142, 8–15.

Engler, A. C., Wiradharma, N., Ong, Z. Y., Coady, D. J., Hedrick, J. L., Yang, Y. Y. (2012). Emerging trends in macromolecular antimicrobials to fight multi-drug-resistant infections. Nano Today, 7, 201–222.

Gamarra-Montes, A., Missagia, B., Morató, J., Muñoz-Guerra, S. (2017). Antibacterial films made of ionic complexes of Poly(γ-glutamic acid) and ethyl lauroyl arginate. Polymers, 10, 1–15.

Hanski, S., Houbenov, N., Ruokolainen, J., Chondronicola, D., Latrou, H., Hadjichristidis, N., Ikkala, O. (2006). Hierarchical ionic self-assembly of rod−comb block copolypeptide-surfactant Complexes. Biomacromolecules, 7, 3379–3384.

Higueras, L., López-Carballo, G., Hernández-Muñoz, P., Gavara, R., Rollini, M. (2013). Development of a novel antimicrobial film based on chitosan with LAE (ethyl-N-dodecanoyl-L-arginate) and its application to fresh chicken. Int. J. Food Microbiol. 165, 339–345.

Kemp, M. M., Kumar, A., Clement, D., Ajayan, P., Mousa, S., Linhardt, R. J. (2009). Hyaluronan- and heparin-reduced silver nanoparticles with antimicrobial properties. Nanomedicine, 4, 421–429.

Lequeux, I., Ducasse, E., Jouenne, T., Thebault, P. (2014). Addition of antimicrobial properties to hyaluronic acid by grafting of antimicrobial peptide. Eur. Polym. J., 51, 182–190.

Liu, L., Liu, Y., Li, J., Du, G., Chen, J. (2011). Microbial production of hyaluronic acid: current state, challenges, and perspectives. Microbiol. Cell Fact., 10, 99–108.

Loeffler, M., Mcclements, D. J., Mclandsborough, L., Terjung, N., Chang, Y., Weiss, J. (2014). Electrostatic interactions of cationic lauric arginate with anionic polysaccharides affect antimicrobial activity against spoilage yeasts. J. Appl. Microbiol., 117, 28–39.

Macknight, W. J., Ponomarenko, E. A., Tirrel, D. A. (1998a). Self-assembled polyelectrolyte-surfactant complexes in nonaqueous solvents and in the solid state. Acc. Chem. Res., 31, 781–788.

Macknight, W. J., Ponomarenko, E. A., Tirrel, D. A. (1998b). Stoichiometric complexes of synthetic polypeptides and oppositely charged surfactants in organic solvents and in the solid state. Macromolecules, 29, 8751-8758.

Necas, J., Bartosikova, L., Brauner, P., Kolar, J. (2008). Hyaluronic acid (hyaluronan): a review. Vet. Med., 53, 397–411.

Otero, V., Becerril, R., Santos, J. A., Rodríguez-Calleja, J. M., Nerín, C., García-López, M. L. (2014). Evaluation of two antimicrobial packaging films against *Escherichia coli* O157: H7 strains in vitro and during storage of a Spanish ripened sheep cheese (Zamorano). Food Control, 42, 296–302.

Pérez-Camero, G., García-Álvarez, M., Martínez de Ilarduya, A., Fernández, C., Campos, L., Muñoz-Guerra, S. (2004). Comb-like complexes of bacterial poly(γ,D-glutamic acid) and cationic surfactants. Biomacromolecules, 5, 144–152.

Ponomarenko, E.A., Alan J. Waddon, David A. Tirrell, MacKnight, W. J. (1996).

Structure and properties of stoichiometric complexes formed by sodium poly(α,L-glutamate) and oppositely charged surfactants. Langmuir, 12, 2169–2172.

Rodriguez, E., Seguer, J., Rocabayera, X., Manresa, A. (2004). Cellular effects of monohydrochloride of L-arginine, N-alpha-lauroyl ethylester (LAE) on exposure to *Salmonella typhimurium* and *Staphylococcus aureus*. J. Appl. Microbiol., 96, 903–912.

Santos, M. R. E., Fonseca, A. C., Mendonça, P. V., Branco, R., Serra, A. C., Morais, P. V., Coelho, J. F. J. (2016). Recent developments in antimicrobial polymers: a review. Materials, 9, 599-632.

Schanté, C. E., Zuber, G., Herlin, C., Vandamme, T. F. (2011). Chemical modifications of hyaluronic acid for the synthesis of derivatives for a broad range of biomedical applications. Carbohyd. Polym., 85, 469-489.

Stern, R., Kogan, G., Jedrzejas, M. J., Šoltés, L. (2007). The many ways to cleave hyaluronan. Biotechnol. Adv., 25, 537–557.

Tolentino, A., Alla, A., Martínez de Ilarduya, A., Muñoz-Guerra, S. (2011). Comb-like ionic complexes of pectinic and alginic acids with alkyltrimethylammonium surfactants. Carbohyd. Polym., 86, 484–490.

Tolentino, A., Alla, A., Martínez de Ilarduya, A., Muñoz-Guerra, S. (2013). Comb-like ionic complexes of hyaluronic acid with alkyltrimethylammonium surfactants. Carbohyd. Polym., 92, 691–696.

Vaara, M. (1992). Agents that increase the permeability of the outer membrane. Microbiol. Rev., 56, 395–411.

General conclusions

I. A series of alkyltrimethylphosphonium bromides (*n*ATMP·Br) including linear alkyl chains with even numbers (*n*) of carbon atoms ranging from 12 to 22 has been synthesized and chemically characterized. These amphiphilic compounds have *Krafft* temperatures and *cmc* values lower than those reported for their alkyltrimethylammonium bromide analogues. *n*ATMP·Br appeared to be highly thermally stable compounds with onset decomposition temperatures close to 400 ºC and they displayed several thermotropic transitions along heating/cooling. At room temperature they all crystallized in a monoclinic lattice, and at increasingly higher temperatures they organized as Smectic-B (90-225 ºC), Smectic-A (225-240 ºC) and isotropic liquid (>225 ºC for n = 12 and 14 and > 240 for $n \geq 16$).

II. Nearly stoichiometric comb-like ionic complexes (*n*ATMP·PGGA) could be readily prepared by mixing aqueous solutions of PGGA and *n*ATMP·Br (n= 12, 14,16,18,20 and 22). These complexes were non-soluble in water and displayed excellent thermal stability with onset decomposition temperatures about 300 ºC. In the solid-state, they adopted the same biphasic layered structure described for their ammonium analogues with an interlayer repeating distance of 3-4.5 nm. *n*ATMP·PGGA with $n \geq 18$ displayed one reversible thermal transition within the 40-80 ºC range involving the melting-crystallization of the paraffinic phase without perceivable alteration of the layered structure. Complexes with $n \leq 16$ displayed strong bactericide activity which confers them high potential for being used in active coating or packaging applications.

III. Nanocomposites of 12ATMP·PGGA and 20ATMP·PGGA complexes with montmorillonite clays modified with 12ATMP and 20ATMP surfactants, respectively, were prepared by blending. XRD and TEM evidenced the occurrence of extensive intercalation which could be further increased by heating treatment. The thermal behavior and layered structure of the *n*ATMP·PGGA complexes was retained in the nanocomposites. The elastic modulus and strength of the complexes were notably enhanced in the nanocomposites although ductility was drastically reduced. It was finally concluded that the efficient mixing of the clay with the polypeptide attained in these nanocomposites was due to the compatibilizing effect of the *n*ATMP·Br surfactants used for both complexation of PGGA and modification of the nanoclays.

IV. Nearly stoichiometric *n*ATMP·HyA complexes have been readily produced by ionic coupling of hyaluronic acid (HyA) with *n*ATMP·Br salts with *n* = 12,14,16,18,20 and 22. Compared to their *n*ATMP·PGGA analogues, these complexes showed noticeable differences as a consequence of the replacement of the polypeptide by the polysaccharide chain: their thermal stability was about 100 ºC lower, their crystallinity was lower, and the biphasic arrangement adopted in the solid state was more complex. Conversely, they decomposed in water in a similar manner and have the same response to pH changes although they showed an extensive degradation in the presence of enzymes. Also the bactericide activity was essentially similar although slightly higher against Gram-positive bacteria. Therefore *n*ATMP·HyA complexes constitute an acceptable option for the design of biocompatible/biodegradable films with antimicrobial properties.

V. *n*ATMP·Br salts (*n* = 16, 18 and 22) were coupled with HyA to obtain *n*ATMP·HyA nanoparticles (*n*ATMP·HyA NPs) using the ionotropic gelation technique in water. These NPs resulted with a hydrodynamic radius of around 100 nm, a negative *ζ*-potential, and a biphasic nanostructure reminiscent of that observed in the films of these complexes. Strikingly, the appearance of these NPs oscillated between banded worm-like to spherical granular depending on value of *n*, composition of the complex, and conditions used for their preparation. All these NPs were effective against *S. aureus* (Gram-positive bacteria) whereas they showed only moderate antimicrobial activity against *E. coli* (Gram-negative bacteria) and the common yeast *C. Albicans*

VI. Nearly stoichiometric ionic complexes of hyaluronic acid and alkanoylcholine surfactants (*n*ACh·HyA with *n* = 12,14,16,18) were successfully synthesized. These complexes were non-water soluble, stable up to around 200 ºC and adopted in the solid state an amphiphilic nanometric structure with the polysaccharide and the alkanoylcholine segregated in two phases that alternate regularly with a periodicity of about 4-5 nm. Spherical nanoparticles with diameters around 150 nm could be prepared by ionotropic gelation from the complexes derived from stearoyl and oleoyl choline with ACh:HyA ratios of 0.5 and 0.25. Cytotoxicity tests demonstrated that these NPs are fully biocompatible. The NPs were stable for a few days in aqueous emulsion and preliminary assays on DOX loaded NPs demonstrated a high loading efficiency and a fast drug delivery upon incubation under physiological conditions. As a result, it

seems that *n*ACh·HyA complexes may be considered a highly promising biocompatible/ biodegradable platform for the design of systems suitable for drug transport and targeted delivery in anticancer chemotherapy.

VII. The widely-known strong antimicrobial agent LAE (ethyl $^{\alpha}$*N*-lauroyl L-arginate) was ionically coupled with both poly(γ-glutamic acid) (PGGA) and hyaluronic acid (HyA) to generate host-guest ionic complexes containing either stoichiometric molar amounts of the two components or an half amount of LAE. All complexes were found to adopt the layered biphasic structure typically observed in the ionic complexes of PGGA and HyA with the lauroyl chains staying in a disordered state. Upon incubation of the complexes in water, LAE was released at a rate dependent on pH, and in a less degree, on its content in the complex. Films of all these complexes displayed antibacterial activity against both Gram-positive and Gram-negative strains but the biocide effect was different according to composition. LAE·PGGA complexes displayed more activity against Gram-positve bacteria whereas the opposite result was observed for LAE·HyA complexes. Since all the components integrating the complexes are of well contrasted biocompatibiliy, and in some cases even edible, these compounds will find applications as both antibacterial food additives or/and packaging materials.

Acknowledgements

En la siguiente sección me gustaría expresar mis agradecimientos a toda la gente que de diferentes maneras me han ayudado durante esta experiencia de desarrollar esta Tesis doctoral.

En primer lugar, me gustaría agradecer al Prof. Dr. Sebastián Muñoz Guerra por su labor como director de la presente Tesis ya que sin su dedicación, apoyo y paciencia esta Tesis no hubiera sido posible finalizarla con tanto éxito.

Además agradecer a toda la gente que forma parte del grupo, especialmente all Dr. Antxon Martínez de Illarduya por su ayuda con los RMNs y al Dr. Abdelillah Alla por su gran ayuda con DSC, TGA y XRD. A la Dr. Lourdes franco y a la Dr. Mª Teresa Casas por su ayuda con las propiedades mecánicas y TEM y su apoyo. Por otro lado agradecer a la Dr. Lourdes Urpí su colacoración en el Sincrotrón ALBA y al Dr. Jordi Bou su compañía hasta largas horas de la tarde.

También agradecer al ministerio de eduación por concederme la beca FPI de investigación “Ayudas para contratos predoctorales para la formación de doctores 2013” y el apoyo financiero de MICINN a mi grupo de investigación para realizar los proyectos MAT2012-38044-C03 y MAT-2016-77345-CO3-03.

Agradecer también al Dr. Kubota of Meiji. Co. (Japan) por proporcionarnos el PGGA utilizado en esta tesis y a Vedepsa (LAMIRSA GROUP, Terrassa, Barcelona, Spain) por proporcionarnos el surfactante LAE.

A la Dr. Christina Kamma-Lorger y el resto de equipo de la línea BL11 del Sincrotrón ALBA por el soporte técnico ofrecido durante las diversas visitas realizadas al Sincrotrón ALBA, Cerdanyola del Vallès, Barcelona.

Al Dr. Jordí Morató y su equipo (en especial a la Dr. Beatriz Missagia y Eva Forés) agradecerles su colaboración para la realización de las pruebas antimicrobianas.

A la Dr. Marta Fernández García del CSIC (Madrid) por sus consejos para la realización de las propiedades antimicrobianas y sus conocimientos aportados sobre materiales con propiedades antimicrobianas.

I wish to express my gratitude to Katharina Landfester and her group for all their kindness, generosity and support during my stay at Max Planck Institute for Polymer Research (Mainz). Thanks to Heloise Thérein-Aubin for her patience and advices for achieving the objectives during my stay. Thanks to Katrin Kirchhoff and Christoph Sieber for their invaluable help in TEM. Eventually I want to thanks to all the staff and partners for the great time I spent there.

Especial agradecimiento a mis padres y hermana por apoyarme durante este largo camino. Es decir, por apoyarme a tomar la decisión, estar siempre cerca a pesar de la distancia, por los múltiples viajes realizados juntos y por su paciencia e interés por escucharme todo el día hablando de la Tesis intentando siempre entender de qué hablaba. Sin vosotros estoy segura de que esta Tesis no hubiera sido posible.

También agradecer a mi familia su apoyo y confianza en mí. En especial agradecer todas esas comidas familiares infinitas para vernos y compartir un rato juntos. Agradecer los diferentes años en las fallas con todos vosotros: mi padrino, y pilar, Paz y David, Paquillo y Mamen, Quique y Chus, mis padres y hermana, Curro, Alfonso, y como no, mi seudo-familia, los Martín.

También agradecer a Sergio Cabezas su apoyo inicial para que realizara la tesis, su paciencia durante todo el camino y todo lo que me ha enseñado durante estos años.

Gracias a mis compis de laboratorio, comidas y cafés por vuestra amistad y todo lo compartido, desde un simple café, hasta babyshowers, bodas y cenas. En especial a Mayka y Angelica por estar siempre atentas conmigo desde el principio, a Elena, Juan Carlos, Ernes y Alberto por sus ratos en el laboratorio y por supuesto a Silvana, Cinthia, Georgina, Neudys, Mar y Yolanda por su amistad y experiencias vividas fuera del laboratorio.

También quiero dar gracias a mis amigos de vermuting que me han ayudado a desconectar y divertirme en medio de estas largas semanas de trabajo. Sin vosotr@s, Brenda, Maria, Marta, Gigi, Clara, Andreu, Andrea, Diego, Carlos, Nacho, Anna y Vero, mi nivel de estrés hubiera estado mucho más alto aunque otros niveles hubieran estado más bajos..

A mis amigas de toda la vida de Medina del Campo quería agradecerles todos estos años juntas y por seguir allí, en la distancia, interesándose por mi tesis y preparándome fiestas sorpresa inexperadas que me han animado a seguir adelante.

A mis amigas de la carrera por siempre escucharme y darme consejos y por seguir siendo igual de locas que cuando nos conocimos durante la carrera.

Por último, agradecer a mi cukiLu por hacer que el último año de tesis, a pesar de ser duro, haya sido inolvidable.

The author

Ana Gamarra Montes was born on 20th of February in 1990 in Medina del Campo. In 2008 she started her bachelor studied on Chemistry Science at the faculty of Chemistry of the Universidad de Valladolid (UVa) in Valladolid and graduated in 2013.

In 2013 she started her master studies on “Química Sintética e Industrial” of the Universidad de Valladolid (UVa) in Valladolid and graduated in 2014. The title at the master dissertation was “Complejos iónicos tipo peine de biopoliácidos y jabones de alquiltrimetilfosfonio” which was realised under the supervision of Prof. Dr. Sebastián Muñoz Guerra and Prof. Pablo Espinet Rubio.

In 2014 she was granted with a FPI from MICINN and started her PhD project entitled “*Ionic complexes of naturally-occurring biopolymers and cationic surfactants: a platform for industrial and biomedical applications*”. During the PhD she performed an international stay for 4 months in the Physical Chemistry of Polymers group of Prof. Dr. K. Landferster at the Max Planck Institute for Polymer Research (Germmany). The results during the intership are included in this Thesis.

Scientific production derived from the Thesis

Scientific papers

1. Gamarra, A., Urpí, L., Martínez de Ilarduya, A., Muñoz-Guerra, S. (2017). Crystalline structure and thermotropic behavior of alkyltrimethylphosphonium amphiphiles. Phys. Chem. Chem. Phys., 19, 4370–4382.
2. Gamarra, A., Martínez de Ilarduya, A., Vives, M., Morató, J., Muñoz-Guerra, S. (2017). Ionic complexes of poly(γ-glutamic acid) with alkyltrimethylphosphonium surfactants. Polymer, 116, 43–54.
3. Gamarra-Montes, A., Missagia, B., Morató, J., Muñoz-Guerra, S. (2017). Antibacterial films made of ionic complexes of poly(γ-glutamic acid) and ethyl lauroyl arginate. Polymers, 10, 1–15.
4. Gamarra, A., Muñoz-Guerra S., Urpí,L.; Galbis, E., Galbis, J.A. (2018). Nanocomposites of microbial polyglutamic acid and nanoclays compatibilized by organophosphonium surfactants. Macromol. Chem. Phys. doi.org/10.1002/macp.201800083.
5. Gamarra, A., Missagia, B., Urpí, L., Morató, J. and Muñoz-Guerra, S. (2018). Ionic coupling of hyaluronic acid with ethyl $^{\alpha}$*N*-lauroyl L-arginate (LAE): Structure, properties and biocide activity of complexes. Carbohydr. Polym. 197 (1), 109-116.
6. Gamarra, A., Therien-Aubin, H., Landfester, K. Comb-like ionic complexes of hyaluronic acid and alkanoylcholine surfactants as platform for drug delivery systems. Submitted to Biomacromolecules.
7. Gamarra, A., Forés, E., Morató, J., Muñoz-Guerra, S. Amphiphilic ionic complexes of hyaluronic acid with organophosphonium compounds and their antimicrobial activity. To be submitted to Int. J. Biolog. Macromol. (Elsevier).
8. Gamarra, A., Forés, E., Morató, J., Muñoz-Guerra, S. Nanoparticles of hyaluronic acid and alkyltrimethylphosphonium salts with antimicrobial properties. To be submitted to Eur. Polym. J. (Elsevier).

Conference proceedings

1. Gamarra, A., Alla, A., Martínez de Ilarduya, A., Muñoz-Guerra, S. Comb-like ionic complexes of microbial poly(gamma-glutamic acid) and alkyltrimethylphosphonium soaps. Poster at “Fourth International Conference on Multifunctional, Hybrid and Nanomaterials”, Sitges, (Spain), 9-13 March, 2015.
2. Gamarra, A., Urpí, L., Alla, A., Muñoz-Guerra, S. Structural characterization of alkyltrimethylphosphonium surfactants by powder real-time and monocrystal XRD analysis. Poster at “VII AUSE Congress and II ALBA User’s Meeting”, ALBA Syncrotron, Cerdanyola del Vallés, (Spain), 16-19 June, 2015.
3. Gamarra, A., Alla, A., Martínez de Ilarduya, A., Muñoz-Guerra, S. Comb-like structures made by ionic coupling of poly(γ-glutamic acid) with alkyltrimethyl-phosphonium surfactants. Oral communication at congress “1st French-Spanish Joint Congress for Young Researchers in Polymers (JIP-JEPO2015)”. San Sebastian, España, 14-18 September, 2015.
4. Gamarra, A., Alla, A., Martínez de Ilarduya, A., Casas, M.T, Muñoz-Guerra, S. Nanostructured amphiphilic systems based on hyaluronic acid ionic complexes. Oral communication at congress “XIV Reunión del grupo especializado de polímeros GEP2016 (RESEQ, RSEF)”, Burgos, (España), 5-8 September 2016.

Annexes

Annex A: Supporting information to Chapter IV

Experimental procedures

1. General procedure for the synthesis of trimethylalkylphosphonium salts (*n*ATMP·Br)

1-bromoalkane (5.5 mmol) was placed in a flask immersed into an oil bath (80 ºC) and under a nitrogen atmosphere. After heating the 1-bromoalkane for several minutes, the trimethylphosphine (TMP) was slowly added (5mL, 5 mmol). The mixture was heated up to 116 ºC and stirred for a period of 12 to 24 h depending on the bromoalkane used. The precipitate, which appeared once the mixture was cooled to room temperature, was collected by filtration, washed several times in order to remove the excess of the alkylbromide and dried over high vacuum.

Dodecyltrimethylphosphonium bromide (12ATMP·Br)

The TMP and 1-bromododecane (1.3 mL, 5.5 mmol) gave after 16h stirring 1.14 g (70%) of the product as a white powder. The chemical structure was ascertained by ^{1}H NMR, ^{13}C NMR, FT-IR and elemental analysis. ^{1}H NMR (300.1 MHz; $CDCl_3$) 2.46 (2H, m, RC**H**$_2$P$^+$), 2.25 and 2.20 (9H, d, P$^+$(C**H**$_3$)$_3$), 1.55 (2H, m, RC**H**$_2$CH$_2$P$^+$),1.25 (18H, m, CH$_3$-(C**H**$_2$)$_9$-CH$_2$ CH$_2$P$^+$), 0.88 (3H, t, C**H**$_3$-(CH$_2$)$_{11}$-P$^+$), ^{13}C NMR (75.5 MHz; $CDCl_3$) 31.9 (CH_2), 30.6 (CH_2), 30.4 (CH_2), 29.6-29.0 (4CH_2), 24.1 (CH_2), 23.4 (CH_2), 22.6 (CH_2), 21.8 (CH_2), 14.1 (CH_3), 9.4 (P$^+$(CH_3)$_3$) and 8.6 (P$^+$(CH_3)$_3$). IR: 2913, 2847, 1471, 972, 705. Elemental analysis: C (%): 55.53; found: 55.53, H (%): 10.59; found: 10.50.

Tetradecyltrimethylphosphonium bromide (14ATMP·Br)

The TMP and 1-bromotetradecane (1.5 mL, 5.5 mmol) gave after 17h stirring 1.43 g (80%) of the product as a white powder. The chemical structure was ascertained by ^{1}H NMR, ^{13}C NMR, FT-IR and elemental analysis. ^{1}H NMR (300.1 MHz; $CDCl_3$) 2.46 (2H, m, RC**H**$_2$P$^+$), 2.25 and 2.20 (9H, d, P$^+$(C**H**$_3$)$_3$), 1.55 (2H, m, RC**H**$_2$CH$_2$P$^+$),1.25 (22H, m, CH$_3$-(C**H**$_2$)$_{11}$-CH$_2$ CH$_2$P$^+$), 0.88 (3H, t, C**H**$_3$-(CH$_2$)$_{13}$-P$^+$), ^{13}C NMR (75.5 MHz; $CDCl_3$) 31.9 (CH_2), 30.6 (CH_2), 30.5 (CH_2), 29.6-29.0 (6CH_2), 24.1 (CH_2), 23.5 (CH_2), 22.7 (CH_2), 21.7 (CH_2), 14.1 (CH_3), 9.3 (P$^+$(CH_3)$_3$) and 8.6 (P$^+$(CH_3)$_3$). IR: 2911, 2856, 1469, 978, 718. Elemental analysis: C (%): 57.92; found: 58.03, H (%): 10.90; found: 10.79.

Hexadecyltrimethylphosphonium bromide (16ATMP·Br)

The TMP and 1-bromohexadecane (1.7 mL, 5.5 mmol) gave after 18h stirring 1.62 g (85%) of the product as a white powder. The chemical structure was ascertained by ^{1}H NMR, ^{13}C NMR, FT-IR and elemental analysis. ^{1}H NMR (300.1 MHz; $CDCl_3$) 2.47 (2H, m, RC**H**$_2$P$^+$), 2.25 and 2.20 (9H, d, P$^+$(C**H**$_3$)$_3$), 1.55 (2H, m, RC**H**$_2$CH$_2$P$^+$),1.25 (26H, m, CH$_3$-(C**H**$_2$)$_{13}$-CH$_2$ CH$_2$P$^+$), 0.88 (3H, t, C**H**$_3$-(CH$_2$)$_{15}$-P$^+$), ^{13}C NMR (75.5 MHz; $CDCl_3$) 31.9 (CH_2), 30.6 (CH_2), 30.5 (CH_2), 29.6-29.0 (8CH_2), 24.1 (CH_2), 23.5 (CH_2), 22.7 (CH_2), 21.7 (CH_2), 14.1 (CH_3), 9.3 (P$^+$(CH_3)$_3$) and 8.6 (P$^+$(CH_3)$_3$). IR: 2912, 2848, 1472, 981, 716. Elemental analysis: C (%): 59.96; found: 60.06, H (%): 11.16; found: 11.00.

Octadecyltrimethylphosphonium bromide (18ATMP·Br)

The TMP and 1-bromooctadecane (1.9 mL, 5.5 mmol) gave after 20h stirring 1.45 g (70%) of the product as a white powder. The chemical structure was ascertained by ^{1}H NMR, ^{13}C NMR, FT-IR and elemental analysis. ^{1}H NMR (300.1 MHz; $CDCl_3$) 2.47 (2H, m, RC**H**$_2$P$^+$), 2.25 and 2.20 (9H, d, P$^+$(C**H**$_3$)$_3$), 1.50 (2H, m, RC**H**$_2$CH$_2$P$^+$),1.26 (30H, m, CH$_3$-(C**H**$_2$)$_{15}$-CH$_2$ CH$_2$P$^+$), 0.88 (3H, t, C**H**$_3$-(CH$_2$)$_{15}$-P$^+$), ^{13}C NMR (75.5 MHz; $CDCl_3$)

31.9 (CH_2), 30.6 (CH_2), 30.5 (CH_2), 29.6-29.0 ($10CH_2$), 24.1 (CH_2), 23.5 (CH_2), 22.7 (CH_2), 21.7 (CH_2), 14.1 (CH_3), 9.3 ($P^+(CH_3)_3$) and 8.6 ($P^+(CH_3)_3$). IR: 2915, 2849, 1472, 991, 714. Elemental analysis: C (%): 61.73; found: 61.56, H (%): 11.38; found: 11.22.

Eicosanetrimethylphosphonium bromide (20ATMP·Br)

The TMP and 1-bromoeicosane (2.0 g, 5.5 mmol) gave after 22h stirring 1.7 g (80%) of the product as a white powder. The chemical structure was ascertained by ^{1}H NMR, ^{13}C NMR, FT-IR and elemental analysis. ^{1} H NMR (300.1 MHz; $CDCl_3$) 2.47 (2H, m, $RC\mathbf{H}_2P^+$), 2.25 and 2.20 (9H, d, $P^+(C\mathbf{H}_3)_3$), 1.50 (2H, m, $RC\mathbf{H}_2CH_2P^+$),1.26 (34H, m, CH_3-$(C\mathbf{H}_2)_{17}$-CH_2 CH_2P^+), 0.88 (3H, t, $C\mathbf{H}_3$-$(CH_2)_{15}$-P^+), ^{13} C NMR (75.5 MHz; $CDCl_3$) 31.9 (CH_2), 30.6 (CH_2), 30.5 (CH_2), 29.6-29.0 ($12CH_2$), 24.1 (CH_2), 23.5 (CH_2), 22.7 (CH_2), 21.7 (CH_2), 14.1 (CH_3), 9.4 ($P^+(CH_3)_3$) and 8.6 ($P^+(CH_3)_3$). IR: 2915, 2848, 1478, 986, 711. Elemental analysis: C (%): 63.26; found: 63.12, H (%): 11.58; found: 11.37.

Docosanetrimethylphosphonium bromide (22ATMP·Br)

The TMP and 1-bromodocosane (2.1 g, 5.5 mmol) gave after 24h stirring 1.6 g (70%) of the product as a white powder. The chemical structure was ascertained by ^{1}H NMR, ^{13}C NMR, FT-IR and elemental analysis. ^{1} H NMR (300.1 MHz; $CDCl_3$) 2.47 (2H, m, $RC\mathbf{H}_2P^+$), 2.25 and 2.20 (9H, d, $P^+(C\mathbf{H}_3)_3$), 1.50 (2H, m, $RC\mathbf{H}_2CH_2P^+$),1.26 (38H, m, CH_3-$(C\mathbf{H}_2)_{19}$-CH_2 CH_2P^+), 0.88 (3H, t, $C\mathbf{H}_3$-$(CH_2)_{15}$-P^+), ^{13} C NMR (75.5 MHz; $CDCl_3$) 31.9 (CH_2), 30.6 (CH_2), 30.5 (CH_2), 29.6-29.0 ($14CH_2$), 24.1 (CH_2), 23.5 (CH_2), 22.7 (CH_2), 21.7 (CH_2), 14.1 (CH_3), 9.4 ($P^+(CH_3)_3$) and 8.6 ($P^+(CH_3)_3$). IR: 2911, 2848, 1474, 989, 716. Elemental analysis: C (%): 64.61; found: 64.70, H (%): 11.75; found: 11.65.

2. Methodology used for the single-crystal analysis

A crystal of 12ATMP·Br was mounted on a D8 Venture diffractometer, the radiation used was from a microfocus with a multilayer monochromator with Mo-Kα radiation (λ = 0.071073 nm), and the diffraction was collected with an area detector Photon 100 CMOS. The unit cell parameters were determined from 7111 reflections (2.23º < θ < 25.14º) and refined by least-squares method. Intensities of 25175 reflections (2.23º < θ < 25.39º) were collected, 3385 of which were unique (R_{int} = 0.0429), and 2530 unique reflections were considered as observed (conditions $I > 2\sigma(I)$). Lorentz-polarization and absorption corrections were made.

The structure was solved by direct methods (SHELXS-97 program)[28] and refined by full-matrix least-squared method (SHELXL-97 program).[28]

The minimized function was $\sum w\left|\left|F_0\right|^2 - \left|F_c\right|^2\right|^2$ where

$$w = [\sigma^2(F_0^2) + (0.1312P)^2 + 1.27P]^{-1} \quad P = (F_0^2 + 2F_c^2)/3.$$

All H atoms were added with idealized geometry and all C-H bond lengths were refined with the constraint that all C-H distances in a group were equal. For all CH_2 (and CH_3) groups, the H isotropic temperature factor has been calculated equal to 1.2 (and 1.5) times the equivalent temperature factor of the atom to which they are linked. The final *R* factors are shown in Table SI-1 together with other details of the quality of the molecule structure.

Figures

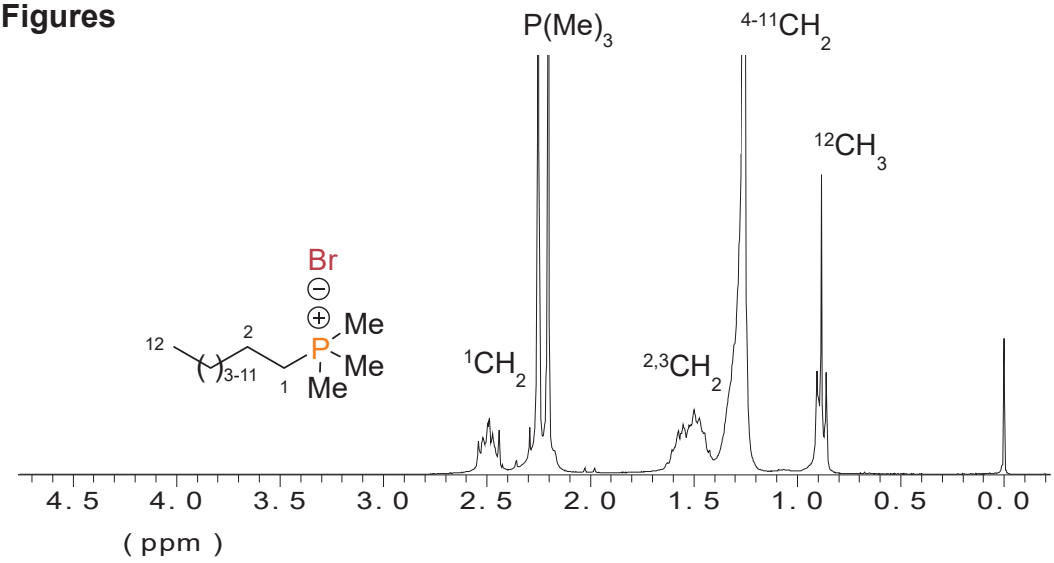
P(Me)3
4-11CH2
12CH3
Br
Me
Me
Me
12
2
3-11
1
1CH2
2,3CH2
4.5 4.0 3.5 3.0 2.5 2.0 1.5 1.0 0.5 0.0
(ppm)

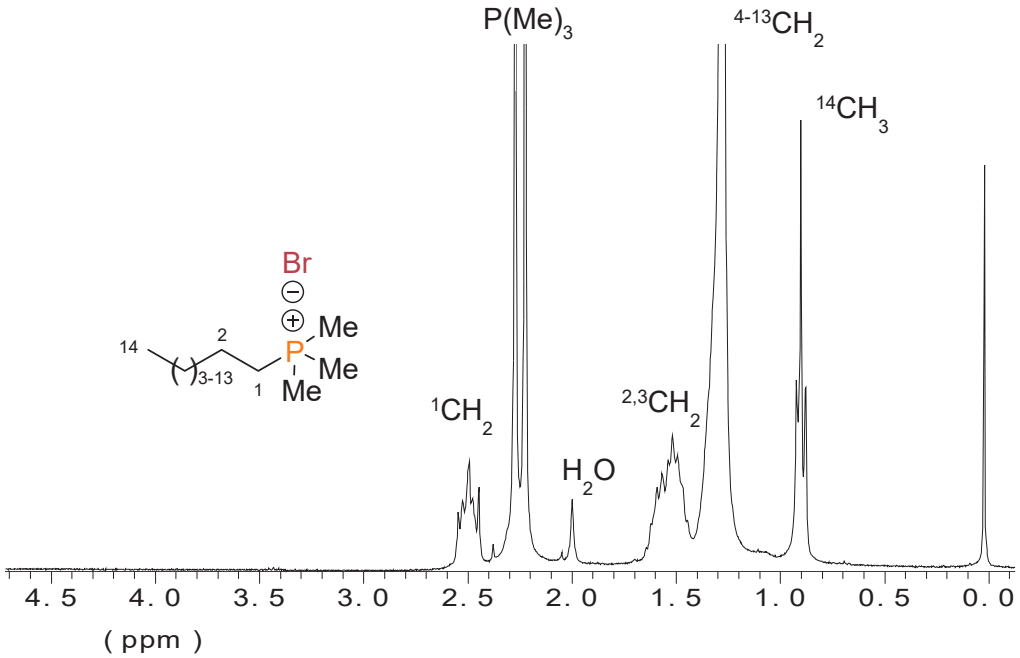
P(Me)3
4-13CH2
14CH3
Br
Me
Me
Me
14
2
3-13
1
1CH2
H2O
2,3CH2
4.5 4.0 3.5 3.0 2.5 2.0 1.5 1.0 0.5 0.0
(ppm)

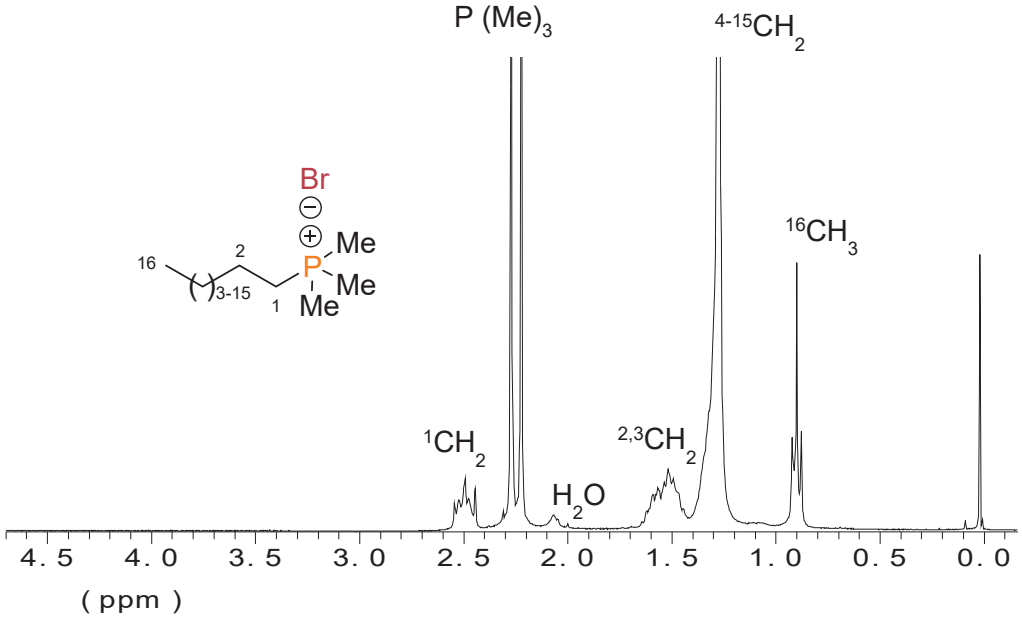
P (Me)3
4-15CH2
16CH3
Br
Me
Me
Me
16
2
3-15
1
1CH2
H2O
2,3CH2
4.5 4.0 3.5 3.0 2.5 2.0 1.5 1.0 0.5 0.0
(ppm)

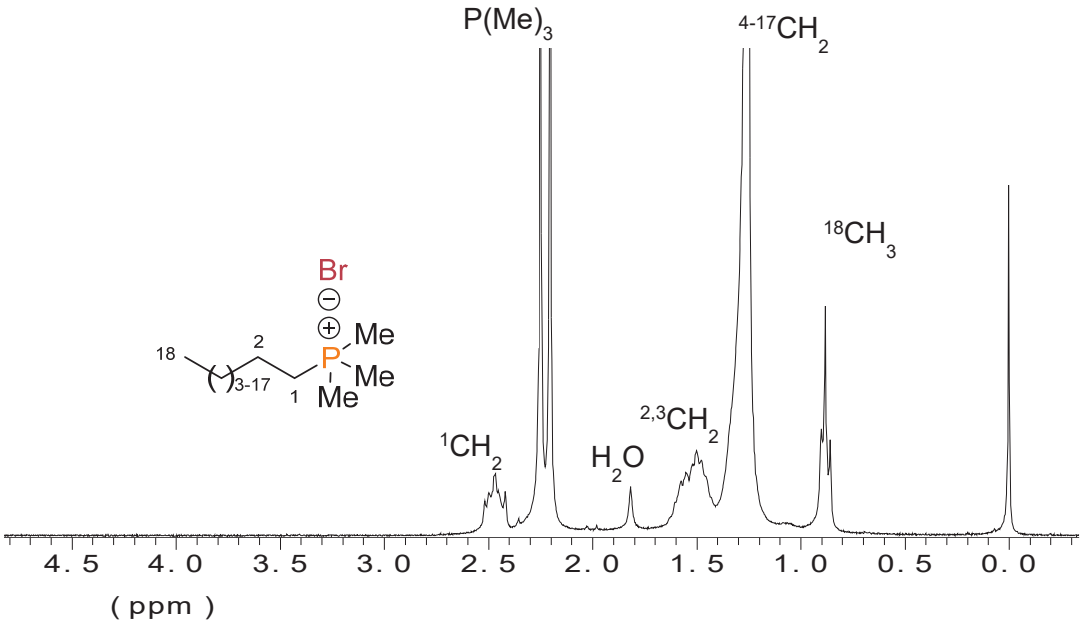

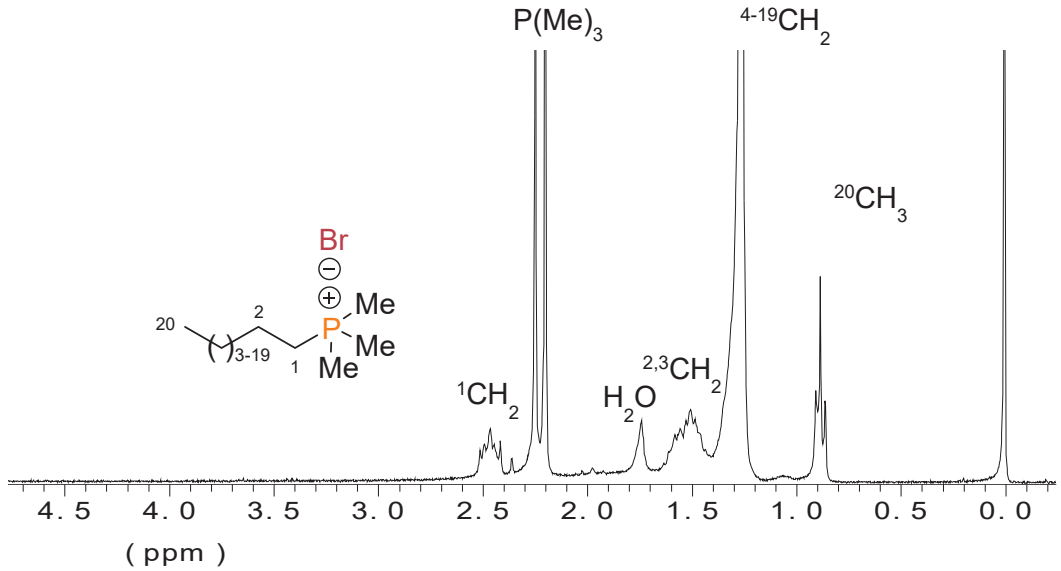

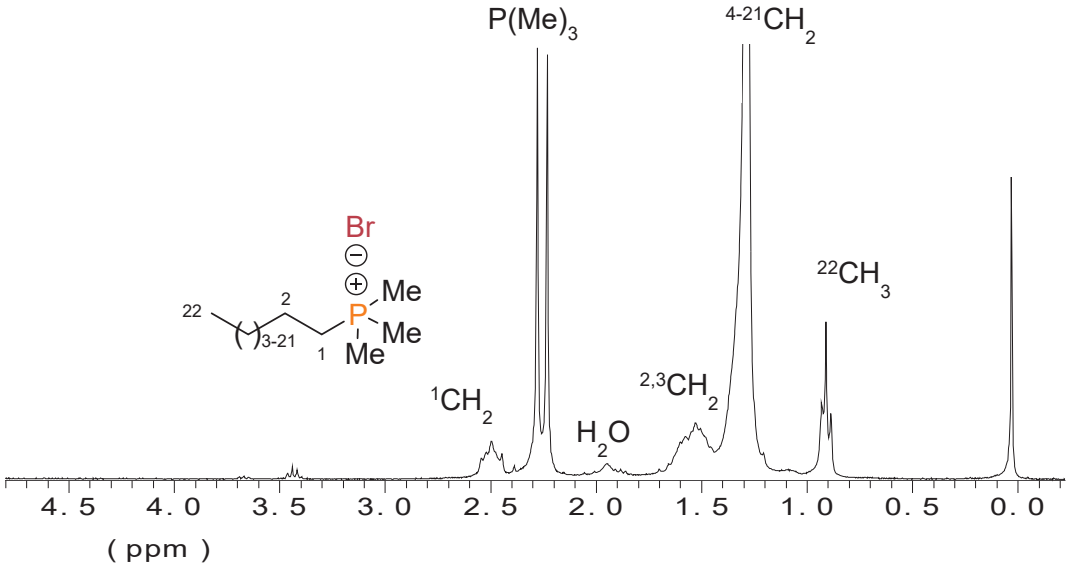

Figure SI-1. ^{1}H NMR spectra of *n*ATMP·Br surfactants.

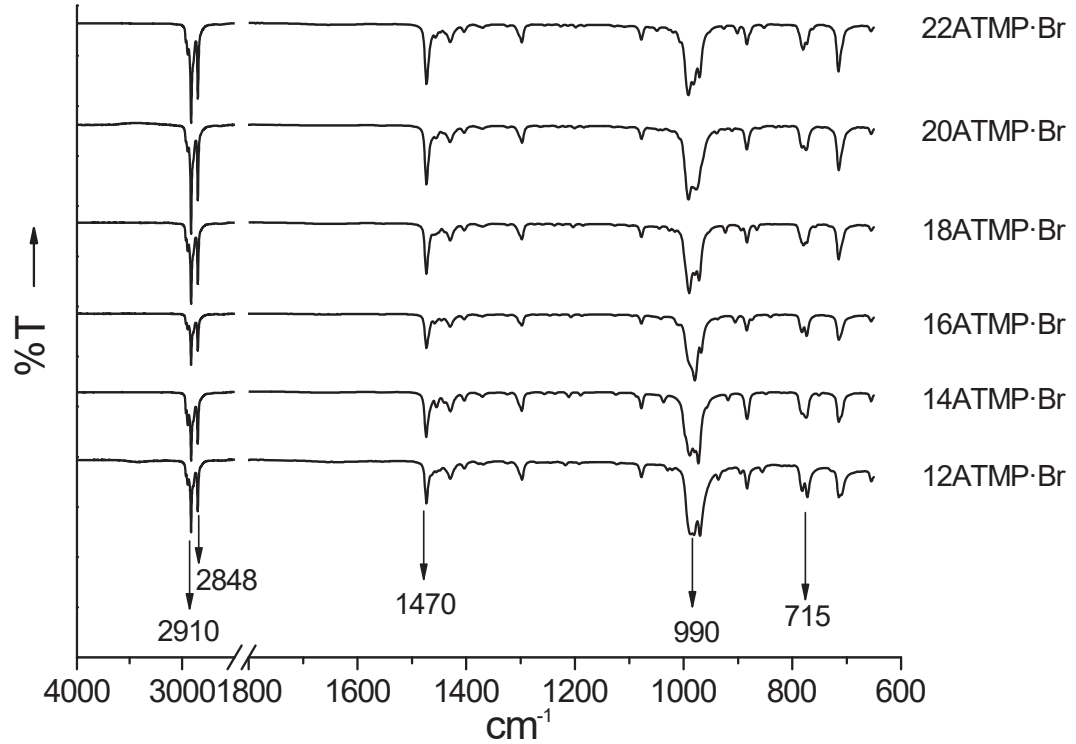

Figure SI-2. Comparison of FT-IR spectra of *n*ATMP·Br surfactants.

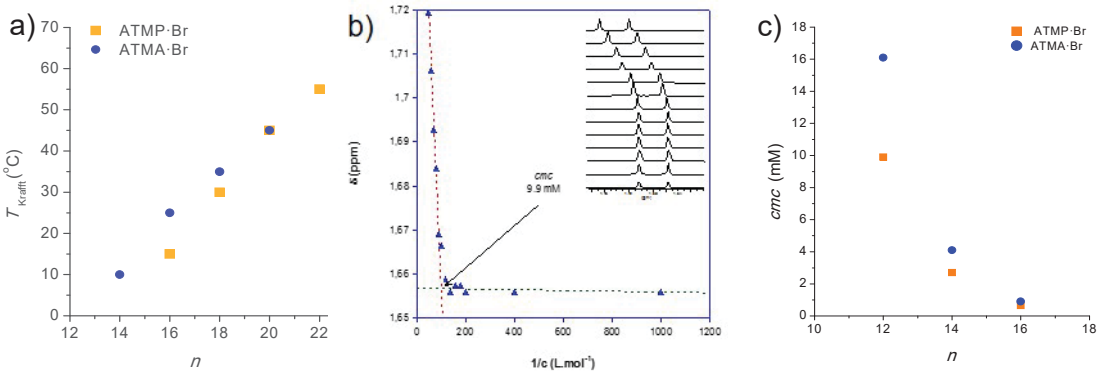

Figure SI-3. Comparison of the above 0 ºC Krafft temperatures for *n*ATMP·Br and *n*ATMA·Br surfactants (a), plot of the methyl chemical shift of 12ATMP·Br against concentration at 25 ºC with indication of the *cmc*; inset: the evolution of the ^{1}H NMR methyl signal of 12ATMP·Br with concentration (b) and comparison of the *cmc* determined by ^{1}H NMR for *n*ATMP·Br and *n*ATMA·Br with *n*=12,14 and 16 (c).

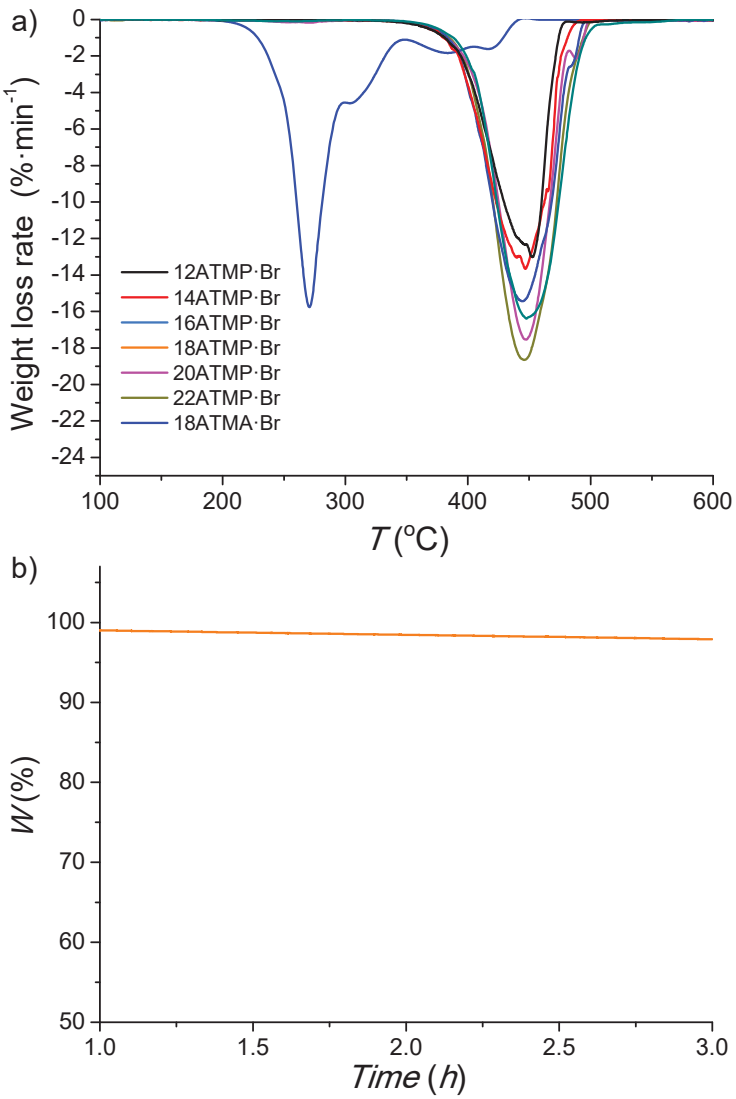

Figure SI-4. TGA derivative curves of *n*ATMP·Br surfactants (a). Isothermal essay realized with 18ATMP·Br at 280 ºC (b).

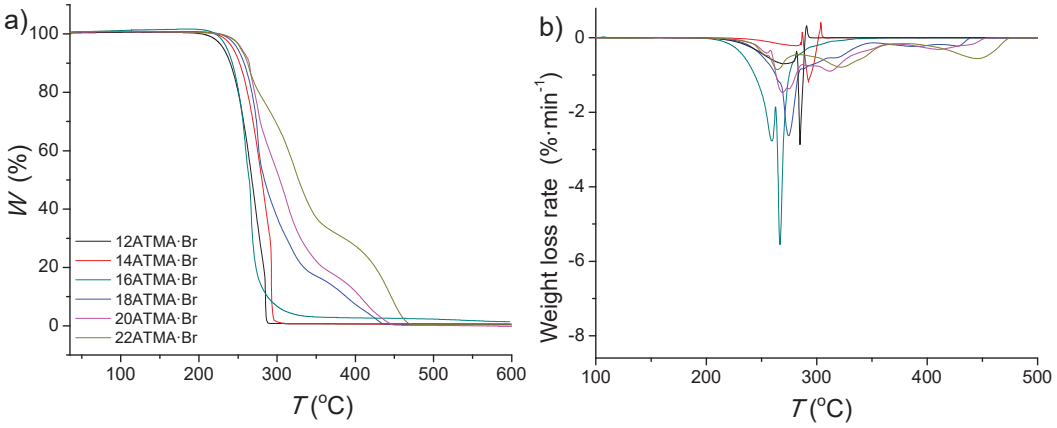

Figure SI-5. TGA traces of *n*ATMA·Br recorded under a nitrogen atmosphere (a) and their corresponding derivative curves (b).

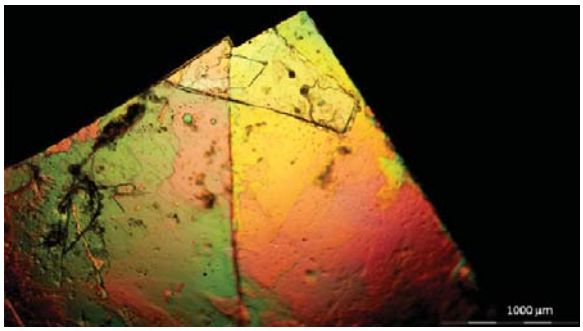

Figure SI-6. Optical micrograph recorded from the single-crystal of 12ATMP·Br wich was obtained by vapor diffusion technique and used for XRD analysis.

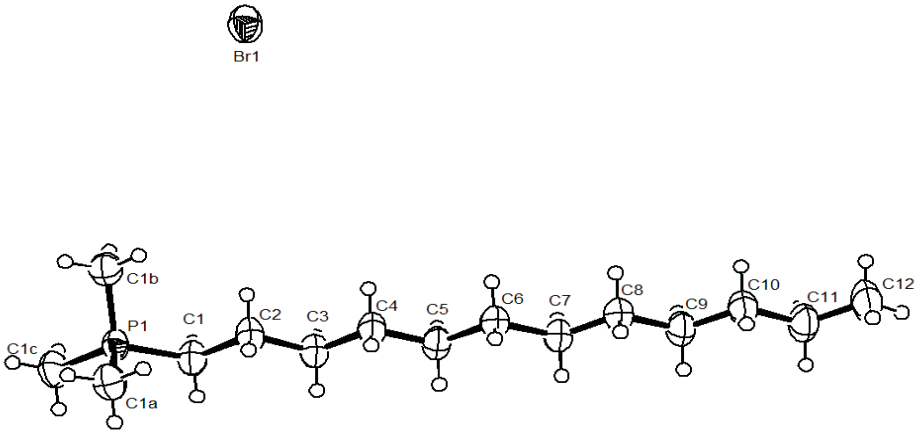

Figure SI-7. ORTEP representation of the 12ATMP·Br molecule in the conformation adopted in the crystal with atom labelling indication. The displacement ellipsoids are drawn at 50% probability levels and H atoms are drawn as small empty circles of arbitrary radius.

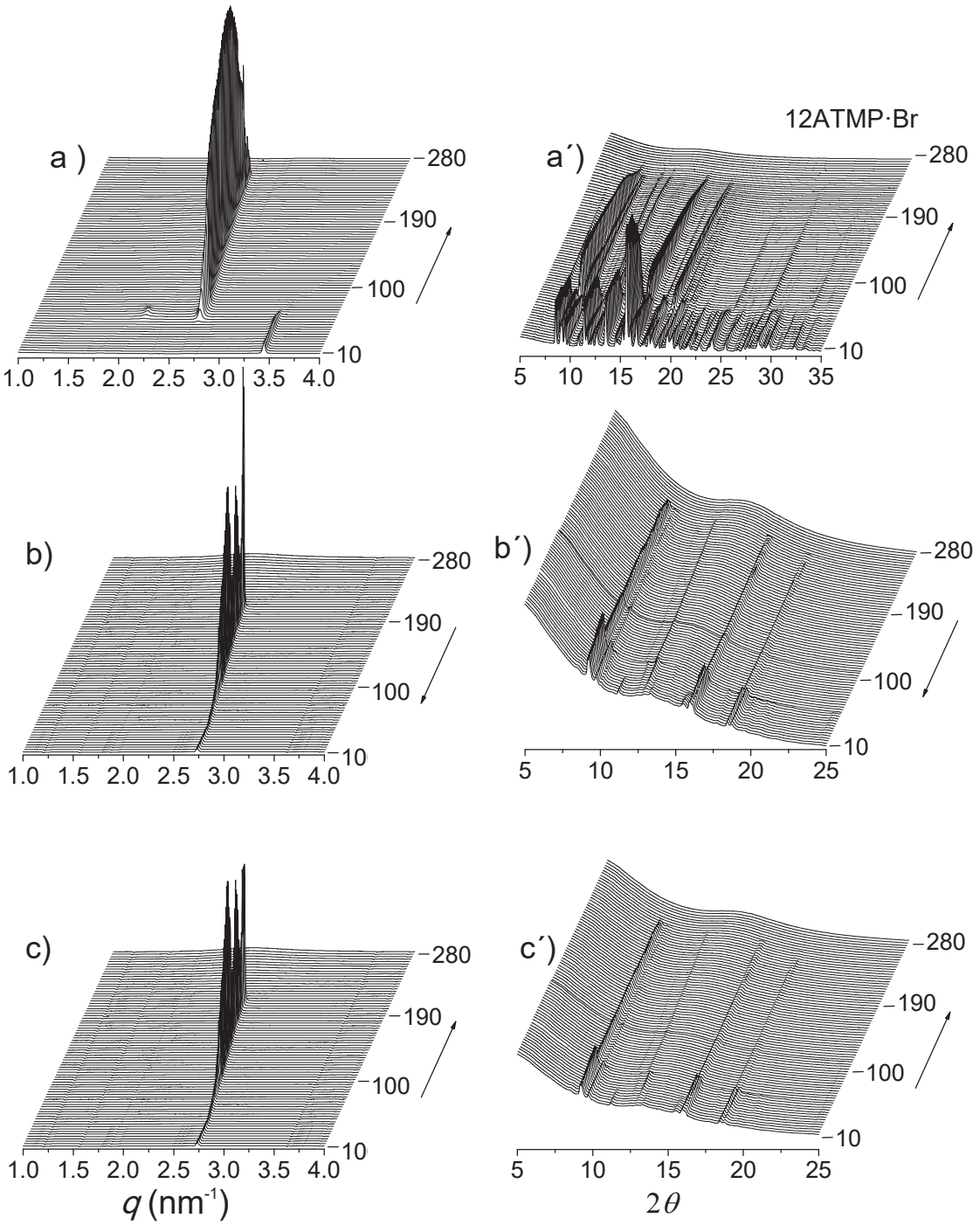

Figure SI-8. SAXS (left) and WAXS (right) plots from 12ATMP·Br registered over the 10-280 ºC interval. a) heating, b) cooling and c) reheating.

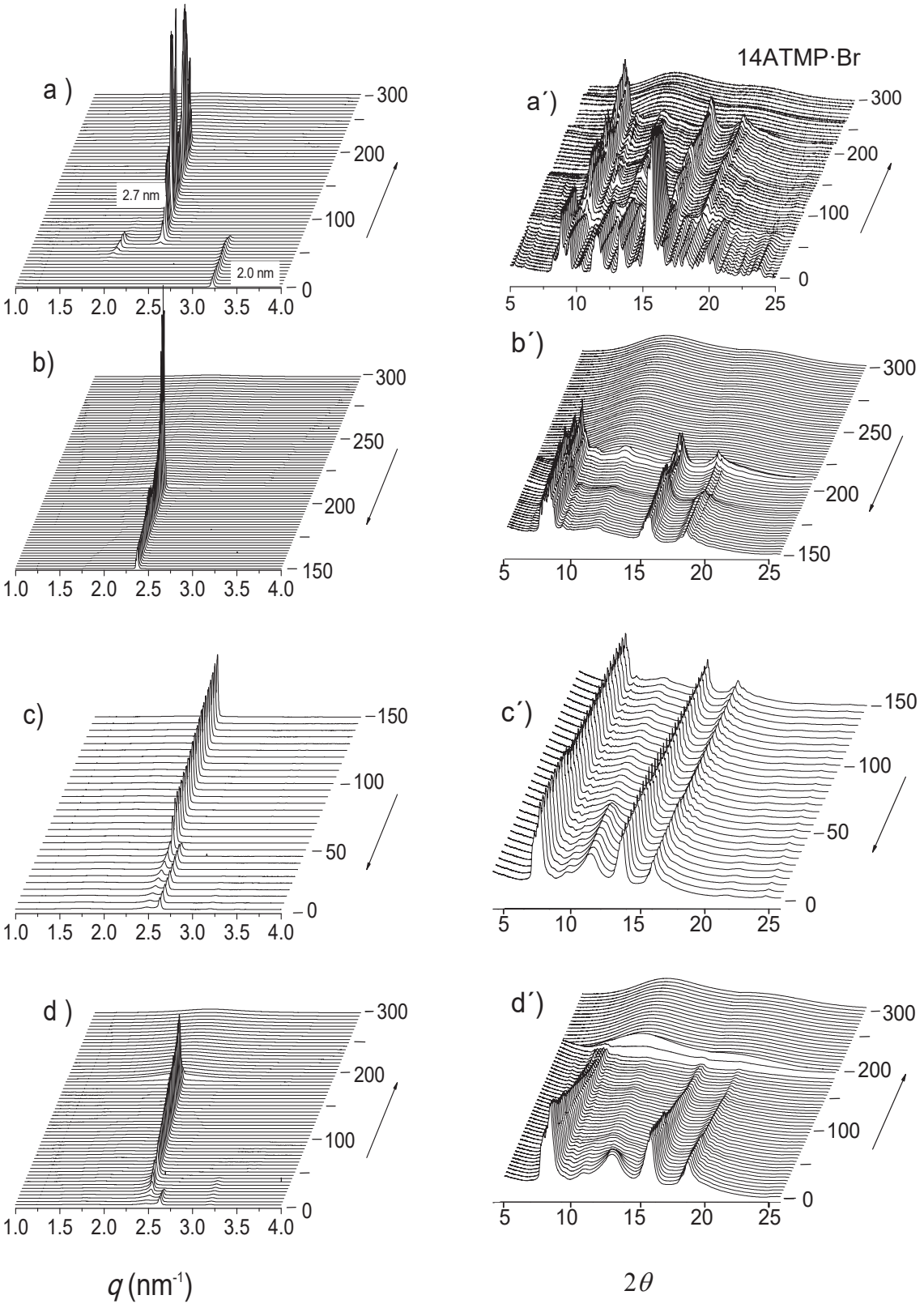

Figure SI-9. SAXS (left) and WAXS (right) plots from 14ATMP·Br registered over the 0-300 ºC interval. a) heating, b) slow cooling, c) fast cooling and d) reheating.

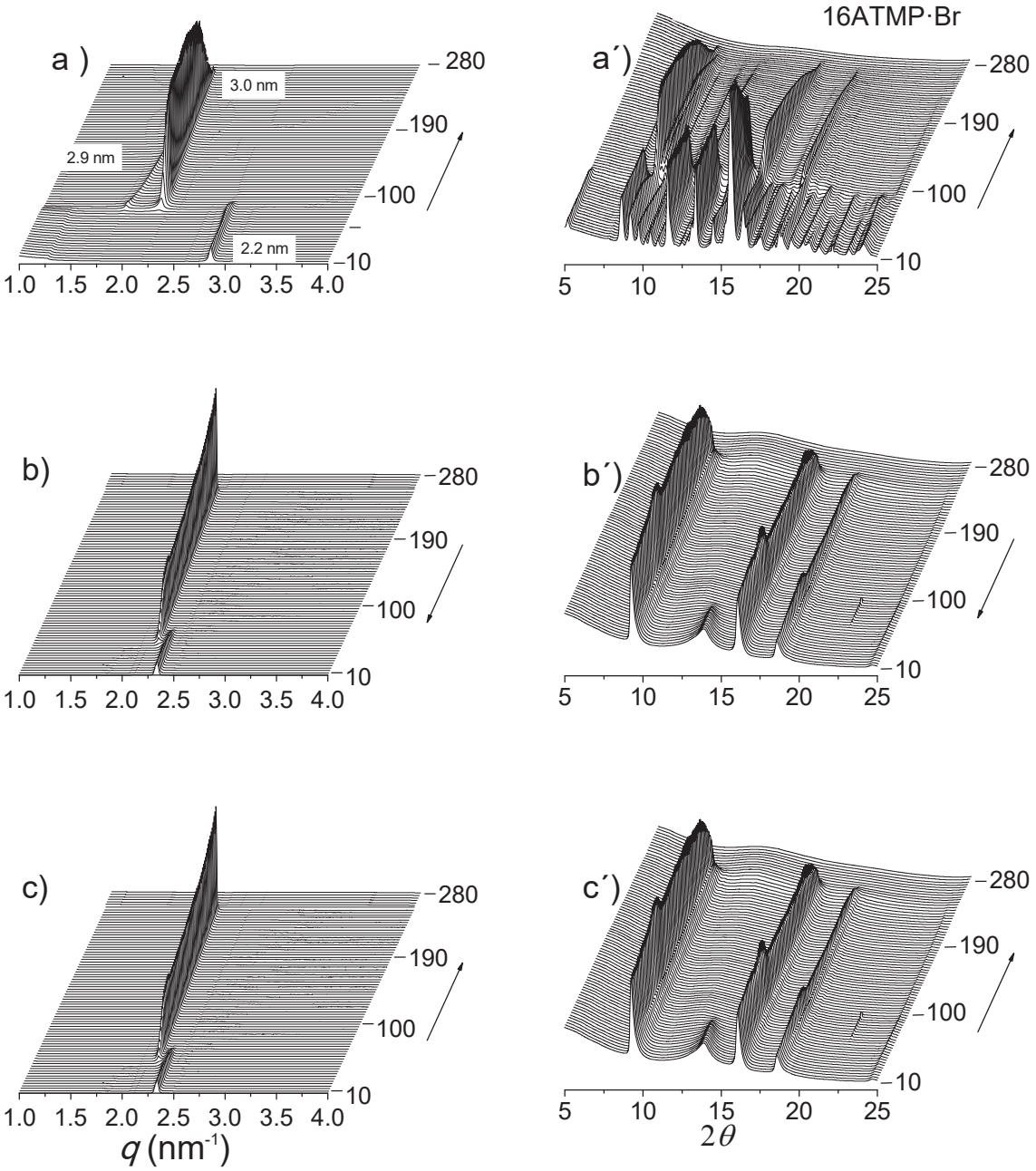

Figure SI-10. SAXS (left) and WAXS (right) plots from 16ATMP·Br registered over the 10-280 ºC interval. a) heating, b) cooling and c) reheating.

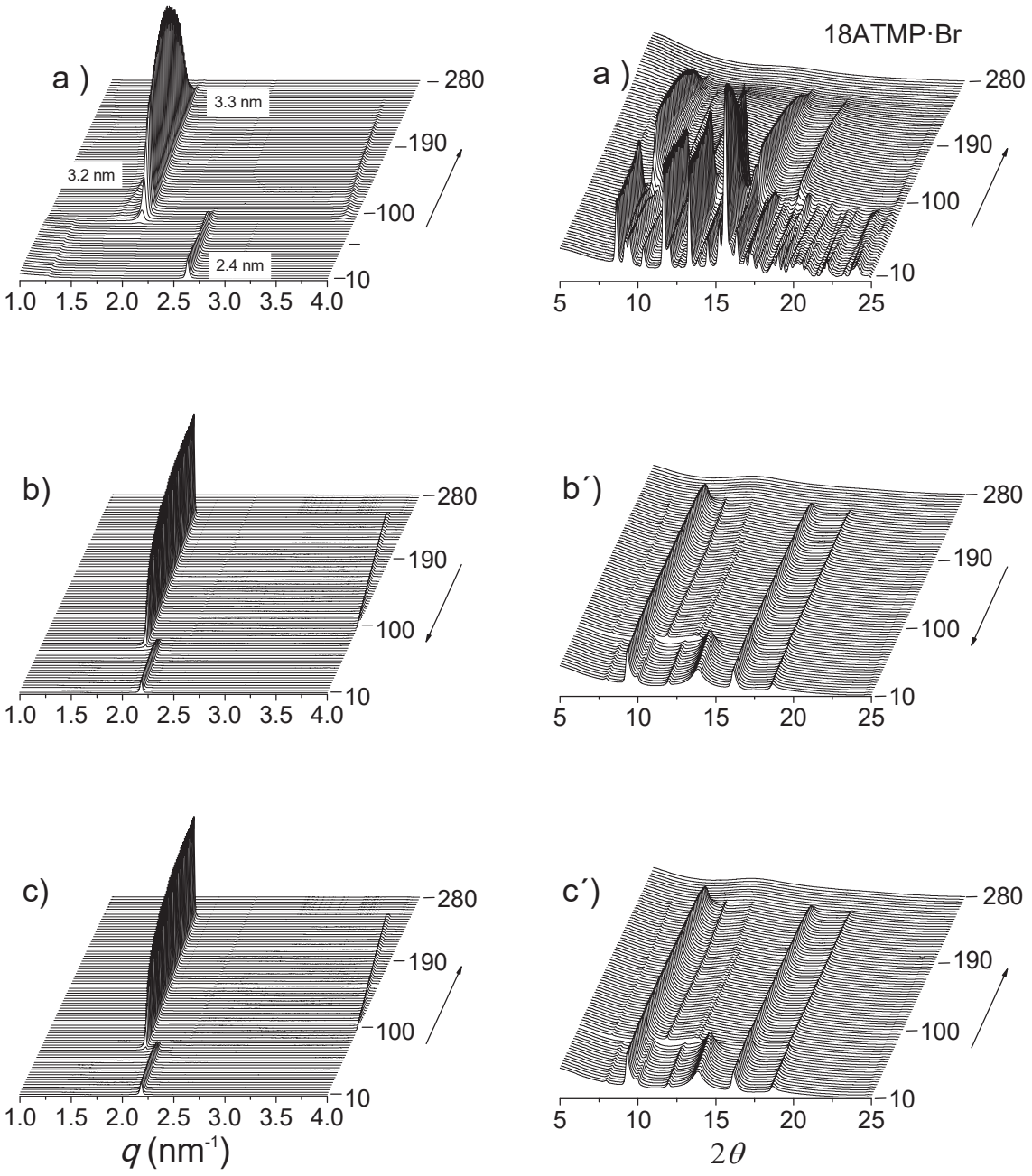

Figure SI-11. SAXS (left) and WAXS (right) plots from 18ATMP·Br registered over the 10-280 ºC interval. a) heating, b) cooling and c) reheating.

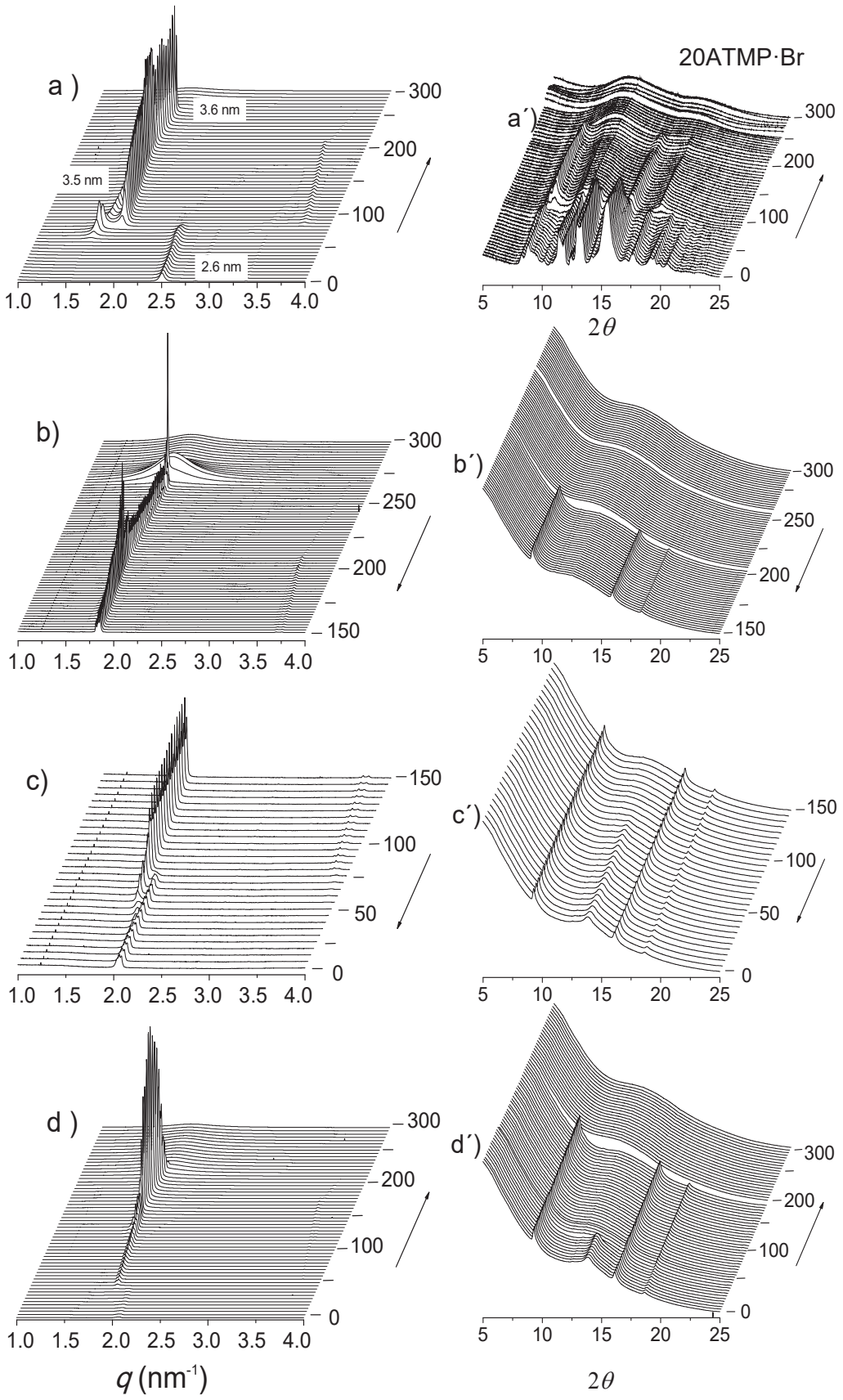

Figure SI-12. SAXS (left) and WAXS (right) plots from 20ATMP·Br registered over the 0-300 ºC interval. a) heating, b) slow cooling, c) fast cooling and d) reheating.

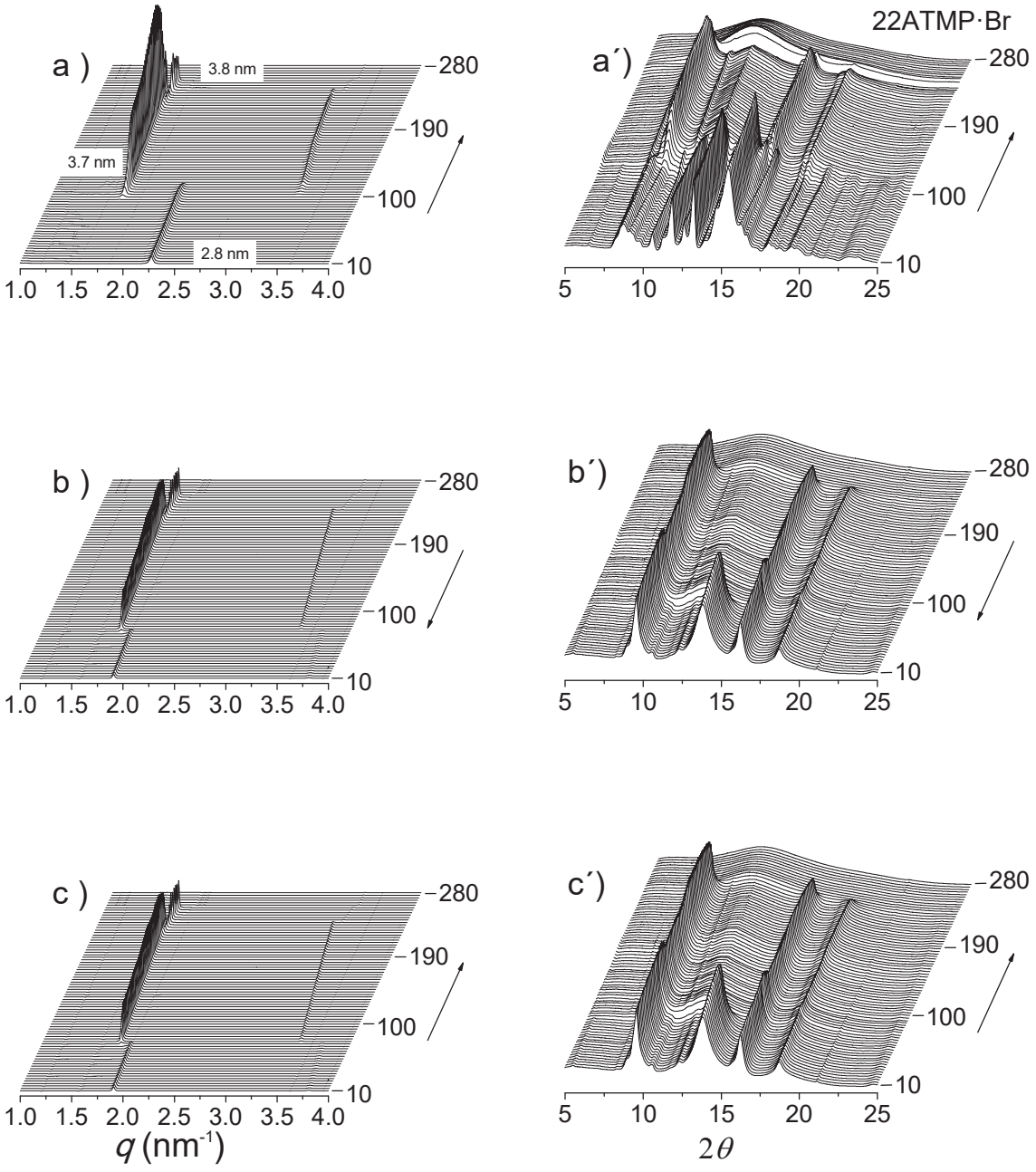

Figure SI-13. SAXS (left) and WAXS (right) plots from 22ATMP·Br registered over the 10-280 ºC interval. a) heating, b) cooling and c) reheating.

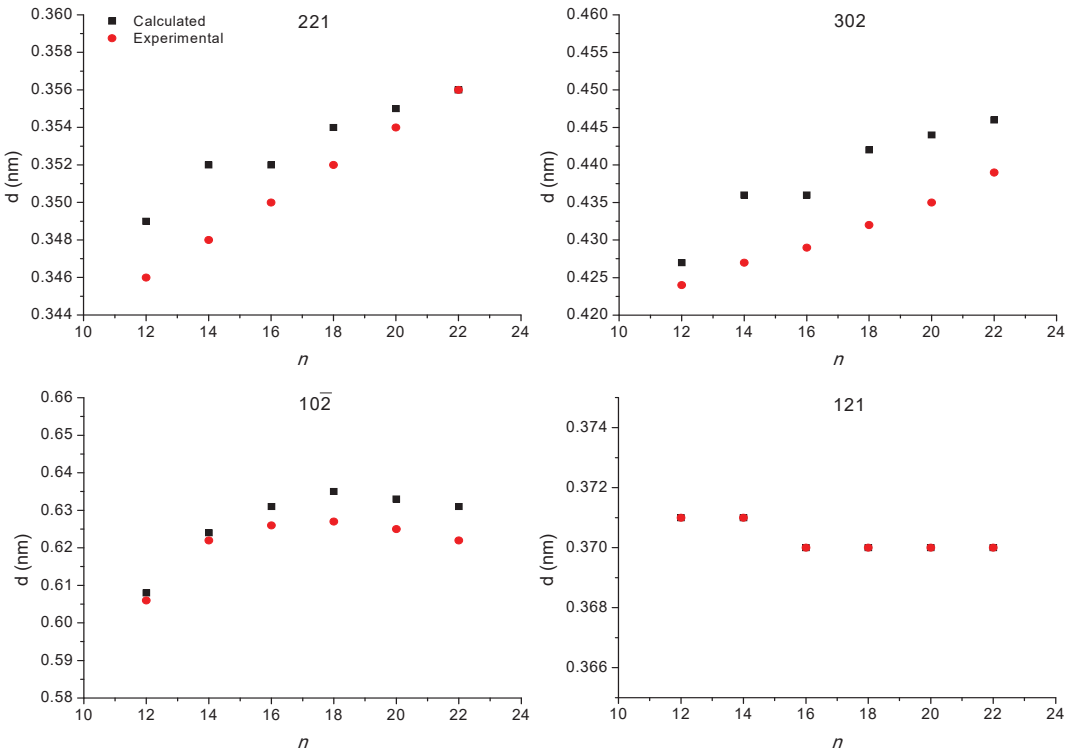

Figure SI-14. Graphical comparison of the observed (at 25 ºC) and calculated main *d*-spacings (nm) with *h*≠0 for *n*ATMP·Br.

12ATMP·Br

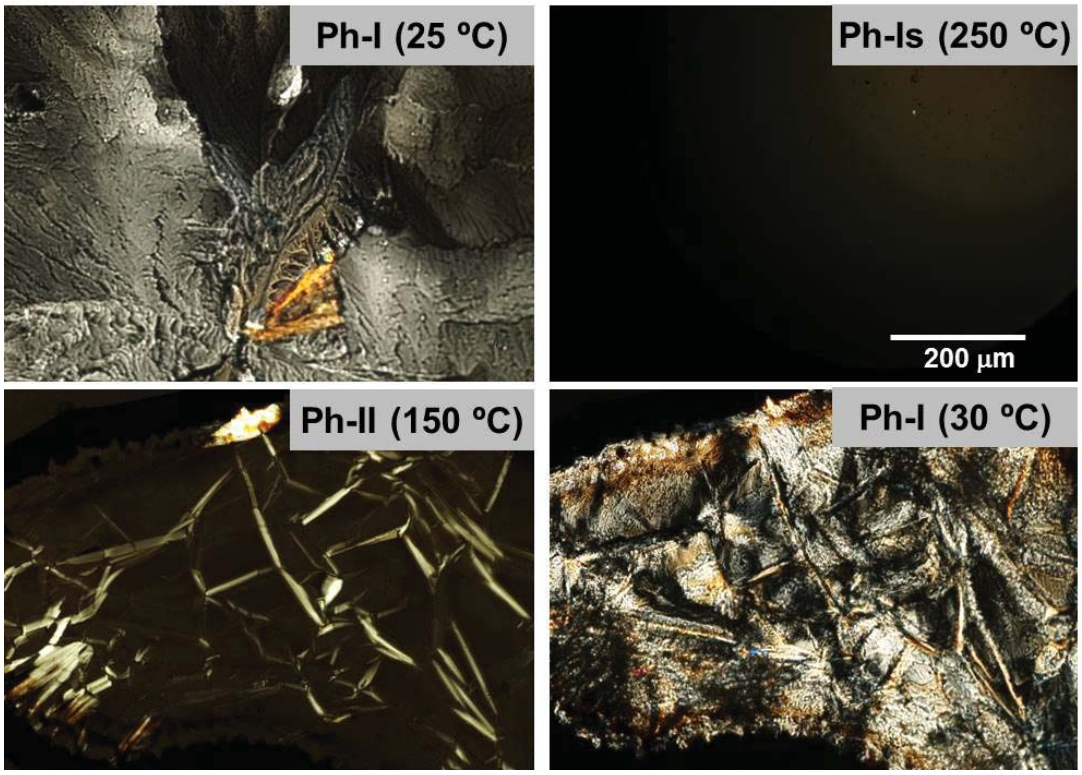

16ATMP·Br

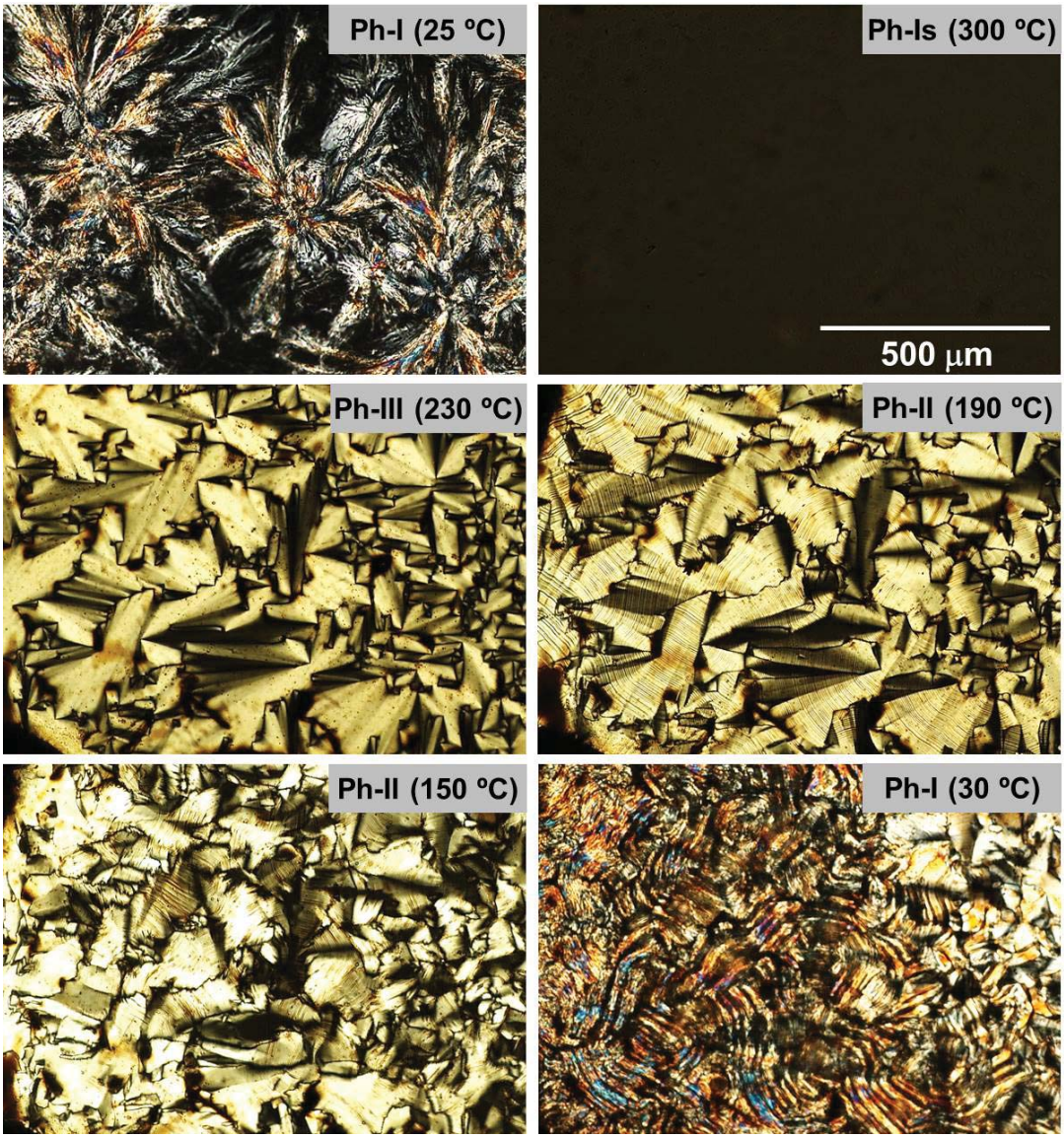
Ph-I (25 ºC)
Ph-Is (300 ºC)
500 μm
Ph-III (230 ºC)
Ph-II (190 ºC)
Ph-II (150 ºC)
Ph-I (30 ºC)

18ATMP·Br

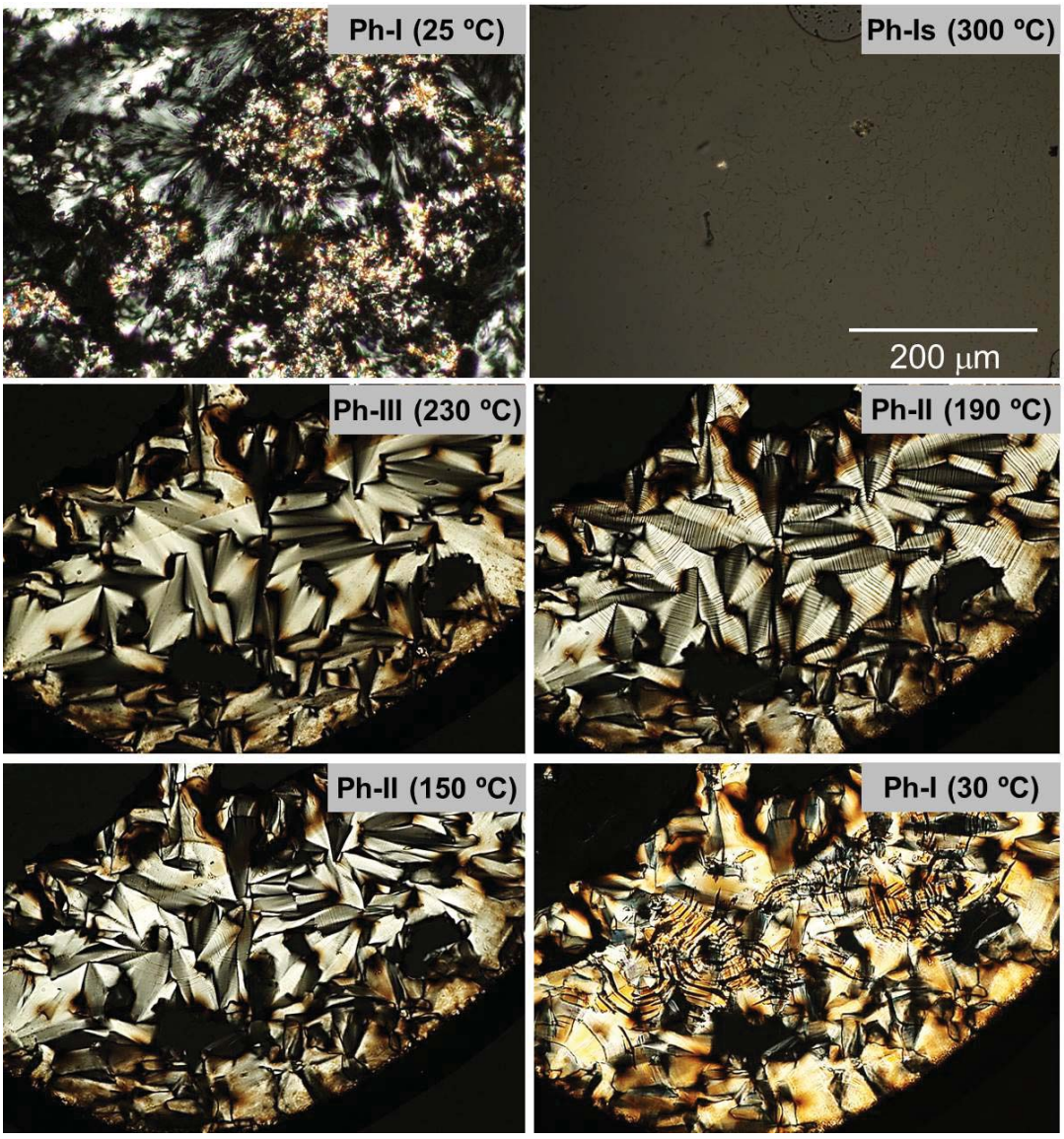
Ph-I (25 ºC)
Ph-Is (300 ºC)
200 μm
Ph-III (230 ºC)
Ph-II (190 ºC)
Ph-II (150 ºC)
Ph-I (30 ºC)

22ATMP·Br

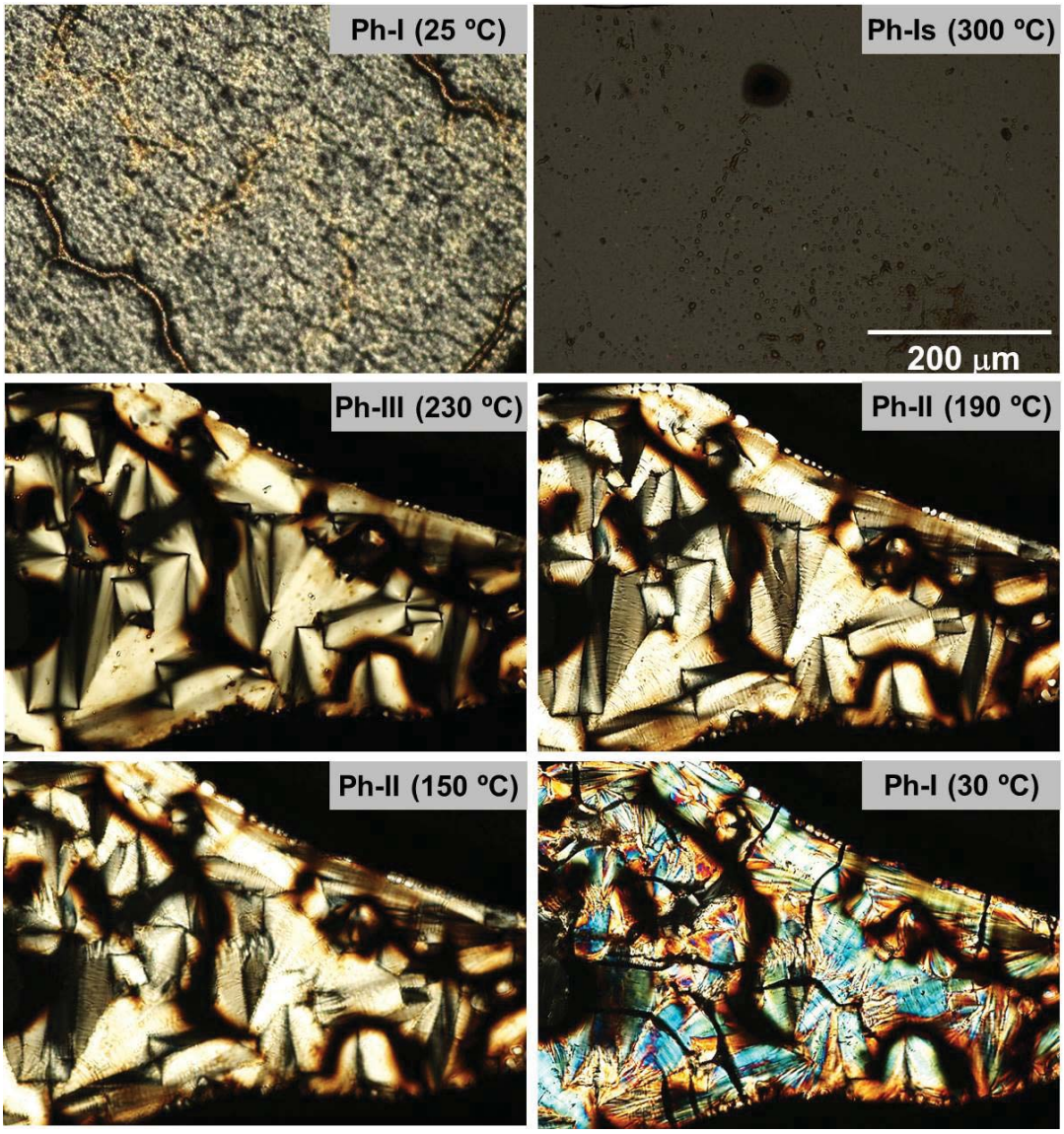

Figure SI-15. POM micrographs recorded from *n*ATMP·Br at the indicated temperatures.

Tables

Table SI-1. Crystal data and structure refinement for 12ATMP·Br.

Empirical formula	C_{15} H_{34} Br P
Formula weight	325.30
Temperature	293(2) K
Wavelength	0.071073 nm
Crystal system, space group	Monoclinic, P 2_1/c
Unit cell dimensions	*a* = 1.82906(10) nm alpha = 90º *b* = 0.79655(4) nm beta = 93.119(2)º *c* = 1.26721(7) nm gamma = 90º
Volume	1843.51(17) Å^3
Z, Calculated density	4, 1.172 Mg/m^3
Absorption coefficient	2.301 mm^{-1}
F(000)	696
Crystal size	0.449 x 0.139 x 0.098 mm
Theta range for data collection	2.230 to 25.393º
Limiting indices	-22<=*h*<=22, -9<=*k*<=9, -15<=*l*<=15
Reflections collected / unique	25175 / 3385 [*R*(int) = 0.0429]
Completeness to theta = 25.242	99.9 %
Absorption correction	Semi-empirical from equivalents
Max. and min. transmission	0.7452 and 0.6345
Refinement method	Full-matrix least-squares on F^2
Data / restraints / parameters	3385 / 0 / 184
Goodness-of-fit on F^2	1.053
Final *R* indices [I>2σ (I)]	*R*1 = 0.0296, w*R*2 = 0.0709
R indices (all data)	*R*1 = 0.0479, w*R*2 = 0.0803
Extinction coefficient	n/a
Largest diff. peak and hole	0.319 and -0.254 e.Å^{-3}

Table SI-2. Atomic coordinates (x 10^4) and equivalent isotropic displacement parameters (Å ^{2} x 10^3) for 12ATMP·Br. U (eq) is defined as one third of the trace of the orthogonalized Uij tensor.

Atom	x	y	z	U(eq)
Br(1)	1173(1)	830(1)	3176(1)	64(1)
P(1)	1077(1)	9047(1)	6693(1)	44(1)
C(1)	2050(1)	8920(3)	6601(2)	52(1)
C(2)	2285(1)	8824(3)	5469(2)	53(1)
C(3)	3108(1)	8874(3)	5373(2)	52(1)
C(4)	3318(1)	8836(3)	4230(2)	53(1)
C(5)	4135(1)	8870(3)	4091(2)	54(1)
C(6)	4340(1)	8855(3)	2953(2)	52(1)
C(7)	5158(1)	8870(3)	2808(2)	54(1)
C(8)	5366(1)	8861(3)	1673(2)	55(1)
C(9)	6188(1)	8880(3)	1543(2)	56(1)
C(10)	6405(1)	8870(3)	409(2)	58(1)
C(11)	7221(2)	8917(3)	285(2)	68(1)
C(12)	7431(2)	8903(4)	-852(3)	96(1)
C(1A)	735(1)	10919(3)	6096(2)	57(1)
C(1B)	654(1)	7295(3)	6042(2)	58(1)
C(1C)	874(2)	9030(3)	8050(2)	60(1)

Table SI-3. Torsion angles (º) for 12ATMP·Br.

C(1A)-P(1)-C(1)-C(2)	-63.2(2)
C(1B)-P(1)-C(1)-C(2)	57.0(2)
C(1C)-P(1)-C(1)-C(2)	176.70(19)
P(1)-C(1)-C(2)-C(3)	174.79(18)
C(1)-C(2)-C(3)-C(4)	-178.0(2)
C(2)-C(3)-C(4)-C(5)	-179.5(2)
C(3)-C(4)-C(5)-C(6)	-179.3(2)
C(4)-C(5)-C(6)-C(7)	-179.4(2)
C(5)-C(6)-C(7)-C(8)	-179.8(2)
C(6)-C(7)-C(8)-C(9)	179.9(2)
C(7)-C(8)-C(9)-C(10)	179.9(2)
C(8)-C(9)-C(10)-C(11)	179.1(2)
C(9)-C(10)-C(11)-C(12)	179.9(2)

Table SI-4. Crystallographic *a* and β values of the *n*ATMP·Br salts used for the simulations of the crystal lattices to obtain their respective SAXS and WAXS profiles.

*n*ATMP·Br	[b]*a* (nm)	β (º)
[a]12	1.83	93.1
14	2.05	97.0
16	2.25	101.0
18	2.47	103.5
20	2.70	106.0
22	2.92	108.0

[a]*a* and β values of 12ATMP·Br are based on the experimental results of 12ATMP·Br.

[b]*b* and *c* parameters and α and γ angles of all the cells are fixed (*b* =0.7965 and *c* = 1.2672 nm, $\alpha = \gamma = 90º$), according to the experimental result of 12ATMP·Br.

Annex B:

B1. Supporting information to Chapter V.1

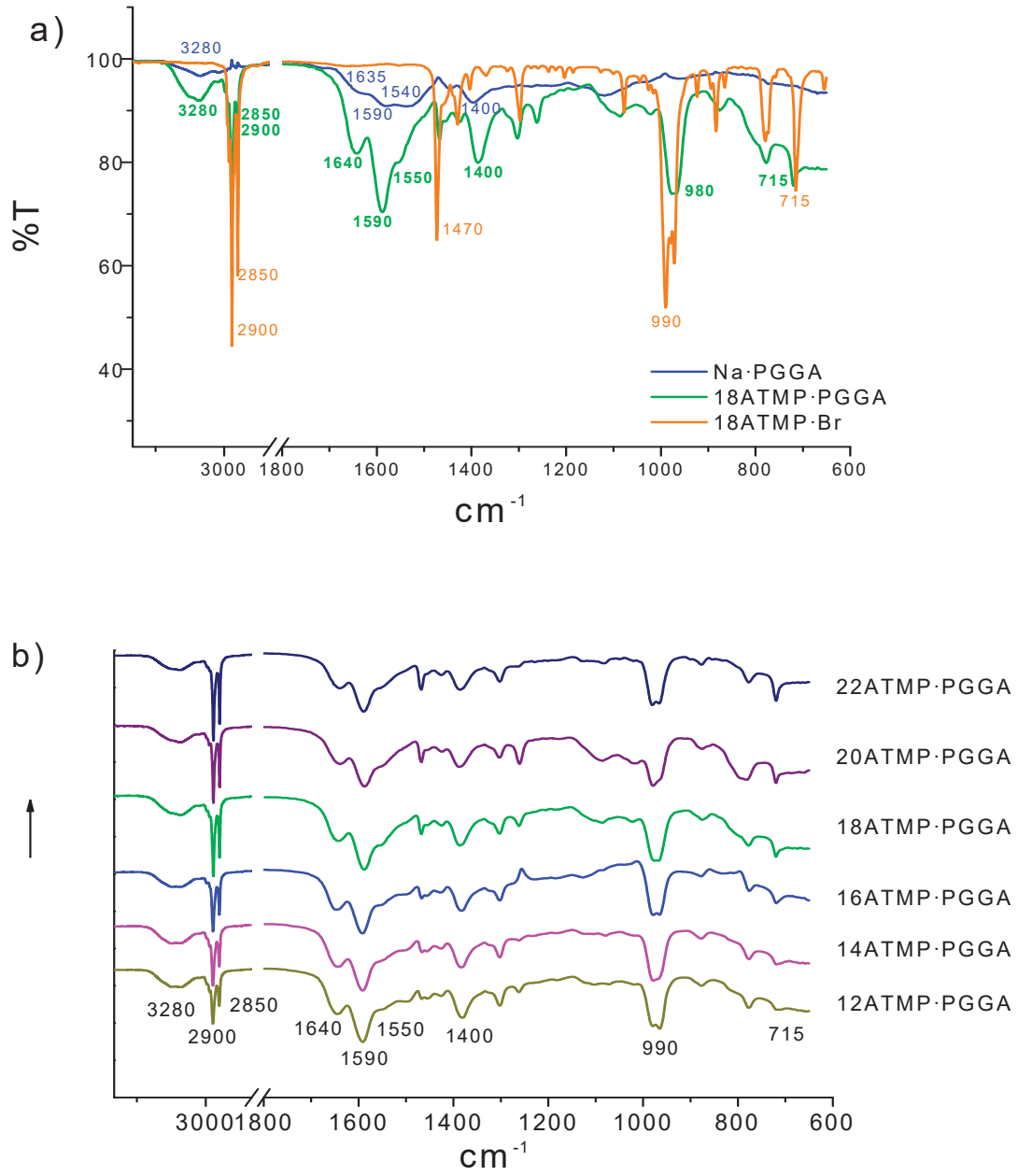

Figure SI-1. FTIR of 18ATMP·Br, PGGA and the complex 18ATMP·PGGA recorded at 25 ºC (a) and comparison of FTIR spectra of the whole series of nATMP·PGGA complexes recorded at 25 ºC (b).

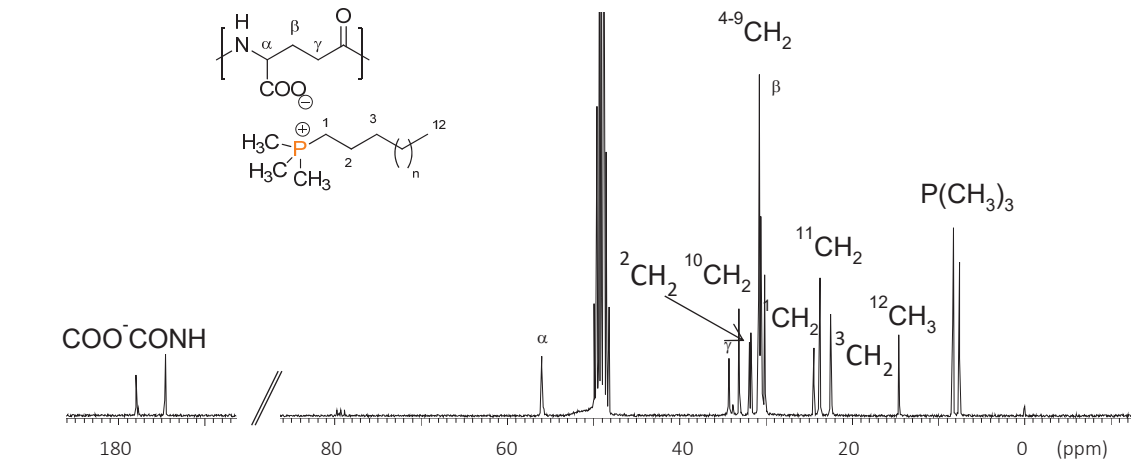
4-9CH2
β
P(CH3)3
11CH2
2CH2
10CH2
12CH3
CH2
3CH2
α
γ
COO-CONH
180
80
60
40
20
0
(ppm)

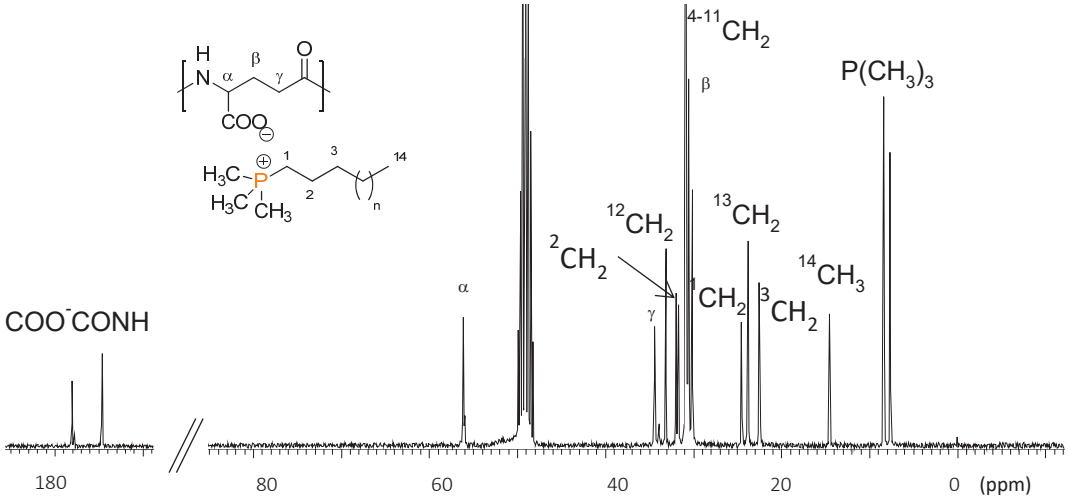
4-11CH2
β
P(CH3)3
12CH2
13CH2
2CH2
14CH3
CH2
3CH2
α
γ
COO-CONH
180
80
60
40
20
0
(ppm)

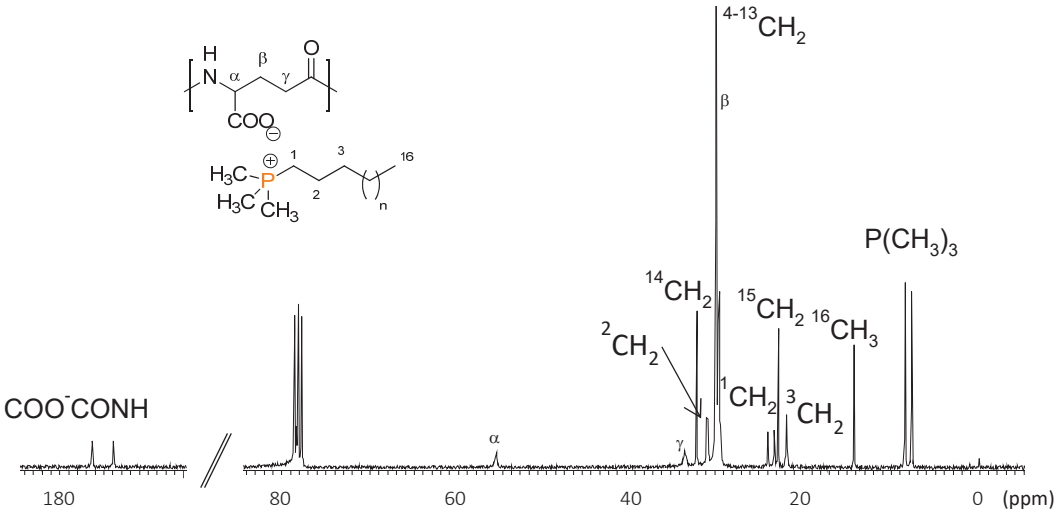
4-13CH2
β
P(CH3)3
14CH2
15CH2
16CH3
2CH2
1CH2
3CH2
α
γ
COO-CONH
180
80
60
40
20
0
(ppm)

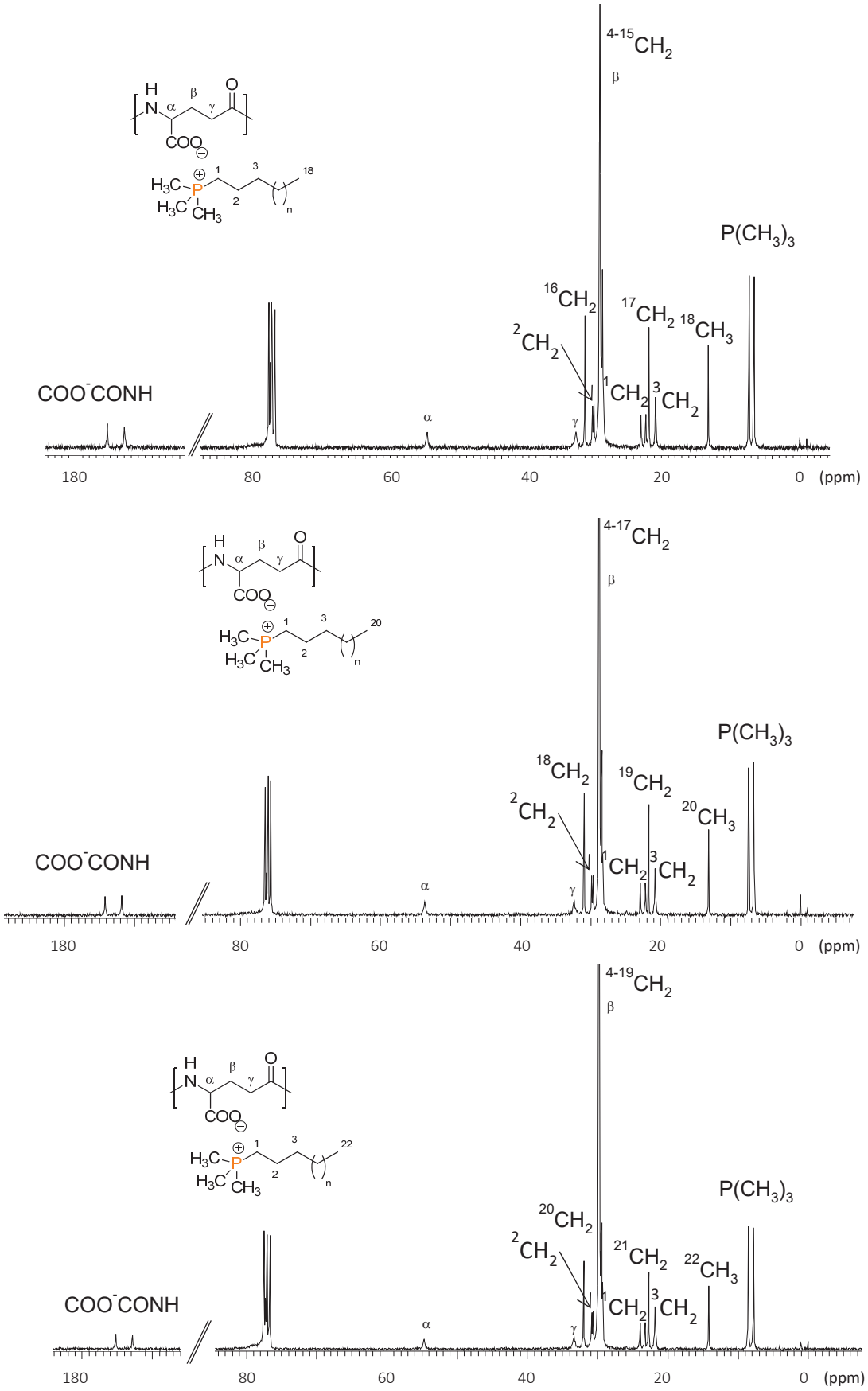

Figure SI-2. ^{13}C NMR spectra of *n*ATMP·PGGA recorded at 25 ºC in MeOH (for *n*=12 and 14) and $CDCl_3$ (for *n*≥16).

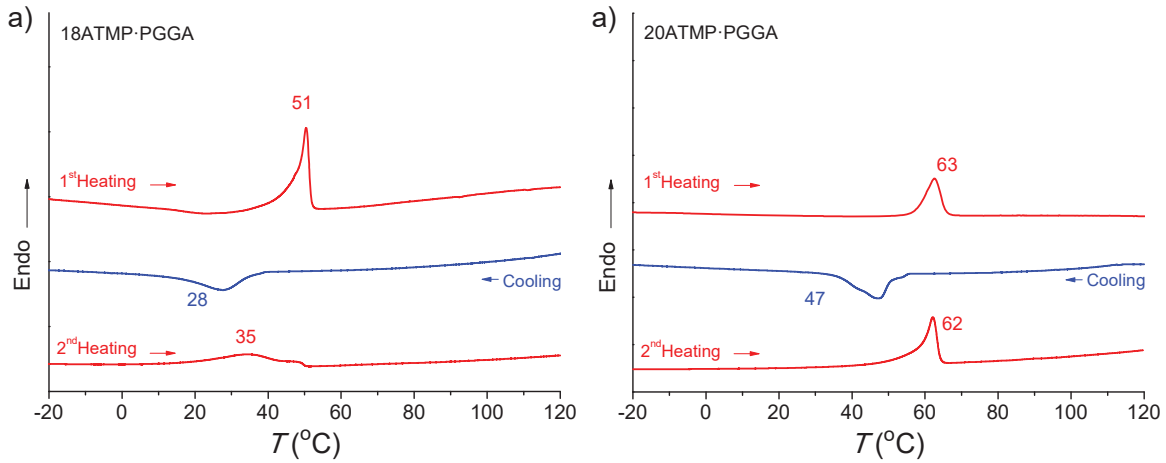

Figure SI-3. DSC traces of 18ATMP·PGGA (a) and 20ATMP·PGGA complexes recorded along the heating-cooling-heating cycles over the -30 ºC to 120 ºC range.

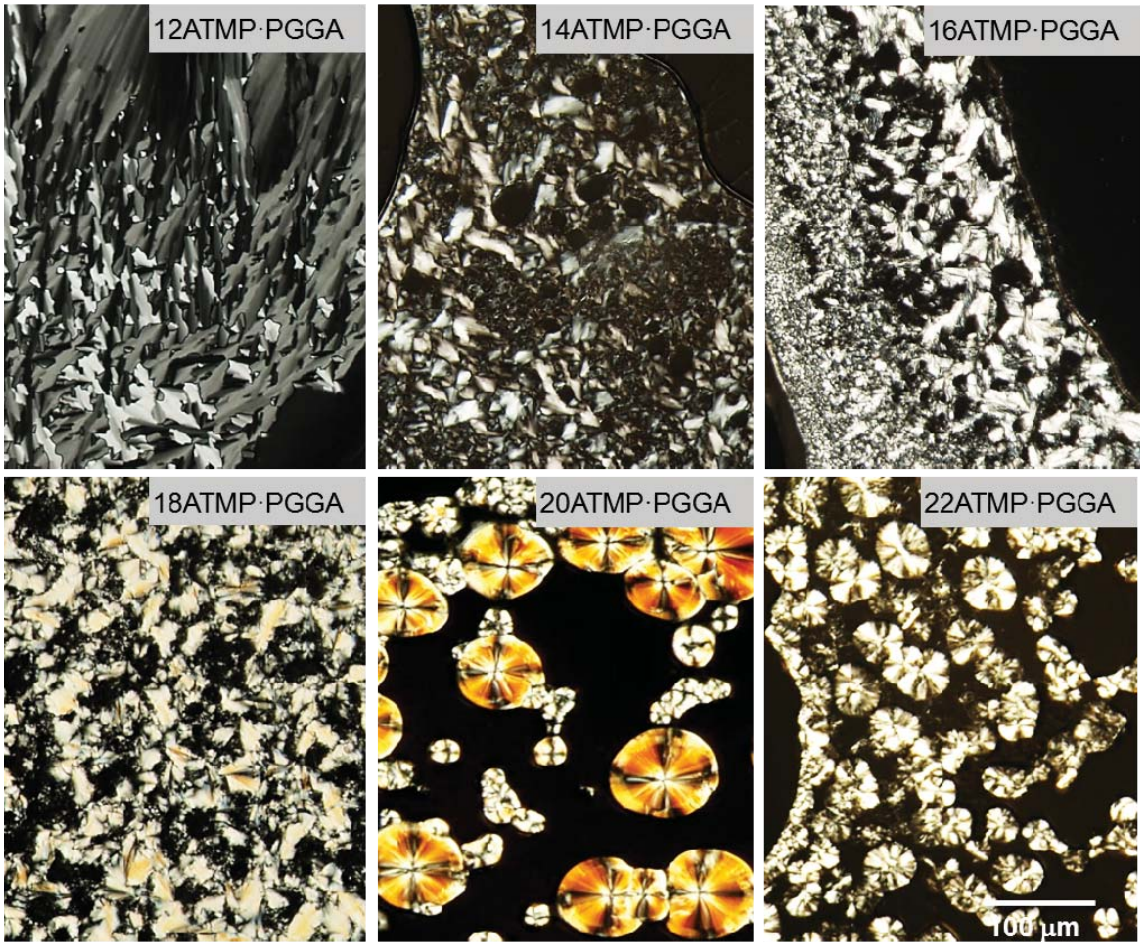

Figure SI-4. An assortment of POM images of *n*ATMP·PGGA complexes films recorded at room temperature illustrating the textures displayed.

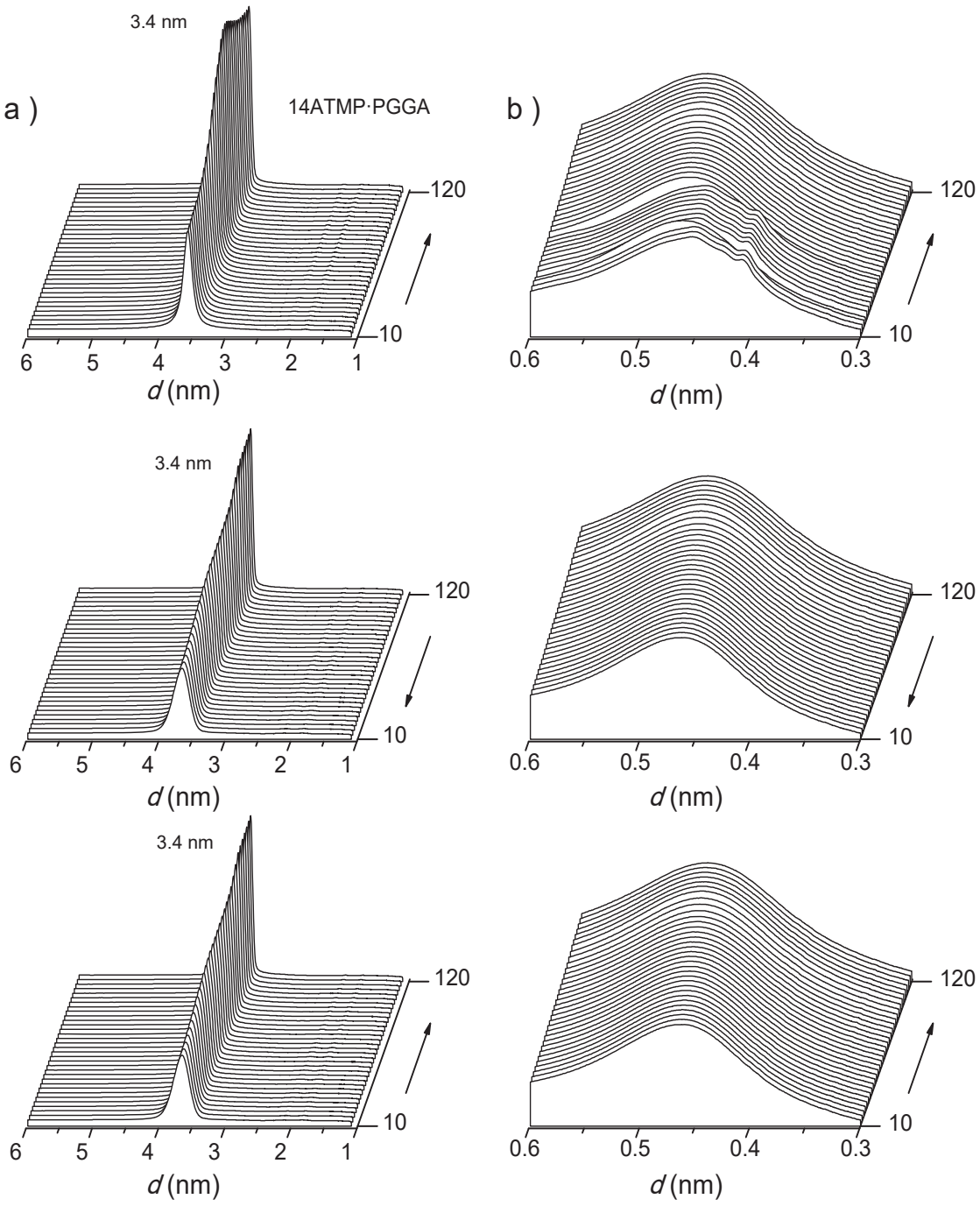

Figure SI-5. SAXS (a) and WAXS (b) profiles of 14ATMP·PGGA at heating (top), cooling (middle) and second heating (bottom).

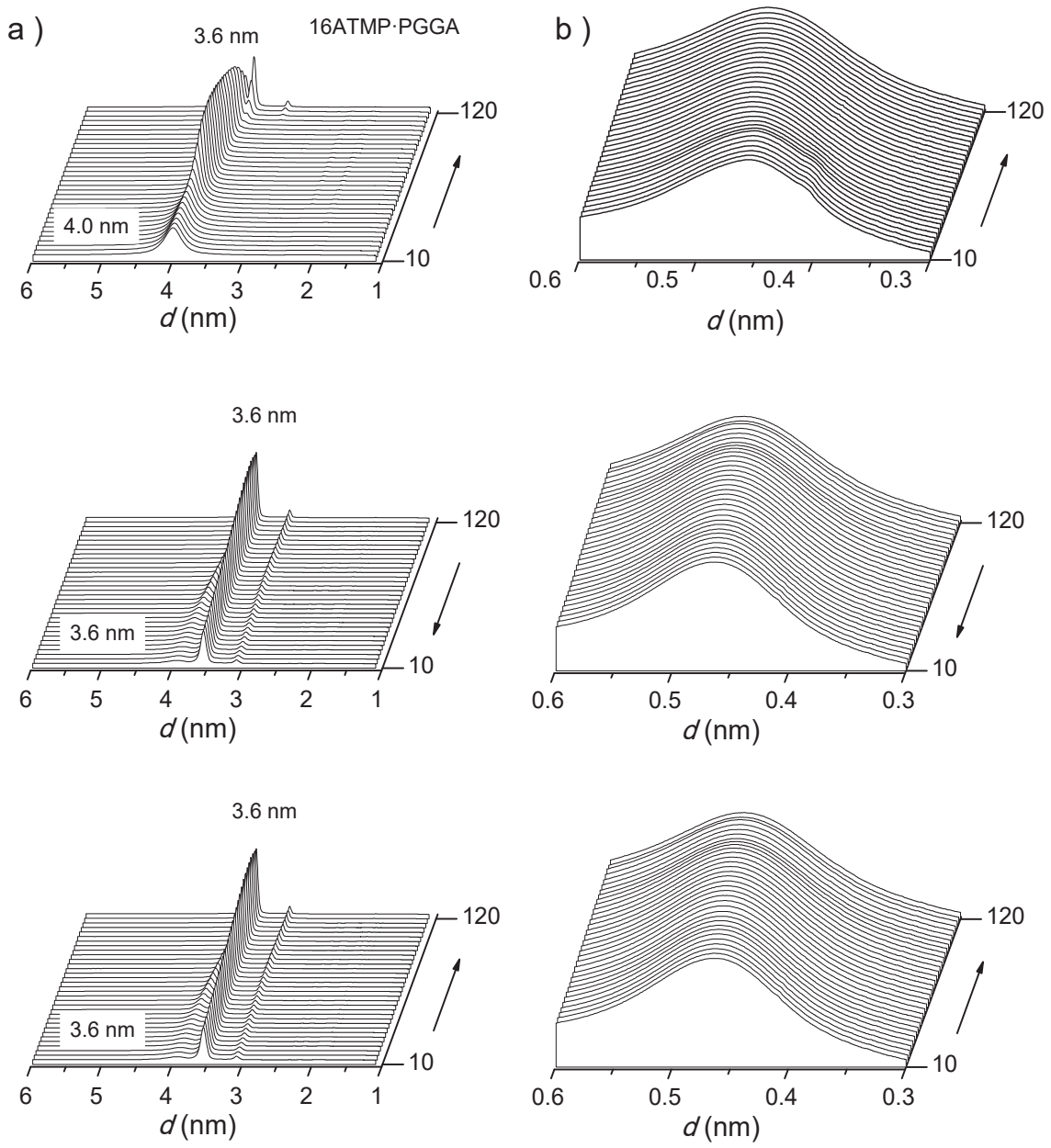

Figure. SI-6. SAXS (a) and WAXS (b) profiles of 16ATMP·PGGA at heating (top), cooling (middle) and second heating (bottom).

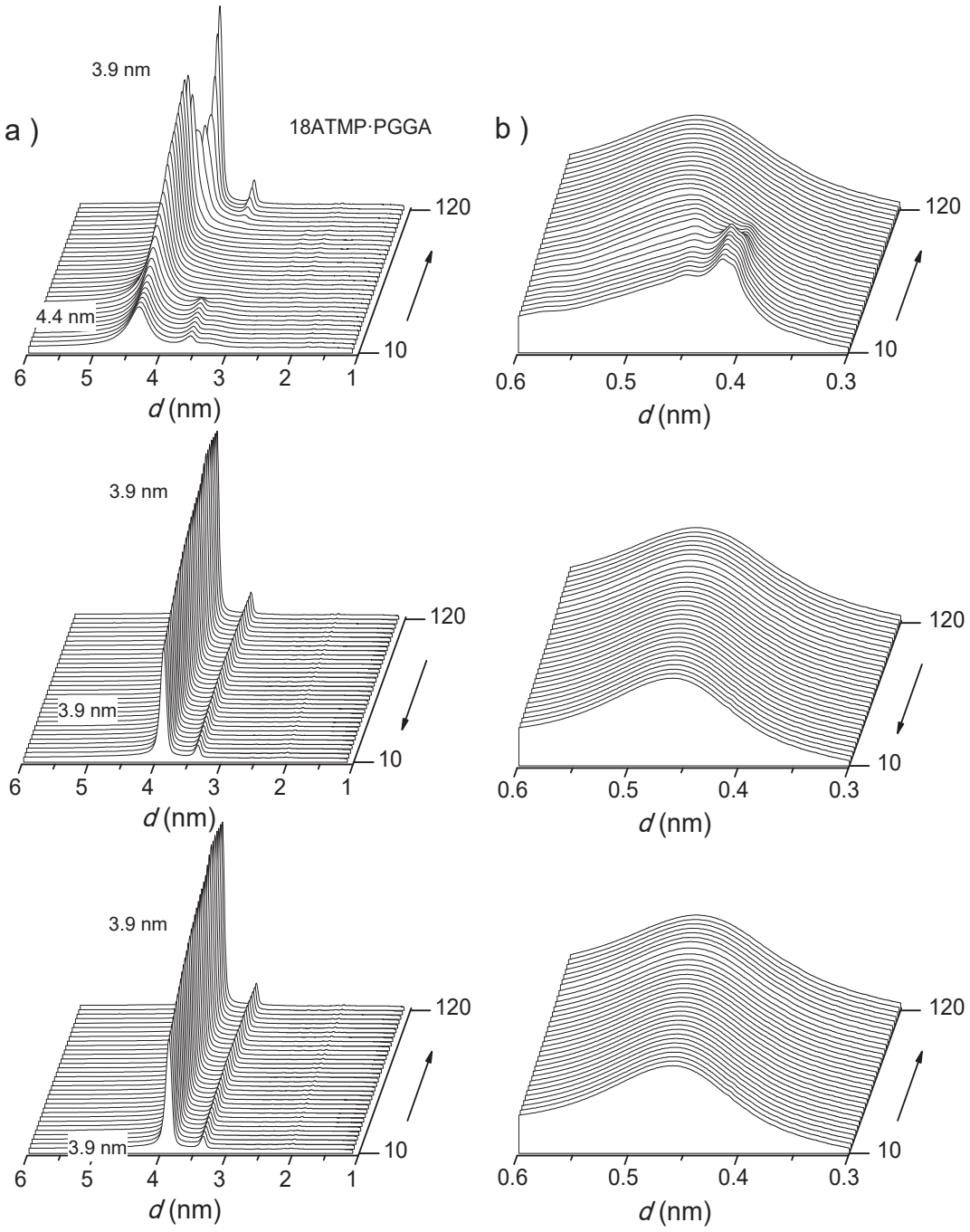

Figure SI-7. SAXS (a) and WAXS (b) profiles of 18ATMP·PGGA at heating (top), cooling (middle) and second heating (bottom).

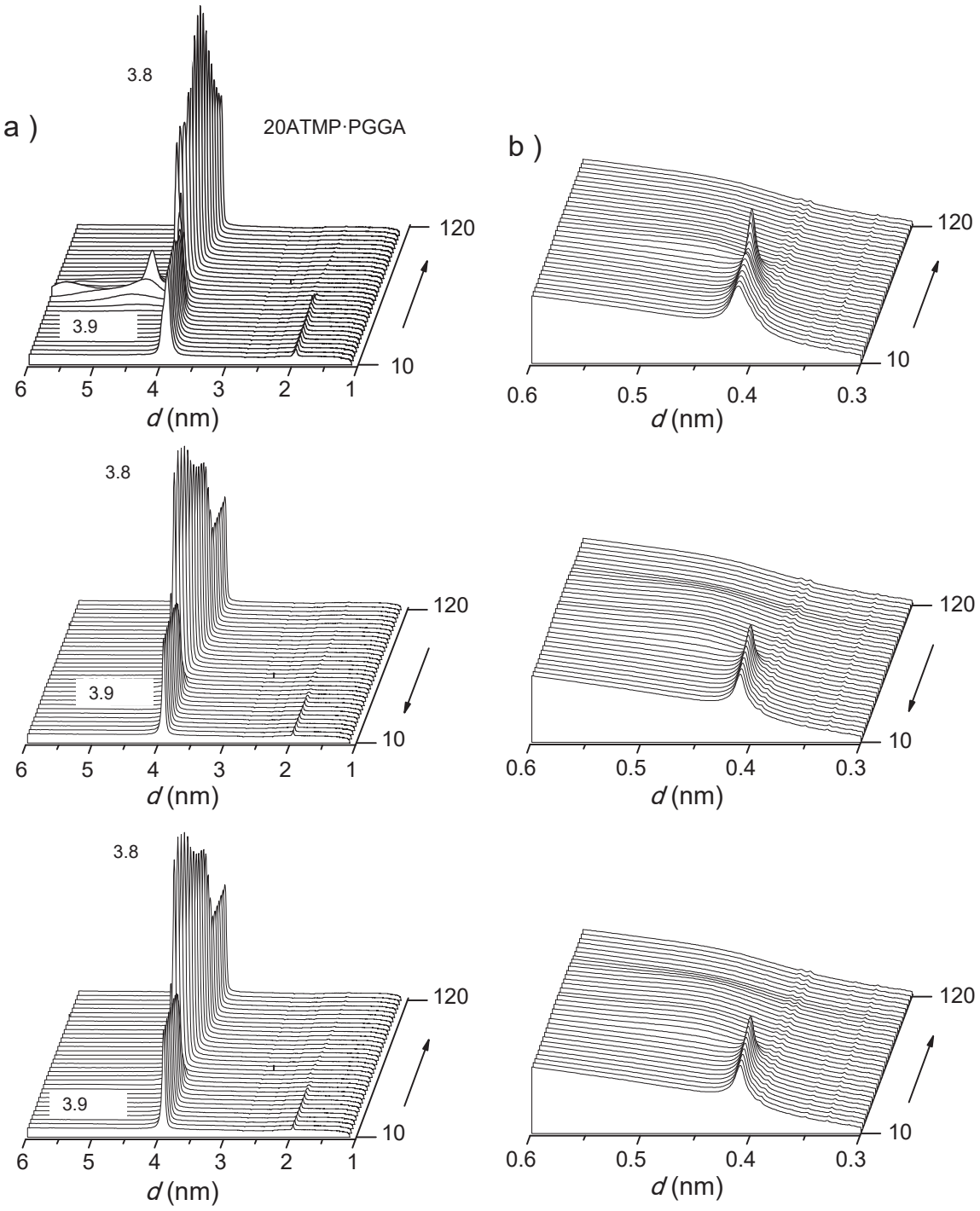

Figure SI-8. SAXS (a) and WAXS (b) profiles of 20ATMP·PGGA at heating (top), cooling (middle) and second heating (bottom).

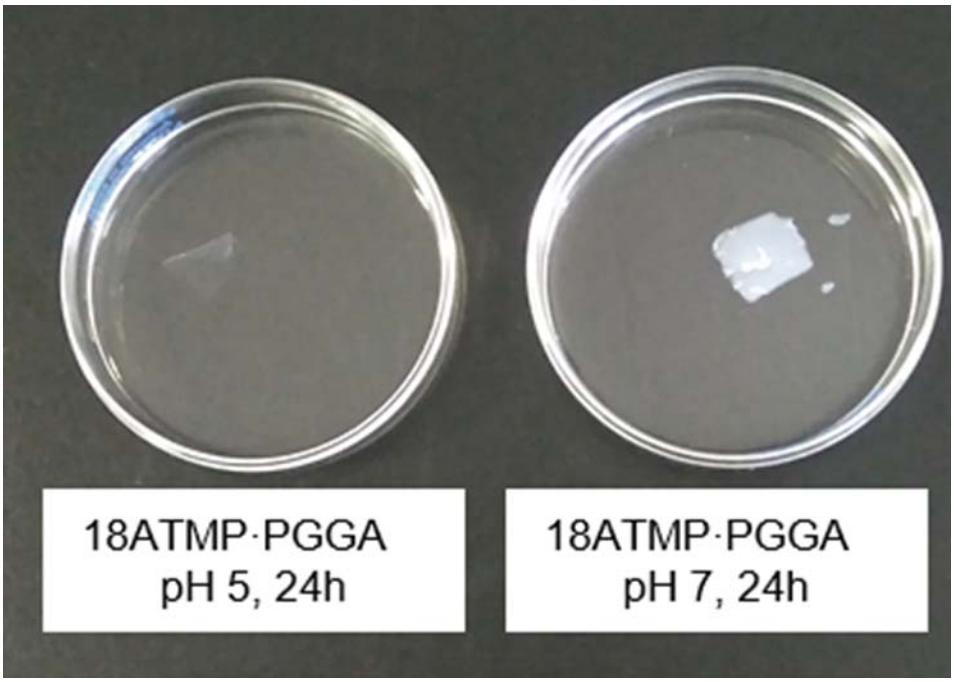

Figure SI-9. 18ATMP·PGGA films immersed in the buffer solution at the indicated pHs after 24 h of incubation.

B2. Supporting information to Chapter V.2

Table SI-1. Tensile properties of *n*ATMP·PGGA·*X*%^{P}MMT nanocomposites.

X% ^{P}MMT	*E* (MPa)	□□□□□$_{max}$ (MPa)	□□□□$_{b}$ (%)
***n*= 12**			
0	2.0	0.17	130
3	2.2	0.13	116
10	3.6	0.23	70
20	21.3	0.35	38
30	21.6	0.42	52
50	48.0	0.72	50
70	101.4	0.83	18
***n*= 20**			
0	16.4	0.83	1513
3	33.3	1.43	1100
10	64.1	2.69	695
20	131.9	3.61	100
30	236.5	5.19	3.8
50	734.5	10.69	1.98
70	1293.0	7.68	0.8

E: Young modulus, □$_{max}$: Maximum tensile stress, □$_{b}$: Strain at break.

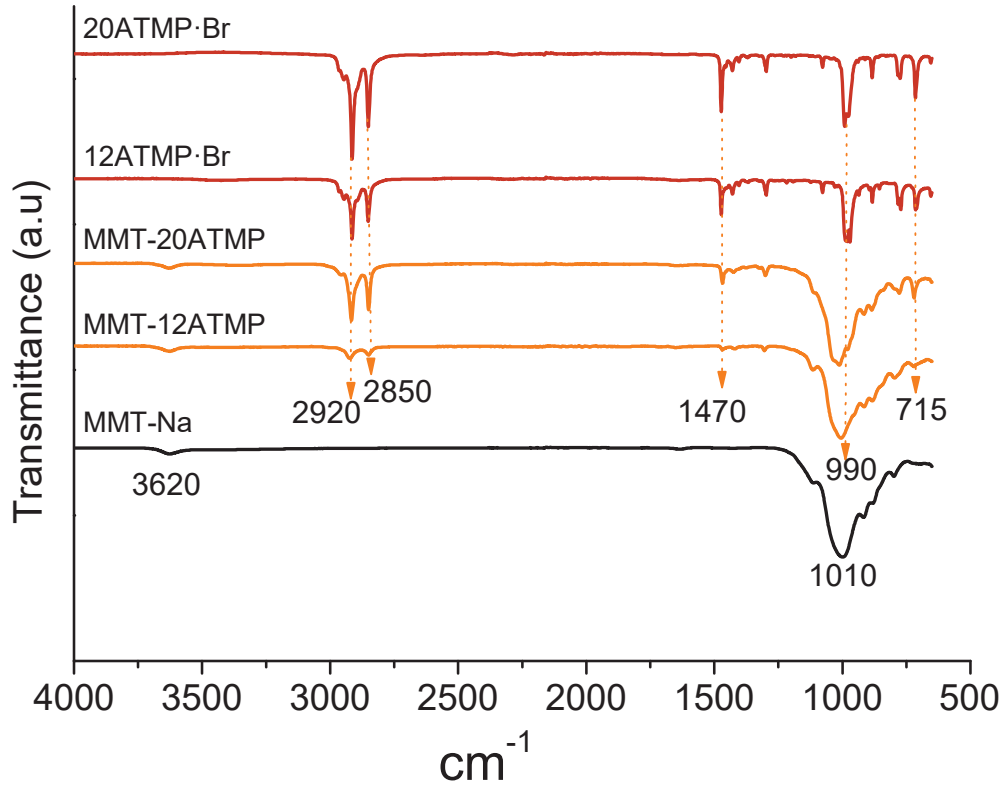

Figure SI-1. FTIR spectra of MMT modified with 12ATMP·Br and 20ATMP·Br surfactants. Spectra of the two surfactants and pristine Na·MMT have been included for comparison.

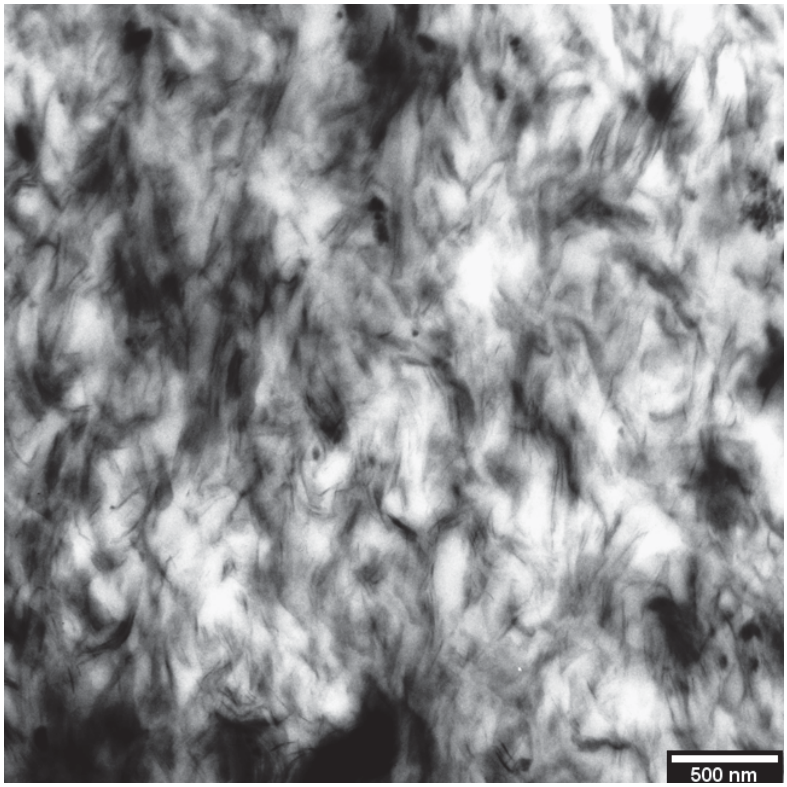

Figure SI-2. Low magnification TEM image recorded from an unstained section of 20ATMP·PGGA·10%^{P}MMT.

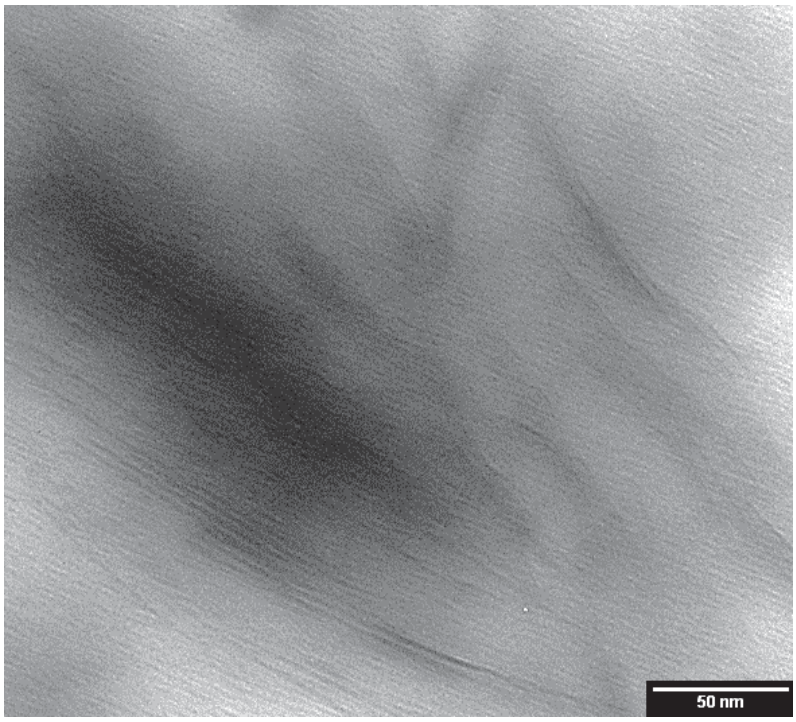

Figure SI-3. High magnification TEM image recorded from an unstained section of 20ATMP·PGGA·10%^{P}MMT

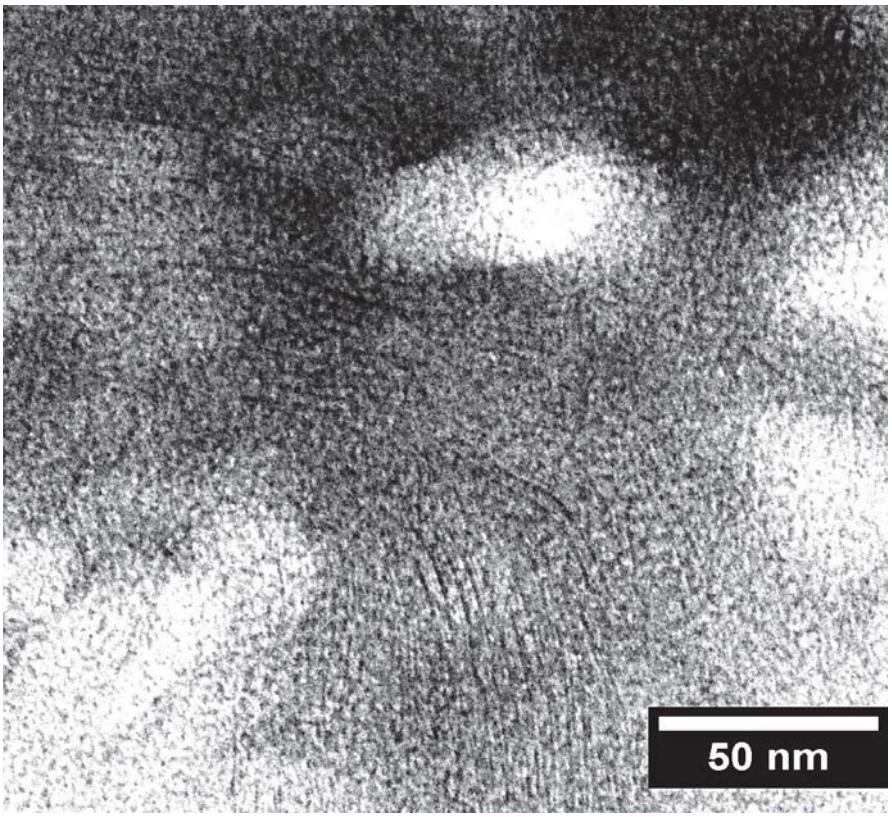

Figure SI-4. High magnification TEM image recorded from a section of 20ATMP·PGGA·50%PMMT stained with uranyl acetate.

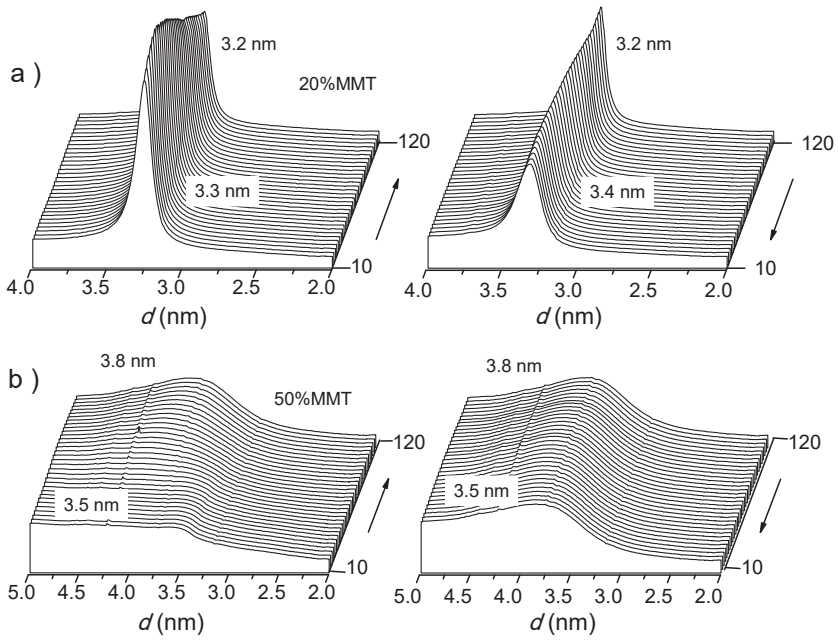

Figure. SI-5. Evolution of SAXS profiles of 12ATMP·PGGA·20%^{P}MMT (a) and 20ATMP·PGGA·50%^{P}MMT (b) at heating (left) and cooling (right).

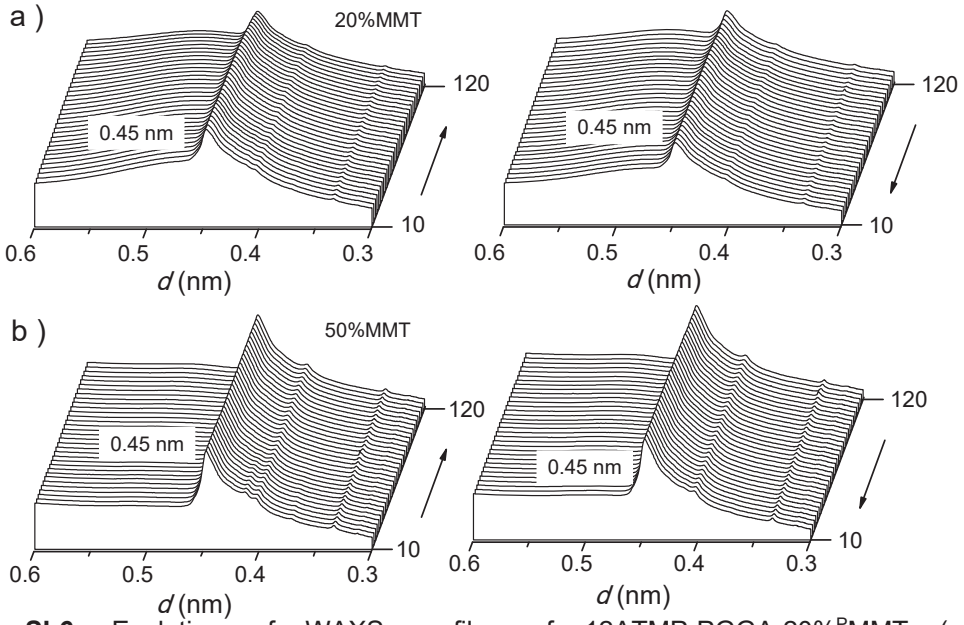

Figure SI-6. Evolution of WAXS profiles of 12ATMP·PGGA·20%^{P}MMT (a) and 20ATMP·PGGA·50%^{P}MMT (b) at heating (left) and cooling (right).

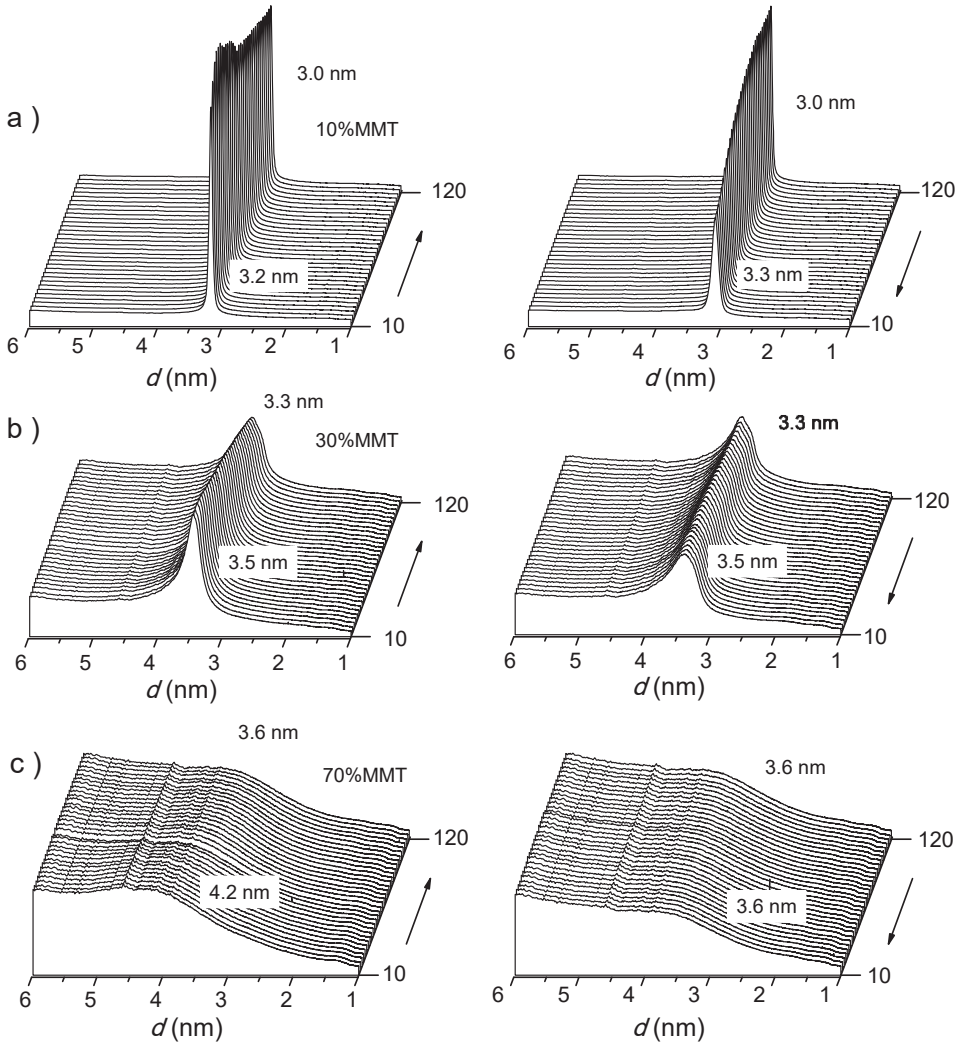

Figure SI-7. Evolution of SAXS profiles of 12ATMP·PGGA·10%^{P}MMT (a), 12ATMP·PGGA·30%^{P}MMT (b) and 12ATMP·PGGA·70%^{P}MMT (c) at heating and cooling.

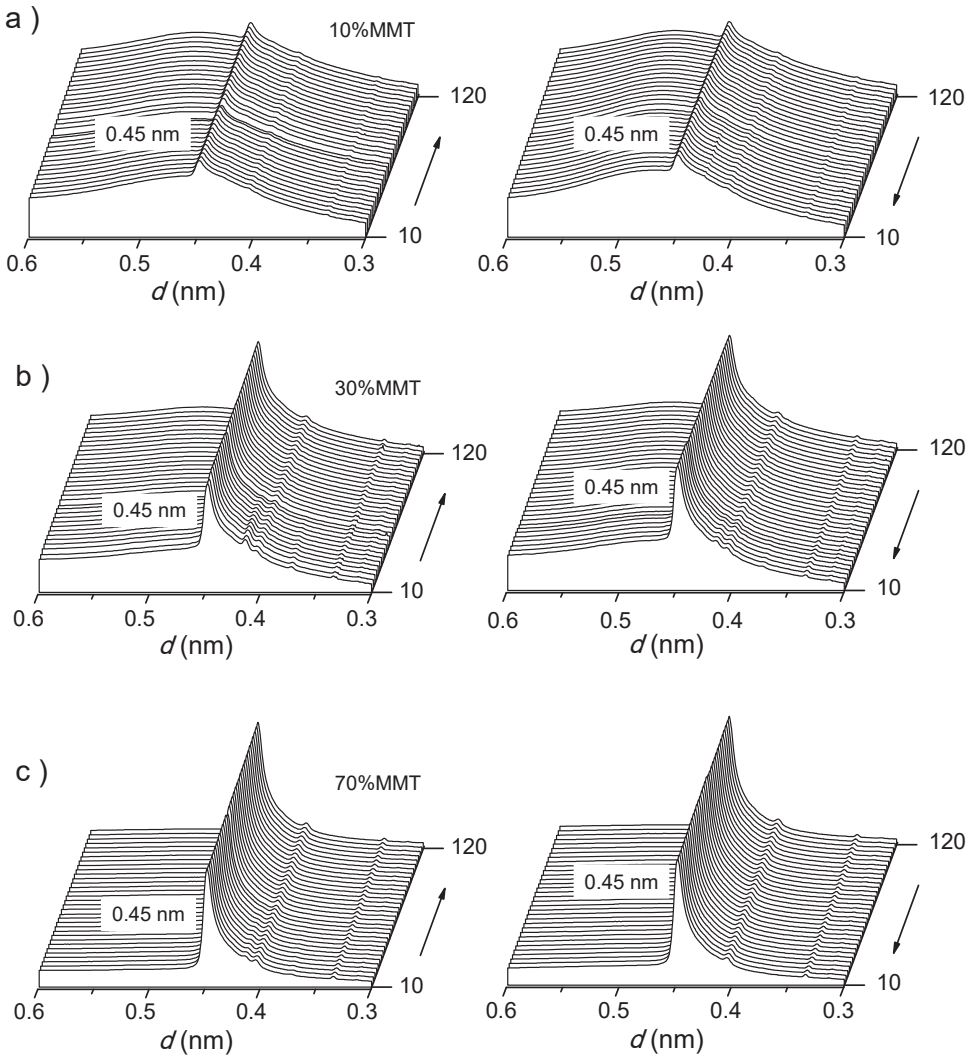

Figure SI-8. Evolution of WAXS profiles of 12ATMP·PGGA·10%^{P}MMT (a), 12ATMP·PGGA·30%^{P}MMT (b) and 12ATMP·PGGA·70%^{P}MMT (c) at heating (left) and cooling (right).

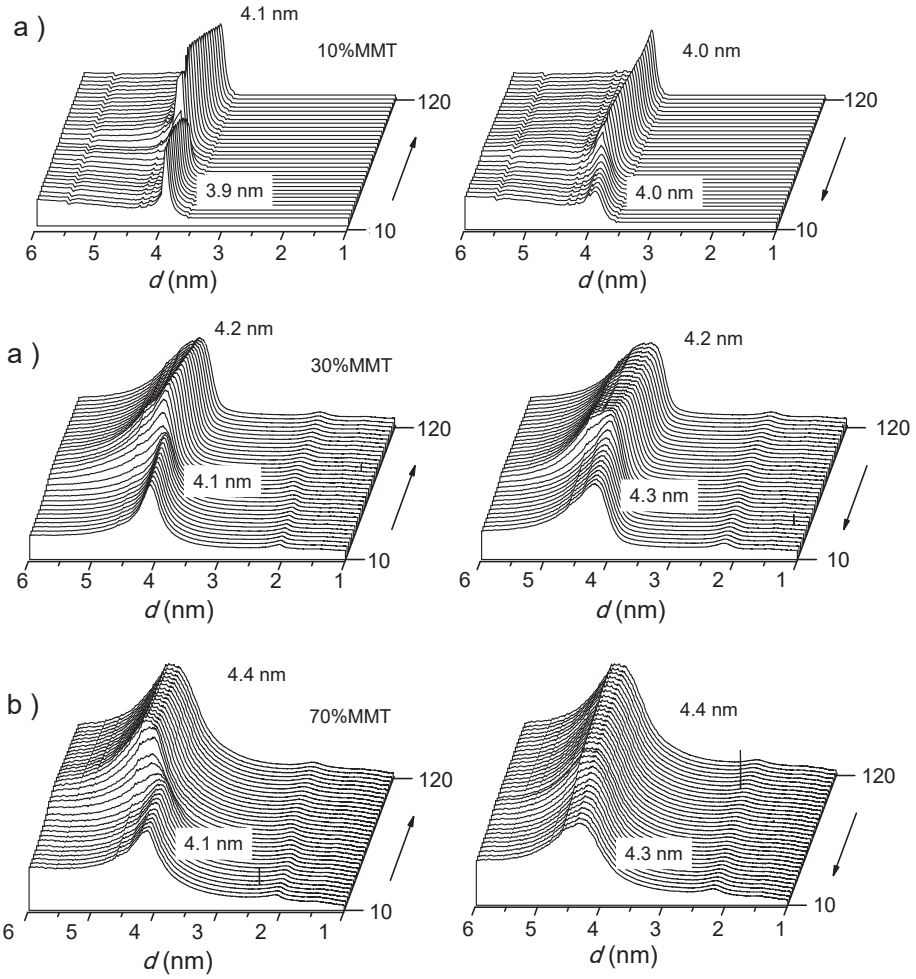

Figure SI-9. Evolution of SAXS profiles of 20ATMP·PGGA·10%^{P}MMT (a), 20ATMP·PGGA·30%^{P}MMT (b) and 20ATMP·PGGA·70%^{P}MMT (c) at heating (left) and cooling (right).

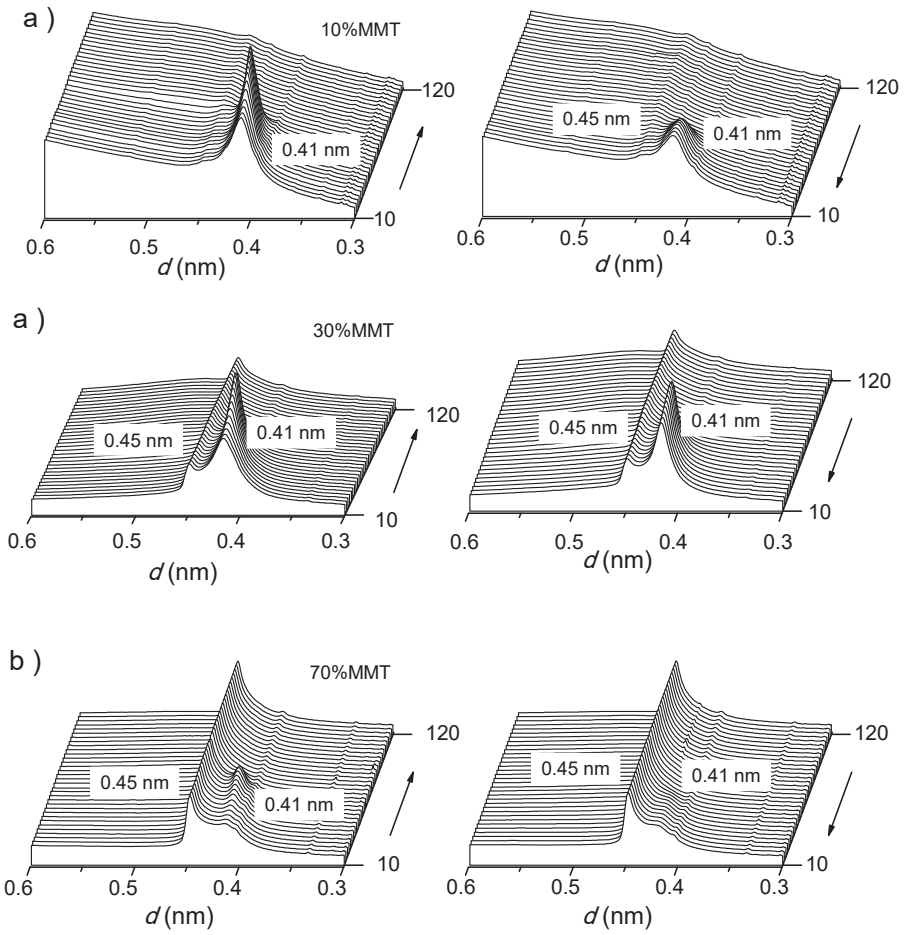

Figure SI-10. Evolution of WAXS profiles of 20ATMP·PGGA·10%^{P}MMT (a), 20ATMP·PGGA·30%^{P}MMT (b) and 20ATMP·PGGA·70%^{P}MMT (c) at heating (left) and cooling (right).

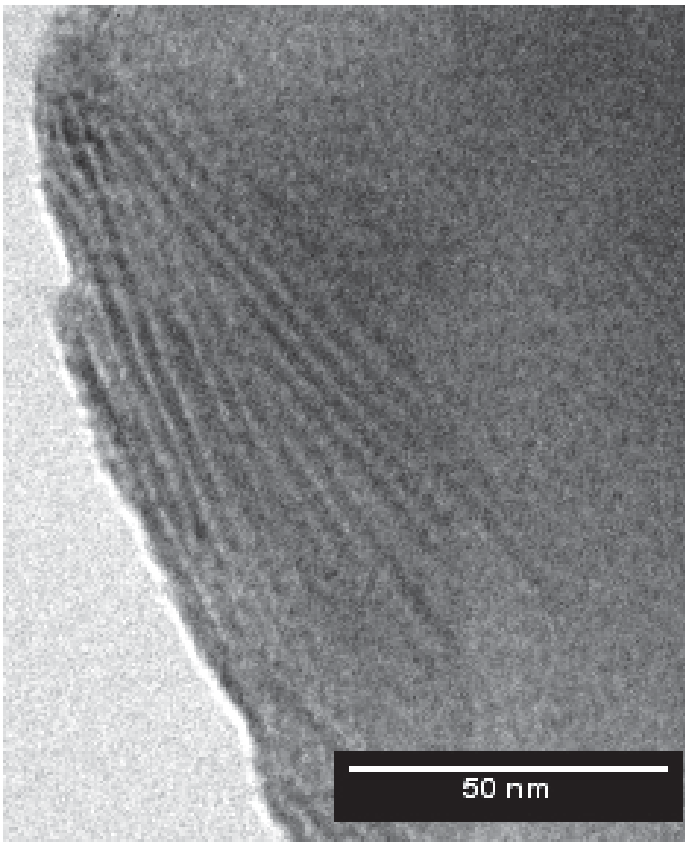

Figure SI-11. High magnification TEM image recorded from a section of 20ATMP·PGGA·50%^{P}MMT after being heated at 100 ºC for 1 h and stained with uranyl acetate.

Annex C:

C1. Supporting information to Chapter VI.1

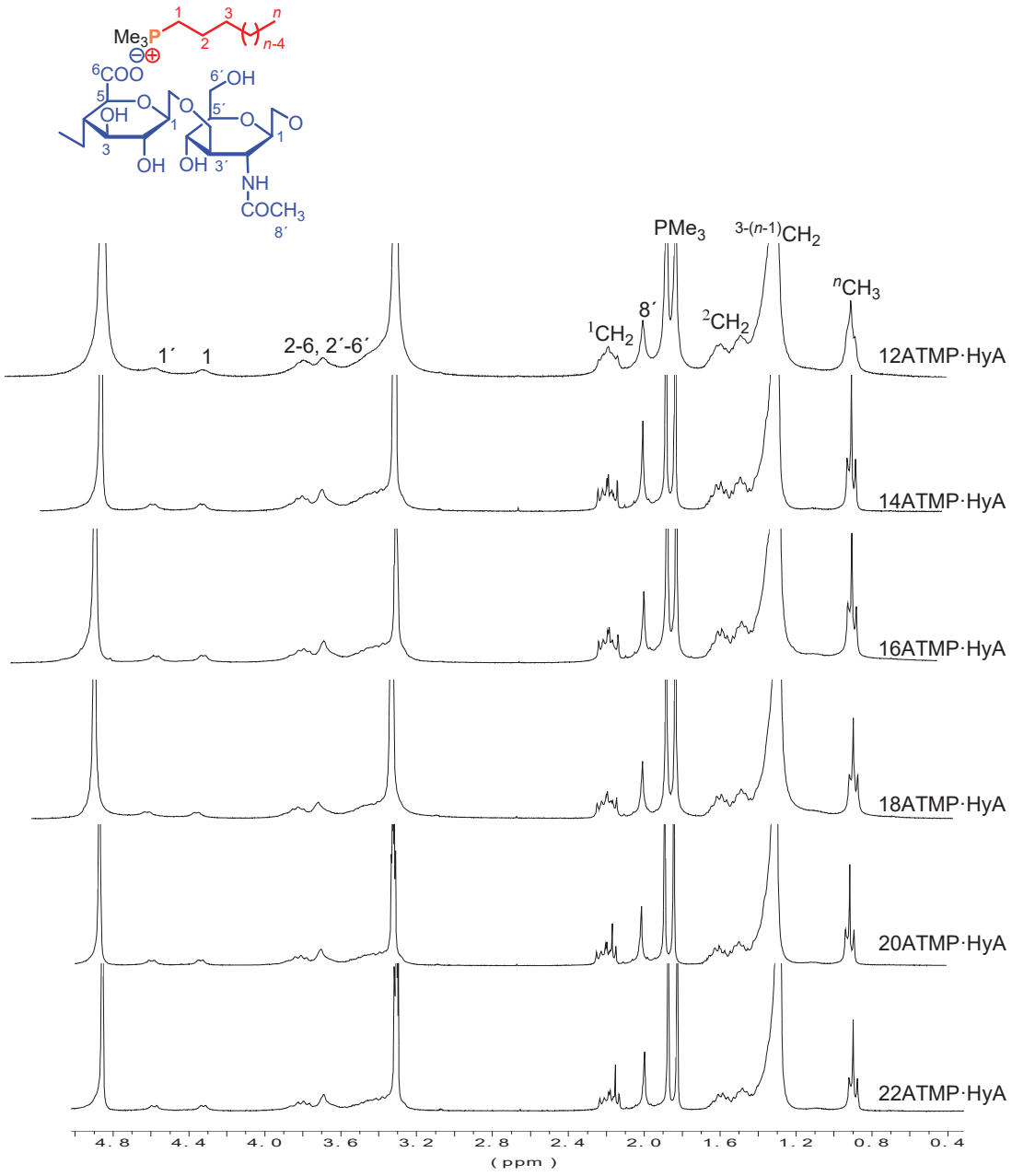

Figure SI-1. ^{1}H NMR spectra of the whole series of *n*ATMP·HyA complexes recorded in MeOD and at 25 ºC.

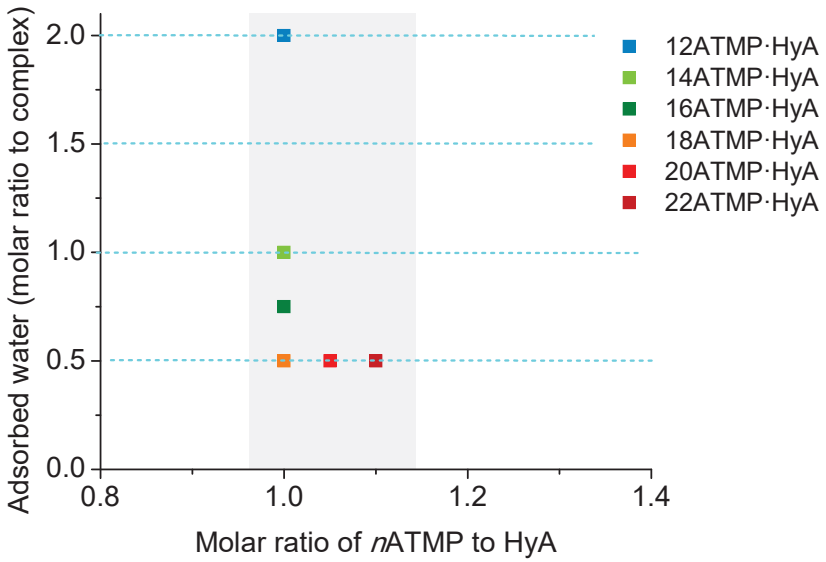

Figure SI-2. Compositions of *n*ATMP·HyA complexes as determined on the basis of elemental analysis data (see Table 1 in the main text). The molar ratio of *n*ATMP to HyA was estimated by including H_2O in the complex in discrete amounts (0.5, 1.0 and 2.0 moles). Intermediate amounts were not considered. The shadowed area delimits approximately the reasonably domain of compositions.

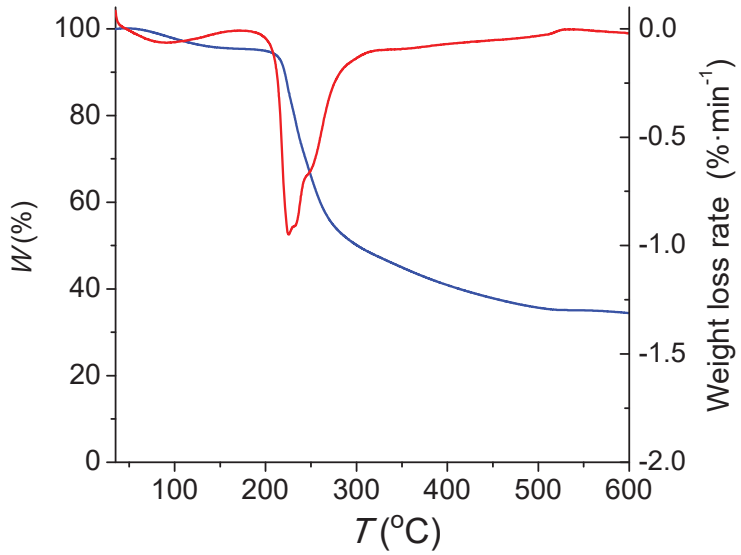

Figure SI-3. TGA trace of hyaluronic acid and its derivative curve.

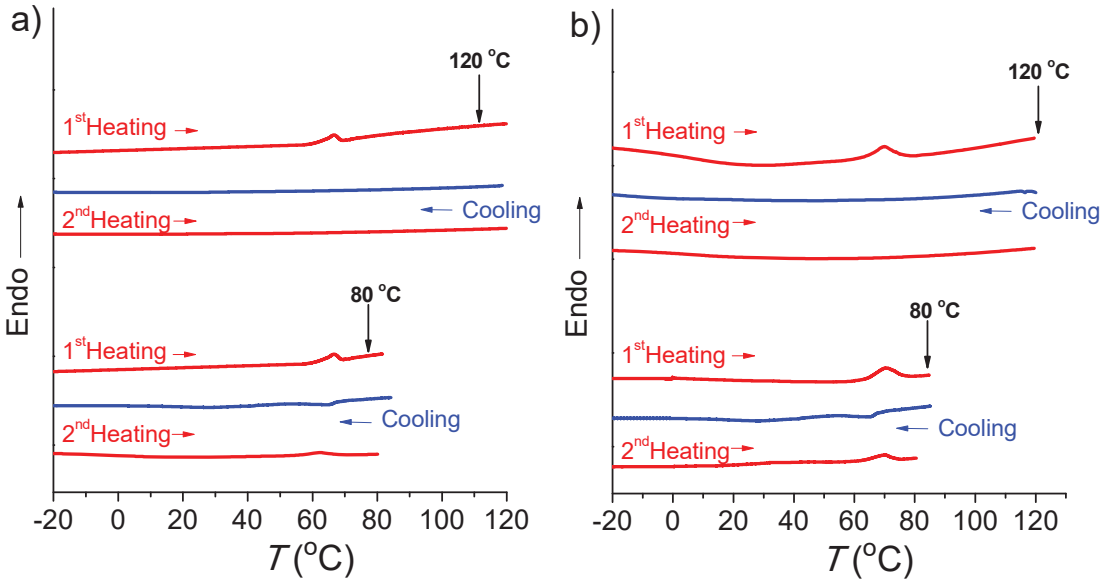

Figure SI-4. DSC traces of 20ATMP·HyA (a) and 22ATMP·HyA (b) complexes along the heating-cooling-heating cycle between -20-120 ºC and -20-80 ºC.

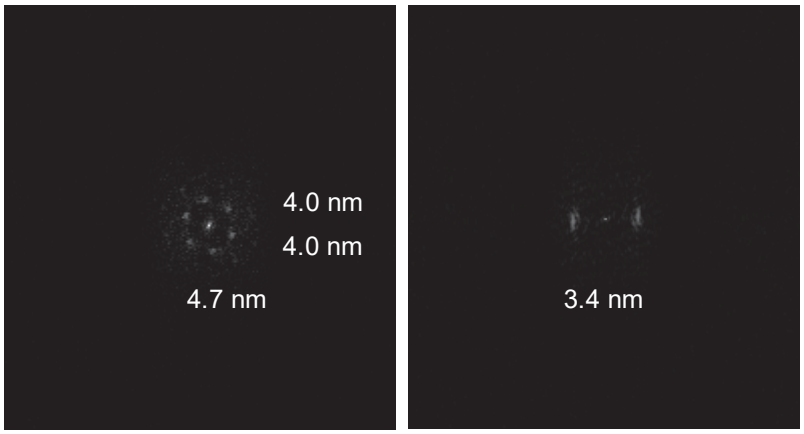

Figure SI-5. Optical diffraction analysis of selected areas to measure the periodical spacings present in 16ATMP·HyA complex.

Figure SI-6. Optical diffraction analysis of selected areas to measure the periodical spacings present in 22ATMP·HyA complex.

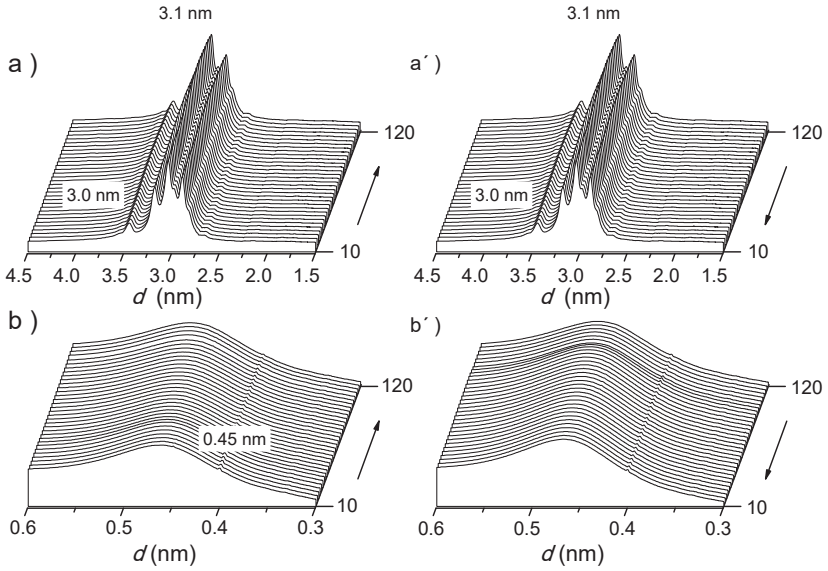

Figure SI-7. SAXS and WAXS profiles of 12ATMP·HyA at heating (a and b) and cooling (a´and b´) along 10-120 ºC range.

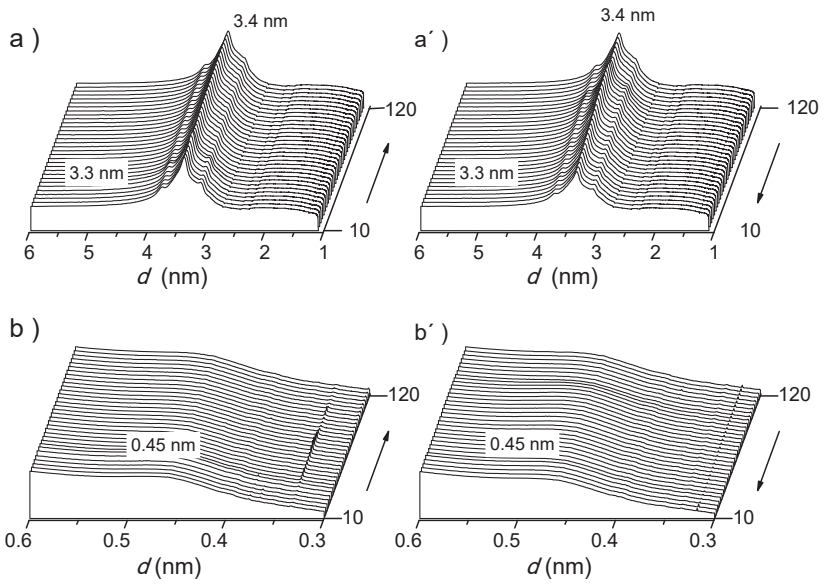

Figure SI-8. SAXS (a) and WAXS (b) profiles of 14ATMP·HyA at heating (a and b) and cooling (a´and b´) along 10-120 ºC range.

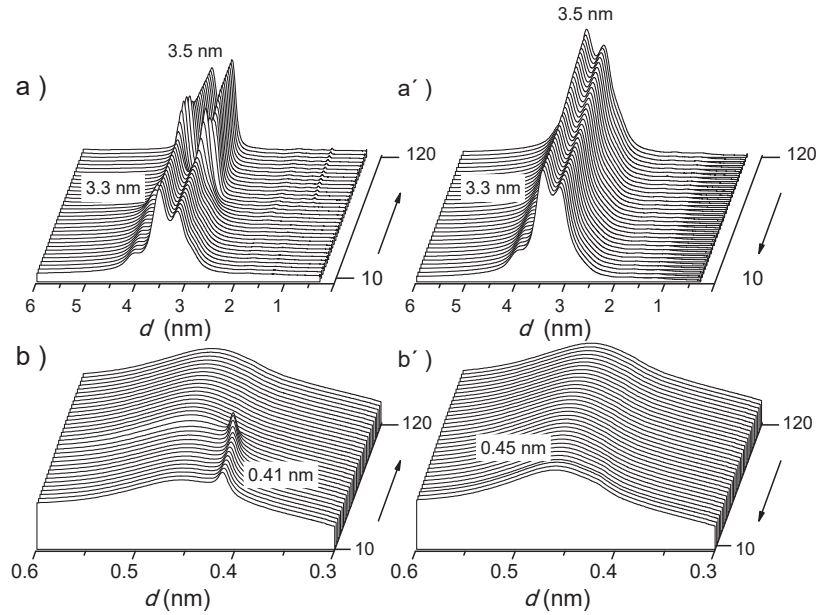

Figure SI-9. SAXS (a) and WAXS (b) profiles of 18ATMP·HyA at heating (a and b) and cooling (a´and b´) along 10-120 ºC range.

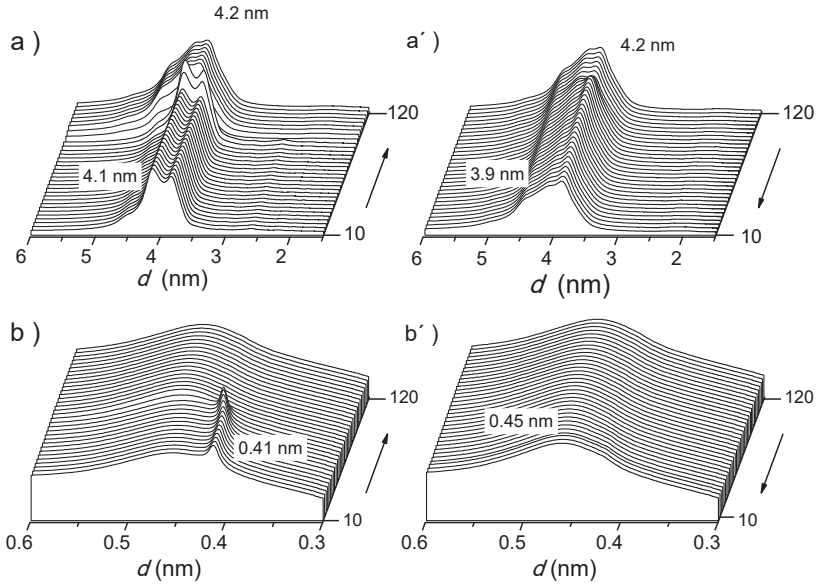

Figure SI-10. SAXS (a) and WAXS (b) profiles of 20ATMP·HyA at heating (a and b) and cooling (a´and b´) along 10-120 ºC range.

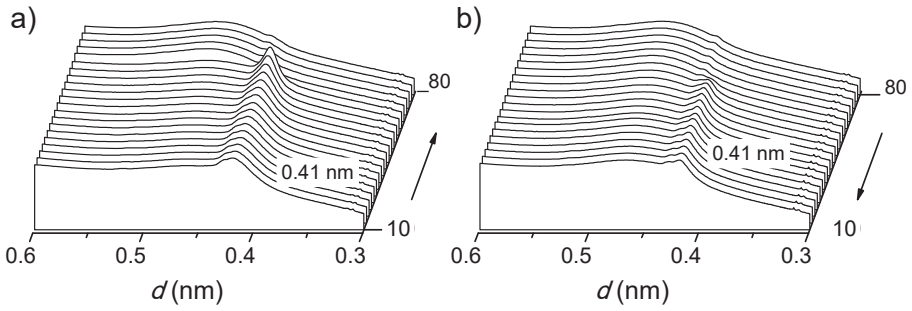

Figure SI-11. WAXS profiles of 22ATMP·HyA at heating (a) and cooling (b) along 10-80 ºC range.

.

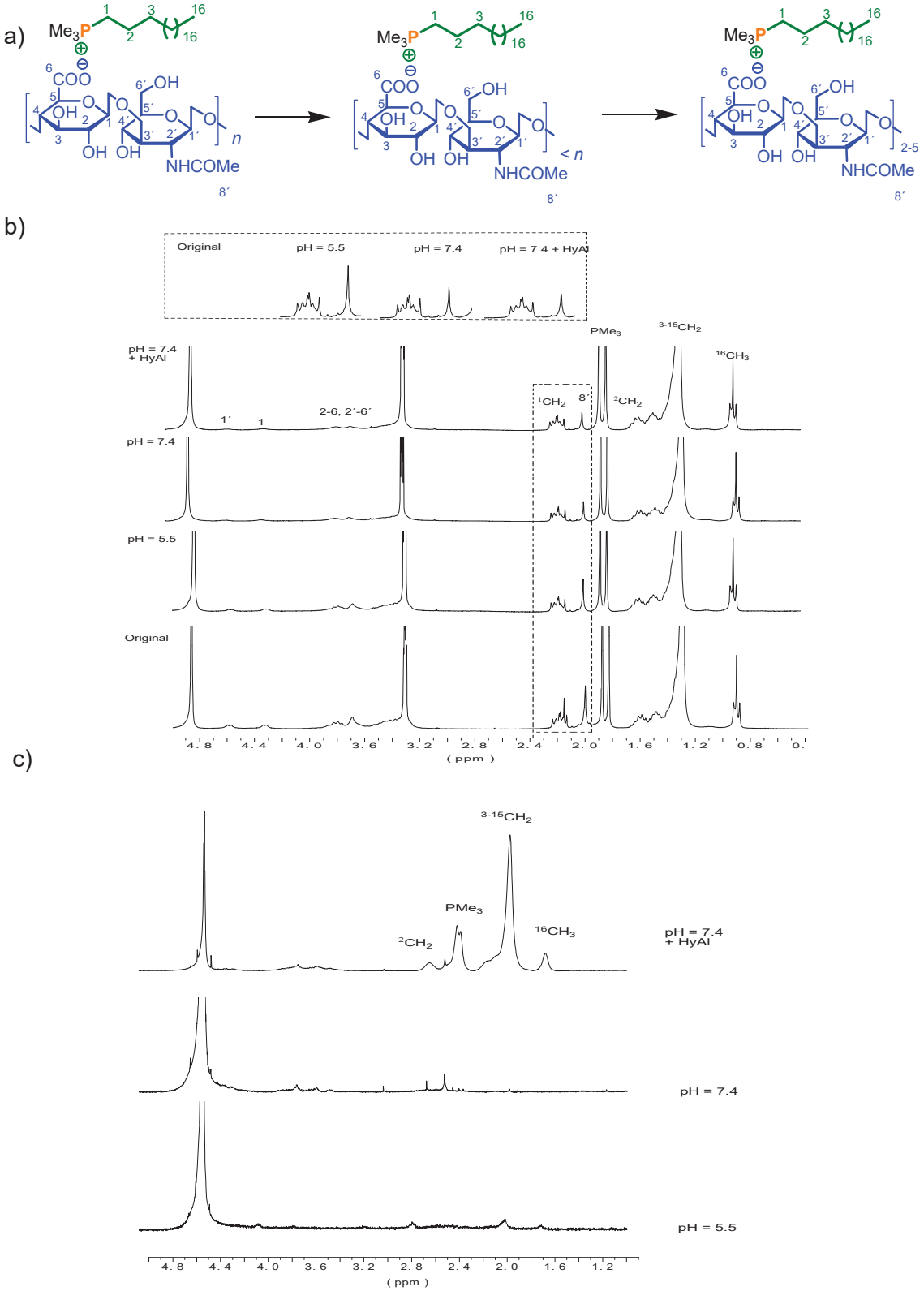

Figure SI-12. Decomposition mechanism of 16ATMP·HyA upon incubation in different buffer solutions at 37 ºC (a); ^{1}H NMR spectra of residual sample at the end of the incubation (b); ^{1}H NMR spectra of products released to the different incubation mediums (c).

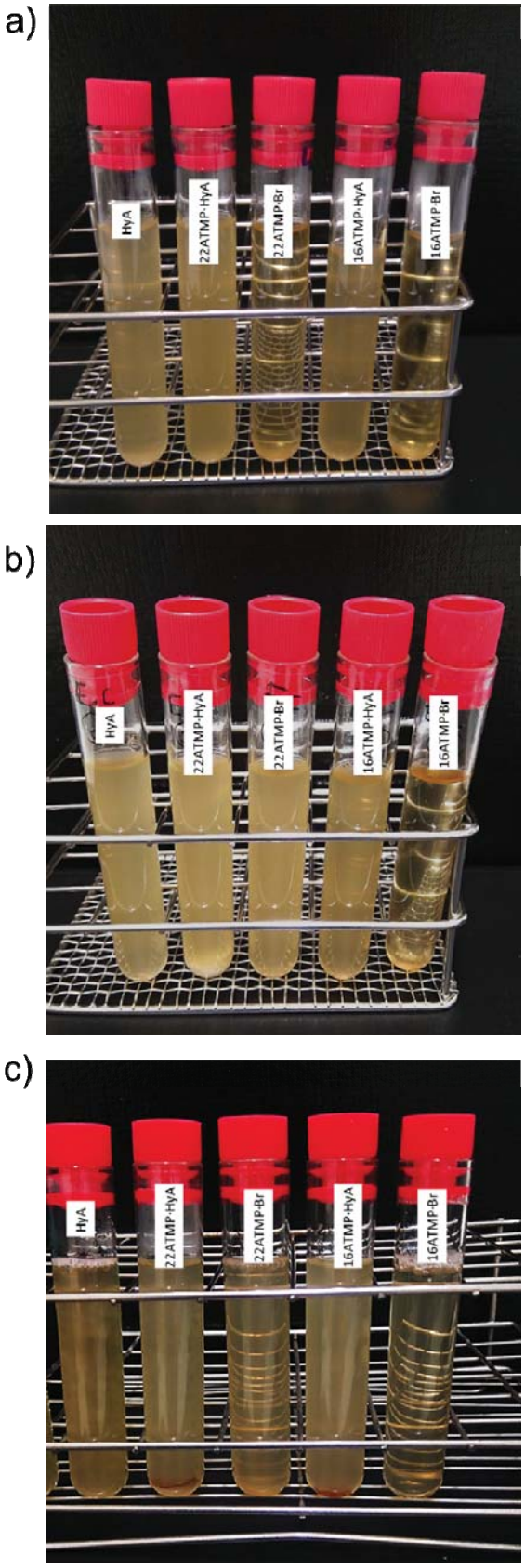

Figure SI-13. Appearance of antimicrobial assays in liquid media after 24 h of 16ATMP·Br, 22ATMP·Br and their complexes with HyA against *S. aureus* (a), *E. coli* (b) and *C. albicans* (c).

Table SI-1. Biocide activity of films made of nATMP·HyA complexes against Gram-negative and Gram-positive bacteria after 0.5, 2, 4 and 24 h of incubation at pH 7.4 and 37 ºC.

		S. aureus			*E. coli*			*C. albicans*		
		2 h	4 h	24 h	2 h	4 h	24 h	2 h	4 h	24 h
HyA	Log (CFU)[a]	4.342	5.253	7.315	6.895	6.491	9.159	3.181	3.029	5.130
	STD [b]	0.139	0.11	0.116	0.037	0.028	0.026	0.035	0.089	0.045
22ATMP·HyA	Log (CFU)	3.461	3.064	2.698	6.764	6.374	9.108	3.634	2.908	5.151
	STD	0.044	0.037	0.048	0.019	0.063	0.078	0.303	0.005	0.217
	Log (RV)[c]	0.881	2.189	4.616	0.131	0.117	0.051	-0.454	0.122	-0.021
	PR (%)[d]	86.864	99.353	99.998	26.017	23.656	11.085	0	24.455	0
22ATMP·Br	Log (CFU)	1.727	Total I.	0.301	6.690	6.286	9.073	2.439	1.802	Total I.
	STD	0.318	0	0.6	0.010	0.039	0.031	0.303	0.084	0.005
	Log (RV)	2.615		7-06	0.205	0.205	0.086	0.742	1.228	
	PR (%)	99.758	100	99.999	37.650	37.634	18.014	81.868	94.081	100
16ATMP·HyA	Log (CFU)	Total I.	Total I.	Total I.	Total I.	0.824	1.1564	3.043	2.861	4.067
	STD	0	0	0	0	0.550	0.281	0.301	0.038	0.058
	Log (RV)					5.667	7.595	0.138	0.168	1.063
	PR (%)	100	100	100	100	99.999	99.998	27.253	32.087	91.358
16ATMP·Br	Log (CFU)	Total I.	Total I.	Total I.	Total I.	Total I.	0.778	Total I.	Total I.	Total I.
	STD	0	0	0	0	0	0.46	0.005	0.005	0.005
	Log (RV)						8.381			
	PR (%)	100	100	100	100	100	99.999	100	100	100

[a] Antimicrobial activity expressed as logarithm of colony forming units.
[b] Standard deviation of each measurement.
[c] Antimicrobial activity expressed as log reduction value.
[d] Percentage of reduction.

C2. Supporting information to Chapter VI.2

Table SI-1. Effects of ratio, concentration and used *n*ATMP surfactant for nanoparticle formation of *n*ATMP·HyA by the ionotropic gelation method.

		conc (mg·mL^{-1})[b]								
		1.0:1.0			0.375:1.0			0.375:0.375		
Ratio[a]	*n*	16	18	22	16	18	22	16	18	22
0.2:1.0		stable	Stable	stable	stable	stable	stable	stable	stable	stable
04:1.0		stable	Stable	stable	stable	stable	stable	stable	stable	stable
0.5:1.0		stable	Stable	stable	stable	stable	stable	stable	stable	stable
0.6:1.0		stable	prec	prec	stable	stable	prec	stable	stable	prec
0.7:1.0		prec	prec	prec	stable	prec	prec	stable	prec	prec
0.8:1.0		prec	prec	prec	prec	prec	prec	stable	prec	prec

[a] Ratio of *n*ATMP to HyA used for the preparation of *n*ATMP·HyA NPs.
[b] Concentration of the twos aqueous solutions, that is *n*ATMP:HyA expressed as mg·mL^{-1}.

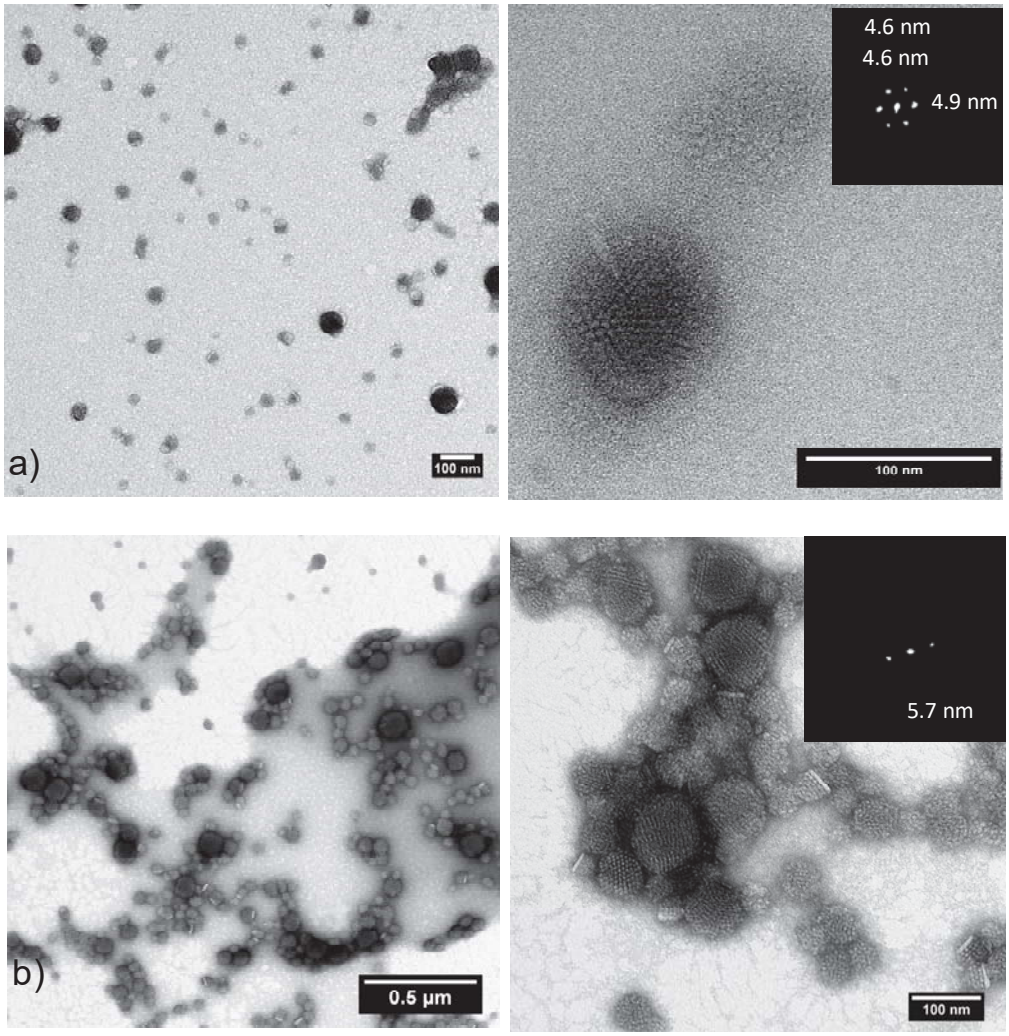

Figure SI-1. TEM micrographs of nanoparticles made of 22ATMP·HyA 0.2H (a) and 0.5L (b). Inset: Optical diffraction analysis of selected areas to measure the periodical spacings present in NPs.

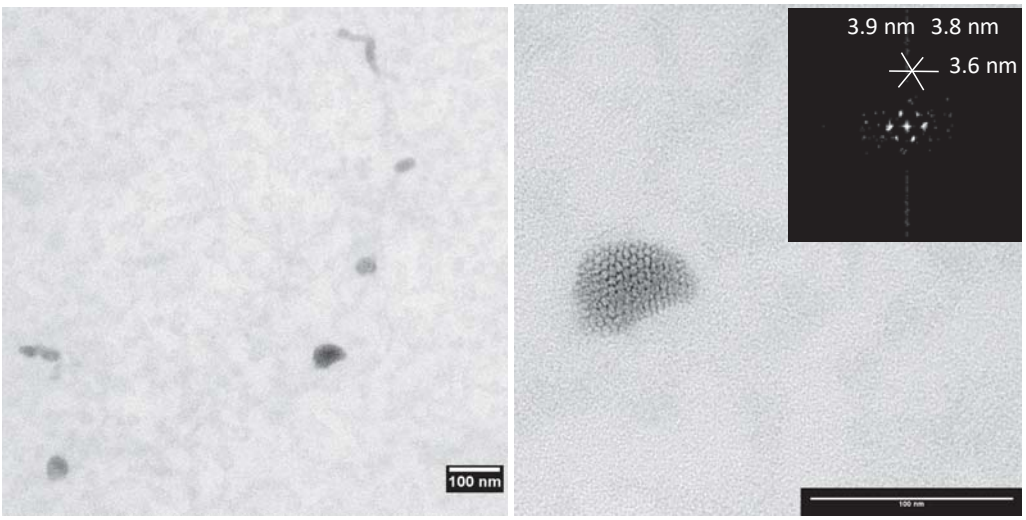

Figure SI-2. TEM micrographs of nanoparticles made of 16ATMP·HyA-0.6. Inset: Optical diffraction analysis of selected areas to measure the periodical spacings present in NPs.

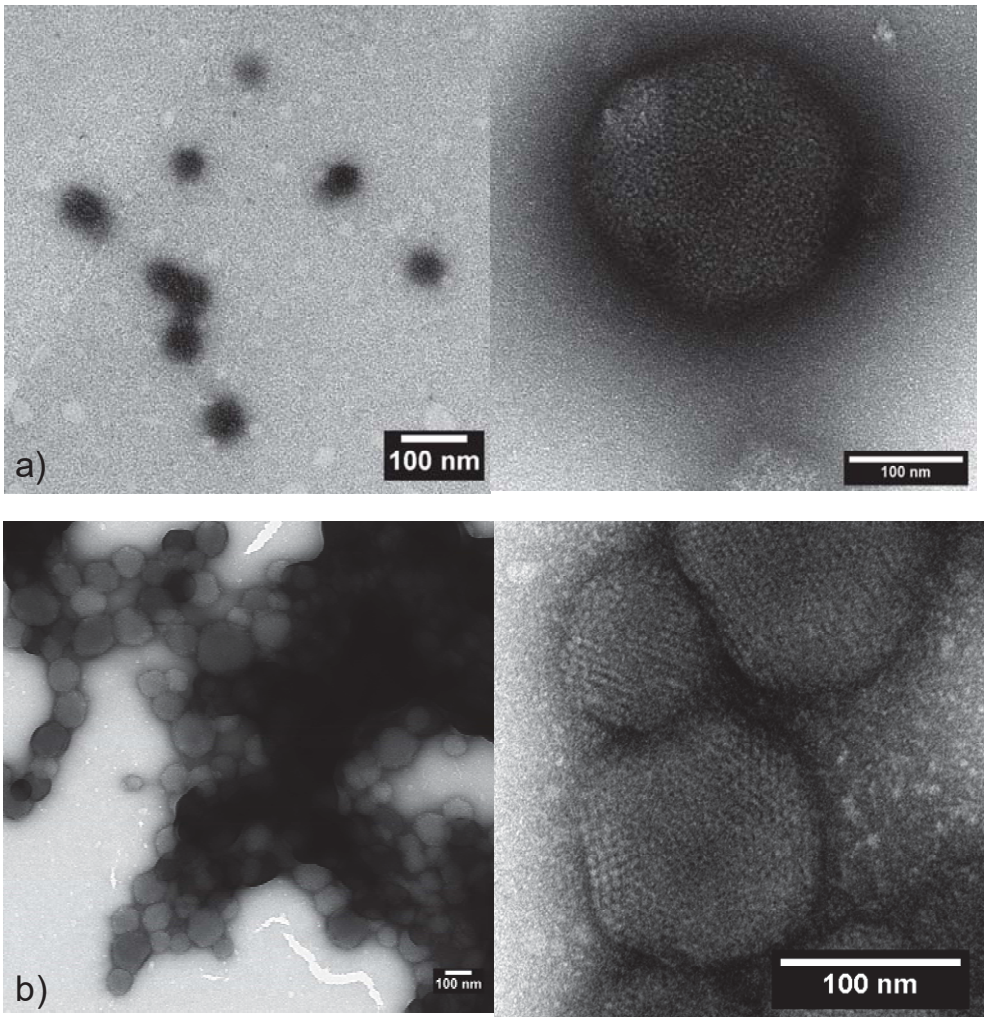

Figure SI-3. TEM micrographs of nanoparticles made of 18ATMP·HyA-0.2H and18ATMP·HyA-0.5H.

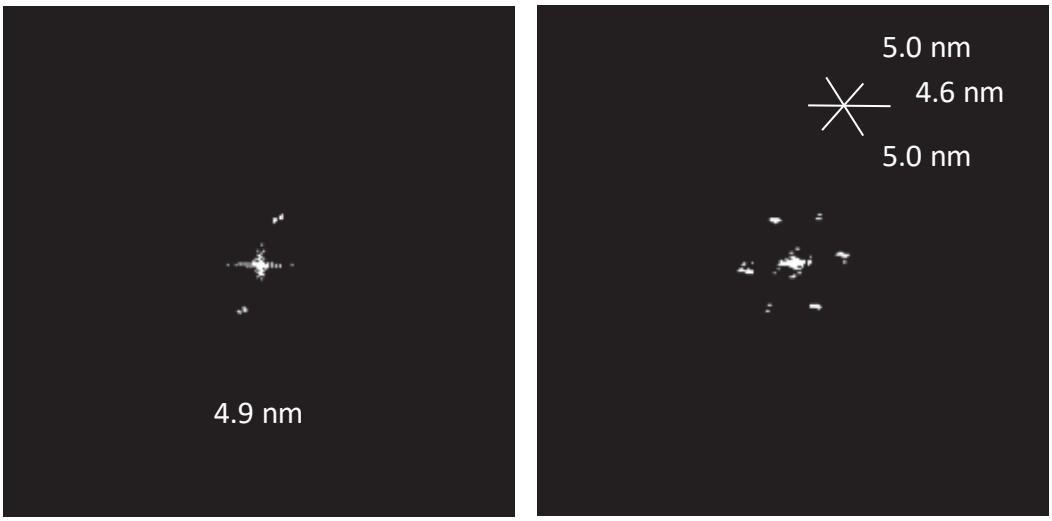

Figure SI-4. Optical diffraction analysis of selected areas to measure the periodical spacings present in nanoparticles made of 18ATMP·HyA-0.5H.

Annex D: Supporting information to Chapter VII

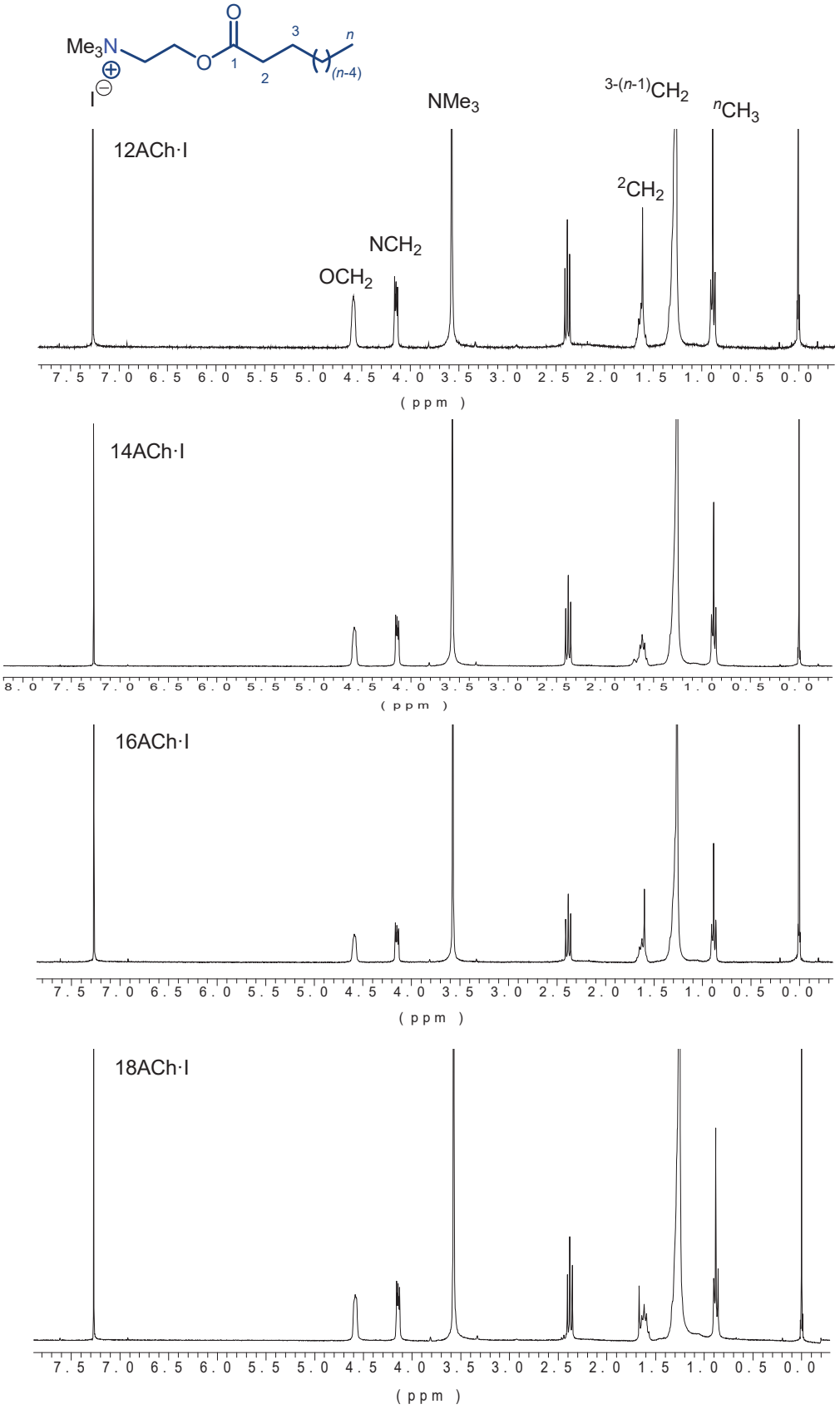

Figure SI-1. ^{1}H NMR spectra of the whole series of *n*ACh·I surfactants in $CDCl_3$.

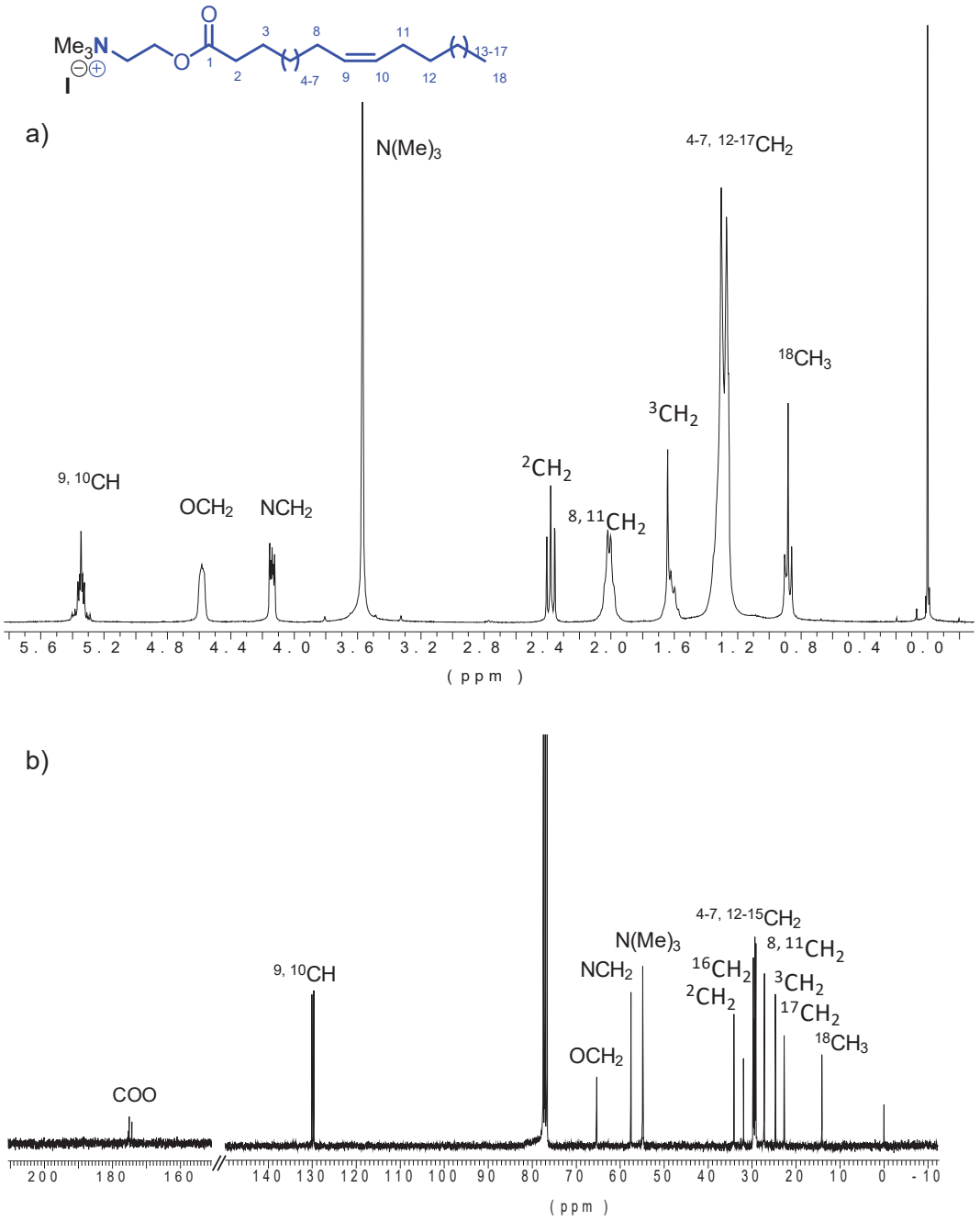

Figure SI-2. ^{1}H NMR (a) and ^{13}C NMR (b) spectra of *cis*18ACh·I surfactant in $CDCl_3$.

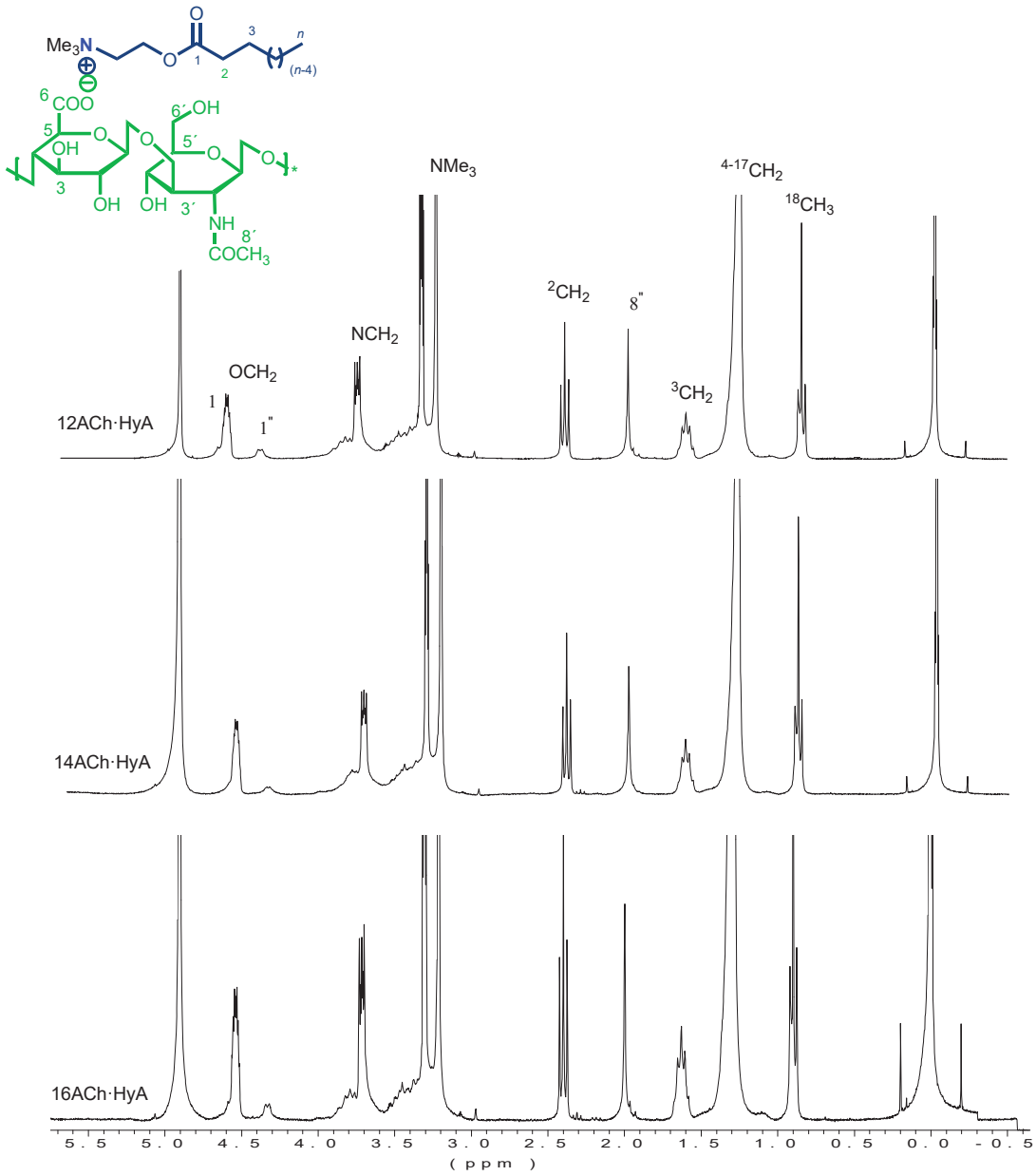

Figure SI-3. ^{1}H NMR spectra of *n*ACh·HyA complexes in MeOD.

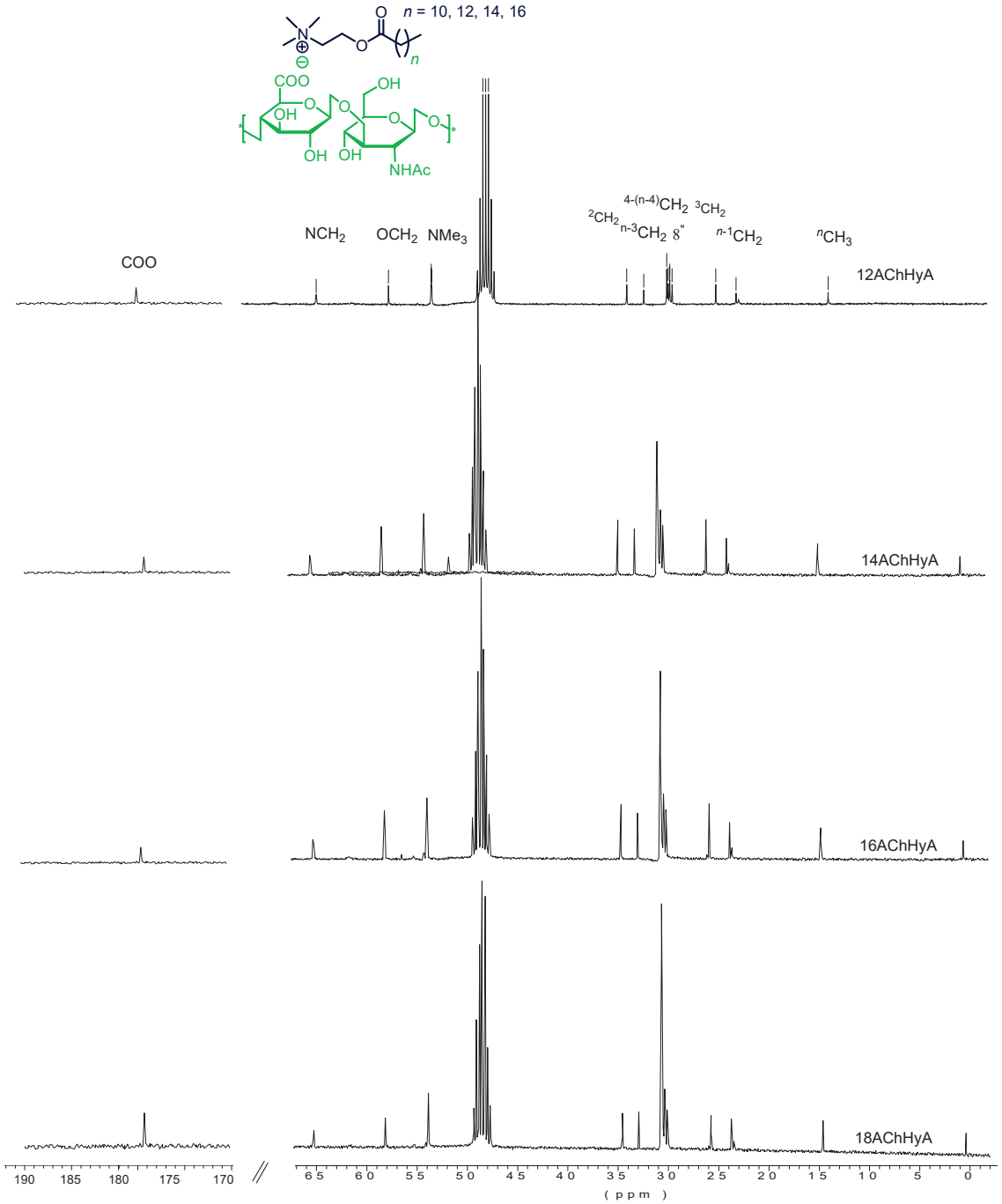

Figure SI-4. ^{13}C NMR spectra of *n*ACh·HyA complexes in MeOD.

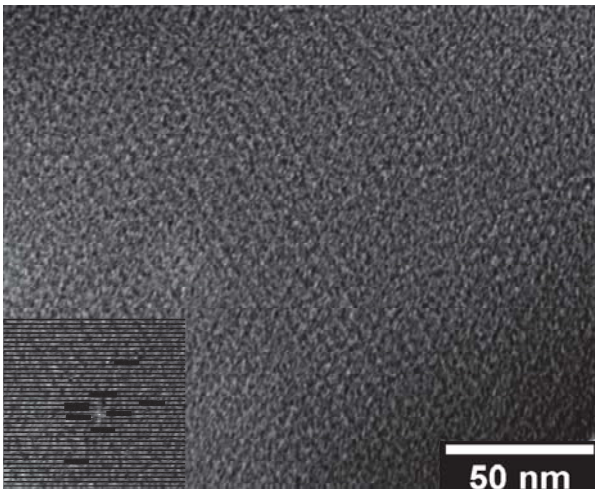

Figure SI-5. TEM micrograph from a film of 18ACh·HyA complex. Inset; OD pattern indicating the periodical spacing displayed on the film.

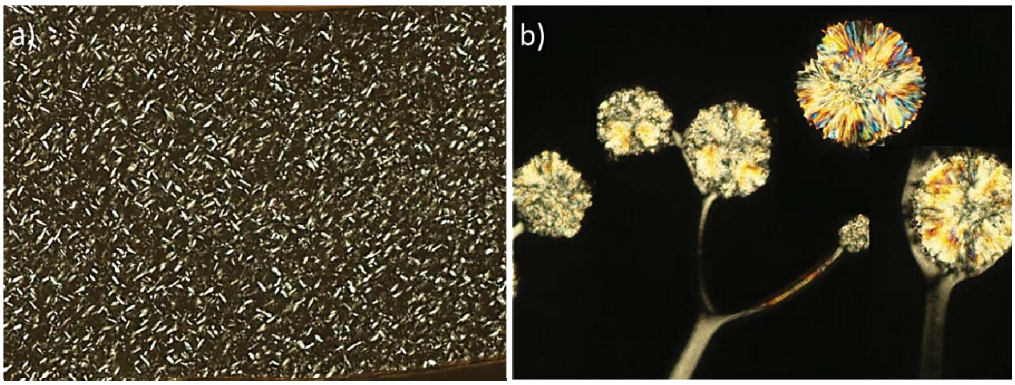

Figure SI-6. POM micrographs of *n*ACh·HyA complexes with *n*= 12 (a) and 18 (b) recorded at 25 ºC.

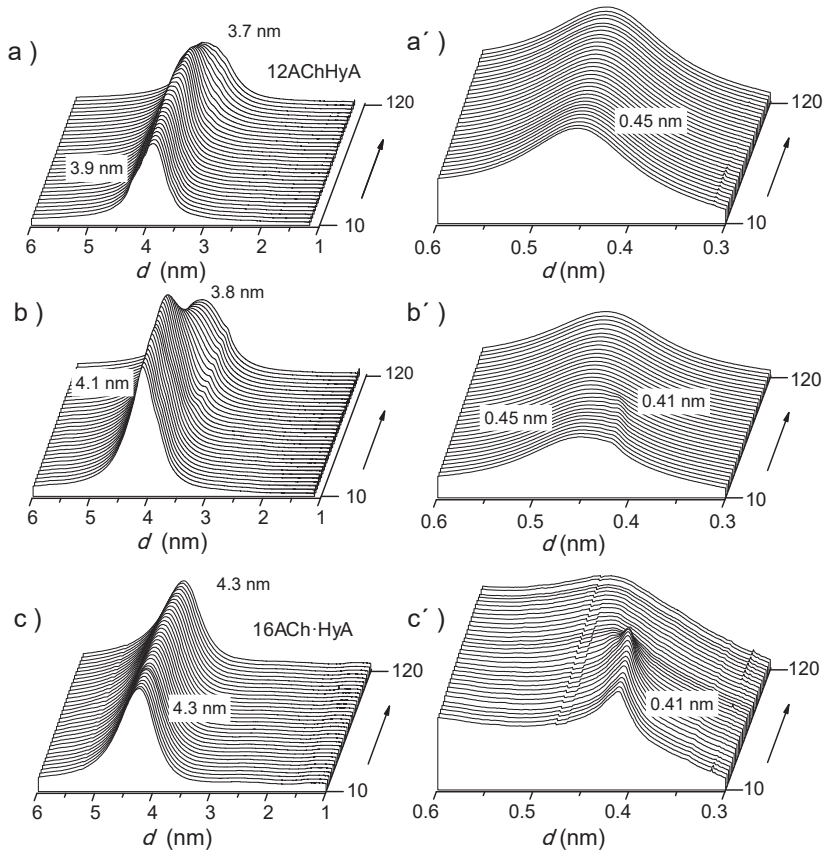

Figure SI-7. SAXS and WAXS profiles of 12ACh·HyA (a and a´), 14ACh·HyA (b and b´) and 16ACh·HyA (c and c´) at heating along the 10-120 ºC range

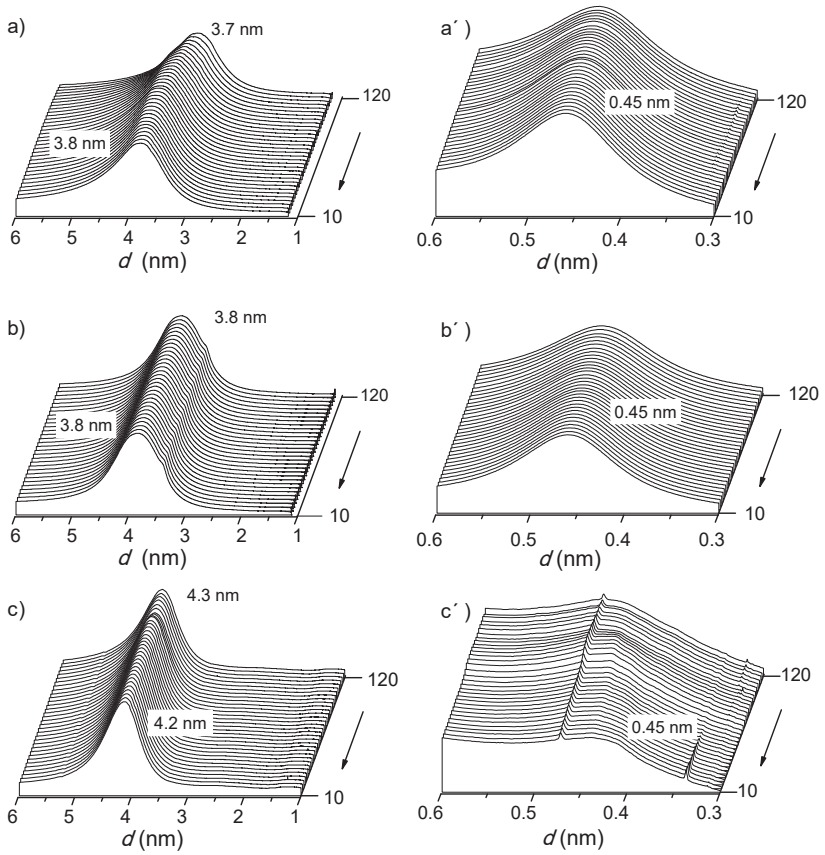

Figure SI-8. SAXS and WAXS profiles of 12ACh·HyA (a and a´), 14ACh·HyA (b and b´) and 16ACh·HyA (c and c´) at cooling along the 120-10 ºC range.

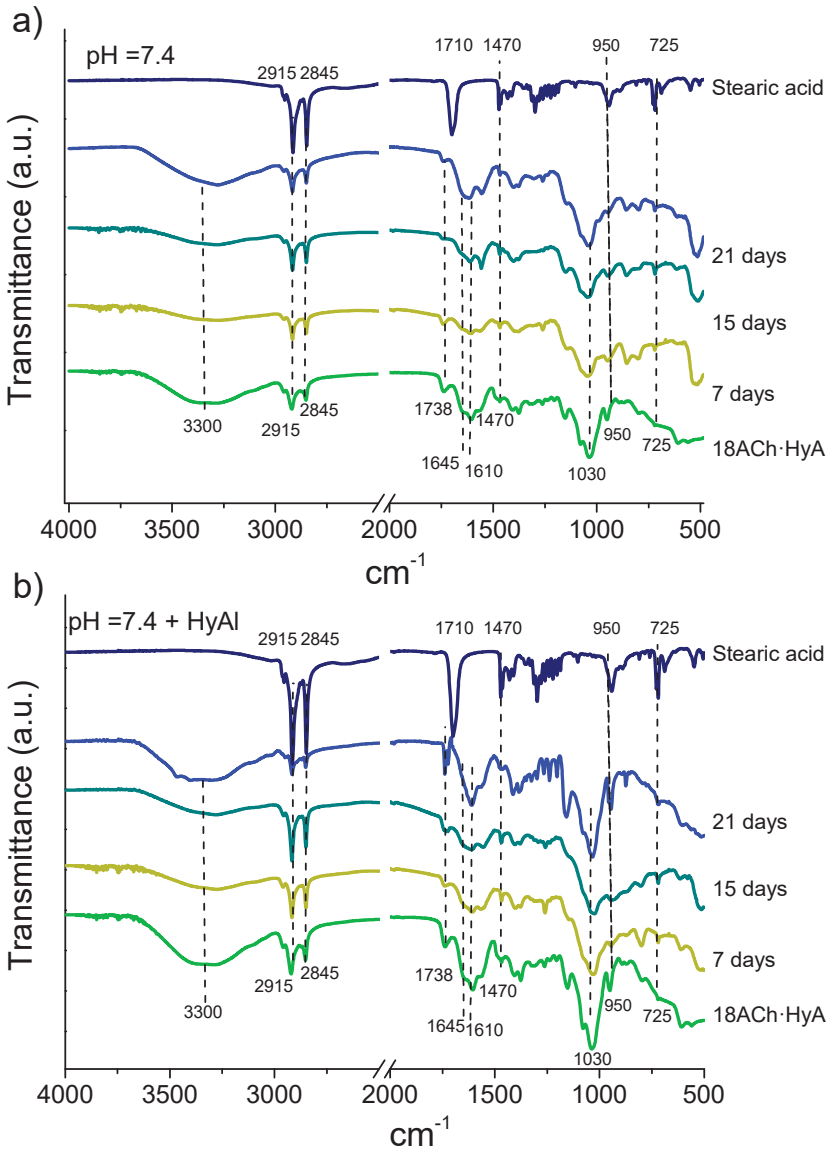

Figure SI-9. FTIR spectra of remaining disc of 18ACh·HyA complex after incubation in aqueous buffer at 37 ºC at the indicated times, in the absence (a) or the presence of HyAl enzymes (b).

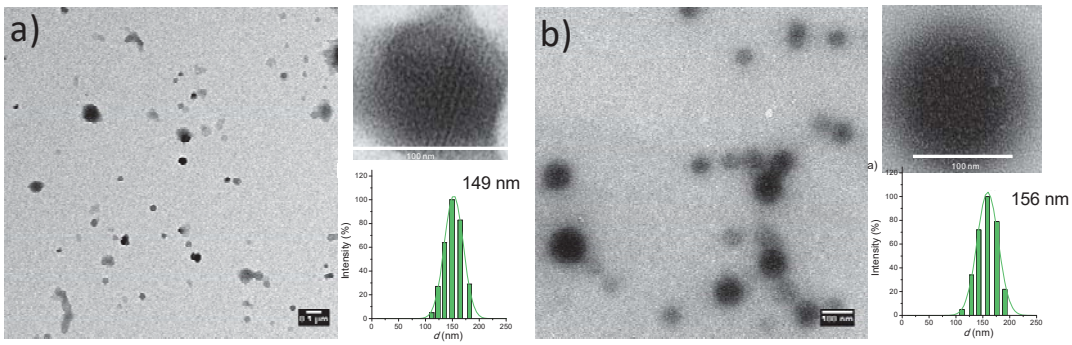

Figure SI-10. TEM micrographs of 18ACh·HyA NPs (a) and *cis*18ACh·HyA NPs (b) with a ACh:HyA:ratio of 0.25:1.0 and obtained using a solutioin concentration of 0.1 (wt-%). High magnification pictures and size distribution plots of NPs are included.

Table SI-1. Results obtained after using the indicated experimental conditions

ACh: HyA ratio	Concentration 18ACh:HyA ($mg \cdot mL^{-1}$)		
	1 : 1	1 : 0.375	0.375 : 0.375
0.2:1.0	119[a]	87,758	469
0.4:1.0	130	92, 432	85, 412
0.5:1.0	143	212	63, 375
0.6:1.0	precipitate	precipitate	241
0.75:1.0	precipitate	precipitate	precipitate
1.0:1.0	precipitate	precipitate	precipitate

[a]Size of nanoparticles formed when it is not obtained a precipitate.

Annex E:

E1. Supporting information to Chapter VIII.1

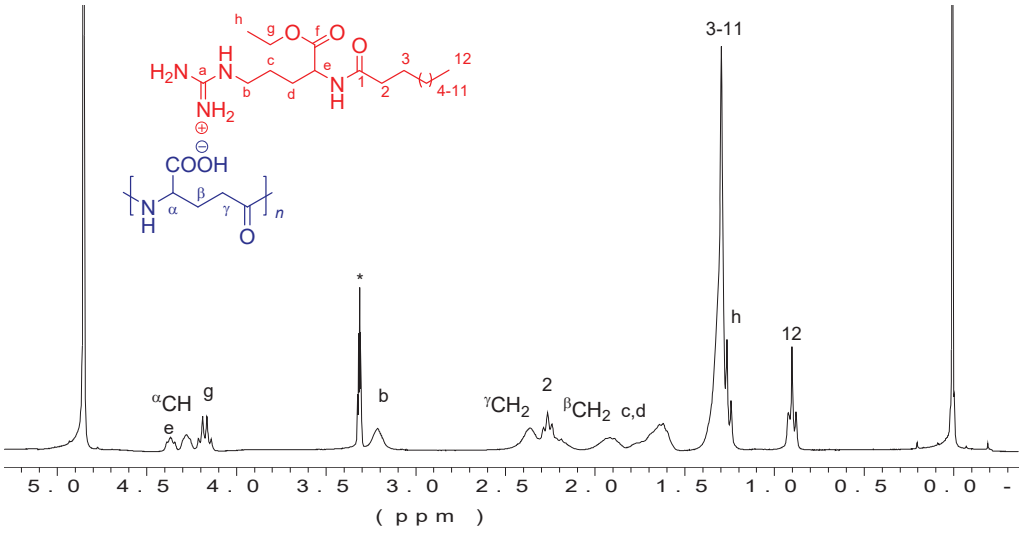

Figure SI-1. ^{1}H NMR spectra of LAE·PGGA-0.5 recorded at 25 ºC in MeOD. *Asterisked signals are those arising from water and non-deuterated solvent.

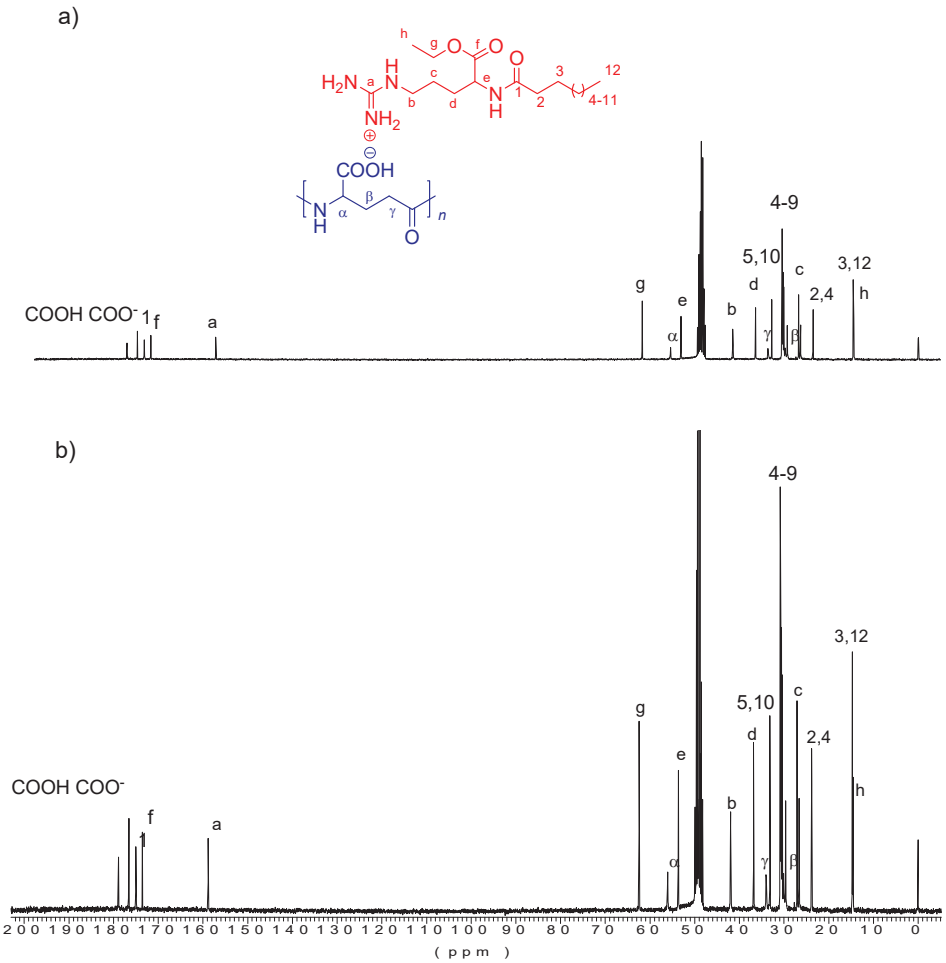

Figure SI-2. ^{13}C NMR spectra of LAE·PGGA-1 (a) and LAE·PGGA-0.5 (b) recorded in MeOD.

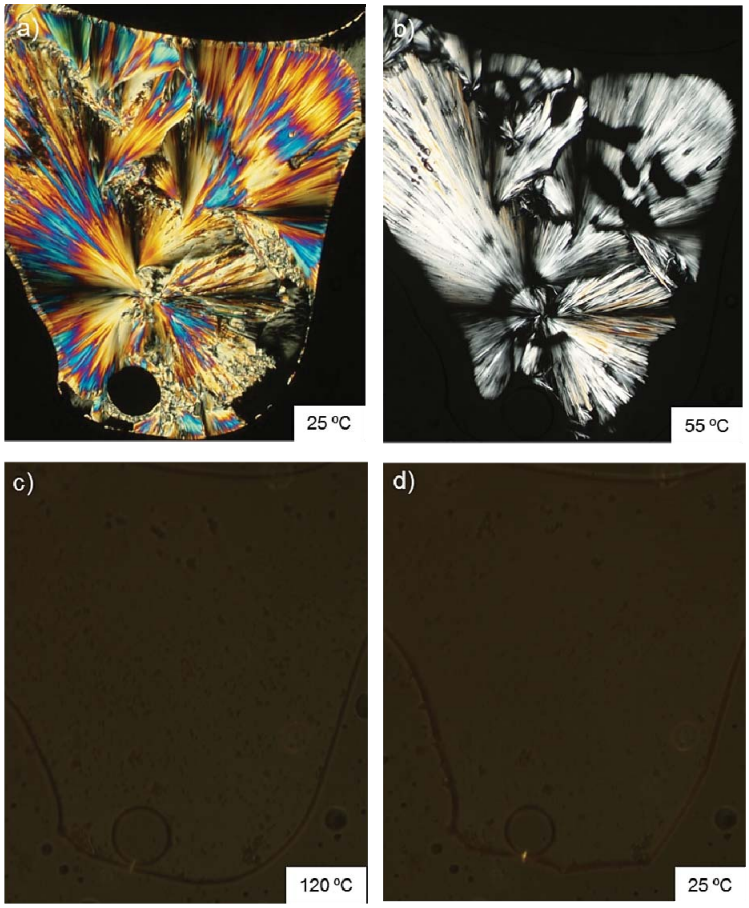

Figure SI-3. POM micrographs recorded from LAE at heating (a,b,c) and after heating (d) at the indicated temperatures.

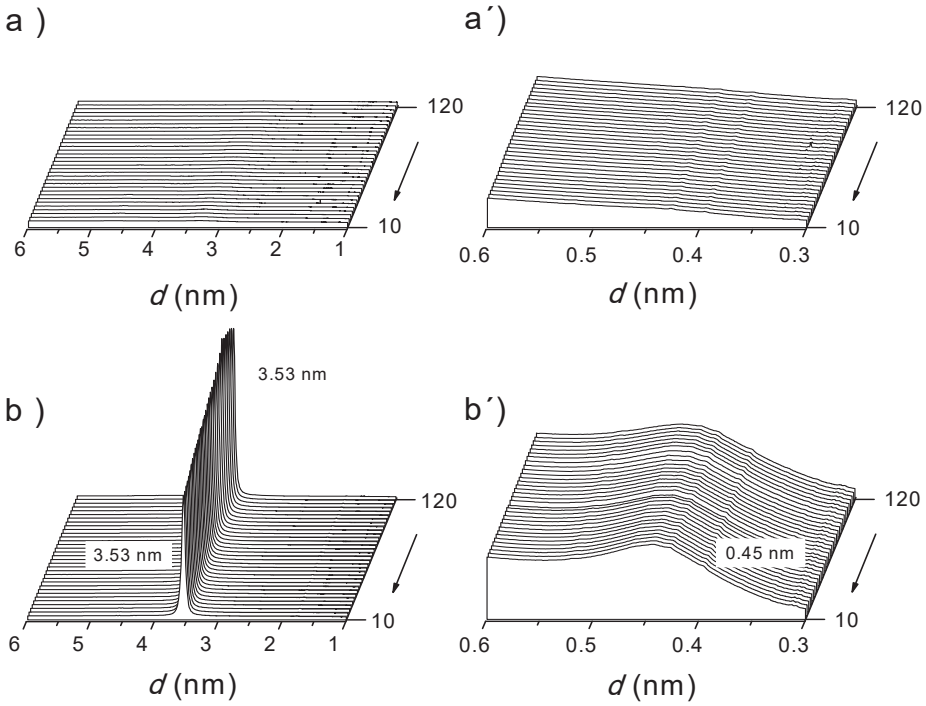

Figure SI-4. Evolution of the SAXS and WAXS profiles of LAE (a and a´) and LAE·PGGA-1 (b and b´) at cooling from 120 to 10 ºC.

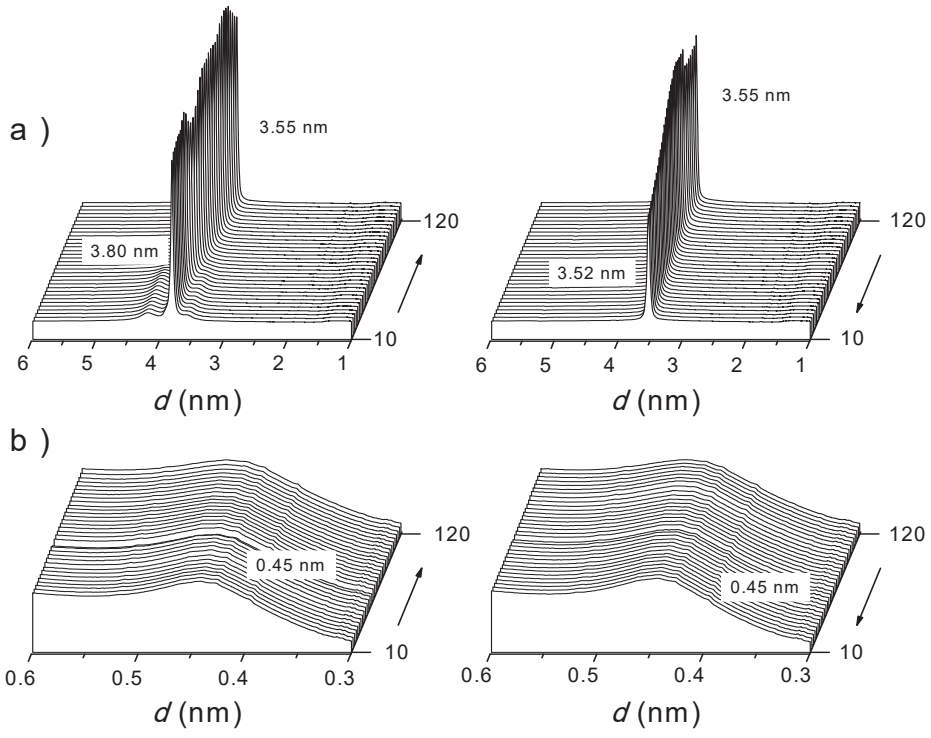

Figure SI-5. SAXS (a) and WAXS (b) profiles of LAE·PGGA-0.5 at heating (left) and cooling (right).

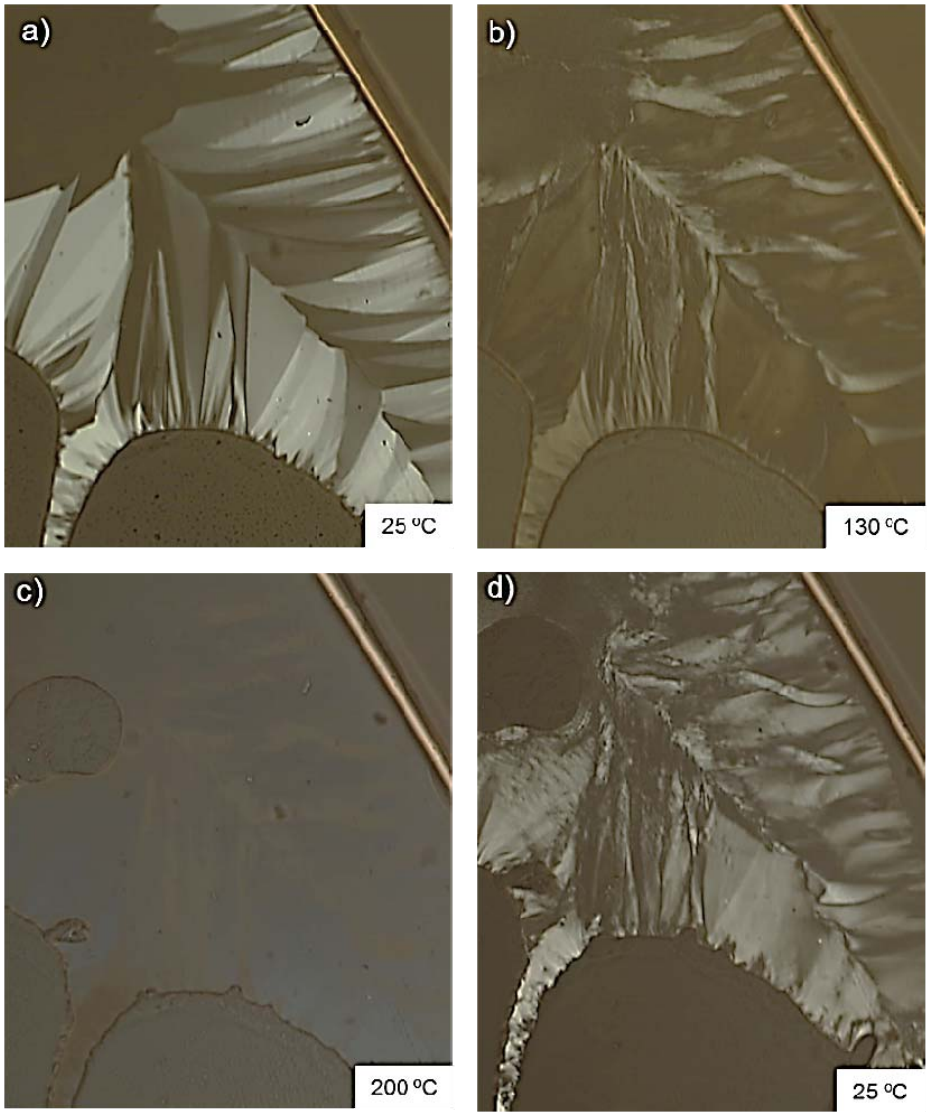

Figure SI-6. POM micrographs recorded from LAE·PGGA-1 at heating (a,b,c) and after heating (d) at the indicated temperatures.

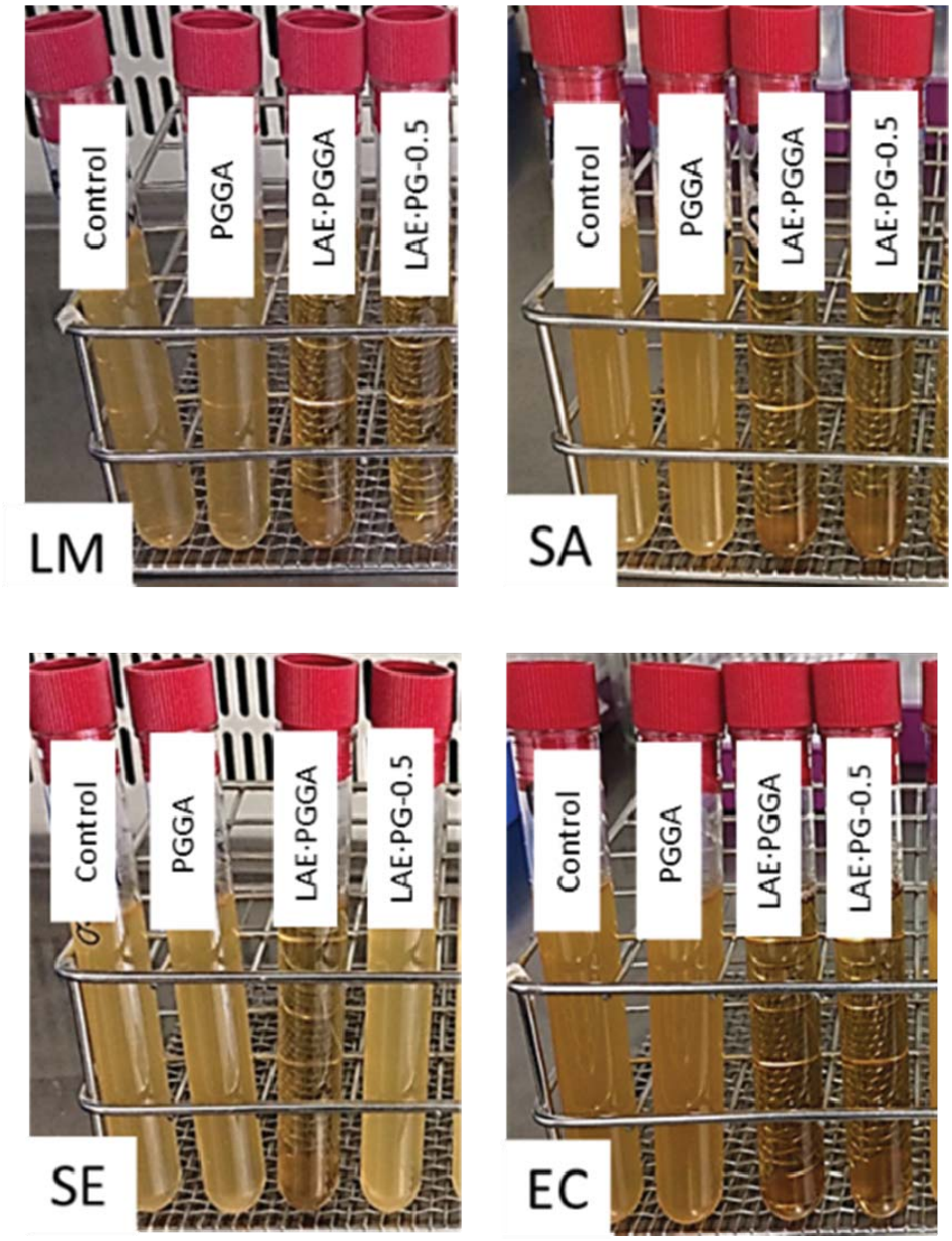

Figure SI-7. Visual appearance of the supernatant of LAE·PGGA-1 and LAE·PGGA-0.5 films incubated with *Listeria monocytogenes* (LM), *Staphylococcus aureus* (SA), *Salmonella enterica* (SE) and *Escherichia coli* (EC).

E2. Supporting information to Chaper VIII.2

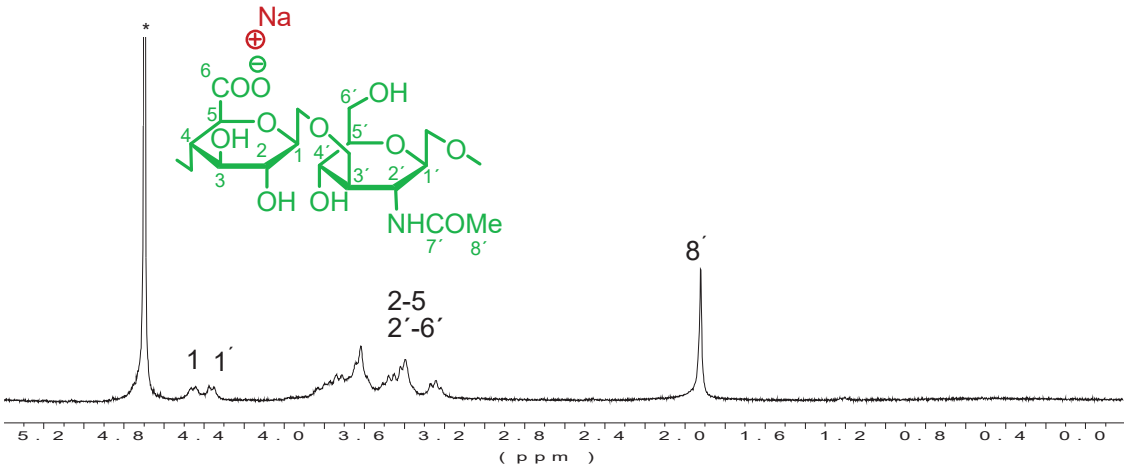

Figure SI-1. ^{1}H NMR spectrum of HyA recorded at 25 ºC in D_2O.

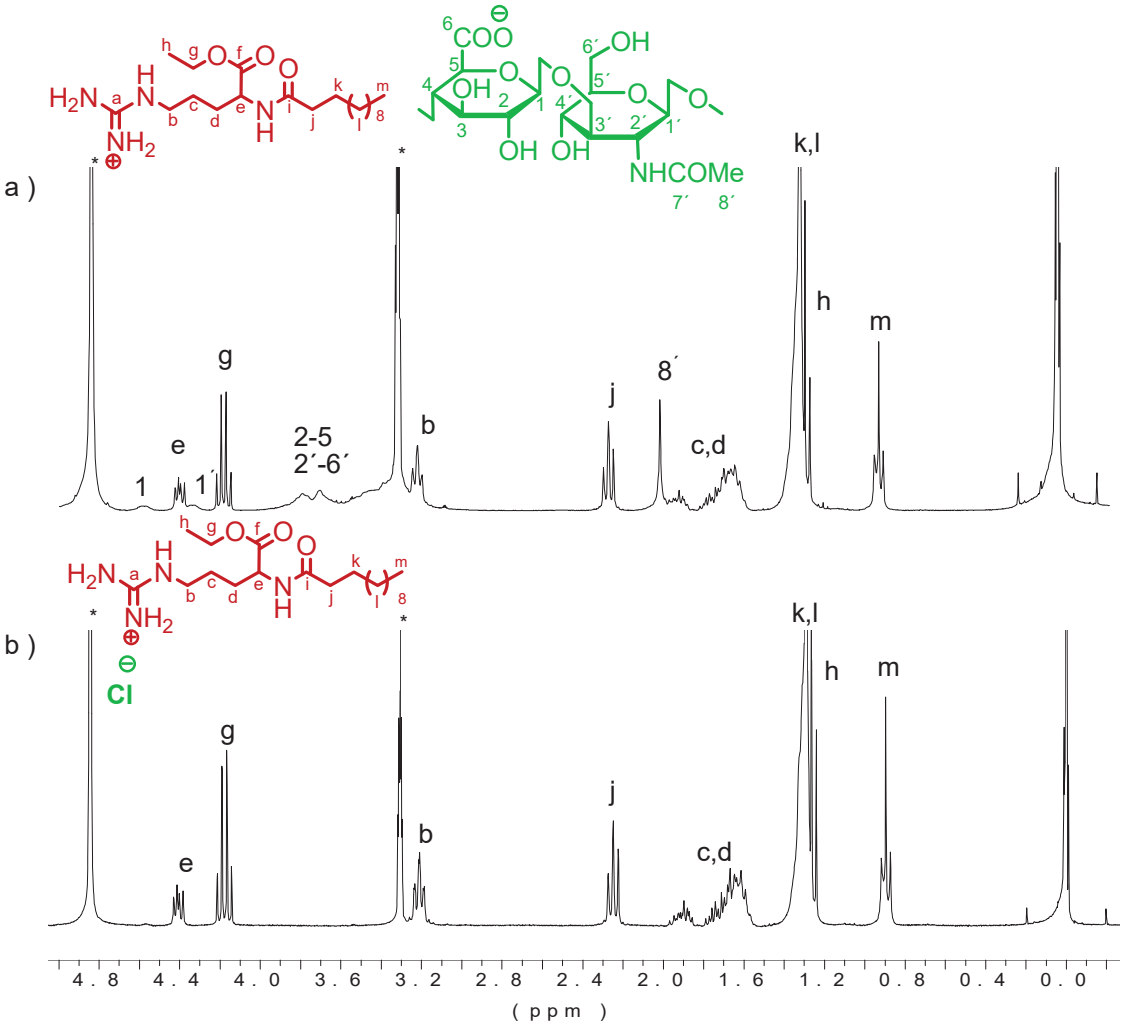

Figure SI-2. ^{1}NMR LAE·HyA-0.5 (a) and LAE (b) recorded at 25 ºC in MeOD.

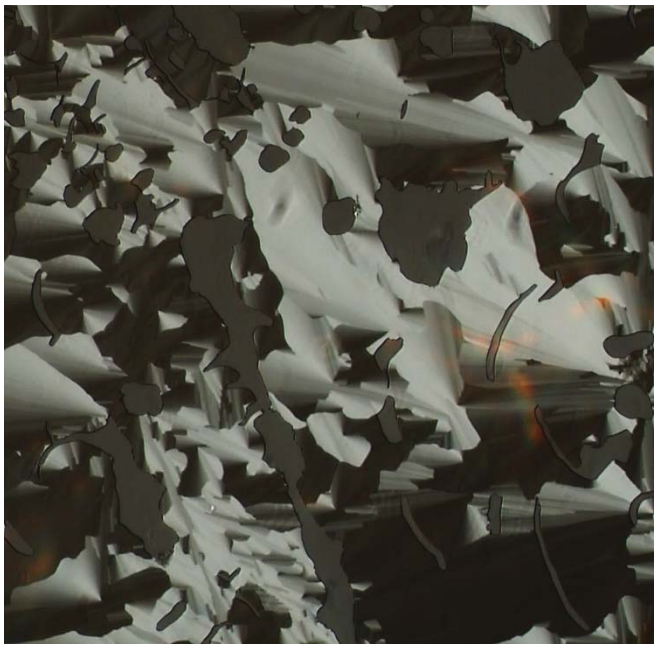

Figure SI-3. POM micrograph recorded from LAE·HyA-0.5.

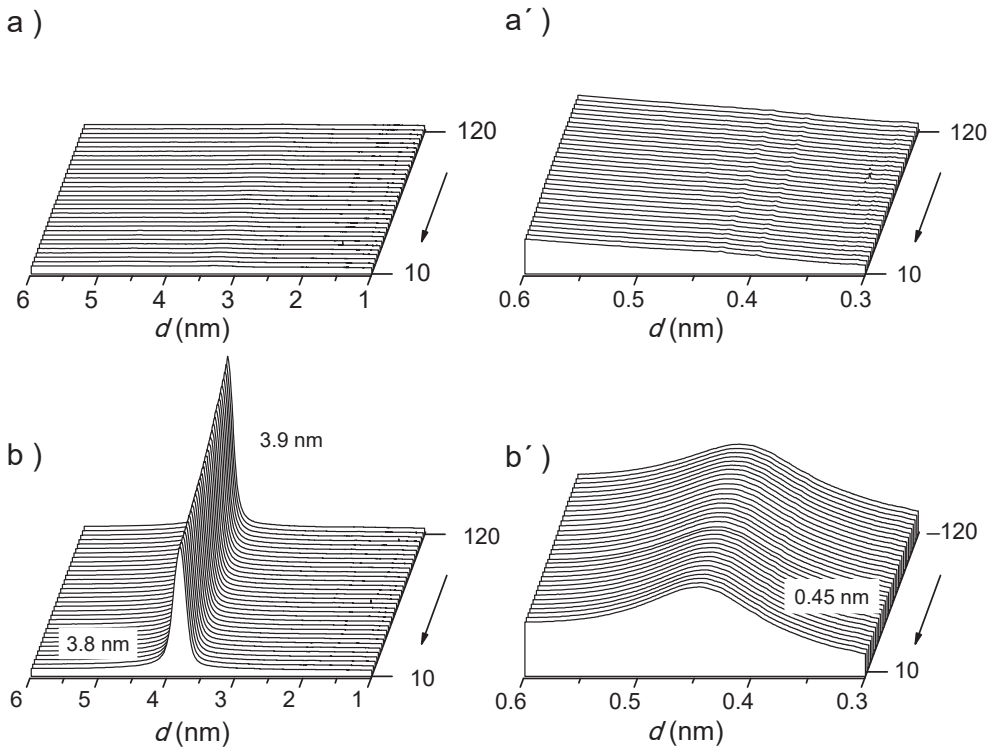

Figure SI-4. Evolution of the SAXS and WAXS profiles of LAE (a and a') and LAE·HyA-1 (b and b') at cooling from 120 to 10 °C.

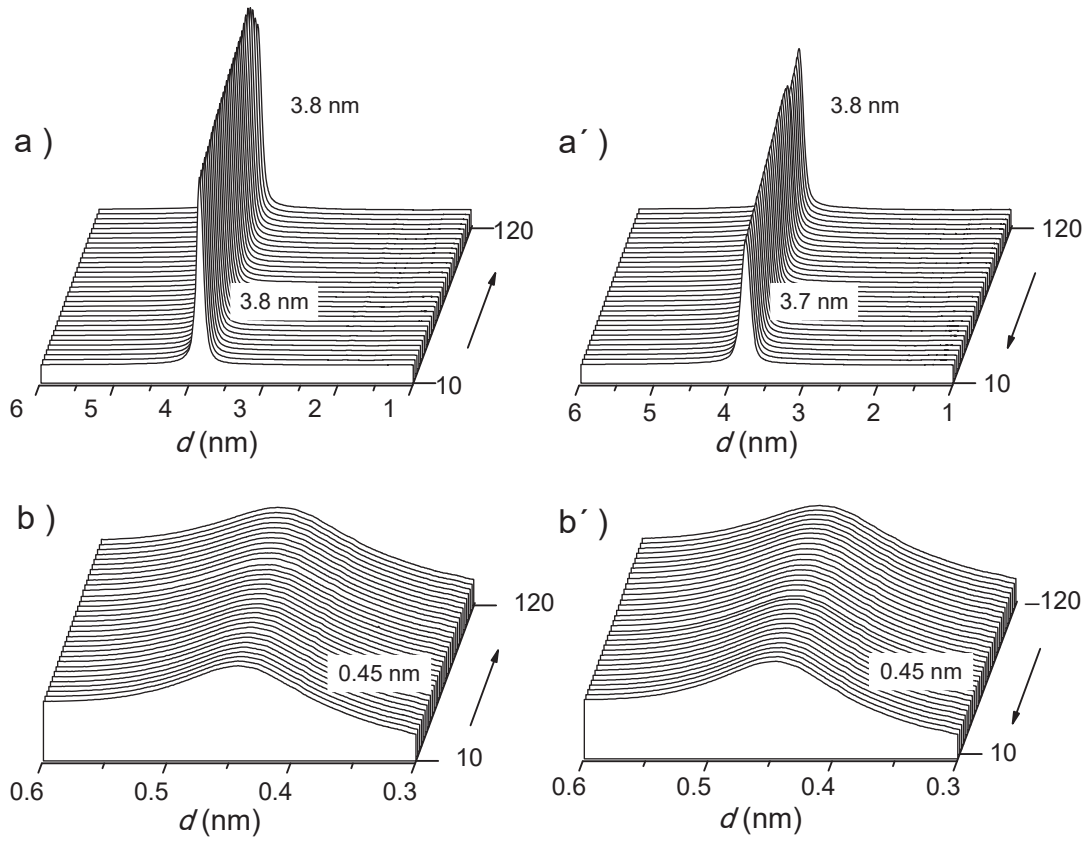

Figure SI-5. Evolution of the SAXS and WAXS profiles of LAE·HyA-0.5 at heating (a, b) and cooling (a´, b´) within the 10-120 °C interval.

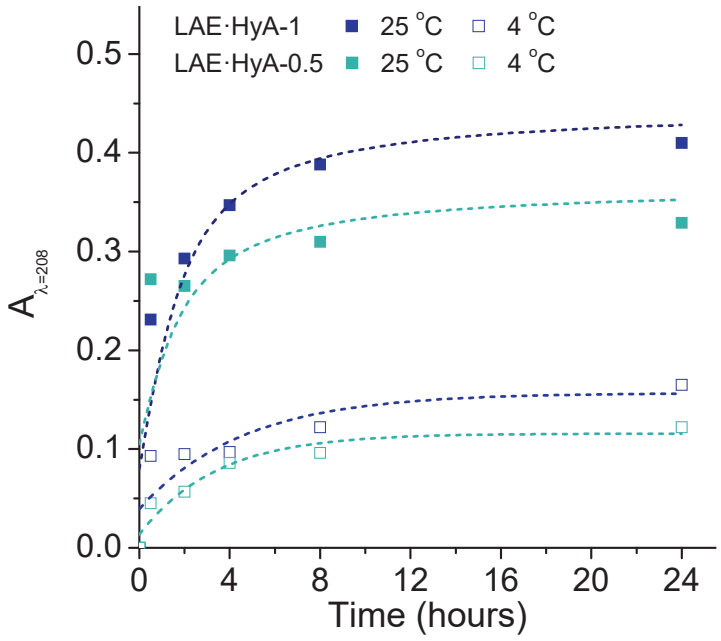

Figure SI-6. Compared dissociation of LAE·HyA complexes upon incubation in aqueous medium (pH= 7.4) at 25 ºC and 4 ºC.

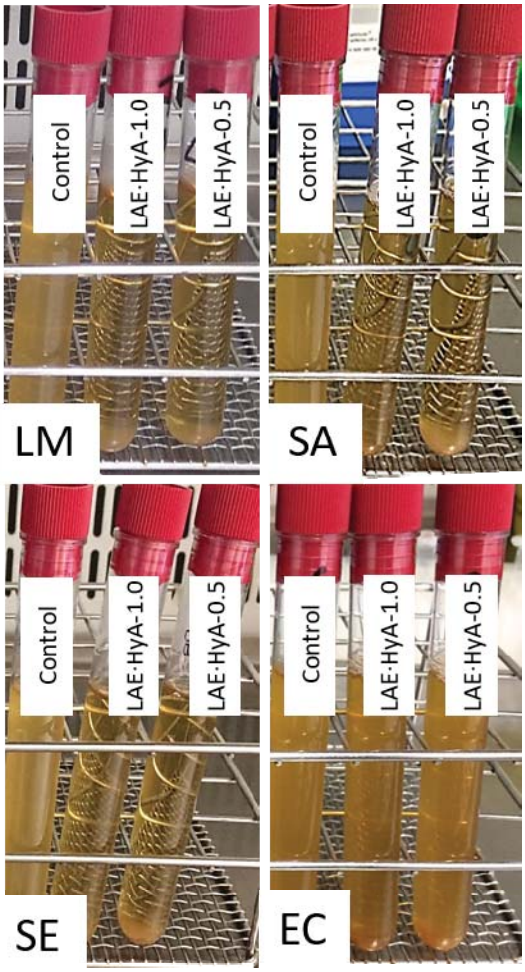

Figure SI-7. Appearance of the bacteria suspensions used for antimicrobial assays of LAE·HyA-1 and LAE·HyA-0.5 films after 24 h of incubation. Complexes films are immersed in the buffer containing the indicated bacteria.

Table SI-1. Biocide activity of films made of LAE·HyA complexes against Gram-negative and Gram-positive bacteria after 2h, 8h and 24 h of incubation at pH 7.4 and 37 °C.

		L. monocytogenes			*S. aureus*			*S. enterica*			*E. coli*		
		2 h	8 h	24 h	2 h	8 h	24 h	2 h	8 h	24 h	2 h	8 h	24 h
HyA	Log (CFU)[a]	5.5	9-4	10.8	6.1	9.0	9.9	6.9	7.7	7.5	6.9	8.7	8.3
LAE·HyA-1	Log (CFU)	5.3	2.3	4.7	5.1	6.4	7	0.3	2.5	2.0	3.3	6.0	6.1
	Log (RV)[b]	0.2	7.1	6.1	1.1	2.6	2.9	6.6	5.2	5.5	3.6	2.7	2.2
	PR (%)[c]	39.39	99.99	99.99	91.26	99.76	99.88	99.99	99.99	99.99	99.98	99.79	99.31
LAE·HyA-0.5	Log (CFU)	5.1	3.3	5.4	5.7	5.4	5.3	2.2	1.1	Total	3.0	6.0	5.2
	Log (RV)	0.4	6.1	5.4	0.4	3.7	4.6	4.7	6.6		3.9	2.7	3.1
	PR (%)	63.63	99.99	99.99	62.71	99.98	99.99	99.99	99.99	100	99.99	99.79	99.91

[a] Antimicrobial activity expressed as logarithm of colony forming units.
[b] Antimicrobial activity expressed as log reduction value.
[c] Percentage of reduction.